NASA CR-54445
PWA FR-1443

FINAL REPORT

INVESTIGATION OF LIGHT HYDROCARBON FUELS WITH FLOX MIXTURES AS LIQUID ROCKET PROPELLANTS

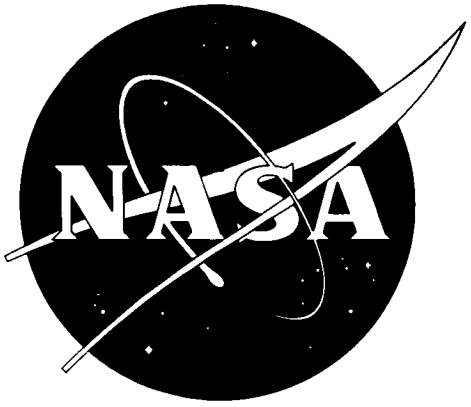

prepared for
NATIONAL AERONAUTICS AND SPACE ADMINISTRATION
CONTRACT NAS3-4195

1 SEPTEMBER 1965

PROGRAM MANAGER
A. I. MASTERS

TECHNICAL MANAGEMENT
NASA LEWIS RESEARCH CENTER
CLEVELAND, OHIO
LIQUID ROCKET TECHNOLOGY BRANCH
JOHN W. GREGORY

Pratt & Whitney Aircraft DIVISION OF UNITED AIRCRAFT CORPORATION
FLORIDA RESEARCH AND DEVELOPMENT CENTER

FOREWORD

This report was prepared by the Pratt & Whitney Aircraft Division of the United Aircraft Corporation under Contract NAS3-4195. The contract was administered by the Lewis Research Center of the National Aeronautics and Space Administration, Cleveland, Ohio. This report is the final report on the subject contract summarizing the technical work during the period 30 June 1964 to 30 June 1965. The NASA Project Manager for the contract was Mr. John W. Gregory.

The following personnel at Pratt & Whitney Aircraft contributed to the technical effort and preparation of this report: D. E. Dahlberg, A. I. Masters (P&WA Program Manager), J. E. Colbert, J. F. Lea, and R. A. Simmons – propellant selection, test, and data analysis; J. F. Butler and R. R. Ramsden – hardware design and test; G. A. Wynne – theoretical performance analysis; M. R. Glickstein, N. W. Barre, and R. H. Whitesides, Jr. – heated tube tests; J. E. Jackson – uncooled test heat transfer analysis; S. A. Mosier, R. E. Dotson, and O. K. Moehrbach – hypergolicity test; R. C. Frink – property determination of hydrocarbon blends; and T. F. Zupnik – nonequilibrium performance analysis. All personnel are employees at Pratt & Whitney Aircraft's Florida Research and Development Center except Mr. Zupnik who is with the P&WA Scientific Staff of the Advanced Power Systems Group in East Hartford, Connecticut.

ABSTRACT

35397

An analysis was completed for determination of the most promising hydrocarbon fuels for use with flox in upper stage rocket engines. Experimental rocket firings in uncooled, transpiration cooled, and regeneratively cooled thrust chambers were conducted using flox with methane, propane, butene-1, and a eutectic blend of pentane and isopentane. Experimental heated tube heat transfer and hypergolicity tests were conducted, and laboratory determinations of physical properties of various blends of hydrocarbon compounds were made.

CONTENTS

SECTION		PAGE
	ABSTRACT	iii
	ILLUSTRATIONS	vii
	TABLES	xi
	NOMENCLATURE	xiii
I	INTRODUCTION	1
II	SUMMARY	5
III	PROPELLANT SELECTION	9
	A. Basis of Selection	9
	B. Fuel Properties	14
	C. Hydrocarbon Blends	14
	D. Theoretical Performance	15
	E. Mission Performance	19
	F. Hypergolic Ignition	21
	G. Heated Tube Tests	21
	H. Transpiration Cooling Analysis	22
	I. Regenerative Cooling Analysis	34
	J. References	37
IV	HARDWARE DESIGN	39
	A. Injector Modification	39
	B. Uncooled Chamber Design	41
	C. Transpiration Cooled Thrust Chamber Design	42
	D. Regeneratively Cooled Thrust Chamber Design	48
V	ROCKET TEST FACILITY	51
VI	TASK II – UNCOOLED PERFORMANCE AND HEAT TRANSFER TESTS	53
	A. Test Description	53
	B. Data Reduction	61
	C. Test Performance	65
	D. Heat Transfer	82
	E. References	105
VII	TASK III – TRANSPIRATION COOLED TESTING	107
	A. Test Description	107
	B. Data Reduction	112
	C. Test Performance	113

CONTENTS (Continued)

SECTION		PAGE
VIII	TASK IV – REGENERATIVE COOLING TESTS	117
	A. Test Description	117
	B. Test Performance	118
	C. Heat Transfer	119
IX	EVALUATION OF TEST RESULTS	121
	A. Injector Performance	121
	B. Heat Transfer	121
	C. Regenerative Cooling	129
	D. Transpiration Cooling	133
	APPENDIX A – Fuel Characteristics	A-1
	APPENDIX B – Determination of Selected Physical Properties of Liquid Hydrocarbon Blends	B-1
	APPENDIX C – Theoretical Performance	C-1
	APPENDIX D – Hypergolic Ignition Tests	D-1
	APPENDIX E – Heated Tube Tests	E-1
	APPENDIX F – Distribution List	F-1

ILLUSTRATIONS

FIGURE		PAGE
1	Coolant Merit Rating vs Fuel Liquid Range for Selected Hydrocarbons	11
2	Generalized Payload Map	19
3	Theoretical Transpiration Cooling Comparison of 82.6% Fluorine – 17.4% Oxygen with Methane	25
4	Theoretical Transpiration Cooling Comparison of 82.6% Fluorine – 17.4% Oxygen with Methane	26
5	Theoretical Transpiration Cooling Comparison of 78.1% Fluorine – 21.9% Oxygen with Ethane	27
6	Theoretical Transpiration Cooling Comparison of 78.1% Fluorine – 21.9% Oxygen with Ethane	28
7	Theoretical Transpiration Cooling Comparison of 76% Fluorine – 24% Oxygen with Propane	29
8	Theoretical Transpiration Cooling Comparison of 76% Fluorine – 24% Oxygen with Propane	30
9	Theoretical Transpiration Cooling Comparison of 70.4% Fluorine – 29.6% Oxygen with Ethylene	31
10	Theoretical Transpiration Cooling Comparison of 70.4% Fluorine – 29.6% Oxygen with Ethylene	32
11	Composite Cooling Scheme	34
12	RL10A-1 Injector	40
13	Injector Area Rework	41
14	Uncooled Chamber Layout	43
15a	Uncooled Chamber with Thermocouple Installation Completed	44
15b	Complete Uncooled Chamber with Fiberglas Covered Insulation	44
16	Transpiration Cooled Chamber Assembly	45
17	Coolant Flow per Unit Area (Constant Pressure – Constant Liner Thickness)	46
18	Coolant Flow per Unit Area (Variable Pressure – Constant Liner Thickness)	46
19	Segment Weld and Thermocouple Installation	47
20	Regenerative Chamber Assembly	49
21	Propellant Supply Area	51
22	Automatic Flow Control System	52
23	Uncooled Chamber Installed in Stand	53
24	RL10A-3 Injector after Test No. 2	55

ILLUSTRATIONS (Continued)

FIGURE		PAGE
25	Oscillograph Trace, Test No. 7	57
26	Injector 3 after Test No. 11	58
27	Soot Formation on Uncooled Chamber after Tests No. 27 through 37 (View from Injector End)	61
28	Flox-Methane Uncooled Test Results (Characteristic Velocity Efficiency vs Mixture Ratio)	70
29	Flox-Methane Uncooled Test Results (Characteristic Velocity Efficiency vs Velocity Ratio)	71
30	Flox-Methane Uncooled Test Results (Characteristic Velocity Efficiency vs Momentum Ratio)	72
31	Flox-Propane Test Results (Characteristic Velocity Efficiency vs Mixture Ratio)	73
32	Flox-Propane Test Results (Characteristic Velocity Efficiency vs Velocity Ratio)	74
33	Flox-Propane Test Results (Characteristic Velocity Efficiency vs Momentum Ratio)	75
34	Flox-Pentane Blend Test Results (Characteristic Velocity Efficiency vs Mixture Ratio)	76
35	Flox-Pentane Blend Test Results (Characteristic Velocity Efficiency vs Velocity Ratio)	77
36	Flox-Pentane Blend Test Results (Characteristic Velocity Efficiency vs Momentum Ratio)	78
37	Flox-Butene-1 Uncooled Test Results (Characteristic Velocity Efficiency vs Mixture Ratio)	79
38	Flox-Butene-1 Uncooled Test Results (Characteristic Velocity Efficiency vs Velocity Ratio)	80
39	Flox-Butene-1 Uncooled Test Results (Characteristic Velocity Efficiency vs Momentum Ratio)	81
40	Comparison of Heat Transfer Coefficients	83
41	Comparison of Heat Transfer Coefficients	84
42	Comparison of Heat Transfer Coefficients	85
43	Comparison of Heat Transfer Coefficients	86
44	Comparison of Heat Transfer Coefficients	87
45	Comparison of Heat Transfer Coefficients	88
46	Comparison of Heat Transfer Coefficients	89
47	Comparison of Heat Transfer Coefficients	90
48	Comparison of Heat Transfer Coefficients	91
49	Comparison of Heat Transfer Coefficients	92

ILLUSTRATIONS (Continued)

FIGURE		PAGE
50	Comparison of Heat Transfer Coefficients	93
51	Comparison of Heat Transfer Coefficients	94
52	Comparison of Heat Transfer Coefficients	95
53	Comparison of Heat Transfer Coefficients	96
54	Comparison of Heat Transfer Coefficients	97
55	Comparison of Heat Transfer Coefficients	98
56	Comparison of Heat Transfer Coefficients	99
57	Comparison of Heat Transfer Coefficients	100
58	Comparison of Heat Transfer Coefficients	101
59	Comparison of Heat Transfer Coefficients	102
60	Comparison of Heat Transfer Coefficients	103
61	Comparison of Heat Transfer Coefficients	104
62	Transpiration Cooled Chamber Mounted in Test Facility	107
63	Separation of Rigimesh Layers after Test No. 1T	108
64	Damage to Chamber after Test No. 10T	110
65	Regenerative Chamber after Test No. 13R (Viewed from Injector End)	119
66	Ratio of Actual to Predicted Film Coefficient vs Axial Location (Flox-Methane, Injector No. 3)	122
67	Ratio of Actual to Predicted Film Coefficient vs Axial Location (Flox-Methane, Injector No. 6)	123
68	Ratio of Actual to Predicted Film Coefficient vs Axial Location (Flox-Propane, Injector No. 7)	124
69	Ratio of Actual to Predicted Film Coefficient vs Axial Location (Flox-Pentane Blend, Injector No. 7)	124
70	Ratio of Actual to Predicted Film Coefficient vs Axial Location (Flox-Butene-1, Injector No. 7)	125
71	Ratio of Measured to Predicted Total Heat Transfer (Uncooled Tests)	126
72	Ratio of Measured to Predicted Total Heat Transfer (Regeneratively Cooled Tests)	127
73	Effect of Fuel Hydrogen-to-Carbon Ratio on Total Chamber Heat Transfer	128
74	Time Variation of Heat Flux and Chamber Pressure (Flox-Methane)	130
75	Time Variation of Heat Flux and Chamber Pressure (Flox-Propane)	131

ILLUSTRATIONS (Continued)

FIGURE		PAGE
76	Time Variation of Heat Flux and Chamber Pressure (Flox-Butene-1)	132
77	Ratio of Measured Heat Flux to Predicted Heat Flux vs Thermocouple Location	134
78	Ratio of Measured Heat Flux to Predicted Heat Flux vs Thermocouple Location	134
79	Ratio of Measured Heat Flux to Predicted Heat Flux vs Thermocouple Location	135
80	Ratio of Measured Heat Flux to Predicted Heat Flux vs Thermocouple Location	135
81	Actual to Predicted c* Ratio vs Chamber Mixture Ratio	136
82	Actual to Predicted c* Ratio vs Chamber Mixture Ratio	136
83	Effect of Mixture Ratio on Experimental c* Loss Due to Transpiration Cooling (Flox-Methane)	137
84	Effect of Mixture Ratio on Experimental c* Loss Due to Transpiration Cooling (Flox-Propane)	138

TABLES

TABLE		PAGE
I	Comparison of Various Cryogenic Oxidizers with Hydrocarbon Fuels	3
II	Design Parameters and Operating Ranges	9
III	Coolant Merit Ratings for Various Light Hydrocarbon Fuels with Flox	11
IV	Selection of Light Hydrocarbon Compounds for Detailed Study (Regenerative Cooling)	13
V	Properties of Light Hydrocarbon Blends	16
VI	Theoretical Vacuum Specific Impulse of Selected Hydrocarbons with Flox	17
VII	Reduction in Vacuum Specific Impulse Due to Reaction Rate Limited Equilibrium During Expansion	17
VIII	Comparison of Sudden Freeze Point Calculations with Kinetic Flow Calculations	18
IX	Relative Impulse for Flox-Light Hydrocarbon Propellants	20
X	Summary of Hypergolic Ignition Test Results	22
XI	Effect of Transpiration Cooling on Flox-Light Hydrocarbon Engine Performance	24
XII	Comparison of Fuels for Composite Cooling Schemes	33
XIII	Gaseous Methane Cooling Configurations	36
XIV	Summary of Injector Modifications	41
XV	Measured Performance Data – Uncooled Tests	66
XVI	Calculated Performance Data – Uncooled Tests	67
XVII	Injector Performance Comparison – Uncooled Tests	68
XVIII	Calculated Heat Loss for Uncooled Tests	105
XIX	Measured Performance Data – Transpiration Cooled Tests	114
XX	Calculated Performance Data – Transpiration Cooled Tests	114
XXI	Effect of Transpiration Cooling on Performance	115
XXII	Coolant Flow and Rigimesh Temperature Data	116

TABLES (Continued)

TABLE		PAGE
XXIII	Measured Performance Data – Regeneratively Cooled Tests	120
XXIV	Calculated Performance Data – Regeneratively Cooled Tests	120
XXV	Injector Performance Comparison – Regeneratively Cooled Tests	120

NOMENCLATURE

SYMBOL	DESCRIPTION	UNITS
AC_D	Effective Injector Flow Area	in^2
c^*	Characteristic Exhaust Velocity	ft/sec
ϵ_e	Nozzle Exit to Throat Area Ratio, A_e/A_t	
η	Efficiency	
F	Thrust	lb_f
I_{sl}	Sea Level Specific Impulse	lb_f-sec/lb_m
I_{vac}	Specific Impulse at $p_a = 0$	lb_f-sec/lb_m
P_c	Chamber Pressure (Throat Total)	psia
ΔP	Pressure Drop (When subscripted refers to injector drop)	psid
Q	Heat Loss to Chamber	Btu/sec
r	Mixture Ratio (Oxidizer-to-Fuel) by Weight	
ρ_b	Propellant Bulk Density	lb_m/ft^3
T	Temperature	°R
V	Propellant Velocity through Injector	ft/sec
$\dot{W}$	Flow Rate	lb_m/sec
$\dot{W}_{f_{inj}}$	Fuel Flow Rate to Injector	lb_m/sec
$\dot{W}_f V_f / \dot{W}_o V_o$	Propellant Momentum Ratio	
Subscripts		
c	Coolant	
f	Fuel	
o	Oxidizer	
p	Propellant	

carbon fuels, the cooling limit is the point where burnout of the thrust chamber coolant passages occurs. When operating below the critical pressure of the coolant, chamber burnout normally occurs in the high heat flux region near the exhaust nozzle throat. This type of burnout usually occurs in the transition region between nucleate boiling and film boiling; however, cooling with film boiling or bulk boiling is possible under some conditions of reduced heat flux. Cracking of the fuel, causing tube fouling, has been suggested as another possible limitation on the cooling capability of hydrocarbon fuels; however, at subcritical pressures cracking will not occur until the fuel is heated well beyond the region of film boiling. For short durations, significant cracking would require temperatures in excess of 2000°R.

When thermally stable fuels are used, transpiration cooling overcomes many of the limitations of ablation and regenerative cooling. Although transpiration cooling involves some unique design problems as well as a potential performance loss due to incomplete mixing between the coolant and the combustion products, the major obstacle to its use has been the lack of applicable experimental data. Light hydrocarbon fuels are ideal transpiration coolants because of (1) good thermal stability, (2) high cooling capacity, and (3) thermodynamic characteristics that give the heated fuel a high specific impulse, even if it is not completely mixed with the combustion products.

For most rocket fuels, fluorine provides a significant increase in theoretical specific impulse over the performance obtained with oxygen. With carbon-hydrogen compounds, even higher theoretical specific impulse is achieved by using fluorine-oxygen blends (or "flox") as the oxidizer. With hydrocarbon fuels, flox will provide a higher theoretical performance than either pure oxygen or fluorine because in combination with carbon oxygen releases more energy than fluorine, whereas, with hydrogen, fluorine releases more energy than oxygen. Flox also provides higher specific impulse than oxygen difluoride with hydrocarbon fuels because of (1) the lower heat of formation of oxygen difluoride and (2) the nonoptimum fluorine concentration in oxygen difluoride for most hydrocarbon fuels. The theoretical specific impulse improvement of flox over oxygen difluoride may be as much as 13 seconds for methane or as little as 2 seconds for hydrocarbons with a hydrogen-to-carbon atomic ratio of 2. Table I gives the theoretical performance of three light hydrocarbon fuels with oxygen, fluorine, flox, and oxygen difluoride. Comparison shows the superiority of the flox combinations.

Program objectives were (1) to evaluate both analytically and experimentally, the ability of light hydrocarbon fuels to cool thrust chambers burning these fuels with flox, and (2) to obtain experimental characteristic velocity, sea level specific impulse, and ignition data for these propellants. Hydrocarbon compounds and blends were selected through detailed analytical and laboratory work, followed by experimental rocket firings using the selected fuels.

SECTION I
INTRODUCTION

Requirements for upper stage rocket engines for future space missions generally include: (1) high specific impulse, (2) high density, (3) hypergolic ignition, (4) space storability, (5) high reliability, and (6) operation for relatively long durations. Although many advanced propellant combinations offer high performance, only a few appear practical from the standpoint of combining high performance with reliable engine operation for long firing times.

Thrust chamber cooling is undoubtedly the most difficult problem that must be solved to permit reliable long duration use of any advanced high energy propellant combination. Most high performance combinations of interest have fluorine as the oxidizer or have an oxidizer containing a high percentage of fluorine, either chemically combined or in solution. These combinations are characterized by high flame temperatures and highly reactive combustion products. Only a few of the high performance rocket fuels under consideration have the physical properties and thermal stability required to provide the necessary thrust chamber cooling with these oxidizers. The most promising of these fuels are low molecular weight carbon – hydrogen compounds such as methane, ethane, ethylene, and propane.

Rocket engines currently in production or under development use ablation or regenerative cooling. Ablation cooling has inherent limits (with regard to flame temperature, duty cycle, and engine operating time) that make this cooling method unsatisfactory for high energy propellants under most conditions. The temperature differential between the flame temperature and the melting point of common ablative materials is almost doubled by changing from current propellants to advanced propellants. Because of this increased temperature difference, ablation rates are increased beyond tolerable limits. In addition, there are the fundamental disadvantages of ablation cooling, i.e., (1) nozzle throat area changes with operating time causing thrust variation and performance loss, (2) chambers are heavy to provide for long operating times, and (3) preflight engine testing either significantly reduces total engine life or necessitates additional ablative material.

Regenerative cooling is the most attractive method of engine cooling. It provides a lightweight design, constant nozzle throat area, and no performance loss. Unfortunately there are also inherent limitations to its use. Some fuels, such as the boron hydrides, decompose so readily that tube fouling will occur under almost any rocket engine conditions. Other fuels, such as hydrazine base fuels, decompose explosively in the vapor phase, thus limiting their applicability to a thrust and chamber pressure where the prevention of fuel vaporization can be assured. With the light hydro-

TABLE I. COMPARISON OF VARIOUS CRYOGENIC OXIDIZERS WITH HYDROCARBON FUELS*

FUELS	OXIDIZERS											
	Oxygen			Fluorine			Oxygen Difluoride			Flox		
	r	ρ_b, lb/ft^3	I_{vac}, sec	r	ρ_b, lb/ft^3	I_{vac}, sec	r	ρ_b, lb/ft^3	I_{vac}, sec	r	ρ_b, lb/ft^3	I_{vac}, sec
Methane	3.52	51.0	364	4.45	61.4	408	5.40	67.6	405	5.75	66.1	417
Ethylene	2.45	55.1	365	2.68	64.8	393	3.85	70.45	407	3.85	66.5	409
Propane	2.82	57.1	359	2.30	68.9	394	4.60	73.8	401	4.50	69.8	408
RP-1	2.60	64.2	352	2.55	75.7	377	3.75	80.0	393	3.75	79.2	396

*Chamber pressure = 100 psia, expansion ratio ϵ_e = 40, shifting equilibrium

The program was divided into four tasks. Task I, "Analytical and Design Activities," included selecting the two most promising fuels for transpiration cooling, and the two most promising fuels for regenerative cooling, and designing hardware for use in the Tasks II, III, and IV experimental tests. Task II, "Uncooled Performance Tests," consisted of short duration uncooled rocket firings with the selected fuels. Task III, "Transpiration Cooling Tests," was an experimental evaluation of the two selected fuels in a transpiration cooled thrust chamber. Task IV, "Regenerative Cooling Tests," was an experimental evaluation of the two selected fuels in a supplementary convectively cooled thrust chamber.

Pertinent to the flox-light hydrocarbon study, Pratt & Whitney Aircraft also conducted several separate Applied Research Programs, which are discussed in this report. These programs are: (1) "Properties of Hydrocarbon Blends," reported under Section III, Paragraph C and Appendix B of this report; (2) "Hypergolicity Tests," Section III, Paragraph F and Appendix D; and (3) "Heated Tube Tests," Section III, Paragraph G and Appendix E.

SECTION II
SUMMARY

The work conducted under NAS3-4195 had two major goals relative to the use of light hydrocarbon fuels with fluorine-oxygen mixtures. The first goal was to select the most promising light hydrocarbon fuels for low chamber pressure (nominal 100 psia) upper stage engines. The second goal was to conduct an experimental evaluation of the heat transfer and cooling characteristics of the selected fuels for both transpiration and regenerative cooling.

The selection of the most promising fuels was to be based on: (1) the cooling ability of the fuel, (2) theoretical performance, (3) space storability, (4) hypergolicity, (5) handling and safety, (6) propellant cost, (7) thermal stability, and (8) bulk density. It was shown early in the study that, because of the similarity of the various hydrocarbon compounds, only the first three items were of major importance to the selection of the most promising fuels. Because of the low chamber pressure, regenerative coolants would be at subcritical pressure, hence the possibility of film or bulk boiling was an important consideration.

Methane was selected on the basis of superior theoretical specific impulse and transpiration cooling capability, as one of the fuels to be evaluated in experimental rocket firings of a transpiration cooled thrust chamber. Because of the clear superiority of methane over other light hydrocarbons for a 100% transpiration cooled engine, the selection of a second fuel for evaluation with transpiration cooling was based on the applicability of the fuel to a composite regenerative – transpiration cooling scheme. Propane was selected as the most desirable fuel for this type of cooling.

To screen the most desirable fuels for regenerative cooling, coolant merit ratings were calculated for ten light hydrocarbon compounds and eight light hydrocarbon blends. The blend merit ratings were based on laboratory determined eutectic diagrams. Propane, propylene, butene-1, methane, and two eutectic blends, 14% n-pentane – 86% isopentane and 48% propane–52% propylene were selected for more detailed analytical studies and heated tube heat transfer tests. Based on the detailed evaluation of these six fuels, butene-1 and the eutectic pentane blend were selected as the two most promising fuels for use in a completely liquid cooled engine. Methane was selected as the most desirable fuel for cooling with boiling and for cooling of higher pressure (pump-fed) engines where the coolant can be maintained above its critical pressure in the heat exchanger.

Using the four selected fuels (methane, propane, butene-1, and the eutectic pentane blend) 43 uncooled rocket firings were made at a nominal 5000-lb vacuum thrust and 100-psia chamber pressure. The first full duration flox-methane test, made with a modified RL10A-3 concentric element injector with swaged oxidizer spuds, showed very high performance (uncorrected characteristic velocity efficiency = 100%), but resulted in burning of the tips of the oxidizer spuds. Tests with RL10A-1 injectors with swaged oxidizer spuds showed good performance at low mixture ratios; however, at high mixture ratios the performance dropped off and oxidizer spud burning again became a problem. The spud burning problem was eliminated by an injector modification using only half of the injector elements without swaging.

The most significant result of the uncooled rocket firings was the low heat fluxes encountered compared to theoretical predictions, and the correlation of the ratio of the measured to theoretically predicted total heat transfer rate to the hydrogen-to-carbon ratio of the fuel. It was found that for butene-1 (hydrogen/carbon ratio equals 2) the total heat transfer rate was only about 15% of the predicted value.

With the greatly reduced heat fluxes encountered in the uncooled tests, regenerative cooling appeared very promising. Propane and the eutectic pentane blend were selected for a series of supplementary fuel-cooled tests. Propane was selected because of its applicability to a composite regenerative-transpiration cooled engine, and the pentane blend was considered to be a better regenerative coolant than butene-1. The selection of the pentane blend over butene-1 was made, however, prior to the uncooled butene-1 firings. Considering the even greater reduction in heat flux encountered in these tests, butene-1 appears to be as good as, or better than, the pentane blend for use in a fully regeneratively cooled chamber.

Thirteen tests, 7 with the eutectic pentane blend and 6 with propane were conducted to verify the practicality of regenerative cooling. Tests were run burning gaseous fuel and liquid flox in the thrust chamber, while subcooled liquid hydrocarbons were supplied to cool the modified RL10 tubular chamber (nozzle area ratio reduced for sea level testing). During the seven cooled tests with pentane the coolant flow was gradually reduced until it was approximately three times the fuel flow to the injector or about 30% greater than the estimated minimum flow required for prevention of film boiling. Test durations were up to 30 seconds, and no hardware damage was encountered. The first four propane cooled tests were of 10-second duration and were made with coolant flows of approximately three times the injector fuel flow. This was approximately twice the coolant flow required to remain in the nucleate boiling region. A 40-second run was then made, during which the coolant flowrate was gradually reduced. For the last 10 seconds of the 40-second test the coolant flowrate was equal to the fuel flowrate through the injector. Although the fuel flow was well into the film boiling regime, as predicted by heated tube data, no hardware damage was incurred.

Twenty-two transpiration cooled 5000-lb thrust rocket firings were made with methane and propane. As in the regeneratively cooled tests the fuel was supplied as a heated gas and the coolant was supplied separately as a subcooled liquid. Ten tests of up to 23-second duration were made with methane. Coolant requirements and performance losses due to incomplete mixing between the coolant and combustion products were equal to or less than the predicted values. Some hardware damage was encountered on the last test; however, this was apparently due to surface irregularities resulting from failure of the coolant supply on previous short duration runs and not due to undercooling during steady-state operation. Twelve transpiration cooled tests including one 30-second and four 20-second tests were made with propane. Good correlation of coolant flowrates with analytical predictions were again obtained; however, the characteristic velocity loss due to transpiration cooling was considerably higher than predicted for propane. No completely satisfactory answer was found for the high characteristic velocity loss; however, it is believed that the loss could be reduced by improved distribution of the coolant flow and a more uniform injector pattern. Also, the effect of incomplete mixing on characteristic velocity does not give a complete picture of the potential performance, because mixing and combustion in the exhaust nozzle could cause the specific impulse reduction to be substantially less than the characteristic velocity reduction.

In addition to the experimental rocket firings and heated tube heat transfer tests, detailed experimental investigations of hypergolic ignition of flox-light hydrocarbon combinations and the physical properties of hydrocarbon blends were also conducted. Methane, propane, ethylene, propylene, butene-1, and a eutectic blend of pentane and isopentane were all shown to be hypergolic over a wide range of conditions. Eutectic freezing points were determined for eight light hydrocarbon blends. Density and viscosity measurements were made of eutectic blends of pentane-isopentane, propane-propylene, and methylcyclopentane – 2-methylpentane.

Numerous conclusions relative to the application of the flox-light hydrocarbon family of propellants to pressure-fed, upper stage rocket engines have been drawn from the work completed to date. Many of the conclusions are listed throughout the text of this report, particularly in Sections III and IX. Some of the major conclusions that have been drawn may be summarized as follows:

1. Methane is the most promising fuel for use in a fully transpiration cooled flox-light hydrocarbon engine, and the development of such an engine is feasible.
2. Development of a composite cooling scheme using partial regenerative and partial transpiration cooling is feasible, and propane appears to be the most promising fuel.

3. Measured heat fluxes are well below analytically predicted values for the flox-hydrocarbon combinations because of carbon deposition on the walls and/or free carbon in the boundary layer. This reduction in heat flux increases markedly with decreasing hydrogen-to-carbon atomic ratio.

4. The reduced heat flux encountered makes full regenerative cooling with butene-1 or a eutectic blend of pentane and isopentane feasible over a wider range of thrust and chamber pressure than predicted theoretically. While exact limits were not determined, 100 psia chamber pressure engines of thrust above 5000 lb appear feasible.

5. All of the flox-light hydrocarbon combinations will be hypergolic under conditions of an ambient sea level start, and there is a strong indication that the propellants will be reliably hypergolic during cold altitude starts.

SECTION III
PROPELLANT SELECTION

A. BASIS OF SELECTION

The selection of fuels for the Task II, III, and IV testing was based primarily on: (1) the ability of the fuels to cool the nozzle and thrust chamber, either regeneratively or with transpiration cooling; (2) the theoretical performance of the fuel with flox; and (3) the space storability of the fuel when used with flox. Also considered in the selection were: hypergolicity, handling and safety, propellant cost, chemical and thermal stability, and propellant bulk density. The design parameters and operating ranges over which these factors were evaluated are listed in table II.

TABLE II. DESIGN PARAMETERS AND OPERATING RANGES

Parameter	Design	Range
Nominal thrust, lb	5000	5000 (maximum)
Chamber pressure, psia	100	50-100
Nozzle area ratio	40	6-60
c* Efficiency, %	95	90-98
Mixture ratio	Optimum	± 50% of optimum
Flox concentration	Optimum for selected fuel	30% to optimum % fluorine by weight
Coolant passage pressure drop, psid	50 (maximum)	100 (maximum)

The initial screening of propellants was accomplished by compiling data for a number of light hydrocarbon compounds and determining which physical and chemical properties are important to achieve the propellant characteristics required. It was found, as will be shown in detail later in this report, that the theoretical specific impulse varies by about 4% for the various hydrocarbon compounds considered. Furthermore, the compounds that provide the lowest specific impulses tend to have the highest densities, so that the performance on a mission basis shows even less variation. On the other hand, a wide variation was found in the hydrocarbon freezing points and boiling points. A low freezing point is important for improved space storability, while a wide liquid range (the temperature difference between the freezing point and the boiling point) was shown to be important for regenerative cooling.

1. CANDIDATES FOR TRANSPIRATION COOLING

All of the hydrocarbon compounds considered appear to be capable of cooling a transpiration cooled engine. It is shown in Section III-D that as the molecular weight of the hydrocarbon fuel increases, the theoretical specific impulse with flox decreases. Similarly, as the molecular weight increases the theoretical specific impulse of the unmixed fuel will decrease.

Thus, while the performance loss associated with transpiration cooling varies only slightly with different hydrocarbons, there is a significant trend toward reduced performance loss (due to incomplete mixing) with increased specific impulse. Thus, the initial screening of fuels for evaluation in a transpiration cooled chamber can be made solely on the basis of theoretical specific impulse and fuel freezing point. Methane, ethane, ethylene, and propane are the four hydrocarbons with the highest specific impulse. These four compounds also have freezing points that are satisfactory for long term space storability (see Section III, paragraph D, and Appendix A, Page A-1). On this basis, methane, ethane, ethylene, and propane were selected as four fuels to be studied in detail for use in a transpiration cooled thrust chamber. The analysis of these four fuels and the selection of two of them for the experimental investigation are presented in paragraph H of this section.

2. *CANDIDATES FOR REGENERATIVE COOLING*

The ability of any particular fuel to be used for regenerative cooling at the specified conditions is not as easily predicted as with transpiration cooling. Coolant merit ratings, defined as the ratio of the enthalpy change of the fuel within its liquid range (from the freezing temperature to the temperature where the vapor pressure equals 150 psia) to the heat transferred to the engine, were calculated for several hydrocarbon compounds as shown in table III. The merit ratings are based on a 5000-lb thrust, 100-psia chamber pressure, area-ratio-of-40 thrust chamber, and on theoretically predicted heat fluxes. For heat exchanger operation at subcritical pressures, a coolant merit rating of 1.0 is a necessary (but not sufficient) criterion for complete regenerative cooling without film boiling. None of the fuels listed have coolant merit ratings above 1.0; this means that none of the fuels are capable of completely cooling a 5000-lb thrust engine if the theoretical heat flux is achieved. Experience with hydrocarbon fuels has shown, however, that the actual heat flux may be considerably less than the predicted value. (This has been substantiated further in the uncooled flox-hydrocarbon tests described in Section VI.) The use of the coolant merit rating as shown here was not intended to prove or disprove the cooling ability of any particular fuel, but rather to determine which fuels appeared most promising.

In figure 1 coolant merit rating is plotted as a function of liquid range. The graph shows that a high coolant merit rating requires a wide liquid range. To assure temperature compatibility between the fuel and oxidizers, thereby greatly improving space storability, no fuel was considered with a freezing point above 200°R, the temperature at which the vapor pressure of flox is approximately 100 psia. It can be seen from table A-1 (Appendix A) that many of the hydrocarbons with freezing points above 200°R have wider liquid ranges than any of the compounds with freezing points below 200°R. One approach to improving the coolant merit rating while maintaining space storability would be to depress the freezing point of hydrocarbons with a wide liquid range.

TABLE III. COOLANT MERIT RATINGS FOR VARIOUS LIGHT HYDROCARBON FUELS WITH FLOX

Fuel	I_{vac},(1) sec	Mixture Ratio	Freezing Point, °R	Liquid Range to Normal Boiling Point, °R	Coolant Merit Rating
Methane	418	5.75	163	38	0.13
Ethylene	409	3.85	187	118	0.24
Ethane	411	4.82	162	170	0.26
Methyl-acetylene	403	3.08	309	141	0.37
Propane	408	4.50	154	262	0.37
Butane	407	4.38	204	267	0.39
Propylene	405	3.85	158	248	0.41
Pentane	404	4.34	258	299	0.48
Butene-1	404	3.85	157	324	0.50
Isopentane	403	4.34	204	338	0.50
Methylcyclopentane	400	3.85	235	385	0.51
2-Methylpentane	404	4.20	215	387	0.59

(1) Based on shifting equilibrium expansion, 100 psia chamber pressure, nozzle exit area ratio of 40, and mixture ratio for maximum specific impulse.

Figure 1
Coolant Merit Rating vs Fuel Liquid Range for Selected Hydrocarbons

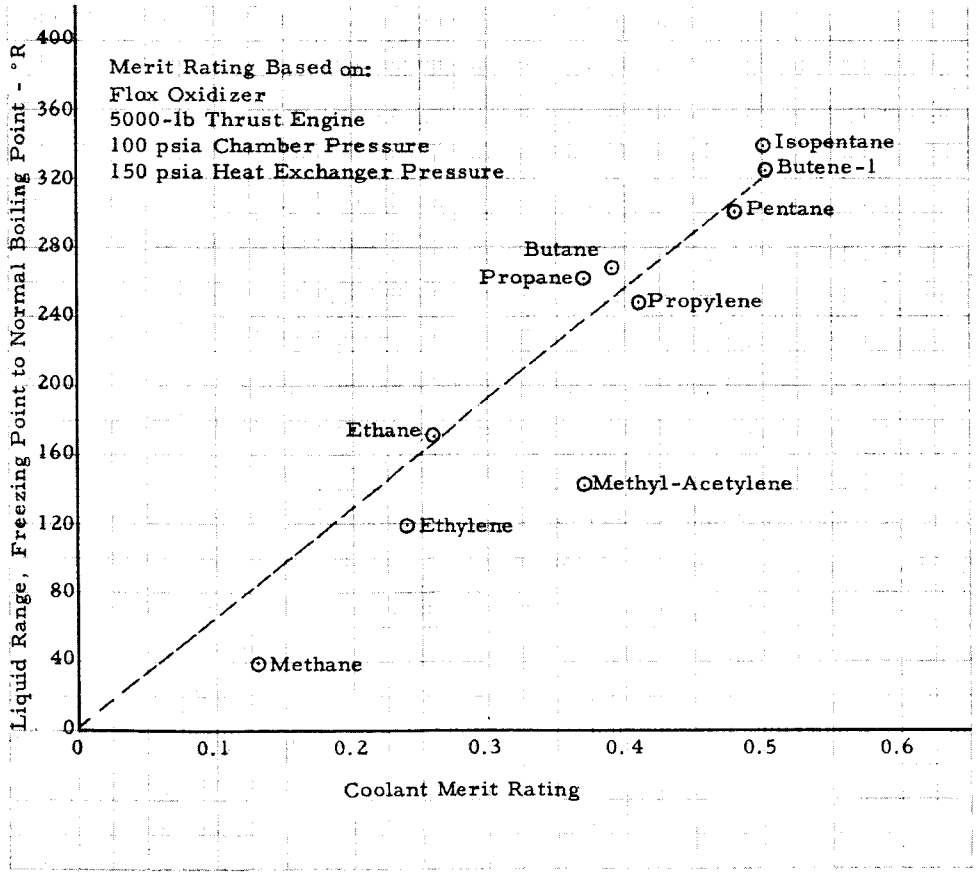

DF 33927

In table IV, the hydrocarbons with freezing points below 260°R (see table A-1) have been listed in order of increasing freezing points and divided into three groups according to their applicability for (1) use as pure compounds, (2) use in blends, and (3) use in blends in small concentrations. Other factors such as liquid range, availability, and viscosity were then considered to determine the propellants that should receive further study.

When two miscible liquids are blended, the freezing point of the blend is normally depressed. The lowest freezing point for any concentration of two compounds is termed the eutectic point. For the light hydrocarbons, the eutectic point is always less than 40°R below the freezing point of the pure compound with the lowest initial freezing point. As the difference between the freezing points of the two compounds increases, the concentration of the higher freezing point compound at the eutectic point decreases. From these considerations, it was concluded that it would not be possible to have a blend with a freezing point below 200°R if one of the major constituents of the blend had a freezing point above 240°R. If a hydrocarbon has a freezing point between 240°R and 260°R, it may be considered for use in a blend in small concentrations, but with freezing points above 260°R a significant quantity of the compound could not be added to any hydrocarbon and still yield a blend with a freezing point below 200°R.

It was decided that a minimum liquid range of 200°R was necessary for a pure compound to yield a high enough coolant merit rating to warrant consideration as a regenerative coolant. In considering compounds for use in blends, the freezing point is not known until the eutectic point is found; therefore, the boiling point was used as the criterion for determining whether the compound is potentially useful in a blend. The minimum boiling points considered satisfactory to warrant further study of the compound were 400°R for group 1, 500°R for group 2, and 550°R for group 3. It was found that unsaturated hydrocarbons tended to have considerably higher viscosities near their freezing points than saturated hydrocarbons. For this reason, the saturated compounds were given preference in the final selection.

As shown in table IV; propane, butene-1, and propylene were selected for further study as pure compounds; propane, butene-1, propylene, isopentane, 2-methylpentane, methylcyclopentane, and n-pentane were selected for study in blends. Methane was also selected for more detailed investigation because of its higher performance and the possibility of its being a superior hydrocarbon coolant in the boiling region.

TABLE IV. SELECTION OF LIGHT HYDROCARBON COMPOUNDS FOR DETAILED STUDY (REGENERATIVE COOLING)

Group(1)	Name	Freezing Point, °R	Boiling Point, °R	Liquid Range, ΔT	ΔT OK(2) for Group 1	B.P. OK(3) for Blends	Available in Test Quantities	Viscosity at Low Temperatures	Coolant Merit Rating (5)	Selected for Study as Pure Compound	Selected for Study as Blends
	Flox	90	155	65							
1	Propane	154	416	262	x	x	x	OK	0.37	x	x
1	Butene-1	157	481	324	x	x	x	High	0.50	x	x
1	Propylene	158	406	248	x	x	x	OK	0.41	x	x
1	Ethane	162	332	170			x	OK	0.26		
1	Methane	163	201	38			x	OK	0.13	x	
1	Cis-pentene-2	169	543	374	x	x					
1	Ethylene	187	305	118			x		0.23		
1	3-Methyl-butene-1	188	528	340	x	x	(4)				
1	Pentene-1	195	545	350	x	x	(4)	High			
2	Iso-butane	204	471	267	-		x				
2	Iso-pentane	204	542	338	-	x	x	OK	0.50		x
2	2-Methyl-pentane	215	602	387	-	x	(4)		0.59		x
2	4-Methyl-pentene-1	217	589	372	-	x	(4)	Probably high			
2	Pentadiene-1, 4	226	539	313	-	x					
2	Methyl-butadiene-1, 3	229	533	304	-	x	x	Probably high			
2	Cis-hexene-2	229	615	386	-	x					
2	Propadiene	229	434	205	-						
2	Methyl-cyclopentane	236	621	385	-	x	(4)		0.51		x
2	Hexadiene-1, 5	239	599	360	-	x					
2	Trans-pentene-2	239	545	306	-	x					
2	2, 3-Dimethyl-butene-1	239	592	353	-	x					
2	Methyl-propene	239	479	240	-		x				
3	Cis-butene-2	242	499	257	-						
3	Hexene-1	242	606	364	-	x					
3	n-Butane	243	491	248	-		x	OK	0.39		
3	2-Methyl-butene-2	243	561	318	-	x					
3	Cis-3-Methyl-pentene-2	243	619	376	-	x					
3	2-Methyl-butene-1	244	548	304	-						
3	Hexyne-1	244	625	381	-	x					
3	Butadiene-1, 2	246	511	265	-		x				
3	Trans-3-methyl-pentene-2	248	614	366	-	x					
3	Cis-hexene-3	249	612	363	-	x					
3	Trans-hexene-2	253	614	361	-	x					
3	n-Pentane	258	557	299	-	x	x	OK	0.48		x

(1) Group 1 - freezing point satisfactory for use as pure compound; group 2 - freezing point satisfactory for use in blends: Group 3 - freezing point satisfactory for use in blends in small concentrations.

(2) 200°R minimum ΔT requirement.

(3) Minimum arbitrarily set at 400°R for group 1, 500°R for group 2 and 550°R for group 3.

(4) Available in small quantities at relatively high cost.

(5) The regenerative coolant merit rating is defined as the heat capacity of the fuel divided by the total heat transferred to a 5K chamber while maintaining a 2160°R wall temperature. The heat capacity of the liquid fuel is taken between its freezing point and its 150 psia boiling point.

B. FUEL PROPERTIES

The freezing points, boiling points, critical constants and densities of 55 selected hydrocarbon compounds are shown in table A-1 of Appendix A. The compounds shown in this table include most stable carbon-hydrogen compounds of 5 carbon atoms or less for which property data are available, and selected carbon-hydrogen compounds with 6 carbon atoms. Flox and RP-1 are shown in the table for comparison. Vacuum specific impulse and coolant merit ratings have been calculated for some of the compounds and are also shown. The data given in table A-1 were used in the initial screening of fuels for both transpiration and regenerative cooling. Appendix A includes detailed property data for all of the fuels selected for study in the transpiration cooling analysis, and as pure compounds or constituents of blends in the regenerative cooling analysis. Properties of butane, methylacetylene, and RP-1 are also included for comparison.

C. HYDROCARBON BLENDS

As described in paragraph A, the compounds selected for study in hydrocarbon blends were propane, butene-1, propylene, isopentane, 2-methylpentane, methylcyclopentane and n-pentane. Before this selection had been completed, some work had also been done with methane and butane. The approach that was followed in selecting and obtaining data for the most promising blends was as follows:

1. The boiling points of the blends are higher than, but approach, the boiling point of the more volatile compound; also, higher boiling point compounds tend to have higher freezing points than compounds with lower boiling points. Blends with potentially the widest liquid range could, therefore, be selected by choosing two hydrocarbons with similar boiling points that appeared as though they might have eutectic freezing points below 200°R. The blends selected were: pentane-isopentane, propylene-propane, propane-pentane, methylcyclopentane-2-methylpentane, 2-methylpentane-isopentane, propane-butene-1, and pentane-butene-1. Eutectic diagrams for propane-methane, methane-ethane, and pentane-butane had been prepared prior to this selection.
2. Eutectic diagrams were prepared for all of the selected blends except the propane-butene-1, and pentane-butene-1. These two blends showed very high viscosities at low temperatures that reduced their useful liquid range and made freezing point determination quite difficult.
3. Coolant merit ratings were calculated for all of the blends as a function of blend concentration.
4. For the most promising blends, density and viscosity were measured as a function of temperature.

5. For a single blend at room temperature, vapor pressure was measured and compared to the theoretically predicted value for a true solution.

The laboratory procedures employed are presented in detail in Appendix B, along with freezing points and coolant merit ratings plotted as a function of blend concentration. The eutectic concentration freezing points and coolant merit ratings are summarized in table V. Of the eight blends listed in table V, pentane-isopentane, propane-propylene, and methylcyclopentane-2-methylpentane were selected for density and viscosity measurements. The density and viscosity of these three blends at their eutectic concentrations are given in Appendix B. It can be seen that the methylcyclopentane-2-methylpentane blend has a higher viscosity near the freezing point than the other two blends. Furthermore both methylcyclopentane and 2-methylpentane are expensive compared to the other light hydrocarbons being considered, and are not readily available in large quantities. With a requirement for quantity production undoubtedly both the cost and availability could easily be improved, but for purposes of this study it was not considered desirable to go into a detailed evaluation of blends containing these two hydrocarbons. Therefore, propane-propylene and pentane-isopentane were selected as the two blends to receive detailed analysis for application to a regeneratively cooled engine.

D. THEORETICAL PERFORMANCE

The theoretical performance of flox with 19 different hydrocarbons has been calculated as shown in table VI and for 8 hydrocarbon blends, as shown in table V. Most of these calculations were based on the mixture ratio optimization techniques outlined in Appendix C of this report. However, complete maps of theoretical performance showing vacuum specific impulse, characteristic velocity, and chamber temperature as a function of mixture ratio for various fluorine concentrations have been prepared for methane, ethylene, butene-1, propane, and the pentane blend. These performance maps are included in Appendix C.

Calculations were performed to determine vacuum specific impulse based on reaction rate limited chemical reaction during expansion. These calculations were based on 100 psia operation of the RL10 thrust chamber (approximately 5000 pounds vacuum thrust and exhaust nozzle area ratio of 40). The calculations determined the magnitude of the reduction in specific impulse due to reaction kinetics and evaluated the variation of this effect with oxidizer-fuel ratio, percent fluorine in the oxidizer, and the hydrogen-to-carbon ratio of the fuel. Calculations were made for methane, propane, and ethylene at the peak specific impulse mixture ratio, and for methane at off mixture ratio conditions, i.e., reduced mixture ratio and reduced percentages of fluorine in the oxidizer. All of the nonequilibrium performance calculations were made using the one-dimensional kinetic flow deck developed for NASA by the United Aircraft Corporation Research Laboratories under contract NAS3-2572 (Reference 1)†. The results of these calculations are shown in table VII.

† *References used in this section are given in Paragraph J.*

TABLE V. PROPERTIES OF LIGHT HYDROCARBON BLENDS

Blend[1] (Weight Percentages) °R	Freezing Point, °R	Normal Boiling Point, °R	Liquid Range ΔT, °R	Cooling Merit Rating[5]	Estimated Fuel Density[2], lb/ft^3	Estimated Propellant Bulk Density[3], lb/ft^3	I_{vac} with Flox[4], sec	Mixture Ratio for Maximum I_{vac}	Weight Percent Fluorine in Oxidizer
14% Pentane 86% Iso-pentane	196	544	348	0.51	48.6	75.7	403 (402)	4.34	74.0
52% Propylene 48% Propane	137	410	273	0.41	46.9	74.5	407 (406)	4.16	73.3
16% Methane 84% Propane	126	227	101	0.19	42.8	74.1	410 (409)	4.70	77.3
31% Methylcyclopentane 69% 2-Methylpentane	197	609	412	0.59	52.9	76.9	403 (402)	4.09	72.6
68% Pentane 32% Butane	221	521	300	0.45	48.4	75.7	405 (404)	4.35	74.3
36% 2-Methylpentane 64% Iso-pentane	184	557	373	0.54	49.6	76.0	403 (402)	4.29	73.8
55% Methane 45% Ethane	133	209	76	0.16	34.4	71.0	415 (415)	5.33	80.8
5% Pentane 95% Propane	148	417	269	0.38	46.1	75.1	408 (407)	4.49	75.9

(1) Weight percentages are at the blend eutectic point
(2) Density taken at the blend freeze point; densities for the pure compound are extrapolated from higher temperatures
(3) Value shown is at the mixture ratio for maximum I_{vac}. Fuel density is taken at the blend freezing point. Oxidizer density is taken at the normal boiling point.
(4) Theoretical values based on both propellants at their normal boiling point, shifting equilibrium expansion, 100 psia chamber pressure, nozzle area ratio of 40, and mixture ratio for maximum specific impulse. Values in parentheses are for liquid fuel taken at its freezing point and liquid flox at its normal boiling point.
(5) The regenerative coolant merit rating is defined as the heat capacity of the fuel divided by the total heat transferred to a 5K chamber while maintaining a 2160°R wall temperature. The heat capacity of the liquid fuel is taken between its freezing point and its 150 psia boiling point.

TABLE VI. THEORETICAL VACUUM SPECIFIC IMPULSE OF SELECTED HYDROCARBONS WITH FLOX

Fuel	F_2 for max I_{vac}, %	r for max I_{vac}	Shifting I_{vac}, sec	Frozen I_{vac}, sec	c* ft/sec	T_c, °R
Methane	82.6	5.75	418	358	6960	7540
Ethane	78.1	4.82	411	354	6880	7530
Propane	76.0	4.50	408	353	6840	7520
Butane	74.8	4.38	407	353	6810	7520
Isobutane	74.8	4.38	407	353	6790	7510
Pentane	74.0	4.34	404	351	6770	7490
Isopentane	74.0	4.34	403	350	6750	7490
2-Methylpentane	73.5	4.20	404	351	6720	7490
Ethylene	70.4	3.85	409	353	6820	7620
Propylene	70.4	3.85	405	351	6770	7600
Butene-1	70.4	3.85	403	350	6780	7560
Methyl-propene	70.4	3.85	403	350	6770	7550
Pentene-1	70.4	3.85	403	350	6760	7550
Cis-pentene-2	70.4	3.85	402	349	6750	7540
3-Methyl butene-1	70.4	3.85	402	349	6750	7540
Cyclopentane	70.4	3.85	400	349	6700	7480
Methylcyclopentane	70.4	3.85	400	349	6690	7480
Methylacetylene	61.3	3.08	403	350	6670	7550
RP-1	69.3	3.75	396	346	6680	7470

NOTE: Pc = 100 psia, ϵ_e = 40, propellants initially at their normal boiling point.

TABLE VII. REDUCTION IN VACUUM SPECIFIC IMPULSE DUE TO REACTION RATE LIMITED EQUILIBRIUM DURING EXPANSION (1)

Fuel	F_2 in Flox,%	Oxidizer/Fuel Ratio	Full Shifting Vacuum Impulse, sec	Kinetic Vacuum Impulse, sec	ΔI_{vac}, sec
Methane	82.6(2)	5.75(2)(3)	418	404	14
	82.6	4.50	405	389	16
	82.6	3.00	386	366	20
	70.0	5.20(3)	407	387	20
	50.0	4.40(3)	392	374	18
	30.0	3.85(3)	380	366	14
Ethylene	70.4(2)	3.85(2)	409	396	13
Propane	76.0(2)	4.50(2)	408	395	13

(1) Theoretical vacuum specific impulse based on 100 psia chamber pressure, nozzle area ratio of 40 and both propellants initially at their normal boiling points.

(2) Values for maximum theoretical shifting vacuum specific impulse.

(3) Peak mixture ratio for the fluorine concentration listed.

From the methane calculations at various oxidizer-to-fuel ratios and various percentages of fluorine in the oxidizer, it can be seen that reducing mixture ratio, whether the percentage of fluorine is held constant or reduced, does not reduce the loss in vacuum specific impulse due to chemical nonequilibrium. Comparison of the ethylene and propane calculations with methane at the peak mixture ratio shows that the carbon-to-hydrogen ratio does not have a significant effect on nonequilibrium losses. It may be concluded from these calculations that when chemical kinetics are considered, the mixture ratio and percentage of fluorine in the oxidizer for maximum specific impulse are not changed significantly from the peak complete-equilibrium values. This conclusion was considered to be true for all of the hydrocarbon compounds of interest in this program.

Frequently in evaluation of nonequilibrium specific impulse losses, a "sudden freeze point approximation" is used. The sudden freeze point approximation has the advantage of greatly reduced calculation time, and has been shown to be reasonably accurate for simple reactions such as oxygen-hydrogen. The validity with C-H-F-O type reactions has never been investigated, therefore, it was considered necessary that a comparison be made before a sudden freezing point analysis was used. The method of calculation used was an extension of Bray's sudden freezing point method (Reference 2) to include nonequilibrium one-dimensional nozzle flows with several concurrent chemical reactions (Reference 3). This method of calculation has been termed a "composite" sudden freeze point analysis. The results of the sudden freeze point calculations are compared with conventional kinetic flow calculations in table VIII.

TABLE VIII. COMPARISON OF SUDDEN FREEZE POINT CALCULATIONS WITH KINETIC FLOW CALCULATIONS

Fuel	F_2 in Oxidizer %	Oxidizer-Fuel Ratio, r	I_{vac} Full Shifting Impulse, sec	I_{vac} Complete Kinetics Calculation	I_{vac} Composite Sudden Freeze Point Approximation, sec	Difference I_{vac}, sec
Methane	82.6	5.75	418	404	390	14
	82.6	4.50	405	389	383	6
	70.0	5.20	407	387	381	6
	50.0	4.40	392	374	372	2
	30.0	3.85	380	366	366	0
Propane	76.0	4.50	408	395	382	13

It can be seen from table VIII that the sudden freeze point calculations give reasonably good agreement with the more rigorous nonequilibrium calculations at low mixture ratios and fluorine concentrations, but are grossly different near the peak specific impulse. It is concluded that because of the complexity of the recombination reactions, the sudden freeze approximation is not valid, even with a composite type of calculation. However, it should also be recognized that all nonequilibrium calculations are based upon partially assumed reaction rates and reaction models that may introduce errors of unknown magnitude.

E. MISSION PERFORMANCE

In addition to theoretical performance and space storability, several other factors were considered from the standpoint of their effect on mission performance. These include: propellant bulk density, handling and storage, and propellant cost.

1. PROPELLANT BULK DENSITY

The relative effect of propellant bulk density and specific impulse on payload was determined by establishing a trade-off factor of the form:

$$I_{relative} = I_{vac}\left(\frac{\rho_{bulk}}{\rho_{reference}}\right)^{k}$$

Where $\rho_{reference}$ is the bulk density of some reference propellant and the exponent k is determined from mission analysis. When this density correlation is used, payload is proportional to the "relative impulse," i.e., higher relative impulses will yield higher payloads for a given gross weight. Exponents determined from two representative space missions were used for comparing the light hydrocarbon-flox propellants; these missions were the Apollo Service Module and the Apollo LEM Descent Stage. Bulk density-specific impulse combinations yielding equal payloads were determined from payload maps of the form shown in figure 2. Because the absolute values of bulk density and specific impulse affect the value of k, only values in the range of the light hydrocarbon-flox combinations were considered. The value of the exponent k was then determined from these density-impulse combinations using the equation:

$$k = \ln(I_{vac_1}/I_{vac_2})/\ln(\rho_2/\rho_1) \ .$$

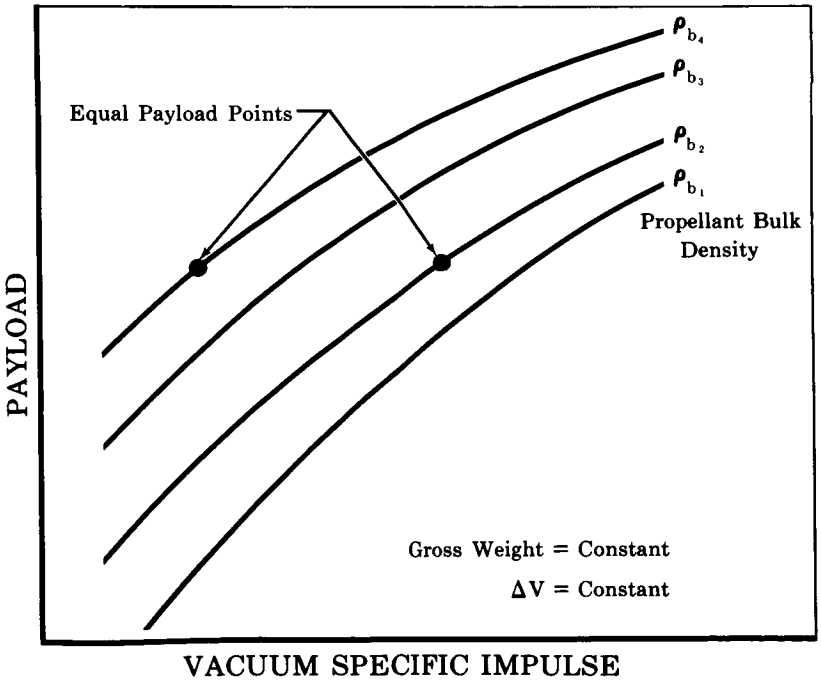

Figure 2. Generalized Payload Map *FD 9560*

Table IX shows the exponents and the relative impulse for all fuels considered for use as pure compounds and all blends at their eutectic point. It can be seen that the effect of the density factor is to bring the relative impulse closer together than the vacuum specific impulse values. This makes it even more difficult to make a propellant selection strictly on mission performance considerations.

TABLE IX. RELATIVE IMPULSE FOR FLOX-LIGHT HYDROCARBON PROPELLANTS

Fuel	Vacuum Specific Impulse, sec (1)	Propellant Bulk Density, lb/ft^3 (2)	Relative Impulse, sec (3) k = 0.05	k = 0.20
Pure Compounds				
Methane (4)	417.4	67.8	417.4	417.4
Propane	407.3	74.9	409.3	415.5
Butene-1	402.4	75.0	404.4	410.6
Propylene	404.5	73.9	406.2	411.5
Ethane	410.9	73.5	412.6	417.6
Ethylene	408.4	70.3	409.1	411.3
Blends				
14% Pentane 86% Isopentane	402.3	75.7	404.5	411.3
52% Propylene 48% Propane	406.2	74.5	408.1	413.9
16% Methane 84% Propane	409.2	74.1	411.0	416.5
31% Methylcyclopentane 69% 2-methylpentane	401.7	76.9	404.2	411.9
68% Pentane 32% Butane	404.0	75.7	406.3	413.0
36% 2-methylpentane 64% Isopentane	402.3	76.0	404.6	411.6
55% Methane 45% Ethane	414.7	71.0	415.7	418.6
5% Pentane 95% Propane	407.1	75.1	409.1	415.5

(1) Theoretical shifting equilibrium value based on liquid fuel at its freezing point and liquid flox at its normal boiling point, 100 psia chamber pressure, exit area ratio of 40 and mixture ratio for maximum specific impulse.

(2) Based on liquid fuel at the freezing point and liquid flox at its normal boiling point.

(3) $I_{relative} = I_{vac}\left(\frac{\rho_{bulk}}{\rho_{reference}}\right)^k$ k = 0.05 is representative of an Apollo Service Module mission. k = 0.20 is representative of an Apollo LEM Descent Stage mission.

(4) Reference propellant, i.e., $\rho_{reference}$ = 67.8 lb/ft^3.

2. *HANDLING AND STORAGE*

From the data in Appendix A, it can be seen that handling and safety procedures are similar for all of the light hydrocarbon fuels. None is more cryogenic than flox and none is toxic, thus, no additional handling problems are encountered with any of these fuels. In addition, the eight blends and six pure compounds shown in table IX can all be considered space storable and, with the exception of the pentane-butane blend, all have liquid ranges compatible with liquid flox pressurized to 100 psia.

3. *COST*

Present costs for the twelve fuels considered for use as pure compounds or blends (Appendix A) range from a few cents per pound (propane, butane) to $3.00 per pound for 2-methylpentane. The high cost of some compounds is due to their limited usage, and could be substantially reduced if larger production quantities were required. The present price of a compound was considered to be a decisive factor in selection of a fuel only if the physical properties closely matched those of a less expensive compound.

F. HYPERGOLIC IGNITION

Only a limited amount of experimental data have been reported on the hypergolicity of flox-hydrocarbon propellant combinations. An experimental ignition program was conducted, therefore, to examine the hypergolicity and relative ignition delay time of the flox-light hydrocarbon combinations over ranges of the following parameters (1) fluorine concentration, (2) propellant precedence, (3) chamber initial pressure, (4) oxidizer and fuel state and temperature, and (5) injector type. The fuels considered were methane, ethylene, propane, propylene, butene-1 and a eutectic blend of 14% pentane and 86% isopentane. For comparison purposes, ignition tests were also conducted with the gaseous fluorine-gaseous hydrogen combination.

In general, the fuels were all found to be hypergolic with flox over the range of variables considered; however, some fuels (particularly methane) are rather sensitive to injection conditions and can produce excessive ignition delays under some conditions. The results of the hypergolicity tests are summarized briefly in table X. The ignition program is described in detail in Appendix D.

G. HEATED TUBE TESTS

Heat transfer tests were conducted with the six hydrocarbon fuels selected for detailed study as regenerative coolants: (1) methane, (2) propane, (3) propylene, (4) butene-1, (5) a eutectic blend of 48% propane and 52% propylene, and (6) a eutectic blend of 14% n-pentane and 86% isopentane. Determinations of the maximum nucleate boiling heat flux, or peak heat flux, were made at fuel inlet temperatures from 160 to 520°R, subcritical

TABLE X. SUMMARY OF HYPERGOLIC IGNITION TEST RESULTS

Fuel Type	Fuel Temperature Range (°R)	Oxidizer Temperature Range (°R)	Oxidizer Composition (%F_2 in Flox)	System Pressure Range (psia)	No. of Tests for each Fuel	Tests with No Ignition (Other than System Malfunction)	Ignition Delay Time Range (millisec)
Methane	280-540	140-540	75-82.6	5.0-14.7	42	9	4-1505
Ethylene	540	140-540	70.4-75	5.5-14.7	15	-	3-515
Propane	200-540	140-540	75-76	4.5-14.7	28	3	10-477
Propylene	540	140-540	70.4-100	5.0-14.7	18	-	8-500
Butene-1	540	140-540	70.4-75	5.0-14.7	23	5	25-994
Pentane Blend	540	140	74	14.7	15	-	20-232
Hydrogen	540	540	100	14.7	23	-	4-59

and supercritical fuel inlet pressures (140 to 800 psia), and fuel inlet velocities of 1.3 to 28 ft/sec. Film boiling heat transfer coefficients were also measured for various fuel flow conditions to obtain data for prediction of wall temperatures at conditions where the maximum nucleate boiling heat flux is exceeded. These data were then correlated for application to the design of cooling systems for liquid propellant thrust chambers.

The upper limit heat flux followed the expected trend of increasing at greater degrees of subcooling and higher velocities. Butene-1 and the eutectic pentane blend had the highest upper limit heat fluxes. All measured upper limit values were somewhat lower than would be predicted using existing empirical relationships such as the Griffith correlation (Reference 4). A detailed description of test procedures and results are included in Appendix E.

H. TRANSPIRATION COOLING ANALYSIS

The four fuels selected for analytical comparison as transpiration coolants for the complete engine were: methane, ethylene, ethane, and propane. These compounds were selected because they have the four highest specific impulses of the light hydrocarbon-flox combinations. Blends were not considered because the properties that make a superior transpiration coolant are diluted by the addition of another compound.

Coolant flows and performance losses were based on a 5000-pound thrust, 100 psia chamber pressure engine with a nozzle area ratio of 40. Coolant flow rates were based on transpiration cooling the complete chamber and nozzle to maintain a 2160°R wall temperature throughout.

Figures 3 through 10 show performance for these propellants based on the assumptions of (1) complete mixing between the coolant and reaction products, and (2) no mixing of the coolant boundary layer and main combustion stream and a coolant boundary temperature equal to the wall temperature. Data are shown to compare the fuel subcooled to its freezing point with fuel maintained at its normal boiling point. These data are summarized in table XI. From the table it can be seen that although the required coolant flow is reduced by subcooling the fuel, the corrected engine specific impulse based on no mixing is very nearly equal for both fuel storage conditions. Vacuum specific impulse losses due to transpiration cooling were predicted to be approximately 0.6 to 0.7% per percent of propellant used for cooling, e.g., if 1 percent of the propellant is used for cooling the loss would be 0.6 to 0.7%, if 2 percent is used the loss would be 1.2 to 1.4%.

Primarily on the basis of these performance data and with some consideration of its good stability, handling,availability, and space storability properties, methane was chosen as one of the two fuels for experimental transpiration evaluation.

Because of the obvious superiority of methane over other light hydrocarbons from the standpoint of theoretical performance and transpiration cooling capability, it was decided to choose the second fuel not on transpiration cooling considerations alone, but rather on applicability to a composite regenerative-transpiration cooling scheme. (See figure 11.) The four fuels chosen for the transpiration cooling studies and the four chosen as regenerative coolants were studied as regenerative coolants in the low heat flux expansion section of the exhaust nozzle. Two of these fuels, propane and methane, were in both categories. A reverse-flow heat exchanger configuration was determined to provide the greatest nozzle area that could be regeneratively cooled considering both the upper limit heat flux and coolant saturation limitations. Table XII shows the area ratio to which the nozzle could be cooled, the percent of total propellant flow required to transpiration cool the remainder of the chamber, and the performance loss due to this cooling flow. These preliminary calculations were performed using Bartz short form heat flux predictions (Reference 5) and upper limit heat fluxes based on Griffith's correlation (Reference 4). The lower heat fluxes encountered in the experimental tests would allow regenerative cooling to lower area ratios; however, any changes in the relative ranking would be small and would tend to increase the advantage of the heavier hydrocarbons. Changes in the experimental values of upper limit heat flux tend to increase the advantage of propane.

TABLE XI. EFFECT OF TRANSPIRATION COOLING ON FLOX-LIGHT HYDROCARBON ENGINE PERFORMANCE

Fuel	Percent Fluorine in Oxidizer	Fuel Inlet Condition(1)	Percent of Total Propellant Required for Cooling(2)	Engine Mixture Ratio	Injector Mixture Ratio	Maximum Theoretical Vacuum Specific Impulse, Sec(3)	Vacuum Specific Impulse with Transpiration Cooling, Sec(4)	Cooling Efficiency(5)
Methane	82.6	NBP	5.94	4.03	5.75	417.6	403.2	0.9655
		FP	5.85	4.05	5.75	417.4	403.2	0.9659
Ethane	78.1	NBP	6.72	3.40	4.82	411.4	393.4	0.9562
		FP	6.35	3.46	4.82	410.9	393.4	0.9575
Propane	76.0	NBP	7.00	3.18	4.50	408.3	387.1	0.9481
		FP	6.43	3.27	4.50	407.3	387.0	0.9502
Ethylene	70.4	NBP	7.73	2.74	3.85	409.4	389.4	0.9511
		FP	7.37	2.78	3.85	408.7	389.4	0.9528

(1) Fuel is in liquid phase at either the normal boiling point (NBP) or the freezing point (FP).

(2) Engine is completely transpiration cooled to the exit expansion ratio of 40.

(3) Based on theoretical shifting equilibrium expansion, 100 psia chamber pressure, nozzle exit area ratio of 40 and mixture ratio for maximum specific impulse.

(4) Transpiration cooling losses are based on calculations assuming no mixing between the mainstream and the coolant stream. This value does not include corrections for combustion and nozzle efficiencies.

(5) Ratio of vacuum specific impulse corrected for cooling to the maximum theoretical value.

Figure 3
Theoretical Transpiration Cooling Comparison of 82.6% Fluorine – 17.4% Oxygen with Methane

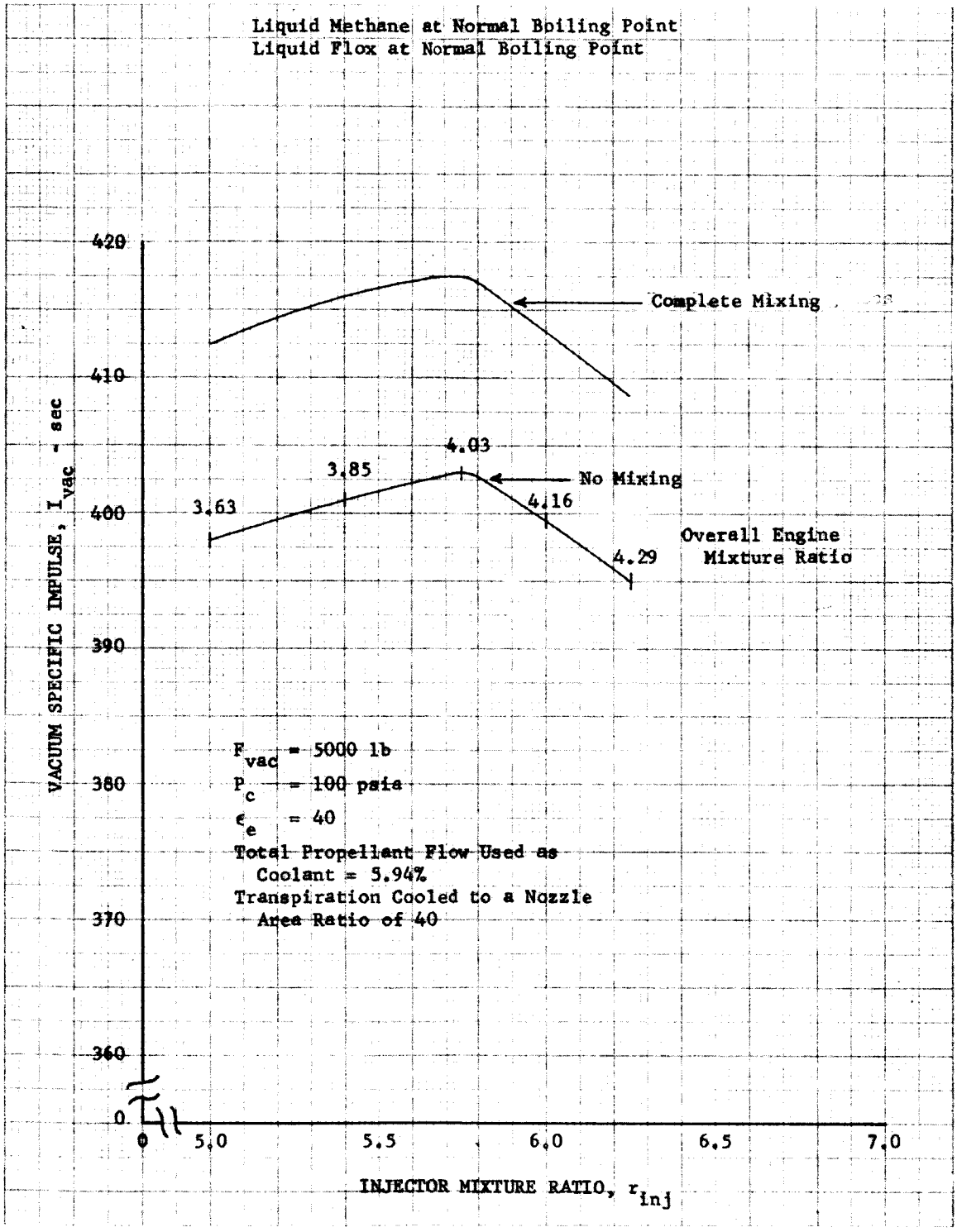

DF 33071
Sheet 1 of 8

Figure 4
Theoretical Transpiration Cooling Comparison of 82.6% Fluorine — 17.4% Oxygen with Methane

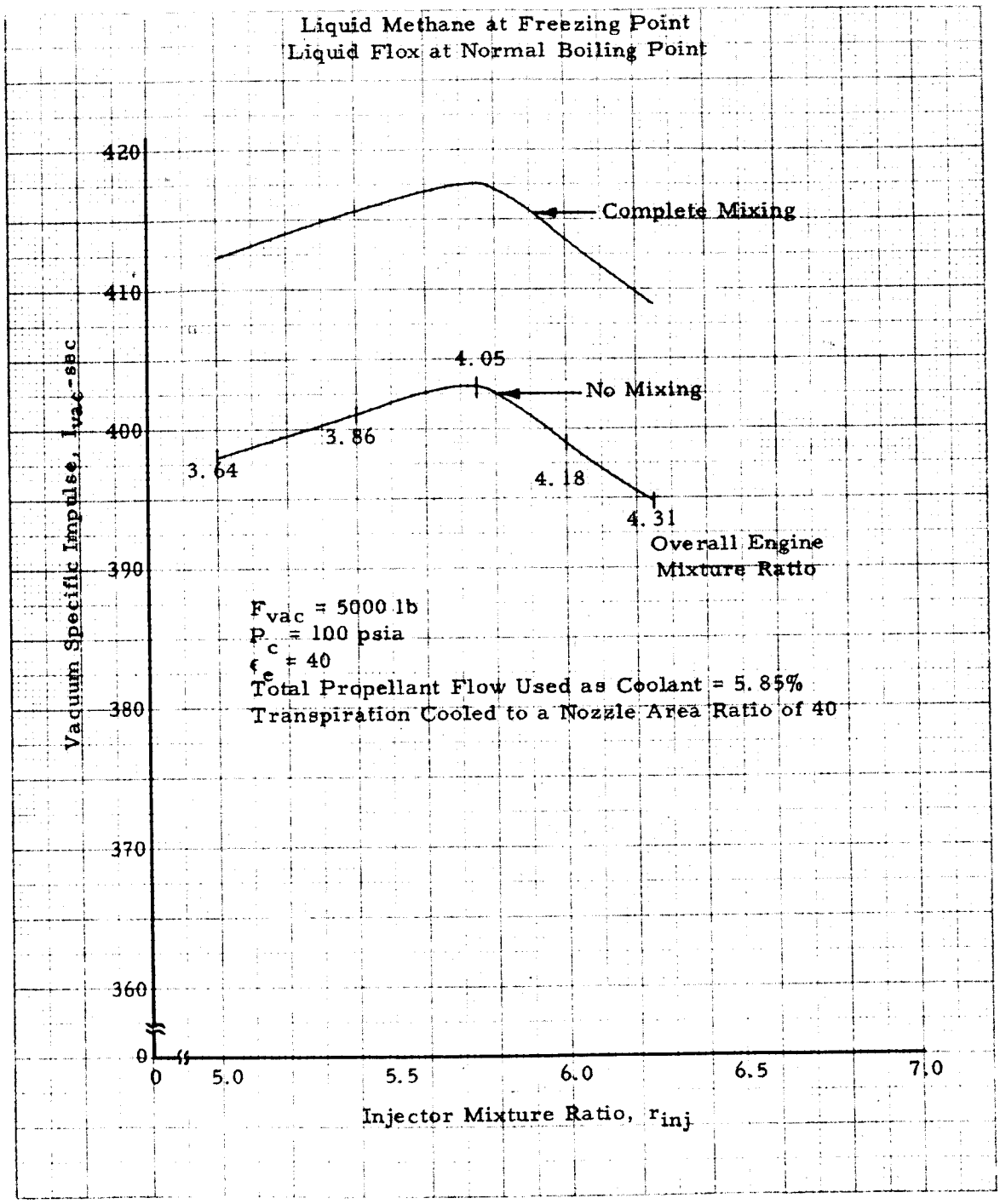

DF 33071
Sheet 2 of 8

Figure 6
Theoretical Transpiration Cooling Comparison of 78.1% Fluorine – 21.9% Oxygen with Ethane

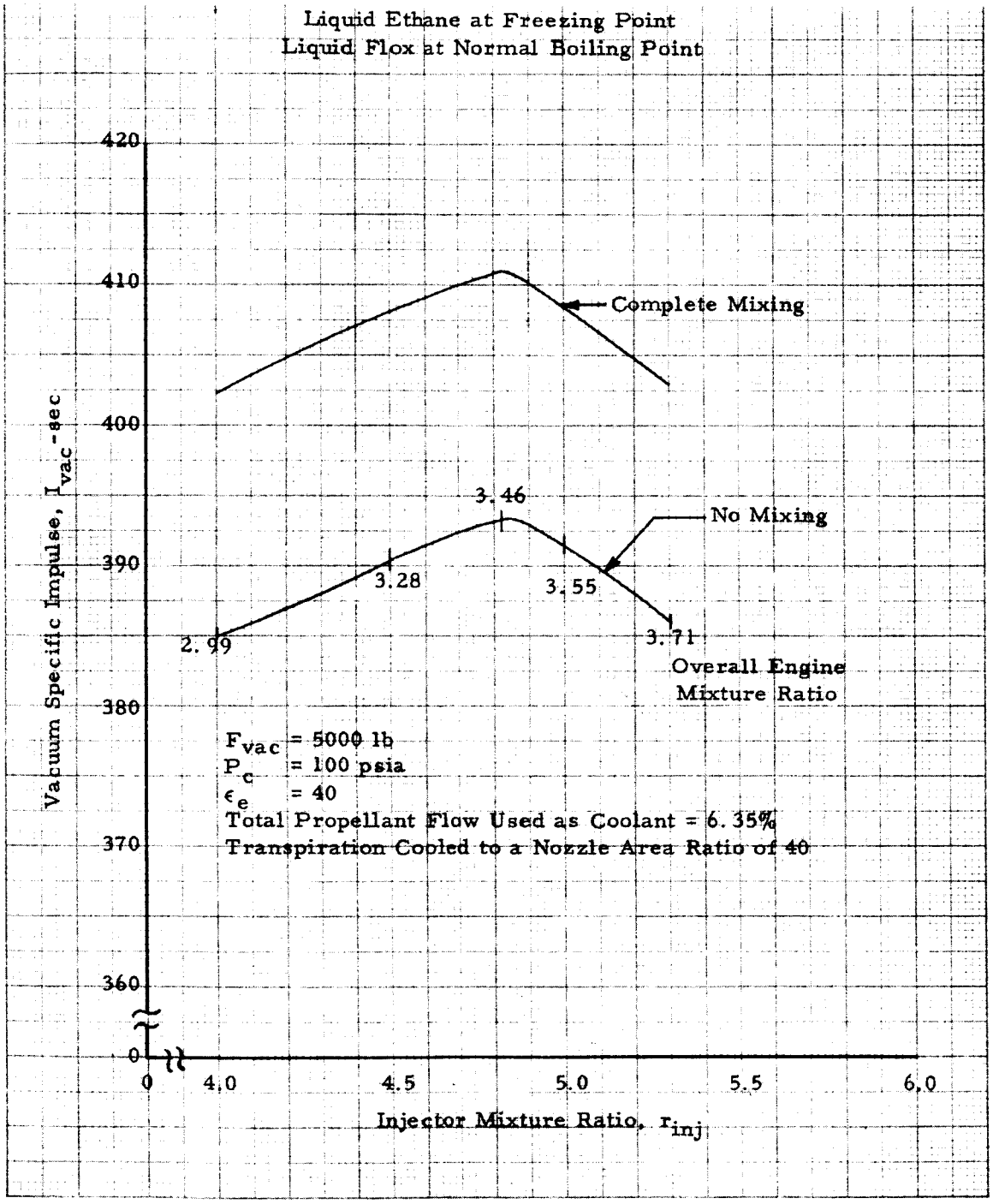

DF 33071
Sheet 4 of 8

Figure 5
Theoretical Transpiration Cooling Comparison of 78.1% Fluorine — 21.9% Oxygen with Ethane

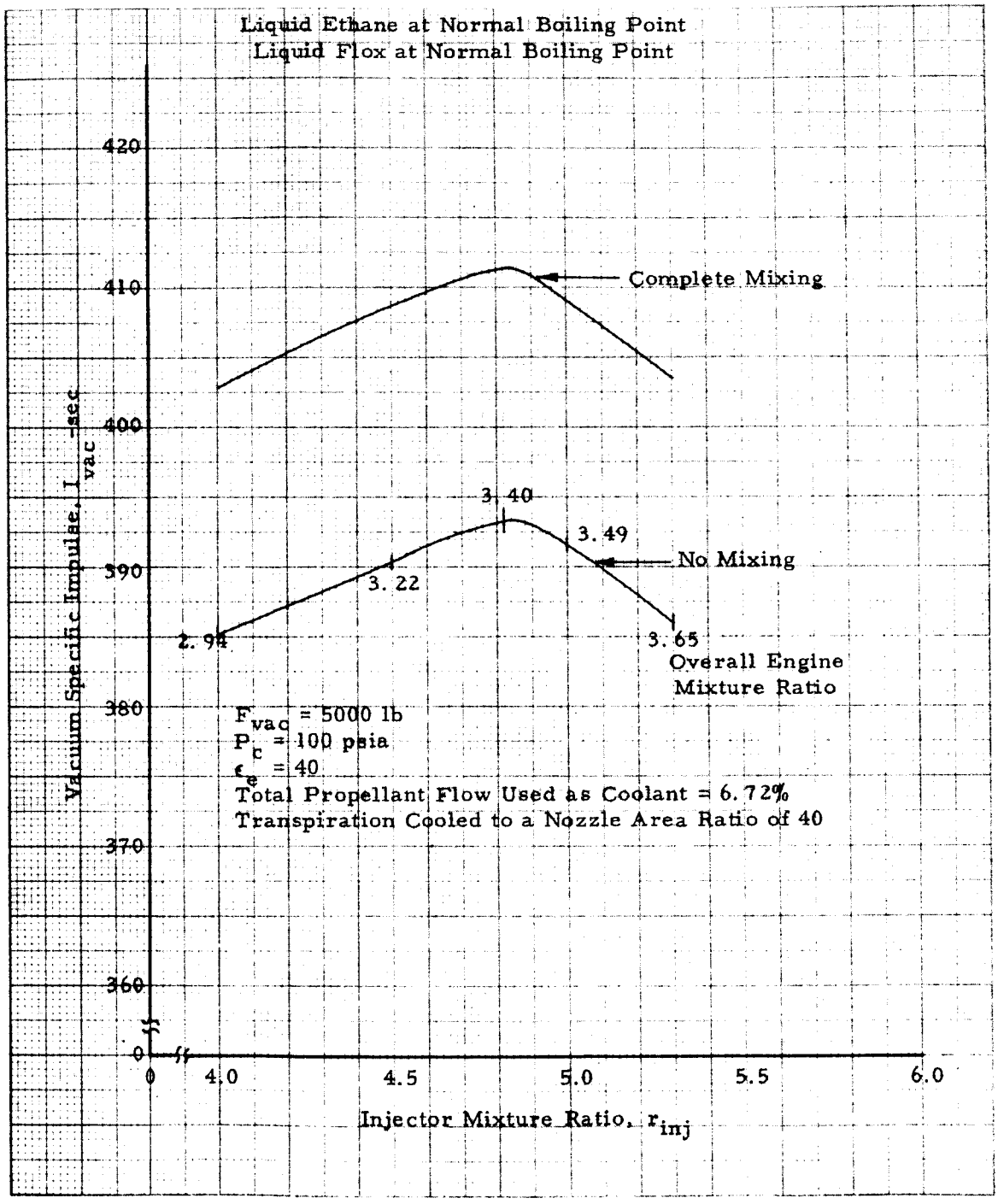

DF 33071
Sheet 3 of 8

Figure 7
Theoretical Transpiration Cooling Comparison of 76% Fluorine — 24% Oxygen with Propane

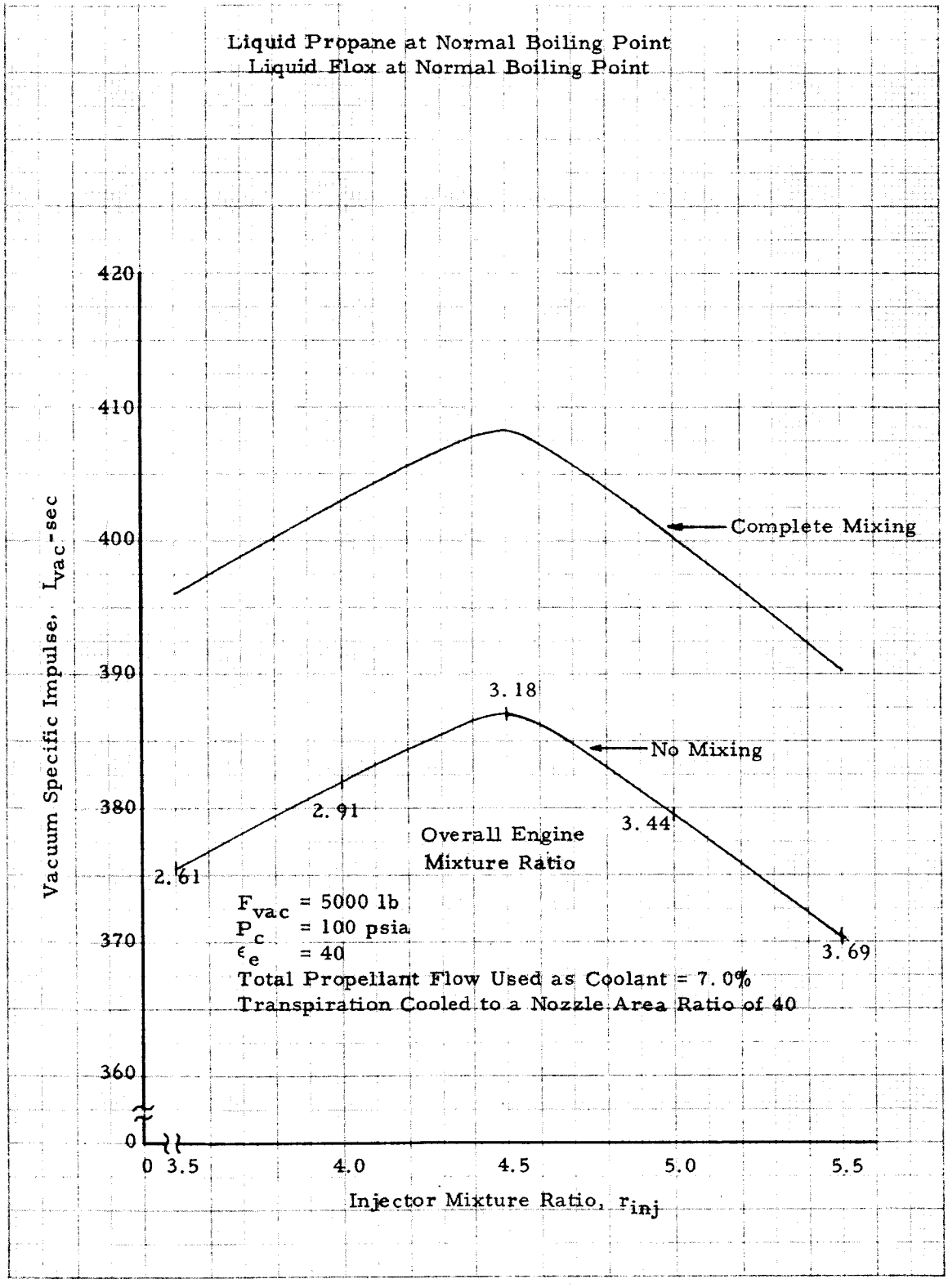

DF 33071
Sheet 5 of 8

Figure 8
Theoretical Transpiration Cooling Comparison of 76% Fluorine — 24% Oxygen with Propane

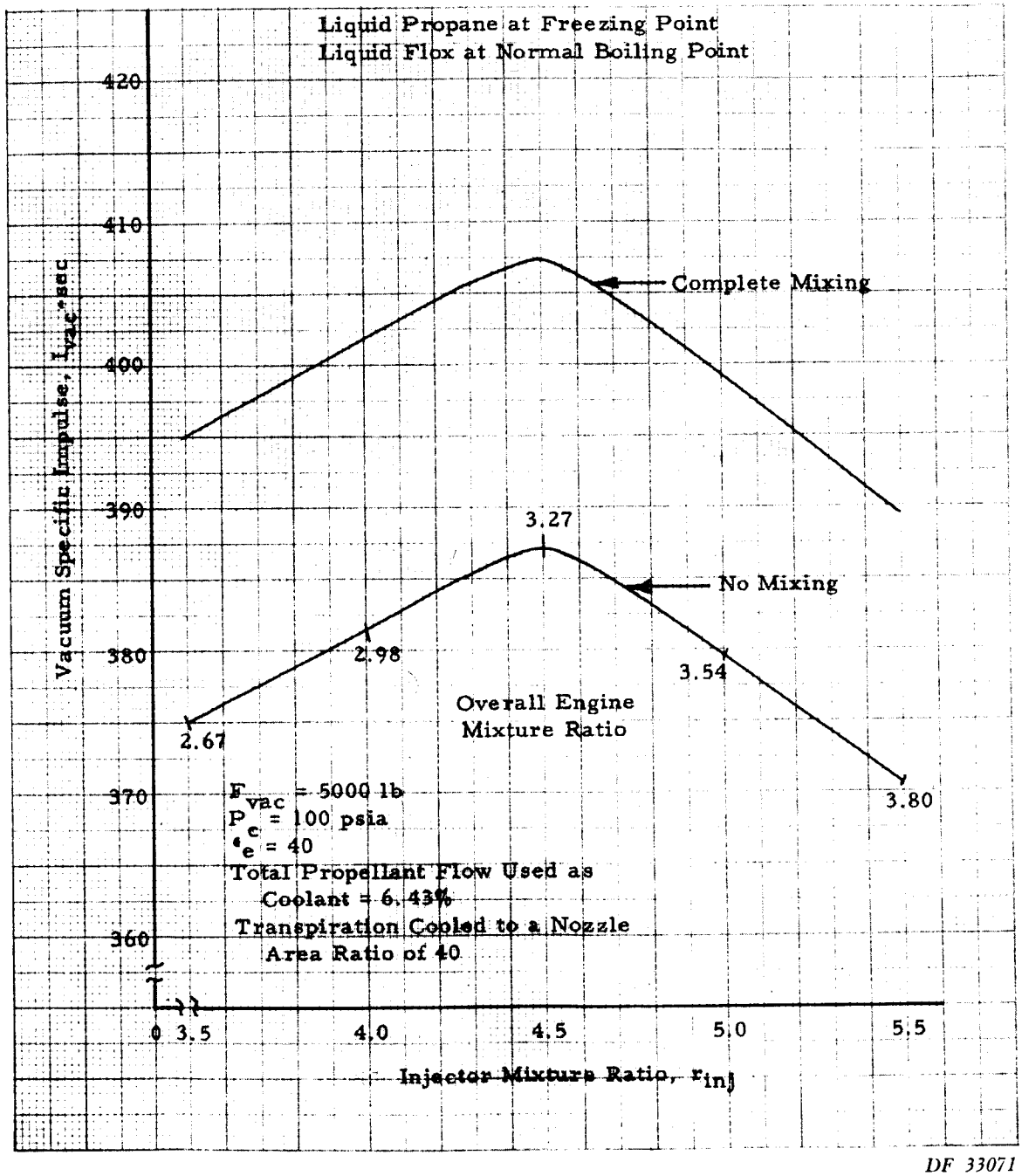

DF 33071
Sheet 6 of 8

Figure 9
Theoretical Transpiration Cooling Comparison of 70.4% Fluorine — 29.6% Oxygen with Ethylene

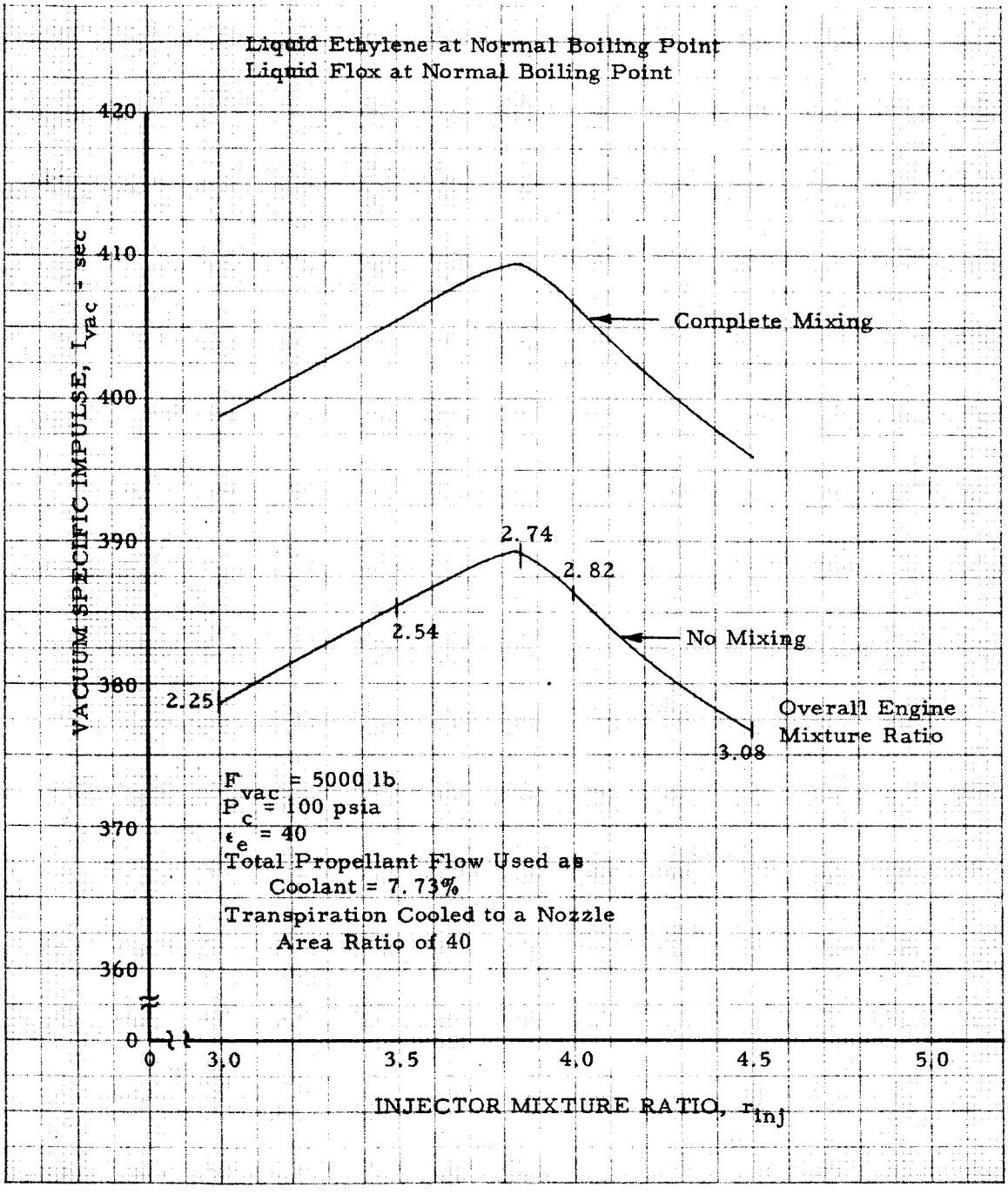

DF 33071
Sheet 7 of 8

Figure 10
Theoretical Transpiration Cooling Comparison of
70.4% Fluorine – 29.6% Oxygen with Ethylene

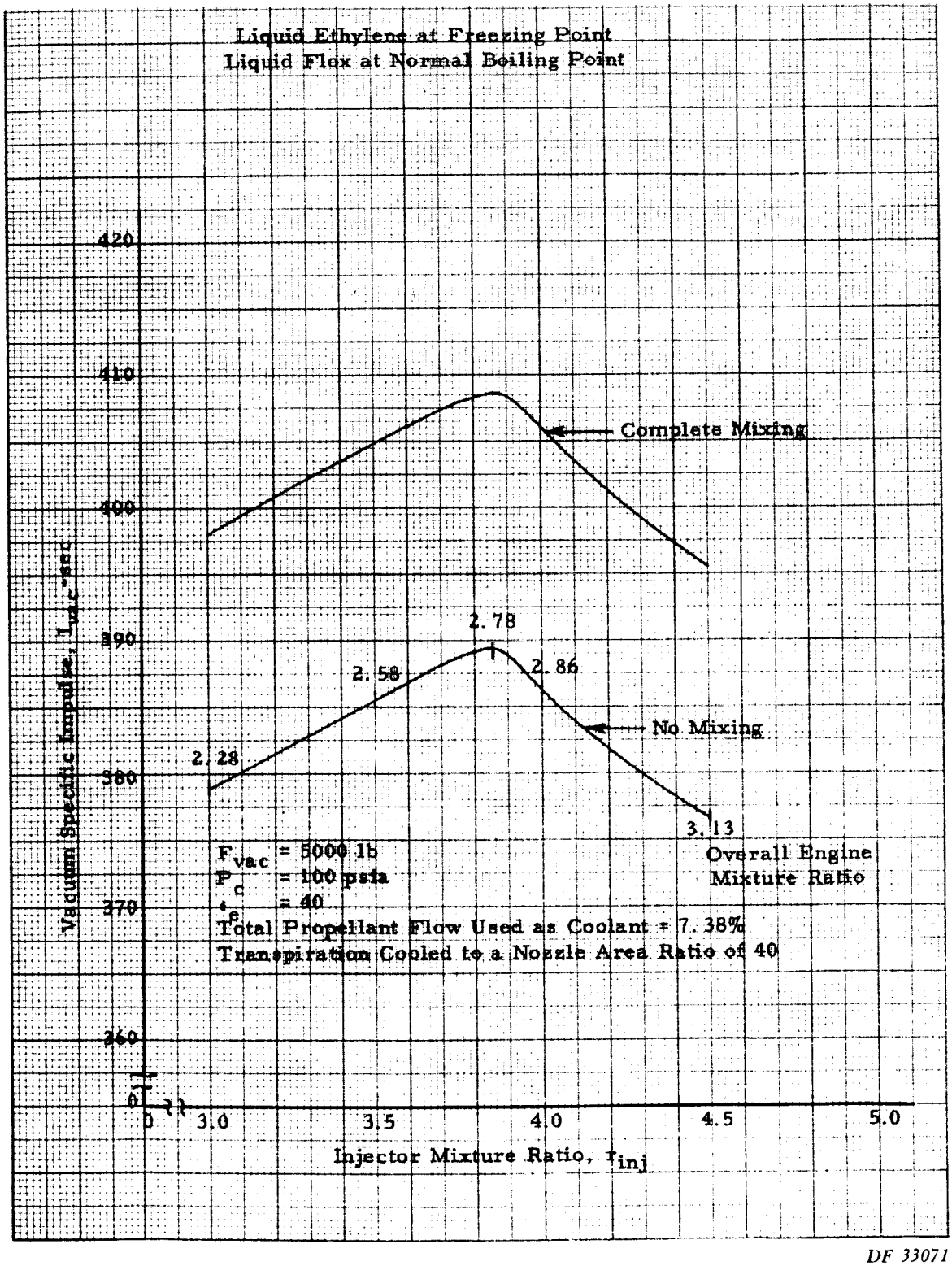

DF 33071
Sheet 8 of 8

TABLE XII. COMPARISON OF FUELS FOR COMPOSITE COOLING SCHEMES

Fuel	Fluorine in Oxidizer, %	Maximum Theoretical Vacuum Specific Impulse, sec (1)	Nozzle Area Ratio at Limit of Regenerative Cooling (2)	Total Propellant Required for Transpiration Cooling, % (3)	Estimated Cooling Efficiency, % (4)	Estimated Vacuum Specific Impulse with Transpiration Cooling, sec (5)
Methane	82.6	417.4	29.3	5.73	96.65	403.5
Ethylene	70.4	408.4	17.2	6.42	95.76	391.1
Ethane	78.1	410.9	17.1	5.6	96.15	395.1
1-Butene	70.4	402.4	6.2	5.5	94.79	381.4
Propylene	70.4	404.5	8.8	5.8	95.32	385.6
Propane	76.0	407.3	10.4	5.3	95.76	390.0

(1) Theoretical shifting equilibrium expansion, 100 psia chamber pressure, nozzle exit area ratio of 40 and mixture ratio for maximum specific impulse. Propellant storage conditions are liquid flox at its normal boiling point and liquid fuel at its freezing point.
(2) Based on a counter flow heat exchanger with inlet at nozzle exit. Coolant is supplied at 150 psia and at its freezing point.
(3) Flow required for cooling the chamber upstream of the regenerative jacket as determined from the saturation limitation. Transpiration coolant heat capacity is taken between the saturated liquid at the jacket outlet temperature and a gas at 2160°R.
(4) Ratio of vacuum specific impulse corrected for cooling to the maximum theoretical value.
(5) Transpiration cooling losses are based on calculations assuming no mixing between the mainstream and the coolant stream. This value does not include corrections for combustion and nozzle efficiencies.

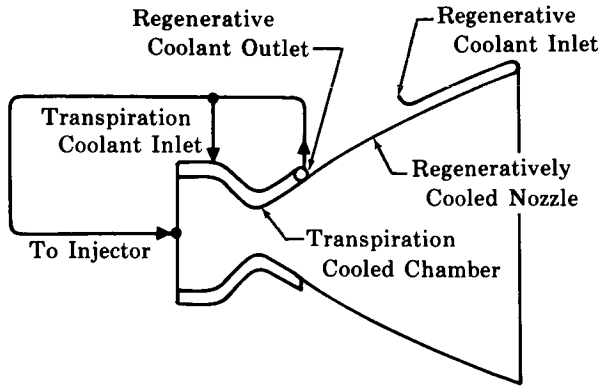

Figure 11. Composite Cooling Scheme *FD 13485*

Choice of the best fuel for a composite cooling scheme was to be based primarily on the nozzle area that could be regeneratively cooled, and secondarily on performance. Greater percentages of regenerative cooling are desired because this is directly related to a simpler design, lighter weight chamber and reduces the amount of coolant which must be injected into the downstream section where performance loss due to incomplete mixing is greatest. It was found that propane, propylene, and butene-1 would regeneratively cool to area ratios between 6 and 10. The selection of one of these three fuels was not clear cut, however, because the problems involved in designing transpiration cooled chambers to an area ratio of 10 is not significantly greater than to an area ratio of 6. Therefore, because the delivered vacuum impulse, fuel cost, and availability favor propane it was selected as the second fuel for transpiration cooled testing.

I. REGENERATIVE COOLING ANALYSIS

Six fuels: methane, propane, propylene, butene-1, a propane-propylene blend and a pentane-isopentane blend were compared to determine the two most desirable for regenerative cooling. Heated tube heat transfer tests were conducted on each (see paragraph G). An examination of the heated tube data and preliminary heat flux data from the methane uncooled tests showed that: (1) none of the fuels had sufficient heat capacity to remain liquid while cooling a complete chamber and nozzle, and (2) the heat flux exceeded the upper limit value in the chamber section for all fuels at thrust levels and chamber pressures of interest.

At this point the regenerative cooling studies did not appear promising; however, small changes in the upper limit heat flux or hot gas film coefficients could substantially affect the cooling requirements. It was decided, therefore, to determine the modifications required to run the experimental chamber and to determine definitely the practicality of regenerative cooling. Candidates for liquid cooling were narrowed down to butene-1, propane, and the pentane blend. These candidate fuels had the highest values of

upper limit heat flux at low values of subcooling. In addition, gaseous methane was studied for cooling the experimental chamber because the narrow liquid range of methane made it the most suitable for vaporizing in the low heat flux expansion section of the nozzle with subsequent gaseous cooling of the chamber.

1. LIQUID COOLANT

Calculations were based on (1) a jacket inlet pressure of 150 psia, (2) a jacket inlet temperature of 10°R above the liquid freezing point, and (3) coolant upper limit heat fluxes estimated from data presented in paragraph G. Each gas side film coefficient was estimated by multiplying the experimental methane hot gas side film coefficient by the ratio of the theoretical coefficient for the fuel being considered to the theoretical coefficient for methane.

Uncooled methane test data showed that heat fluxes were highest near the injector. A parallel flow coolant direction was, therefore, most effective because the highest upper limit heat fluxes correspond to the greatest degree of subcooling. Even with the coolant flow rates greater than 10 times the injector fuel flow, none of the liquid fuels being considered could cool the existing RL10 chambers without modification.

Because coolant velocity has a direct effect on upper limit heat flux, calculations were repeated considering the effect of partial blockage of the coolant flow area; this was done by inserting triangular and square shaped wires into the coolant tubes from the injector end. Using square wires with the largest cross sectional area that could be inserted, it was found that to cool with propane, the pentane blend, and with butene-1, respectively, coolant flows of 5, 8, and 12 times the injector fuel flow were necessary. Wires with a constant cross sectional area were found to be satisfactory in all cases because the most stringent velocity requirements occur at the injector end of the chamber and no reduction in the coolant flow rate could be achieved by using tapered wires inserted further into the tubes.

The relatively better results achieved with propane over butene-1 were due to the extrapolated effect of coolant velocity on upper limit heat flux as determined from the heated tube tests. Two uncertainties affected the validity of these calculations. First, the effect of coolant velocity on upper limit heat flux was based on data obtained at much lower coolant velocities than those used for these calculations. Secondly, the hot gas side film coefficients were estimated on the basis of methane tests. Later uncooled tests showed that the heat flux used in these calculations was higher than the actual values.

2. *GASEOUS METHANE*

Gaseous methane at 537°R and an inlet pressure of 200 psia was used in these calculations. This inlet pressure was considered to be the maximum practicable for a pressure-fed chamber; high inlet pressures permit higher coolant flow rates to be used without choking in the tubes. Table XIII indicates the configurations investigated in determining the required chamber modifications. Flow area reductions were based on square wires of the same maximum size considered for liquid cooling. Table XIII shows that the test chamber can be successfully cooled by gaseous methane, but with a high pressure drop. Cooling of a complete engine appears to be practical if the methane, after boiling, enters the high heat flux region below 537°R. The additional analysis required to assess the feasibility of this method of cooling was beyond the scope of this program.

TABLE XIII. GASEOUS METHANE COOLING CONFIGURATIONS

Coolant Multiple, $\frac{\dot{W}_c}{\dot{W}_{f_{inj}}}$	Flow Direction	Comments
1	Parallel	Excessive wall temperatures near injector
2	Counter	Flow choked before throat section
1.5	Parallel with flow areas reduced in first 8 inches	Choked before area transition
1	Parallel with flow areas reduced in first 8 inches	Flow choked before throat – high wall temperatures near injector
1.5	Counter with flow areas reduced in last 8 inches	Flow choked at area transition
1.5	Counter with flow areas reduced in last 5 inches	Marginal success – maximum wall temperatures of 2100°R exit pressure 75 psia

3. *CONCLUSIONS*

Of all the light hydrocarbons and hydrocarbon blends studied, the eutectic pentane-isopentane blend, propane, and butene-1 were the most promising for regenerative cooling without film or bulk boiling. Cooling with methane with boiling also appeared promising; however, investigation of this cooling scheme was not possible because it would require that boiling occur in the high area ratio portion of the exhaust nozzle and high area ratio nozzle testing was beyond the scope of this program. Cooling of a modified RL10 thrust chamber with gaseous methane was shown to be marginal and facilities were not available without modification. Since propane and methane had already been selected for the uncooled ex-

perimental rocket firings, butene-1 and the eutectic pentane blend were selected as the other two fuels to be tested in uncooled hardware. The selection of these four fuels not only allowed evaluation of the four most promising fuels for transpiration cooling, regenerative cooling, or any combination of the two cooling methods; but also provided a wide range of physical and chemical properties. Propane and the eutectic pentane blend were selected as the two fuels to be tested in a regeneratively cooled chamber.

J. REFERENCES

The following references are used in this section.

1. Sarli, V. J., "Investigation of Nonequilibrium Flow Effects in High Expansion Ratio Nozzles," UAC Research Laboratories Report B910056-12, September 1964.

2. Bray, K. N. C., and J. P. Appleton, "Atomic Recombination in Nozzles, Methods of Analysis for Flows with Complicated Chemistry," University of Southhampton, Department of Aeronautics and Astronautics, May 1961.

3. Hofland, R. Jr., and W. G. Burwell, "Development and Evaluation of Sudden Freezing Criteria for Predicting Nonequilibrium Mixture Properties in Expanding One-Dimensional Flow Fields," UAC Research Laboratories Report No. C110035-1, July 1964.

4. Griffith, P., "Correlation of Nucleate Boiling Burnout Data," ASME Paper No. 57-HJ-21, 19 August 1957.

5. Bartz, D. R., "An Approximate Solution of Compressible Turbulent Boundary Layer Development and Convective Heat Transfer in Convergent-Divergent Nozzles." Transactions of the ASME-77, pp 1235-1245.

SECTION IV
HARDWARE DESIGN

A. INJECTOR MODIFICATION

All tests with the uncooled, transpiration cooled, and regeneratively cooled thrust chambers were conducted using modified RL10 injectors. The injector modifications were necessary to improve combustion efficiency with the low volumetric flow rates encountered at 100 psia operation with the flox-hydrocarbon combinations. It was also shown from test experience that the welds attaching the backplate of the injector to the posts that support the backplate were not fluorine-compatible in many instances. All injector modifications made during the latter part of the program included removing and replacing the injector backplate using fluorine-compatible welding techniques. Figure 12 shows an RL10 injector prior to modification.

The initial injector rework consisted of swaging the oxidizer spuds of an RL10A-3 injector to reduce the oxidizer flow area by approximately 50%, and replacing the Rigimesh faceplate to provide a fuel annulus that conformed to the geometry of the oxidizer spud and reduced the fuel flow area. Figure 13 shows an oxidizer spud and adjacent Rigimesh before and after this modification.

Testing with the swaged RL10A-3 type injector showed severe burning of the ends of the oxidizer spuds. The swirlers in the oxidizer spuds were believed to have contributed to the burning of the spuds. Therefore, similar modifications were made to two RL10A-1 injectors. The RL10A-1 injectors, which do not have swirlers, are easier to swage because the spud diameter before swaging is smaller than the RL10A-3 spud diameter.

Several tests with the swaged RL10A-1 type injectors showed the importance of a high propellant momentum ratio to achieve high efficiency. Injectors with several different fuel and oxidizer orifice areas were tested. Although one of these injectors proved satisfactory at low mixture ratios, none of the swaged injectors were able to attain the optimum mixture ratio without some spud burning.

A different modification was tested and shown to be satisfactory for high mixture ratio operation. Only half the oxidizer spuds were used; the others were welded shut. On one injector the existing stainless steel spuds were used, whereas on another the spuds were replacd with nickel spuds. Nickel is more compatible with fluorine, particularly at high temperatures; its use was considered to be desirable with such heated fuels as propane and the eutectic blend of pentane and isopentane.

Seven different modifications of four injectors, listed in table XIV, were used to complete the program. Test results given in Sections VI, VII, and VIII are referenced to these seven modifications by number.

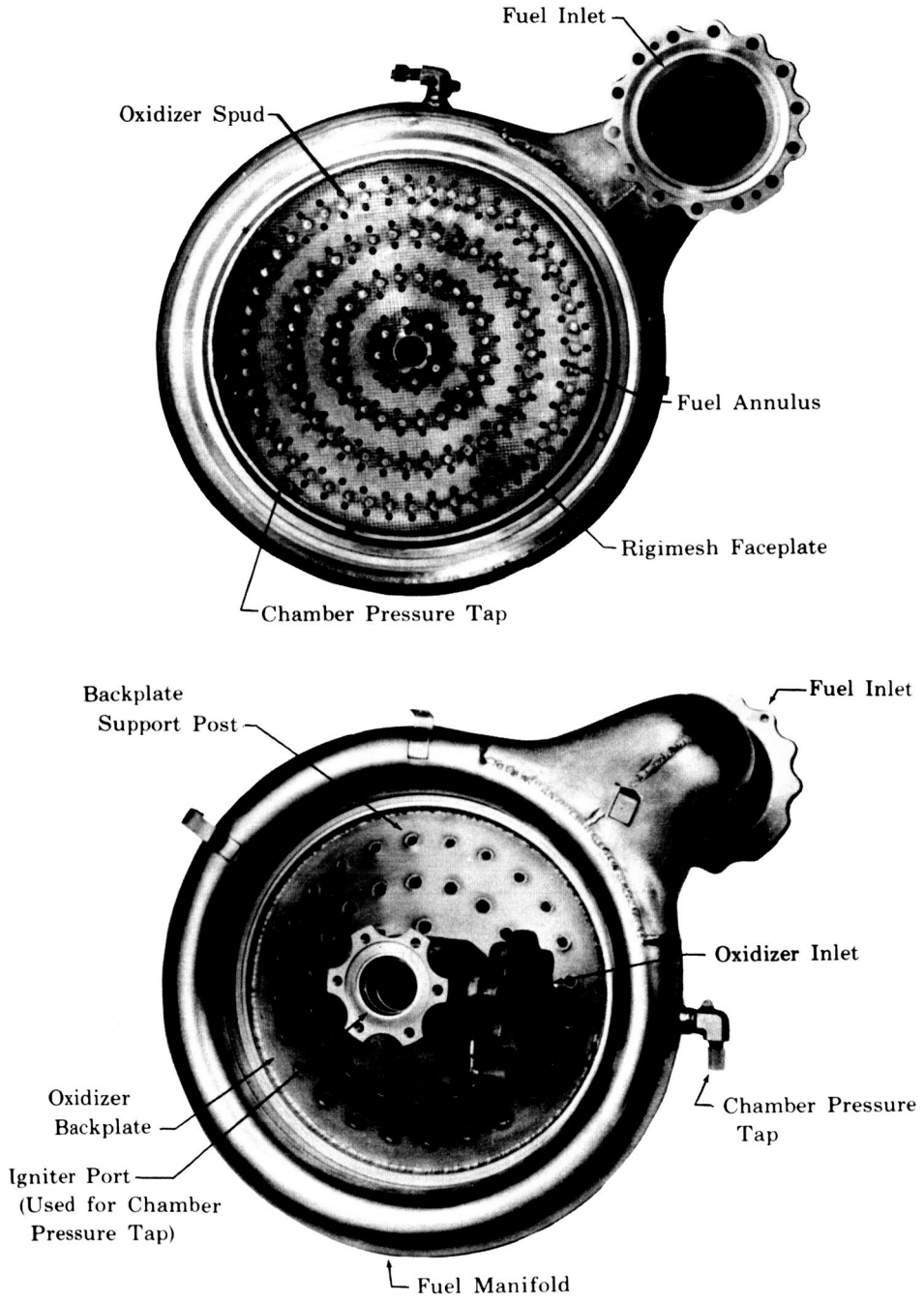

Figure 12. RL10A-1 Injector *FD 12777 A*

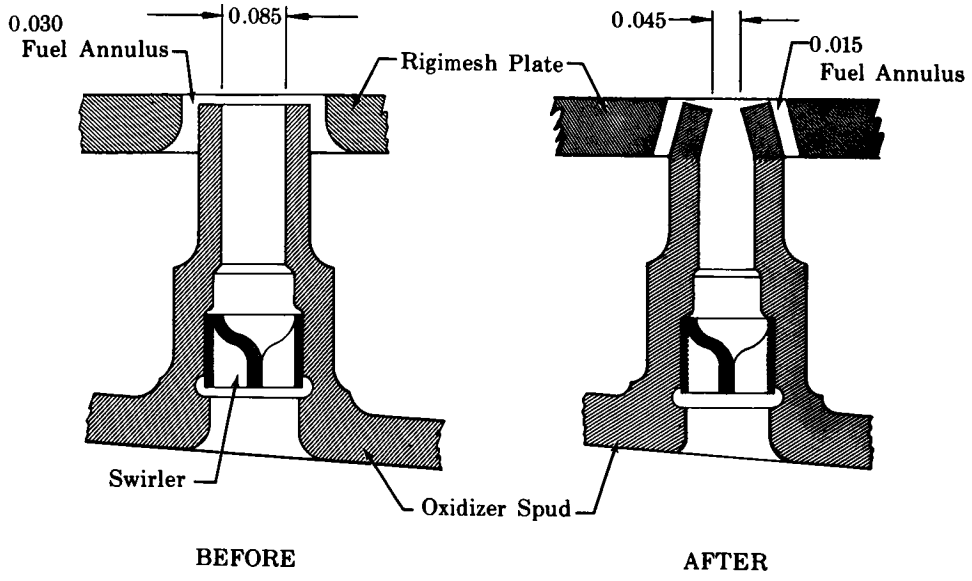

Figure 13. Injector Area Rework *FD 9564*

TABLE XIV. SUMMARY OF INJECTOR MODIFICATIONS

Injector No.	Model	Serial No.	No. of Elements	Type Elements	AC_{D_f}	AC_{D_o}	Comments
1	RL10A-3	HK 740	216	Swaged with swirlers	1.1	0.40	
2	RL10A-1	DW 670	216	Swaged	1.6	0.28	
3	RL10A-1	DW 670	216	Swaged	1.5	0.41	Same injector as 2 with the oxidizer spuds swaged open.
4	RL10A-1	IF 289	216	Swaged	1.0	0.29	
5	RL10A-1	JX 767	108	Standard A-1	0.89	0.43	50% of elements removed. Oxidizer backplate replaced with fluorine compatible welds.
6	RL10A-1	JX 767	108	Swaged open	0.89	0.44	Same injector as 5 except the oxidizer spuds were swaged open and more accurately centered.
7	RL10A-1	IF 289	108	Nickel	0.73	0.38	50% of elements on injector 4 were replaced with nickel spuds and 50% were welded shut. Oxidizer backplate replaced with fluorine compatible welds.

B. UNCOOLED CHAMBER DESIGN

The uncooled chambers were fabricated from high purity oxygen-free copper. Copper was selected because of its high thermal conductivity, high specific heat, and satisfactory yield strength at elevated temperatures. The chamber contour is similar to that of the RL10 thrust chamber. The major dimensions are:

1. Injector diameter – 10 inches
2. Throat diameter – 5.98 inches
3. Nozzle exit diameter – 11.27 inches.

This exit diameter provides an exhaust nozzle area ratio of 3.54, which is approximately the maximum possible area ratio for sea level expansion without flow separation for a 100-psia chamber pressure. The chamber length is 12.35 inches from the injector to the throat; the total length is 16.85 inches. Wall thickness is 0.50 inch in a plane perpendicular to the chamber centerline. This thickness was chosen to keep predicted maximum wall temperatures below 1600°R and still provide good transient temperature measurements on the outside wall surface. An assembly drawing of the copper chamber, with stainless steel mounting lugs and a stainless steel injector mounting flange, is shown in figure 14.

The copper chamber is instrumented with 54 chromel-alumel thermocouples imbedded in slots in the chamber outside surface. Thermocouples are placed every 30 degrees around the throat section and also along a line at the top of the chamber. The imbedded thermocouple wires are copper-flame sprayed to provide high conductivity and strong junctions. The thermocouple installation is shown in figure 15a. The chamber is wrapped with an insulation blanket and given a protective glass-fiber coating. The insulation is necessary to maintain a heat balance for data reduction. The completed chamber is shown in figure 15b.

C. TRANSPIRATION COOLED THRUST CHAMBER DESIGN

The transpiration cooled thrust chamber was designed with eight segments of approximately equal length to permit local variation of coolant flow. The segments were held in position by a stainless steel cylinder and clamped at the exit to prevent axial movement. The exit clamp and flange also served as a junction point for segment temperature and pressure connections. Each segment was machined to permit both axial and radial coolant flow throughout the chamber. An assembly view of the complete chamber assembly is shown in figure 16. The predicted and required cooling flows for methane and propane are shown in figures 17 and 18. Figure 17 shows predicted coolant with the orifices sized for constant back pressure on the Rigimesh, and figure 18 shows the required flowrate and resulting back pressure for an optimized distribution.

Rigimesh liner material capable of satisfying the flow requirements was available in many combinations of thickness and number of mesh layers. Material selection was thus largely dependent upon strength requirements under operating conditions, the most stringent of which was at the weld joining the Rigimesh to adjacent parts of the chamber. (See figure 19). Design studies were made using 8-layer 12 x 64 mesh material, which had previously been used to establish coolant flows. These studies showed that, although the greatest stress occurred during shutdown at the segment to Rigimesh weld, it was less than the maximum permissible. Using the strength and cooling requirements as criteria, 0.120-inch thick, 8-layer, 12 x 64 mesh material was selected.

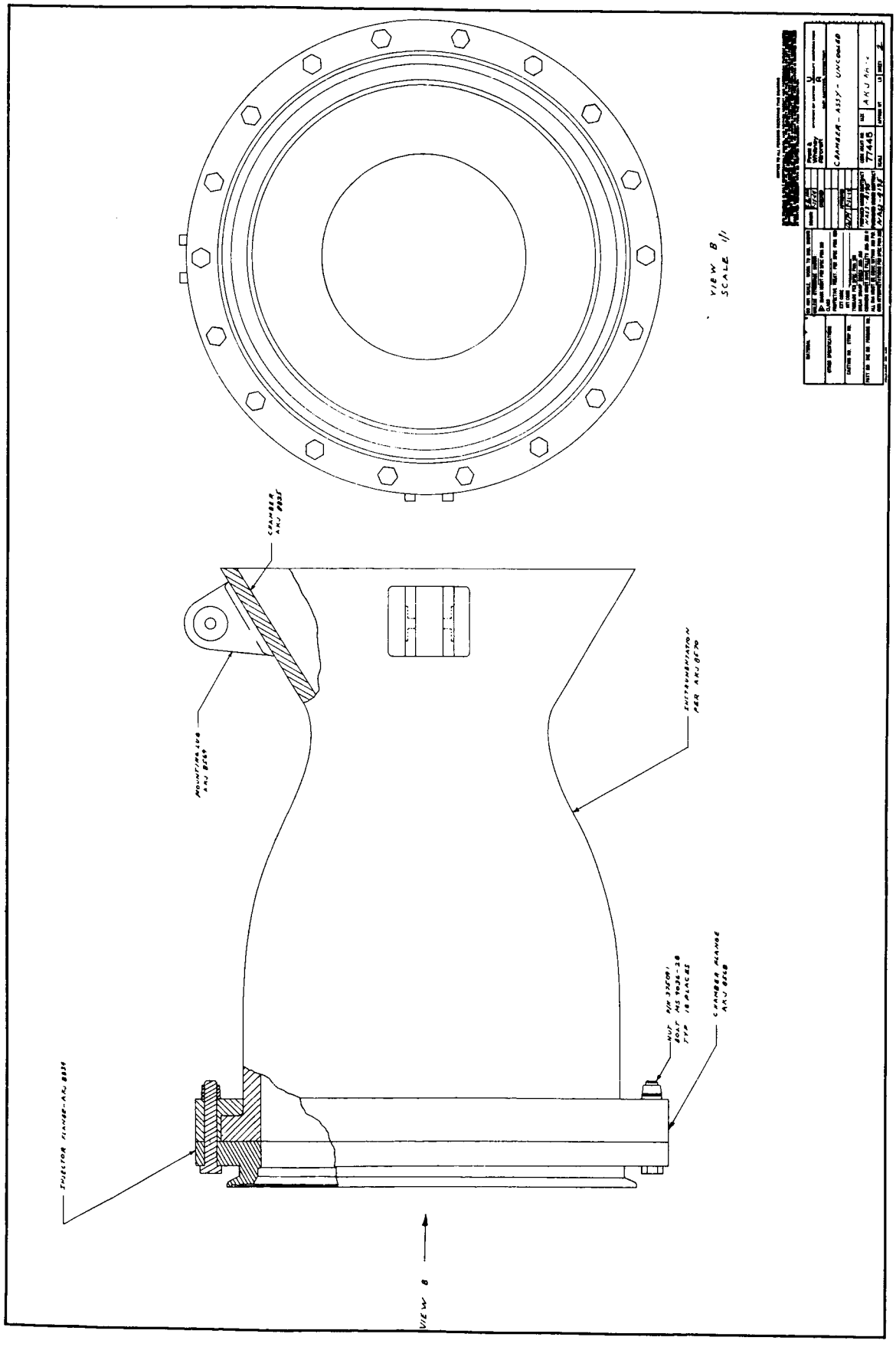

Figure 14. Uncooled Chamber Layout

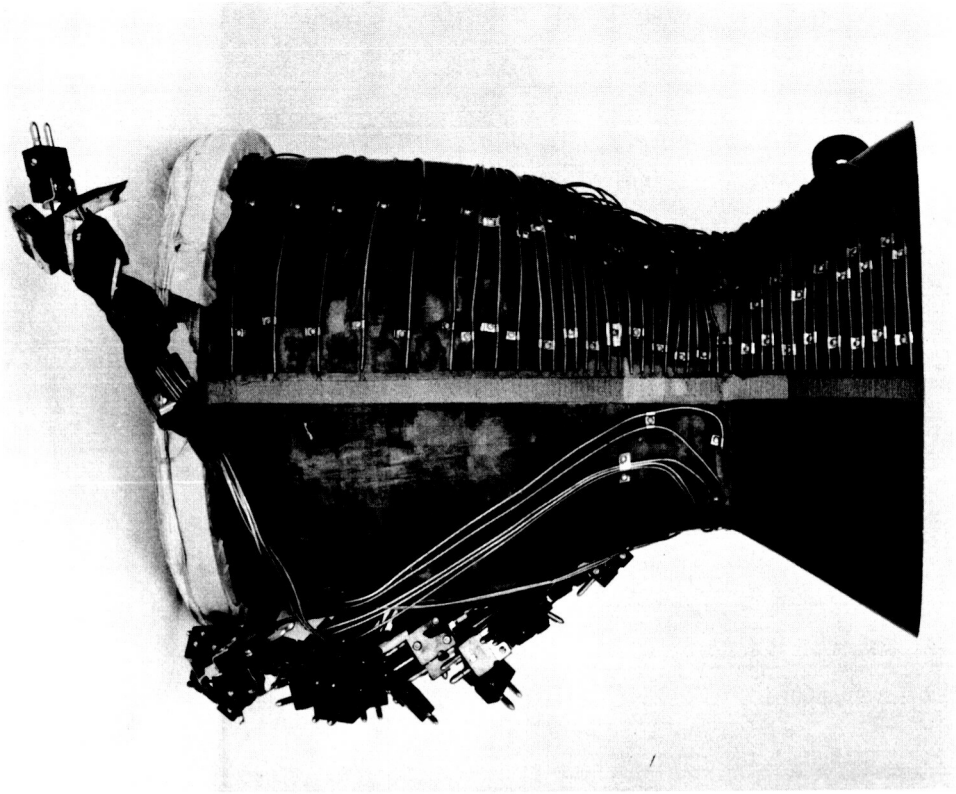

Figure 15a. Uncooled Chamber with Thermocouple Installation Completed FE 46722

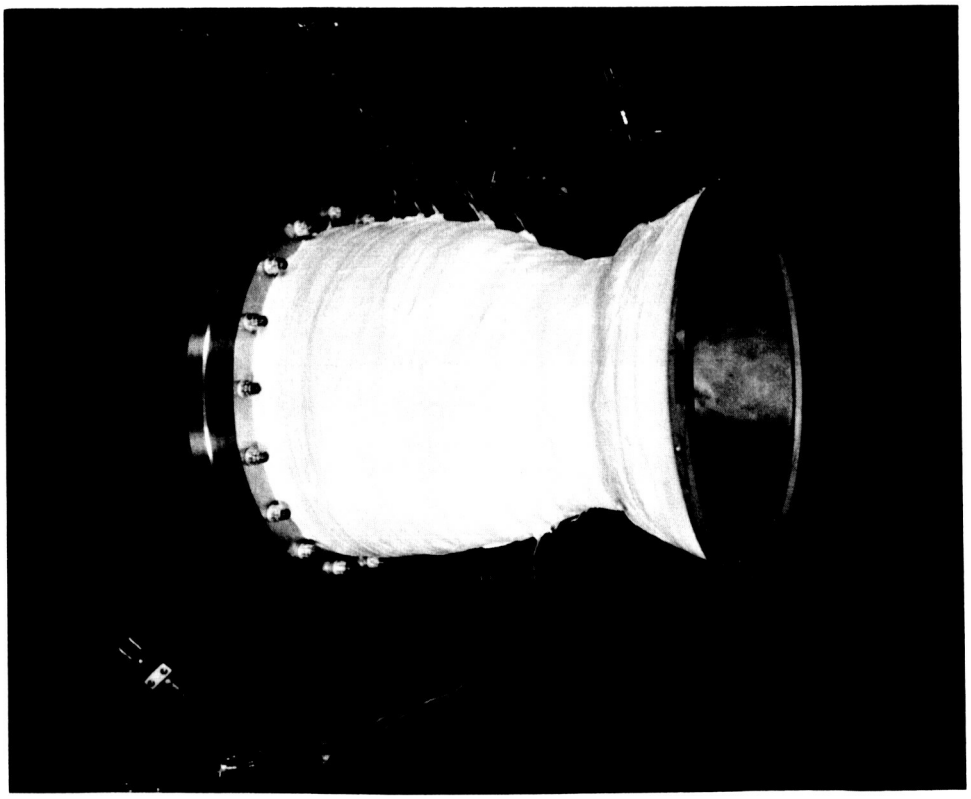

Figure 15b. Complete Uncooled Chamber with Fiberglas Covered Insulation FE 46884

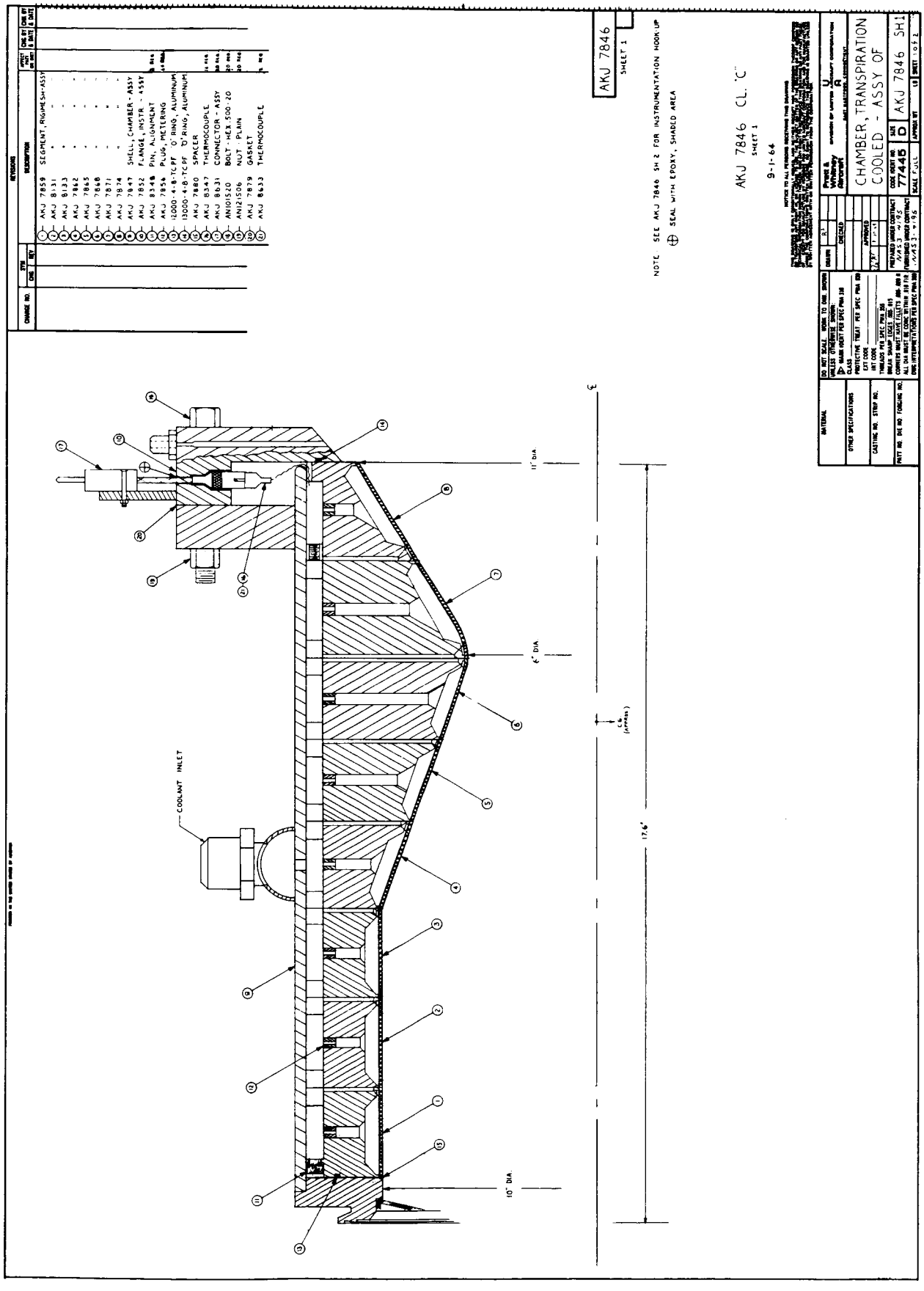

Figure 16. Transpiration Cooled Chamber Assembly

Figure 17
Coolant Flow Per Unit Area (Constant Pressure—Constant Liner Thickness)

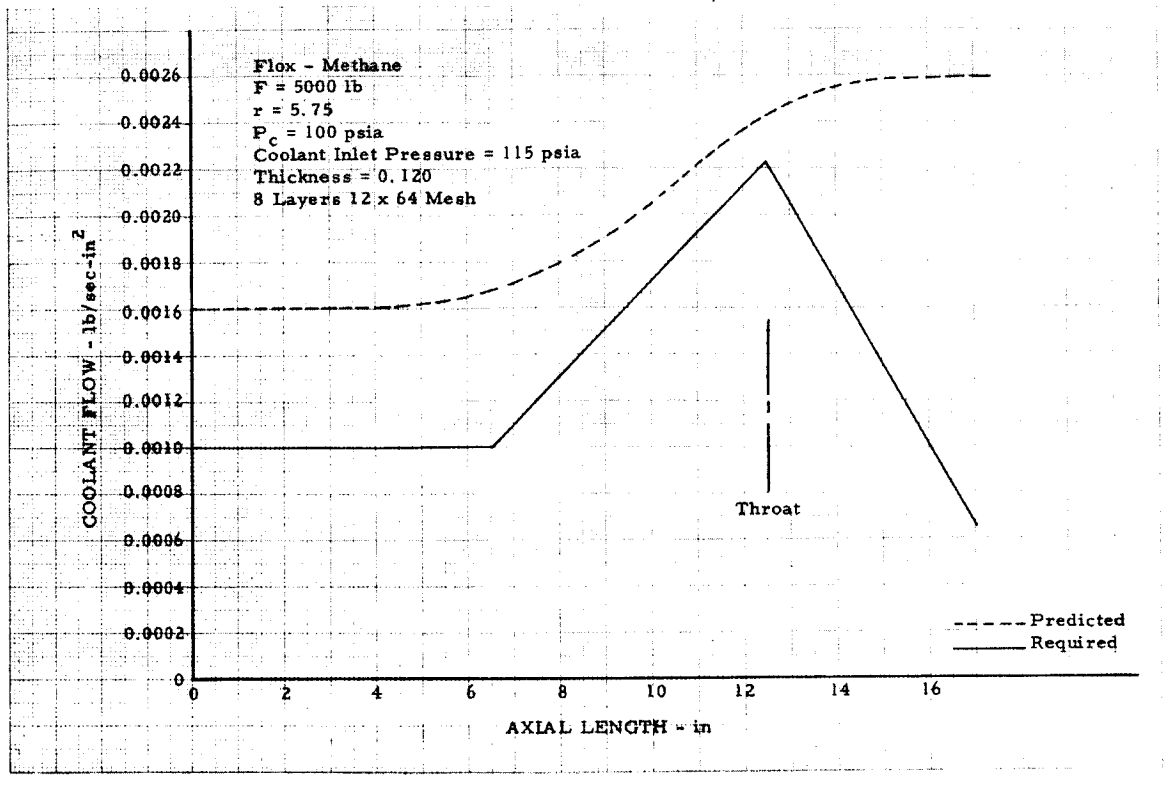

DF 33929

Figure 18
Coolant Flow Per Unit Area (Variable Pressure—Constant Liner Thickness)

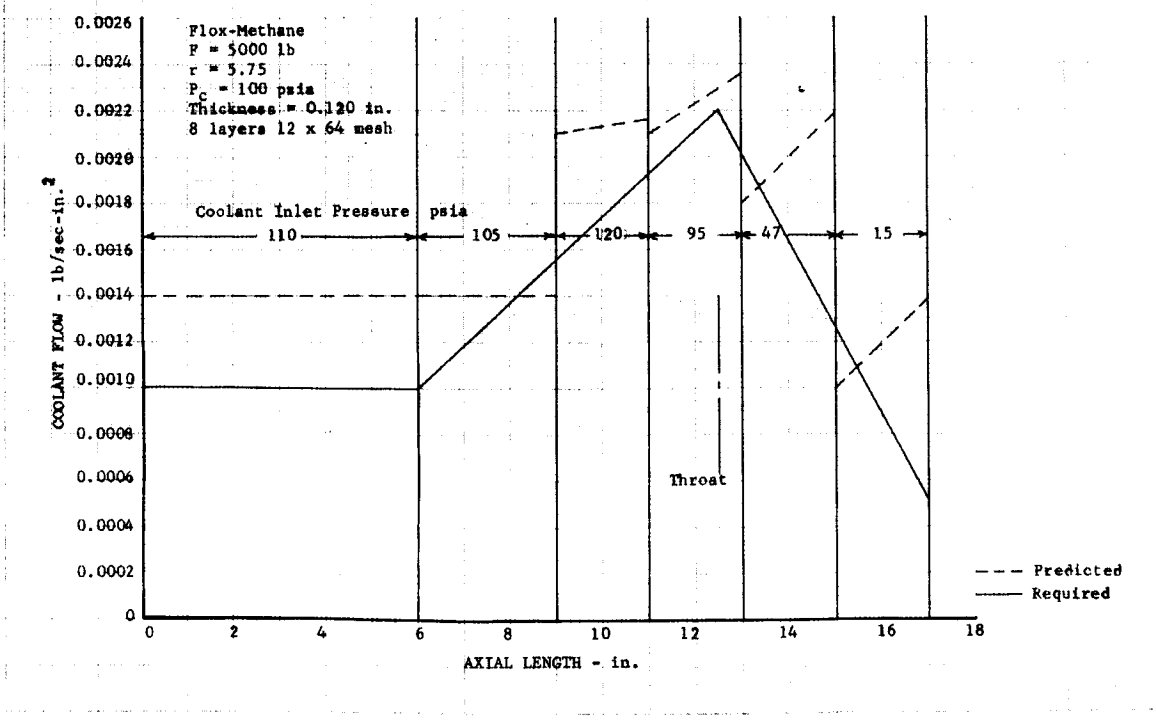

DF 40654

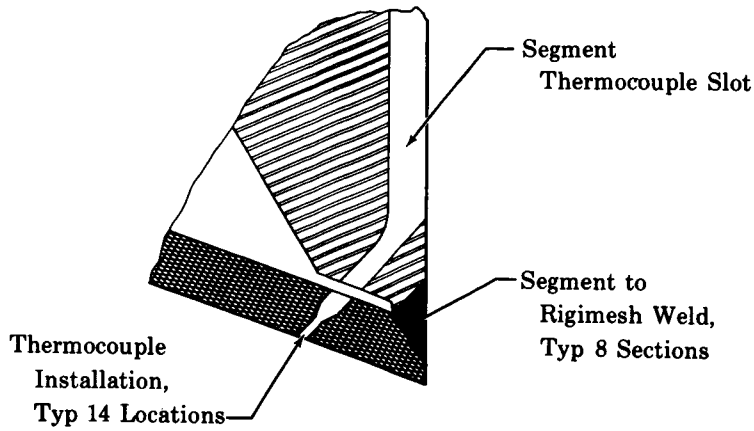

Figure 19. Segment Weld and Thermocouple Installation *FD 12774*

Because of the need to vary coolant flow along the chamber length, the transpiration chamber was divided into eight sections approximately 2 inches long. Each section consists of a stainless steel segment and a Rigimesh liner, as well as temperature and pressure measurement provisions. The liner was formed to the proper inside diameter and hand-fitted to the segment before mating the segment and liner by butt-welding. Also, the liner was spiral-welded thus allowing coolant to flow over the weld (preventing hot spots). Both welds were permitted to penetrate through only part of the Rigimesh, allowing coolant to flow over the entire Rigimesh face.

Segments were made from individual solid pieces of stainless steel, machined to provide axial and radial coolant passages. Coolant flow to the Rigimesh was controlled by eight orifices around the OD of each segment. The orifices could be drilled to any desired diameter up to 0.150 inch, and could be changed as required to vary the Rigimesh inlet pressure. The eight sections were constructed so that the downstream edge of any two adjacent liners was always at least 0.005 inch greater in diameter than the preceding edge. This feature ensured that there would be no exposed edges as the expanding gases proceeded toward the exit. Rigimesh thermocouples were installed by machining a radial slot from ID to OD, inserting the thermocouple, filling the slot with braze, and machining it smooth (figure 19). Both sides of each segment were then coated with copper, 0.001-0.003 inch thick, to provide better sealing between segments.

The eight sections were stacked in a stainless steel cylinder. The injector end of the cylinder was welded to the injector flange, which is machined to accept standard RL10 injector seals and clamps. The segments were held in place at the exit end by a flange bolted to a second flange welded to the exit end of the cylinder. Sealing was provided between the flanges and between the flange and first coolant section by aluminum

O-rings. This retaining flange also acted as an instrumentation terminus, which was drilled and machined to accept 20 subminiature thermocouple connectors. These connectors, held in place by epoxy, provided great flexibility in the handling and assembly of the chamber.

Instrumentation consisted of 16 chromel-alumel metal-sheathed thermocouples, 3 Rigimesh upstream pressure taps, and coolant inlet temperature and pressure measurements. The 16 Rigimesh thermocouples were 0.040 inch in diameter, tapered to 0.020 inch at the junction; 14 of these provide chamber ID temperatures and 2 provide liner OD temperatures. The ID thermocouples were installed after the cooling segment and liner had been welded together. A small hole approximately 0.050 inch in diameter was drilled through the segment cover at a 45-degree angle and about halfway through the Rigimesh. The 0.050-inch hole was then tapered to 0.025 inch and drilled through. The junction was then brazed to the Rigimesh. The thermocouple was then led to the chamber OD through the radial slot cut in the segment. Chamber ID temperatures were measured in one location at the first, third, fourth, fifth, sixth, and eighth segments. At the second and seventh segments they were measured in four locations, 90 degrees apart. The Rigimesh OD temperature was measured at the third and sixth segments by welding the junction to the liner OD after forming but prior to welding to the segment. The metal-covered sheath was then fed through the 45-degree segment hole and out the radial slot to the chamber OD. All thermocouple wires at the segment OD were distributed around the circumference and led to the flange-mounted instrumentation ring through the coolant passages. Rigimesh upstream pressure was measured on the second, fourth, and eighth segments.

D. REGENERATIVELY COOLED THRUST CHAMBER DESIGN

The regeneratively cooled thrust chamber design was a basic RL10A-1 chamber cut off downstream of the throat. A coolant manifold was then installed, giving an expansion ratio of 3.54. (See figure 20). Coolant flow in either direction was possible with this design. The chamber was subsequently modified to incorporate tube fillers as a means of increasing coolant velocity in the tubes. These fillers, constructed of copper and twisted one turn per inch of length, were inserted into all 180 chamber tubes. They extended approximately 8 inches into the tube and were twisted to provide coolant mixing, thus preventing hot spots. The swirlers were held in position by first brazing a length of 0.030-inch diameter wire to the swirler and then welding the wire at the injector end.

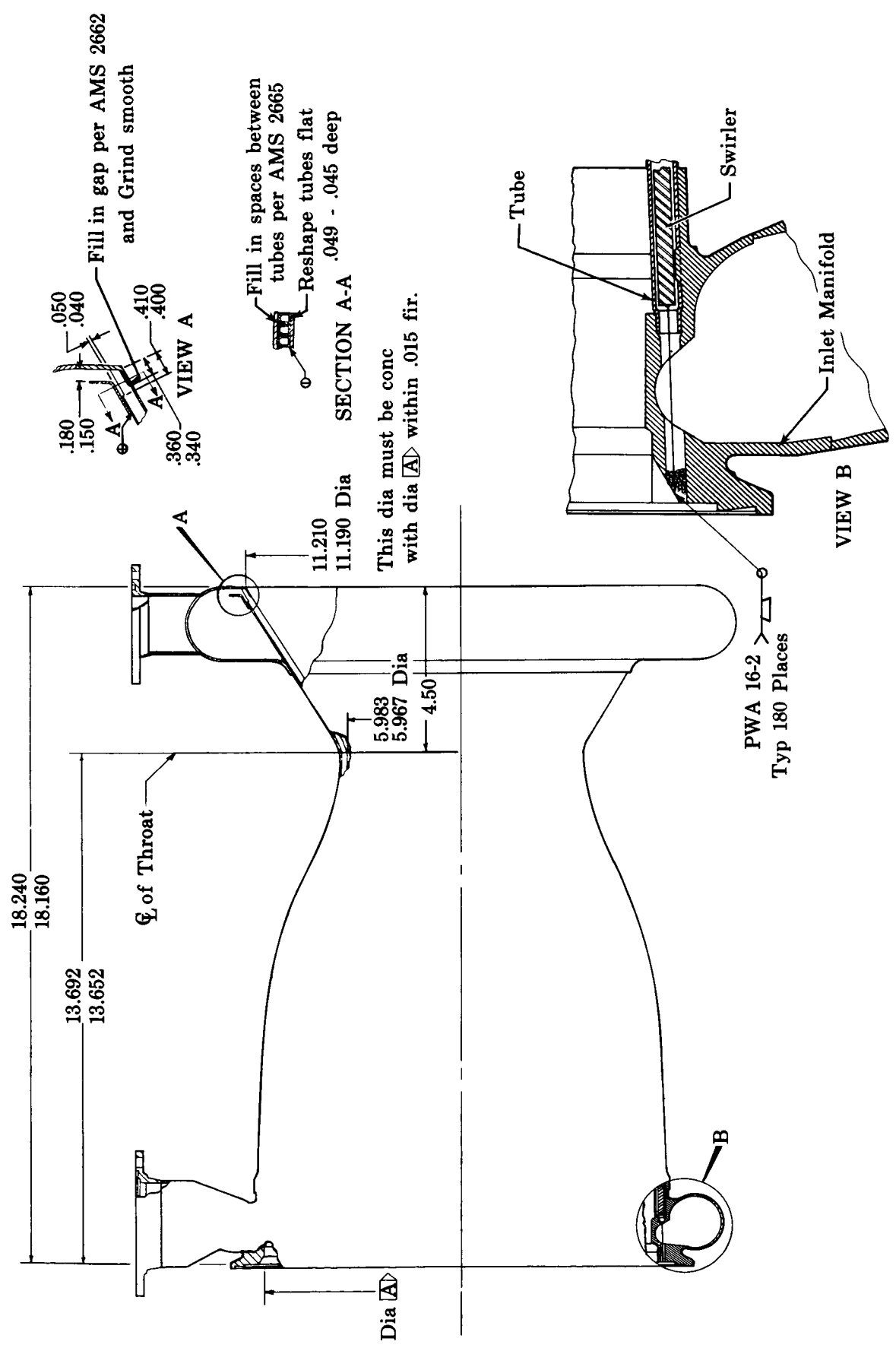

Figure 20. Regenerative Chamber Assembly

FD 10571B

SECTION V
ROCKET TEST FACILITY

All rocket chamber firings made under Contract NAS3-4195 were conducted in stand B-27 of Pratt & Whitney Aircraft's Liquid Propellant Research Facility. The propellant supply system components for this stand are shown in figure 21. All tests used gaseous fuel injection, supplied from a 700-gallon run tank. This tank has an insulated outer and an inner jacket that is heated by a circulating heated oil system. The fuel run line also has a high-temperature circulating oil jacket and insulated outer jacket. The system is capable of handling gaseous fuels at temperatures up to 950°R and pressures up to 800 psig. Methane, propane and a eutectic pentane blend were supplied from this tank at super-critical temperatures.

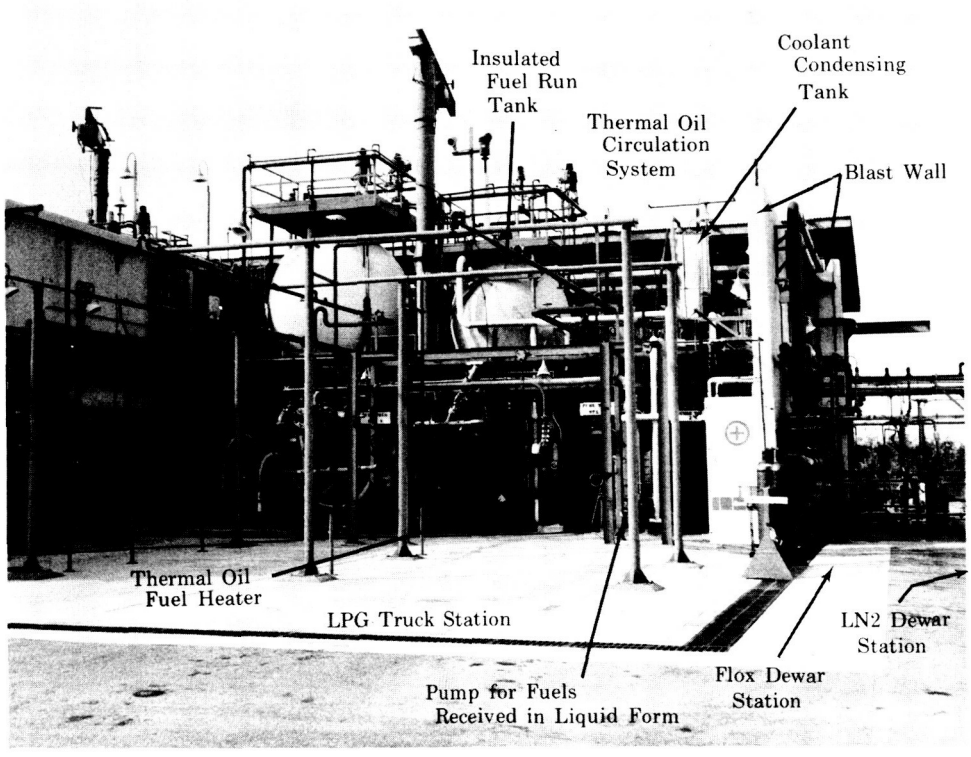

Figure 21. Propellant Supply Area *FD 10567*

The liquid flox was supplied from a 500-gallon, vacuum-jacketed, roadable dewar. The dewar has an operating pressure of 300 psig and a liquid nitrogen cooling coil to maintain the oxidizer in the liquid state. The oxidizer run line is liquid-nitrogen jacketed.

The liquid hydrocarbon coolant was supplied from a 250-gallon, liquid nitrogen jacketed dewar with a maximum operating pressure of 300 psig. The liquid nitrogen jacket could be operated at pressures up to 100 psig, thereby providing temperature control of the coolant tank from 140°R to

184°R. Control of the jacket tank temperature was used to liquefy gaseous methane for the transpiration cooled tests as well as for temperature conditioning of all hydrocarbon coolants prior to running. Coolant run lines were vacuum jacketed and were precooled with liquid nitrogen prior to testing.

The automatic propellant control system consists of servo-operated control valves, an analog computer and a digital sequencer. The automatic fuel and oxidizer portions of the system are illustrated schematically in figure 22. Through the analog computer, the valve controlling reference is selected as (1) downstream pressure control, (2) flow control, or (3) chamber pressure control. A position control mode (not shown on the diagram) was also used during the start transient on many of the tests to prevent abrupt changes in valve position during the transition from gaseous to liquid oxidizer as the oxidizer inlet line cooled down. The digital sequencer can be programed in one-millisecond intervals to operate any one of 40 relay channels over a maximum time interval of 2000 seconds. This unit provides for desired valve operation before and after firing, initiation and shutdown of the test, and timing of controlling parameter changes during test in conjunction with the analog computer. By interrogation of preselected go/no-go parameters the test is allowed to proceed for the programed duration or advanced to a controlled abort shutdown.

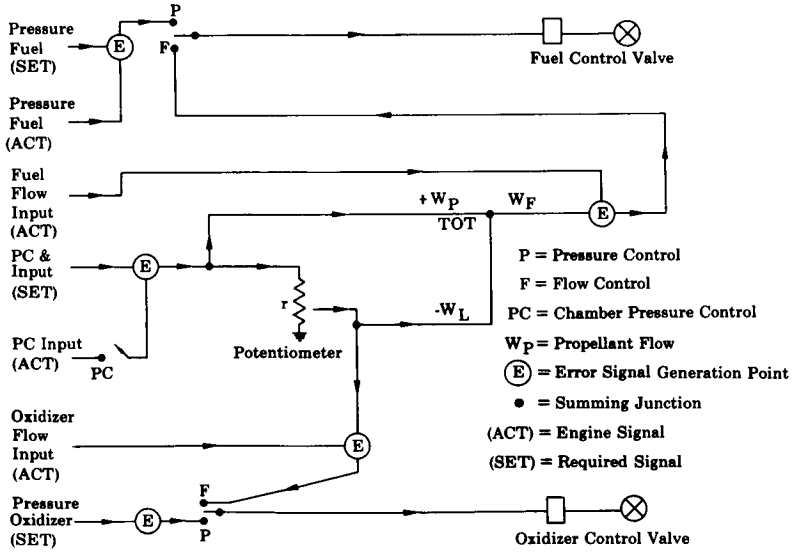

Figure 22. Automatic Flow Control System *FD 8201*

Over 100 instrumentation channels are available for each test. Recorded data included pressure, temperature, thrust, and flow. The data recording system consisted of a 96-channel low-level multiplex system with digital tape recording, high speed recording oscillographs, strip chart recorders, and a 14-channel high speed tape recorder for high frequency measurements. Digital data was processed and reduced to engineering units by an IBM 7090 computer.

SECTION VI

TASK II — UNCOOLED PERFORMANCE AND HEAT TRANSFER TESTS

A. TEST DESCRIPTION

A total of 43 uncooled firings were conducted: 26 with methane, 6 with propane, 5 with a pentane blend (86% isopentane — 14% n-pentane), and 6 with butene-1. The uncooled chamber is shown mounted in the test facility in figure 23. During the initial tests, severe injector burning problems were encountered. Several design modifications were included in later injectors and this problem was eliminated. No other recurring problems were encountered in the uncooled testing. The following paragraphs describe each of the tests and the injector modifications included.

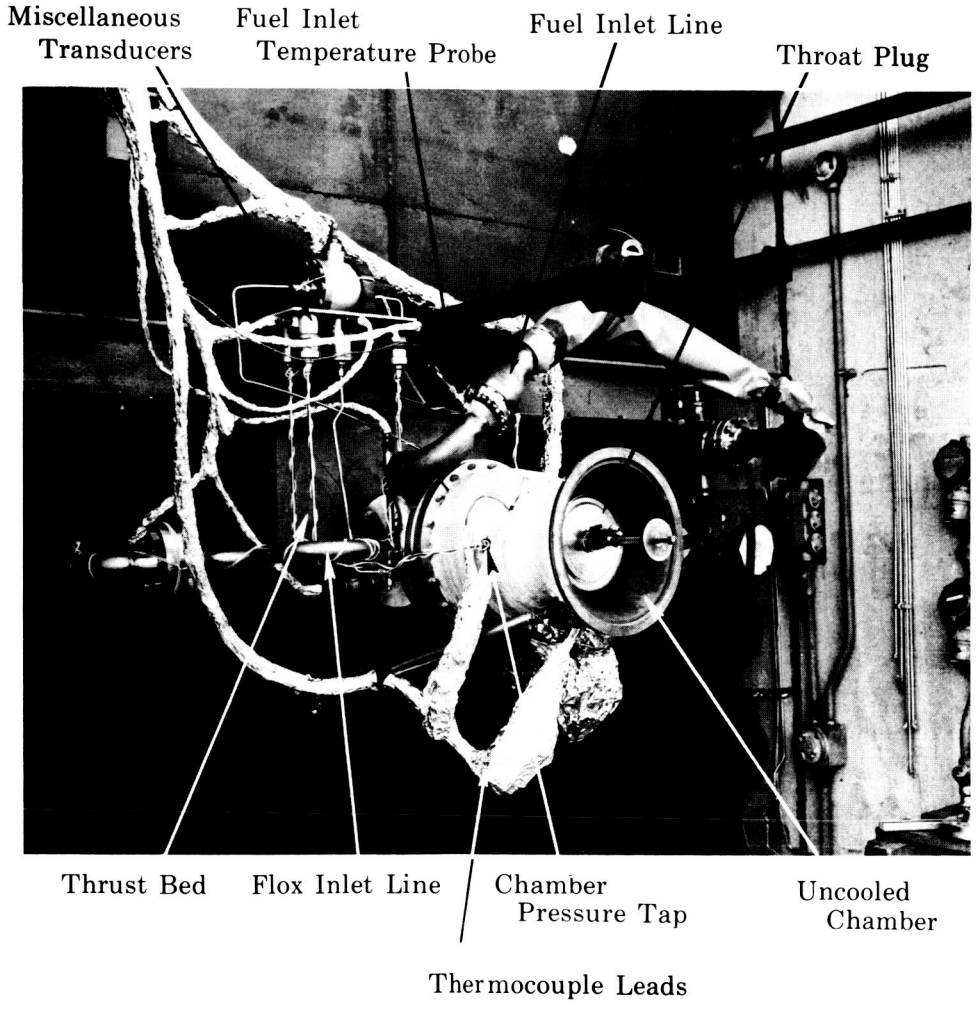

Figure 23. Uncooled Chamber Installed in Stand FD 10570

1. METHANE TESTS (FLOX WAS 82.6% FLUORINE UNLESS NOTED)

Test No. 1 — This test was a scheduled 0.40 second ignition check (time measured from start signal to beginning of oxidizer ramp down). From the oscillograph recording, ignition was clearly shown at 65 milliseconds after the first indication of movement on the oxidizer run valve and oxidizer injector manifold pressure traces. Actual ignition delay would be somewhat less than this by the fill time of the oxidizer side of the injector. During this short run the flox was vaporizing in the inlet line and liquid flox flow through the injector was not obtained. The start-transient with the gaseous flox was smooth without sharp pressure peaks. Injector No. 1, an RL10A-3 injector with swaged oxidizer spuds to reduce the oxidizer flow area and a new Rigimesh faceplate to reduce the fuel flow area, was used for this test. (See table XIV). There was no damage to either the injector or the copper chamber.

Test No. 2 — This test was a 2-second test using the same hardware as test No. 1. The control system for this test was set to open the run valves over a 0.5-second interval by feedback from the run valve downstream pressure. The control system then remained in this pressure control mode for an additional 0.5 second. After 1.0 second the control system switched to flow control, i.e., controlling from the ΔP of the flow measuring devices. With only gaseous oxidizer flow into the chamber at the start of the test the chamber pressure, and hence the valve downstream pressure, remained low and the valve opened completely during pressure control. This caused the oxidizer flow rate to be very high and resulted in a high mixture ratio. The measured performance for this test was satisfactory during transient conditions about 1.2 to 1.4 seconds after test start. At 1.4 seconds the performance declined sharply.

Approximately 30% of the oxidizer spuds were badly burned. (See figure 24). It is believed that the majority of this burning occurred at about 1.4 seconds after the test start and that this accounted for the sudden decline in performance. The cause of the burning has been attributed to a combination of the following four factors.

1. This particular injector was badly dished from previous RL10 tests. This made it difficult to control the gap between the oxidizer spud and the Rigimesh so that insufficient cooling of the spud may have occurred in some places. Also, because of the dished effect, several of the spuds were appreciably below the Rigimesh surface and these seemed to burn more readily than those that were flush with or above the surface of the Rigimesh.
2. The high mixture ratio during the start-transient provided a much more severe condition than normal operation.

3. The swirlers apparently contributed to the damage because none of the inner and outer row spuds, which did not have swirlers, were burned as badly as many of the spuds with swirlers.

4. The swaging operation left a rather rough surface on the tips of the spuds that may have been more susceptible to fluorine than a smooth surface.

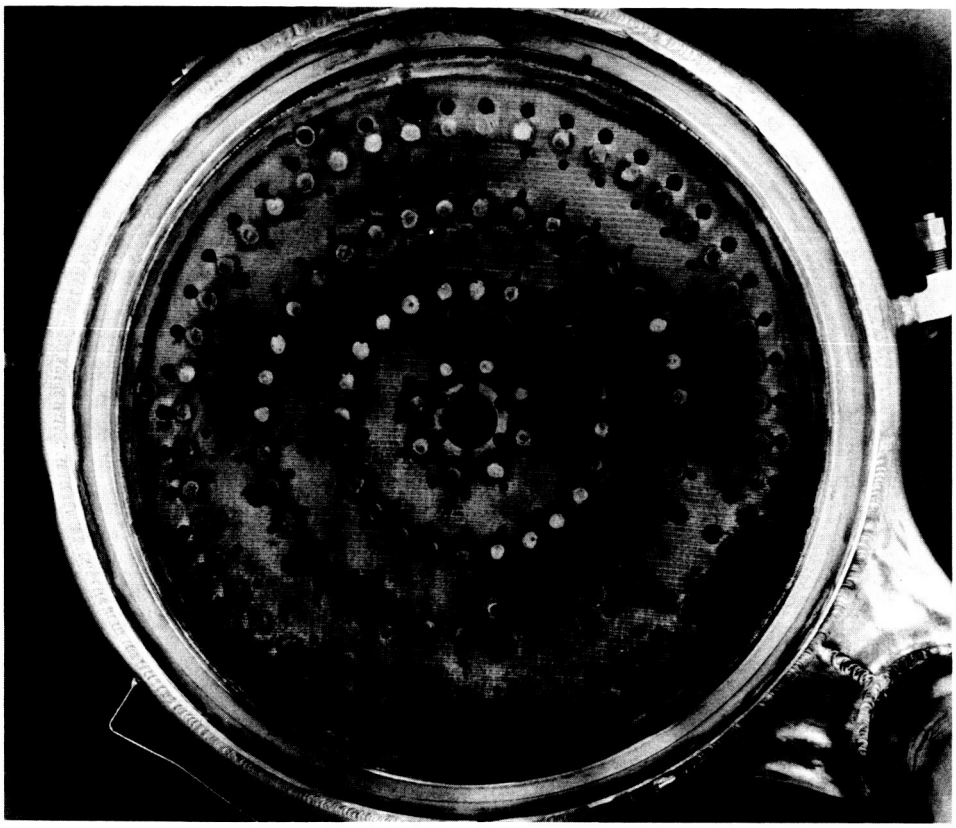

Figure 24. RL10A-3 Injector after Test No. 2 *FE 47785*

Test No. 3 — This test was conducted to compare a swaged RL10A-1 injector (injector No. 2) with the RL10A-3 injector tested in test No. 2. The RL10A-1 injector had no swirlers and the original spud diameter was smaller, therefore the swaging did not roughen the surface as much. The centering of the spuds within the fuel annulus was also much better than the first injector. The control system was changed to switch from pressure control to flow control at 0.45 second instead of 1.0 second to prevent the high mixture ratio during start. This test was advanced to the shutdown-transient after 1.0 second by a low chamber pressure signal to the abort system. The difficulty was caused by a longer start-transient resulting from the early change over to flow control.

Test No. 4 — The same hardware and control scheme as test No. 3 were used. The only change was increasing the timing of the low chamber pressure advance to be activated if chamber pressure did not reach 50 psia at 1.5 seconds. Test duration was 2 seconds. Post-test inspection showed a slight burning that enlarged the inside diameter on three oxidizer spuds; otherwise no change was found.

Test No. 5 — Prolonged oscillation of the oxidizer run valve after the start-transient in test No. 4, necessitated a change in the oxidizer start control mode. The control was programed to ramp up on position control of the oxidizer run valve to be 40% open at 0.45 second, hold at 40% for 0.85 second and switch to flow control at 1.3 seconds. The fuel start control was not changed. Both fuel and oxidizer controls were changed to ramp down on flow control. Test duration was 2.5 seconds and no further burning of the injector spuds was noted.

Test No. 6 — This test was programed for a mixture ratio of 4.03 compared to a mixture ratio of 5.18 for tests No. 1 through 5. Test No. 6 was automatically advanced to the shutdown mode at 1.0 seconds. The advance was due to the burnwire being intact at the end of this time. The burnwire is a weighted wire hung across the nozzle exit. If this wire has not burned through at some set time the test is automatically advanced to shutdown. From the data it was determined that ignition did occur; however, at the lower mixture ratio the burnwire required more time to burn. The sequencer was reset to sample the burnwire at 1.5 seconds.

Test No. 7 — This test was conducted at the same conditions as test No. 6 with the exception of the increased burnwire sampling time. Test duration was 4 seconds. The test was stable and resulted in efficiencies of about 93%. An oscillograph trace of this test is shown in figure 25.

Test No. 8 — The same control sequence used for tests No. 6 and 7 was used for this test. Mixture ratio was increased to 4.60. Test duration was 4 seconds. Combustion efficiency decreased slightly from test No. 7.

Test No. 9 — The only change between this and the previous two tests was increasing the mixture ratio to 5.18. The test was stable; however, combustion efficiency was lower than test No. 8.

Test No. 10 — This was of 4.0 seconds duration using injector No. 3. This was the same as injector No. 2 used for tests No. 3 through 9, except prior to this test, the oxidizer spuds were opened to provide lower oxidizer velocities and higher fuel velocities than those obtained with injector No. 2. This modification had a substantial effect on injector performance, and the resulting efficiencies were the highest obtained to date with an RL10A-1 type injector.

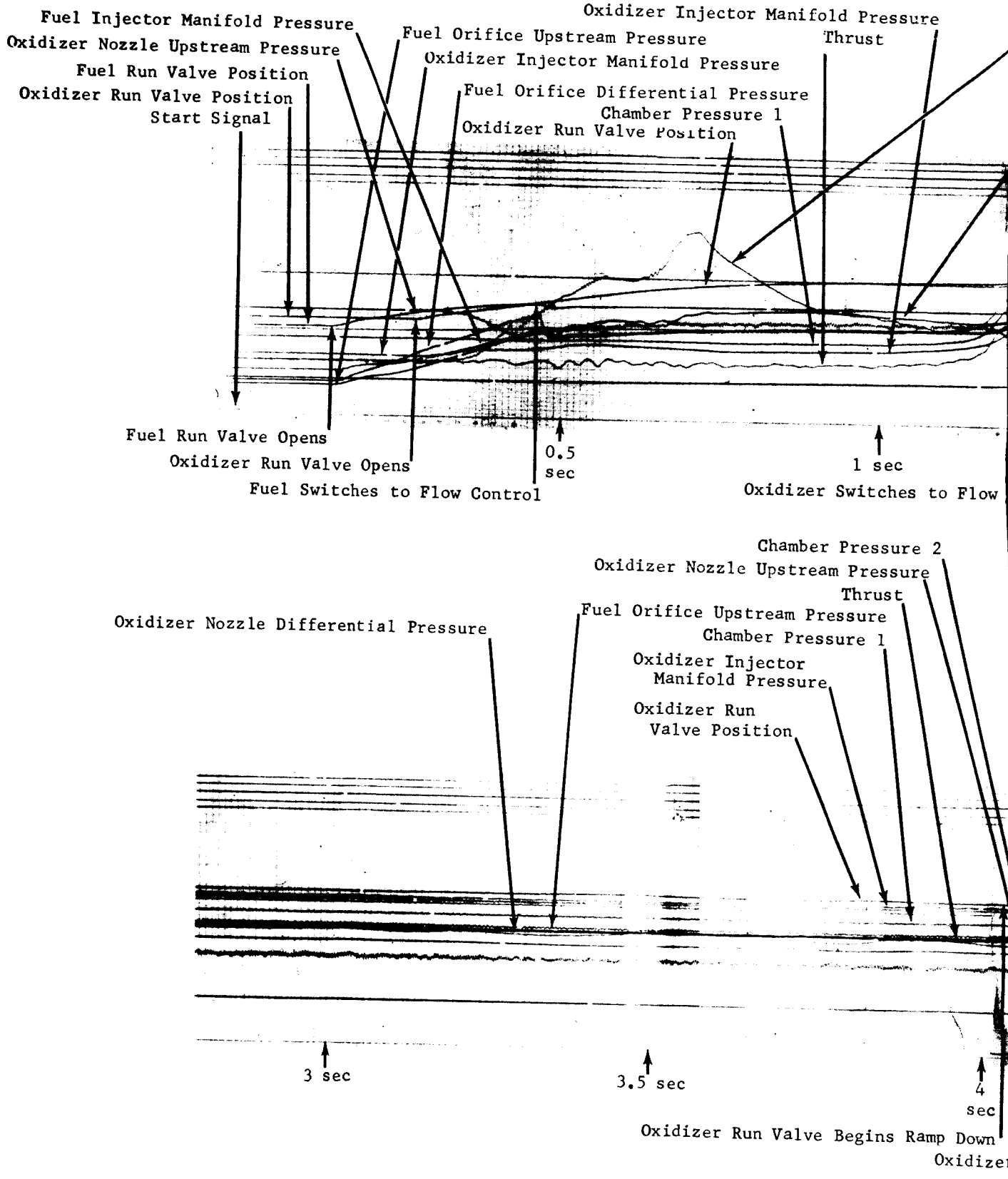

Figure 25. Oscillograph Trace, Test No. 7

2

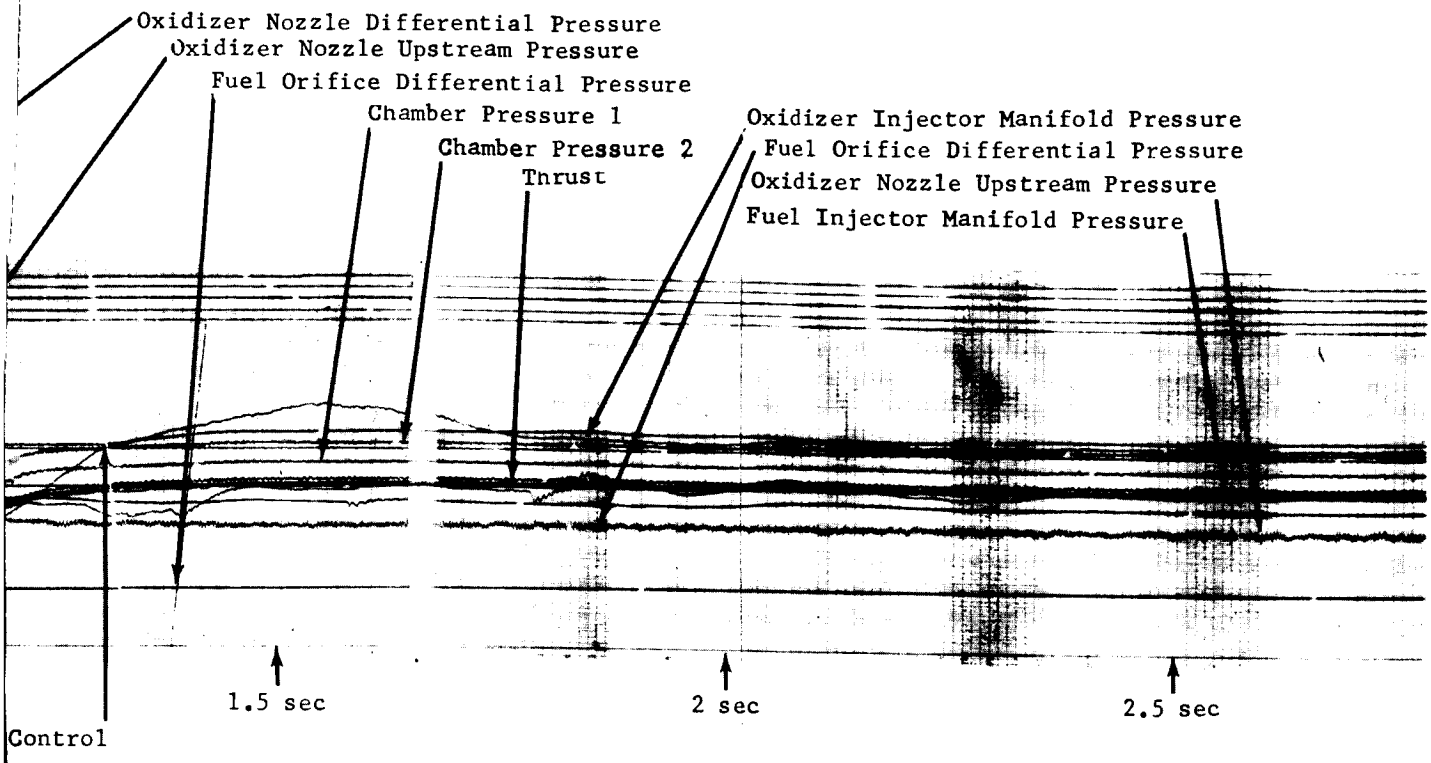
Oxidizer Nozzle Differential Pressure
Oxidizer Nozzle Upstream Pressure
Fuel Orifice Differential Pressure
Chamber Pressure 1
Chamber Pressure 2
Thrust
Oxidizer Injector Manifold Pressure
Fuel Orifice Differential Pressure
Oxidizer Nozzle Upstream Pressure
Fuel Injector Manifold Pressure
1.5 sec
2 sec
2.5 sec
Control

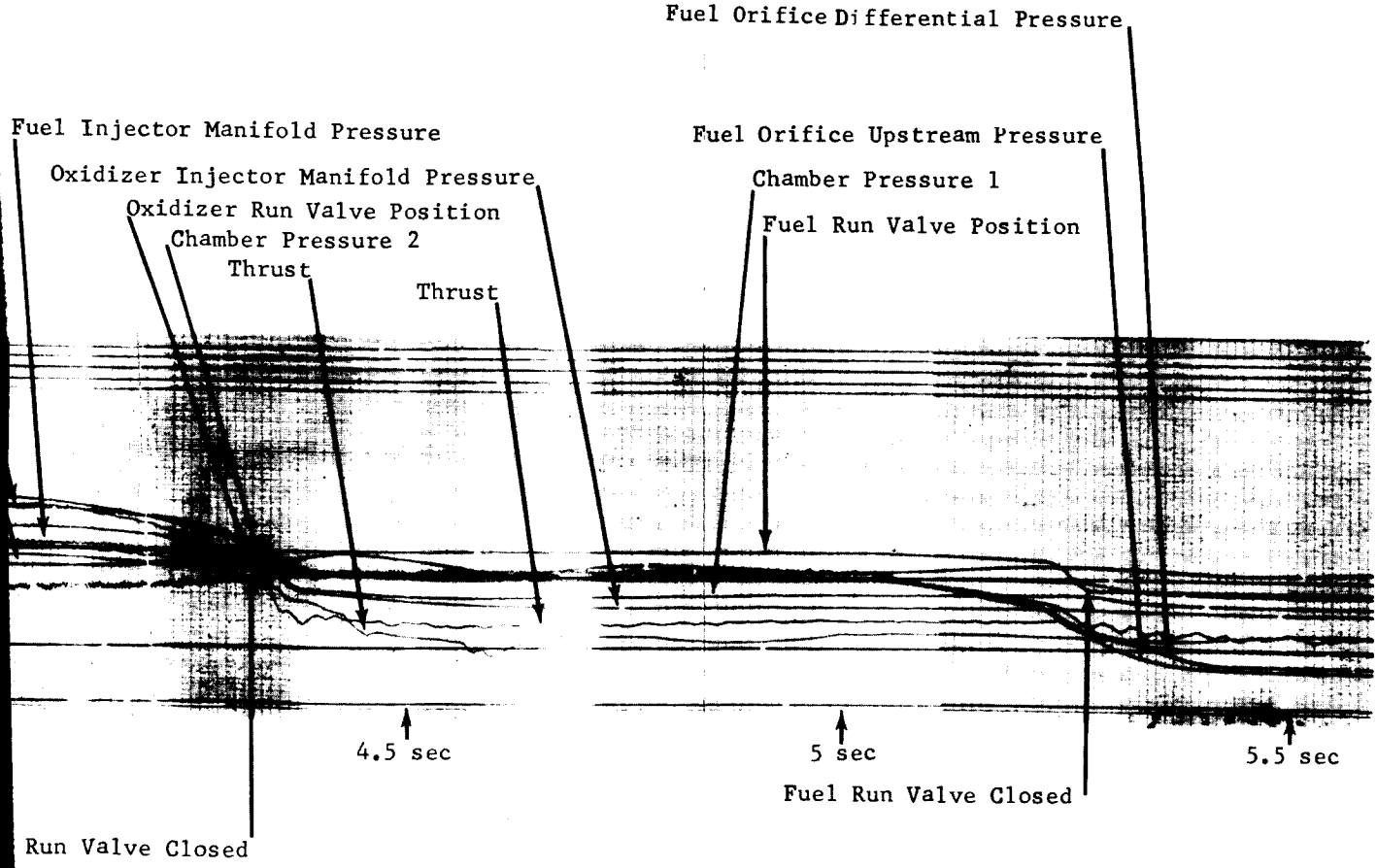
Fuel Orifice Differential Pressure
Fuel Injector Manifold Pressure
Oxidizer Injector Manifold Pressure
Oxidizer Run Valve Position
Chamber Pressure 2
Thrust
Thrust
Fuel Orifice Upstream Pressure
Chamber Pressure 1
Fuel Run Valve Position
4.5 sec
5 sec
5.5 sec
Fuel Run Valve Closed
Run Valve Closed

FD 10566

Test No. 11 – Two instrumentation failures during this test resulted in severe hardware damage. Incorrect control signals from the fuel orifice (because of an incorrect transducer hookup) and from the oxidizer nozzle (because of transducer damage during the start-transient) caused the fuel valve to open fully at 0.40 second after start and the oxidizer valve to close at 1.30 seconds. Fuel was forced into the oxidizer manifold because of transient conditions resulting from the control failure, as well as an aspirating effect of the concentric injector orifices (which caused evacuation of the oxidizer manifold under high fuel and low oxidizer flow conditions). Resulting damage to a section of the injector backplate (figure 26) was repaired and the injector was used in later tests. After test No. 11 the following actions were taken to prevent future similar control system failures.

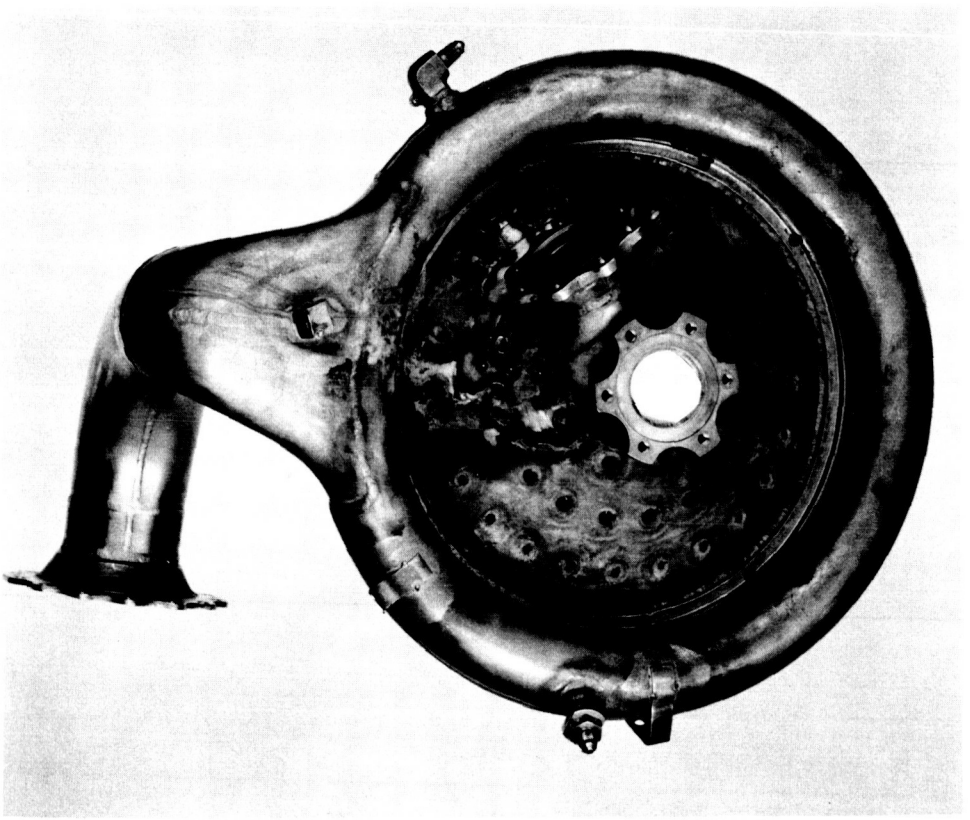

Figure 26. Injector 3 after Test No. 11 *FE 47975*

1. A higher range ΔP transducer was installed on the oxidizer nozzle to prevent overscaling during the start-transient.
2. The nitrogen purge through the oxidizer inlet was set to open automatically whenever the valve position dropped below 5% open. This control on the purge valve is in addition to the automatic sequencing of the valve previously used.
3. The nitrogen pressure used for the oxidizer purge was increased from 25 to 40 psia.

Test No. 12 – Injector No. 4 was used in this test (4.0 seconds duration). Both oxidizer and fuel flow areas were smaller than those of injector No. 3 used in test No. 10. The fuel-to-oxidizer velocity ratio was approximately the same. The characteristic velocity efficiency for the run was low; 12 oxidizer spuds were burned below the surface of the Rigimesh.

Test No. 13 – The same injector was used in this test as in the previous test. A lower mixture ratio ($r = 4.03$ as compared to 4.92) provided higher injector velocity ratios and the characteristic velocity efficiency increased significantly. Six more oxidizer spuds were burned below the surface of the Rigimesh.

Test No. 14 – With the injector utilized in the previous two tests was again employed. At the higher mixture ratio used in this test ($r = 5.67$) the efficiency again dropped off and 36 more spuds were burned below the surface of the Rigimesh. During shutdown a small oxidizer leak developed in the rear of the injector around one of the plate supporting post welds; this failure has been attributed to a poor weld penetration at the post weld and a chemical reaction around it, causing a local overpressure at that location. This injector was later repaired and used in the propane and pentane blend tests (Injector No. 7).

Test No. 15 – Injector No. 3, which had been damaged during test No. 11, was repaired and used in this test. The fluorine concentration in the oxidizer was 55%. The mixture ratio, higher than planned ($r = 5.10$ instead of 4.75), coupled with a fluorine concentration lower than expected, resulted in a mixture ratio slightly higher than stoichiometric (as the fluorine concentration is decreased the stoichiometric mixture ratio is also lowered). High combustion efficiency was obtained. In addition, ignition was hypergolic and smooth despite the lower fluorine concentration and there was no carbon deposited on combustion chamber walls as had occurred in all previous tests.

Test No. 16 – In this test, the same injector used in the previous test was employed, and the flox concentration was increased to 70%. Combustion efficiency was good (although lower than that in test No. 15). There was a heavy carbon deposit on the chamber walls.

Test No. 17 – The flox concentration was increased to 82%. Injector No. 3 was again used. Tests No. 15, 16, and 17 demonstrated the suitability of this injector for providing high performance at low mixture ratios without injector damage. The injector was removed after this test and used for initial low mixture ratio firings of the transpiration cooled chamber.

Test No. 18 – Injector No. 5 incorporating the modifications listed in Table XIV was used. Duration of this test was 4 seconds. No injector damage was visible; however, performance was not as high as expected.

Test No. 19 — This was another 4-second test using injector No. 5. Again there was no visible change in the injector. Performance was not improved.

Test No. 20 — This test (using injector No. 5) was made at the peak mixture ratio for flox-methane. There was no injector damage. After this test the injector was removed for modification of the spud flow areas in an attempt to improve engine performance.

Test No. 21 — Prior to this test, injector No. 5 was swaged to increase the oxidizer flow area, thereby decreasing the fuel area and increasing the fuel-oxidizer velocity ratio. The identification number after modification was changed to injector No. 6. The data indicate that combustion efficiency was approximately 4% higher after the swaging operation.

Tests No. 22, 23, 24 — These were all normal 4-second methane runs at 82.6% fluorine in the flox. Chamber pressure was steady. No hardware damage was noted.

Tests No. 25 and 26 — These two tests were conducted using 90% fluorine in the flox. Chamber pressure was steady and combustion efficiency was good. No hardware damage was noted.

2. PROPANE TESTS (FLOX WAS 75% FLUORINE FOR ALL PROPANE TESTS)

Test No. 27 — This was a 2.7-second propane ignition check. The control sequence used for all propane tests was identical to that initiated after methane test No. 4. Injector No. 7 was used. This was a rebuild of injector No. 4, which was used in methane tests 12, 13, and 14. Modifications included: (1) reducing the number of injector spuds from 216 to 108, (2) using nickel oxidizer spuds and (3) incorporating 100% penetration-fluorine welds on the injector backplate. Propane ignition was smooth.

Tests No. 28, 29, 30, 31, 32 — These were normal 4-second propane runs. No hardware damage was noted.

3. PENTANE BLEND TESTS (FLOX WAS 75% FLUORINE FOR ALL TESTS)

Tests No. 33, 34, 35, 36, 37 — These were all 4-second runs. The pentane blend tests were conducted with the same control sequence used for the later methane tests and all propane tests. All pentane blend tests were characterized by a fuel-rich start-transient. It is believed that this could have been eliminated by a controls sequence change; however, the pressure overshoot was not considered deleterious to hardware or test data and no controls changes were made. The same injector (injector No. 7) used in the propane tests was used in all pentane blend tests. Figure 27 is a post-run photograph showing carbon soot formation on the chamber walls after the series of tests.

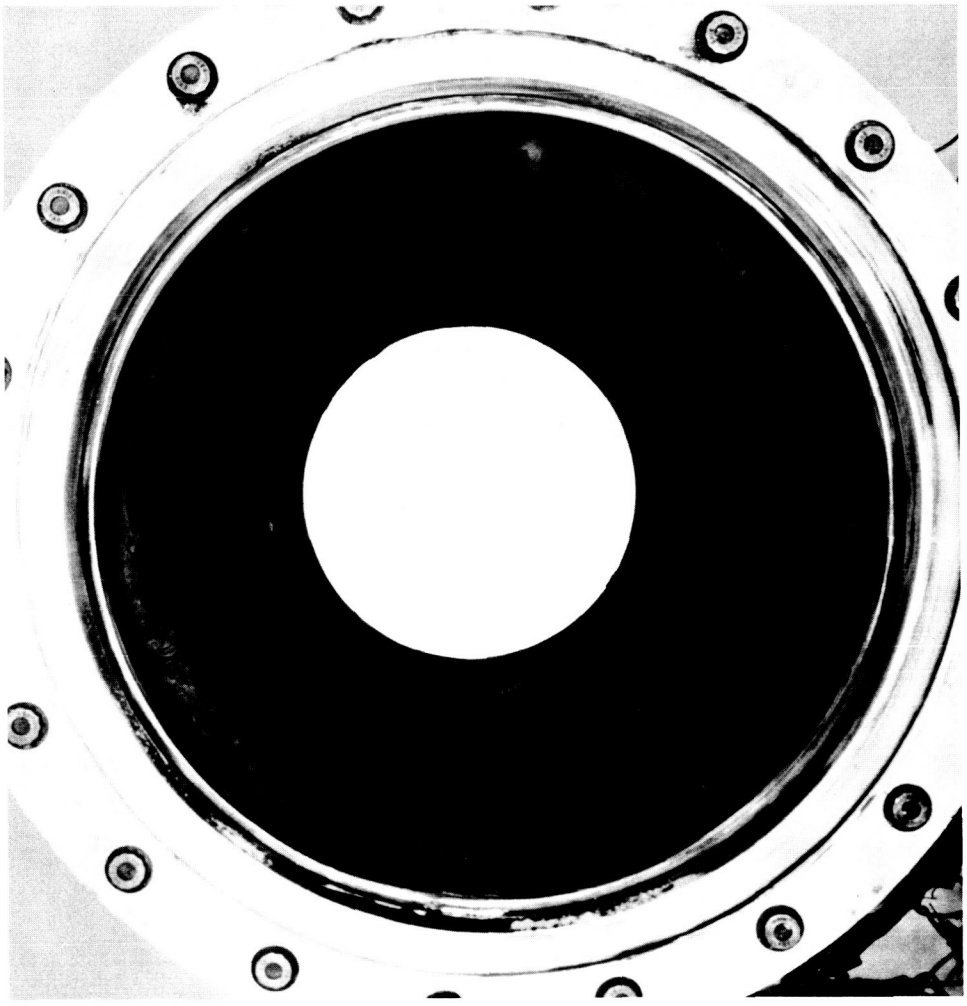

Figure 27. Soot Formation on Uncooled Chamber after Tests No. 27 through 37 (View from Injector End) *FE 50548*

4. BUTENE-1 TESTS (FLOX WAS 70.4% FLUORINE FOR ALL TESTS)

Tests No. 38, 39, 40, 41, 42, 43 – These were all 4-second runs. The butene-1 tests were conducted with the same control sequence used for all uncooled tests after test No. 4. The start-transient was very similar to that encountered in the pentane blend tests. As in those tests, the fuel-rich start was not considered important to test results and the control sequence was not changed. The same injector (injector No. 7) used in the propane and pentane blend tests was used for all butene-1 tests.

B. DATA REDUCTION

Measured performance parameters were recorded every 0.0125 second. Every eight scans of recorded data were averaged to provide an average data value for each 0.10 second interval. These average values were then used in determining the calculated performance parameters and efficiencies every 0.10 second over the stable portion of each run.

The following is a list of symbols and subscripts utilized in the following calculations.

A_e	Nozzle Exit area, in^2
A_t	Throat area, in^2
C_F	Thrust coefficient
C_P	Constant pressure specific heat, $Btu/lb_m-°R$
C_s	Stream thrust coefficient
c*	Characteristic exhaust velocity, ft/sec
ϵ_e	Nozzle exit to throat area ratio, A_e/A_t
F	Thrust, lb
g_o	Gravitational constant - 32.174 lb_m-ft/lb_f-sec^2
I_{sl}	Sea level specific impulse, lb_f-sec/lb_m
I_{vac}	Specific impulse at $P_a = 0$, lb_f-sec/lb_m
P_a	Ambient pressure, psia
P_c	Chamber pressure, psia
P_T	Chamber pressure corrected for momentum loss, psia
r	Mixture ratio, (oxidizer/fuel)
$\dot{w}$	Flow rate, lb_m/sec
η	Efficiency
Δ	Indicates difference
'	Indicates theoretical value

Subscripts:

vac	Value at $P_a = 0$
(C_s)	Corrected for C_s
(cor)	Corrected for momentum loss, heat loss, and C_s
o	Oxidizer
f	Fuel
p	Propellant

The thrust coefficient was calculated from test data as follows:

$$C_F = \frac{F}{A_t P_c} \qquad (1)$$

The experimental thrust coefficient was compared to a theoretical value calculated as follows:

$$C_{F_{vac}} = \frac{F_{vac}}{A_t P_c} = \frac{F + P_a A_e}{A_t P_c} = \frac{F}{A_t P_c} + \frac{P_a \epsilon_e}{P_c} \qquad (2)$$

for these test $A_t = 28.2$ square inches and $\epsilon_e = 3.54$. Also from the above:

$$C_F = C_{F_{vac}} - \frac{3.54\ P_a}{P_c} \qquad (3)$$

For the flox-LPG combinations considered in the range of mixture ratios and chamber pressures of interest, the use of constant value of 1.597 for theoretical $C_{F_{vac}}$ introduces negligible error. Thus, using $P_a = 14.696$ psia:

$$C_F' = 1.597 - \frac{51.726}{P_c} \qquad (4)$$

where the prime denotes a theoretical value.

The value of C_F may be corrected for nozzle friction and divergence losses through use of a calculated stream thrust coefficient efficiency, C_s.

$$C_s = \frac{C_{F_{vac}}}{C_{F_{vac}}'} \qquad (5)$$

For nozzles with a 30-degree half angle and area ratio of 3.54, C_s has been calculated to be 0.905. These calculations were based on the method of characteristics including effects of wall friction. Values of C_s calculated by this method have proved to be quite accurate in numerous research and development programs. Thus:

$$C_{F_{(C_s)}}' = 1.4453 - \frac{51.726}{P_c} \qquad (6)$$

Characteristic exhaust velocity is calculated in two ways:

$$c^*_{P_c} = \frac{A_t\ g_o\ P_c}{\dot{w}_p} = \frac{907.31\ P_c}{\dot{w}_p} \qquad (7)$$

The subscript $_{P_c}$ is used to denote that c* has been calculated from chamber pressure. For comparison, c* may also be calculated from thrust measurements by assuming that a theoretical C_F corrected for nozzle divergence and friction losses is an accurate estimate of the experimental C_F.

$$c^*_F = \frac{I_s \, g_o}{C'_F \, (C_s)} \tag{8}$$

Equation (6) indicates that small changes in $_{P_c}$ have only a small effect on c^*_F. c^*_F is proportional to thrust, hence comparison of c^*_F and $c^*_{P_c}$ provides a check on the consistency of the thrust and chamber pressure measurements.

The theoretical performance data (prime superscript) used for comparison with measured data was based on propellant enthalpies corresponding to the actual propellant inlet conditions.

For calculating sea level specific impulse:

$$I_{sl}' = I_{vac}' - \frac{P_a \, A_e}{\dot{w}_p} \tag{9}$$

$$\dot{w}_p = \frac{A_t \, P_c \, g_o}{c^*} \tag{10}$$

$$I_{sl}' = I_{vac} - \frac{P_a \epsilon_e \, c^*}{g_o \, P_c} = I_{vac} - 1.6078 \frac{c^*}{P_c} \tag{11}$$

correcting I_{vac}' for stream thrust coefficient efficiency

$$I_{sl}'(C_s) = 0.905 \, I_{vac}' - 1.6078 \frac{c^*}{P_c} \tag{12}$$

The following efficiencies were then calculated:

$$\eta_{c^*_{P_c}} = \frac{c^*_{P_c}}{c^{*\prime}}$$

$$\eta_{c^*_F} = \frac{c^*_f}{c^{*\prime}}$$

$$\eta I_s = \frac{I_{sl}}{I_{sl}'}$$

$$\eta C_F = \frac{C_F}{C_F'}$$

In estimating the performance of a propellant in an ideal engine, it is assumed that burning takes place at zero velocity. In an actual engine there is a loss in total pressure because burning takes place at velocities other than zero. Momentum losses were calculated over the range of mixture ratios and chamber pressures of interest. From these calculations it was determined that the total pressure after burning may be found with sufficient accuracy from:

$$P_T = 0.974\ P_c$$

Heat lost to the engine walls was calculated from the rate of temperature rise of the chamber skin thermocouples. This heat loss was then accounted for by adjusting the propellant inlet enthalpies in calculating theoretical performance values.

The efficiencies shown below were then calculated using theoretical and experimental values corrected for momentum loss by replacing P_c with P_T in all calculations, basing the theoretical values on corrected inlet enthalpy, and correcting for nozzle divergence and friction effects through the use of $I_{sl}'_{(C_s)}$ and $C_F'_{(C_s)}$ in place of I_{sl}' and C_F'.

$$\eta_{c^*_P\,(cor)} = \frac{c^*_{P_c}}{c^{*\prime}}$$

$$\eta_{c^*_F(cor)} = \frac{c^*_F}{c^{*\prime}}$$

$$\eta_{I_s(cor)} = \frac{I_{sl}}{I_{sl}'_{(C_s)}}$$

$$\eta_{C_F(cor)} = \frac{C_F}{C_F'_{(C_s)}}$$

C. TEST PERFORMANCE

Table XV presents measured performance data for all uncooled tests, table XVI presents performance data calculated from the preceding equations, and table XVII contains injector performance data. Poor agreement between $\eta c^*_{P_c}$ and ηc^*_F in tests 4 through 10 was attributed to nozzle separation. After test number 10 the propellant flow rate was increased by 10% to raise chamber pressure and prevent separation. There was satisfactory agreement between performance based on chamber pressure and thrust in most of the tests having a chamber pressure above approximately 105 psia.

TABLE XV. MEASURED PERFORMANCE DATA – UNCOOLED TESTS

Test No.	Fuel	Percent F_2 in Flox	Test Duration, sec	P_c, psia	F, lb	$\dot{W}_o$, lb/sec	$\dot{W}_f$, lb/sec	T_o, °R	T_f, °R	ΔP_o, psi	ΔP_f, psi	Injector[3]	Comments
1[1]	Methane	82.6	0.4	33	462			200+	537	9	90	1	Ignition check
2		82.6	2.0	115	3130	12.7	2.08	194	524	40	28	1	Checkout run, injector spuds burned
3[1]		82.6	1.0	93	2000	17.2	3.24	200+	556	20	20	2	Premature shutdown, low P_c abort
4		82.6	2.0	90	2170	13.4	2.12	183	552	65	15	2	Checkout run
5		82.6	2.5	88	2250	11.9	2.15	175	523	44	16	2	Checkout run
6[2]		82.6	1.0									2	Planned 4.0 second run, burnwire abort
7		82.6	4.0	97	2520	11.3	2.76	160	567	44	23	2	
8		82.6	4.0	92	2390	11.3	2.44	164	532	49	19	2	
9		82.6	4.0	85	2190	11.5	2.11	164	556	49	16	2	
10		82.6	4.0	102	2708	11.3	2.60	171	508	24	16	3	
11[2]		82.6	1.5									3	Burned out injector
12		82.6	4.0	108	2814	12.8	2.59	164	583	40	53	4	Ends of 12 spuds burned
13		82.6	4.0	104	2739	11.3	2.80	168	579	26	64	4	Ends of 6 spuds burned
14		82.6	4.0	98	2554	12.0	2.11	168	583	31	41	4	Small hole in back of injector, ends of 36 spuds burned
15		55.0	4.0	111	2935	12.8	2.51	164	588	42	44	3	
16		70.0	4.0	110	2859	12.8	2.58	164	589	37	27	3	
17		82.6	4.0	111	2988	12.7	2.55	171	590	36	27	3	
18		82.6	4.0	106	2787	12.4	2.56	186	572	28	44	5	
19		82.6	4.0	103	2726	12.3	2.38	170	571	26	40	5	
20		82.6	4.0	104	2746	12.8	2.23	168	572	27	34	5	
21		82.6	4.0	103	2771	11.9	2.23	167	605	19	48	6	
22		82.6	4.0	107	2888	12.4	2.32	166	608	20	50	6	
23		82.6	4.0	111	3018	12.1	2.94	163	611	19	74	6	
24		82.6	4.0	107	2922	12.6	2.20	166	614	23	45	6	
25		90.0	4.0	106	2868	12.3	2.45	165	613	18	55	6	
26		90.0	4.0	103	2810	12.1	2.31	165	614	17	51	6	
27	Propane	75.0	2.7	105	2724	11.7	2.74	169	756	18	63	7	
28		75.0	4.0	108	2891	11.8	2.95	169	750	18	82	7	Checkout run, ignition smooth
29		75.0	4.0	105	2783	11.9	2.73	169	760	17	67	7	No visible hardware damage on any propane tests
30		75.0	4.0	103	2727	12.0	2.57	169	763	18	56	7	
31		75.0	4.0	103	2748	12.3	2.46	166	767	17	52	7	
32		75.0	4.0	102	2690	11.9	2.57	171	771	18	63	7	
33	Pentane Blend	75.0	4.0	101	2604	11.5	3.48	176	861	21	54	7	Very fuel-rich start on all pentane tests
34		75.0	4.0	104	2672	11.7	3.83	173	866	18	65	7	No visible hardware damage on any pentane tests
35		75.0	4.0	101	2598	12.1	3.05	172	862	22	49	7	
36		75.0	4.0	102	2633	12.3	3.08	170	864	21	44	7	
37		75.0	4.0	106	2782	13.2	2.97	165	866	19	42	7	
38	Butene-1	70.4	4.0	119	3182	12.3	4.49	168	790	23	88	7	Very fuel-rich start on all Butene-1 tests.
39		70.4	4.0	115	3083	11.8	4.83	167	795	23	107	7	No visible damage on any Butene-1 tests.
40		70.4	4.0	115	3096	12.3	3.88	168	795	23	89	7	
41		70.4	4.0	116	3157	12.7	3.78	161	796	22	84	7	
42		70.4	4.0	117	3167	12.3	4.34	165	798	23	90	7	
43		70.4	4.0	120	3330	13.1	3.57	159	800	29	67	7	

(1) Values given are transient values near end of tests.

(2) Data not reduced.

(3) See Table XIV

TABLE XVI. CALCULATED PERFORMANCE DATA – UNCOOLED TESTS

Test No.	Fuel	r	$\dot{w}_p$, lb/sec	c*, ft/sec	I_{sl}', sec	C_F'	$c^*_{P_c}$, ft/sec	c^*_F, ft/sec	Q, Btu/sec	$\eta_{c^*P_c}$	η_{c^*F}	$\eta_{c^*P_{c(cor)}}$	$\eta_{c^*F(cor)}$	I_{sl}, sec	η_{I_s}	$\eta_{I_{s(cor)}}$	C_F	η_{C_F}	$\eta_{C_{F(cor)}}$	Δt Used,(1) sec
2	Methane	6.10	14.8	6951	246.5	1.147	6980	6860		1.00	0.986			211	0.857		0.974	0.849		0.10
4		6.34	15.5	6863	216.9	1.020	5190	5220		0.756	0.760			146	0.675		0.907	0.890		0.10
5		5.55	14.1	6983	216.1	1.002	5570	5830		0.797	0.835			160	0.742		0.926	0.925		0.70
7		4.11	14.1	6835	228.6	1.077	6350	6270	619	0.929	0.917	0.907	0.934	179	0.784	0.931	0.908	0.843	1.029	1.50
8		4.64	13.8	6916	224.2	1.047	6140	6250	625	0.887	0.904	0.867	0.922	173	0.772	0.923	0.907	0.866	1.064	1.10
9		5.43	13.6	6982	216.3	1.004	5770	6130	625	0.827	0.878	0.808	0.898	161	0.746	0.901	0.900	0.896	1.112	1.60
10		4.34	13.9	6877	235.3	1.102	6780	6637	653	0.986	0.965	0.963	0.982	195	0.830	0.981	0.926	0.840	1.019	1.40
12		4.92	15.4	6970	241.3	1.120	6360	6100	650	0.912	0.877	0.891	0.892	183	0.759	0.895	0.927	0.823	1.001	2.10
13		4.03	14.1	6831	234.3	1.104	6690	6600	709	0.980	0.967	0.957	0.983	194	0.830	0.981	0.935	0.847	1.027	1.30
14		5.67	14.1	6992	232.2	1.073	6290	6350	650	0.900	0.908	0.879	0.925	183	0.779	0.927	0.925	0.862	1.058	1.30
15		5.09	15.3	6537	229.4	1.137	6620	6300	972	1.013	0.963	0.989	0.978	192	0.837	0.983	0.933	0.821	0.989	1.40
16		4.97	15.4	6781	237.1	1.131	6490	6130	683	0.957	0.904	0.935	0.918	186	0.784	0.921	0.921	0.814	0.982	1.50
17		4.96	15.3	6969	244.2	1.134	6600	6460	650	0.947	0.927	0.925	0.942	196	0.804	0.945	0.957	0.844	1.018	1.00
18		4.82	14.9	6957	239.2	1.107	6423	6292	700	0.923	0.904	0.902	0.920	187	0.781	0.922	0.936	0.845	1.020	1.40
19		5.17	14.7	6990	237.4	1.089	6371	6324	700	0.911	0.905	0.891	0.921	186	0.782	0.925	0.937	0.855	1.034	1.70
20		5.73	15.0	6994	239.0	0.937	6278	6224	750	0.898	0.890	0.877	0.906	183	0.766	0.906	0.939	0.855	1.032	1.80
21		5.35	14.1	6999	237.6	1.095	6604	6681	558	0.944	0.954	0.922	0.971	196	0.824	0.975	0.954	0.871	1.054	1.30
22		5.36	14.7	7004	241.5	1.112	6571	6563	525	0.938	0.937	0.916	0.953	196	0.811	0.957	0.960	0.863	1.040	1.00
23		4.10	15.0	6848	241.6	1.131	6714	6608	525	0.981	0.965	0.958	0.980	201	0.833	0.978	0.964	0.852	1.023	1.00
24		5.73	14.8	6998	242.8	1.115	6585	6594	517	0.941	0.942	0.919	0.958	197	0.813	0.959	0.965	0.865	1.042	0.70
25		5.02	14.8	6834	235.5	1.109	6538	6503	629	0.957	0.952	0.935	0.968	193	0.822	0.969	0.952	0.858	1.035	1.40
26		5.25	14.4	6832	232.5	1.095	6478	6565	650	0.948	0.961	0.926	0.978	193	0.828	0.980	0.956	0.873	1.056	1.60
27	Propane	4.27	14.4	6822	234.4	1.103	6588	6391	300	0.966	0.937	0.943	0.952	189	0.807	0.951	0.923	0.836	1.010	0.60
28		4.00	14.8	6788	236.3	1.118	6666	6538	328	0.982	0.963	0.959	0.979	196	0.831	0.977	0.937	0.848	1.021	1.50
29		4.36	14.6	6836	234.9	1.105	6506	6411	293	0.952	0.938	0.929	0.953	190	0.808	0.953	0.928	0.850	1.026	1.40
30		4.68	14.6	6823	232.0	1.095	6408	6360	293	0.936	0.932	0.914	0.948	186	0.804	0.949	0.927	0.856	1.035	0.90
31		5.02	14.8	6747	230.0	1.096	6335	6318	276	0.939	0.937	0.917	0.952	186	0.808	0.954	0.943	0.860	1.039	2.40
32		4.65	14.5	6832	231.5	1.092	6399	6341	300	0.936	0.928	0.914	0.944	185	0.800	0.945	0.932	0.854	1.033	1.60
33	Pentane Blend	3.32	15.0	6687	225.1	1.087	6122	5968	209	0.916	0.893	0.893	0.907	173	0.770	0.910	0.911	0.839	1.016	0.90
34		3.05	15.5	6644	225.3	1.098	6059	5849	170	0.912	0.895	0.889	0.894	172	0.764	0.900	0.914	0.832	1.005	1.10
35		3.80	15.2	6726	227.5	1.084	5981	5858	178	0.889	0.880	0.887	0.885	170	0.746	0.881	0.913	0.842	1.021	0.80
36		4.00	15.4	6746	229.2	1.089	5994	5864	188	0.889	0.871	0.866	0.883	171	0.745	0.879	0.917	0.842	1.019	0.80
37		4.44	16.2	6763	233.2	1.110	5957	5778	188	0.881	0.869	0.859	0.867	172	0.738	0.867	0.929	0.838	1.010	1.00
38	Butene-1	2.73	16.8	6616	238.5	1.161	6424	6058	325	0.971	0.916	0.947	0.928	190	0.797	0.929	0.951	0.820	0.979	1.4
39		2.45	16.6	6597	234.6	1.147	6252	5979	425	0.948	0.906	0.925	0.919	185	0.788	0.921	0.952	0.830	0.994	1.6
40		3.18	16.2	6660	238.7	1.145	6422	6201	525	0.964	0.931	0.941	0.944	191	0.802	0.938	0.959	0.838	1.004	0.5
41		3.38	16.5	6692	241.8	1.152	6396	6152	500	0.956	0.919	0.933	0.932	191	0.791	0.924	0.962	0.835	0.999	0.4
42		2.82	16.6	6622	237.8	1.155	6394	6124	540	0.966	0.925	0.943	0.938	191	0.803	0.937	0.961	0.832	0.9951	1.2
43		3.67	16.7	6731	245.3	1.164	6522	6364	550	0.969	0.946	0.946	0.959	200	0.816	0.951	0.988	0.849	1.014	0.5

(1) Δt used, is the amount of time over which the performance figures are averaged.

TABLE XVII. INJECTOR PERFORMANCE COMPARISON – UNCOOLED TESTS

Test No.	Fuel	Injector[1]	$\dot{w}_f$, lb/sec	$\dot{w}_o$, lb/sec	V_f, ft/sec	V_o, ft/sec	r	$\dot{w}_f V_f$, lb-ft/sec^2	$\dot{w}_o V_o$, lb-ft/sec^2	$\eta_{c^*} P_c$	P_c, psia	V_f/V_o	$\dot{w}_f V_f / \dot{w}_o V_o$
2	Methane	1	2.08	12.7	855	52	6.10	1780	692	1.00	115	16.5	2.57
4		2	2.12	13.4	785	73	6.34	1640	935	0.756	90	10.5	1.75
5		2	2.16	11.9	805	68	5.55	1740	810	0.797	87	11.8	2.15
7		2	2.76	11.3	1030	65	4.11	2840	735	0.929	97	15.8	3.87
8		2	2.44	11.3	909	65	4.64	2220	735	0.887	92	14.0	3.02
9		2	2.11	11.5	815	66	5.43	1740	759	0.827	85	12.3	2.29
10		3	2.60	11.3	834	45	4.34	2170	509	0.986	102	18.5	4.27
12		4	2.59	12.8	1350	72	4.92	3500	922	0.912	108	18.8	3.80
13		4	2.80	11.3	1505	63	4.03	4220	712	0.980	104	23.9	5.93
14		4	2.11	12.0	1212	67	5.67	2560	804	0.900	98	18.1	3.18
15		3	2.51	12.8	930	58	5.09	2340	742	1.013	111	16.0	3.15
16		3	2.58	12.8	966	55	4.97	2490	704	0.957	110	17.6	3.54
17		3	2.55	12.7	949	54	4.96	2420	686	0.947	111	17.6	3.53
18		5	2.56	12.4	1499	47	4.82	3837	583	0.923	106	31.9	6.58
19		5	2.38	12.3	1432	46	5.17	3408	566	0.911	103	31.1	6.02
20		5	2.23	12.8	1331	48	5.73	2968	614	0.898	104	27.7	4.83
21		6	2.23	11.9	1420	43	5.35	3170	519	0.944	103	33.1	6.10
22		6	2.32	12.4	1425	45	5.36	3290	561	0.938	107	31.6	5.87
23		6	2.92	12.1	1750	44	4.10	5090	480	0.981	111	39.8	10.6
24		6	2.20	12.6	1365	46	5.73	3000	534	0.941	107	29.7	5.63
25		6	2.45	12.3	1530	44	5.02	3750	540	0.957	106	34.8	6.96
26		6	2.31	12.1	1490	43	5.25	3440	522	0.948	103	34.6	6.59
27	Propane	7	2.74	11.7	944	53	4.27	2580	615	0.966	105	18.1	4.22
28		7	2.95	11.8	980	53	4.00	2890	626	0.982	108	18.5	4.52
29		7	2.73	11.9	949	54	4.36	2590	637	0.952	105	17.7	4.07
30		7	2.57	12.0	910	54	4.68	2340	646	0.936	103	16.9	3.63
31		7	2.46	12.3	880	55	5.02	2165	680	0.939	103	15.9	3.19
32		7	2.57	11.9	922	54	4.65	2365	637	0.936	102	17.3	3.72
33	Pentane Blend	7	3.48	11.5	882	52	3.32	3070	595	0.916	101	17.0	5.16
34		7	3.83	11.7	935	53	3.05	3580	615	0.912	104	17.7	5.82
35		7	3.05	12.1	763	54	3.80	2325	655	0.889	101	14.1	3.55
36		7	3.08	12.3	765	55	4.00	2360	680	0.889	102	13.9	3.48
37		7	2.97	13.2	711	59	4.44	2110	780	0.881	106	12.1	2.70
38	Butene-1	7	4.49	12.3	1125	56	2.73	5050	690	0.971	119	20.0	7.32
39		7	4.83	11.8	1260	53	2.45	6080	625	0.948	115	23.8	9.74
40		7	3.88	12.3	1010	56	3.18	3880	689	0.964	115	18.1	5.63
41		7	3.78	12.7	979	58	3.38	3710	736	0.956	116	16.9	5.03
42		7	4.34	12.3	1115	55	2.82	4850	675	0.966	117	20.3	7.18
43		7	3.57	13.1	895	59	3.67	3190	772	0.969	120	15.2	4.14

[1] See Table XIV

Figure 28
Flox-Methane Uncooled Test Results (Characteristic Velocity Efficiency vs Mixture Ratio)

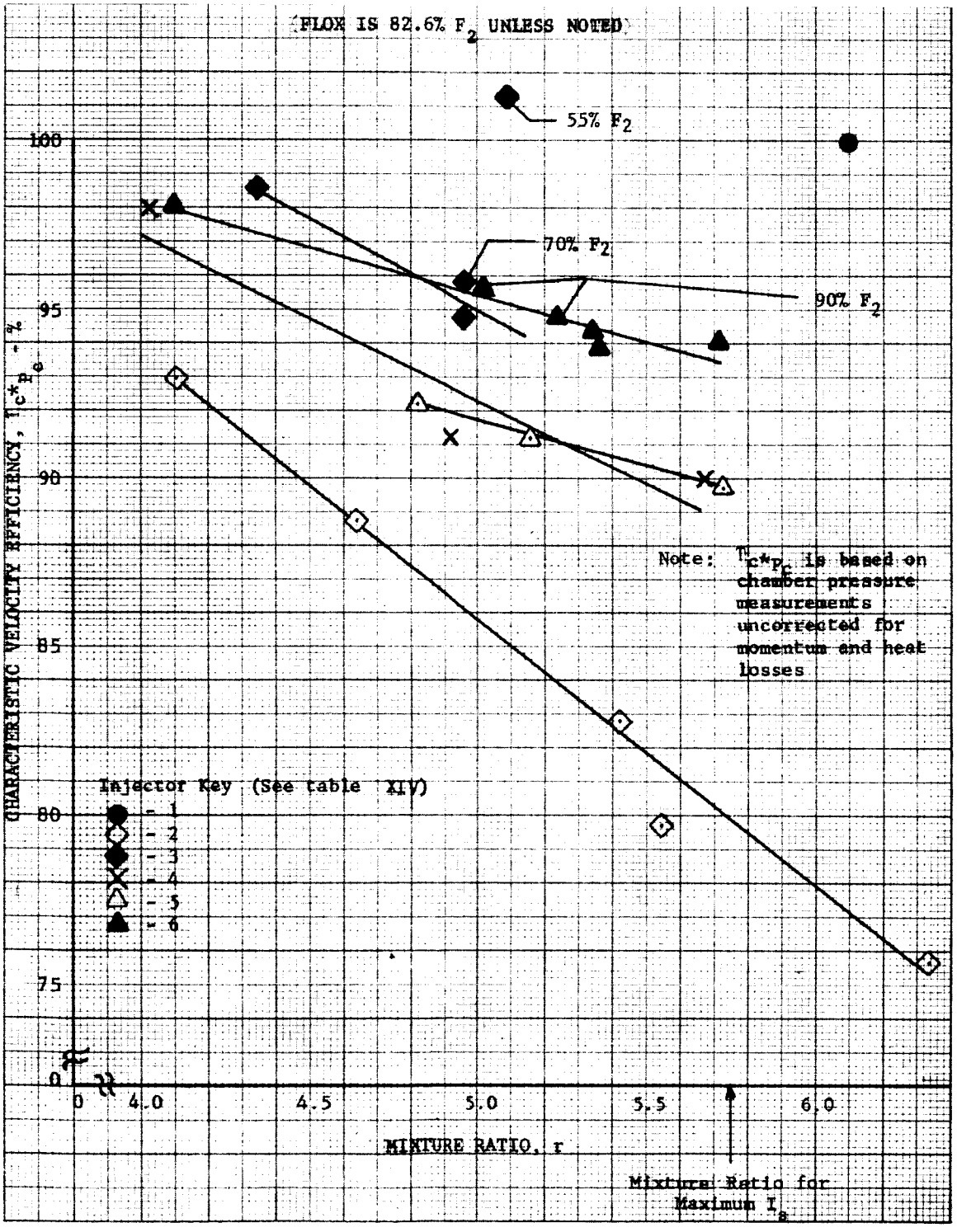

DF 38416A
Sheet 1 of 3

Characteristic velocity efficiency has been plotted as a function of mixture ratio, velocity ratio, and momentum ratio for methane (figures 28 through 30), propane (figures 31 through 33), the pentane blend (figures 34 through 36), and butene-1 (figures 37 through 39). The propane and pentane blend curves also present data from the regeneratively cooled tests. It can be seen from these figures that for a given injector a satisfactory linear correlation was obtained between characteristic velocity efficiency and any of the other three parameters.

From the tests completed prior to test No. 18, three conclusions were drawn regarding injector performance.

1. Increasing the fuel and oxidizer velocity did not improve the injector efficiency unless a substantial increase in fuel-oxidizer velocity ratio resulted. This was determined comparing the efficiencies and injector velocity ratios from tests No. 10, 12, 13, and 14. (Refer to table XVII.) Surprisingly, it was indicated that for a given velocity ratio a low oxidizer velocity is desirable.
2. A high oxidizer velocity contributed significantly to increased oxidizer spud burning. Swaging the oxidizer spuds appeared to increase spud burning. In the first 17 tests the six spuds in the row closest to the center of the injector were not swaged; none of these unswaged spuds were damaged.
3. The welds around the posts of the oxidizer cavity of the injector were not satisfactory for reliable fluorine service. (This conclusion is based upon the injector failure that occurred during test No. 14.)

On the basis of the above conclusions, injector No. 5 (JX767-1) was modified as follows:

1. The injector backplate was removed and replaced using welds suitable for fluorine service.
2. Oxidizer spuds were not swaged.
3. The number of spuds was reduced by 50% to maintain a reasonable pressure drop through the orifices. (While the backplate was removed, half of the oxidizer spuds were plugged with fluorine compatible welds.)
4. The width of the fuel annulus around each oxidizer spud was reduced to an average value of 0.018 inch. (This was done to provide a fuel-to-oxidizer velocity ratio from 20 to 30 for the flox-methane tests.)

This injector (injector No. 5) was used in tests 18, 19, and 20. Data for these tests in table XVII show that the performance of this injector was not as high as expected; however, the condition of the oxidizer spuds after these high mixture ratio tests proved the structural stability of this design. After test No. 20 the spud flow areas in this injector were modified to increase the velocity ratio by decreasing the oxidizer velocity. The injector (No. 6) was then used for uncooled flox-methane tests No. 21 through 26, and later for transpiration cooled tests. After this latter modification the characteristic velocity efficiency was increased approximately 2%.

Figure 29
Flox-Methane Uncooled Test Results (Characteristic Velocity Efficiency vs Velocity Ratio)

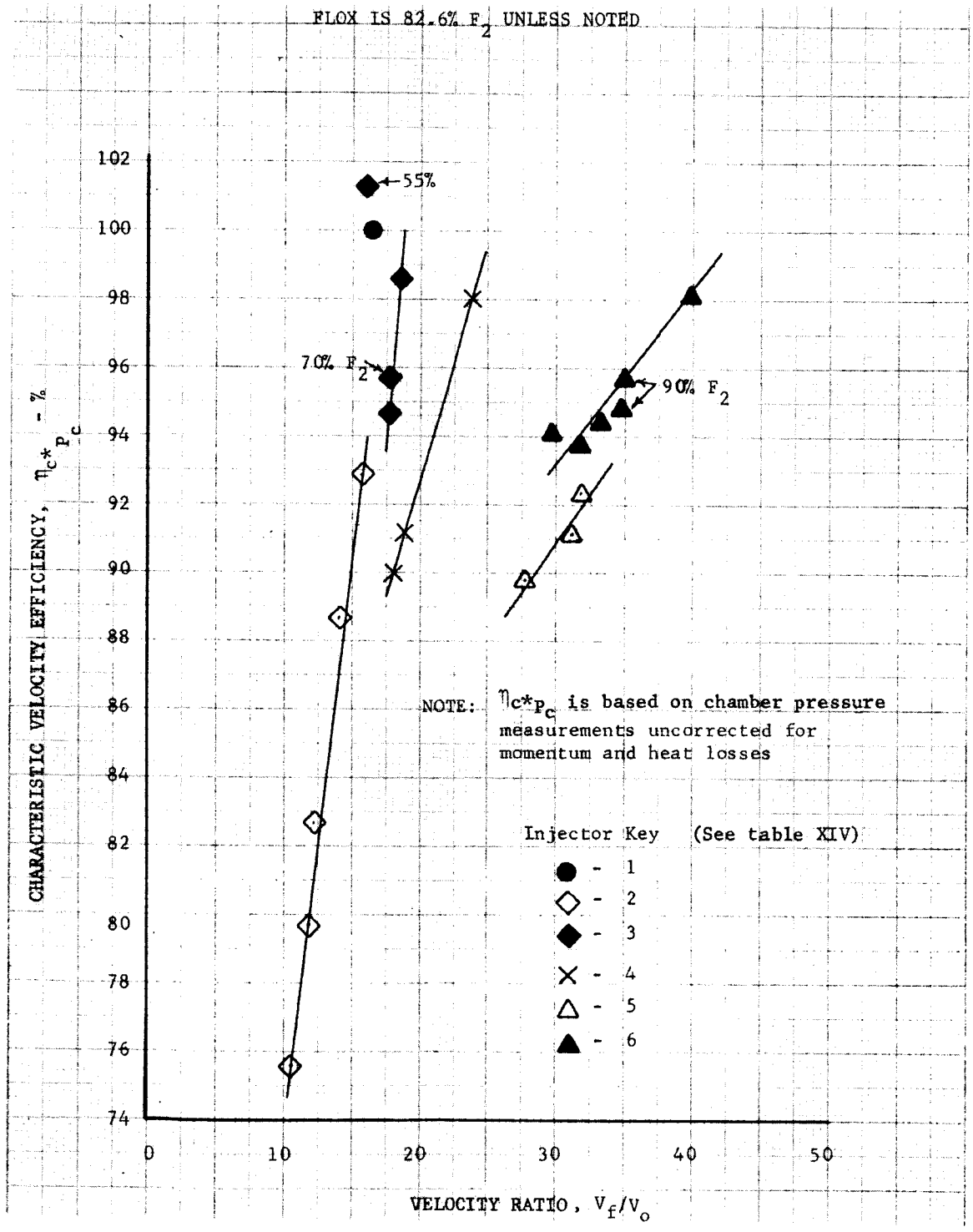

DF 38416A
Sheet 2 of 3

Figure 30

Flox-Methane Uncooled Test Results (Characteristic Velocity Efficiency vs Momentum Ratio)

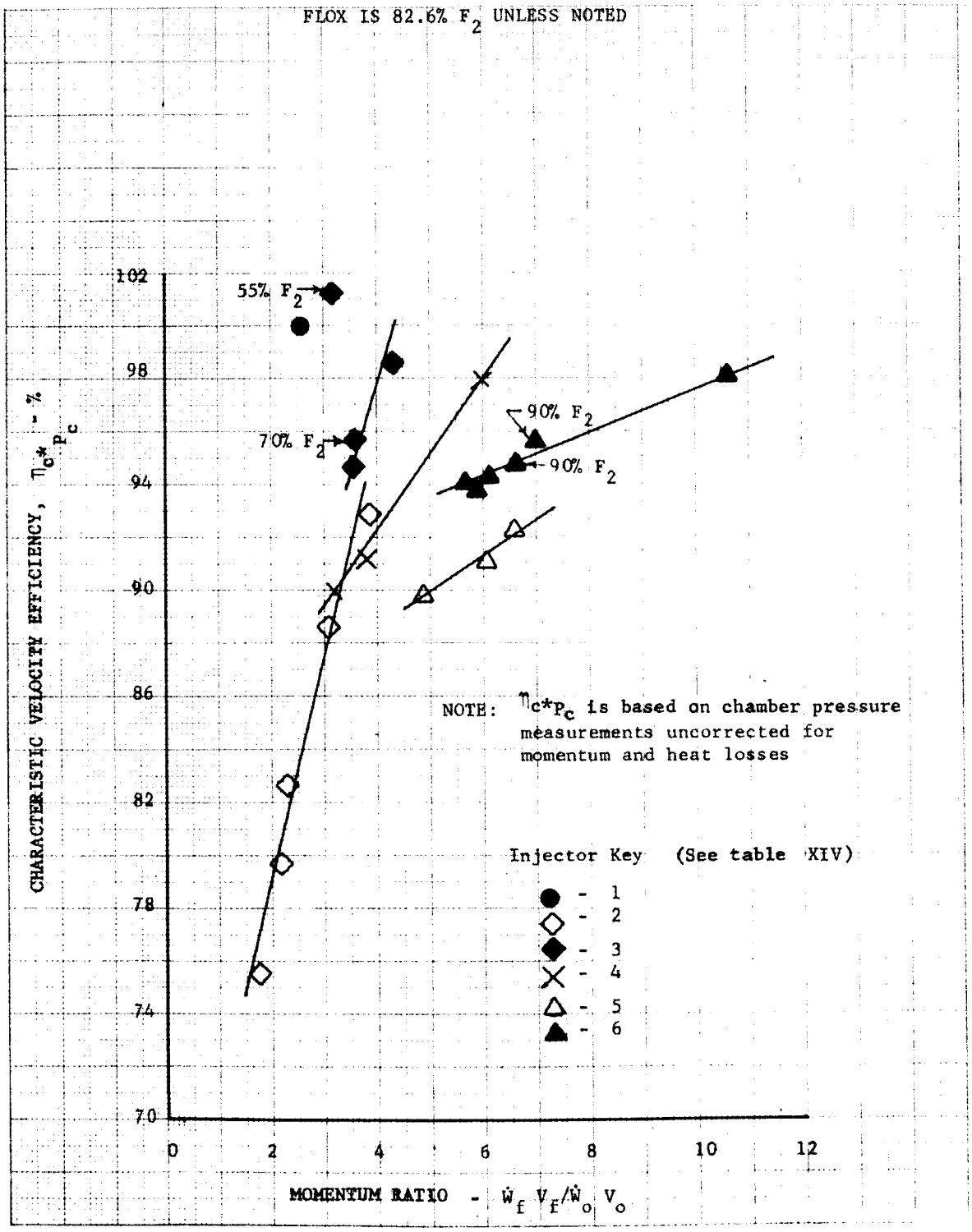

DF 38416A
Sheet 3 of 3

Figure 32
Flox-Propane Test Results (Characteristic Velocity Efficiency vs Velocity Ratio)

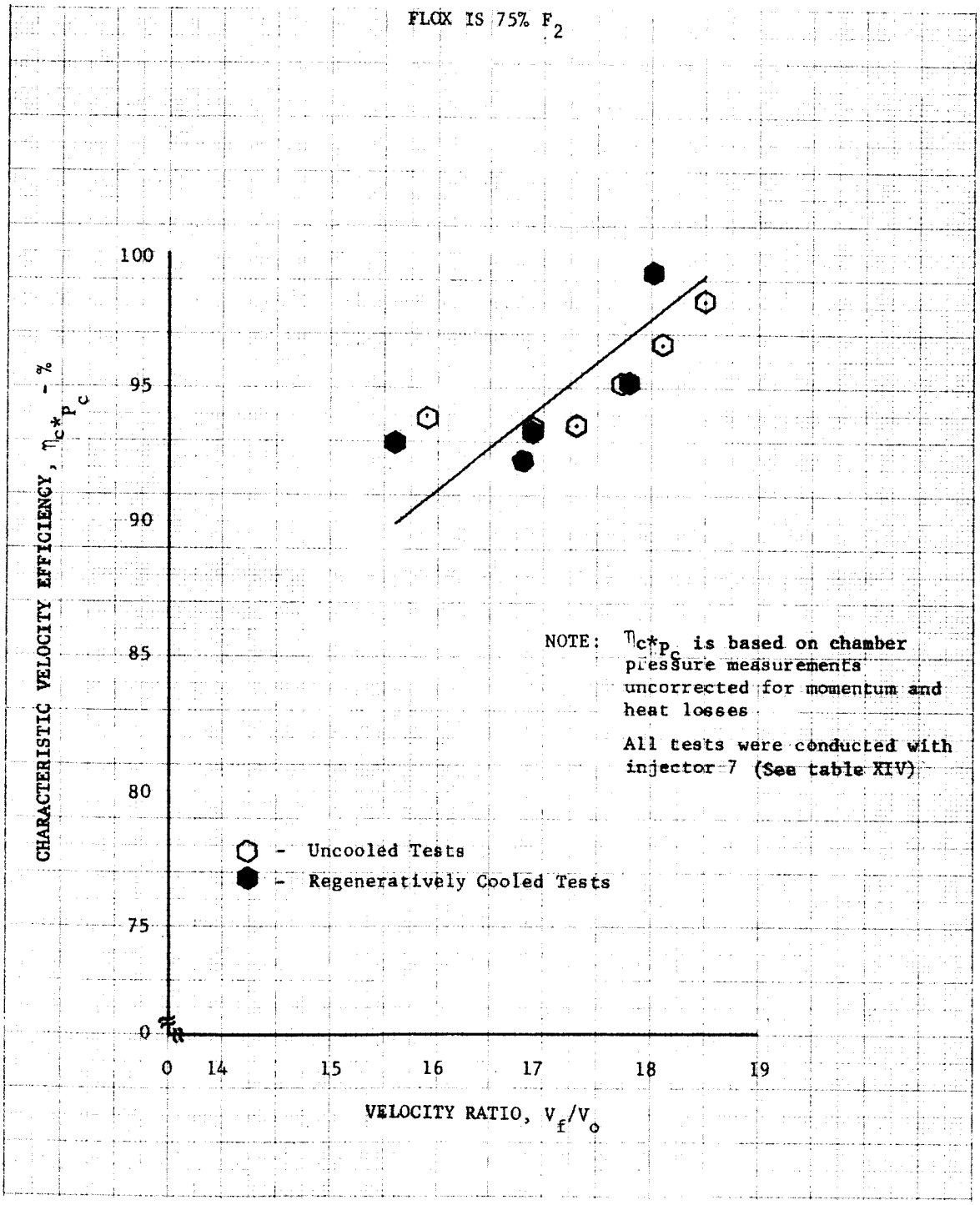

DF 39446
Sheet 2 of 3

Figure 31
Flox-Propane Test Results (Characteristic Velocity Efficiency vs Mixture Ratio)

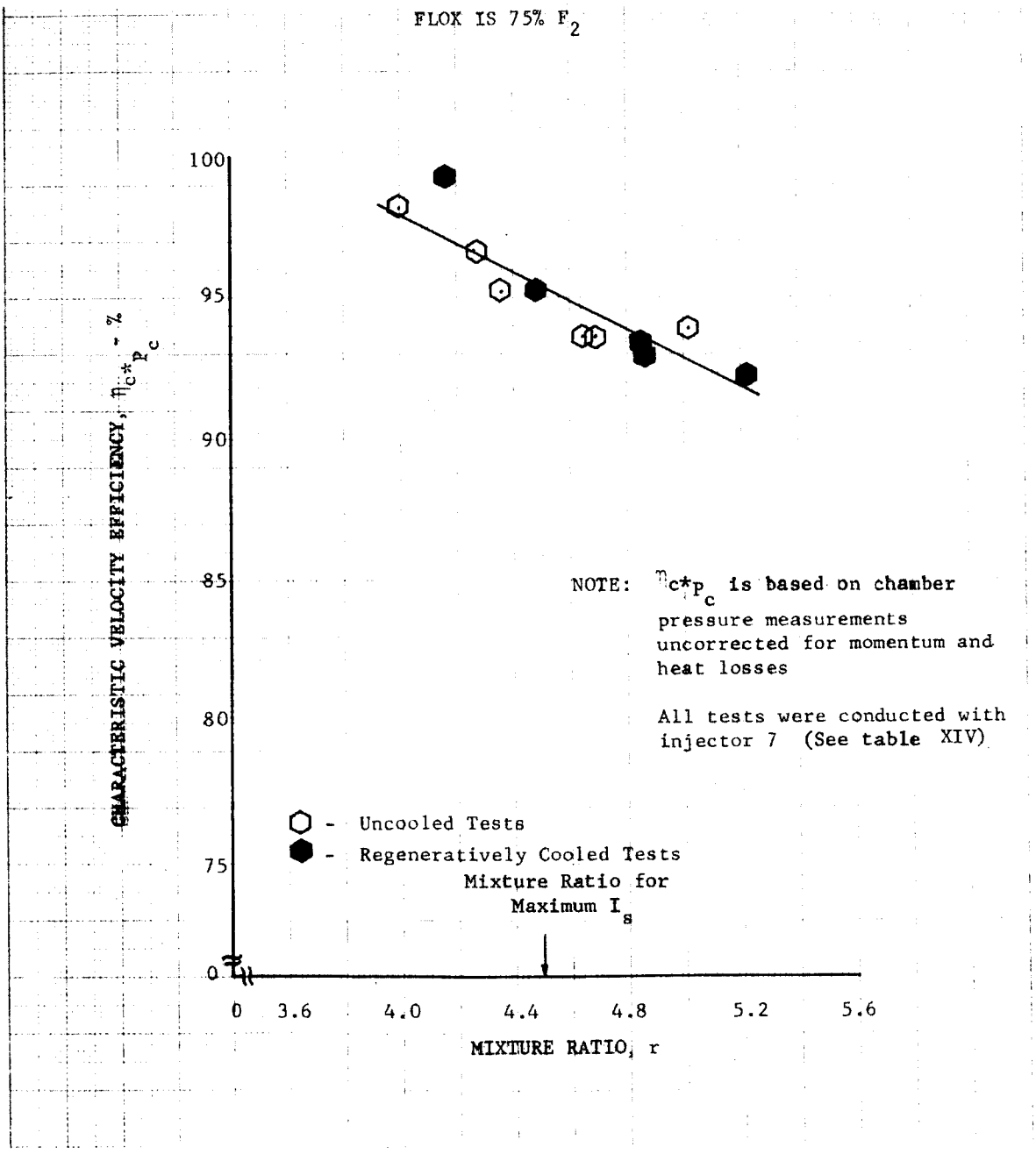

DF 39446
Sheet 1 of 3

Figure 33
Flox-Propane Test Results (Characteristic Velocity Efficiency vs Momentum Ratio)

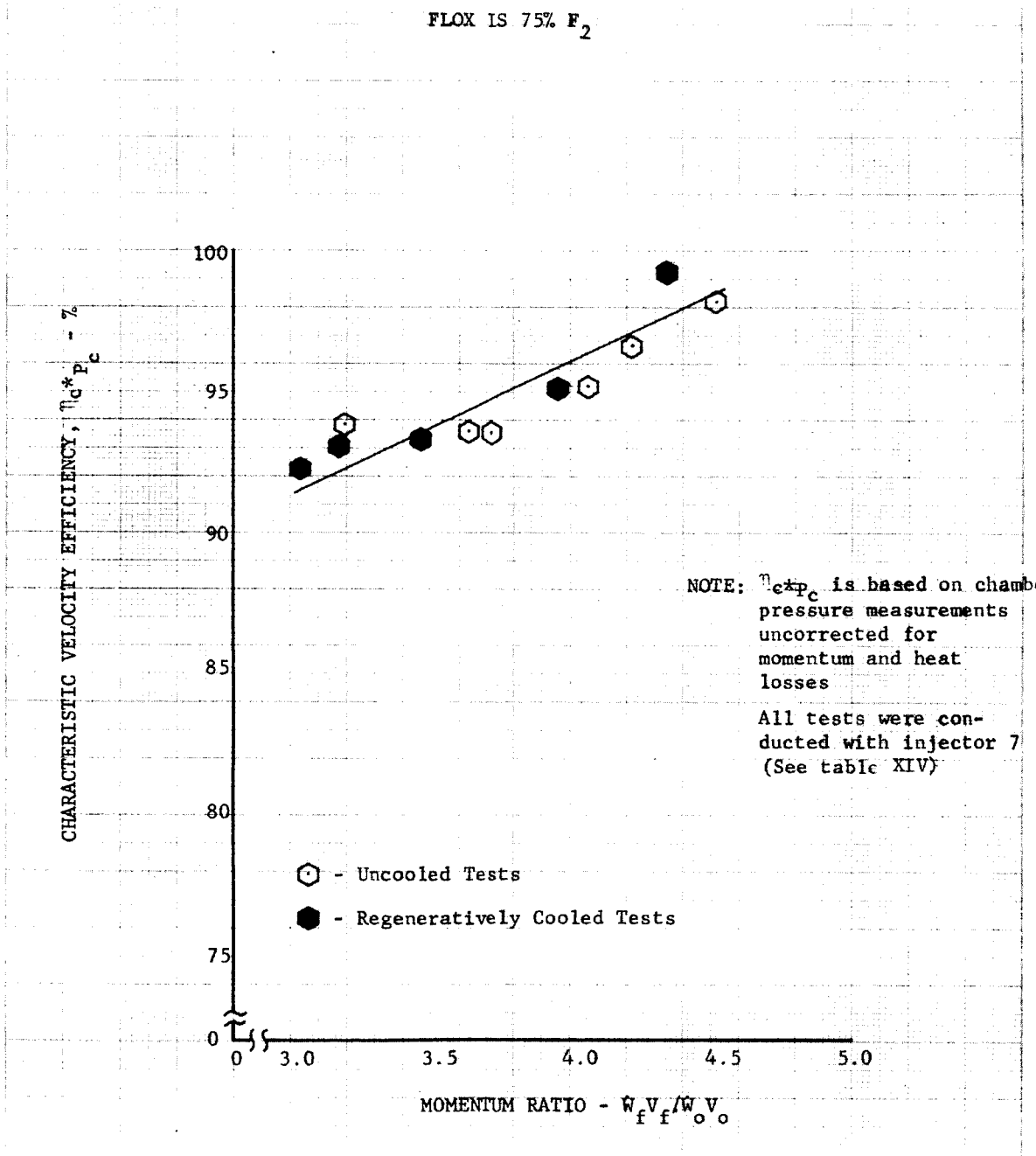

DF 39446
Sheet 3 of 3

Figure 34
Flox-Pentane Blend Test Results (Characteristic Velocity Efficiency vs Mixture Ratio)

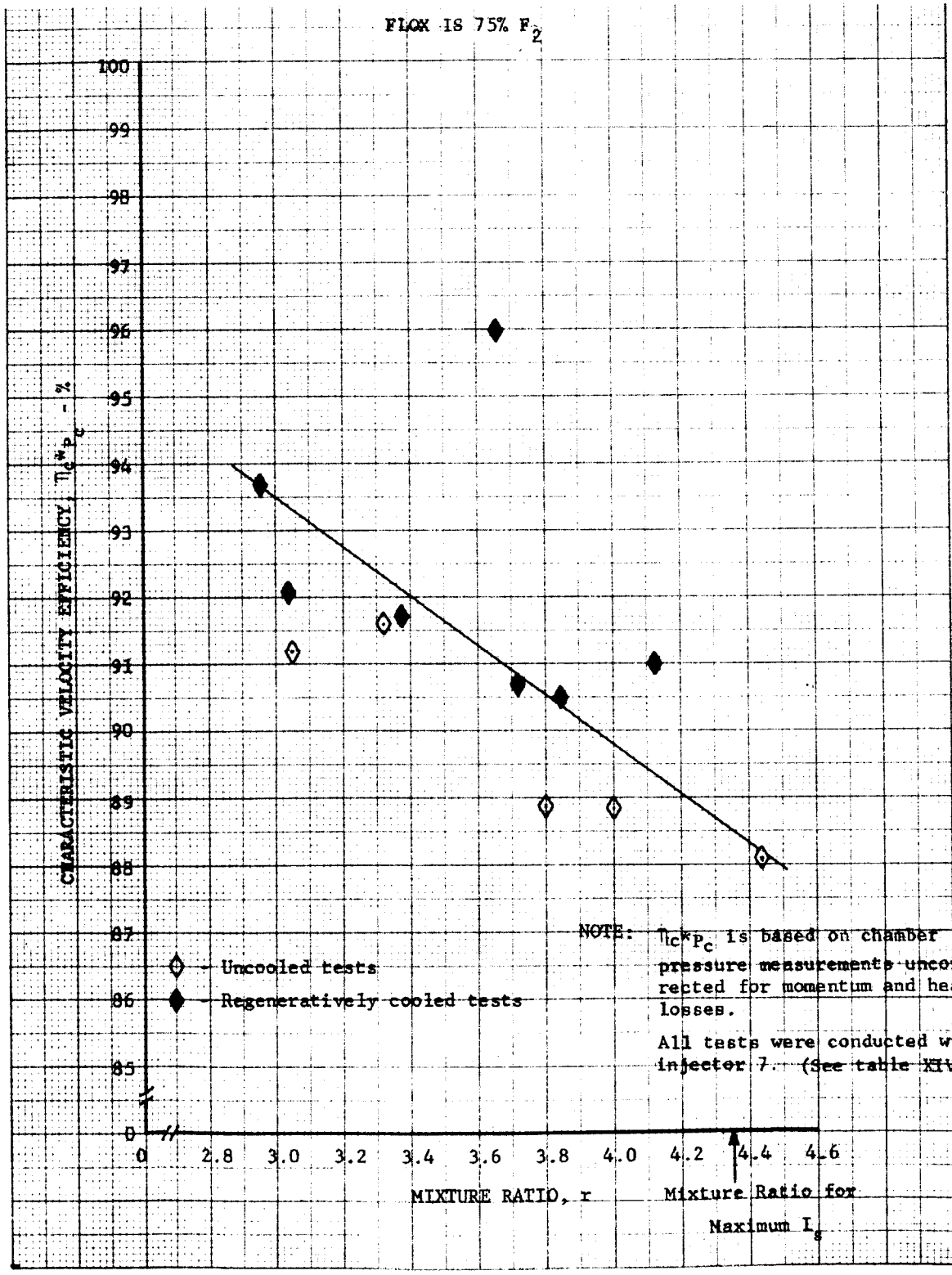

DF 39445
Sheet 1 of 3

Figure 35
Flox-Pentane Blend Test Results (Characteristic Velocity Efficiency vs Velocity Ratio)

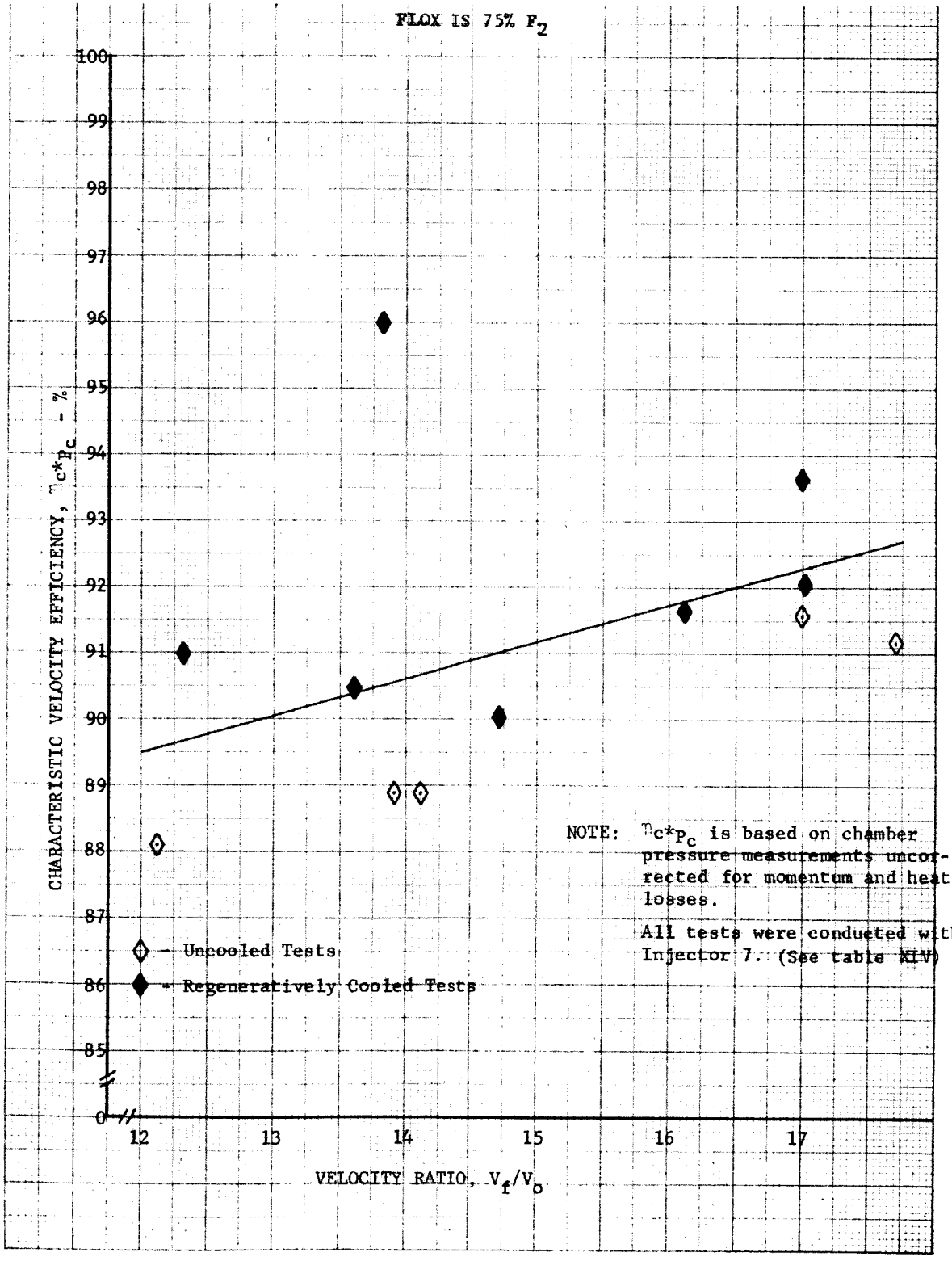

Figure 36
Flox-Pentane Blend Test Results (Characteristic Velocity Efficiency vs Momentum Ratio)

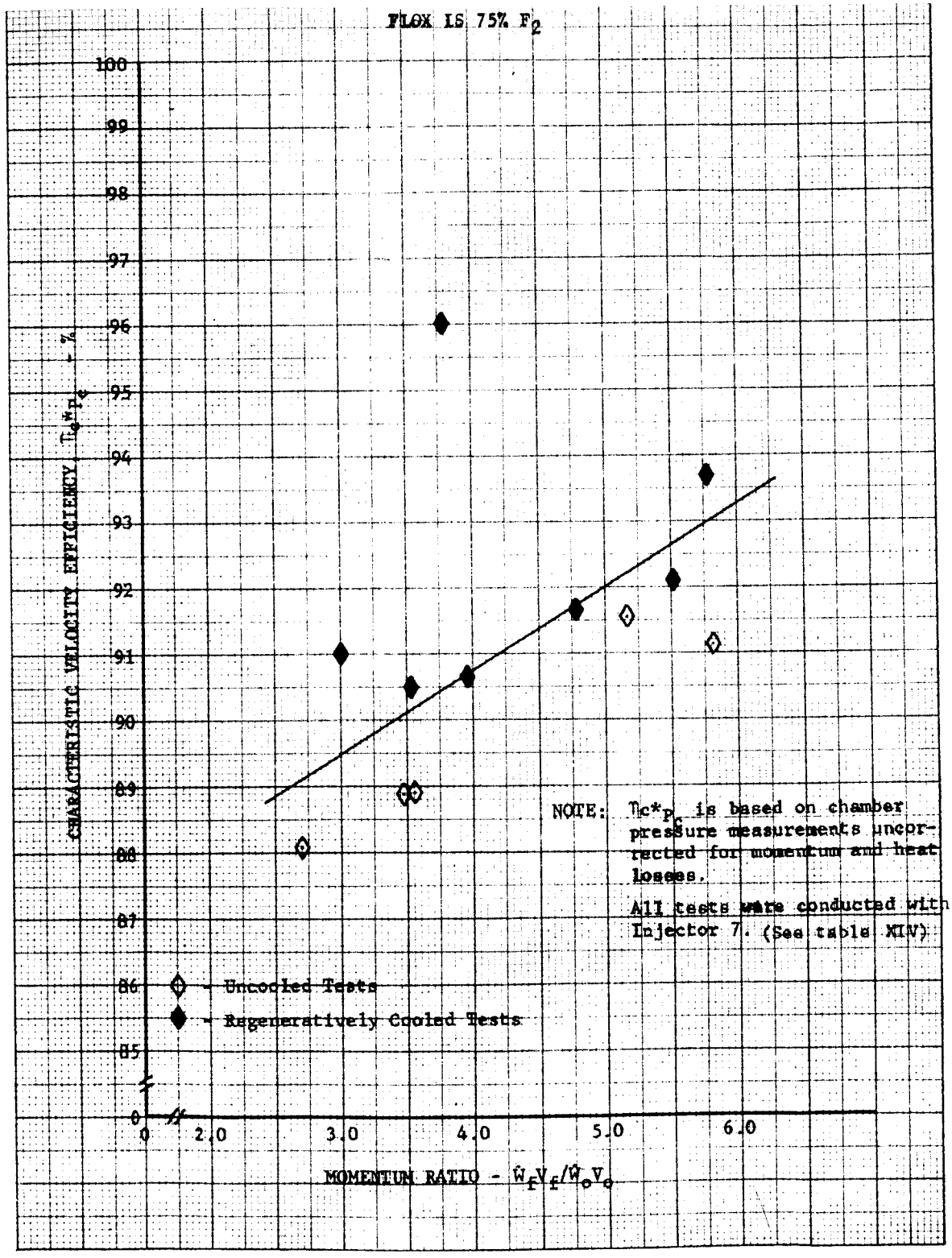

DF 39445
Sheet 3 of 3

Figure 37
Flox-Butene-1 Uncooled Test Results (Characteristic Velocity Efficiency vs Mixture Ratio)

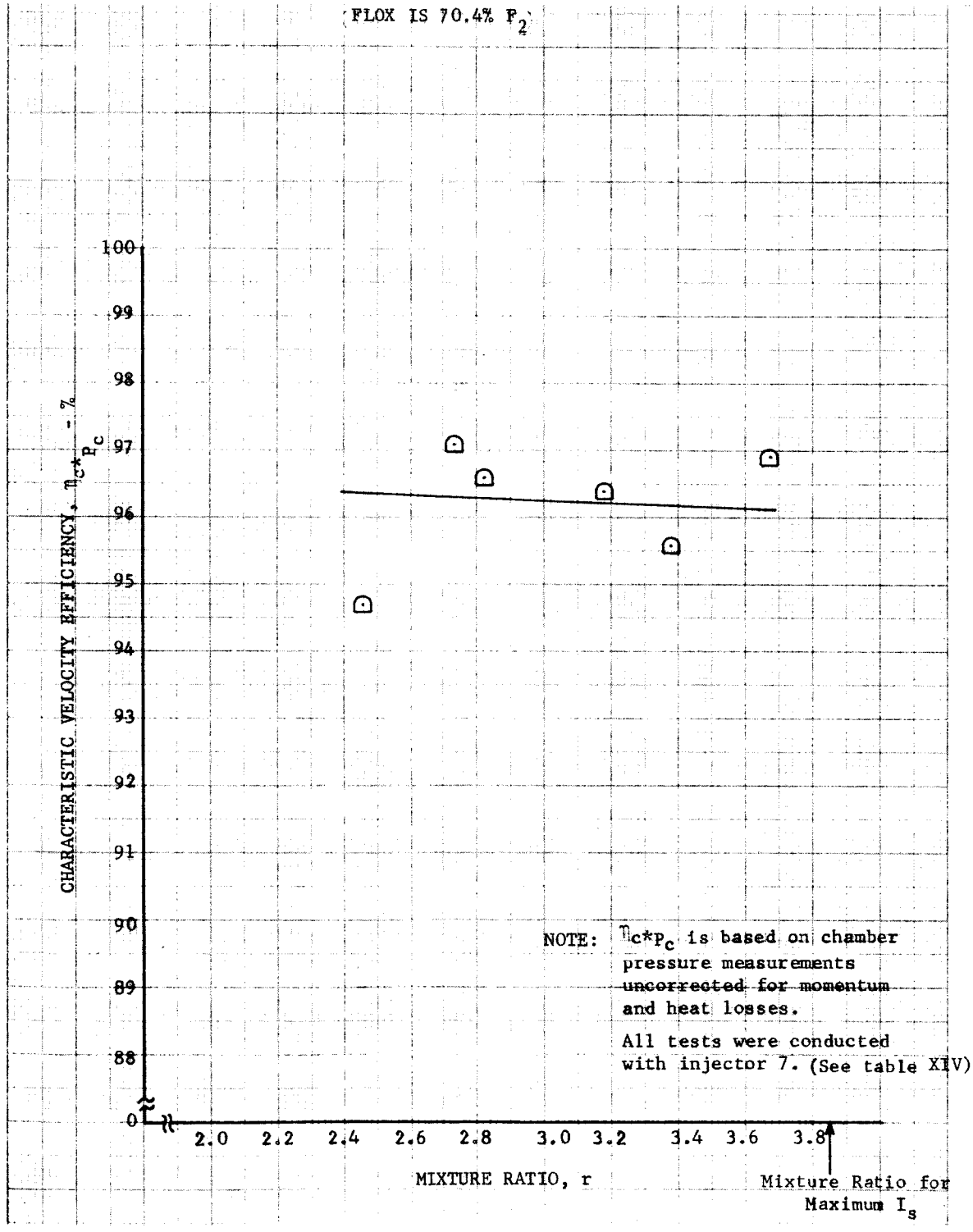

DF 40656
Sheet 1 of 3

Figure 38
Flox-Butene-1 Uncooled Test Results (Characteristic Velocity Efficiency vs Velocity Ratio)

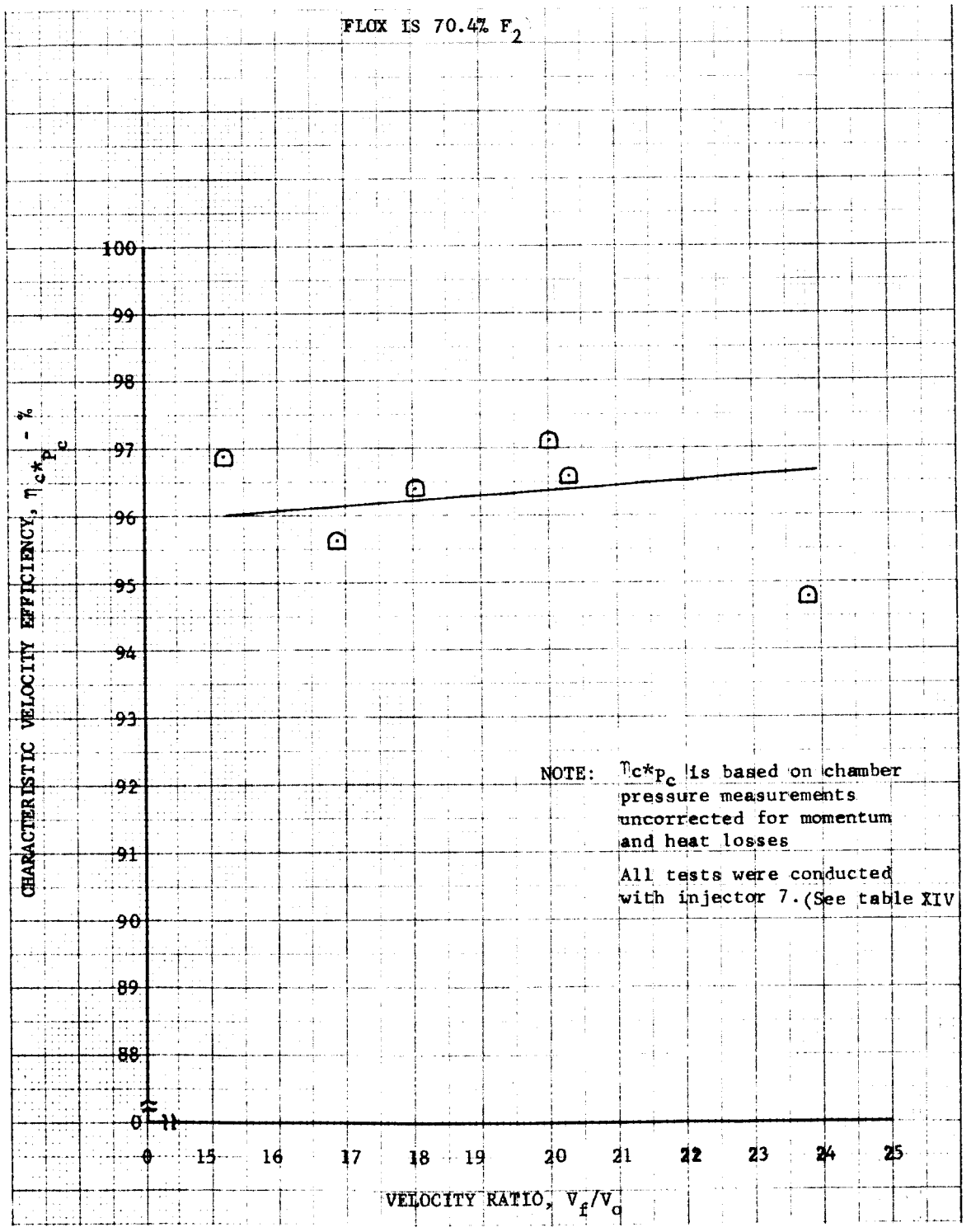

DF 40656
Sheet 2 of 3

Figure 39
Flox-Butene-1 Uncooled Test Results (Characteristic Velocity Efficiency vs Momentum Ratio)

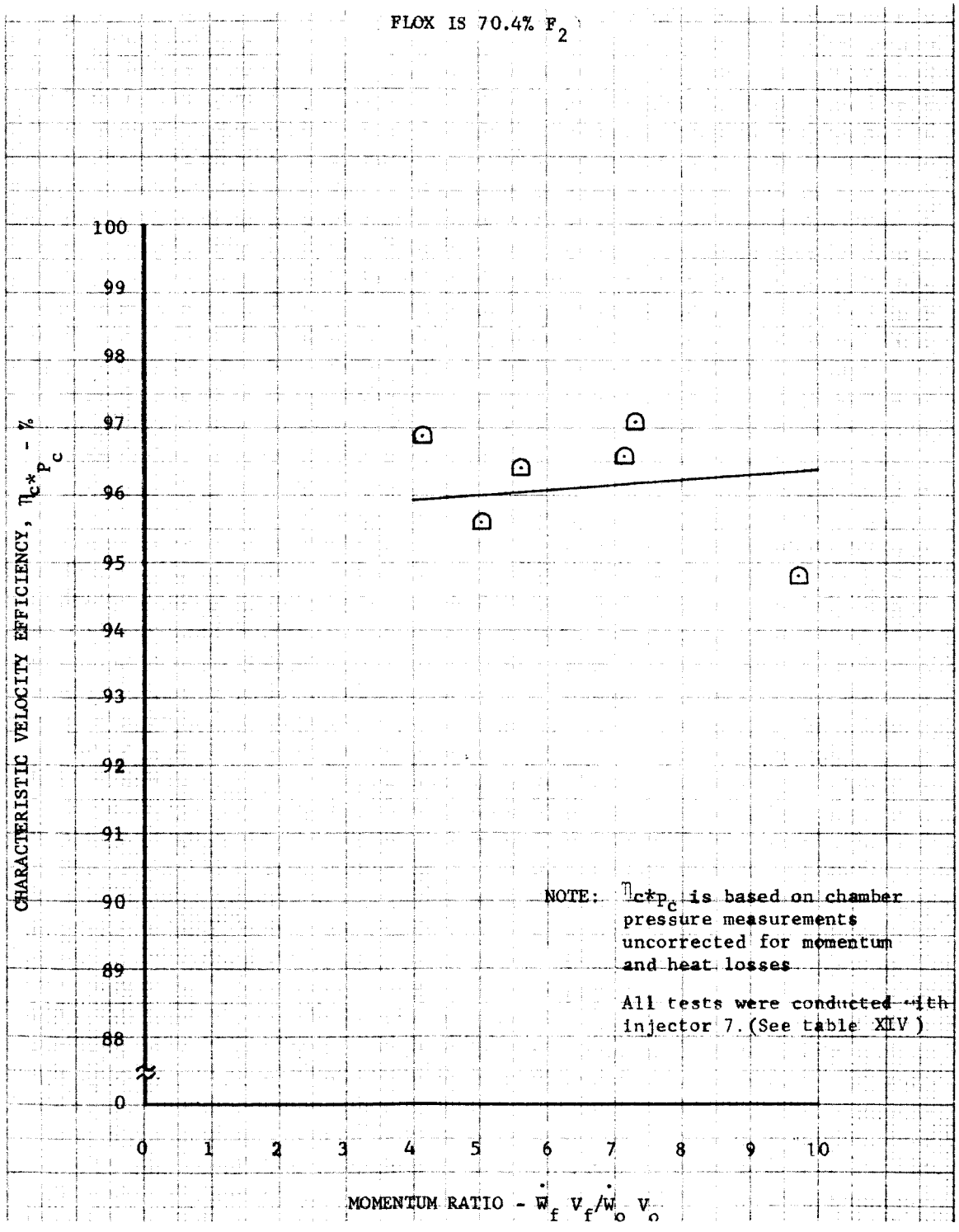

DF 40656
Sheet 3 of 3

D. HEAT TRANSFER

Comparison of experimentally measured heat transfer coefficients with those predicted by the Bartz short form equation (Reference 1) are shown in figures 40 through 61. The origin of the axial coordinate scale on these curves corresponds to the location of the most upstream thermocouple on the nozzle wall; this is approximately 2 inches from the injector face. Film coefficients shown in the figures represent statistical mean values over the duration of the test. The numerical technique used in determining heat transfer coefficients from experimental data is discussed in detail in Reference 2.

The value of the chamber coefficient in tests No. 7 through 16 (see figures 41 through 45) was higher in relation to the throat coefficient than normally expected. This high chamber coefficient can probably be attributed to the use of an RL10A-1 injector in these tests. The high chamber coefficient was not encountered in test No. 2 (figure 40) where an RL10A-3 injector was used. Because the axial velocity of the injected oxidizer streams is higher for the RL10A-1 injector than for the RL10A-3 (which has swirlers in the oxidizer spuds), there is a greater tendency for recirculation of combustion products along the chamber wall resulting in higher chamber heat transfer for the RL10A-1 injector. The uniform pattern of the RL10A-3 injector accounts for the close agreement of experimental with theoretical film coefficients for test No. 2. Test No. 21 through 37 (see figures 46 through 57) were conducted using unswaged RL10A-1 injectors having half the number of elements used in previous tests. This modification apparently removed the cause of the high chamber film coefficients.

In all tests, except 2 and 15, the total heat transferred was significantly lower than that predicted by the Bartz Short Form calculations. This attributed largely to the formation of heavy carbon deposits on the chamber walls; in test No. 15 (55% F_2) (figure 44) there was very little carbon formation and the film coefficients were close to the predicted values, in the propane, pentane blend, and butene-1 tests the carbon formation was heavier than in the methane tests and the heat transfer was correspondingly lower.

The total heat loss per second to the thrust chamber and exhaust nozzle, computed from the experimental data is shown in table XVIII.

Figure 40
Comparison of Heat Transfer Coefficients

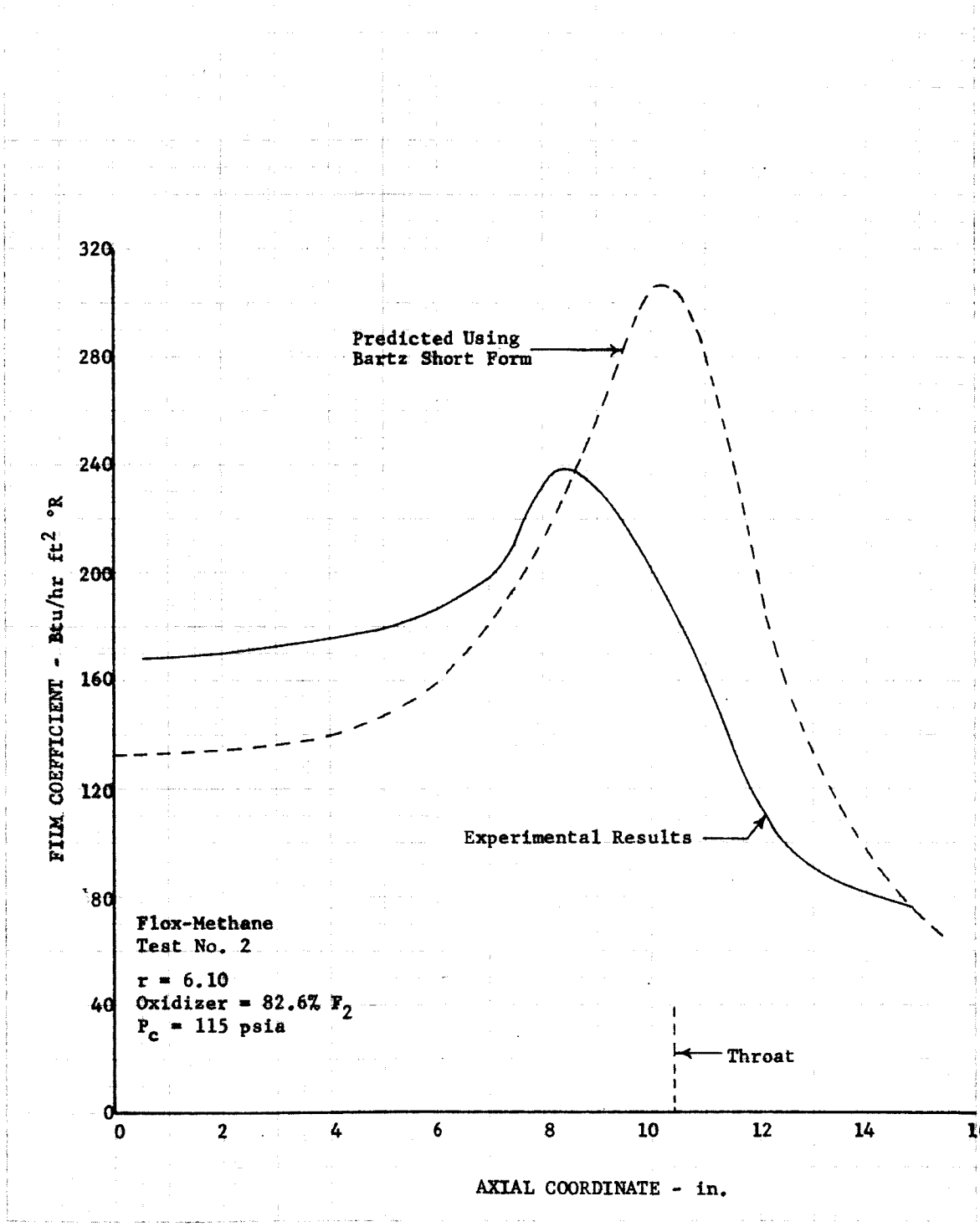

DF 37604

Figure 41
Comparison of Heat Transfer Coefficients

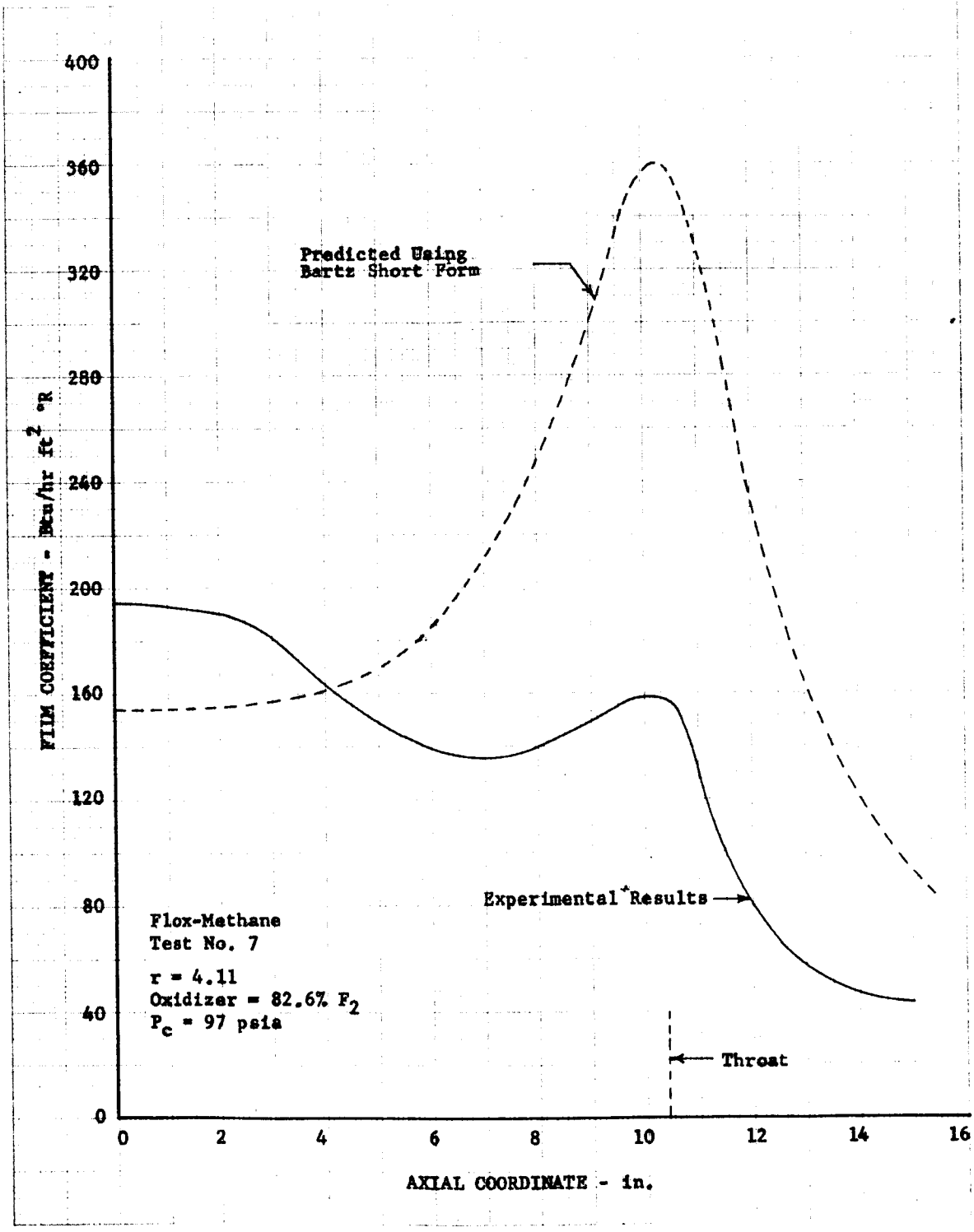

DF 37607

Figure 42
Comparison of Heat Transfer Coefficients

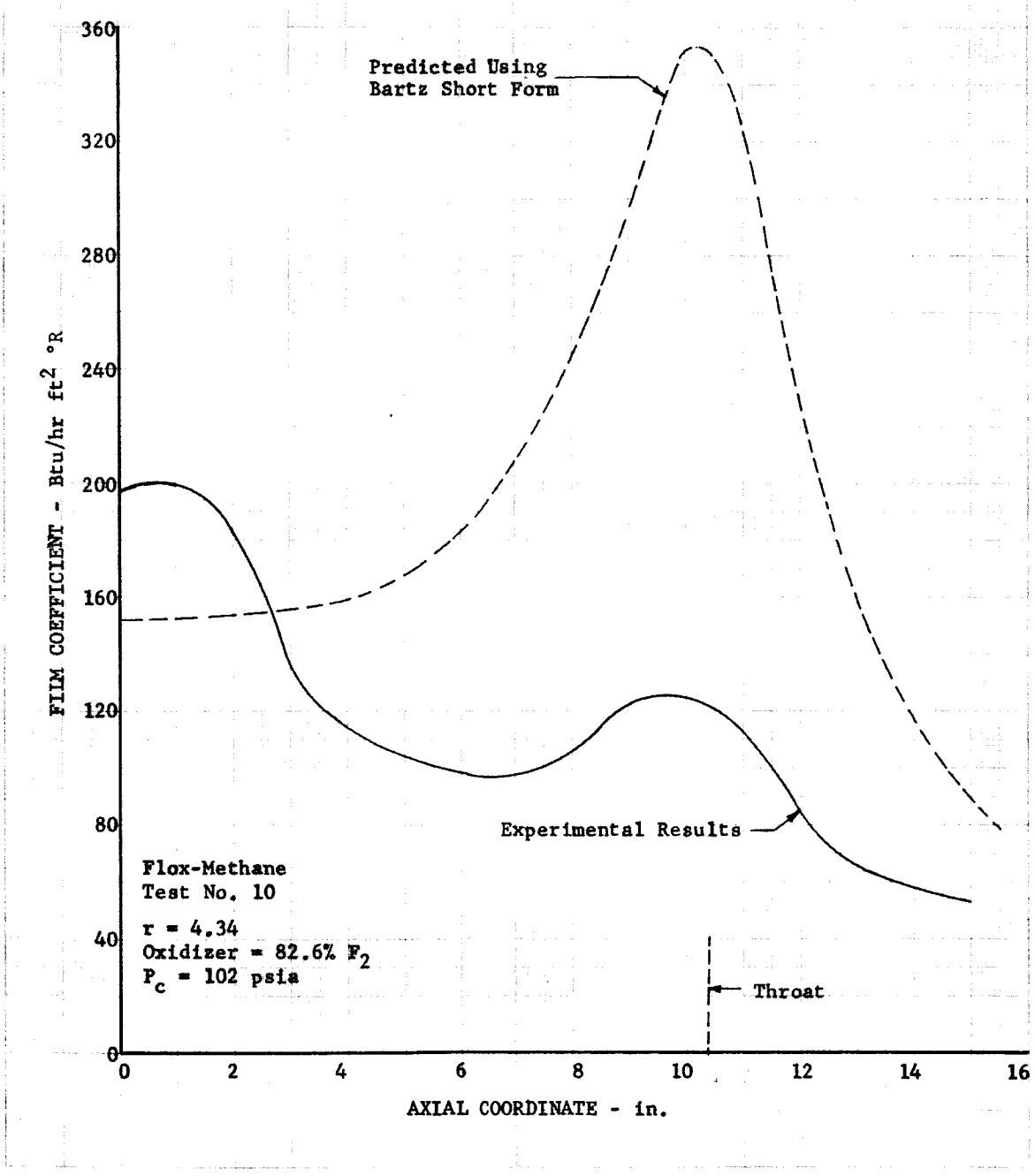

DF 37610

Figure 43
Comparison of Heat Transfer Coefficients

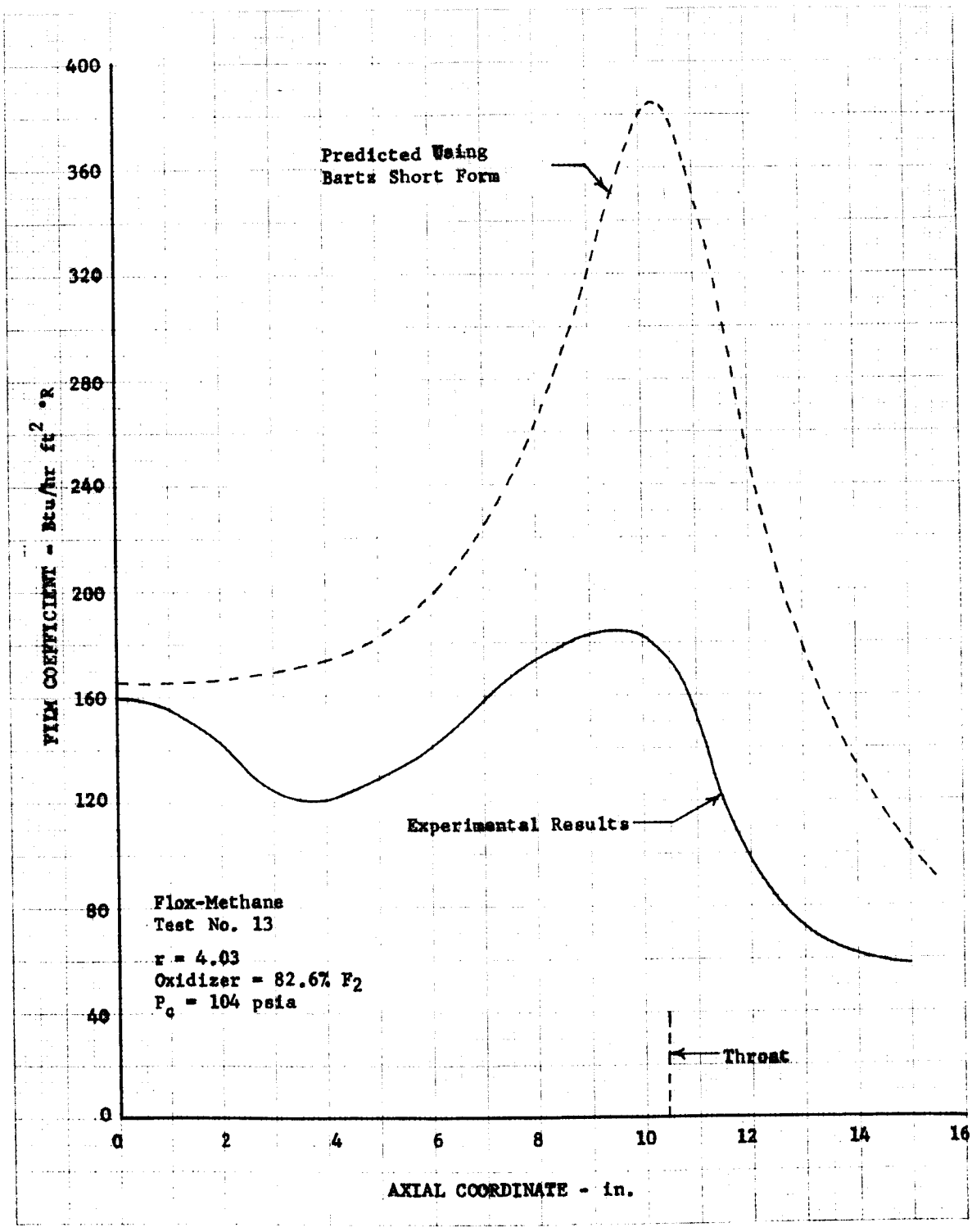

DF 37613

Figure 44
Comparison of Heat Transfer Coefficients

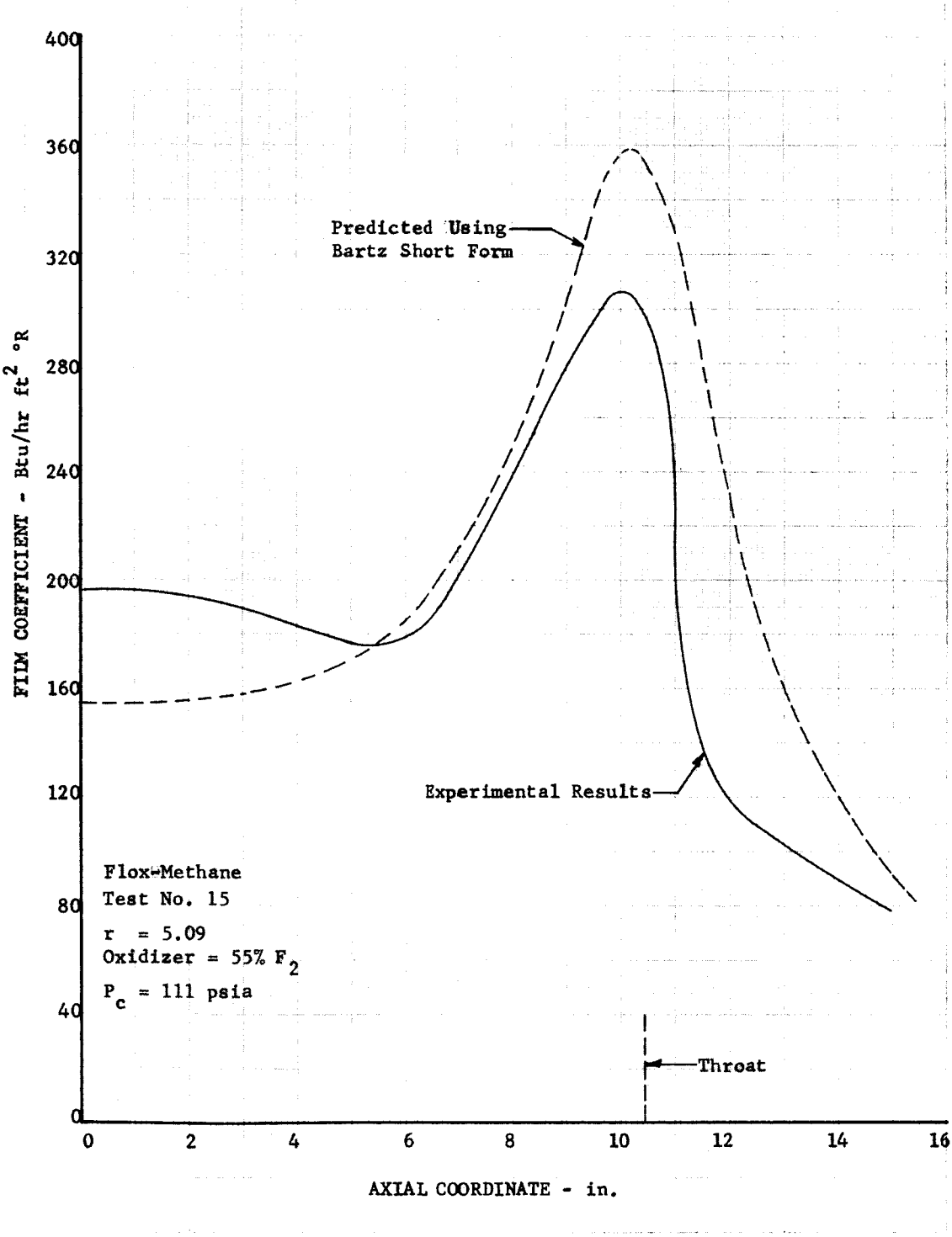

DF 37616

Figure 45
Comparison of Heat Transfer Coefficients

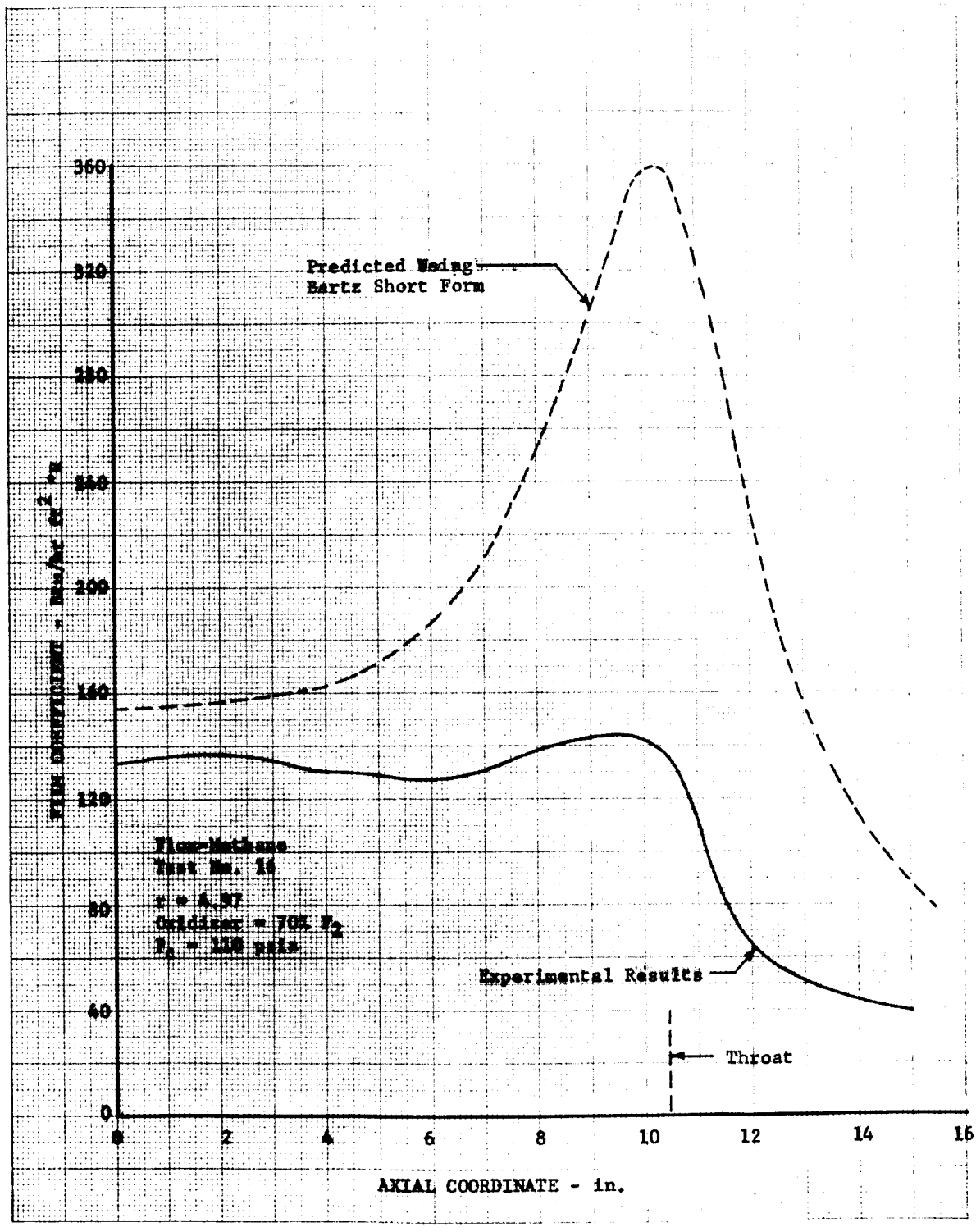

DF 37619

Figure 47
Comparison of Heat Transfer Coefficients

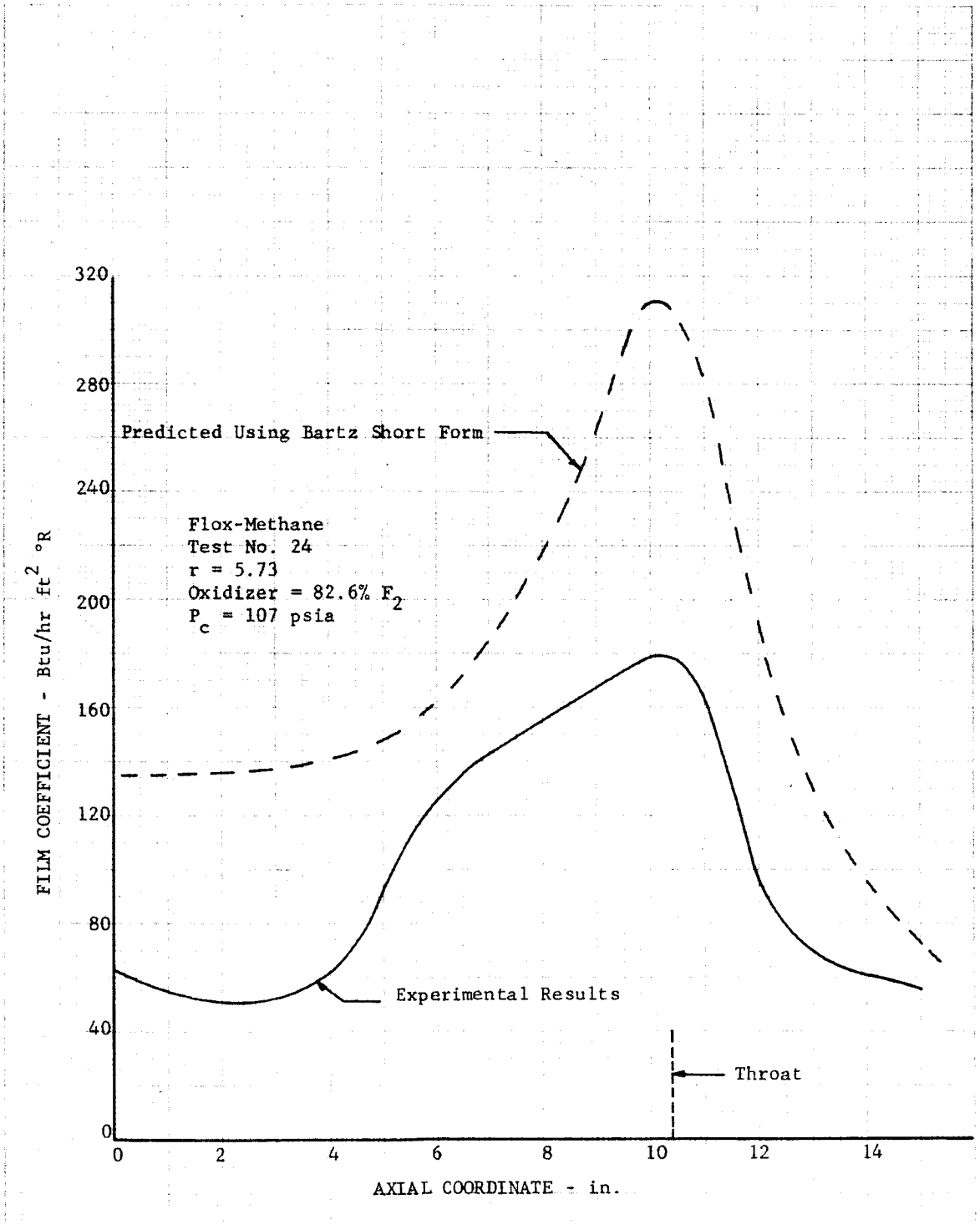

DF 38673

Figure 46
Comparison of Heat Transfer Coefficients

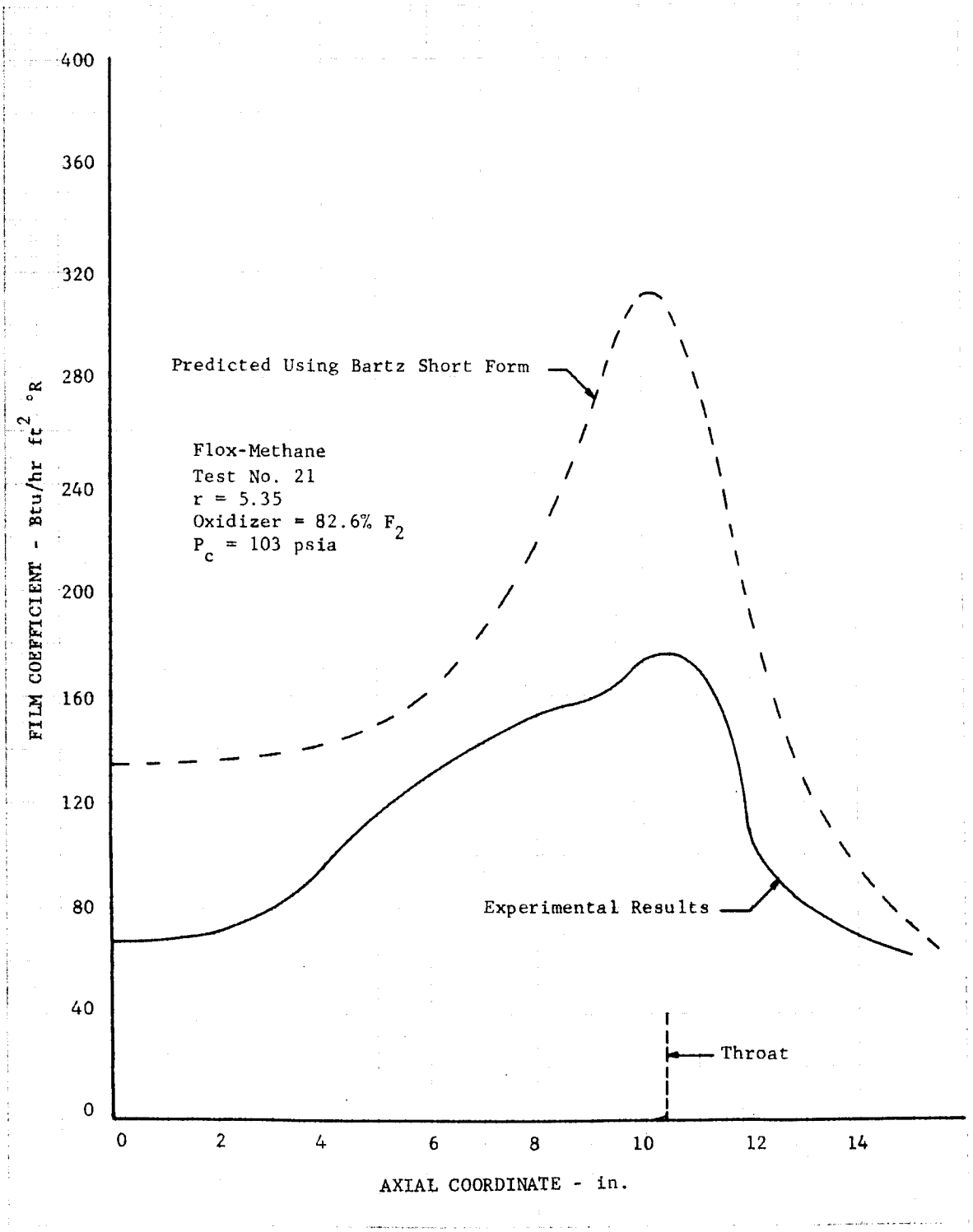

DF 40669

Figure 48
Comparison of Heat Transfer Coefficients

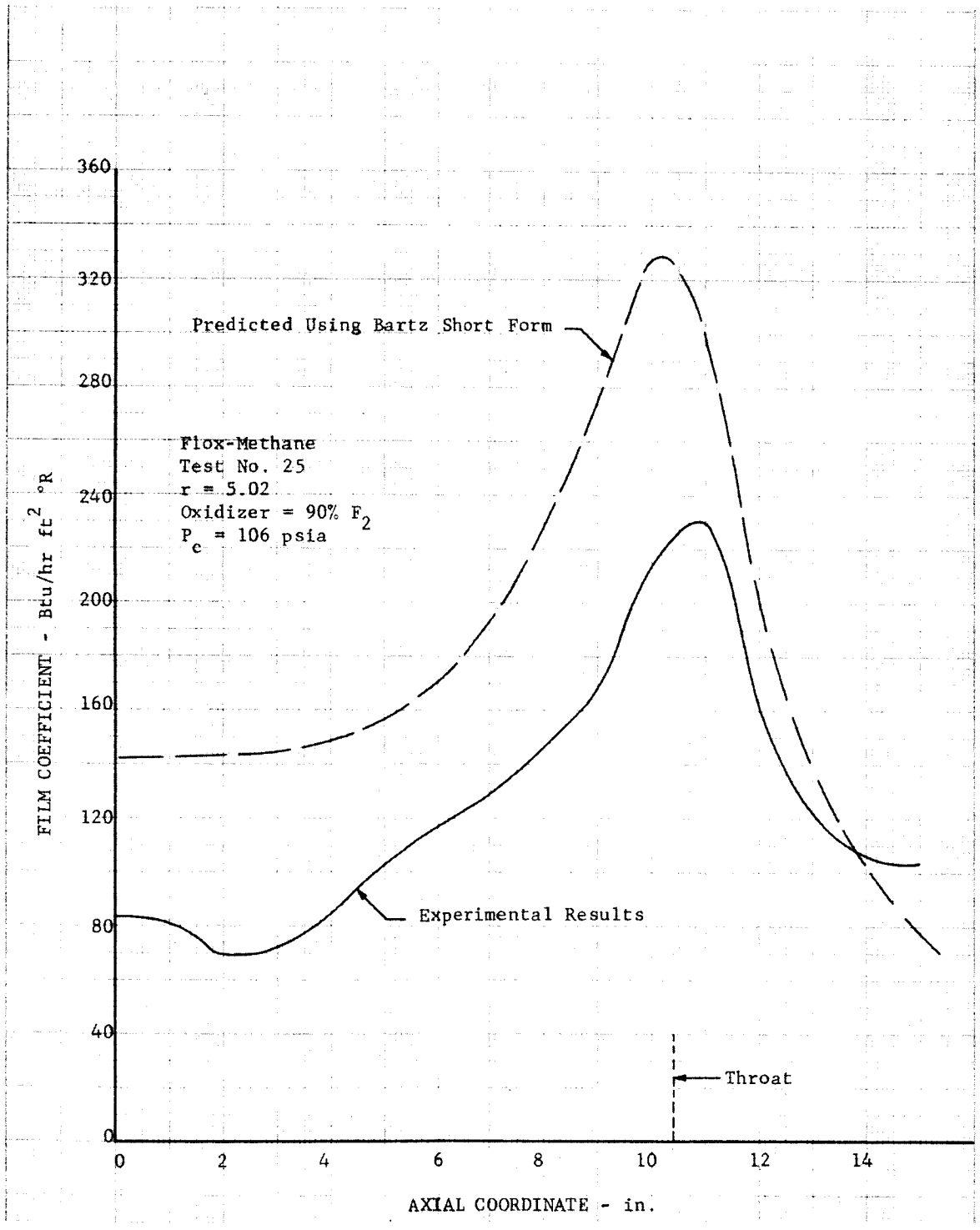

DF 38690

Figure 49
Comparison of Heat Transfer Coefficients

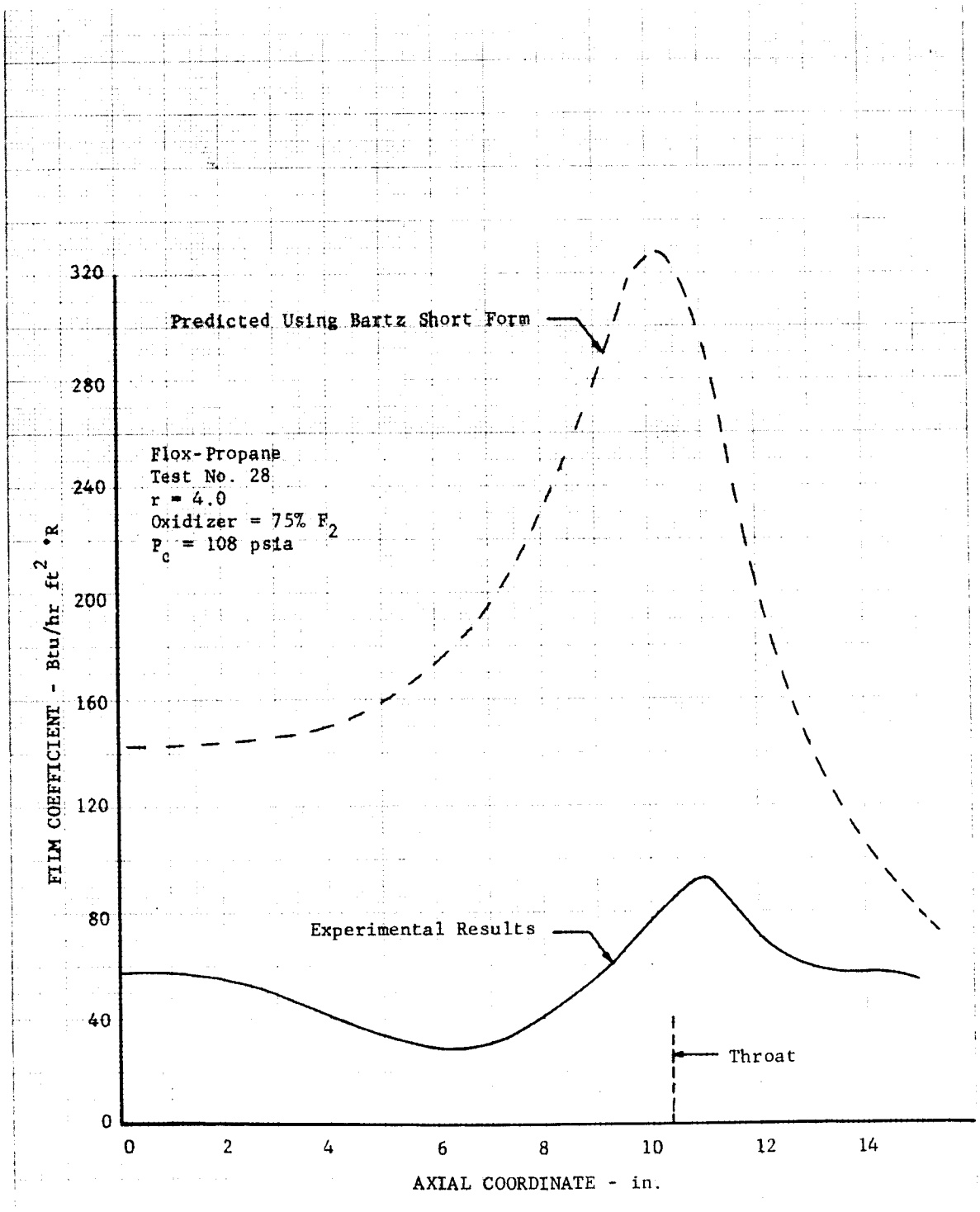

DF 39156

Figure 50
Comparison of Heat Transfer Coefficients

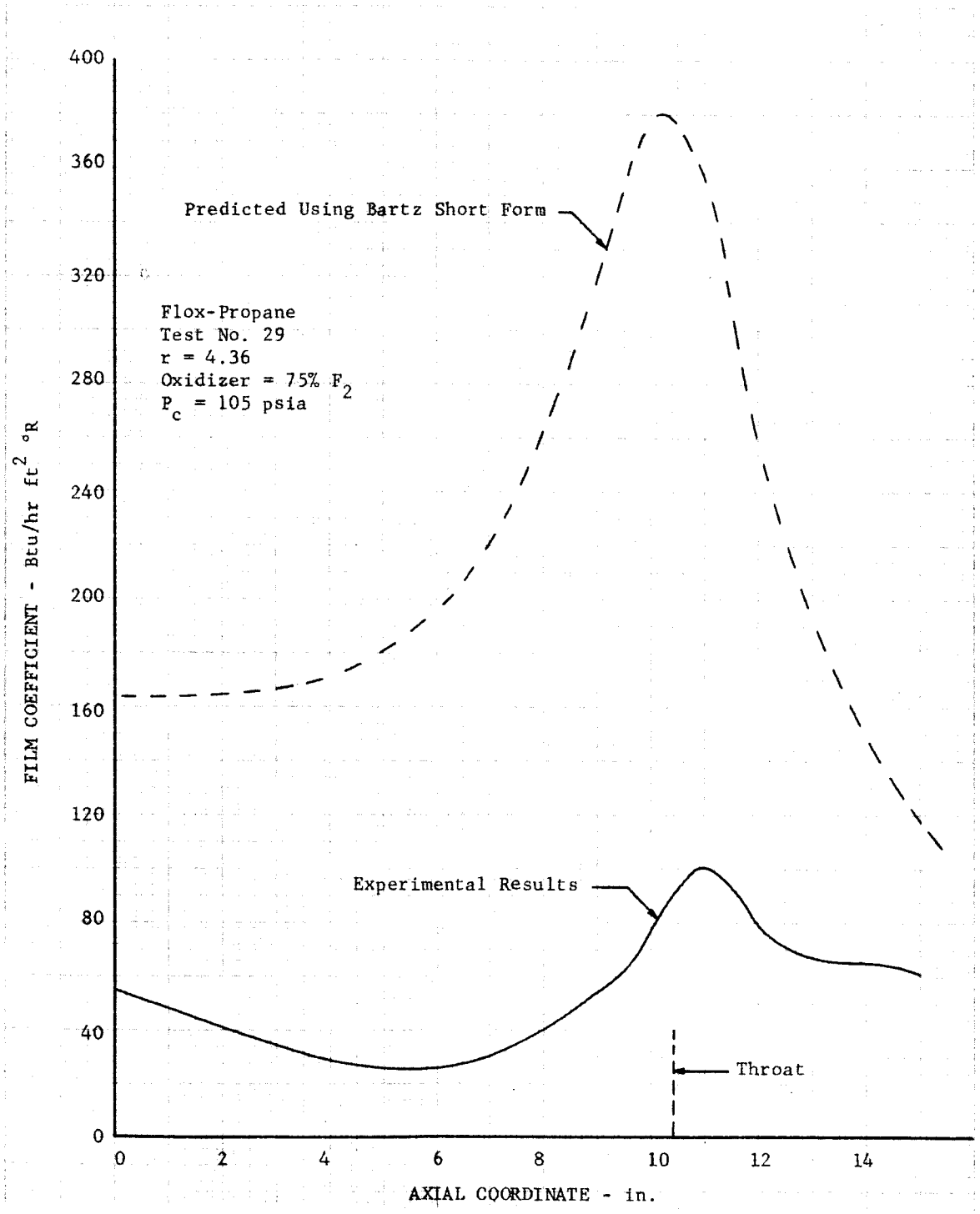

DF 39178

Figure 51
Comparison of Heat Transfer Coefficients

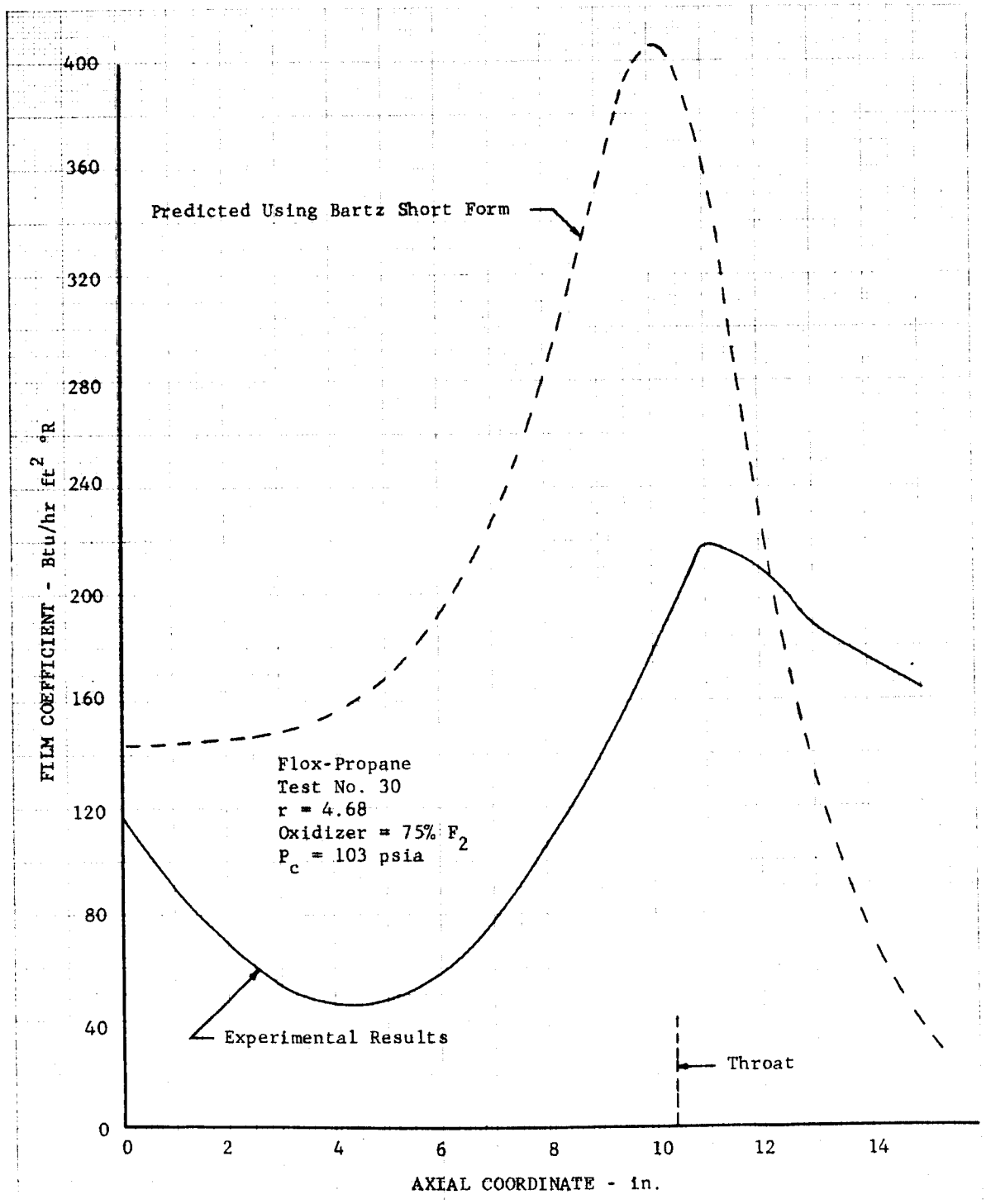

DF 38674

Figure 52
Comparison of Heat Transfer Coefficients

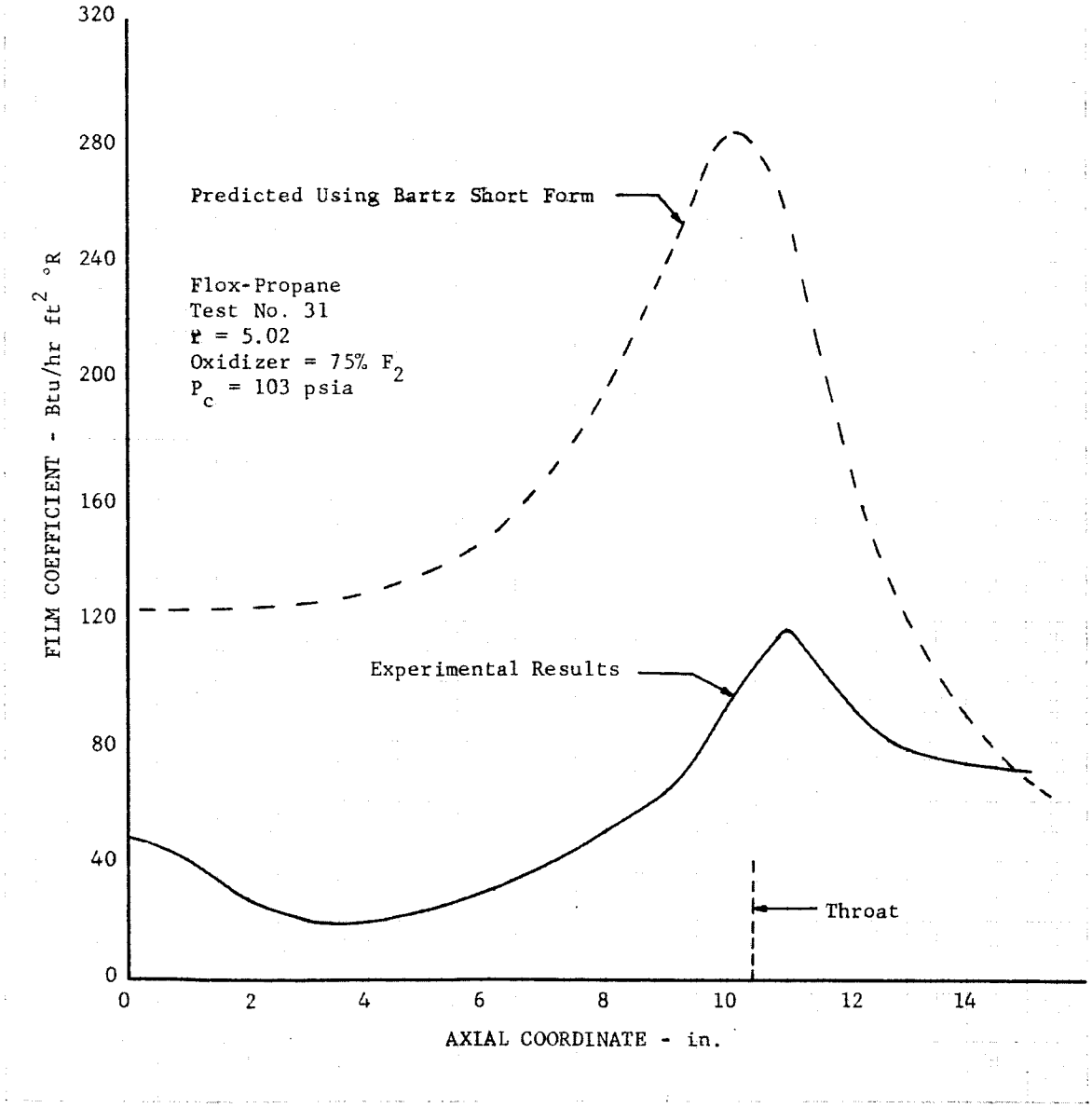

DF 40670

Figure 53
Comparison of Heat Transfer Coefficients

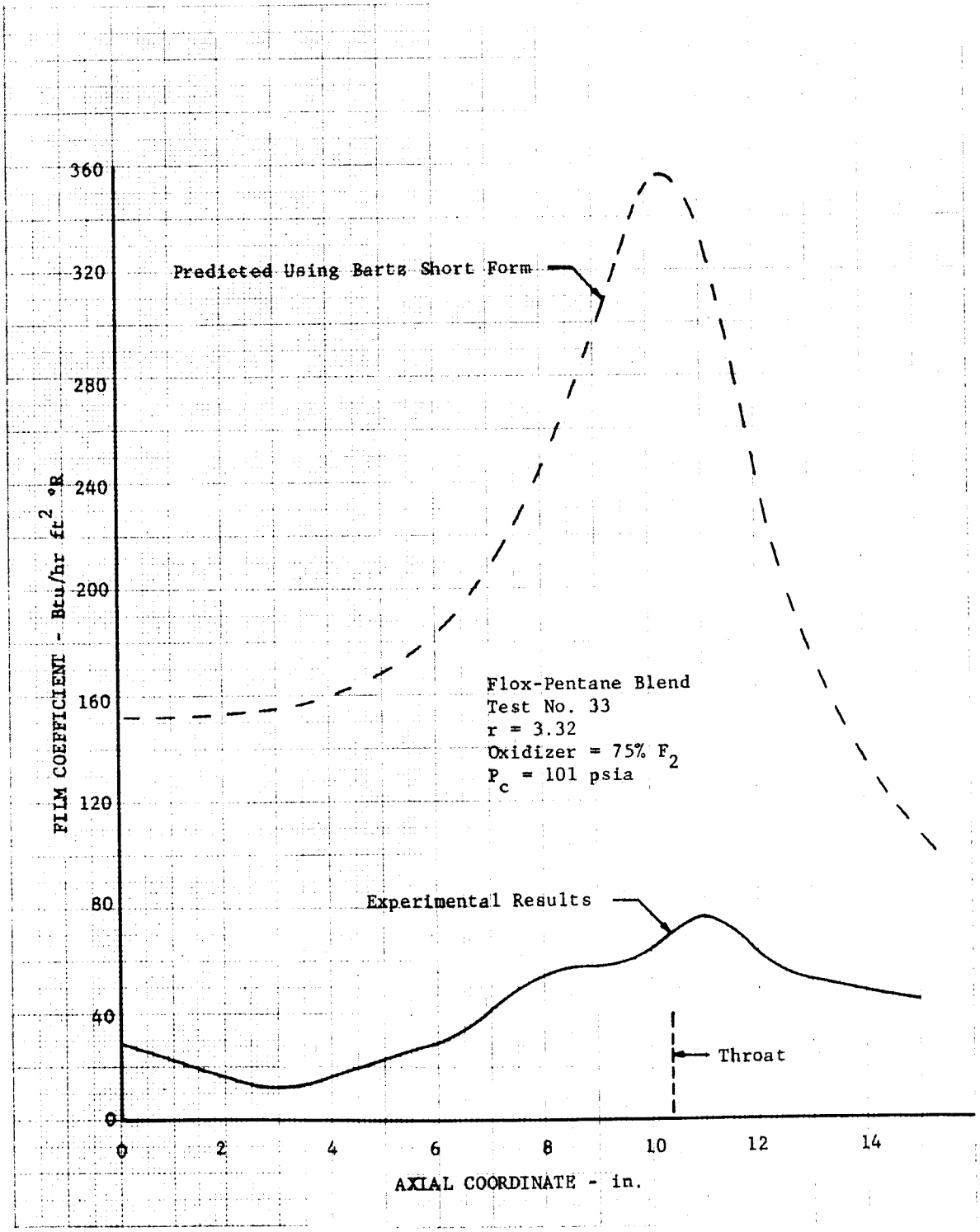

DF 40671

Figure 54
Comparison of Heat Transfer Coefficients

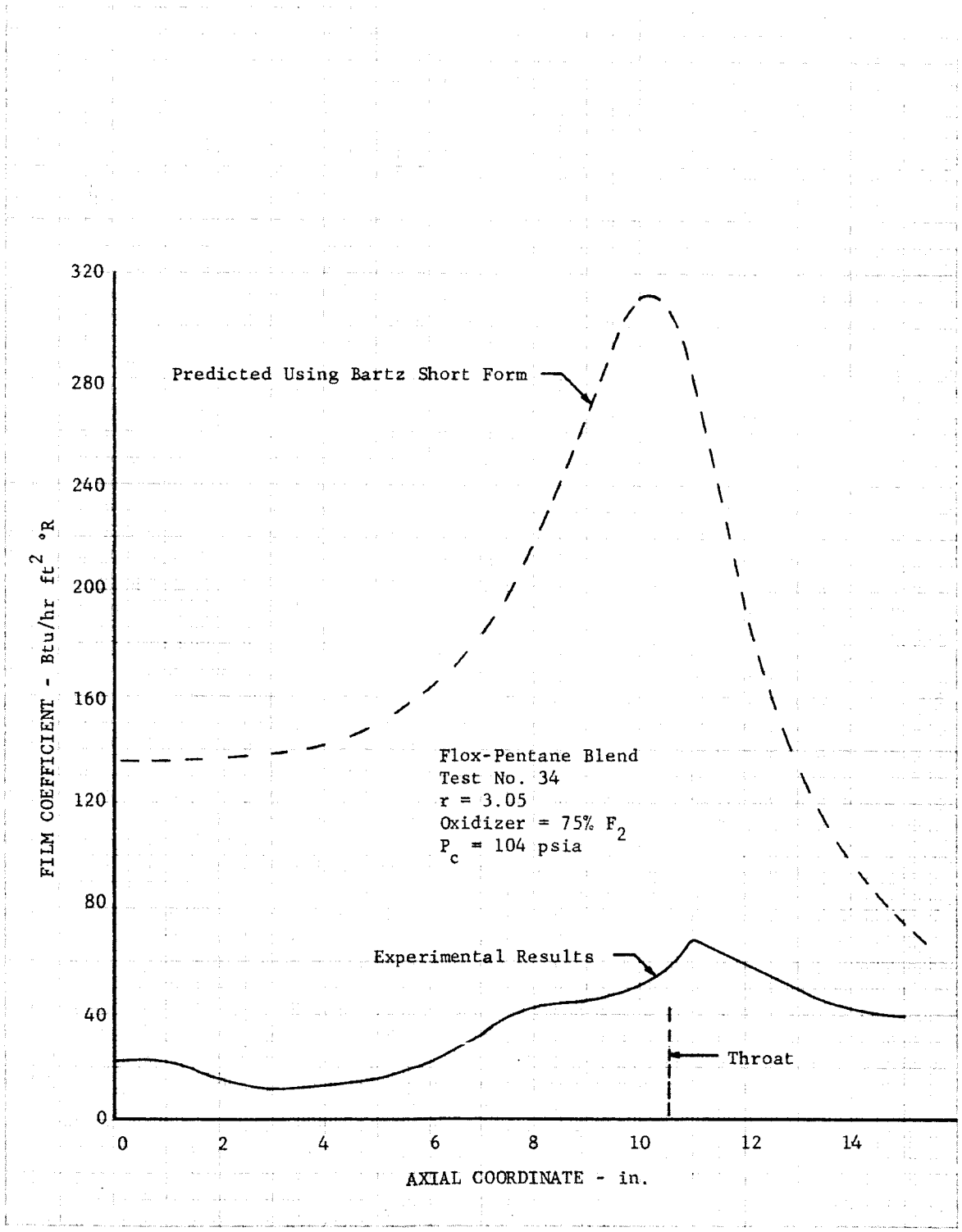

DF 40672

Figure 55
Comparison of Heat Transfer Coefficients

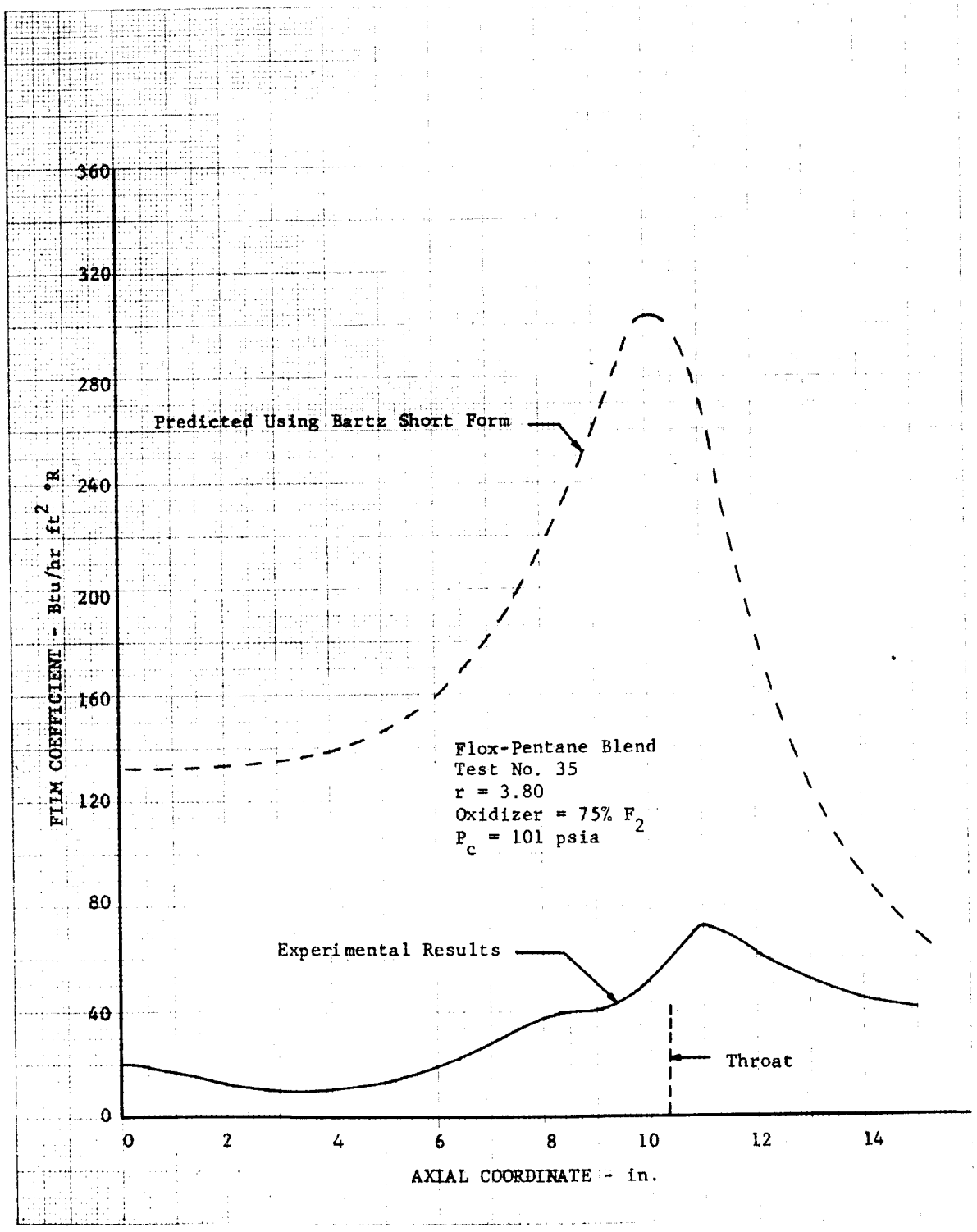

DF 40673

Figure 56
Comparison of Heat Transfer Coefficients

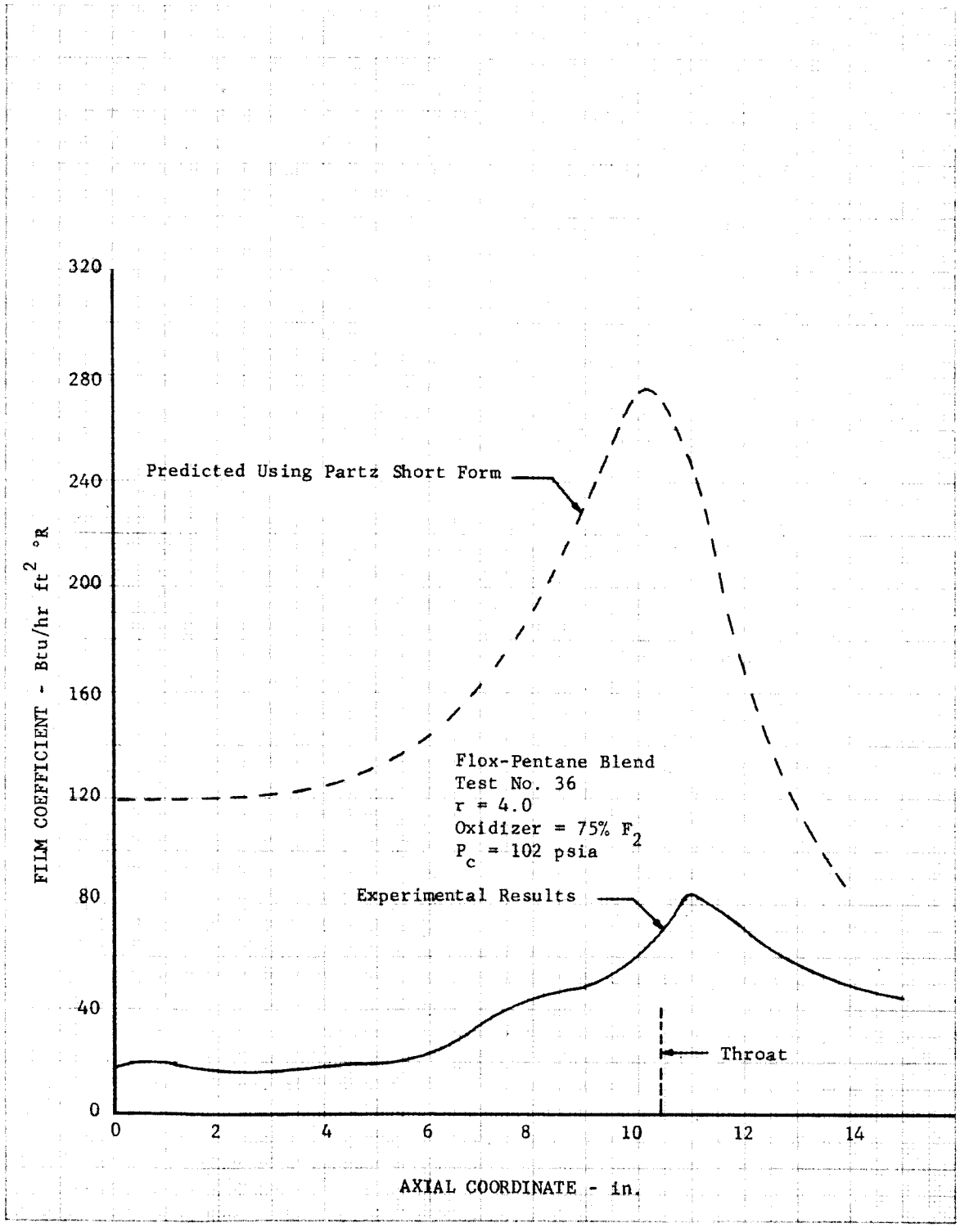

DF 41398

Figure 57
Comparison of Heat Transfer Coefficients

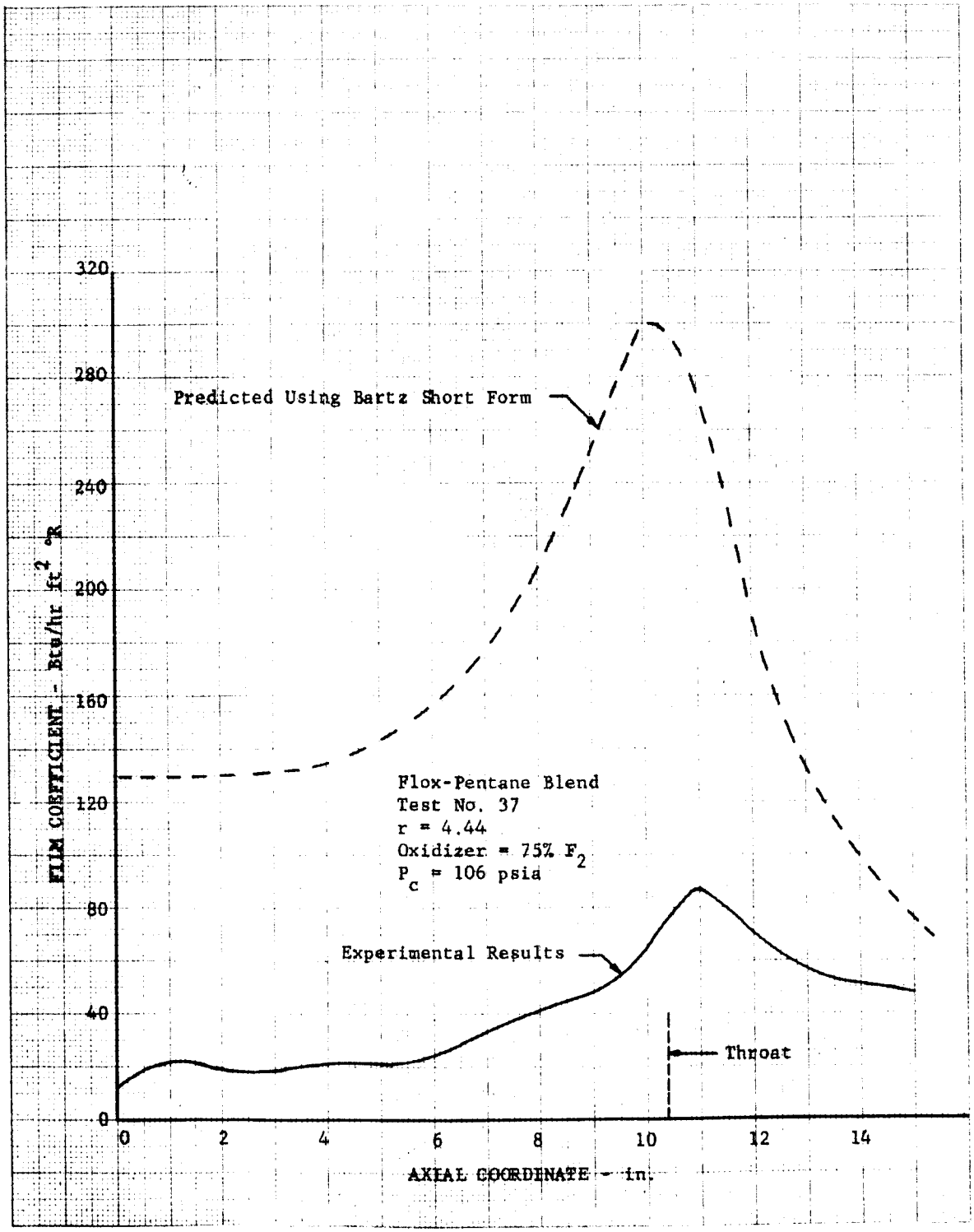

DF 41399

Figure 58
Comparison of Heat Transfer Coefficients

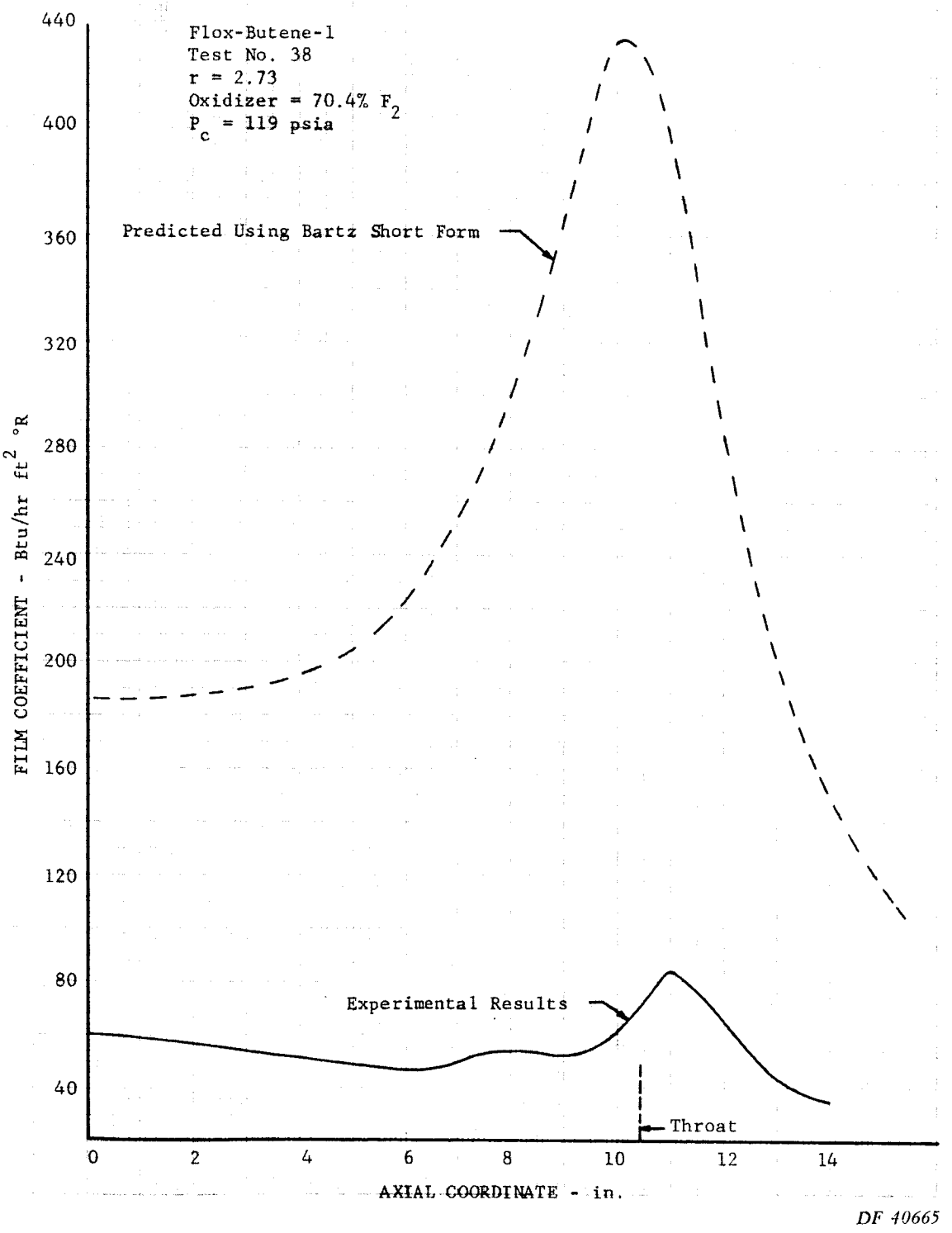

DF 40665

Figure 59
Comparison of Heat Transfer Coefficients

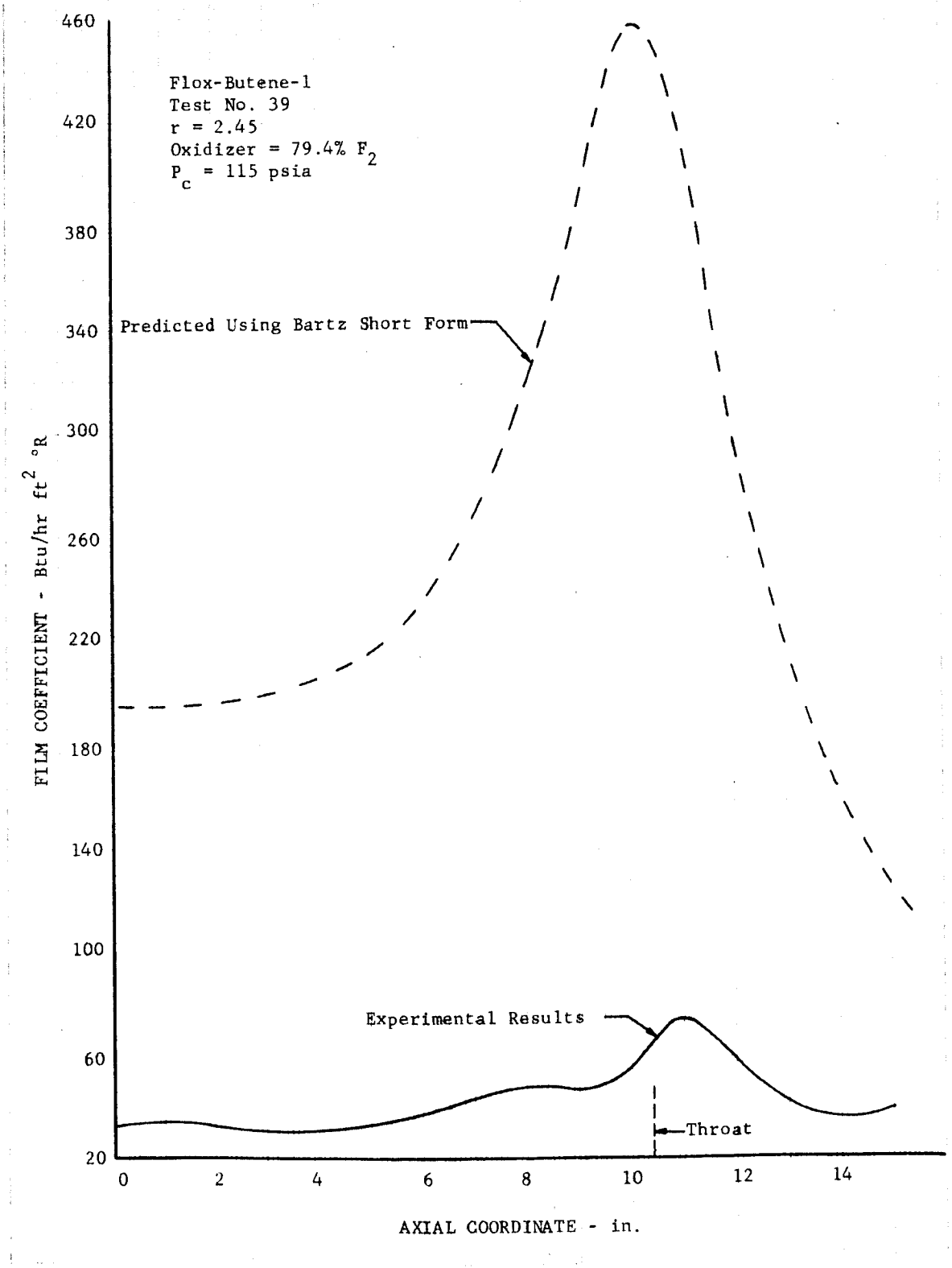

DF 40666

Figure 60
Comparison of Heat Transfer Coefficients

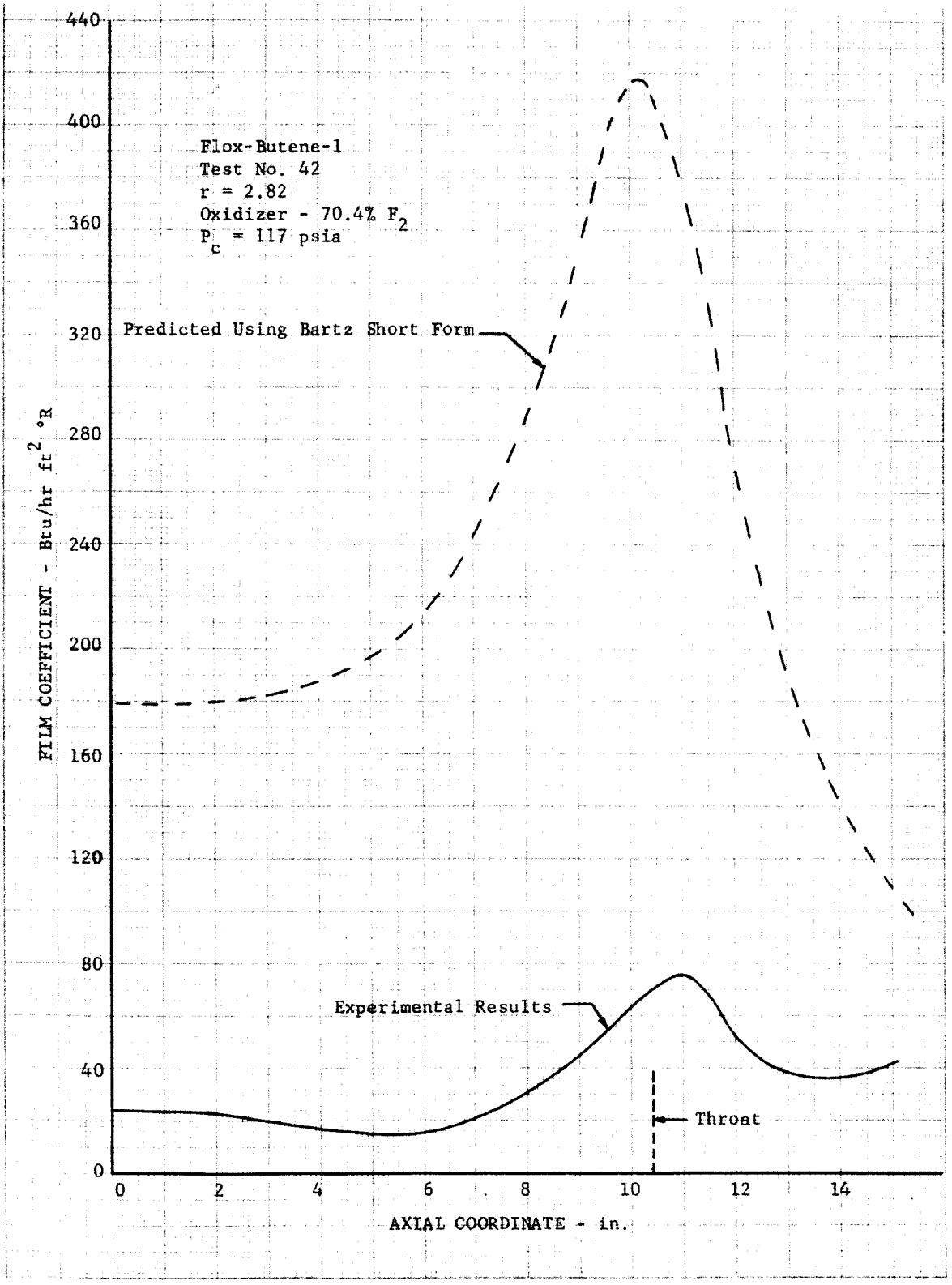

DF 40667

Figure 61
Comparison of Heat Transfer Coefficients

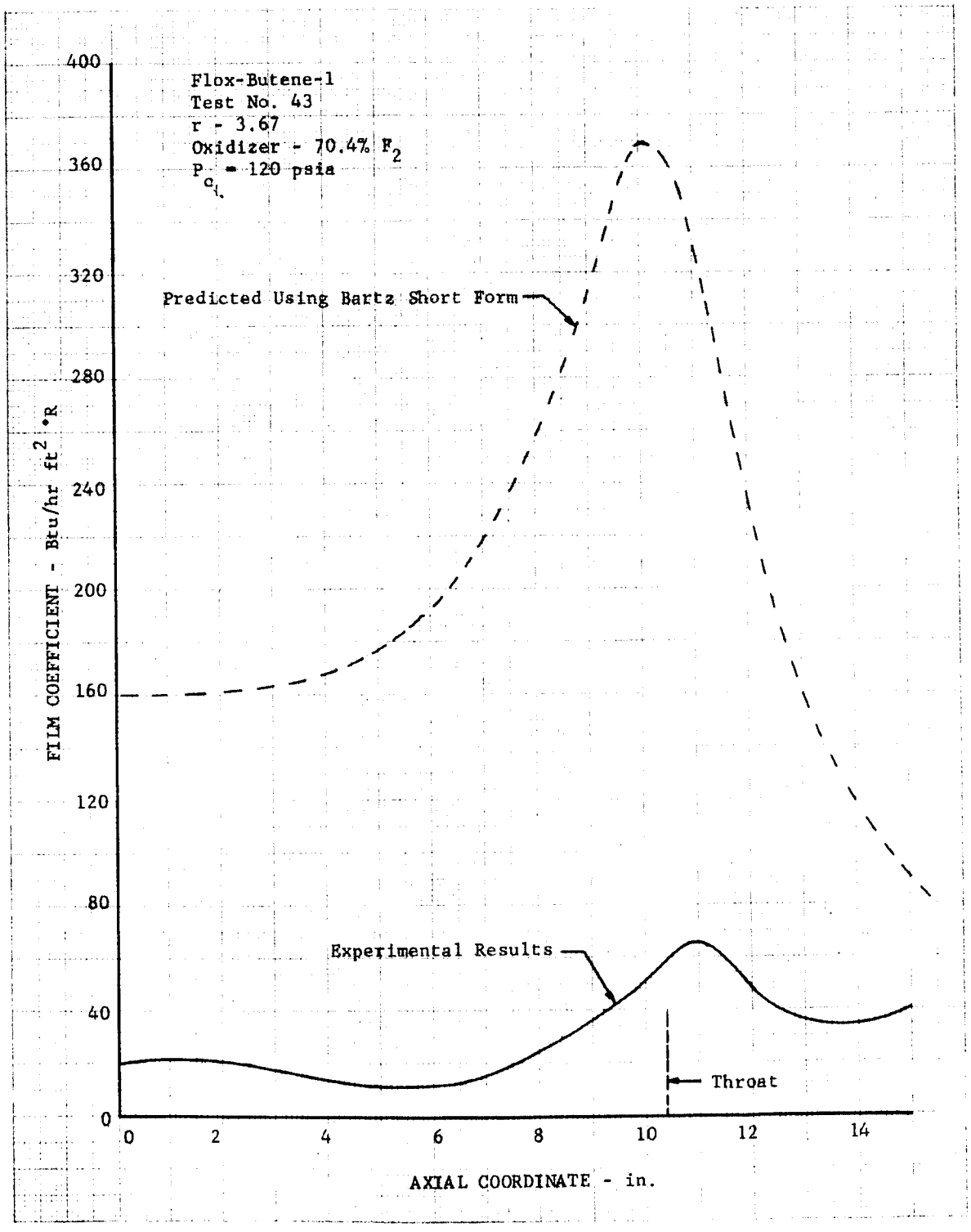

DF 40668

TABLE XVIII. CALCULATED HEAT LOSS FOR UNCOOLED TESTS

Test No.	Fuel	Heat Loss Rate, Btu/sec.
2	Methane	1005
7	Methane	979
10	Methane	706
13	Methane	707
15	Methane	974
16	Methane	677
21	Methane	550
24	Methane	500
28	Propane	320
29	Propane	291
30	Propane	292
31	Propane	275
33	Pentane Blend	208
34	Pentane Blend	169
35	Pentane Blend	177
26	Pentane Blend	186
37	Pentane Blend	184
38	Butene-1	296
39	Butene-1	207
42	Butene-1	176
43	Butene-1	161

E. REFERENCES

1. Bartz, D. R., "An Approximate Solution of Compressible Turbulent Boundary Layer Development and Convective Heat Transfer in Convergent-Divergent Nozzles," Transactions of the ASME-77, 1955, pp 1235-1245.

2. Glickstein, M. R., and Jackson, J. E., "Two Dimensional Heat Flux Measurements in Uncooled Rocket Nozzles," Bulletin of the 6th Liquid Propulsion Symposium, Vol. II, CPIA, September, 1964.

SECTION VII

TASK III — TRANSPIRATION COOLED TESTING

A. TEST DESCRIPTION

A total of 22 transpiration cooled tests were conducted: 10 with methane and 12 with propane. The chamber is shown mounted in the test stand in figure 62. The injector propellant control sequence initiated after uncooled test No. 4 was used for all transpiration cooled tests. The coolant control valve was opened in a position control mode and held at the 100 percent open position until steady-state chamber conditions were achieved. The valve was then automatically sequenced to switch to a flow control mode, i.e., controlling to a preset value of coolant flow orifice differential pressure.

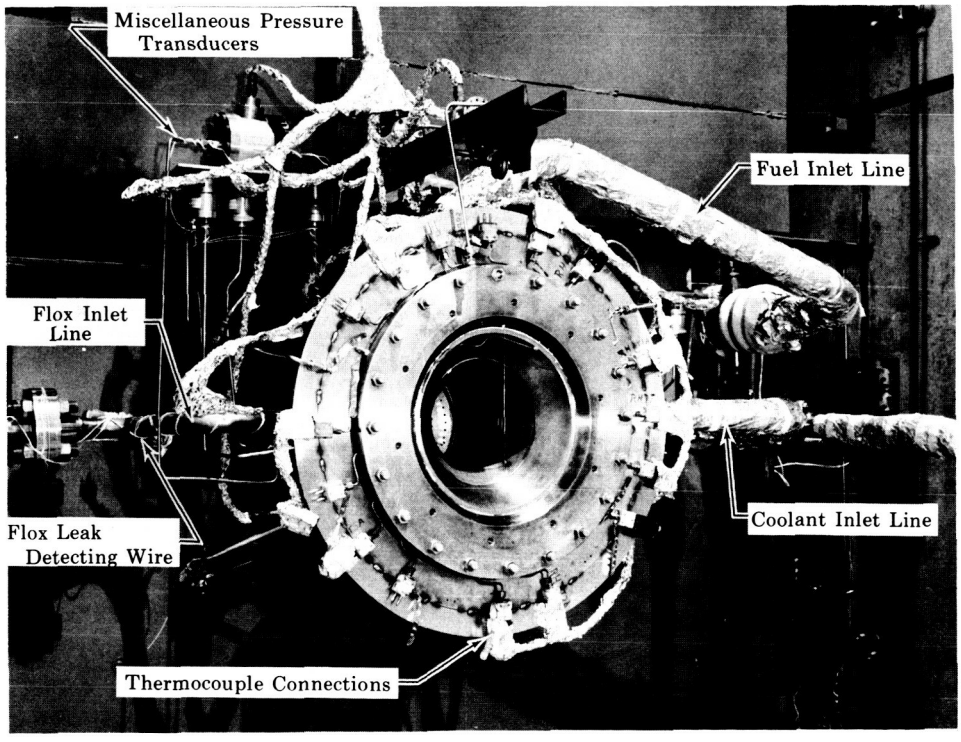

Figure 62. Transpiration Cooled Chamber Mounted in Test Facility FD 12776

During the methane tests problems with localized freezing of methane within the coolant line caused aborts of tests No. 6, 7, and 8. Subsequent modifications to cooldown and start procedures and removal of a coolant line filter remedied this problem.

1. METHANE TESTS (FLOX WAS 82.5% F_2)

Test No. 1T — Test No. 1T was conducted using the transpiration cooled chamber and the injector No. 3, which had been used for most of the early uncooled low mixture ratio flox-methane tests. This planned 2.0-second checkout firing was terminated after 1.7 seconds because of low

coolant flow, resulting from failure of the coolant valve to open fully. During the start transient, Rigimesh temperature rise and pressure drop followed expected trends. At the end of the test there was some separation of the Rigimesh layers (figure 63) at the edge of three of the segments; this was easily repaired by rewelding the edge of the segment and did not recur. Rigimesh replacement was not necessary.

Figure 63. Separation of Rigimesh Layers after Test No. 1T *FD 11731*

Test No. 2T — Test No. 2T, of 3.0-second duration, was made using the same hardware and test conditions as in test No. 1T. Maximum temperature for the thermocouples imbedded in the Rigimesh surface was 1925°R. Temperatures recorded at most of the hot side thermocouples were between 1200 and 1500°R. In the divergent section of the nozzle the temperature peaked at 540°R. The low temperatures in the divergent section were expected because the metering orifices were sized for constant Rigimesh upstream pressure rather than optimum coolant distribution.

Test No. 3T – Test No. 3T was to be of 10.0-second duration under the same conditions as the two previous firings. At the start of the test the oxidizer flow nozzle ΔP transducer failed, causing the oxidizer control valve to open fully, thereby resulting in a mixture ratio higher than planned. The test was aborted at 3.0 seconds because of a 1700°R temperature reading at one of two Rigimesh hot side thermocouples which were being monitored. This abort was only partially caused by the high mixture ratio. Temperature readings were probably appreciably higher than the actual Rigimesh temperature (because of the installation of the thermocouples within the Rigimesh). This abort temperature, 1700°R, was a very conservative operating limit set for initial checkout runs.

Test No. 4T – Test No. 4T was a successful 10.0 second firing; Rigimesh temperature limit aborts were set for 2100°R for this test. One Rigimesh hot side thermocouple reached 2300°R during the shutdown transient; however, most temperatures were between 1100 and 1400°R. Excessive overcooling in the exhaust nozzle divergent section was again indicated; temperature at this section was only 290°R.

Test No. 5T – Test No. 5T, an attempted firing of 10.0-second duration at a lower mixture ratio (30 percent less than optimum), was terminated at 4.0 seconds because of low coolant flow. The low coolant flow signal was apparently caused by incomplete purging of liquid nitrogen in the coolant line after cooldown and by nitrogen boiling in the coolant flow measuring orifice, which caused a fluctuation in the indicated coolant flow. Despite the shortened run duration, good steady-state performance data were obtained.

Test No. 6T – This was the first transpiration cooled test run using injector No. 6 (108 elements). This injector was used in uncooled tests No. 21 through 26. Coolant distribution orifices had been changed from that used in tests No. 1 through 5 to provide a more uniform wall temperature. The test was aborted after 0.7 second due to inadequate coolant flow to the chamber. A small amount of Rigimesh erosion was found at one small spot in transpiration cooled segment No. 6 at the nozzle throat.

Test No. 7T – The same hardware and coolant distribution as test No. 6T was again used. This test was also aborted after 0.7 second due to inadequate coolant flow. The chamber damage incurred in test No. 6T appeared to be slightly enlarged. After the run a filter in the coolant line was removed and a piece of solid methane was found in the filter blocking the fuel line. This filter was removed for the remaining tests and additional coolant line purge procedures were instituted.

Test No. 8T – This firing ran 5.7 seconds before being aborted by a high temperature indication from the chamber segment that had been damaged in test No. 6T and 7T. There was no appreciable increase in the

erosion previously noted. It was surmised that this was caused by one of two things: (1) a bad thermocouple damaged in tests No. 6T and 7T or (2) partial blocking of the distribution orifices to this segment by solidified methane.

Test No. 9T — Low coolant flow caused this test to be aborted at 2.9 seconds. The coolant flow was adequate at the start of the run and gradually dropped off, indicating partial rather than complete plugging of the methane run line due to freezing of the methane. Slight additional erosion of the transpiration cooled liner was again noticed in the same location as tests No. 6T and 7T.

Test No. 10T — This was a planned 30.0-second test that was manually aborted at 23.4 seconds because of high temperature indications from the throat segment. The first 10.0 seconds of the firing were made using the same control setting as all previous tests, i.e., the coolant control valve was set in position control at 100% open. After the first 10.0 seconds the coolant system was switched to flow control of a coolant flow rate of 1.09 lb/sec (6.87 percent of the total propellant flow). Inspection of the chamber after the test showed that the throat segment was badly damaged and that the Rigimesh liners in three other segments had minor damage, figure 64. It was impossible to tell from the data exactly where burnthrough of the Rigimesh occurred, but the failure apparently progressed gradually between 20 seconds after the start of the run and the end of the run.

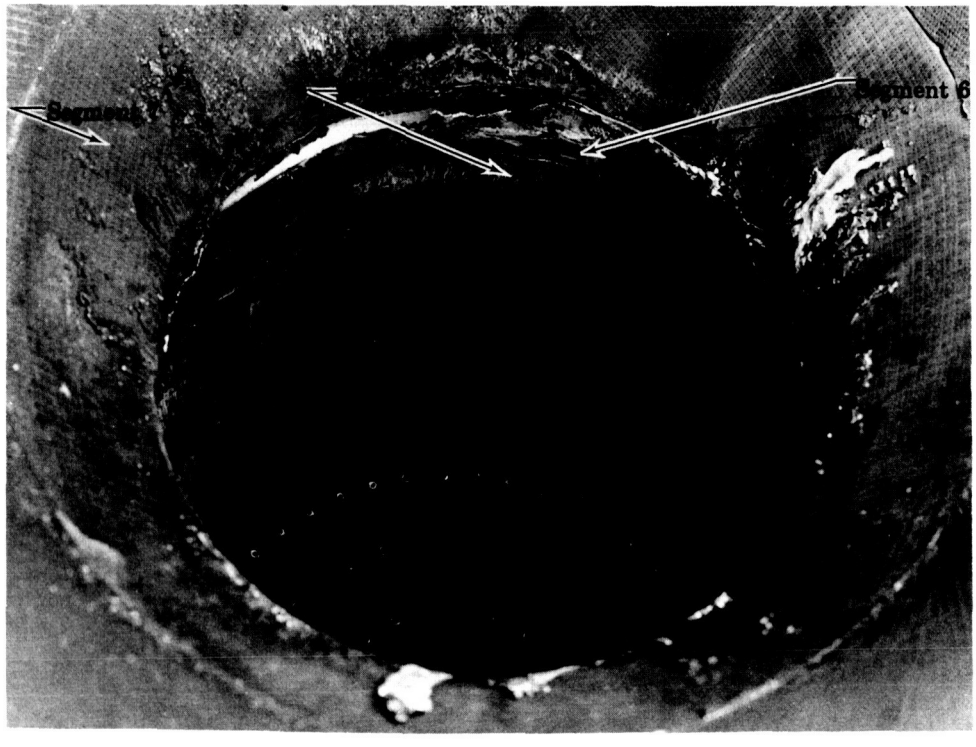

Figure 64. Damage to Chamber after Test No. 10T FD 12775

The damage to the thrust chamber encountered during tests No. 8T, 9T, and 10T was apparently due primarily to local disturbances around the area of erosion caused by inadequate cooling on tests No. 6T and 7T. Similar results have also been noted in transpiration cooled high pressure oxygen-hydrogen engines being tested under Air Force Contract, i.e., surface irregularities tend to increase local heat transfer, thereby causing localized burning. An additional contribution to the burnout may have been localized hot spots caused by the injector.

2. PROPANE TESTS (FLOX WAS 75% F_2)

Test No. 11T – This planned 10-second test was advanced to shutdown at 1.3 seconds by a high Rigimesh temperature indication. The high temperature was due to low coolant flow resulting from an insufficient coolant line prerun purge. The prerun procedures were changed to allow a longer line fill period.

Test No. 12T – This was a scheduled 10-second test. It was advanced to shutdown at 4.9 seconds by high Rigimesh temperatures. The high temperatures were caused by a low coolant flow which occurred because a coolant line bypass valve was leaking thereby diverting flow from the rig. (The leaking valve was not discovered until after test No. 13T.)

Test No. 13T – This scheduled 10-second test was advanced at 1.3 seconds by high Rigimesh temperatures. The coolant line bypass valve was found to be leaking thereby depleting the coolant supply to the chamber. The valve was repaired prior to additional testing.

Test No. 14T – This was a full duration test manually advanced to shutdown at 10.8 seconds. Maximum Rigimesh temperature was 2050°R and occurred in segment 7 just downstream of the throat. No hardware damage was visible.

Test No. 15T – This was a scheduled 10-second test which was advanced to shutdown at 7.8 seconds. Early shutdown was caused by a high Rigimesh temperature indication. The coolant line bypass valve was again found to be leaking and was repaired. No further trouble with this valve was encountered.

Test No. 16T – This was a full duration 30-second test. Maximum Rigimesh temperature was 2100°R at a point just downstream of the nozzle throat. No hardware damage was noted.

Test No. 17T – This was a full duration test which was manually advanced at 11.3 seconds. Maximum temperature was 2030°R just downstream of the nozzle throat. No hardware damage was noted.

Test No. 18T – This was a full duration 20-second test. Mixture ratio was varied during the test. Maximum Rigimesh temperature was 1900°R. No hardware damage was noted.

Test No. 19T – This was a planned 20-second test which was advanced at 4.8-seconds. Attempted coolant flow was 17 percent lower than tests 11T through 18T. Premature advance was due to low coolant flow which was caused by excessive closing of the coolant control valve when the valve switched to flow control. For future tests the valve gain was reduced. No hardware damage was noted.

Test No. 20T – This was a full duration 20-second test with a mixture ratio switch at 10 seconds. Coolant flowrate was 18 percent lower than tests 11T through 18T. Maximum temperature was 1930°R just downstream of the throat. No hardware damage was noted.

Test No. 21T – This was a 20-second test at a coolant flow rate 33 percent lower than that used in tests 11T through 18T. Maximum indicated temperature was 2800°R just downstream of the nozzle throat. Mixture ratio was switched at 10 seconds.

Test No. 22T – This was a 20-second test. Coolant flow was 50 percent lower than tests 11T through 18T. Mixture ratio was varied during the test. After this test some erosion of the Rigimesh was noted in segments 6 and 7 near the throat. The erosion was due primarily to the reduced coolant flow; however, it is believed that with better coolant distribution and a more uniform injector pattern the coolant flowrate could be reduced even more.

B. DATA REDUCTION

Transpiration cooled chamber performance parameters are calculated, using equations similar to those used for the uncooled chamber (Section VI, paragraph B) with the following changes and additions:

Delivered performance parameters are based on total propellant flow rate including coolant flow:

$$\dot{w}_p = \dot{w}_o + \dot{w}_f + \dot{w}_c$$

Two mixture ratios

$$r_{chamber} = \frac{\dot{w}_o}{\dot{w}_f + \dot{w}_c}$$

$$r_{inj} = \dot{w}_o/\dot{w}_f$$

and the percent of total propellant used for cooling

$$P_p = \frac{\dot{w}_c}{\dot{w}_c + \dot{w}_o + \dot{w}_f}(100)$$

are also calculated.

Theoretical performance parameters are calculated at the chamber mixture ratio, $r_{chamber}$, with propellant enthalpies corrected to the actual injector and coolant flow inlet conditions. The corrected values include momentum loss corrections identical to the uncooled corrections; however, because all heat is transferred to the coolant there is no heat loss correction.

List of Symbols

P_p	percent of total propellant used for cooling
$r_{chamber}$	chamber mixture ratio, (oxidizer/fuel + coolant)
r_{inj}	injector mixture ratio (oxidizer/fuel)

Subscripts

c	coolant
f	injector fuel flow
o	oxidizer

C. TEST PERFORMANCE

Tables XIX and XX show measured test data and calculated performance data, respectively, for the transpiration cooled tests. Table XXI shows the breakdown of injector efficiency and performance loss incurred by incomplete propellant mixing. Estimated injector efficiencies were based on uncooled tests with the same injector. Efficiency was correlated with injector fuel-oxidizer momentum ratio.

The apparent disagreement of cooling loss in test No. 4T compared with the other methane tests is either due to a faulty chamber pressure calibration or to excessive coolant flow through the divergent portion of the nozzle. Low temperature measurements in the divergent portion of the nozzle during test No. 4T tend to substantiate the latter premise.

Table XXII presents coolant flow and hot side Rigimesh temperatures for each chamber segment. Coolant flows are per unit of Rigimesh surface area. Rigimesh temperatures are taken during the stable portion of the test and are averages for some segments, hence, they may not agree with the individual readings mentioned in the test discussion.

TABLE XIX. MEASURED PERFORMANCE DATA – TRANSPIRATION COOLED TESTS

Test No.	Fuel	Percent F_2 in Flox	Test Duration, sec	P_c, psia	F, lb	$\dot{w}_o$, lb/sec	$\dot{w}_f$, lb/sec	$\dot{w}_c$, lb/sec	T_o, °R	T_f, °R	T_c, °R	ΔP_o, psi	ΔP_f, psi	Injector[4]	Comments
1T[1]	Methane	82.6	1.7	112	2877	12.0	2.66	0.94	156	566	190	29	23	3	Planned 2.0 sec checkout
2T		82.6	3.0	116	3147	12.3	2.69	0.98	151	590	190	30	26	3	3.0 sec checkout
3T		82.6	3.0	123	3355	14.2	2.63	1.04	148	587	195	41	22	3	Planned 10 sec run, high temperature abort
4T		82.6	10.0	114	3140	12.5	2.69	1.24	150	592	192	28	27	3	Full duration run
5T		82.6	4.0	123	3343	12.1	3.18	1.07	149	576	198	32	32	3	Planned 10 sec run, low coolant flow abort
6T		82.6	0.7	19	353	11.7	2.00	0.0	400	584	202		114	6	Planned 10 sec run, low coolant flow abort
7T		82.6	0.7	22	404	11.8	2.31	0.0	400	580	194		91	6	Planned 10 sec run, low coolant flow abort
8T		82.6	5.7	111	2986	12.1	2.58	1.10	164	604	188	14	70	6	Planned 10 sec run, high temperature abort
9T		82.6	2.9	112	2927	12.4	2.29	1.25	166	598	191	16	53	6	Planned 10 sec run, low coolant flow abort
10T		82.6	23.4	109	2771	12.4	2.34	1.09	170	605	198	14	54	6	Planned 30 sec run, high temperature abort
11T[2]	Propane	75.0	1.3											7	Planned 10 sec run, high temperature abort
12T		75.0	4.9	116	3189	12.2	3.81	1.48	156	770	184	19	87	7	Planned 10 sec run, high temperature abort
13T[2]		75.0	1.3											7	Planned 10 sec run, high temperature abort
14T		75.0	10.8	112	2962	12.2	3.37	1.48	160	787	251	24	77	7	Full duration run, no hardware damage
15T		75.0	7.8	107	2920	12.0	3.02	0.838	173	783	203	23	61	7	Planned 10 sec run, high temperature abort
16T		75.0	30.0	108	2905	12.7	2.85	1.32	175	787	238	25	57	7	Full duration run, no hardware damage
17T		75.0	11.3	110	2887	13.2	2.67	1.43	163	789	306	34	43	7	Full duration run, no hardware damage
18T[3]		75.0	20	112	3012	12.0	3.68	1.44	186	795	282	26	78	7	Full duration run, mixture ratio switch at 10 sec, no hardware damage
				105	2863	12.1	3.04	1.46	177	795	254	25	65		
19T		75.0	4.8	109	2869	12.5	3.02	1.44	164	793	312	23	59	7	Planned 20 sec test, low coolant abort
20T[3]		75.0	20	110	2877	12.5	3.02	1.30	157	792	364	21	59	7	Full duration test, mixture ratio switch at 10 sec, no hardware damage
				105	2824	12.7	2.77	1.18	170	803	293	24	54		
21T[3]		75.0	20	110	2908	12.0	3.00	0.925	153	782	359	21	56	7	Full duration test, mixture ratio switch at 10 sec, no hardware damage
				105	2836	12.7	2.78	0.929	164	788	316	21	55		
22T[3]		75.0	20	108	2823	12.0	2.97	0.707	182	790	333	24	62	7	Full duration test, slight Rigimesh erosion mixture ratio switch at 10 sec.
				105	2769	12.6	2.76	0.702	176	794	325	22	53		

(1) Values given are transient values near the end of test.

(2) Data not reduced.

(3) Mixture ratio was varied during run. Data is shown separately for each mixture ratio.

(4) See Table XIV

TABLE XX. CALCULATED PERFORMANCE DATA – TRANSPIRATION COOLED TESTS

Test No.	Fuel	Chamber, r	Injector, r	c*',[1] ft/sec	I_{sl},[1] sec	C_F',[1] ft/sec	c*P_c, ft/sec	c*F, ft/sec	$\eta_{c^*P_c}$	η_{c^*F}	$\eta_{c^*P_{c(cor)}}$	$\eta_{c^*F(cor)}$	I_{sl}, sec	η_{I_s}	$\eta_{I_{s(cor)}}$	C_F	η_{C_F}	$\eta_{C_{F(cor)}}$	Δt Used,[2] sec
1T	Methane	3.34	4.52	6762	236.0	1.134	6504	6041	0.962	0.893	0.937	0.905	185	0.782	0.915	0.913	0.805	0.966	0.3
2T		3.37	4.60	6768	239.3	1.150	6547	6336	0.967	0.936	0.942	0.948	196	0.821	0.958	0.966	0.840	1.006	0.9
3T		3.87	5.41	6823	249.3	1.177	6249	5895	0.916	0.864	0.892	0.874	188	0.753	0.875	0.967	0.822	0.979	0.9
4T		3.17	4.64	6724	235.9	1.142	6294	6223	0.936	0.925	0.912	0.937	192	0.812	0.948	0.979	0.857	1.028	3.7
5T		2.87	3.81	6637	240.5	1.287	6806	6422	1.026	0.968	0.999	0.979	204	0.848	0.987	0.966	0.822	0.979	0.9
8T		3.28	4.69	6749	235.0	1.133	6413	6210	0.950	0.920	0.926	0.932	189	0.806	0.943	0.950	0.839	1.007	2.2
9T		3.53	5.44	6782	236.9	1.133	6333	6006	0.934	0.886	0.910	0.897	183	0.773	0.905	0.931	0.821	0.986	1.4
10T		3.61	5.29	6795	236.0	1.124	6285	5798	0.925	0.853	0.901	0.865	175	0.743	0.871	0.897	0.798	0.960	12.5
12T	Propane	2.30	3.20	6415	227.9	1.149	6010	5895	0.937	0.919	0.913	0.931	183	0.802	0.936	0.979	0.852	1.020	2.9
14T		2.52	3.62	6488	227.9	1.135	5979	5693	0.922	0.878	0.898	0.889	174	0.764	0.893	0.937	0.825	0.990	2.9
15T		3.11	3.98	6670	230.4	1.115	6150	6150	0.922	0.922	0.899	0.935	184	0.800	0.938	0.964	0.865	1.041	3.2
16T		3.05	4.46	6652	229.9	1.116	5769	5736	0.867	0.862	0.845	0.874	172	0.748	0.878	0.959	0.859	1.035	15.8
17T		3.22	4.94	6699	233.3	1.125	5760	5529	0.860	0.825	0.838	0.837	167	0.717	0.840	0.934	0.831	0.999	5.4
18T		2.35	3.32	6431	225.4	1.133	5941	5778	0.924	0.899	0.900	0.915	176	0.782	0.915	0.955	0.843	1.013	8.7
		2.68	3.97	6537	223.9	1.107	5767	5813	0.882	0.889	0.860	0.902	173	0.770	0.906	0.962	0.870	1.049	5.0
19T		2.81	4.16	6581	229.0	1.124	5842	5584	0.888	0.849	0.865	0.860	169	0.737	0.864	0.930	0.827	0.995	2.9
20T		2.89	4.13	6606	230.0	1.126	5932	5659	0.898	0.857	0.875	0.868	171	0.744	0.872	0.929	0.826	0.992	2.5
		3.20	4.56	6697	229.0	1.104	5732	5746	0.856	0.858	0.834	0.870	170	0.743	0.873	0.955	0.865	1.044	6.7
21T		3.06	4.00	6658	231.9	1.125	6258	6040	0.940	0.908	0.916	0.920	183	0.788	0.923	0.940	0.836	1.005	3.8
		3.42	4.56	6750	230.9	1.105	5848	5870	0.866	0.870	0.844	0.883	173	0.752	0.886	0.958	0.874	1.059	7.3
22T		3.25	4.03	6713	232.1	1.116	6250	6022	0.931	0.897	0.907	0.910	181	0.778	0.913	0.929	0.833	1.003	3.4
		3.64	4.56	6787	232.8	1.106	5962	5814	0.879	0.857	0.856	0.869	173	0.741	0.871	0.931	0.842	1.015	3.6

(1) Based on chamber mixture ratio.

(2) Δt used, is the increment of time over which the performance figures are averaged.

TABLE XXI. EFFECT OF TRANSPIRATION COOLING ON PERFORMANCE

Test No.	Fuel	Injector[3]	Estimated Injector Efficiency[1]	Measured Efficiency, $\eta_{c^*P_{c(cor)}}$	Cooling Loss Efficiency[2]	Percent of Total Propellant Used for Cooling
1T	Methane	3	0.955	0.937	0.981	6.03
2T		3	0.953	0.942	0.988	6.14
3T		3	0.882	0.892	1.011	5.82
4T		3	0.961	0.912	0.949	7.55
5T		3	0.981	0.999	1.018	6.47
8T		6	0.940	0.926	0.985	6.99
9T		6	0.920	0.910	0.989	7.80
10T		6	0.924	0.901	0.975	6.87
12T	Propane	7	0.992	0.913	0.920	8.49
14T		7	0.973	0.898	0.922	8.68
15T		7	0.955	0.899	0.941	5.28
16T		7	0.931	0.845	0.908	7.82
17T		7	0.898	0.838	0.933	8.25
18T		7	0.987	0.900	0.912	8.44
			0.955	0.860	0.901	8.82
19T		7	0.957	0.865	0.904	8.48
20T		7	0.958	0.875	0.913	7.73
			0.928	0.834	0.899	7.09
21T		7	0.953	0.916	0.961	5.81
			0.927	0.844	0.910	5.67
22T		7	0.953	0.907	0.952	4.52
			0.929	0.856	0.921	4.37

[1] This corresponds to $\eta_{c^*P_{c(cor)}}$ estimated for the injector used at the injector momentum ratio.

[2] Cooling loss efficiency = measured efficiency/estimated injector efficiency.

[3] See Table XIV

TABLE XXII. COOLANT FLOW AND RIGIMESH TEMPERATURE DATA (1)

Run No.	Fuel	Segment 1 Temperature, °R	Segment 1 $(\dot{w}_c/A)\times10^3$, lb/sec-in^2 (2)	Segment 2 Temperature, °R	Segment 2 $(\dot{w}_c/A)\times10^3$, lb/sec-in^2	Segment 3 Temperature, °R	Segment 3 $(\dot{w}_c/A)\times10^3$, lb/sec-in^2	Segment 4 Temperature, °R	Segment 4 $(\dot{w}_c/A)\times10^3$, lb/sec-in^2	Segment 5 Temperature, °R	Segment 5 $(\dot{w}_c/A)\times10^3$, lb/sec-in^2	Segment 6 Temperature, °R	Segment 6 $(\dot{w}_c/A)\times10^3$, lb/sec-in^2	Segment 7 Temperature, °R	Segment 7 $(\dot{w}_c/A)\times10^3$, lb/sec-in^2	Segment 8 Temperature, °R	Segment 8 $(\dot{w}_c/A)\times10^3$, lb/sec-in^2
2	Methane	1486	2.14	1318	1.66	1084	1.57	1067	1.91	1037	1.98	1188	2.50	1027	2.48	250	2.90
3		1638	2.16	1986	1.66	1285	1.59	1240	1.91	1693	1.98	1507	2.50	1272	2.48	308	1.77
4		1246	2.44	1503	1.83	1220	1.74	1151	2.11	1152	2.18	1457	2.74	1109	1.93	203	3.46
5			1.87	973	1.41	1176	1.33	1192	1.32	1148	1.65	1089	2.10	1100	2.10	247	4.74
8			2.31	1540	2.22	1058	2.22	(4)	2.03	1128	1.62	2001	2.66	1490	2.09	766	2.19
9			2.83	950	2.72	942	2.72	1325	2.50	1102	2.00	766	3.28	1425	2.58	790	2.18
10			2.31	507	2.23	636	2.23	1410	2.04	1272	2.20	(4)	1.98	1799	2.16	813	1.24
14	Propane	943	2.275	1400	2.275	1169	2.31	1613	2.55	NO	4.43	1519	6.51	1800	4.58	NO	1.68
15		1168	2.24	1091	2.24	1027	2.36	1307	2.50	THERMOCOUPLE	4.35		6.46	1806	4.50	THERMOCOUPLE	1.71
16		921	2.47	1534	2.47	1208	2.60	1077	2.77		4.80		7.14	1882	2.14		1.675
17		875	2.245	1059	2.245	991	2.38	1376	2.60		4.37		6.50	1509	2.33		1.62
18-1		941	2.20	888	2.20	1020	2.33	1514	2.47		4.27	720	6.92	1718	4.42		1.67
18-2		893	2.39	1163	2.39	995	2.52	1413	2.67		4.64	782	7.50	1645	4.78		1.655
19		934	2.35	934	2.35	966	2.48	1267	2.63		4.55		7.42	1428	4.72		1.645
20-1		913	2.03	868	2.03	1089	2.14	1655	2.27		3.94		6.64	1675	4.07		1.605
20-2		861	2.11	1467	2.11	1405	2.21	1688	2.35		4.075		6.60	1900	4.23		1.640
21-1		1006	1.54	716	1.54	1223	1.63	1810	1.725		2.99	861	4.83	1405	3.09		1.605
21-2		1157	1.64	1213	1.64	1416	1.735	1779	1.84		3.19	1011	5.14	1800	3.30		1.615
22-1		875	1.21	988	1.21	1126	1.28	1830	1.355		2.35	1229	3.79	1700	2.43		1.615
22-2		889	1.255	1015	1.255	1146	1.331	1851	1.412		2.45	1542	3.96	1800	2.54		1.63

(1) Data taken at steady-state portion of run

(2) $\dot{w}_c/A$ = Coolant flow (lb/sec) over area of Rigimesh (in^2) per segment

(3) Average segment temperature

(4) Overscale (no reading)

SECTION VIII

TASK IV — REGENERATIVE COOLING TESTS

A. TEST DESCRIPTION

Thirteen supplementary convectively cooled tests were conducted to evaluate the regenerative cooling ability of liquid light hydrocarbon fuels. Seven of the tests were conducted using a eutectic blend of pentane and isopentane and 6 tests were conducted using propane. All tests were made with an oxidizer of 75% fluorine in the flox, heated gaseous fuels supplied to the injector, and liquid fuels cooled to 10°R to 120°R above their freezing point as coolants. All tests were conducted using the same injector (7) and fuel and oxidizer injection conditions as had been used in the uncooled tests with these fuels (tests 27 through 37). The thrust chamber was a modified RL10A-1 tube wall combustion chamber cut off at a nozzle expansion area ratio of 3.54 to allow sea level testing without flow separation, and with copper swirlers installed in a short section of the tubes at the injector end of the chamber. (See Section IV-D for complete description.

The control sequence used for the injector propellants was identical to that used for the uncooled tests. The coolant was a subcooled liquid supplied from a pressurized tank and controlled by two control valves. One valve, upstream of the coolant jacket, was operated in the flow control mode, and therefore regulated flow to a preset value based on a signal from the coolant flowmeter. The second valve, downstream of the coolant jacket was in pressure control and was set to maintain a 150 psia back pressure on the jacket discharge.

Minimum coolant flowrates required for remaining in the nucleate boiling regime were estimated using the film coefficients determined from the uncooled tests and the upper limit heat flux data from the heated tube tests.

1. PENTANE BLEND TESTS (FLOX WAS 75% F_2 FOR ALL TESTS)

Test No. 1R — This was a 3.3-second checkout run using the pentane blend. Coolant flowrate was 27.8 lb_m/sec which is approximately 3 times the flow rate predicted (based on uncooled combustion tests and heated tube tests) to be a minimum for maintaining nucleate boiling. The coolant flow was steady. The initial high fuel flowrate encountered in the pentane blend uncooled tests also occurred in all pentane regenerative tests. No visible hardware damage was noted.

Test No. 2R — This was a 10-second pentane blend run with approximately the same coolant flow as test No. 1R. No visible hardware damage was noted.

Tests No. 3R, 4R, and 5R – These were 10-second pentane blend runs with a coolant flowrate approximately twice that predicted to be a minimum for remaining in the nucleate boiling regime. No visible hardware damage was noted.

Test No. 6R – This was a 30-second pentane blend run. Coolant flow was again twice that required to stay in the nucleate boiling regime. No visible hardware damage was noted.

Test No. 7R – This was a 10-second pentane blend run. Coolant flow was approximately 30% higher than that required to maintain nucleate boiling. No visible hardware damage was noted.

2. PROPANE TESTS (FLOX WAS 75% F_2 IN ALL TESTS)

Tests No. 8R, 9R, 10R, and 11R – These were 10-second propane runs. Coolant flowrate was approximately 2 times that estimated as a minimum for remaining in the nucleate boiling regime. No hardware damage was noted after tests.

Test No. 12R – This was a 40-second propane run. The initial coolant flow was slightly lower than that used for tests No. 8R through 11R. At 10 seconds the coolant flowrate was reduced to a value approximately 25% greater than that estimated to be a minimum for nucleate boiling. At 20 seconds the coolant flow was reduced to a value approximately 10% below that estimated as the nucleate boiling requirement. At 30 seconds the coolant flowrate was reduced to a value equal to the injector fuel flowrate at the optimum mixture ratio. This was approximately 60% of the flowrate estimated to be a minimum for maintaining nucleate boiling. No coolant instability was encountered and there was no visible hardware damage.

Test No. 13R – This was a planned 10-second propane run. The coolant flowrate was scheduled to be equal to the lowest flowrate used in test No. 12R. During the start transient the coolant upstream valve closed while attempting to adjust to the low flowrate. The jacket downstream valve then closed attempting to maintain backpressure with a no flow condition. As the upstream valve closed, a pressure surge caused by the sudden termination of flow, ruptured a burst disk in the coolant line. This diverted the coolant flow from the rig to a vent line. The lack of coolant flow caused the chamber burnout shown in figure 65.

B. TEST PERFORMANCE

Tables XXIII, XXIV, and XXV present measured and calculated performance data for all regeneratively cooled runs. Data reduction methods are identical to those shown in Section VI, paragraph B. The effect of mixture ratio, velocity ratio and momentum ratio on characteristic velocity efficiency is presented in figures 31 through 36 along with the uncooled data.

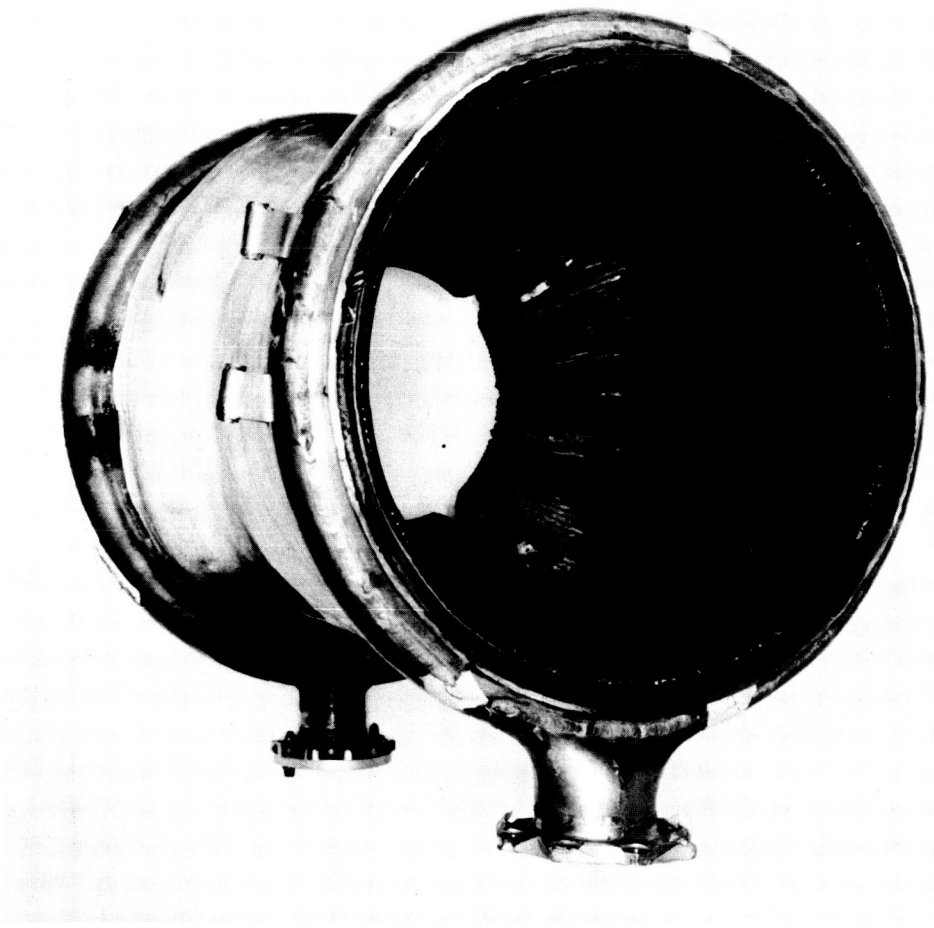

Figure 65. Regenerative Chamber after Test No. 13R (Viewed from Injector End) *FE 50969*

C. HEAT TRANSFER

Heat transfer to the coolant was calculated from coolant flowrate and temperature rise. Total heat transfer (shown in table XXIV) in the pentane tests was approximately 30% greater than that predicted from the uncooled data. For the propane tests the heat transfer was approximately 25% greater than predictions based on uncooled film coefficient data.

TABLE XXIII. MEASURED PERFORMANCE DATA – REGENERATIVELY COOLED TESTS

Test No.	Fuel	Test Duration, sec	P_c, psia	F, lb	$\dot{w}_o$, lb/sec	$\dot{w}_f$, lb/sec	T_o, °R	T_f, °R	ΔP_o, psi	ΔP_f, psi	Injector[3]	Coolant Inlet Temperature, °R	Coolant Outlet Temperature, °R	Coolant Flow Rate, lb/sec	Coolant Inlet Pressure, psia	Coolant Exit Pressure, psia	Coolant Flow Multiple[2]	Comments[1]
1R	Pentane	3.3	113	3090	12.4	4.21	163	869	25	73	7	243	280	27.8	282	149	6.6	Checkout test
2R	Blend	10.0	110	2906	12.3	4.03	163	869	19	61	7	287	315	28.2	267	150	7.0	No visible hardware damage on any pentane tests
3R		10.0	108	2774	12.1	3.59	167	877	16	50	7	248	297	18.9	227	154	5.3	
4R		10.0	104	2666	12.2	3.29	170	867	21	44	7	225	269	19.1	231	151	5.8	
5R		10.0	107	2813	12.8	3.10	154	837	20	38	7	217	260	19.5	233	153	6.3	
6R		30.0	108	2879	12.8	3.32	168	856	17	44	7	245	282	19.2	218	153	5.8	
7R		10.0	111	2921	12.3	3.38	155	846	21	43	7	212	284	12.6	192	151	3.7	
8R	Propane	10.0	109	2875	11.9	2.85	167	773	17	76	7	191	303	8.3	166	145	2.9	No visible hardware damage on tests 8 through 12
9R		10.0	104	2667	11.9	2.66	169	775	15	68	7	184	290	8.5	179	158	3.2	
10R		10.0	102	2634	12.1	2.49	172	778	17	56	7	178	281	9.1	161	139	3.6	
11R		10.0	100	2583	12.4	2.37	173	780	20	52	7	184	280	9.2	161	134	3.9	
12R		40.0	102	2677	12.1	2.49	168	784	18	57	7	180	297	8.2	156	142	3.3	Coolant flow at 10 sec
												180	327	5.7	145	139	2.3	Coolant flow at 20 sec
												180	375	4.2	131	129	1.7	Coolant flow at 30 sec
												180	452	2.7	162	161	1.1	Coolant flow at 40 sec
13R		10.0									7							Tube burnout due to no coolant flow.

[1] Flox was 75% F_2 for all tests.

[2] Coolant flow rate/injector fuel flowrate

[3] See Table XIV

TABLE XXIV. CALCULATED PERFORMANCE DATA – REGENERATIVELY COOLED TESTS (1)

Test No.	Fuel	r	$\dot{w}_p$, lb/sec	c*', ft/sec	I_{s1}', sec	C_F'	c^*P_c, ft/sec	Q, Btu/sec	$\eta_{c^*P_c}$	η_{c^*F}	$\eta_{c^*P_{c(cor)}}$	$\eta_{c^*F(cor)}$	I_{s1}, sec	η_{I_s}	$\eta_{I_{s(cor)}}$	C_F	η_{C_F}	$\eta_{C_{F(cor)}}$	Δt Used,[2] sec
1R	Pentane	2.95	16.6	6612	233.1	1.141	6193	433	0.937	0.916	0.914	0.929	186	0.798	0.934	0.967	0.848	1.016	0.8
2R	Blend	3.04	16.3	6636	230.8	1.126	6406	338	0.921	0.888	0.899	0.901	178	0.773	0.907	0.939	0.834	1.003	7.2
3R		3.38	15.7	6691	230.3	1.109	6387	395	0.917	0.888	0.895	0.901	177	0.768	0.903	0.927	0.835	1.007	7.5
4R		3.72	15.5	6718	230.3	1.100	6313	355	0.907	0.869	0.885	0.883	172	0.747	0.881	0.908	0.826	0.998	7.0
5R		4.13	15.9	6750	234.2	1.114	6400	348	0.910	0.880	0.888	0.894	177	0.758	0.891	0.932	0.839	1.012	5.4
6R		3.85	16.1	6731	234.9	1.119	6245	300	0.905	0.883	0.883	0.896	179	0.761	0.893	0.944	0.844	1.016	11.7
7R		3.66	15.7	6709	236.6	1.132	6653	385	0.960	0.911	0.936	0.924	186	0.787	0.922	0.931	0.824	0.990	8.5
8R	Propane	4.16	14.8	6806	238.0	1.124	6756	492	0.993	0.951	0.970	0.967	196	0.829	0.966	0.932	0.829	0.997	7.0
9R		4.47	14.6	6829	233.2	1.099	6492	479	0.951	0.913	0.929	0.928	184	0.787	0.929	0.909	0.827	0.999	7.4
10R		4.86	14.6	6786	229.2	1.088	6341	498	0.934	0.917	0.912	0.933	181	0.790	0.933	0.919	0.845	1.022	7.9
11R		5.22	14.8	6696	224.4	1.081	6180	468	0.923	0.908	0.901	0.923	176	0.782	0.926	0.914	0.845	1.025	8.4
12R		4.87	14.6	6779	228.7	1.087	6306	444	0.930	0.930	0.908	0.946	183	0.802	0.948	0.936	0.861	1.043	38.9

[1] Methods for calculating the various performance parameters are given in Section VI, Paragraph B.

[2] Δt used, is the amount of time over which the performance figures are averaged.

TABLE XXV. INJECTOR PERFORMANCE COMPARISON – REGENERATIVELY COOLED TESTS

Test No.	Fuel	Injector[1]	$\dot{w}_f$, lb/sec	$\dot{w}_o$, lb/sec	V_f, ft/sec	V_o, ft/sec	r	$\dot{w}_f V_f$, lb-ft/sec^2	$\dot{w}_o V_o$, lb-ft/sec^2	$\eta_{c^*P_c}$	P_c, psia	V_f/V_o	$\dot{w}_f V_f / \dot{w}_o V_o$
1R	Pentane	7	4.21	12.4	950	56	2.95	3990	692	0.937	113	17.0	5.78
2R	Blend	7	4.03	12.3	935	55	3.04	3780	685	0.921	110	17.0	5.52
3R		7	3.59	12.1	872	54	3.38	3130	655	0.917	106	16.1	4.78
4R		7	3.29	12.2	806	55	3.72	2650	669	0.907	104	14.7	3.96
5R		7	3.10	12.8	713	58	4.13	2210	736	0.910	107	12.3	3.00
6R		7	3.32	12.8	775	57	3.85	2560	722	0.905	108	13.6	3.54
7R		7	3.38	12.3	759	55	3.66	2570	680	0.960	111	13.8	3.78
8R	Propane	7	2.85	11.9	968	54	4.16	2760	638	0.993	109	18.1	4.34
9R		7	2.66	11.9	950	54	4.47	2525	638	0.951	104	17.8	3.95
10R		7	2.49	12.1	912	54	4.86	2270	655	0.934	102	16.9	3.47
11R		7	2.37	12.4	887	56	5.22	2095	692	0.923	100	16.8	3.03
12R		7	2.49	12.1	842	54	4.87	2097	655	0.930	102	15.6	3.18

[1] See Table XIV

SECTION IX
EVALUATION OF TEST RESULTS

A. INJECTOR PERFORMANCE

The purpose of the experimental program was not to demonstrate high performance, but rather to use existing injectors with minor modifications to provide adequate performance for evaluation of the heat transfer characteristics and cooling ability of light hydrocarbon fuels. Nevertheless, several important conclusions can be drawn from the experimental performance data regarding requirements for gaseous hydrocarbon fuel – liquid flox injection. From the data given in Section VI, the importance of a high velocity ratio or momentum ratio for providing high performance is evident. Although only one test was completed with swirlers installed, their beneficial effect on performance is clearly indicated. The use of fluorine-compatible materials and installation techniques for the swirlers should eliminate spud burning, making the use of swirlers practical. The methane data give an indication of the performance improvement of a 216-element injector over a 108-element injector for the conditions tested. These data provide some insight into injector element density requirements for similar gas-liquid injectors.

Some information on injector fabrication techniques is also apparent from the testing. The use of Rigimesh to provide transpiration cooling of the injector face, a well-proved method for hydrogen fuel, has been proved to be equally satisfactory with gaseous hydrocarbon fuels. Post-firing inspection of injectors has substantiated the anticipated improvement in durability of nickel spuds over stainless steel spuds, even though the nickel spuds were tested under more severe conditions.

B. HEAT TRANSFER

Figures 66 through 70 summarize the ratio of the experimentally-determined to the analytically-predicted film coefficient as a function of axial location along the chamber for each of the four fuels tested. Note that the measured film coefficients are all well below the predicted values, although the theoretical value is approached in the divergent portion of the nozzle. Figures 66 and 67 show the effect of injector design on the chamber film coefficient. Note that, as expected, the effect of the injector on the film coefficient is greatest near the injector. Comparing figures 68, 69, and 70, it can be seen that the ratio of the actual to predicted film coefficient is higher in the chamber than near the nozzle throat for propane, but remains relatively constant for the butene-1 and the eutectic pentane blend. This provides an indication that the effect of injector design on the chamber film coefficient becomes less significant as the fuel hydrogen/carbon ratio decreases.

Figure 66
Ratio of Actual to Predicted Film Coefficient vs Axial Location (Flox-Methane, Injector No. 3)*

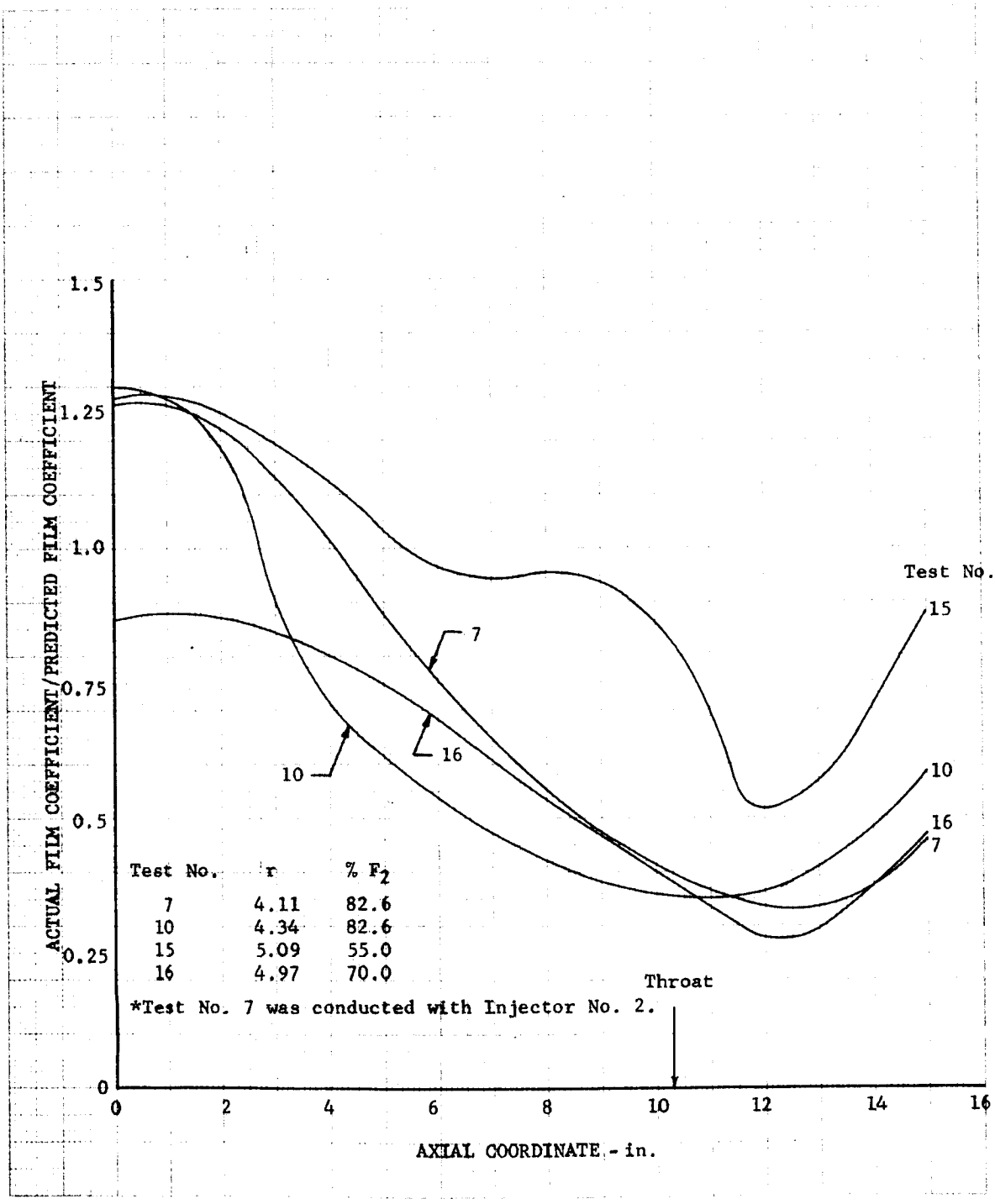

DF 40655

Figure 67
Ratio of Actual to Predicted Film Coefficient vs Axial Location (Flox-Methane, Injector No. 6)

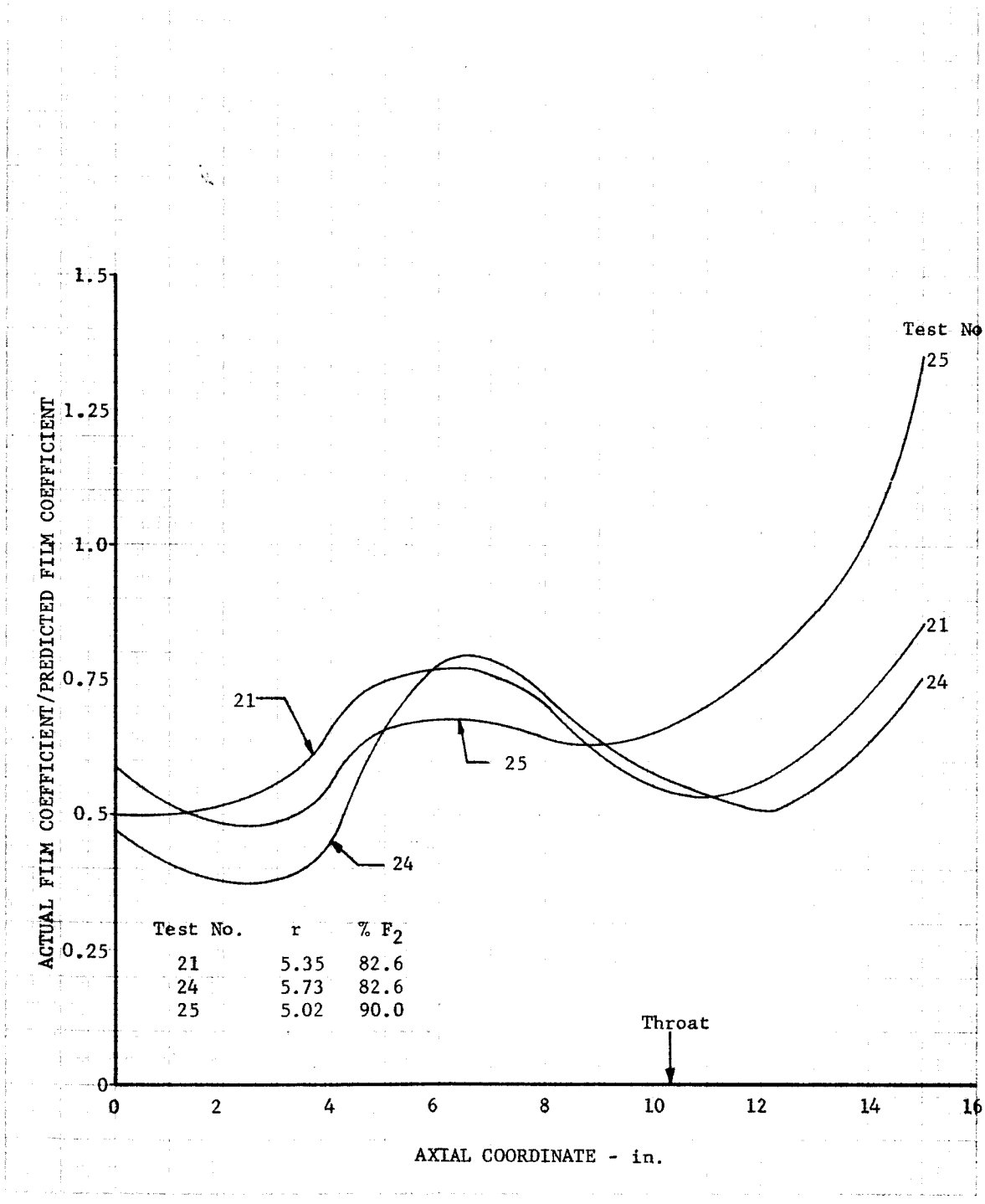

DF 41400

Figure 68
Ratio of Actual to Predicted Film Coefficient vs Axial Location (Flox-Propane, Injector No. 7)

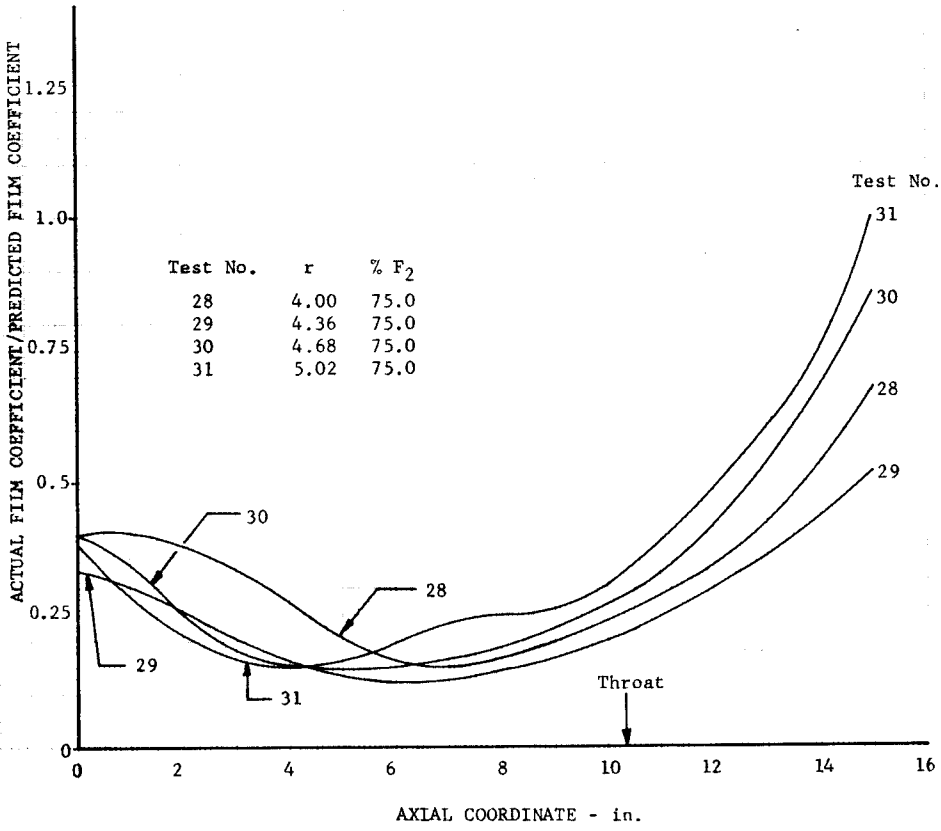

DF 41401

Figure 69
Ratio of Actual to Predicted Film Coefficient vs Axial Location (Flox-Pentane Blend, Injector No. 7)

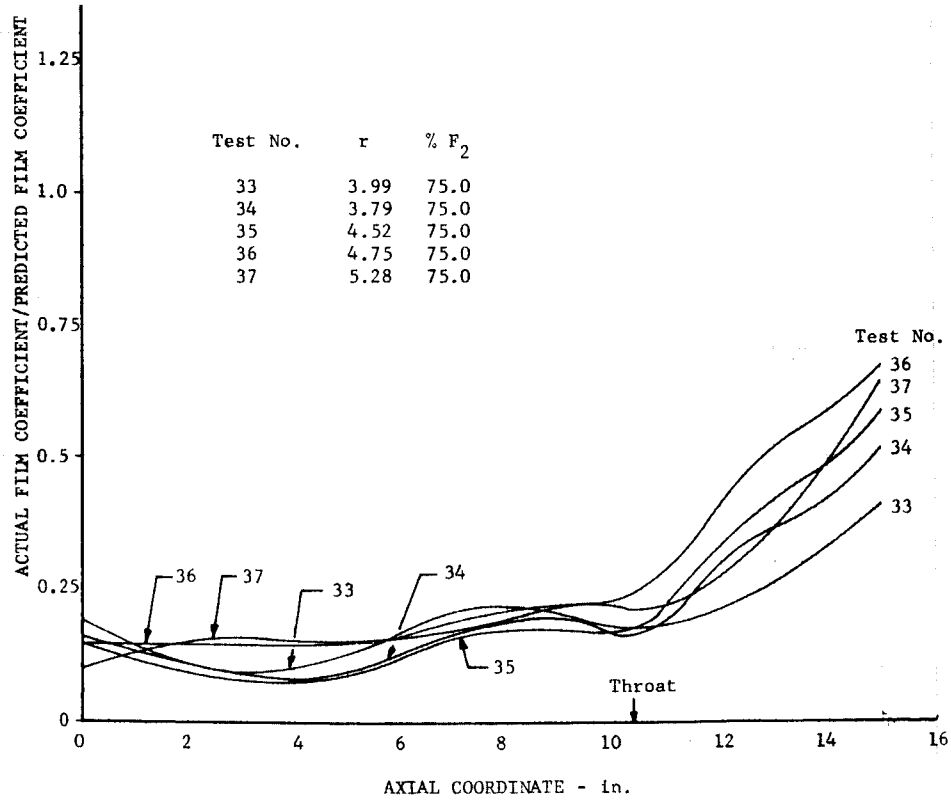

DF 41402

Figure 70
Ratio of Actual to Predicted Film Coefficient vs Axial Location (Flox-Butene-1, Injector No. 7)

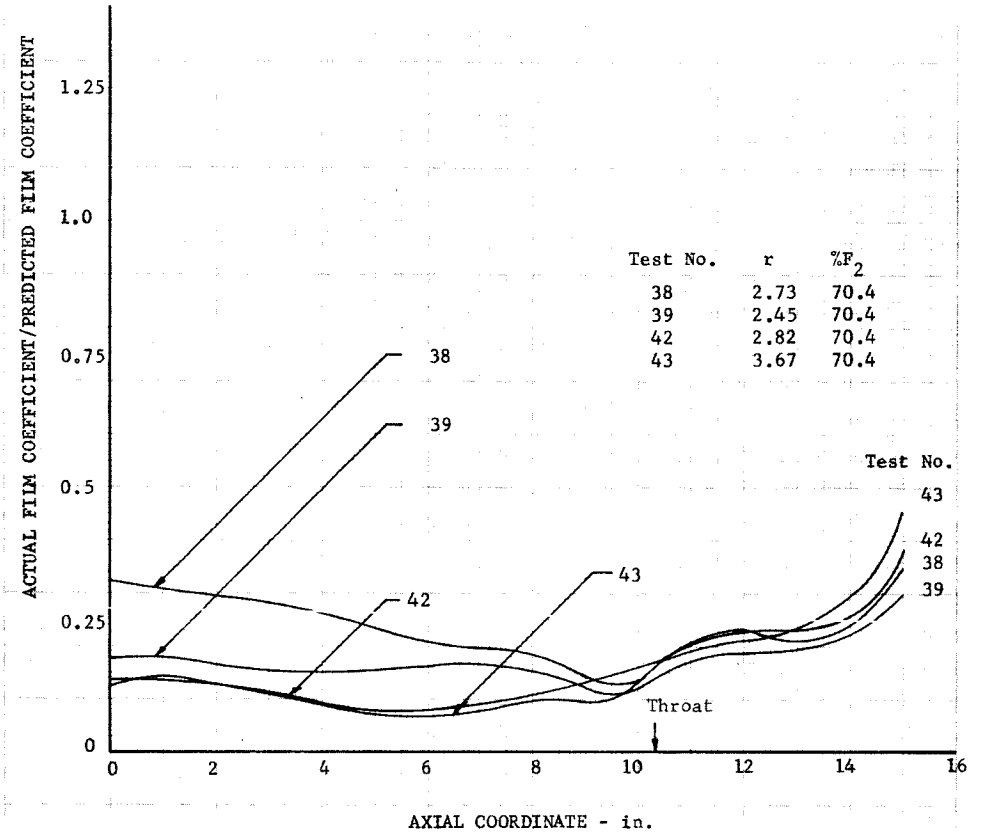

DF 41403

Figure 71 shows the ratio of experimental-to-predicted total heat transfer rate plotted as a function of mixture ratio for the uncooled tests. Figure 72 shows this same data for the regeneratively cooled tests. The "X" on each of the curve shows the interpolated value of the ratio of experimental-to-predicted total heat transfer rate at the mixture ratio for maximum theoretical specific impulse. Figure 73 shows the interpolated ratio of actual-to-predicted total heat transfer rate as a function of hydrogen/carbon atomic ratio for each of the four fuels tested. The curve shows a remarkably good correlation of the effect of decreasing hydrogen/carbon ratio on reducing the heat transfer rate to the chamber walls. The difference in magnitude shown in the cooled and uncooled data is probably due primarily to the integrating effect of the cooled data, i.e., uncooled temperature measurements are taken along one axial line and do not show the effects of hot spots due to injector nonuniformity. The trends shown in the two curves are, however, quite similar. The reduction in heat transfer rate is almost certainly due to increased carbon on the walls and free carbon in the boundary layer at decreased hydrogen-to-carbon ratios.

Figure 71
Ratio of Measured to Predicted Total Heat Transfer (Uncooled Tests)*

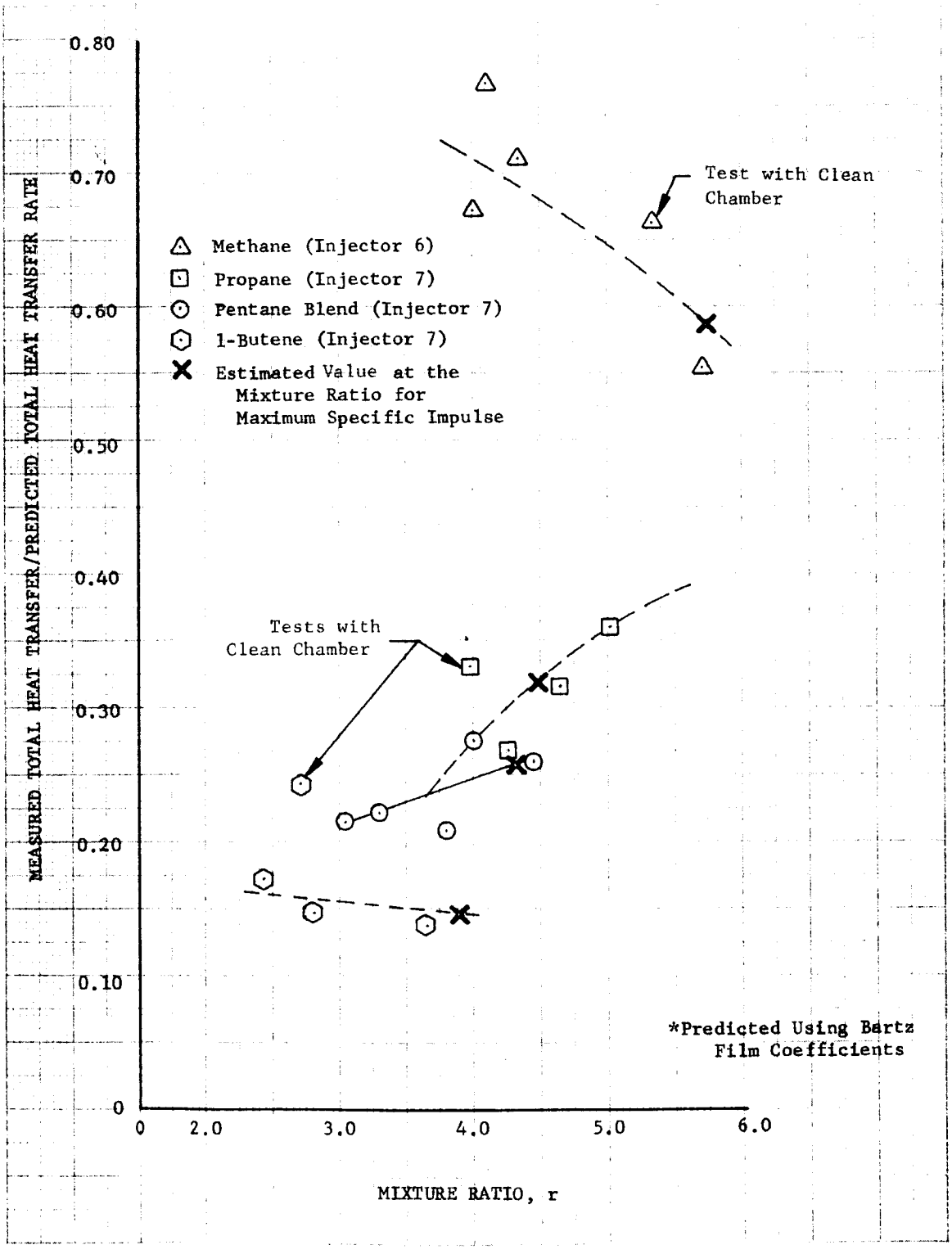

DF 41404

Figure 72
Ratio of Measured to Predicted Total Heat Transfer (Regeneratively Cooled Tests)*

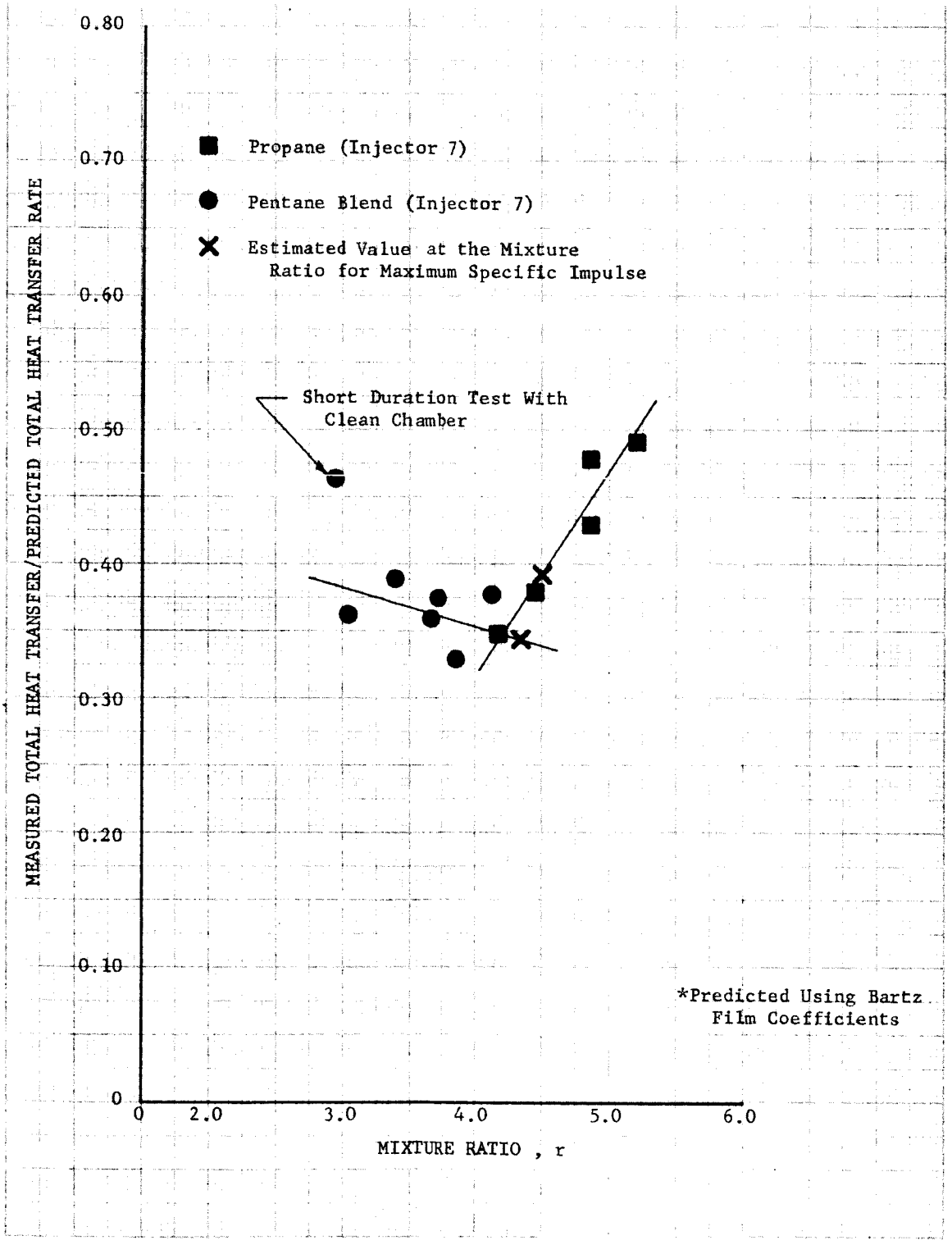

DF 41405

Figure 73
Effect of Fuel Hydrogen-to-Carbon Ratio on Total Chamber Heat Transfer

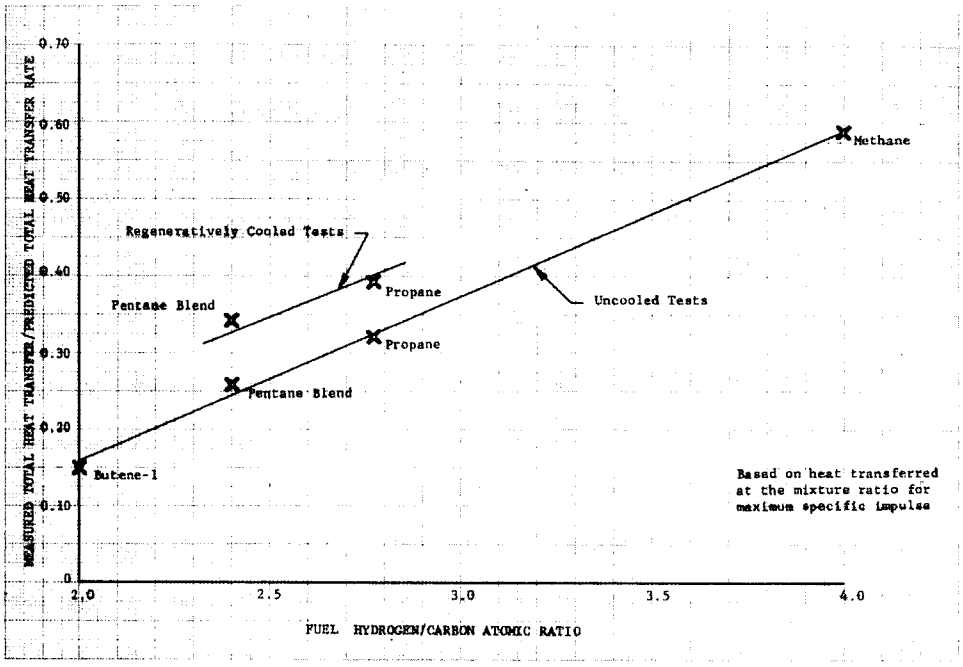

DF 40661

Injector design will have a major effect on the total heat transfer and on the distribution of the heat transfer. Combustion efficiency can also be a major factor in influencing heat transfer rates. These effects did not, however, significantly influence the trends in figure 73. All of the test data summarized in figure 73 were obtained with similar injectors (the pentane, propane, and butene-1 data were obtained with the same injector). Combustion efficiencies near the maximum specific impulse mixture ratio were nearly the same for the methane, propane, and butene-1 tests. In addition, all calculations of predicted heat transfer were corrected for the combustion efficiency measured in that test. For all four of the fuels, a substantial change in combustion efficiency over the mixture ratio range investigated shows a small change in the ratio of actual to predicted heat flux compared to the very large change in this ratio between the various fuels. While a radically different injector design might greatly change the ratio of actual to predicted heat flux obtained, it would be expected that the tendency of the ratio to decrease significantly with decreasing hydrogen-to-carbon ratio in the fuel would always be observed. Also, since high performance and low heat flux was obtained with both propane and butene-1 it would be expected that any new injector required for any flox-hydrocarbon combination could be developed to produce reduced heat fluxes comparable to those obtained in this program.

The effect of carbon buildup on heat transfer rate may be seen in figures 74 through 76 showing the heat flux versus time curves for points near the injector, nozzle throat, and nozzle exit. The solid lines in figures

74 and 76 show the heat flux measured with a clean copper chamber while the dotted lines show the heat flux measured on subsequent firings after a carbon deposit was present on the walls. The solid line in figure 75 shows the heat flux measured with a relatively light carbon deposit (one two-second ignition check has previously been made with the chamber), and the dotted line shows the next succeeding test, where a heavier deposit was present at the start of the test. Examination of these curves leads to two conclusions:

1. As the hydrogen-to-carbon ratio of the fuel decreases (with consequent reduction of the percentage of theoretical heat flux), the time dependent effect of carbon buildup increases. Eventually a steady-state layer is built up and the heat flux remains constant with time. The curves shown in figures 74 through 76 for "dirty" chambers approach this steady-state value.
2. The effect on heat transfer of carbon buildup with time is greatest in the chamber, decreases in the throat and is quite small in the exhaust nozzle.

C. REGENERATIVE COOLING

The ability to cool the thrust chamber in either the nucleate or film boiling regimes, as demonstrated in twelve successful tests with propane and the eutectic pentane blend, is due to the low experimental heat fluxes encountered. Previous calculations had clearly shown that regenerative cooling of a 5000-lb thrust 100-psia chamber with film boiling was impossible and that film boiling would cause chamber burnout, if the calculated theoretical heat fluxes were correct. The low heat fluxes measured with propane, butene-1, and the pentane blend greatly reduced the coolant flowrates required to prevent film boiling from occurring and also reduced the wall temperatures to below the point of tube burnout when film boiling did occur.

It may be concluded that the development of a regenerative cooled 5000-lb thrust 100-psia chamber pressure flox-light hydrocarbon engine is feasible using either butene-1 or a eutectic blend of pentane and isopentane as the fuels. While cooling with propane has also been shown to be possible, the propane would leave the heat exchanger at near saturation conditions, and boiling of the propane in the injector would cause severe problems in injector design and engine control. The use of ablation cooled exhaust nozzles or partial film or transpiration cooling could, however, be used to reduce the total heat transferred to the propane, thereby making a 5000-lb thrust flox-propane engine feasible. Also, larger engines would result in less heat transferred per pound of coolant so that for 100-psi engines above 8000 to 10,000 pounds thrust, full regenerative cooling with propane would be possible.

Figure 74
Time Variation of Heat Flux and Chamber Pressure
(Flox-Methane)

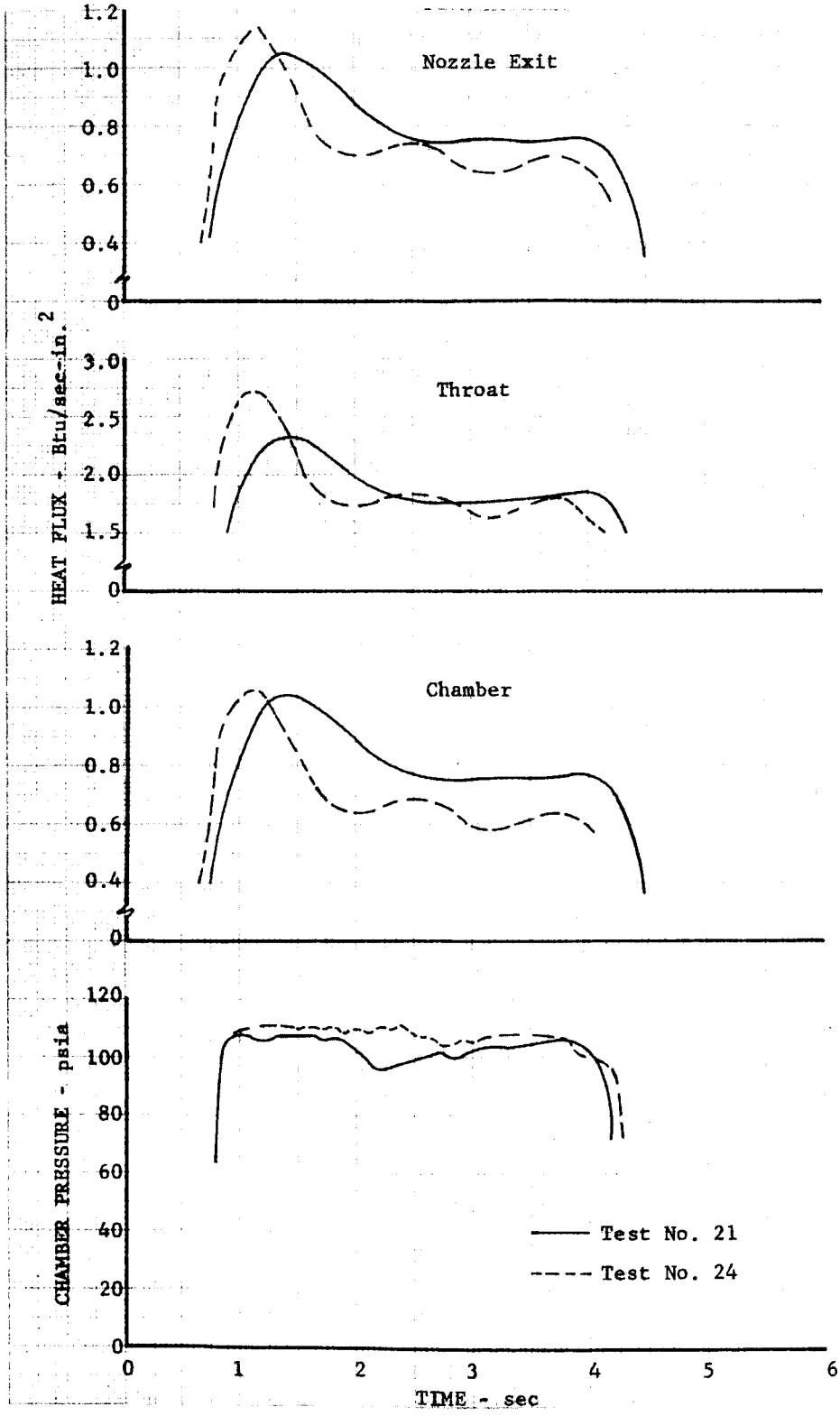

DF 42077

Figure 75
Time Variation of Heat Flux and Chamber Pressure
(Flox-Propane)

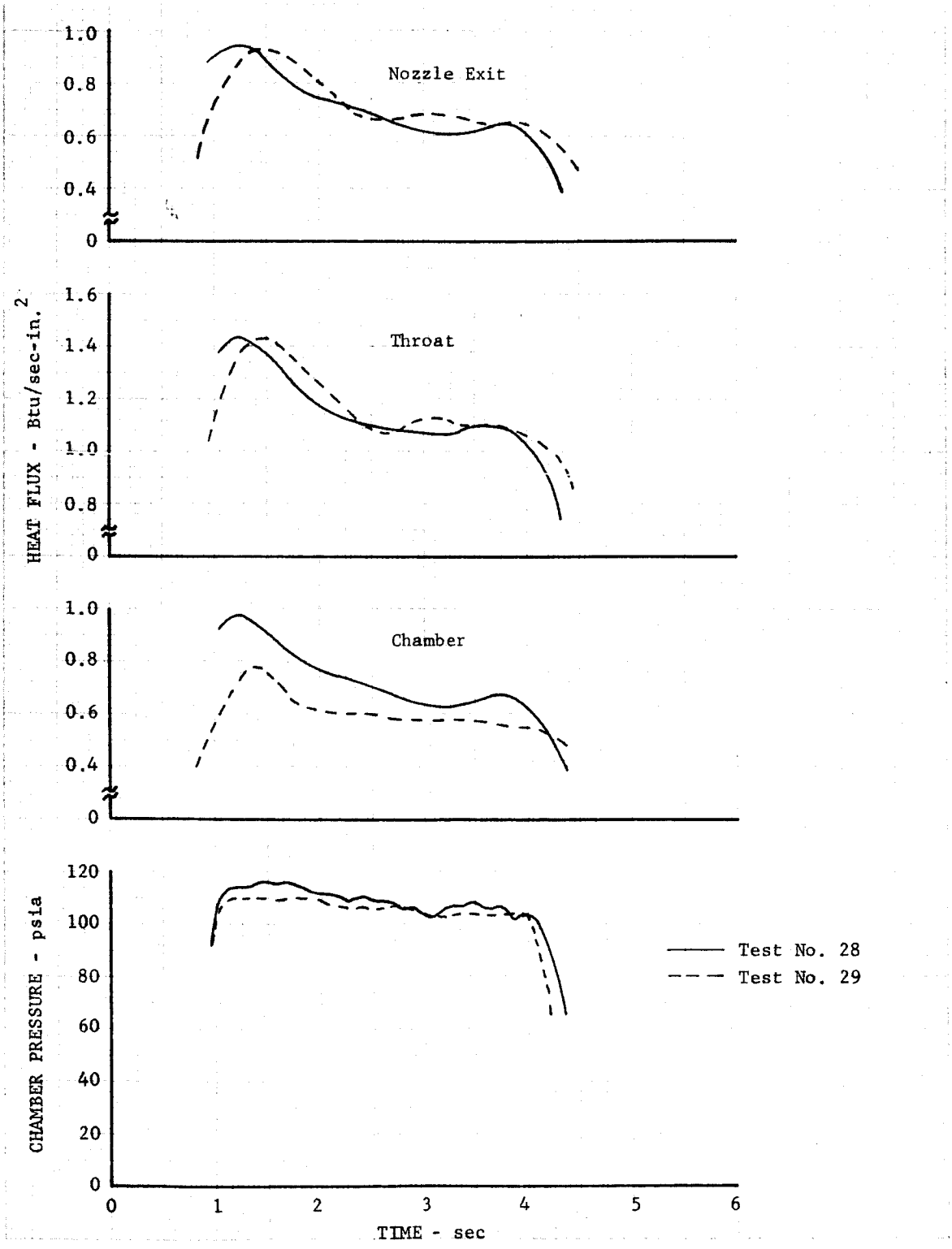

DF 42078

Figure 76
Time Variation of Heat Flux and Chamber Pressure
(Flox-Butene-1)

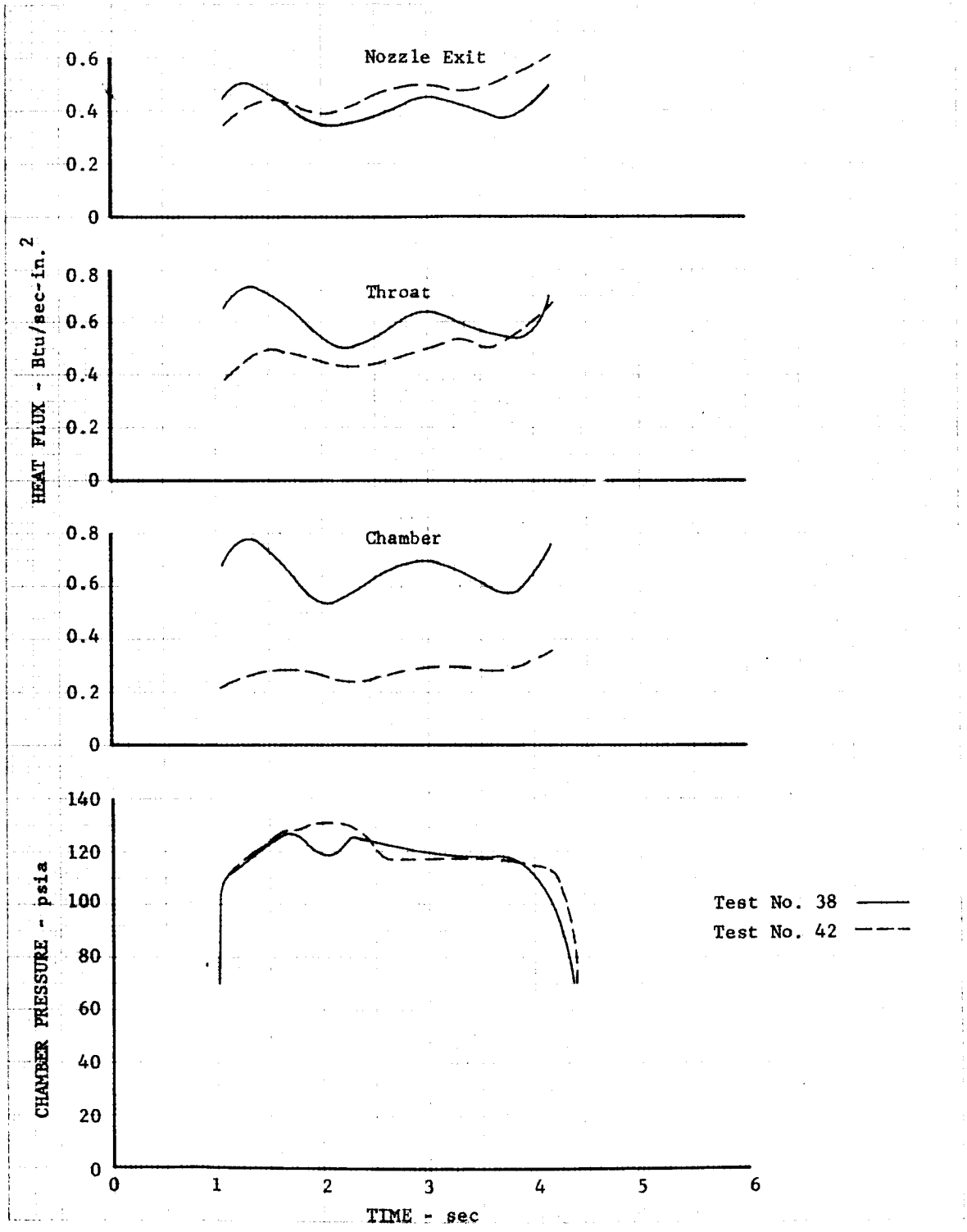

DF 42079

D. TRANSPIRATION COOLING

Two correlations of the data from the transpiration cooled flox-methane and flox-propane tests were used to evaluate the data. The first correlation (figures 77 through 80) is an evaluation of the cooling ability of the fuels, while the second correlation (figures 81 through 84) is an evaluation of the performance loss due to incomplete mixing between the coolant flowing through the porous walls and the burning propellants from the injector.

Figure 77 shows the ratio of the measured heat flux to the chamber walls, as determined from a heat balance based on measured coolant flow and measured surface temperature, to the predicted heat flux based on results of the uncooled thrust chamber firings. Figure 78 shows the same ratio for the same tests, except that the predicted heat flux is based on analytically determined values using the Bartz short form method. Except for the two segments nearest the injector (where the experimental heat flux from the uncooled tests was higher than the predicted heat fluxes) figure 78 shows values closer to the anticipated value of 1.0 (or slightly less) than figure 77. Figures 79 and 80 show the same data for the flox-propane transpiration cooled tests. Again the ratios based on the analytically predicted film coefficient show much better agreement. The data tend to indicate that the factors causing a reduction in uncooled heat transfer (presumably carbon deposition on the wall or free carbon in the boundary layer) are partially negated by the transpiration coolant flow and that analytically predicted film coefficients based on the Bartz short form method are more valid.

Figures 81 and 82 show the ratio of experimental characteristic velocity (c*) to the predicted c* for methane and propane, respectively. The predicted c* includes correction of injector c* for combustion efficiency as determined in the uncooled tests, and correction of measured c* and mixture ratio to include only the coolant flow introduced upstream of the throat. (All results in Section VII use total coolant flow rather than coolant flow upstream of the nozzle throat.) For methane the actual c* is greater than the predicted c* in all cases but one, and this case is within one percent of the predicted value – within the experimental accuracy of the data. With propane, the opposite is true. The actual c* losses are in all cases equal to or greater than the predicted losses. Figures 83 and 84 show the percent characteristic velocity loss due to transpiration cooling to the percentage of coolant used. As would be predicted both coolants show a tendency for increasing loss per percent coolant as mixture ratio is increased.

Figure 77
Ratio of Measured Heat Flux to Predicted Heat Flux vs Thermocouple Location*

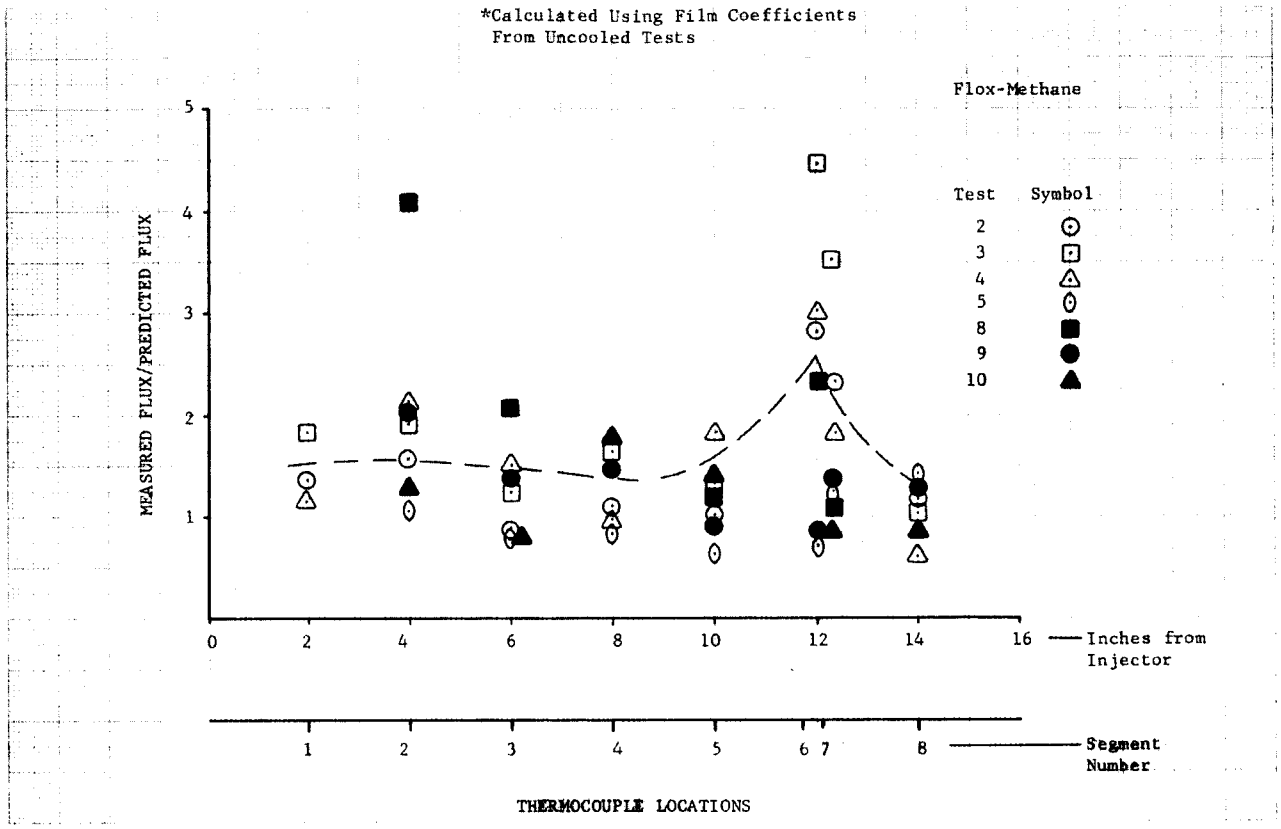

Figure 78
Ratio of Measured Heat Flux to Predicted Heat Flux vs Thermocouple Location*

DF 39398
Sheet 1 of 2

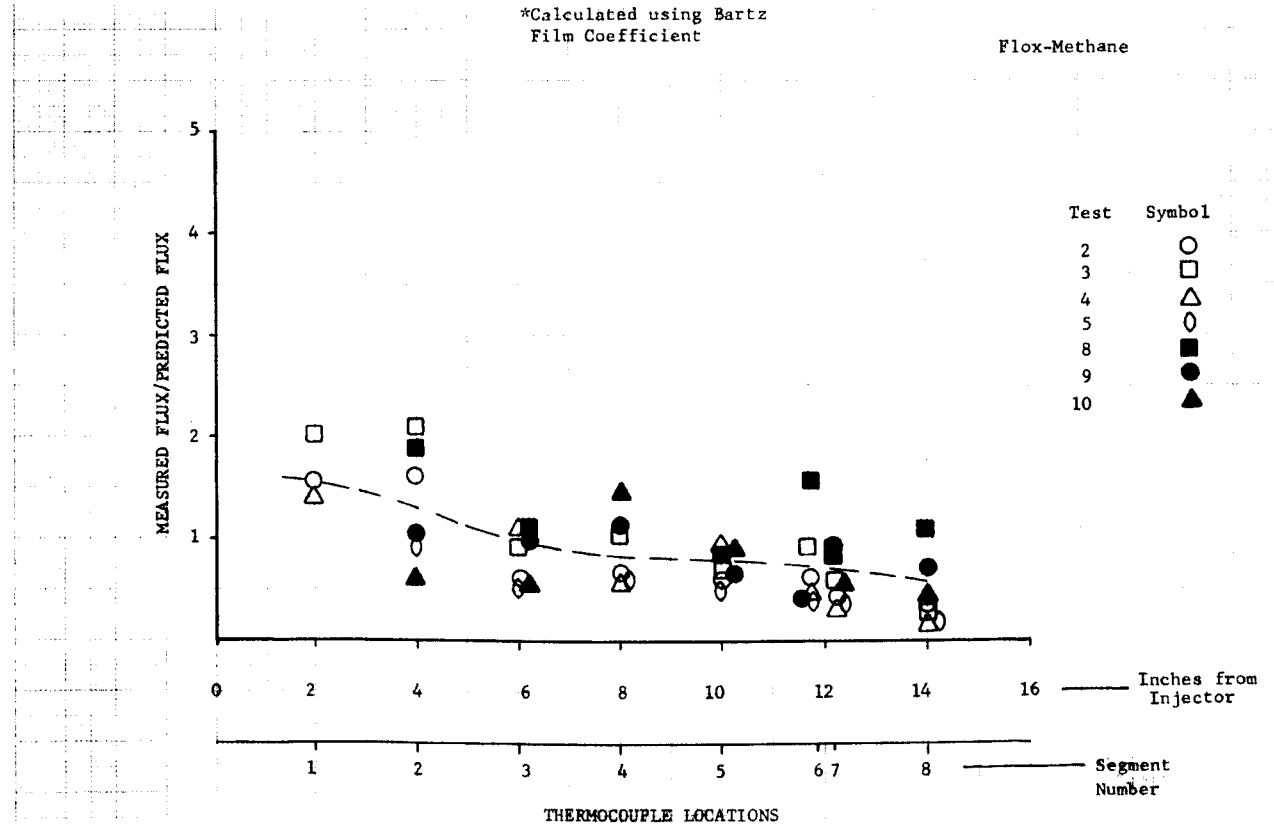

DF 39398
Sheet 2 of 2

Figure 79
Ratio of Measured Heat Flux to Predicted Heat Flux vs Thermocouple Location*

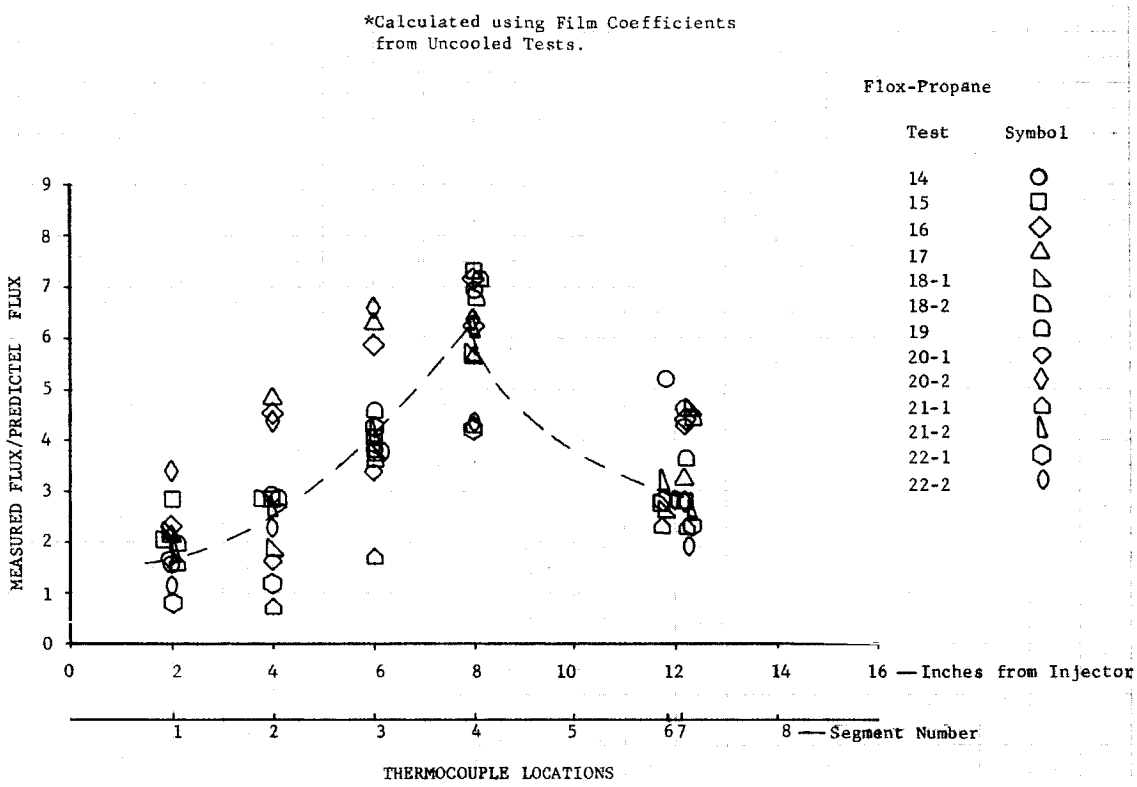

DF 41406

Figure 80
Ratio of Measured Heat Flux to Predicted Heat Flux vs Thermocouple Location*

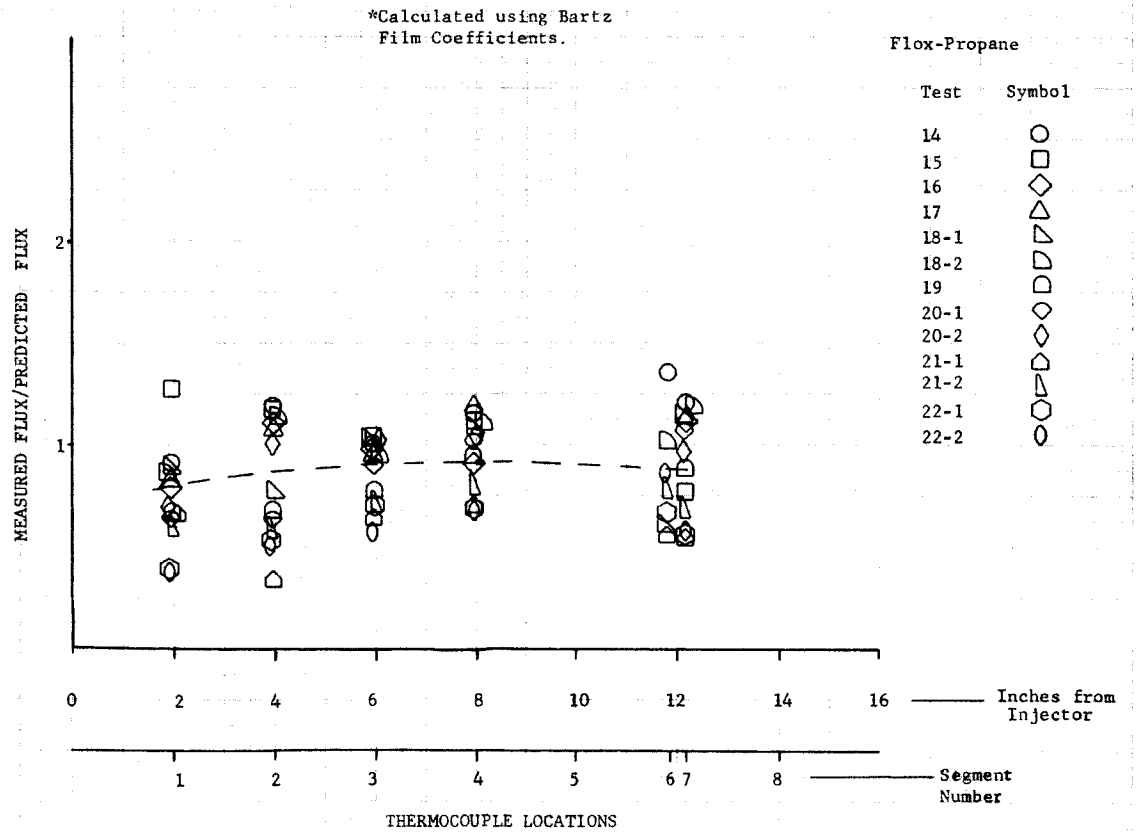

DF 41407

Figure 81
Actual to Predicted c Ratio vs Chamber Mixture Ratio*

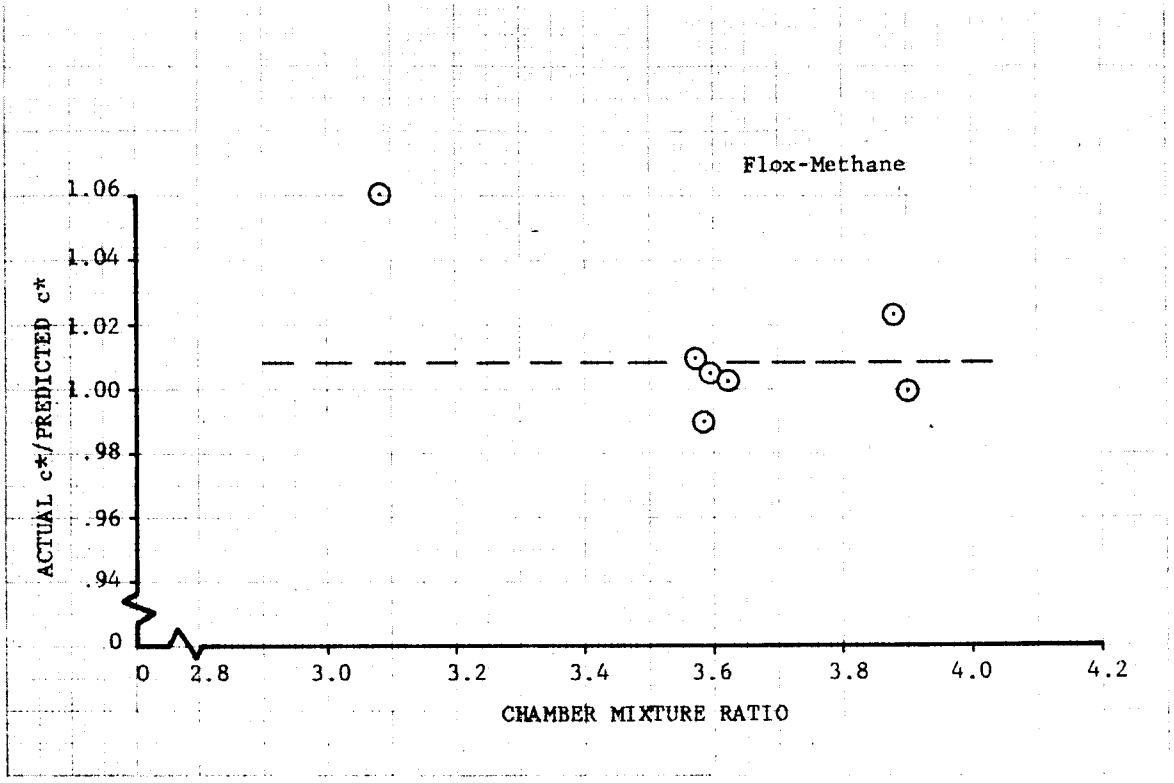

DF 42235

Figure 82
Actual to Predicted c Ratio vs Chamber Mixture Ratio*

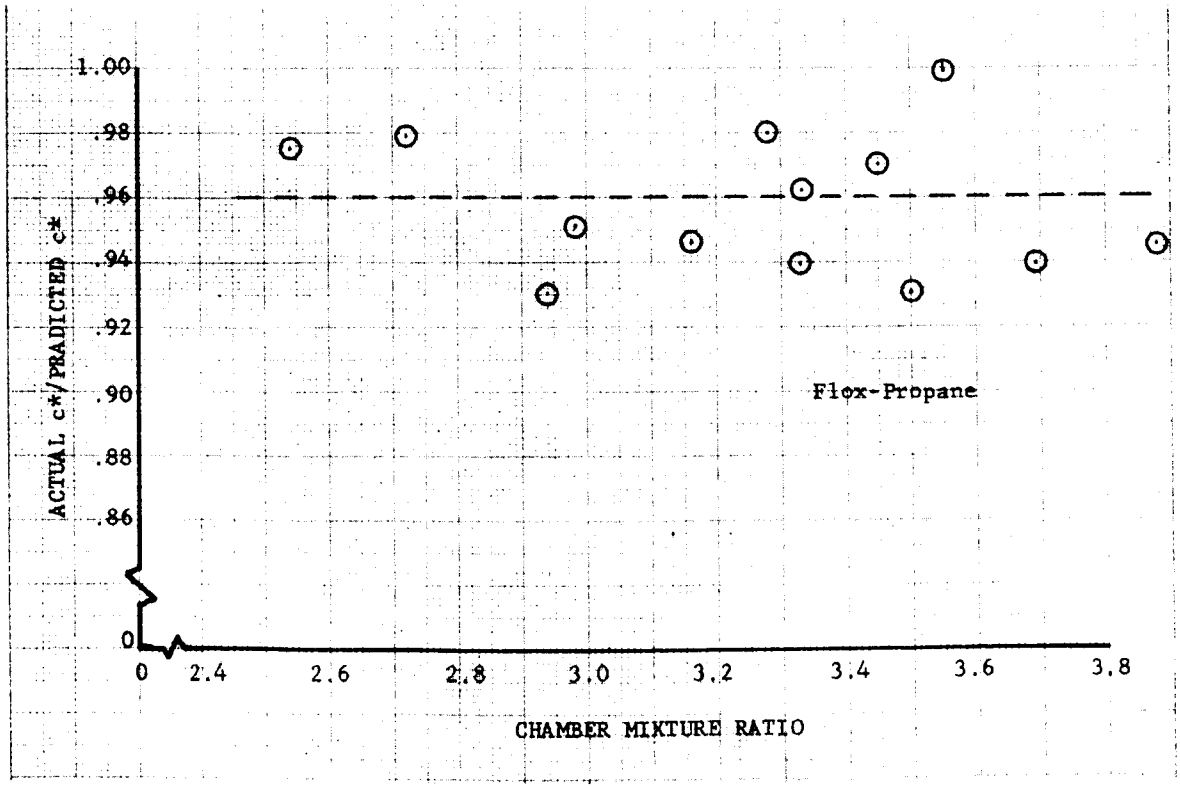

DF 42236

Figure 83
Effect of Mixture Ratio on Experimental c Loss Due to Transpiration Cooling (Flox-Methane)*

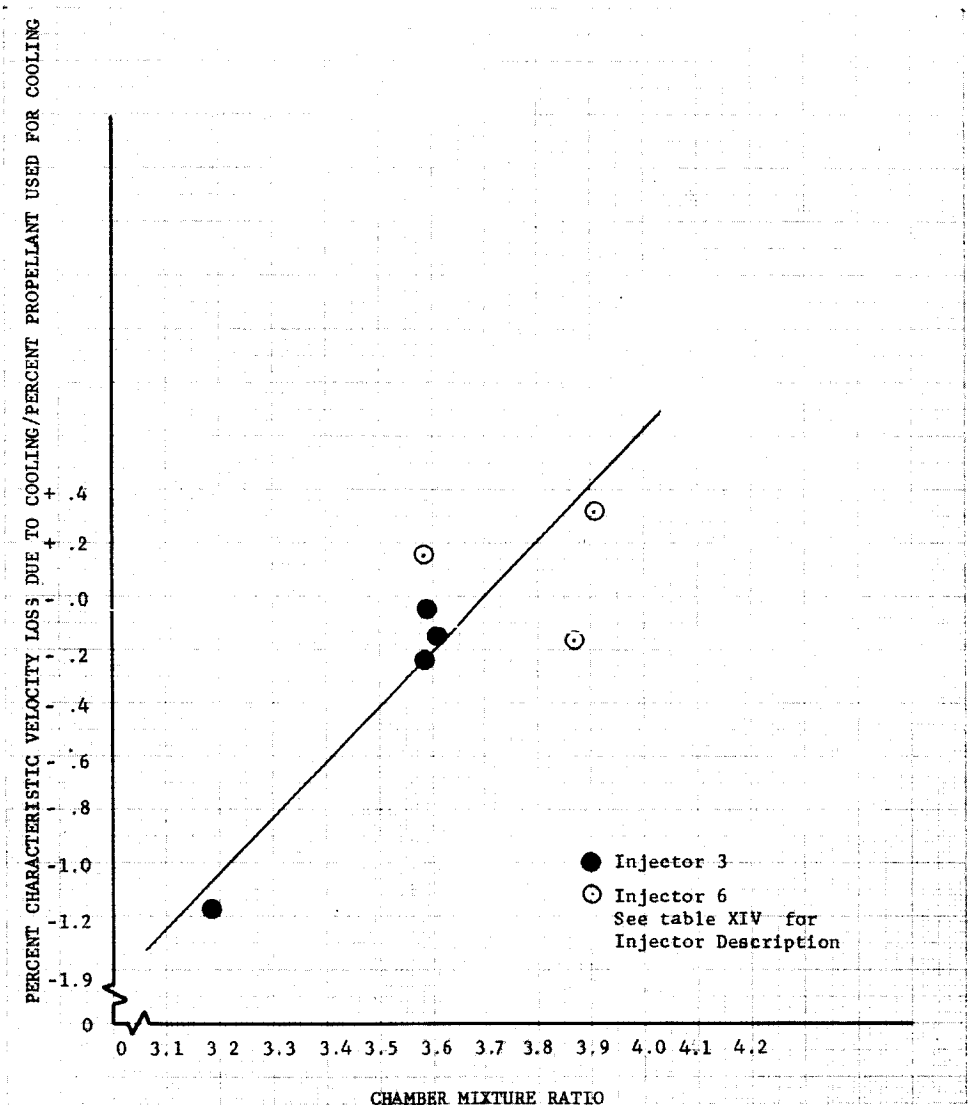

DF 40658

No good explanation is currently available for the high c* losses encountered with the propane tests. There are indications of a nonuniform injector pattern which would increase losses by allowing some of the propane to expand without being heated to a temperature where it could contribute substantially to performance. Another explanation might be that cracking of the propane in the boundary layer was releasing substantial quantities of free solid carbon that could have had a high velocity lag relative to the exhaust gas, thereby reducing the characteristic velocity. It would be expected, however, that a large amount of cracking of the propane would increase its cooling capacity, thereby reducing cooling requirements. This was not the case.

Figure 84
Effect of Mixture Ratio on Experimental c Loss Due to Transpiration Cooling (Flox-Propane)*

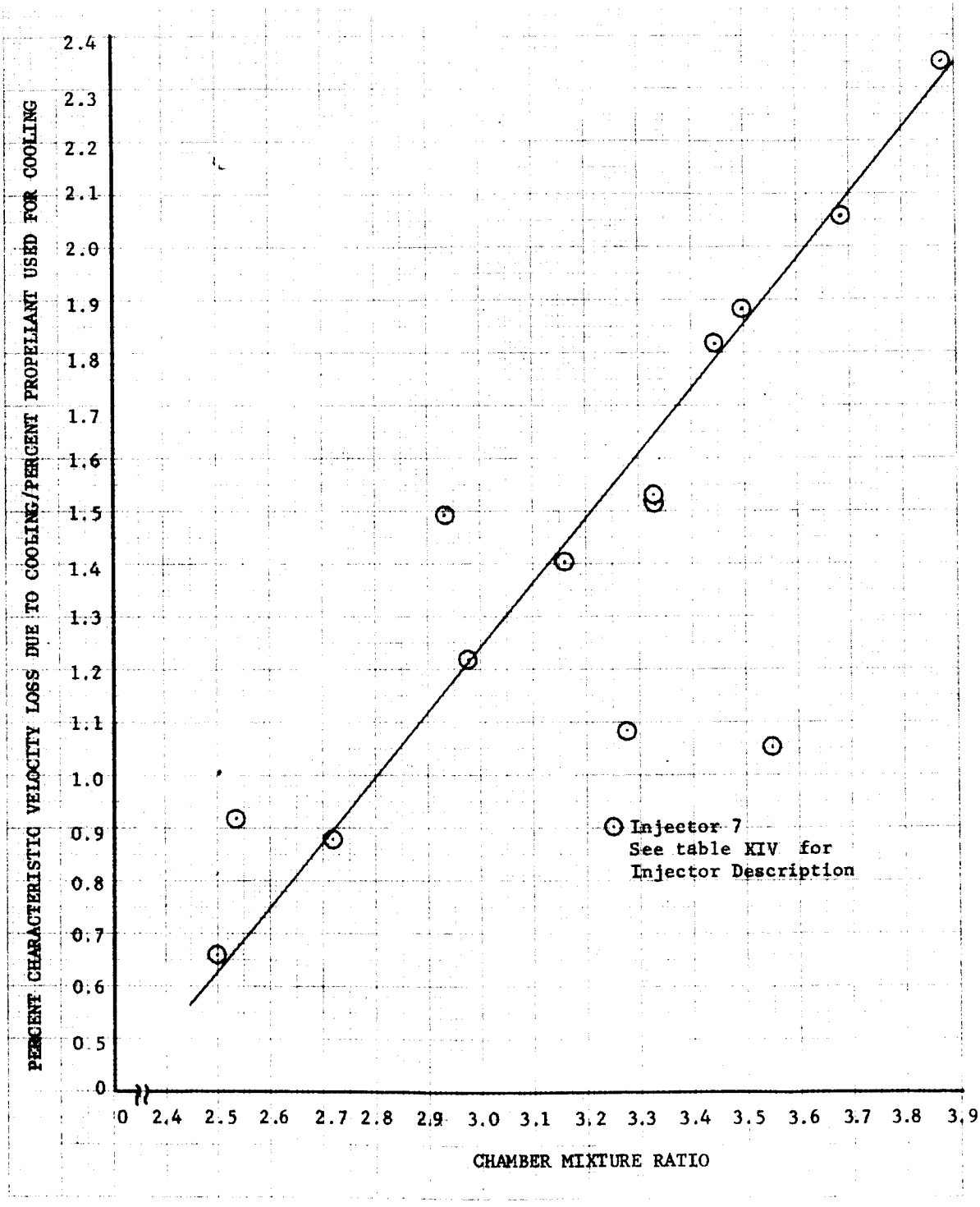

TABLE A-I. PHYSICAL PROPERTIES OF SELECTED HYDROCARBON COMPOUNDS

Appendix Index Number	Name	Chemical Symbol	Molecular Weight	Freezing[4] Point, °R	Boiling[4] Point, °R	Liquid[4] Range, °T	Critical Temperature, °R	Critical Pressure, psia	Liquid[1] Density lb/ft3	Ivac[2] with Flox	Mixture Ratio for Max Ivac	Weight Percent Fluorine in Flox	Cooling[5] Merit Rating
	Flox[3] (fluorine-oxygen blends)	$F_2 + O_2$	≈36.3	90	≈155	≈ 65	≈266	≈788	≈ 87.4				
A-1	Methane	CH_4	16.04	163	201	38	343	673	26.5	418	5.75	82.6	0.13
	Acetylene	C_2H_2	26.04	344	341	- 3	563	910	26.0			54.3	
A-2	Ethylene (ethene)	C_2H_4	28.05	187	305	118	510	750	35.5	409	3.85	70.4	0.23
A-3	Ethane	C_2H_6	30.07	162	332	170	550	708	34.1	411	4.82	78.1	0.26
A-4	Methyl-acetylene (allylene)	C_3H_4	40.06	309	450	141	722	866	42.1	403	3.08	61.3	0.37
	Propadiene (allene)	C_3H_4	40.06	229	434	205	709	1030	37.1			61.3	
A-5	Propylene (propene)	C_3H_6	42.08	158	406	248	656	667	38.0	405	3.85	70.4	0.41
	Cyclopropane	C_3H_6	42.08	262	432	170	716	793	44.9			70.4	
A-6	Propane	C_3H_8	44.09	154	416	262	666	619	36.4	408	4.5	76.0	0.37
	Diacetylene (butadiyne)	C_4H_2	50.06	427	508	81						37.3	
	Butyne-1 (ethyl-acetylene)	C_4H_6	54.09	266	507	241	835	955	40.6			64.1	
	Butyne-2 (Crotonylene)	C_4H_5	54.09	434	540	106	880	891	43.3			64.1	
	Butadiene-1, 2 (methy-allene)	C_4H_6	54.09	246	511	265	803	653	40.7			64.1	
	Butadiene-1, 3 (erythrene)	C_4H_6	54.09	296	484	188	768	661	38.8			64.1	
A-7	Butene-1 (α - butylene)	C_4H_8	56.10	158	480	324	755	583	38.6	404	3.85	70.4	0.50
	Cis-butene-2	C_4H_8	56.10	242	499	257	776	544	39.0			70.4	
	Trans-butene-2	C_4H_8	56.10	302	495	193	770	544	38.0			70.4	
	Methyl-propene (iso-butylene)	C_4H_8	56.10	239	479	240	752	580	37.4	403	3.85	70.4	
	Cyclobutane	C_4H_8	56.10	338	512	174	845	734	43.9			70.4	
	Methyl-cyclopropane	C_4H_8	56.10		500				43.1			70.4	
A-8	n-Butane (butane)	C_4H_{10}	58.12	243	491	248	766	550	37.5	407	4.38	74.8	0.39
	Iso-butane (methyl propane)	C_4H_{10}	58.12	204	471	267	735	529	34.8	407	4.38	74.8	
	Pentyne-1 (propyl-acetylene)	C_5H_8	68.12	301	565	264	889	588	43.1			65.5	
	Pentyne-2 (valerylene)	C_5H_8	68.12	312	592	280	920	610	44.4			65.5	
	Pentadiene-1, 3	C_5H_8	68.12	375	568	193	880		42.2			65.5	
	Pentadiene-1, 4	C_5H_8	68.12	226	539	313	810	550	41.5			65.5	
	Methyl-butadiene-1, 3 (isoprene)	C_5H_8	68.12	229	533	304	855	558	42.5			65.5	
	Methyl-butadiene-2, 3 (dimethyl-allene)	C_5H_8	68.12	273	564	291			42.5			65.5	
	Pentene-1 (amylene)	C_5H_{10}	70.14	195 (233)	545	350 (312)	845	529	40.0	403	3.85	70.4	
	Cis-pentene-2	C_5H_{10}	70.14	169 (220)	543 (559)	374 (339)	858	513	41.0	402	3.85	70.4	
	Trans-pentene-2	C_5H_{10}	70.14	239 (249)	545 (557)	306 (305)	856	513	40.5			70.4	
	2-Methyl-butene-1	C_5H_{10}	70.14	244	548	304	847	529	40.6			70.4	
	2-Methyl-butene-2	C_5H_{10}	70.14	243 (251)	561	318 (310)	861	513	41.3			70.4	
	3-Methyl-butene-1 (iso-amylene)	C_5H_{10}	70.14	188	528	340	823	544	39.1	402	3.85	70.4	
	Cyclopentane	C_5H_{10}	70.14	322	581	259	930	675	46.5	400	3.85	70.4	
A-9	n-Pentane-(pentane)	C_5H_{12}	72.15	258	557	299	846	479	38.7	404	4.34	74.0	0.48
A-10	Iso-pentane (methyl-butane)	C_5H_{12}	72.15	204	542	338	829	476	38.3	403	4.34	74.0	0.50
	Dimethyl-propane (neo-pentane)	C_5H_{12}	72.15	459	509	50	789	514	38.3			74.0	
	Hexyne-1	C_6H_{10}	82.15	244	625	381	966	513	44.9			66.4	
	Hexadiene-1, 5 (diallyl)	C_6H_{10}	82.15	239	599	360	938	500	43.1			66.4	
	Hexene-1 (α-hexylene)	C_6H_{12}	84.16	242	606	364	923	500	42.0			70.4	
	Cis-hexene-2	C_6H_{12}	84.16	229	615	386	933	500	43.0			70.4	
	Trans-hexene-2	C_6H_{12}	84.16	253	614	361	932	500	42.6			70.4	
	Cis-hexene-3	C_6H_{12}	84.16	249	612	363	932	500	42.7			70.4	
	Trans-hexene-3	C_6H_{12}	84.16	288	614	326	933	500	42.6			70.4	
	2, 3 - Dimethyl-butene-1	C_6H_{12}	84.16	239	592	353	902	470	42.3			70.4	
	3, 3 - Dimethyl-butene-1	C_6H_{12}	84.16	284	566	282	882	457	40.8			70.4	
	Cis-3-methyl-pentene-2	C_6H_{12}	84.16	243	619	376	932	476	43.6			70.4	
	Trans-3-methyl-pentene-2	C_6H_{12}	84.16	248	614	366	939	478	43.3			70.4	
	4-Methyl-pentene-1	C_6H_{12}	84.16	217	589	372						70.4	
A-11	Methyl-cyclopentane	C_6H_{12}	84.16	235	621	385	959	549	46.4	400	3.85	70.4	0.51
	n-Hexane (hexane)	C_6H_{14}	86.17	320	615	295	915	432	41.1			73.5	
A-12	2-Methyl-pentane	C_6H_{14}	86.17	215	600	387	897	455	40.5	404	4.2	73.5	0.59
	3-Methyl-pentane (neo-pentane)	C_6H_{14}	86.17	280	606	326	503	440	41.5			73.5	
	2, 3 - Dimethyl-butane	C_6H_{14}	86.17	261	596	335	501	455	41.3			73.5	
A-13	RP-1[3]	$(CH_{1.9})_n$	172	420	882	472	1218	315	49.7	396	3.75	69.3	0.80

(1) Values taken at the normal boiling point or 537°R, whichever is lower.
(2) Based on shifting equilibrium expansion with both propellants at their normal boiling points, 100 psia chamber pressure, nozzle exit area ratio of 40 and mixture ratio for maximum specific impulse.
(3) Listed for comparison
(4) Numbers in parentheses indicate conflicting data from two sources that are considered equally reliable.
(5) The regenerative coolant merit rating is defined as the heat capacity of the fuel divided by the total heat transferred to a 5K chamber (100 psia chamber pressure - expansion area ratio of 40) while maintaining a 2160°R wall temperature. The heat capacity of the liquid fuel is taken between its freezing temperature and the temperature at which the vapor pressure equals 150 psia.

APPENDIXES

APPENDIX A
FUEL CHARACTERISTICS

This appendix presents physical property data for twelve of the light hydrocarbon compounds that are considered to have the properties most desirable in rocket fuels to be used with fluorine-oxygen (flox) oxidizer blends. Selection of these fuels was based on their liquid range compatibility with flox either individually or in blends, their cost and availability, their high performance and their capability for use as regenerative or transpiration coolants. Data on RP-1 is also included for comparison. The following liquid properties are plotted as a function of temperature: vapor pressure, density, specific heat, viscosity and thermal conductivity. Origin of the data shown on these curves is coded as follows: (1) solid line-experimental data from the references given at the end of the Appendix, (2) dashed line-extrapolated and (3) dot dash line-estimated. The heats of formation presented are based on the elements in their reference state at 537°R. In cases where conflicting property data were found, the reference believed to be most accurate was used. In addition to physical property data, a summary of shipping, handling, toxicity and cost information is presented. Cost data are estimates from various manufacturers and in most cases are not from quotations.

Shipping, handling and storage problems and materials compatibility are similar for all of the compounds presented; therefore, this information is summarized here to avoid repetition on the individual data sheets.

1. SHIPPING

The fuels presented here can be classified into either of two shipping categories: (1) flammable liquid or (2) flammable compressed gas. All require an Interstate Commerce Commission (I.C.C.) red label for shipping. Requirements for shipping such materials are detailed in reference 13.

a. Flammable Liquids – Those compounds with normal boiling points above 537°R are classified as flammable liquids. They are shipped in tightly closed steel containers under their own vapor pressure. The exception is RP-1 which has an extremely high boiling point and can be shipped and handled in the same manner as kerosene or other common jet fuels.

b. Flammable Compressed Gases – Those compounds with normal boiling points below 537°R are classified as compressed gases and are shipped in pressurized steel containers.

2. HANDLING AND STORAGE

The major hazard in handling these compounds is attributed to their extreme flammability. They should be kept away from ignition sources, and flames should never be used for leak detection. All equipment should be grounded. The storage area should be well ventilated to prevent ac-

cumulation of combustible mixtures. They should not be stored with oxygen, chlorine or other oxidizing materials. Containers should be protected from excessive temperature increases by shielding them from radiators, the direct rays of the sun or other sources of heat. In addition, the general rules for handling and storing compressed gas cylinders should be followed (reference 12).

3. CONSTRUCTION MATERIALS

None of these compounds are considered corrosive and any common or commercially available metal may be used. The exception to this is methylacetylene which should not be used with copper, silver or magnesium.

Some non-metallic compounds are attacked by petroleum compounds. The attack occurs in one of the following two forms:

1. The material becomes spongy. Natural rubber is one material affected in this manner.
2. In some plastics one component is dissolved out leaving a brittle base material.

Selection of non-metallic materials will be greatly influenced by the intended use and required length of service. In general, the following materials are acceptable for gasket, seal or coating purposes: neoprene, cork, white asbestos, phenolic asbestos, nylon, fluorocarbon plastics (Teflon and Kel-F) and most epoxy coatings (reference 2). Natural rubber, polypropylene, and glass fabrics with silicone elastomers should be avoided.

METHANE

SUMMARY OF PROPERTIES

		Reference
Chemical formula	CH_4	
Molecular weight	16.042	
Freezing point (normal), °R	163.2	5
Boiling point (normal), °R	200.8	5
Liquid density (at NBP), lb/ft^3	26.48	4
Critical temperature, °R	343.4	5
Critical pressure, psia	673.	5
Critical volume, ft^3/lb	0.0989	5
Heat of vaporization, (at NBP), BTU/lb	219.22	7
Heat of fusion, BTU/lb	25.25	2
Heat of formation (liquid at NBP), BTU/lb	—2400.	8
Autoignition temperature, °R	1630.	2
Flammability limits in air, volume percent	5.3 — 14.	12

I.C.C. CLASSIFICATION—

Flammable compressed gas "Red Gas Label"

TOXICITY

Methane is a non-poisonous, odorless, tasteless gas whose primary danger is as a simple asphyxiant by oxygen displacement. Concentrations up to 9% have not produced apparent effects. Above that percent a pressure on the forehead and eyes is noticed; however, this disappears on breathing fresh air.

COST AND AVAILABILITY

Methane gas is easily obtained in large quantities in cylinders, tube trailers, and tank cars. Liquid methane has only recently become commercially available in this country. Current prices may range from $8.00 to $2.00 per gallon (plus shipping charges) for quantities on the order of several hundred to several thousand gallons. Prices should drop to below $.025/ gallon for very large quantities of commercial grade liquid. Prices given below are for gaseous methane.

Shell Oil Co. (Price FOB Sheridan, Texas)

(95% purity) Tank car lots $100/car (850/lb car)
Transportation – $1,146/car – to WPB, Fla.
Demurrage – $4/car-day after 48 hours

Olefins Div. of Union Carbide (Price FOB Charleston W. Va.)

(95% purity) $0.015/ft^3 ($\approx$ 24 ft^3/lb)
Transportation – furnish own trailers at Charleston, W. Va.

Phillips Petroleum Co. (Prices FOB Borger, Texas unless noted)

(99% purity) tube trailer 60,000 ft^3 (2,500 lb) – $15,000
260 ft^3 cylinder (11 lb) – $75/cyl (FOB WPB, Fla)

(95% purity) 260 ft^3 cylinder (11 lb) – $25/cyl (FOB WPB, Fla)

Transportation $1,120/tractor round trip (48 hr max. turnaround)
$15/day trailer rental

cylinder return $2.65/cylinder
demurrage $2.00/month after 4 months

The Matheson Co. (Prices FOB East Rutherford, New Jersey)

(95% purity) 11 lb/cyl – $36/cyl
$30.00/cyl for more than 6 cylinders
$24.00 for more than 20 cylinders

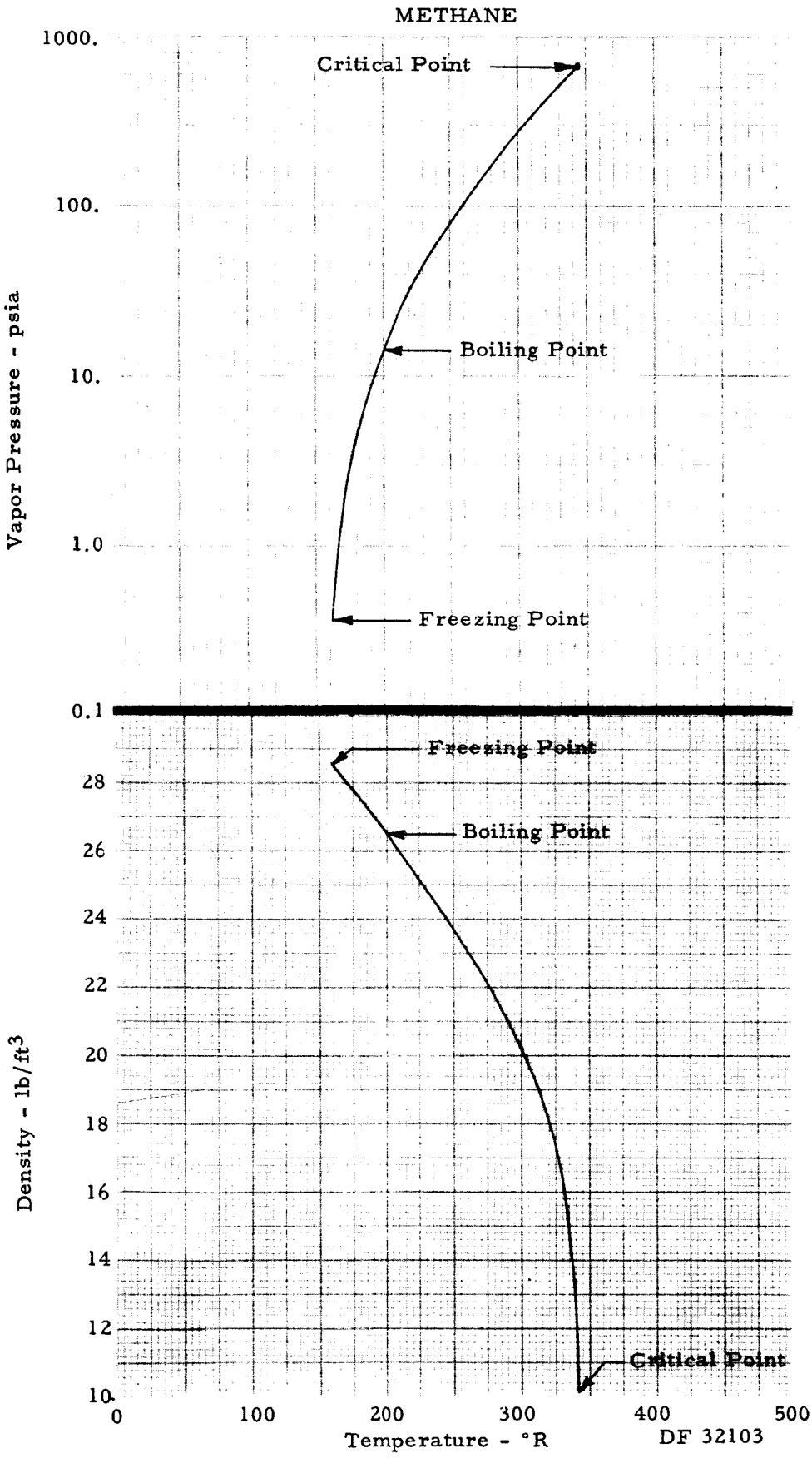
METHANE
1000.
100.
10.
1.0
0.1
Vapor Pressure - psia
Critical Point
Boiling Point
Freezing Point
28
26
24
22
20
18
16
14
12
10
Density - lb/ft3
Freezing Point
Boiling Point
Critical Point
0
100
200
300
400
500
Temperature - °R
DF 32103

METHANE

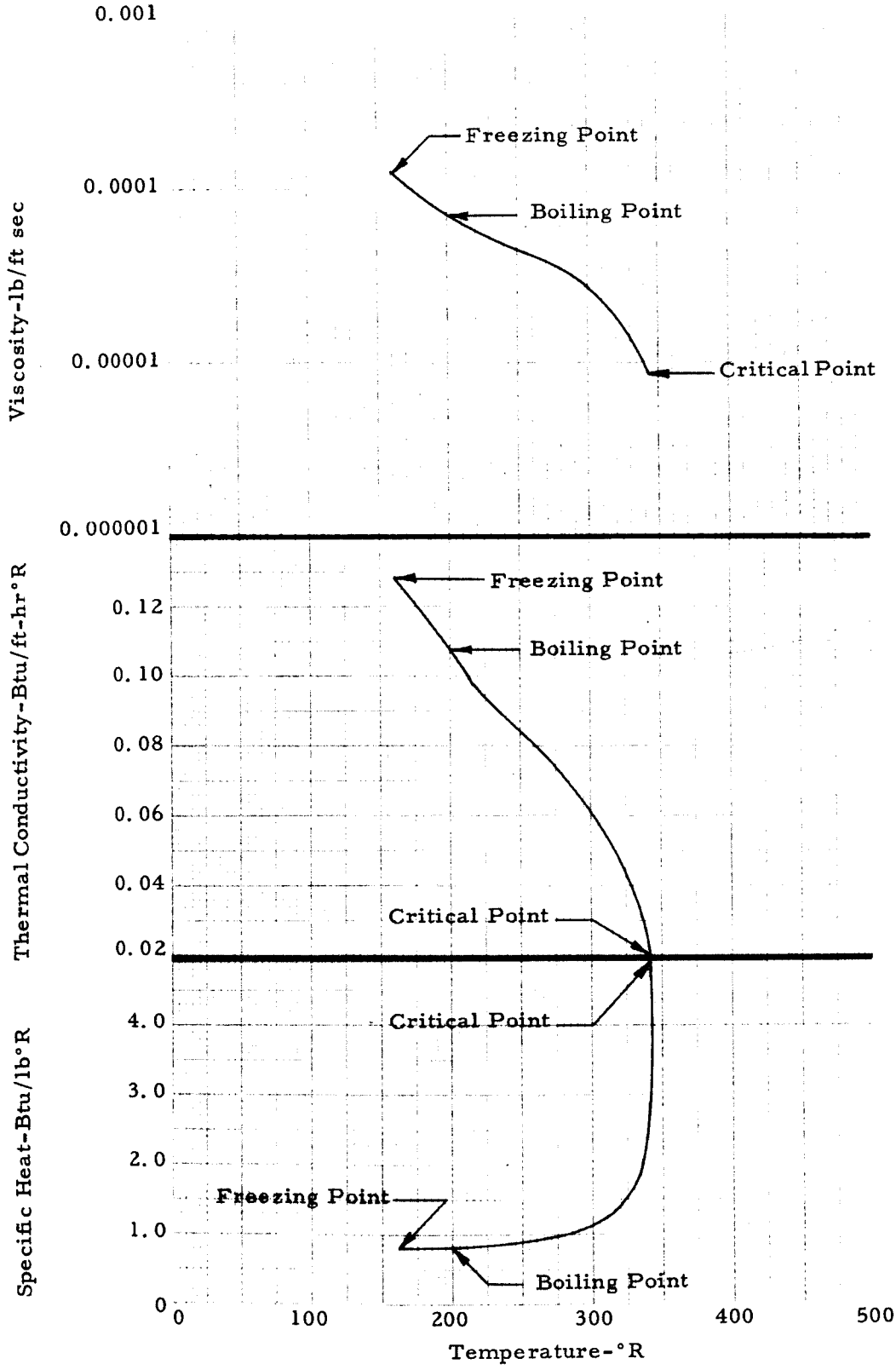
Viscosity-lb/ft sec
0.001
0.0001
0.00001
0.000001
Freezing Point
Boiling Point
Critical Point
Thermal Conductivity-Btu/ft-hr°R
0.12
0.10
0.08
0.06
0.04
0.02
Freezing Point
Boiling Point
Critical Point
Specific Heat-Btu/lb°R
4.0
3.0
2.0
1.0
0
Critical Point
Freezing Point
Boiling Point
0
100
200
300
400
500
Temperature-°R

ETHYLENE
(ETHENE)

SUMMARY OF PROPERTIES

		Reference
Chemical formula	C_2H_4	
Molecular weight	28.052	
Freezing point (normal), °R	187.2	5
Boiling point (normal), °R	305.0	5
Liquid density (at NBP), lb/ft^3	35.486	2
Critical temperature, °R	509.7	5
Critical pressure, psia	750.	5
Critical volume, ft^3/lb	0.0728	5
Heat of vaporization, (at NBP), BTU/lb	207.56	7
Heat of fusion, BTU/lb	51.39	2
Heat of formation (liquid at NBP), BTU/lb	536.	8
Autoignition temperature, °R	1469.	12
Flammability limits in air, volume percent	3.1 – 32.0	12

I.C.C. CLASSIFICATION–

Flammable compressed gas "Red Gas Label"

TOXICITY

Ethylene is a colorless gas with a sweet odor and taste. The toxicity is low, but excess inhalation may cause asphyxia. When inhaled it acts as an anesthetic and depressant. Maximum permissible workroom concentration should not exceed 5500 ppm.

COST AND AVAILABILITY

Phillips Petroleum Co. (Prices FOB Pasadena, Texas)

(99% purity) 30 lb/cyl – $22.50/cyl

Transportation – $5.50/cyl – to WPB, Fla.
$3.66/cyl to return
Cylinder demurrage $2.00/month after 4 months
Tube trailer not recommended for less than 6,000 lb/shipment

Shell Oil Co.

Long term contract would be required on high volume basis. Approximate price $0.05/lb – FOB Texas Gulf Plants

Gulf Oil Co.

Available on Gulf Coast by pipeline at approximately $0.05/lb

The Matheson Co. (Prices FOB East Rutherford, N.J.)

(95% purity) 28 lb/cyl – $26.00/cyl
$20.16/cyl in lots of 6 or more

Phillips Petroleum Co. (Prices FOB Borger, Texas)

(99.8% purity) 30 lb/cyl – $37.50/cyl

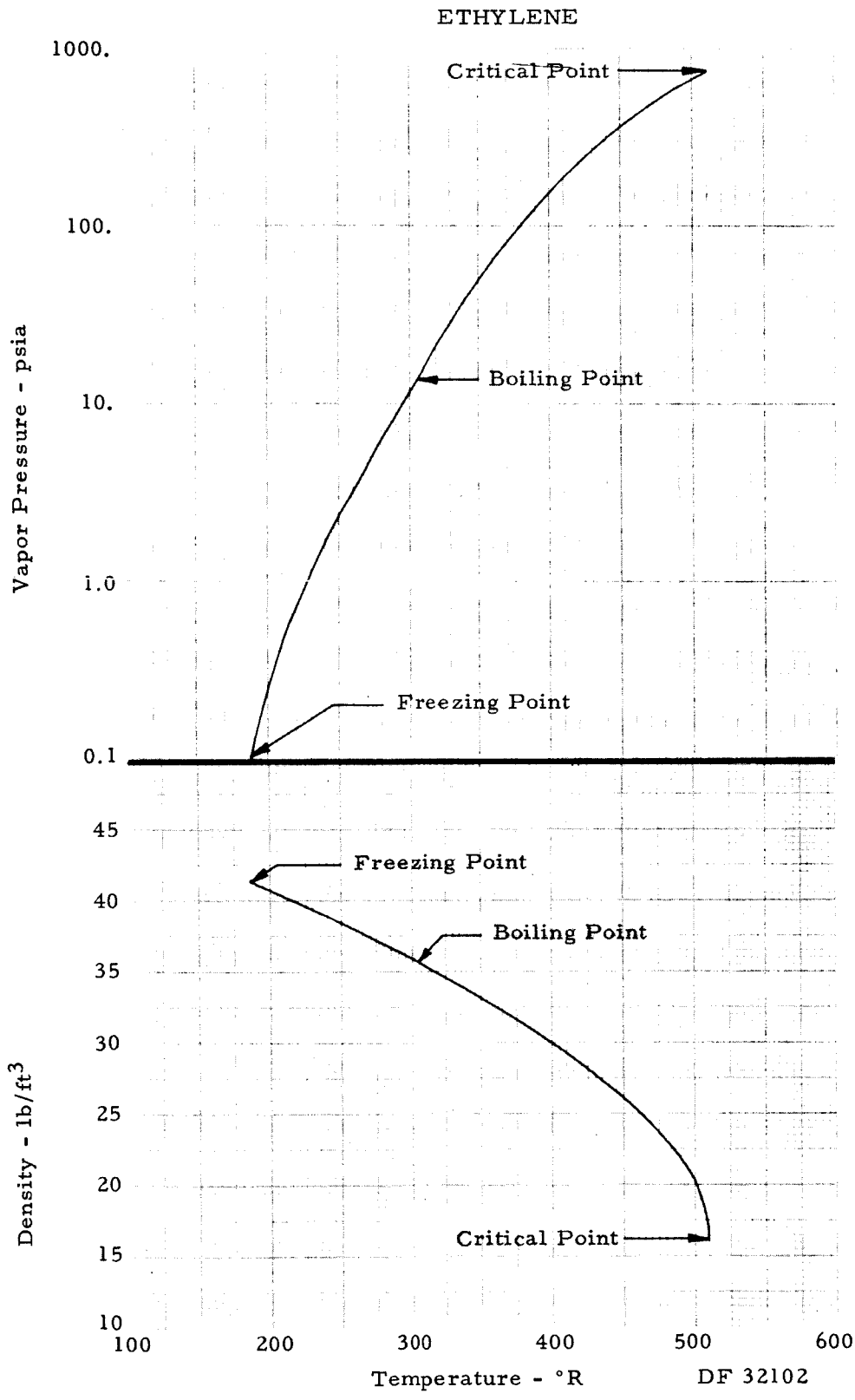
ETHYLENE
1000.
100.
10.
1.0
0.1
Vapor Pressure - psia
Critical Point
Boiling Point
Freezing Point
45
40
35
30
25
20
15
10
Density - lb/ft3
Freezing Point
Boiling Point
Critical Point
100
200
300
400
500
600
Temperature - °R
DF 32102

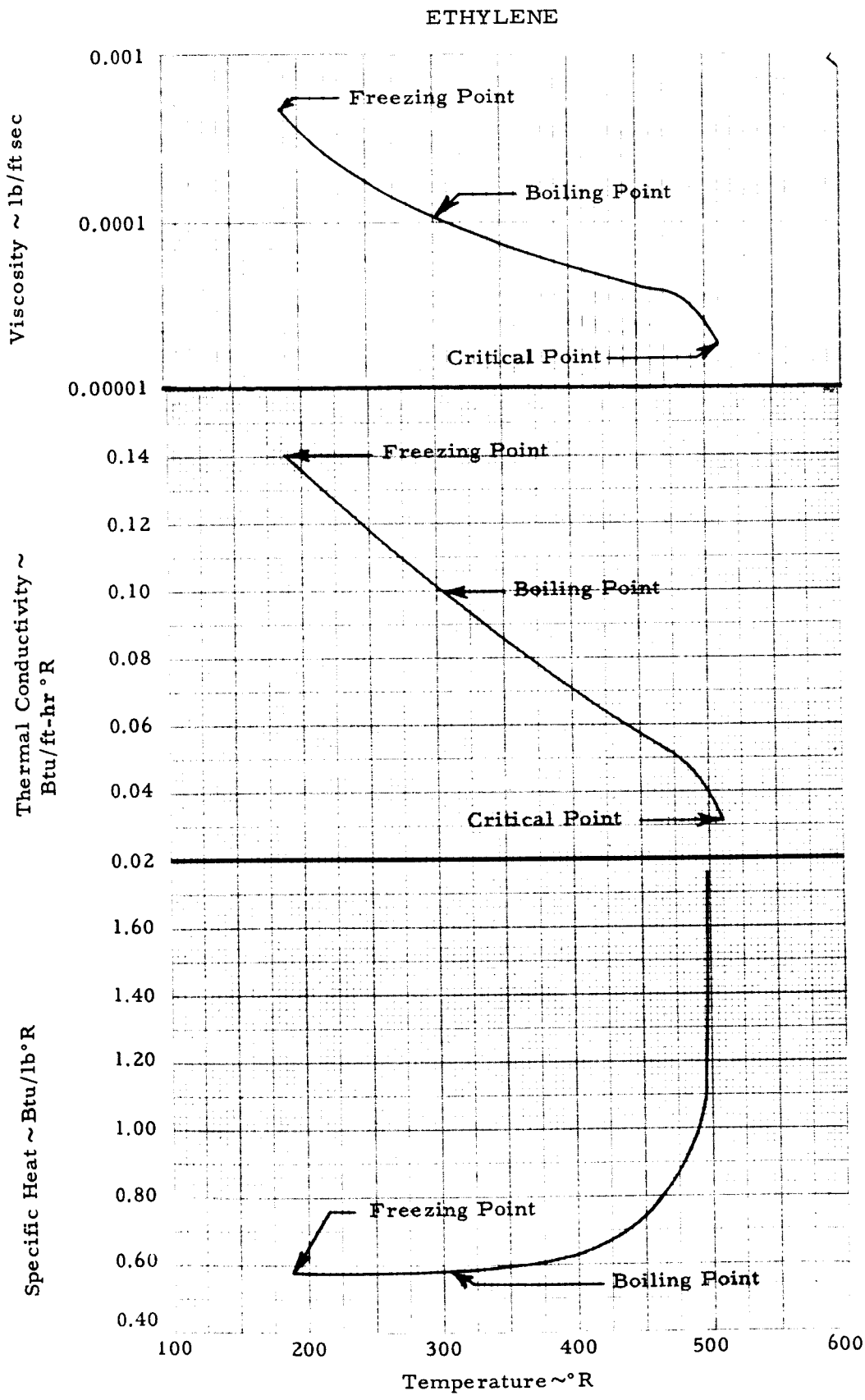
ETHYLENE
Viscosity ~ lb/ft sec
0.001
0.0001
0.00001
Freezing Point
Boiling Point
Critical Point
Thermal Conductivity ~ Btu/ft-hr °R
0.14
0.12
0.10
0.08
0.06
0.04
0.02
Freezing Point
Boiling Point
Critical Point
Specific Heat ~ Btu/lb °R
1.60
1.40
1.20
1.00
0.80
0.60
0.40
Freezing Point
Boiling Point
100
200
300
400
500
600
Temperature ~ °R

ETHANE

SUMMARY OF PROPERTIES

		Reference
Chemical formula	C_2H_6	
Molecular weight	30.068	
Freezing point (normal), °R	161.9	5
Boiling point (normal), °R	331.7	5
Liquid density (at NBP), lb/ft³	34.15	4
Critical temperature, °R	549.8	5
Critical pressure, psia	708.	5
Critical volume, ft³/lb	0.0789	5
Heat of vaporization, (at NBP), BTU/lb	210.41	7
Heat of fusion, BTU/lb	40.88	2
Heat of formation (liquid at NBP), BTU/lb	−1500.	8
Autoignition temperature, °R	1410.	12
Flammability limits in air, volume percent	3.0 – 12.5	12

I.C.C. CLASSIFICATION–

Flammable compressed gas "Red Gas Label"

TOXICITY

Ethane is colorless, odorless and non-poisonous. However, it does have an anesthetic effect in concentrations greater than 50,000 ppm (5%) for exposures over 2 hours. Concentrations greater than 70% by volume can be fatal due to asphyxiation.

COST AND AVAILABILITY

Phillips Petroleum Co. (Prices FOB Sweeny, Texas)

(99% purity) 32 lb/cyl – $72.00/cyl
(95% purity) 32 lb/cyl – $28.80/cyl

Transportation $5.80/cylinder to WPB, Fla.
$3.90/cylinder to return
Cylinder demurrage $2.00/month after 3 mo.

The Matheson Co. (Price FOB East Rutherford, N.J.)

(95% purity) 32 lb/cyl – $44.80/cyl

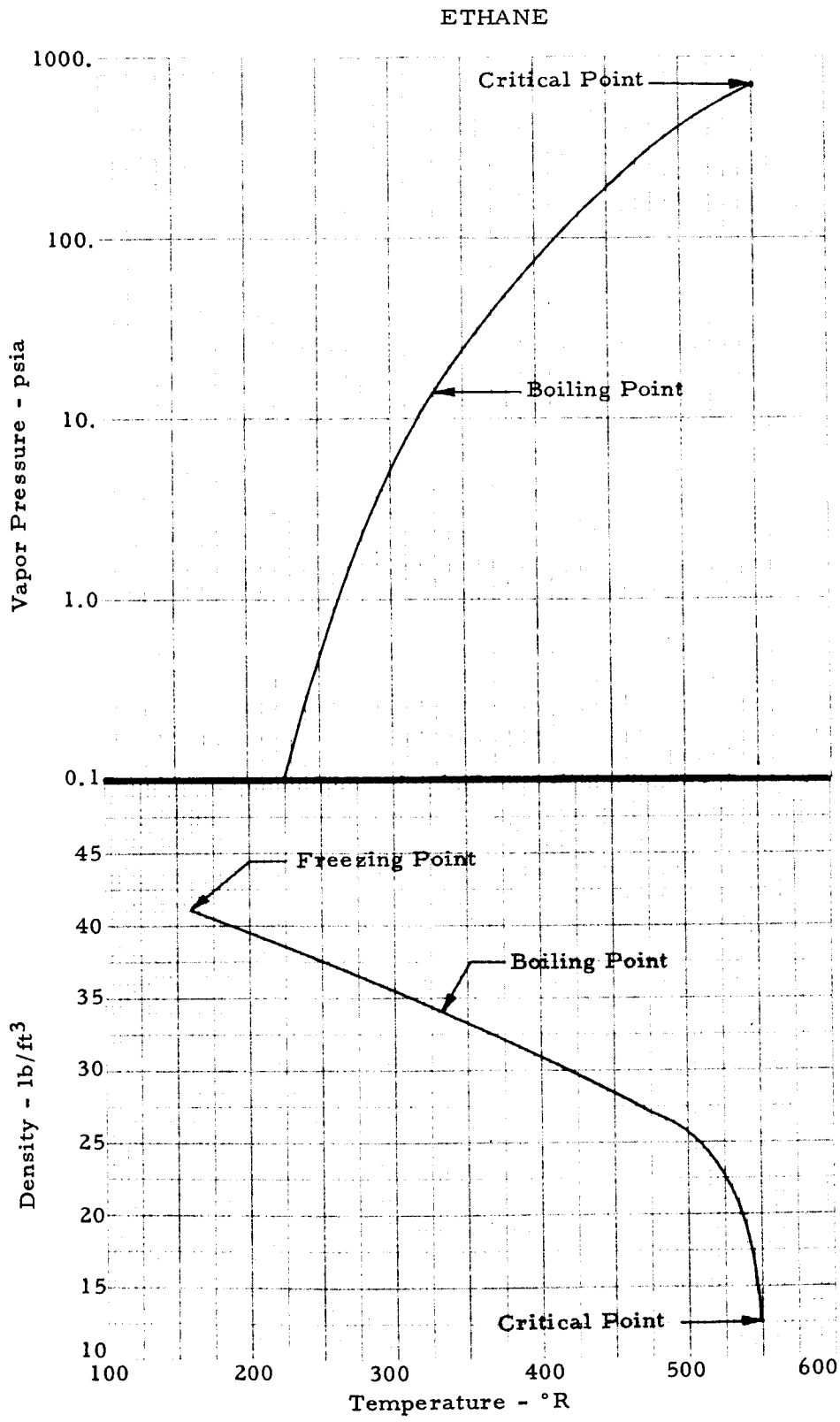
ETHANE
1000.
100.
10.
1.0
0.1
Vapor Pressure - psia
Critical Point
Boiling Point
45
40
35
30
25
20
15
10
Density - lb/ft3
Freezing Point
Boiling Point
Critical Point
100
200
300
400
500
600
Temperature - °R

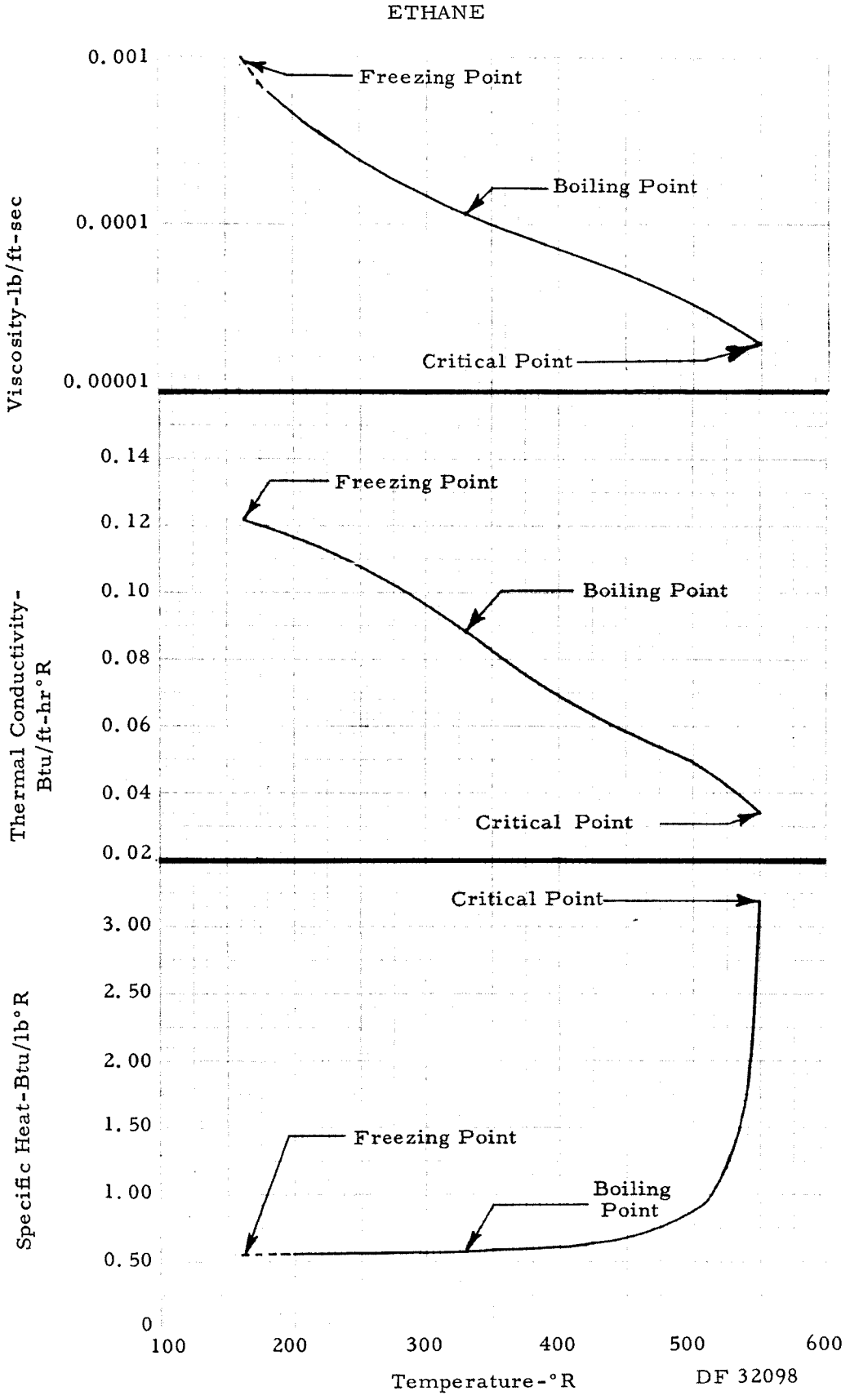
ETHANE
Viscosity-lb/ft-sec
0.001
0.0001
0.00001
Freezing Point
Boiling Point
Critical Point
Thermal Conductivity-
Btu/ft-hr°R
0.14
0.12
0.10
0.08
0.06
0.04
0.02
Freezing Point
Boiling Point
Critical Point
Specific Heat-Btu/lb°R
3.00
2.50
2.00
1.50
1.00
0.50
0
Critical Point
Freezing Point
Boiling Point
100
200
300
400
500
600
Temperature-°R
DF 32098

METHYLACETYLENE
(PROPYNE)

SUMMARY OF PROPERTIES

		Reference
Chemical formula	C_3H_4	
Molecular weight	40.062	
Freezing point (normal), °R	309.	12
Boiling point (normal), °R	450.1	12
Liquid density (at NBP), lb/ft^3	42.1	1
Critical temperature, °R	722.1	12
Critical pressure, psia	866.	15
Critical volume, ft^3/lb	0.0656	14
Heat of vaporization, (at NBP), BTU/lb	234.7	12
Heat of fusion, BTU/lb		
Heat of formation (liquid at NBP), BTU/lb		
Autoignition temperature, °R		
Flammability limits in air, volume percent	2.4 – 11.7	12

I.C.C. CLASSIFICATION–

Flammable compressed gas "Red Gas Label"

TOXICITY

This compound is a simple anesthetic and in high concentrations is an asphyxiant. Threshold limit value is 1000 ppm in air for 8 hour daily exposure.

COST AND AVAILABILITY

The Matheson Co. – (Prices FOB East Rutherford, N.J.)

(96% purity) 15 lb/cyl – $95.25

Air Reduction Chemical & Carbide Co. (Prices FOB Bound Beach, N.J.)

(purity not stated) 100 lb/cyl – $1500.00

METHYLACETYLENE

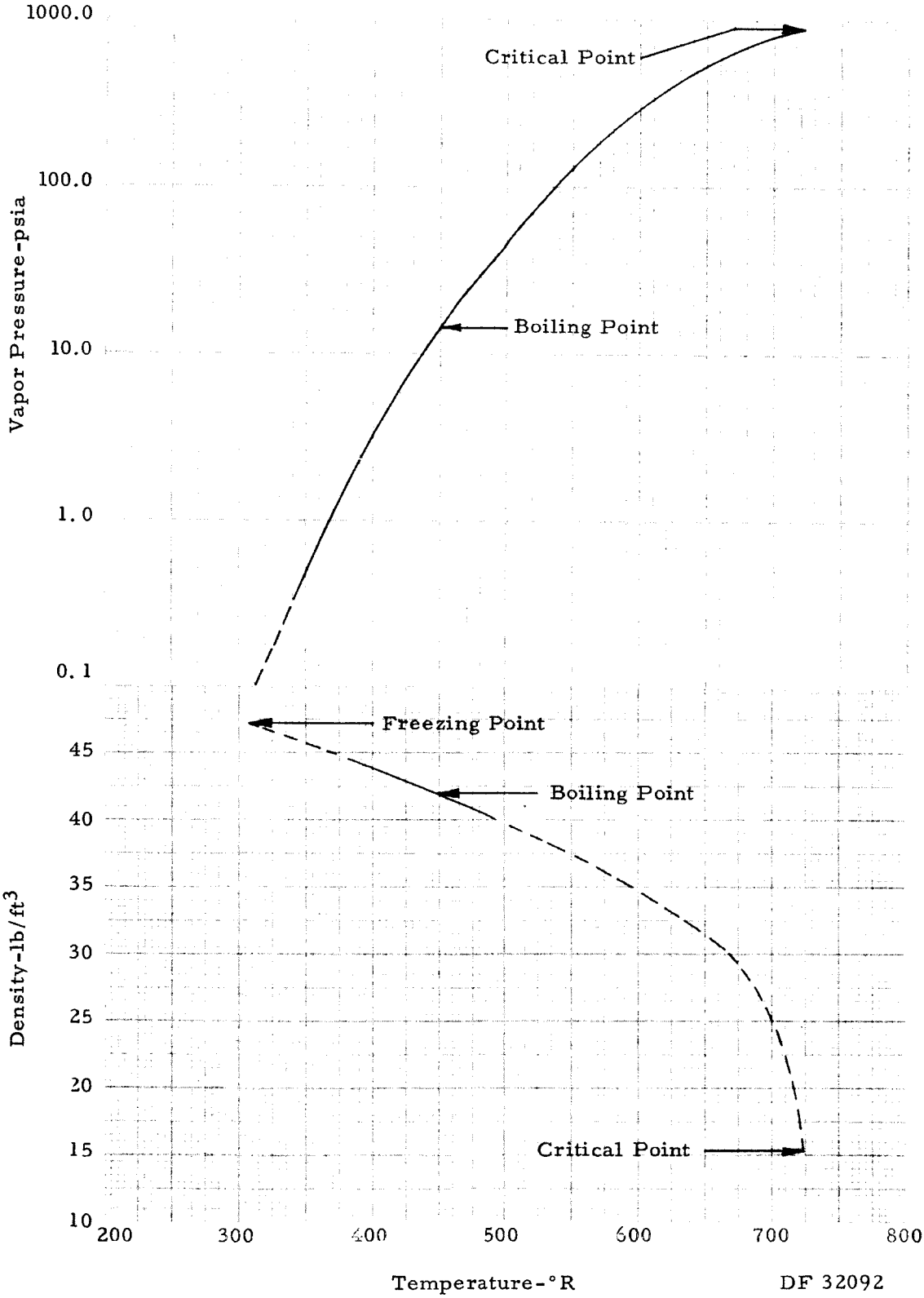

Viscosity-lb/ft sec

Experimental data for viscosity and thermal conductivity are not available and no analytical prediction methods are considered sufficiently reliable for acetylenic compounds.

Thermal Conductivity-Btu/ft-hr°R

Experimental data for viscosity and thermal conductivity are not available and no analytical prediction methods are considered sufficiently reliable for acetylenic compounds.

Specific Heat-Btu/lb°R

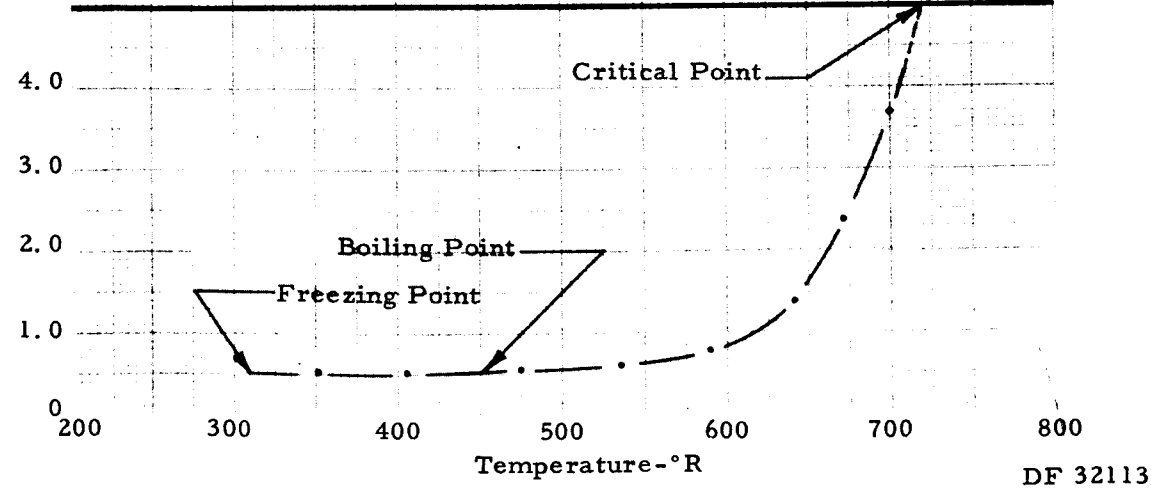

DF 32113

PROPYLENE
(PROPENE)

SUMMARY OF PROPERTIES

		Reference
Chemical formula	C_3H_6	
Molecular weight	42.078	
Freezing point (normal), °R	158.3	5
Boiling point (normal), °R	405.8	5
Liquid density (at NBP), lb/ft³	38.0	3
Critical temperature, °R	656.2	5
Critical pressure, psia	667.	5
Critical volume, ft³/lb	0.0687	5
Heat of vaporization, (at NBP), BTU/lb	188.19	7
Heat of fusion, BTU/lb	30.70	2
Heat of formation (liquid at NBP), BTU/lb	—75.	8
Autoignition temperature, °R	1316.	2
Flammability limits in air, volume percent	2.4 — 10.3	12

I.C.C. CLASSIFICATION—

Flammable compressed gas "Red Gas Label"

TOXICITY

Propylene is a simple asphyxiant which can cause death in concentrations greater than 75% by volume in air. No irritating effects occur from lesser concentrations in gaseous form.

COST AND AVAILABILITY

Phillips Petroleum Co. (Prices FOB Borger, Texas)

(99% purity) 105 lb/cyl — $42.00
$31.50 in lots of 50 or more

Transportation — $10.90/cyl — FOB West Palm Beach, Fla.
$ 7.30/cyl — return
Cylinder demurrage $2.00/month after 4 months

Gulf Oil Co. (Prices FOB Gulf Coast)

(Commercial) approximately $0.035/lb

The Matheson Co. (Price FOB East Rutherford, N.J.)

(95% purity) 105 lb/cyl — $57.75/cyl

PROPYLENE

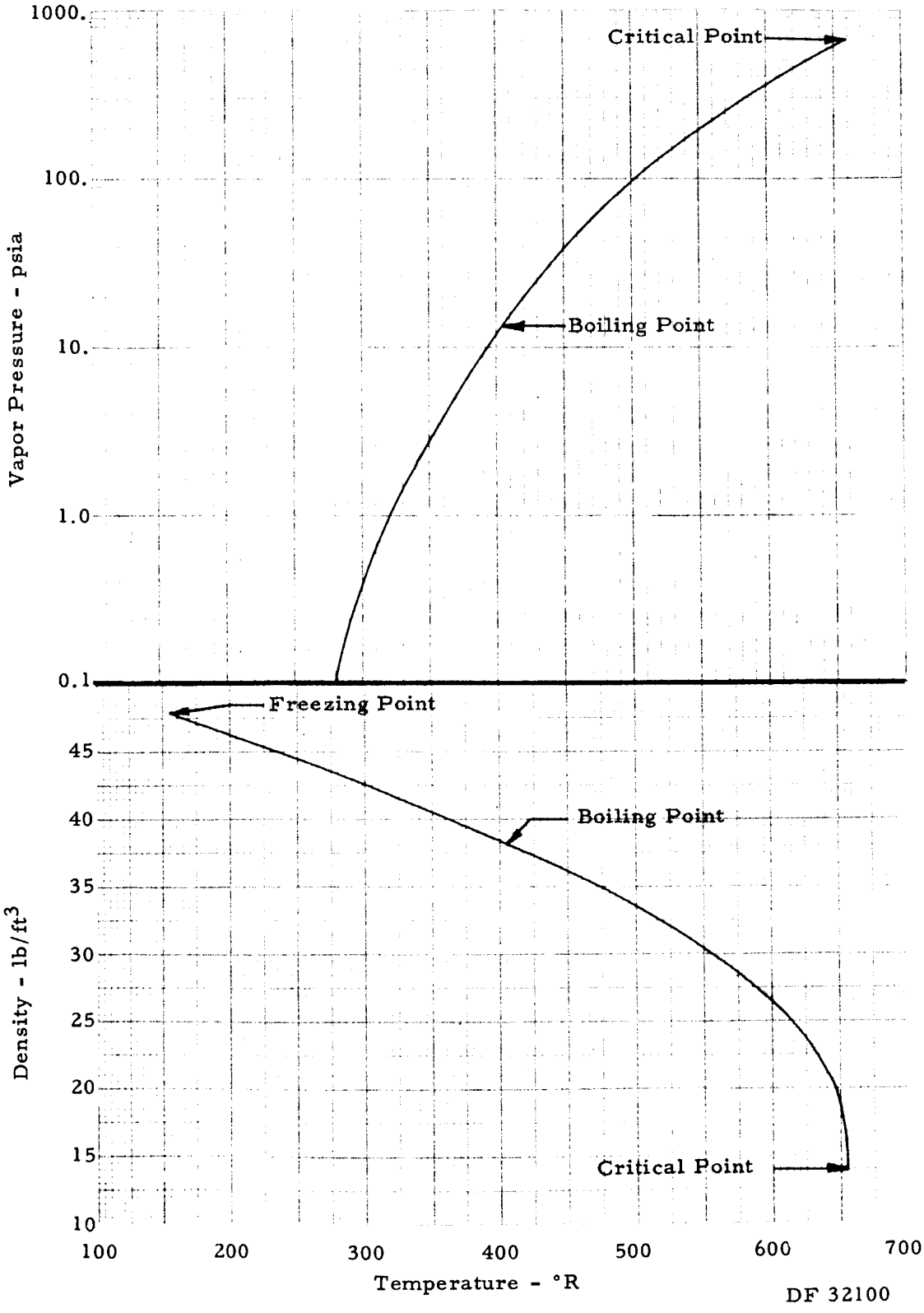
Vapor Pressure - psia
1000.
100.
10.
1.0
0.1
Critical Point
Boiling Point
Freezing Point
Density - lb/ft3
45
40
35
30
25
20
15
10
Boiling Point
Critical Point
100
200
300
400
500
600
700
Temperature - °R
DF 32100

PROPYLENE

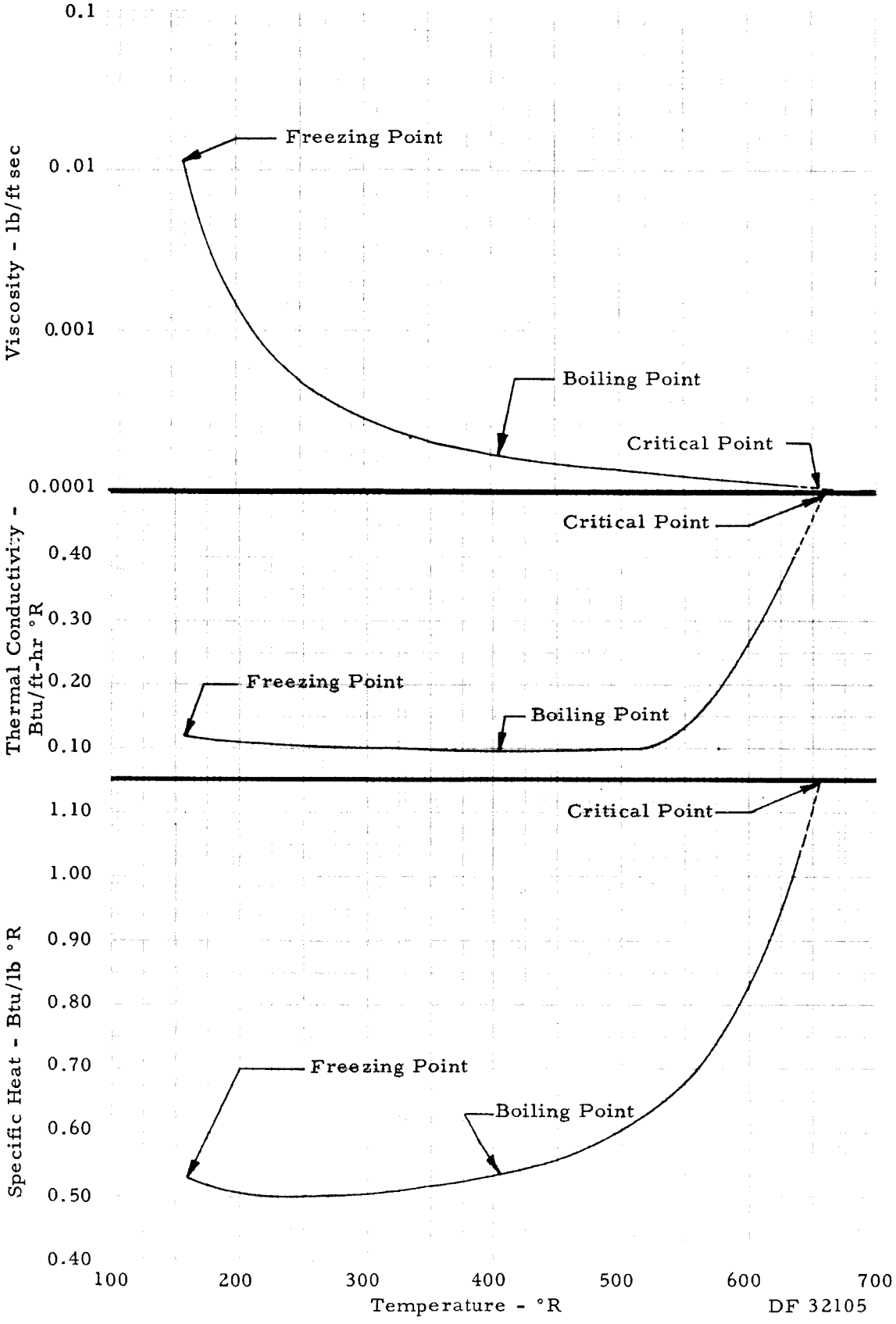
Viscosity - lb/ft sec
0.1
0.01
0.001
0.0001
Freezing Point
Boiling Point
Critical Point
Thermal Conductivity - Btu/ft-hr °R
0.40
0.30
0.20
0.10
Critical Point
Freezing Point
Boiling Point
Specific Heat - Btu/lb °R
1.10
1.00
0.90
0.80
0.70
0.60
0.50
0.40
Critical Point
Freezing Point
Boiling Point
100
200
300
400
500
600
700
Temperature - °R
DF 32105

PROPANE

SUMMARY OF PROPERTIES

		Reference
Chemical formula	C_3H_8	
Molecular weight	44.094	
Freezing point (normal), °R	154.0	5
Boiling point (normal), °R	415.9	5
Liquid density (at NBP), lb/ft³	36.4	4
Critical temperature, °R	666.0	4
Critical pressure, psia	618.7	4
Critical volume, ft³/lb	0.0709	5
Heat of vaporization, (at NBP), BTU/lb	183.05	7
Heat of fusion, BTU/lb	34.38	2
Heat of formation (liquid at NBP), BTU/lb	—1240.	8
Autoignition temperature, °R	1334.	12
Flammability limits in air, volume percent	2.2 — 9.5	12

I.C.C. CLASSIFICATION—

Flammable compressed gas "Red Gas Label"

TOXICITY

Propane is not considered toxic. It does have an anesthetic action in concentrations exceeding 50,000 ppm (5%) for exposures greater than 2 hours. It has the characteristic odor of natural gas and can cause death by oxygen exclusion in concentration exceeding 70% by volume in air.

COST AND AVAILABILITY

Shell Oil Co.

(Commercial) approximately $0.01/lb — FOB Tulsa, Okla.
approximately $0.02/lb — FOB East Coast

The Matheson Co. (Prices FOB East Rutherford, N. J.)

(96% purity) 100 lb/cyl — $25.00
35 lb/cyl — $12.25

Phillips Petroleum Co. (Prices FOB Borger, Texas)

(95% purity) 200 lb/cyl — $28.00

PROPANE

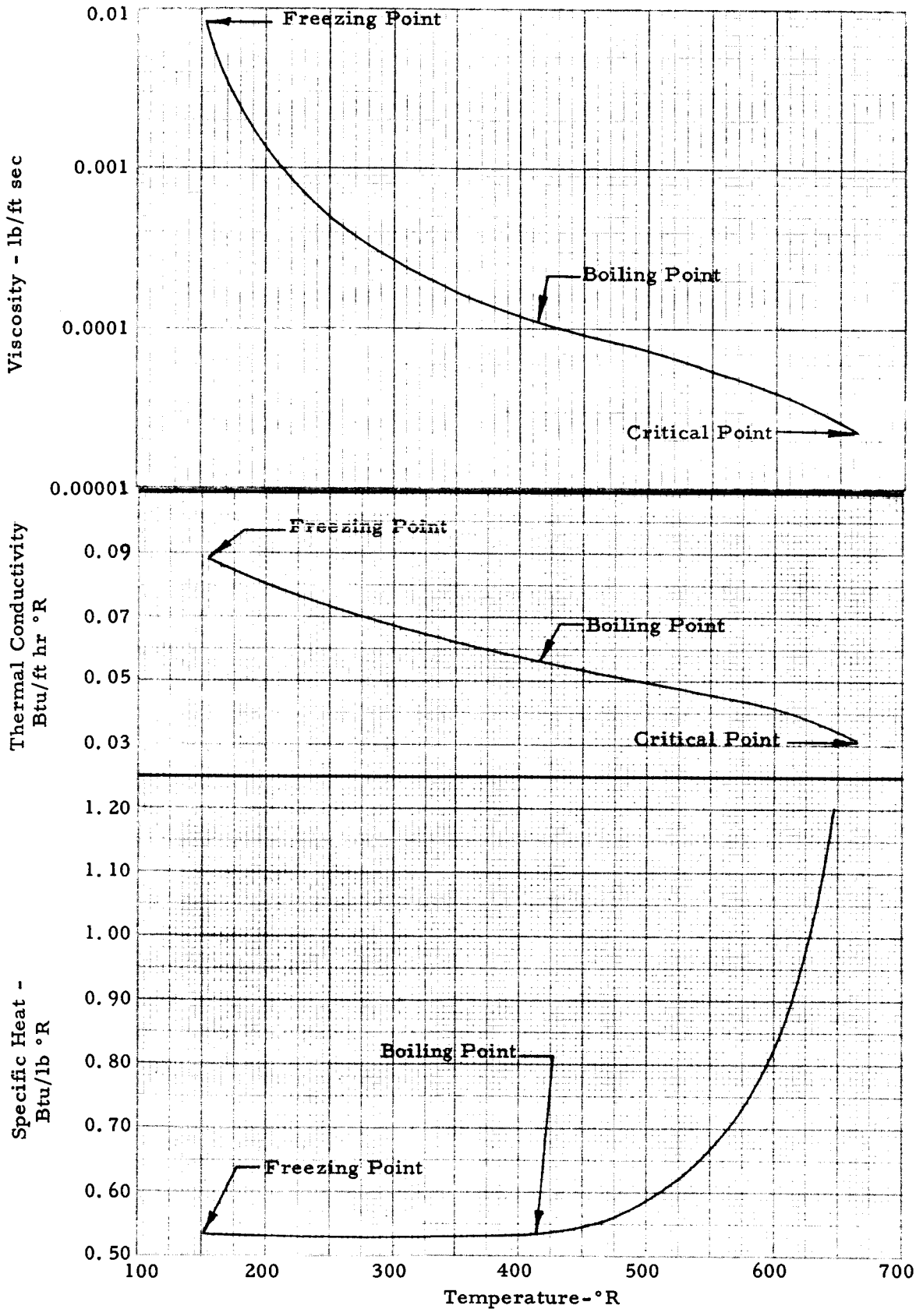
Viscosity - lb/ft sec
0.01
0.001
0.0001
0.00001
Freezing Point
Boiling Point
Critical Point
Thermal Conductivity Btu/ft hr °R
0.09
0.07
0.05
0.03
Freezing Point
Boiling Point
Critical Point
Specific Heat - Btu/lb °R
1.20
1.10
1.00
0.90
0.80
0.70
0.60
0.50
Boiling Point
Freezing Point
100
200
300
400
500
600
700
Temperature-°R

PROPANE

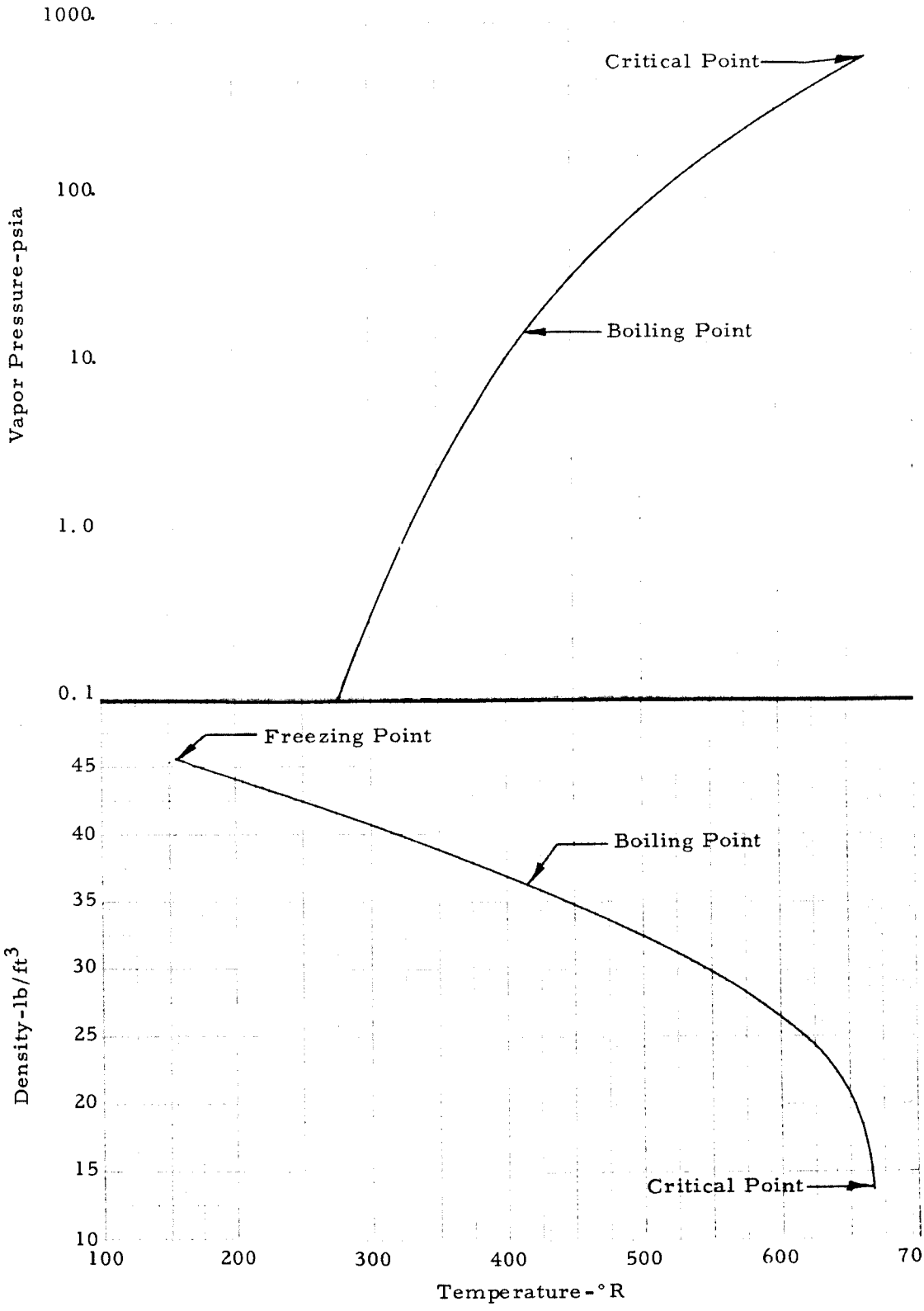

DF 32108

The Matheson Co. (Prices FOB East Rutherford, N.J.)

(95% purity) 129 lb/cyl $82.56/cyl
$77.40/cyl in lots of 6 or more

Sinclair Refining Co.

(95% purity) Tank truck quantities (14,000 lb) – $0.10/lb
FOB WPB, Fla.

BUTENE-1
(α-BUTYLENE)

SUMMARY OF PROPERTIES

		Reference
Chemical formula	C_4H_8	
Molecular weight	56.104	
Freezing point (normal), °R	158.0	2
Boiling point (normal), °R	480.4	5
Liquid density (at NBP), lb/ft³	38.6	5
Critical temperature, °R	755.3	7
Critical pressure, psia	583.	7
Critical volume, ft³/lb	0.0690	7
Heat of vaporization, (at NBP), BTU/lb	167.93	7
Heat of fusion, BTU/lb	29.51	2
Heat of formation (liquid at NBP), BTU/lb	−179.	8
Autoignition temperature, °R		
Flammability limits in air, volume percent	1.6 – 9.3	12

I.C.C. CLASSIFICATION–

Flammable compressed gas "Red Gas Label"

TOXICITY

Butylene is moderately toxic by inhalation and has an anesthetic effect. In high concentrations it is dangerous as an asphyxiant by oxygen depletion.

COST AND AVAILABILITY

Phillips Petroleum Co. (Prices FOB Borger, Texas)

(99% purity) 129 lb/cyl – $258/cyl
(95% purity) 129 lb/cyl – $ 51.60/cyl
258 lb/cyl – $102.20/cyl
Tank truck quantities (approximately 14,000 lb) – $0.0625/lb

Transportation 129 lb/cyl $11.28/cyl – FOB WPB, Fla.
$ 8.80/cyl – return
258 lb/cyl $20.44/cyl – FOB WPB, Fla.
$13.66/cyl – return
Cylinder demurrage $2.00/month after 4 months
Tank truck (round trip) – $1,089 to WPB, Fla.

1 - BUTENE

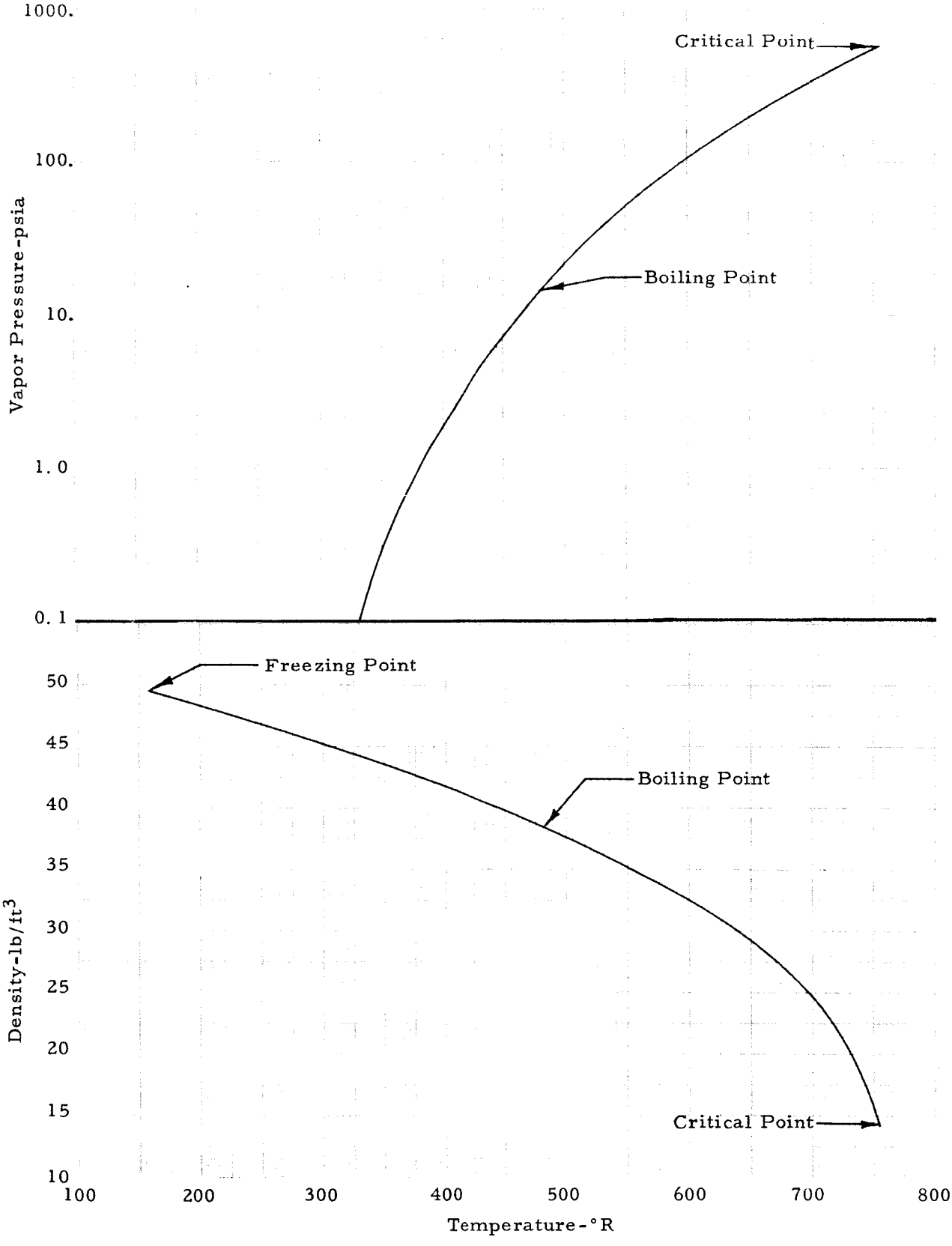

DF 32106

1 - BUTENE

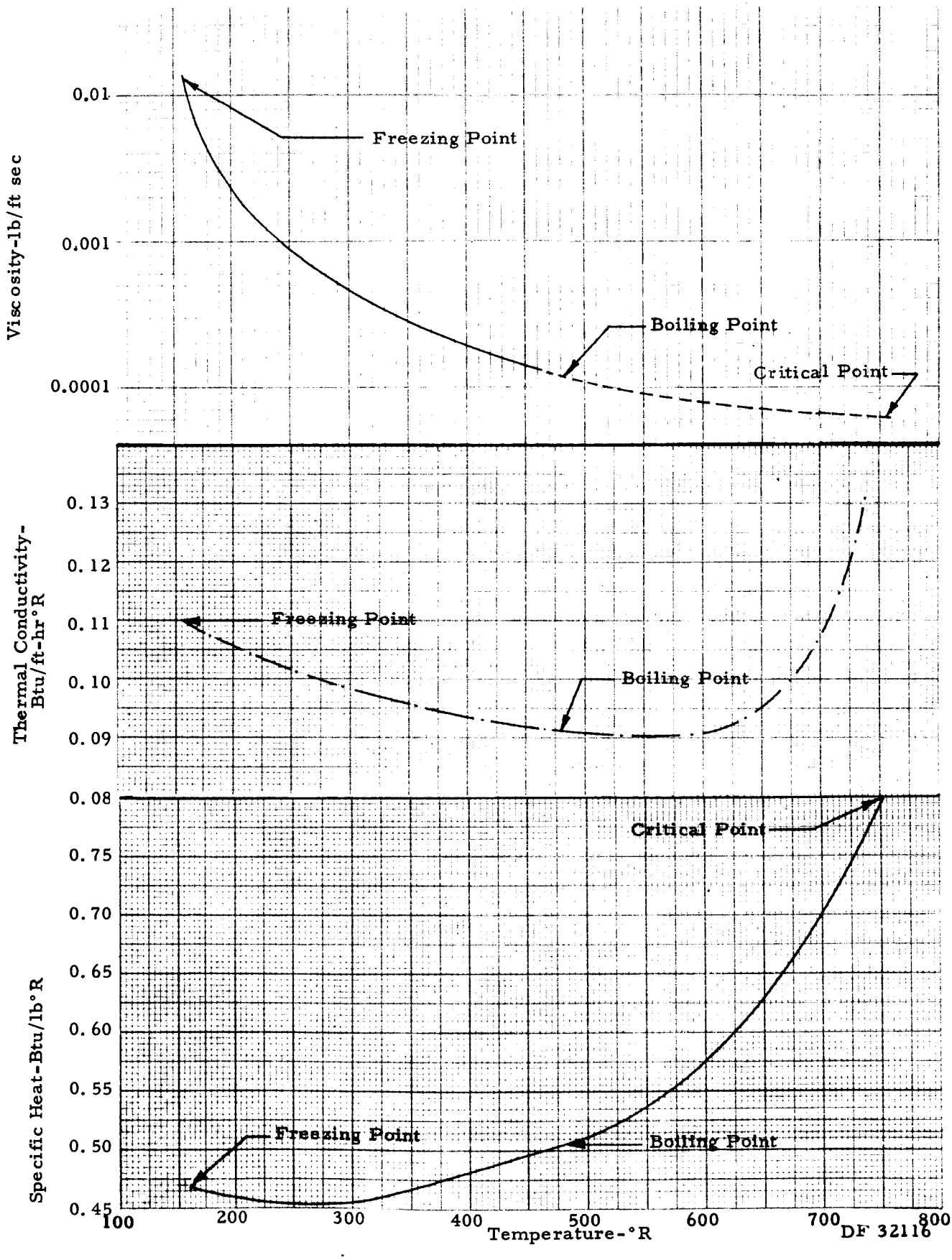
Viscosity-lb/ft sec
0.01
0.001
0.0001
Freezing Point
Boiling Point
Critical Point
Thermal Conductivity-
Btu/ft-hr°R
0.13
0.12
0.11
0.10
0.09
Freezing Point
Boiling Point
Specific Heat-Btu/lb°R
0.08
0.75
0.70
0.65
0.60
0.55
0.50
0.45
Critical Point
Freezing Point
Boiling Point
100
200
300
400
500
600
700
800
Temperature-°R
DF 32116

BUTANE

SUMMARY OF PROPERTIES

		Reference
Chemical formula	C_4H_{10}	
Molecular weight	58.120	
Freezing point (normal), °R	242.8	5
Boiling point (normal), °R	490.8	5
Liquid density (at NBP), lb/ft^3	37.5	3
Critical temperature, °R	766.	5
Critical pressure, psia	550.	5
Critical volume, ft^3/lb	0.0712	5
Heat of vaporization, (at NBP), BTU/lb	165.64	7
Heat of fusion, BTU/lb	34.50	2
Heat of formation (liquid at NBP), BTU/lb	−1092.6	2, 5
Autoignition temperature, °R	1221.	12
Flammability limits in air, volume percent	1.9 - 8.5	12

I.C.C. CLASSIFICATION—

Flammable compressed gas "Red Gas Label"

TOXICITY

Butane is a colorless gas with a characteristic natural gas odor. It may produce drowsiness but is primarily a simple asphyxiant which can cause death by oxygen exclusion above 70% volume concentrations in air. Concentrations up to 5% do not produce injuries on exposures up to 2 hours.

COST AND AVAILABILITY

Shell Oil Co. (FOB Texas refinery)

(Commercial) approximately 1.6 to 3. cents/lb

The Matheson Co. (FOB East Rutherford, N.J.)

(95% purity) 122 lb/cyl — $43.93

Phillips Petroleum Co. (Prices FOB Borger, Texas)

(99% purity) 244 lb/cyl — $110.00
(95% purity) 244 lb/cyl — $ 47.00

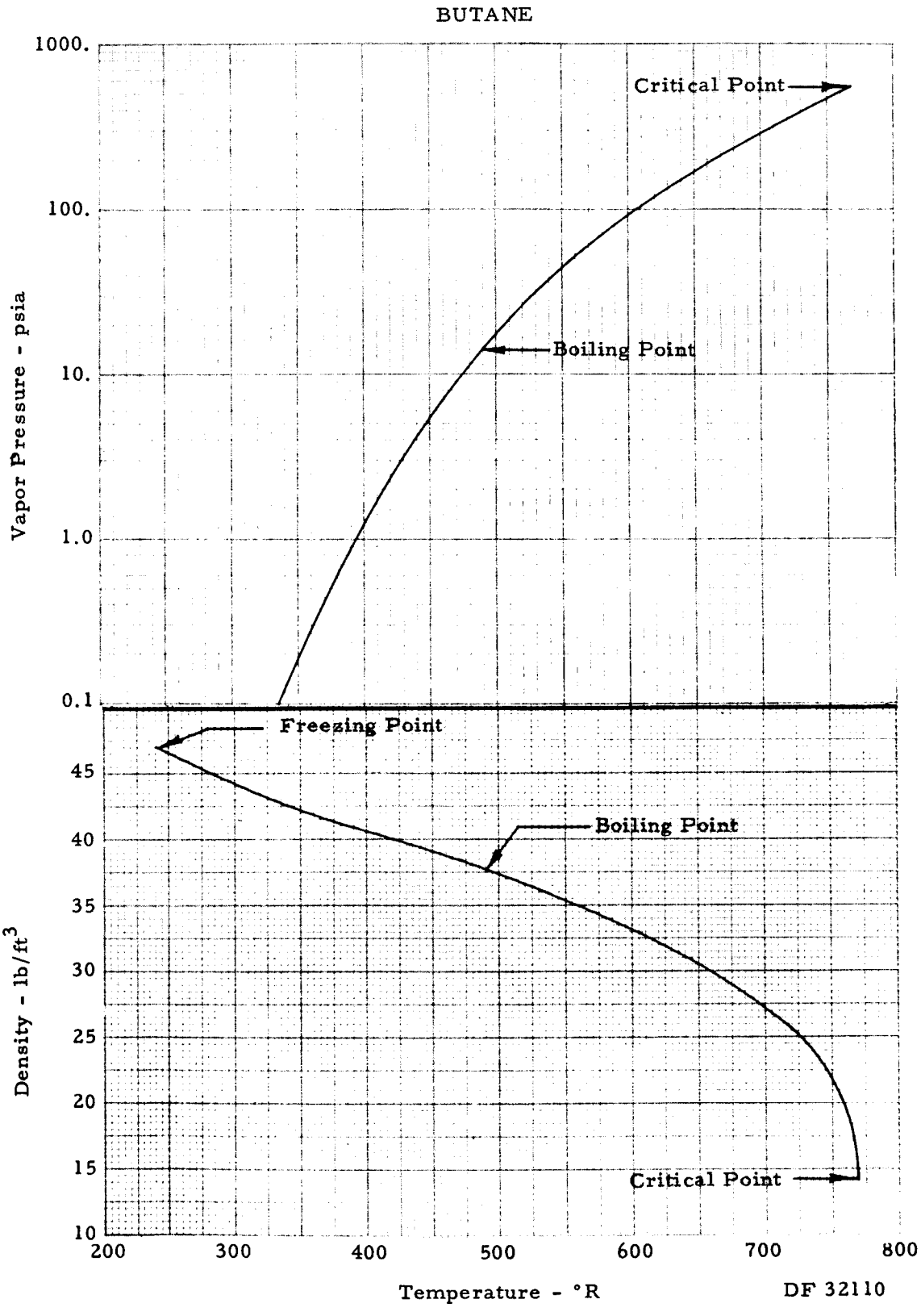
BUTANE
1000.
100.
10.
1.0
0.1
Vapor Pressure - psia
Critical Point
Boiling Point
Freezing Point
Boiling Point
Critical Point
45
40
35
30
25
20
15
10
Density - lb/ft3
200
300
400
500
600
700
800
Temperature - °R
DF 32110

BUTANE

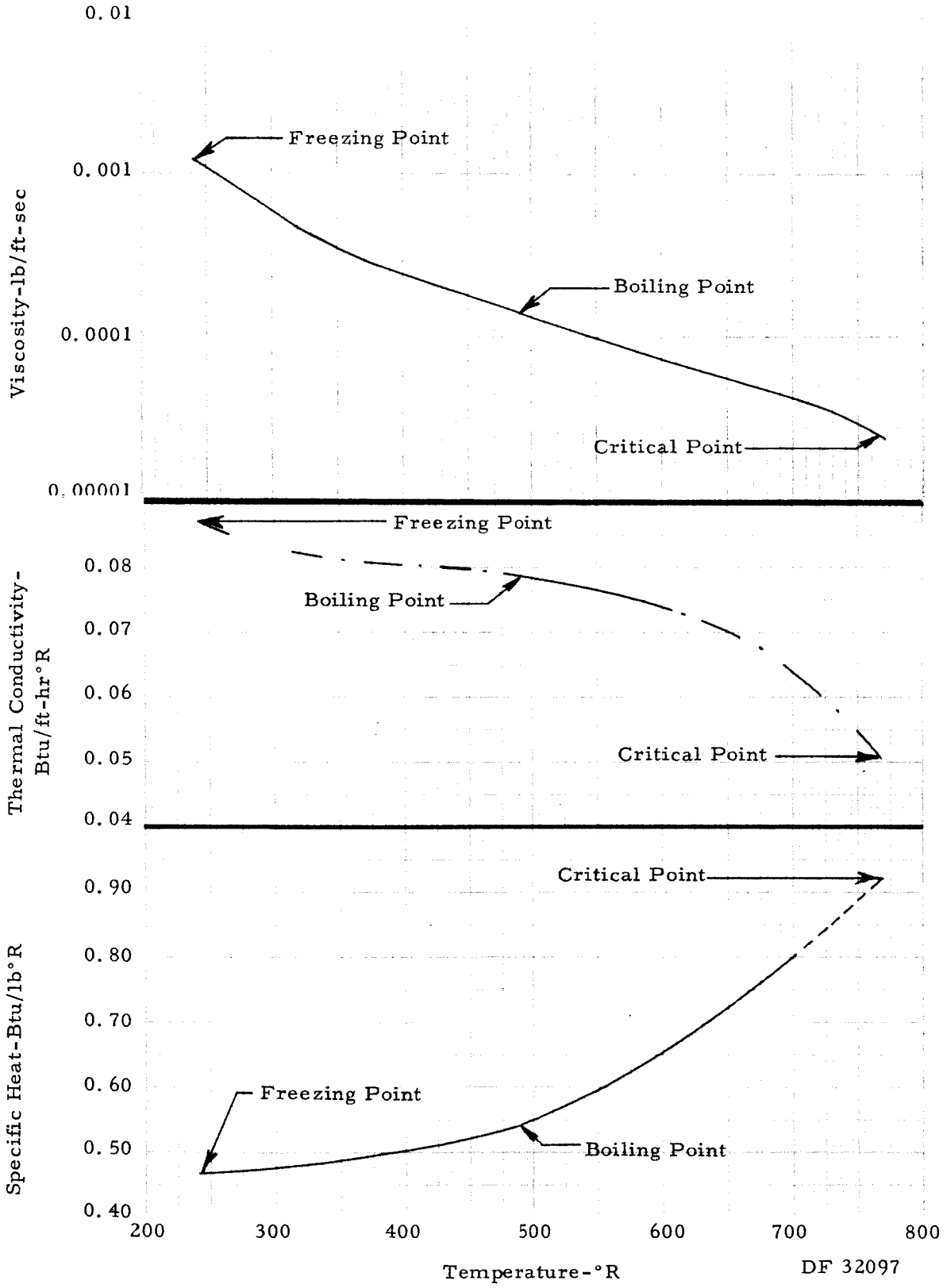
Viscosity-lb/ft-sec
0.01
0.001
0.0001
0.00001
Freezing Point
Boiling Point
Critical Point
Thermal Conductivity-
Btu/ft-hr°R
0.08
0.07
0.06
0.05
0.04
Freezing Point
Boiling Point
Critical Point
Specific Heat-Btu/lb°R
0.90
0.80
0.70
0.60
0.50
0.40
Critical Point
Freezing Point
Boiling Point
200
300
400
500
600
700
800
Temperature-°R
DF 32097

PENTANE

SUMMARY OF PROPERTIES

		Reference
Chemical formula	C_5H_{12}	
Molecular weight	72.146	
Freezing point (normal), °R	258.2	5
Boiling point (normal), °R	556.6	5
Liquid density (at 537°R), lb/ft³	38.7	14
Critical temperature, °R	846.2	5
Critical pressure, psia	479.09	5
Critical volume, ft³/lb	0.0690	5
Heat of vaporization, (at NBP), BTU/lb	153.59	7
Heat of fusion, BTU/lb	50.17	2
Heat of formation (liquid at 537°R), BTU/lb	−1032.	2, 5
Autoignition temperature, °R	987.	2
Flammability limits in air, volume percent	5.3 - 14.	12

I.C.C. CLASSIFICATION–

Flammable liquid "Red Label"

TOXICITY

Pentane is a colorless liquid. It is slightly toxic and has a narcotic effect when inhaled.

COST AND AVAILABILITY

Phillips Petroleum Co. (Prices FOB Borger, Texas)

(99% purity) 54 gallon drum (283 lb) – $142.00
(95% purity) 54 gallon drum (283 lb) – $ 71.00
(commercial) 54 gallon drum (283 lb) – $ 32.40
– $ 23.80 2 to 4 drums
– $ 22.20 5 to 39 drums
– $ 20.00 40 or more drums

Tank car quantities (approx. 42,000 lb) – $ 0.027/lb

Transportation – tank car $1.46/cwt – to WPB, Fla.
tank truck $2.44/cwt – to WPB, Fla.
drums are non-returnable

PENTANE

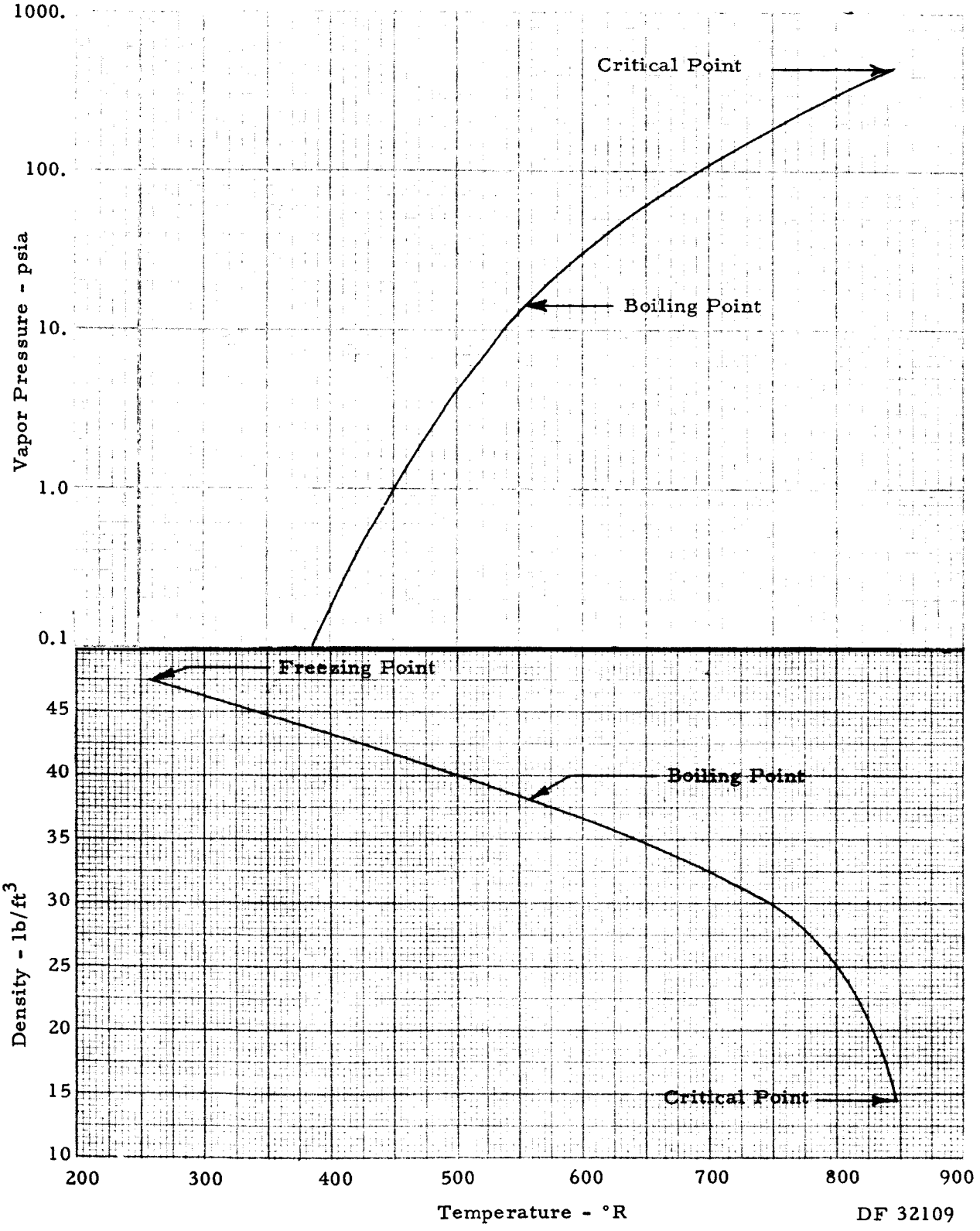
1000.
100.
10.
1.0
0.1
Vapor Pressure - psia
Critical Point
Boiling Point
Freezing Point
Boiling Point
Critical Point
45
40
35
30
25
20
15
10
Density - lb/ft3
200
300
400
500
600
700
800
900
Temperature - °R
DF 32109

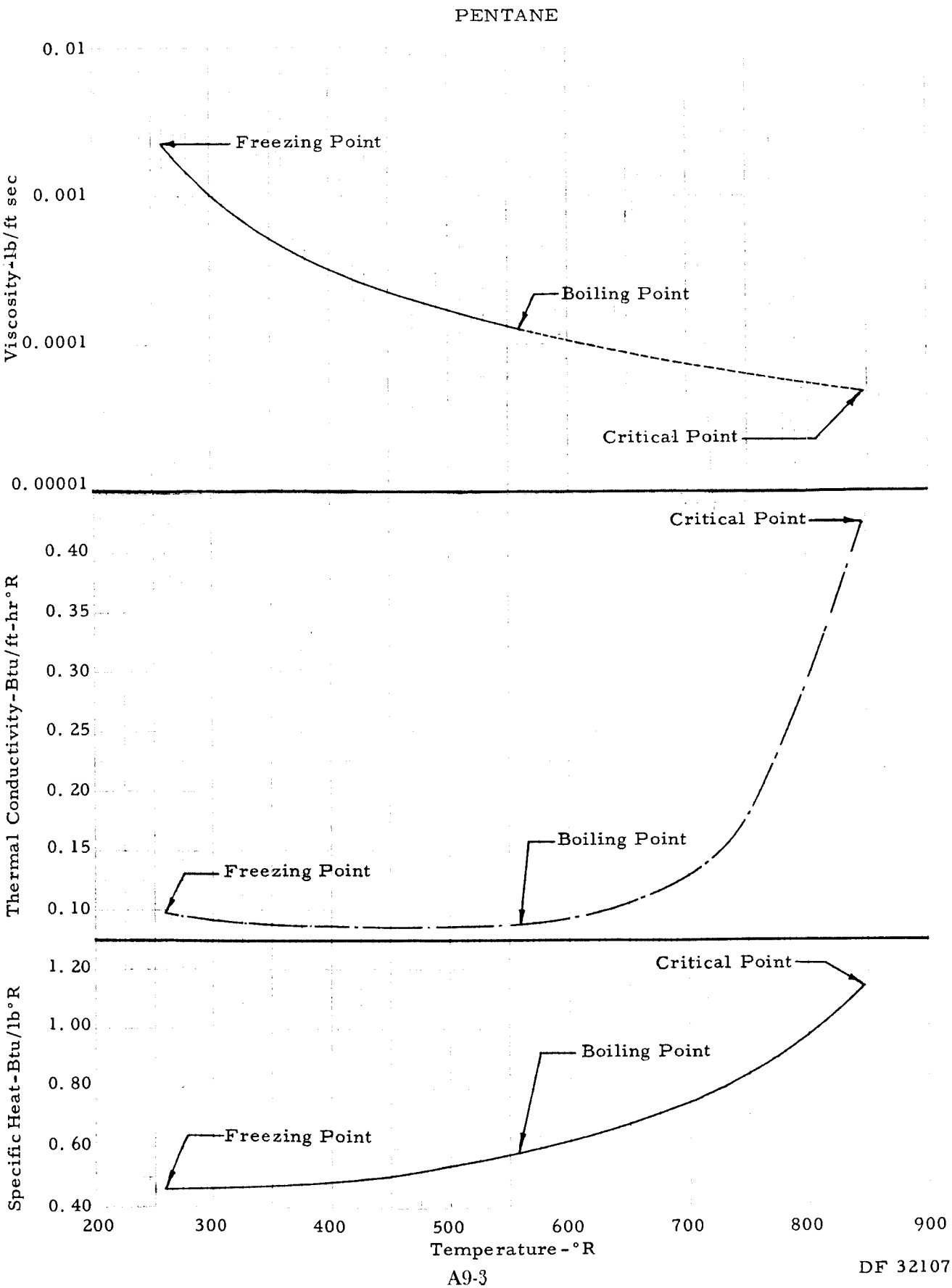
PENTANE
0. 01
0. 001
0. 0001
0. 00001
Viscosity-lb/ft sec
Freezing Point
Boiling Point
Critical Point
0. 40
0. 35
0. 30
0. 25
0. 20
0. 15
0. 10
Thermal Conductivity-Btu/ft-hr°R
Critical Point
Boiling Point
Freezing Point
1. 20
1. 00
0. 80
0. 60
0. 40
Specific Heat-Btu/lb°R
Critical Point
Boiling Point
Freezing Point
200
300
400
500
600
700
800
900
Temperature-°R

DF 32107

ISO-PENTANE
(2-METHLYBUTANE)

SUMMARY OF PROPERTIES

		Reference
Chemical formula	C_5H_{12}	
Molecular weight	72.146	
Freezing point (normal), °R	204.2	5
Boiling point (normal), °R	541.9	5
Liquid density (at 537°R), lb/ft³	38.3	14
Critical temperature, °R	829.2	5
Critical pressure, psia	476.	5
Critical volume, ft³/lb	0.0685	5
Heat of vaporization, (at NBP), BTU/lb	145.7	2
Heat of fusion, BTU/lb	30.74	2
Heat of formation (liquid at 537°R), BTU/lb	−1069.	2, 5
Autoignition temperature, °R		
Flammability limits in air, volume percent	1.32 - 8.3	2

I.C.C. CLASSIFICATION–

Flammable liquid "Red Label"

TOXICITY

Iso-Pentane is a colorless liquid with a pleasant odor. It is slightly toxic and has a narcotic effect when inhaled.

COST AND AVAILABILITY

Philips Petroleum Co. (Prices FOB Borger, Texas)

(99% purity) 54 gallon drum (279 lb) – $140.00
(95% purity) 54 gallon drum (279 lb) – $ 70.00
(commercial) 54 gallon drum (279 lb) – $ 32.40
– $ 25.40 2 to 4 drums
– $ 23.80 5 to 39 drums
– $ 21.60 40 or more drums

Tank car quantities (approximately 42,000 lb) – $0.032/lb

Transportation – tank car $1.46/cwt – to WPB, Fla.
tank truck $2.44/cwt – to WPB, Fla.
drums are non-returnable

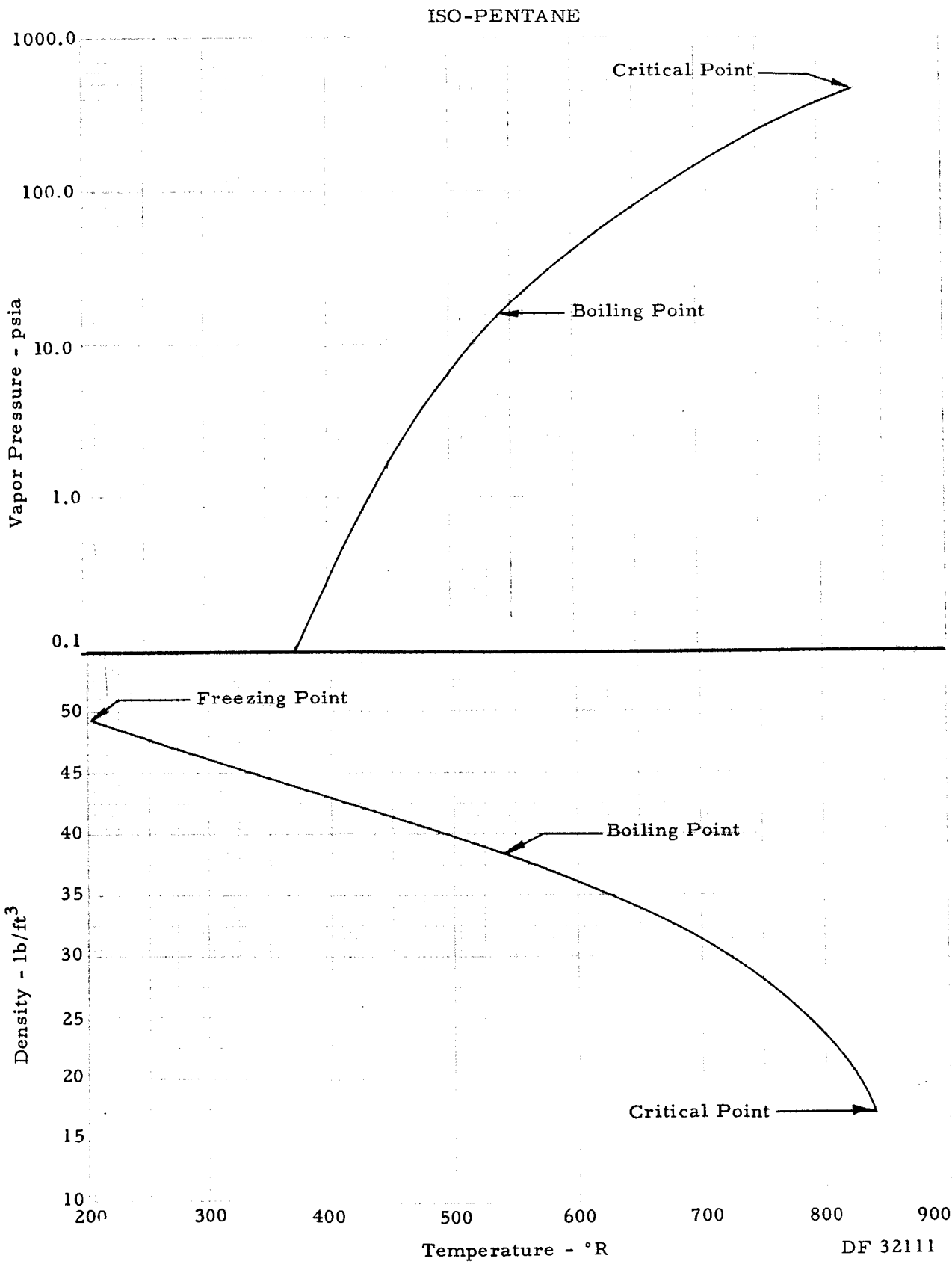
ISO-PENTANE
1000.0
100.0
10.0
1.0
0.1
Vapor Pressure - psia
Critical Point
Boiling Point
50
45
40
35
30
25
20
15
10
Density - lb/ft3
Freezing Point
Boiling Point
Critical Point
200
300
400
500
600
700
800
900
Temperature - °R
DF 32111

METHYLCYCLOPENTANE

SUMMARY OF PROPERTIES

		Reference
Chemical formula	C_6H_{12}	
Molecular weight	84.156	
Freezing point (normal), °R	235.3	14
Boiling point (normal), °R	621.0	14
Liquid density (at 537°R), lb/ft³	46.4	14
Critical temperature, °R	959.0	14
Critical pressure, psia	549.0	14
Critical volume, ft³/lb	0.0607	14
Heat of vaporization, (at NBP), BTU/lb	147.83	14
Heat of fusion, BTU/lb	35.42	2
Heat of formation (liquid at 537°R), BTU/lb	—707.5	2
Autoignition temperature, °R	1084.	2
Flammability limits in air, volume percent	1.2 - 8.35	14

I.C.C. CLASSIFICATION—

Flammable liquid "Red Label"

TOXICITY

Unknown

COST AND AVAILABILITY

Phillips Petroleum Co. (Prices FOB Borger, Texas)

(95% purity) 54 gallon drum (340 lb) — $340.00
in large quantities the price would reduce to approximately — $0.50/lb

Transportation — tank car quantities (1300 lb) $1.46/cwt to WPB, Fla.

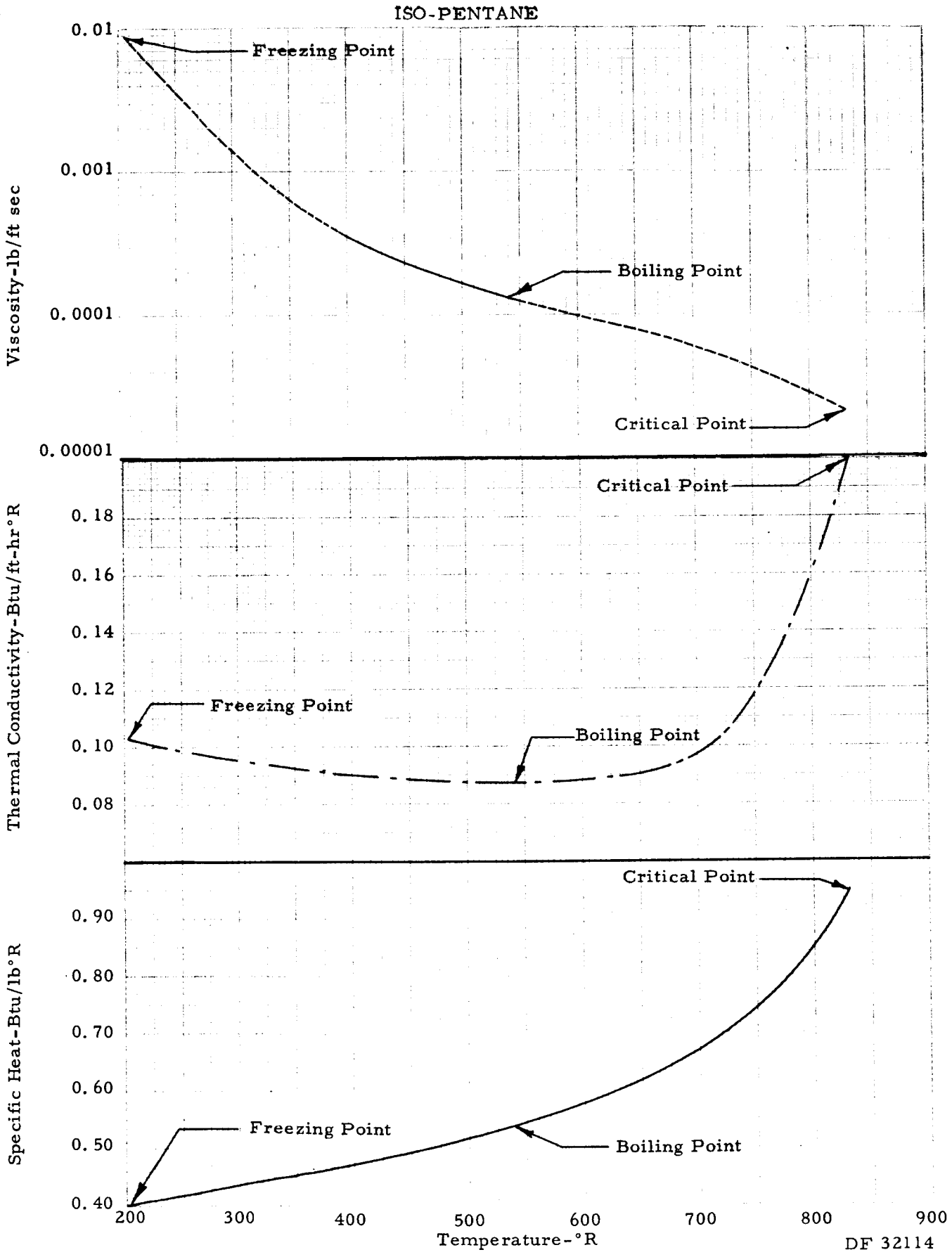
ISO-PENTANE
Viscosity-lb/ft sec
0.01
0.001
0.0001
0.00001
Freezing Point
Boiling Point
Critical Point
Thermal Conductivity-Btu/ft-hr°R
0.18
0.16
0.14
0.12
0.10
0.08
Critical Point
Freezing Point
Boiling Point
Specific Heat-Btu/lb°R
0.90
0.80
0.70
0.60
0.50
0.40
Critical Point
Freezing Point
Boiling Point
200
300
400
500
600
700
800
900
Temperature-°R
DF 32114

METHYLCYCLOPENTANE

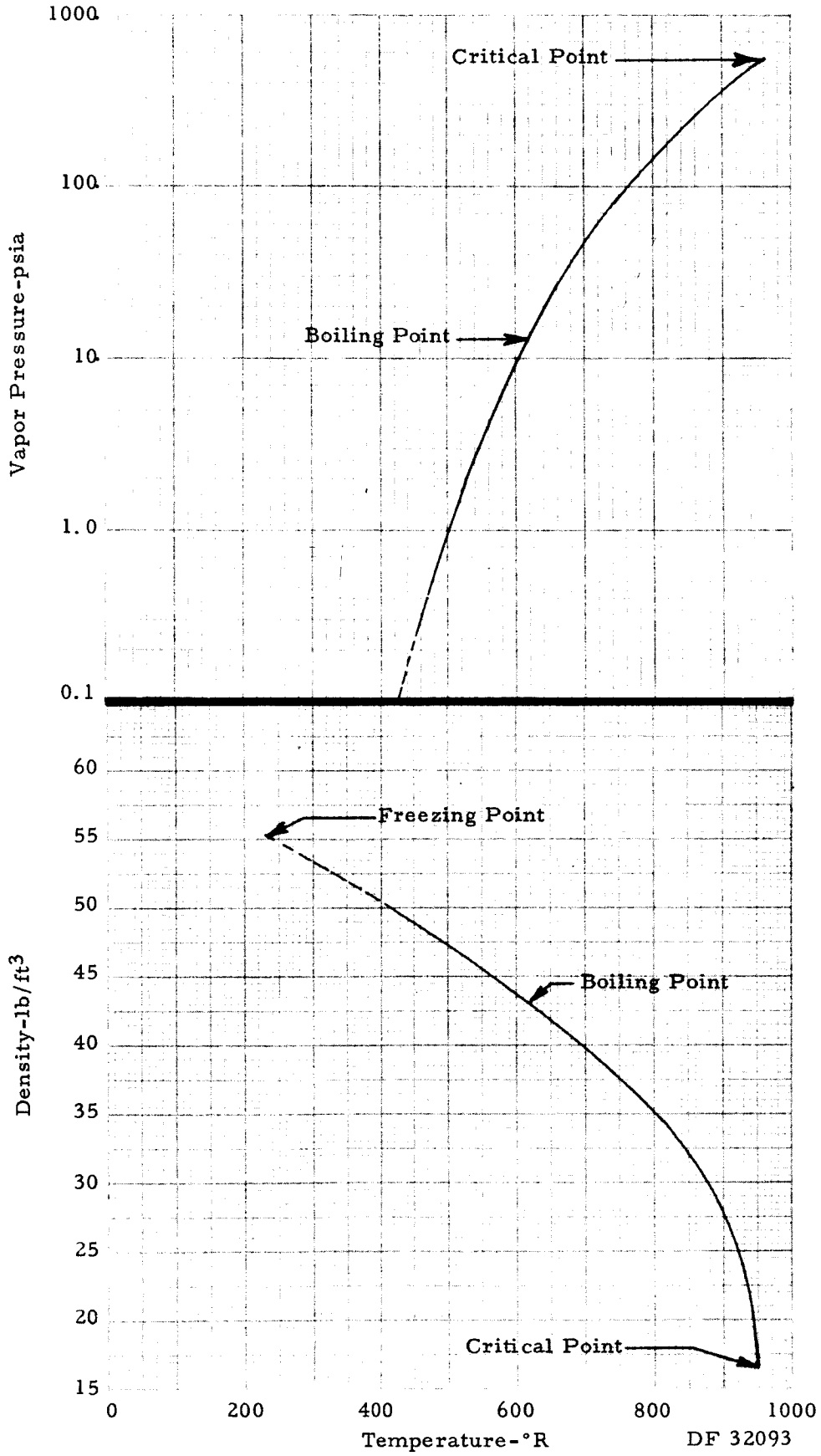

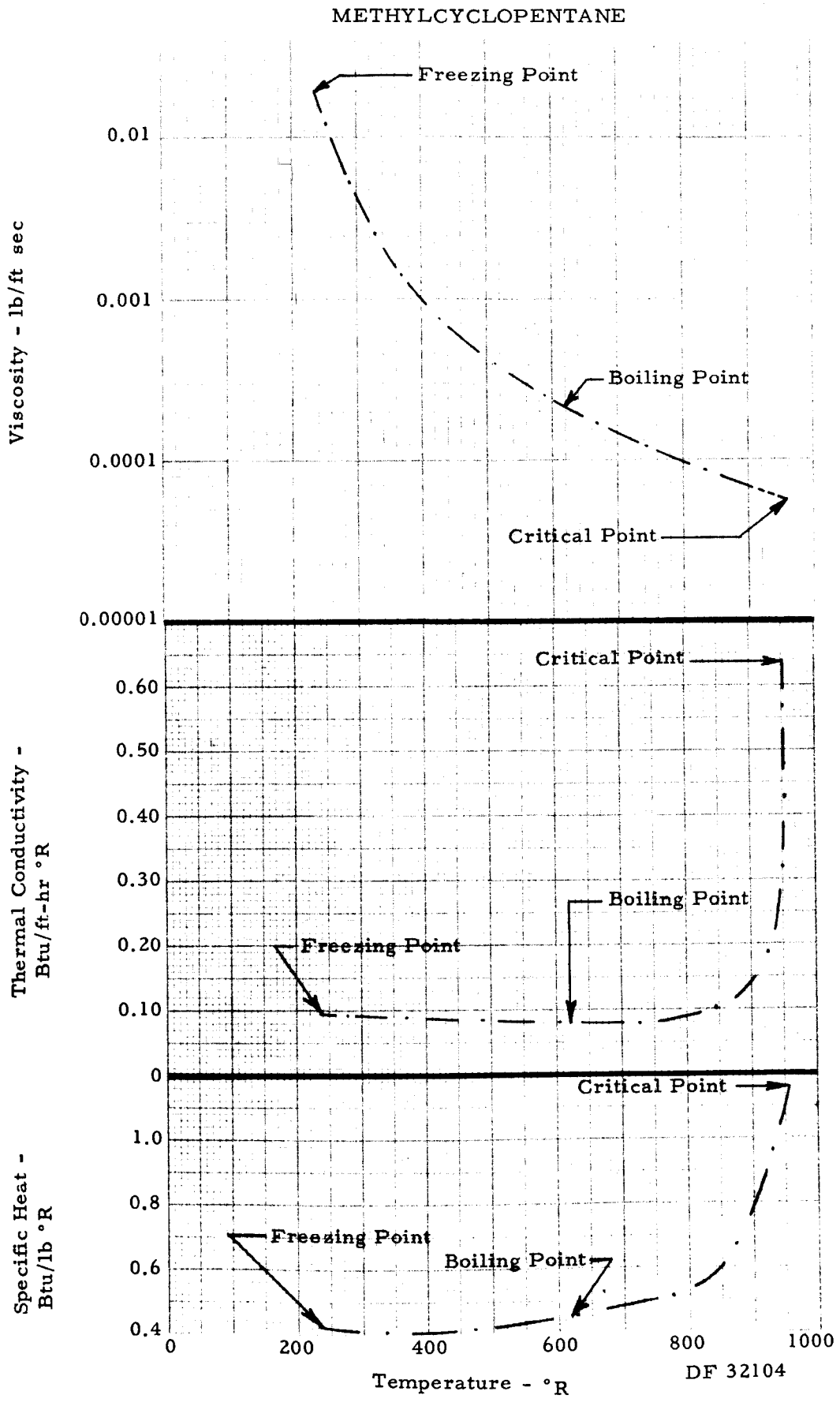
METHYLCYCLOPENTANE
Freezing Point
Boiling Point
Critical Point
Viscosity - lb/ft sec
0.01
0.001
0.0001
0.00001
Critical Point
Boiling Point
Freezing Point
Thermal Conductivity - Btu/ft-hr °R
0.60
0.50
0.40
0.30
0.20
0.10
0
Critical Point
Freezing Point
Boiling Point
Specific Heat - Btu/lb °R
1.0
0.8
0.6
0.4
0
200
400
600
800
1000
Temperature - °R
DF 32104

2-METHYLPENTANE
(ISO-HEXANE)

SUMMARY OF PROPERTIES

		Reference
Chemical formula	C_6H_{14}	
Molecular weight	86.172	
Freezing point (normal), °R	215.1	14
Boiling point (normal), °R	600.2	14
Liquid density (at 537°R), lb/ft³	40.4	14
Critical temperature, °R	896.6	14
Critical pressure, psia	440.1	14
Critical volume, ft³/lb	0.0681	14
Heat of vaporization, (at NBP), BTU/lb	138.67	14
Heat of fusion, BTU/lb	31.33	2
Heat of formation (liquid at 537°R), BTU/lb	—1020.	2
Autoignition temperature, °R		
Flammability limits in air, volume percent	1.2 - 7.7	14

I.C.C. CLASSIFICATION–

Flammable liquid "Red Label"

TOXICITY

Details unknown, may have narcotic or anesthetic properties.

COST AND AVAILABILITY

Phillips Petroleum Co. (Prices FOB, Borger, Texas)

(95% purity) 54 gallon drum (296 lb) — $740.00

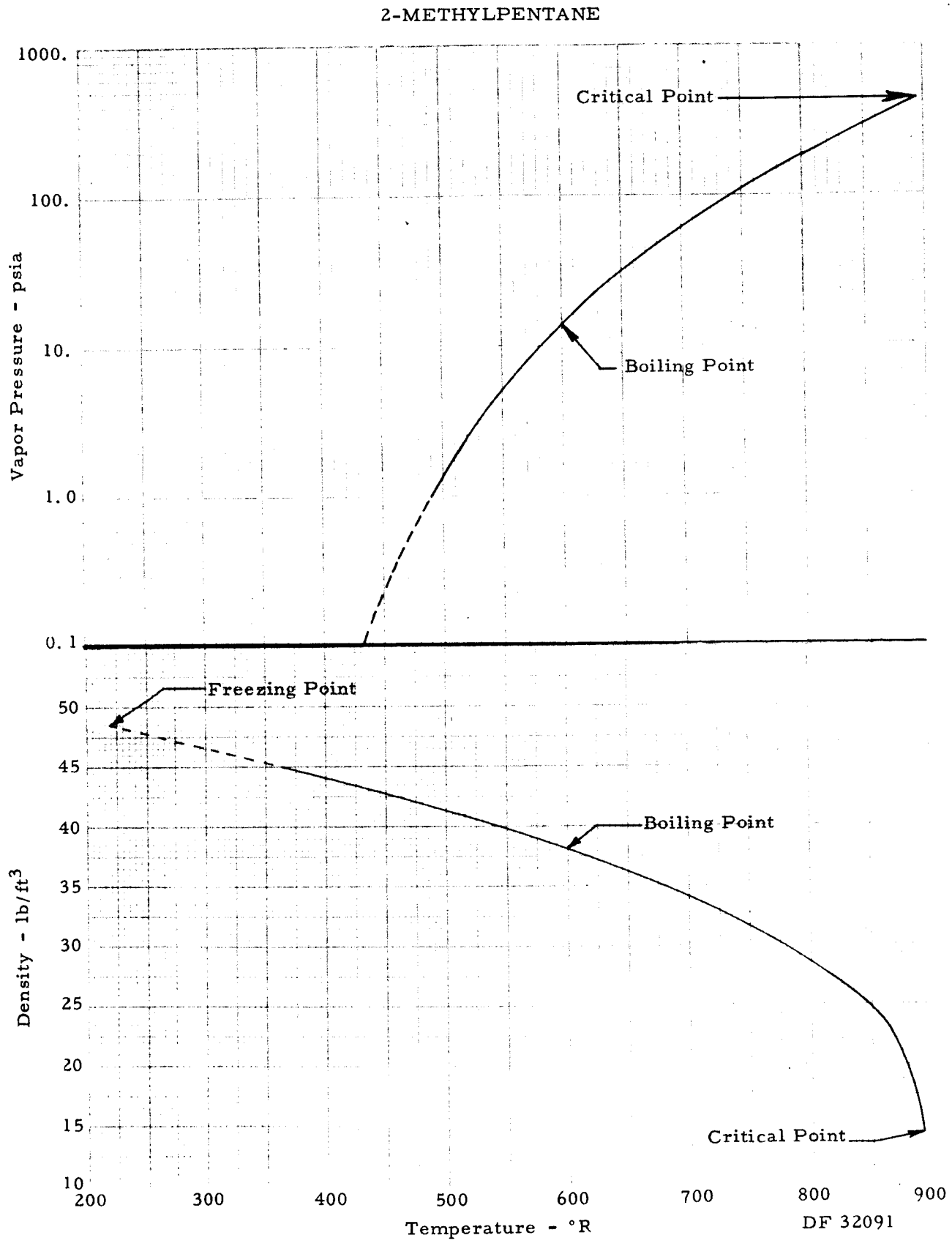
2-METHYLPENTANE
1000.
100.
10.
1.0
0.1
Vapor Pressure - psia
Critical Point
Boiling Point
Freezing Point
50
45
40
35
30
25
20
15
10
Density - lb/ft3
Boiling Point
Critical Point
200
300
400
500
600
700
800
900
Temperature - °R
DF 32091

2-METHYLPENTANE

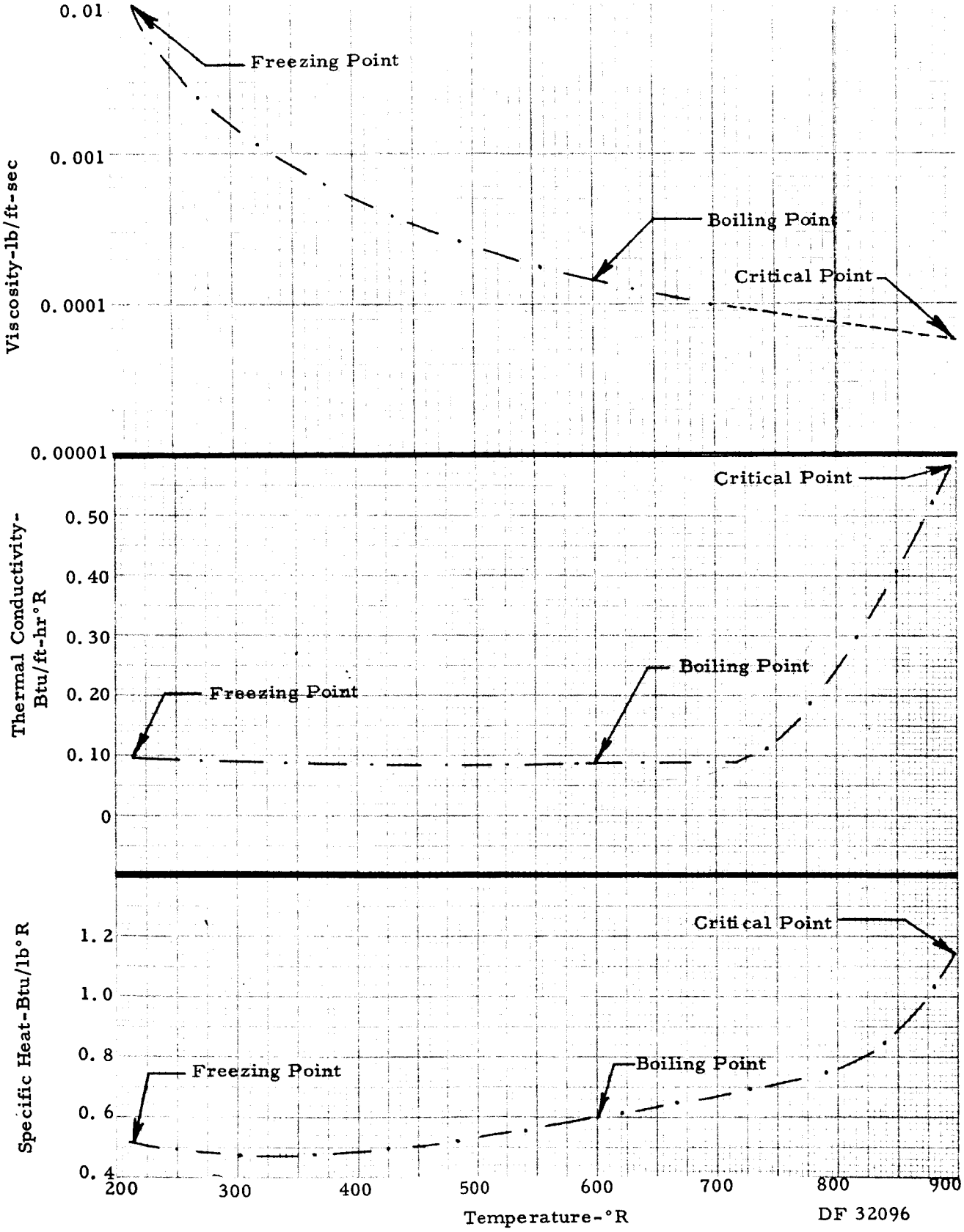

RP-1

SUMMARY OF PROPERTIES

		Reference
Chemical formula	$CH_{1.9063}$	9
Molecular weight	172.	9
Freezing point (normal), °R	420.	10
Boiling point (normal), °R	882.	9
Liquid density (at 537°R), lb/ft³	44.9	9
Critical temperature, °R	1218.	9
Critical pressure, psia	315.	9
Critical volume, ft³/lb	0.060	9
Heat of vaporization, (at NBP), BTU/lb	125.	9
Heat of fusion, BTU/lb	20.	9
Heat of formation (liquid at 537°R), BTU/lb	−757.	8
Autoignition temperature, °R		
Flammability limits in air, volume percent		

I.C.C. CLASSIFICATION—

Flammable liquid "Red Label"

TOXICITY

The Toxicity of RP-1 is low; problems are similar to gasoline and kerosene.

COST AND AVAILABILITY

About $0.015 to $0.02 per pound in tank car quantities.

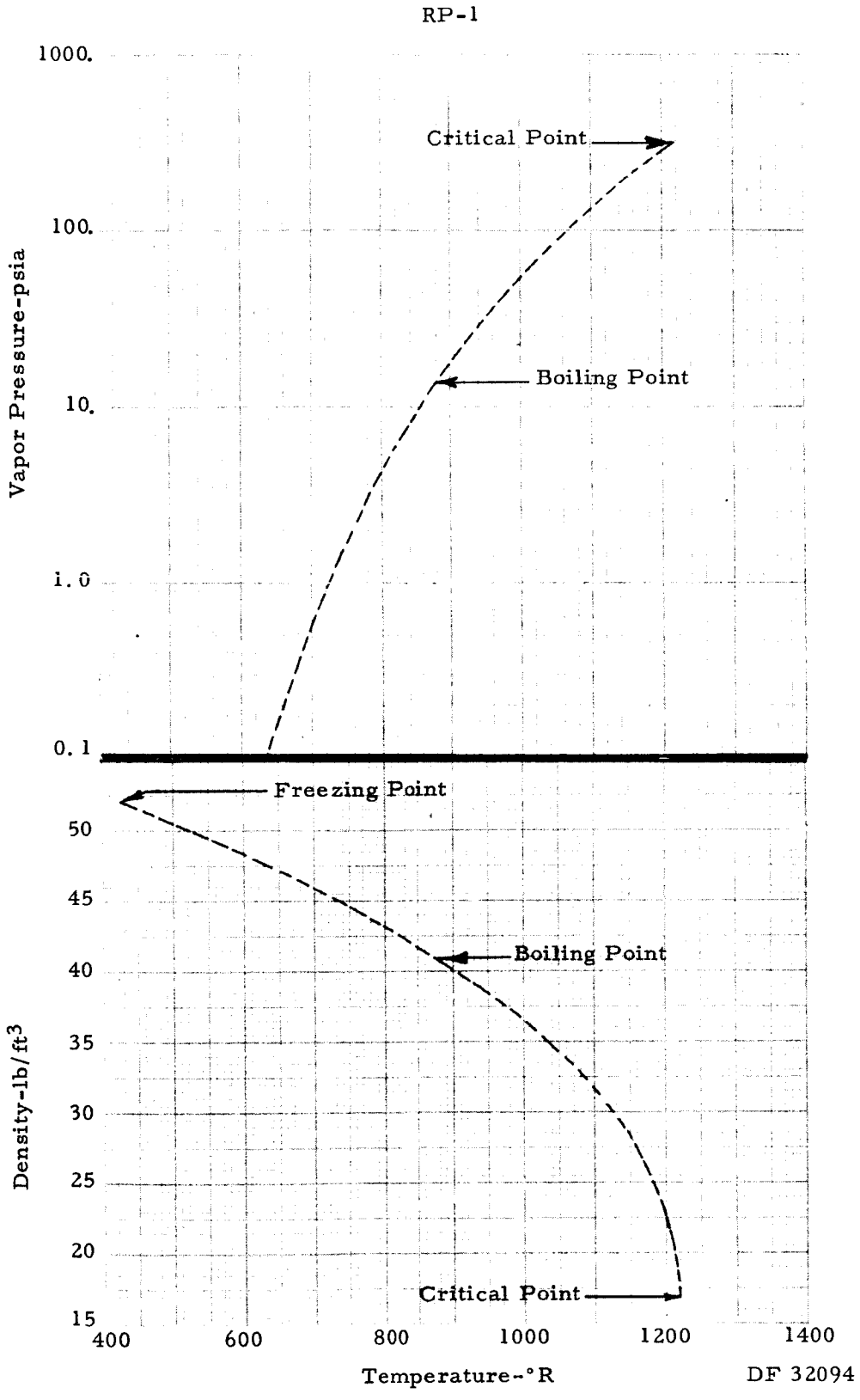
RP-1
1000.
100.
10.
1.0
0.1
Vapor Pressure-psia
Critical Point
Boiling Point
Freezing Point
Boiling Point
Critical Point
50
45
40
35
30
25
20
15
Density-lb/ft3
400
600
800
1000
1200
1400
Temperature-°R
DF 32094

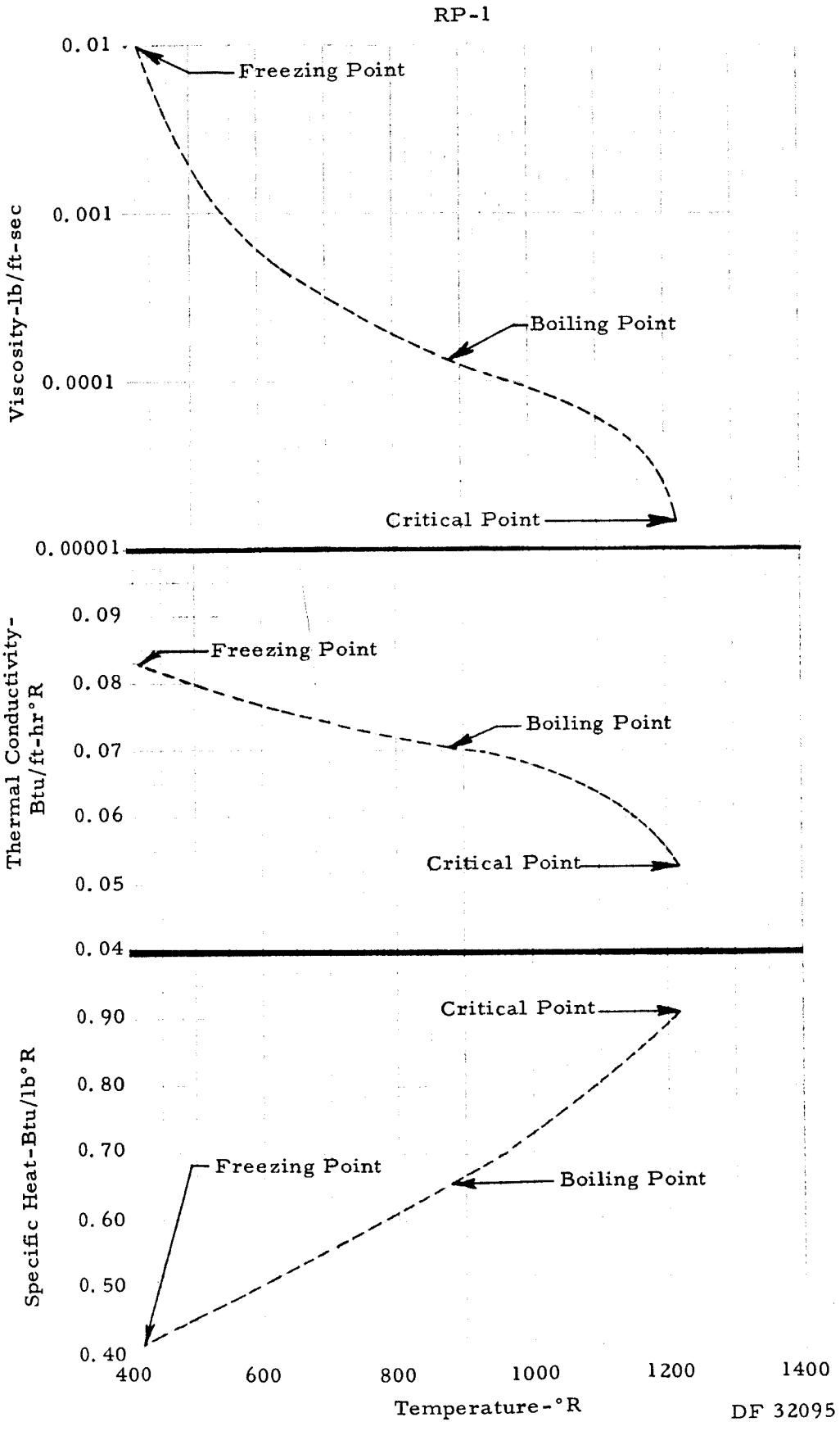
RP-1
0.01
0.001
0.0001
0.00001
Viscosity-lb/ft-sec
Freezing Point
Boiling Point
Critical Point
0.09
0.08
0.07
0.06
0.05
0.04
Thermal Conductivity-
Btu/ft-hr°R
Freezing Point
Boiling Point
Critical Point
0.90
0.80
0.70
0.60
0.50
0.40
Specific Heat-Btu/lb°R
Critical Point
Freezing Point
Boiling Point
400
600
800
1000
1200
1400
Temperature-°R
DF 32095

REFERENCES

1. Evered, Douglas S. and Boris Kit, "Rocket Propellant Handbook," New York, (The Macmillan Company), 1960

2. Perry, J. H. (Ed.), "Chemical Engineers' Handbook," New York, (McGraw-Hill Book Company), 1963

3. Jenkin, D. B. "The Properties of Liquified Petroleum Gases," London, Shell International Petroleum Company Limited, Oil Products Development Division; Sept. 1962

4. Din, F. (Ed.) "Thermodynamic Functions of Gases," London (Butterworths), 1961

5. Maxwell, J. B., "Data Book on Hydrocarbons," New York (D. Van Nostrand Company, Inc.) 1950

6. Timmermans, J., "Physico-Chemical Constants of Pure Organic Compounds," New York (Elsevier Publishing Co., Inc.) 1950

7. American Petroleum Institute Project 44, "Selected Values of Physical & Thermodynamic Properties of Hydrocarbons and Related Derivatives," New York (Elsevier Publishing Co., Inc.) 1950

8. B. Williams and G. Wynne "Composition and Thermodynamic Properties of Propellants," January 20, 1964 DF-19284

9. Petrozzi, P. J. and L. E. Dean, Report No. LRP 178, "Physical Properties of Liquid Propellants," Sacramento, California, Aerojet-General Corporation, 1960

10. Military Specification, "Rocket Fuel, RP-1," MIL-R-25576B 3 January 1957

11. Sax, N. Irving, "Dangerous Properties of Industrial Materials Second Edition," Reinhold Publishing Corporation, New York, 1963

12. The Matheson Company, Inc., "Gas Data Book," New York, N.Y. 1961

13. "Interstate Commerce Commission Regulations," Agent T. C. George's, Tariff No. 13, issued by T. C. George, Agent, 30 Vesey Street, New York 7, New York

14. "Reference Data for Hydrocarbons and Petro-Sulfur Compounds," Phillips Petroleum Company, Special Products Division, Bartlesville, Oklahoma 1962

15. "Alkyl Acetylenes Product Data Sheet," Air Reduction Chemical and Carbide Co. 150 East 42nd Street, New York, N.Y. MDD Technical Bulletin C-1

APPENDIX B
DETERMINATION OF SELECTED PHYSICAL PROPERTIES OF LIQUID HYDROCARBON BLENDS

1. EUTECTIC DIAGRAMS

Analysis of the cooling curve for a binary hydrocarbon solution of definite composition allows the determination of the freezing point of that solution and the eutectic temperature for the system. By plotting the freezing points of a series of binary mixtures against their known compositions, the composition of the eutectic solution was determined graphically. Several experimental considerations tend to limit the accuracy of the procedure. The most significant of these are:

1. Equilibrium Kinetics: In the determination of a freezing point, the temperature should be changed as slowly as practicable to provide enough time for different phases in the system to come to equilibrium. The time required for equilibrium to be attained appeared to be closely related to viscosity. The more viscous samples did not come to equilibrium even after several hours of repeated seeding, stirring, and waiting. In less severe cases, the time required for crystals to form or melt at a given temperature was sometimes great compared to the temperature stability of the apparatus, resulting in a slight scattering of the data.
2. Supercooling: In general, the solutions had to be cooled below their melting points before freezing began. The amount of supercooling required depended on the rate of cooling, manner of stirring, nature of temperature gradients, and the presence of suitable crystal nuclei. Usually, if a sample had been frozen and carefully warmed to its melting point, freezing could proceed with very little supercooling. This was due to the presence of tiny crystal nuclei. The term "melting point" refers to the lowest temperature at which any frozen solids were suspended in a mixture melt. This is the same temperature as the freezing point provided proper techniques were employed to minimize supercooling.

a. Apparatus

Samples were placed in a double walled glass vessel. Cooling was accomplished by surrounding the vessel with liquid nitrogen. By adjusting the pressure of helium gas between the two glass walls surrounding the sample, the rate of heat exchange between the sample and its surroundings could be quickly adjusted. Temperature was measured with calibrated copper-constantan thermocouples connected to a one-millivolt recorder with adjustable zero point. Freezing points were observed visually or defined as plateaus on the temperature-time recorder trace.

A closed freezing point apparatus (figure B-1) was used for mixtures composed of two liquefied gases or one liquefied gas and one normal liquid. Mixtures were cooled to 125°R by evacuating the space above the liquid nitrogen. An effective vacuum seal over the liquid nitrogen was obtained by sealing the glassware to an aluminum plate with epoxy adhesive and clamping the plate, sealed with a neoprene gasket, onto the liquid nitrogen dewar. A heating coil of Nichrome wire was included to reflux vapors frozen in the inlet tube back into the sample solution. Stirring was accomplished by bubbling helium through the sample.

An open freezing point apparatus (figure B-2) was used for mixtures composed of two normal liquids. A blanket of helium kept air and moisture out of the sample. The lower temperature was limited to 160°R since there was no provision for changing the pressure on the liquid nitrogen. A stainless steel stirring ring was operated electrically.

For temperature measurement in both apparatus, two copper-constantan thermocouples were fabricated from the same spools of wire. Initial calibration was made with a resistance thermometer as a reference in liquid oxygen and liquid nitrogen. When extended calibration became necessary, the melting points of several pure hydrocarbons, whose melting points were known from the literature, were measured in the closed glass cryostat. These two sets of data overlapped quite well and thereby provided calibration in the range 125 to 270°R.

The two thermocouples were arranged in a circuit designed to provide several cross checks in order to assure accuracy. Both thermocouple reference junctions were placed in a test tube half full of mercury suspended in an ice bath. The mercury acted as a heat sink and prevented thermal transients in the junctions. One of the thermocouple read-out junctions was placed in liquid nitrogen and the other in the sample to be measured. When the potential from the thermocouple in boiling liquid nitrogen remained at a constant temperature equilibrium in the ice bath (as read on the millivolt potentiometer) reference was assumed. This output was then switched to a strip recorder through switch "A" (figure B-3). Then by throwing switch "B," the sample temperature could be recorded as a function of time. Frequent cross checks with the liquid nitrogen reference and potentiometer allowed detection of recorder drift, which was usually negligible.

b. Procedure

(1) Methane-Propane

A six liter stainless steel cylinder was dried and evacuated. Gaseous methane and propane were mixed in the cylinder to the desired composition by adjusting their partial pressures.

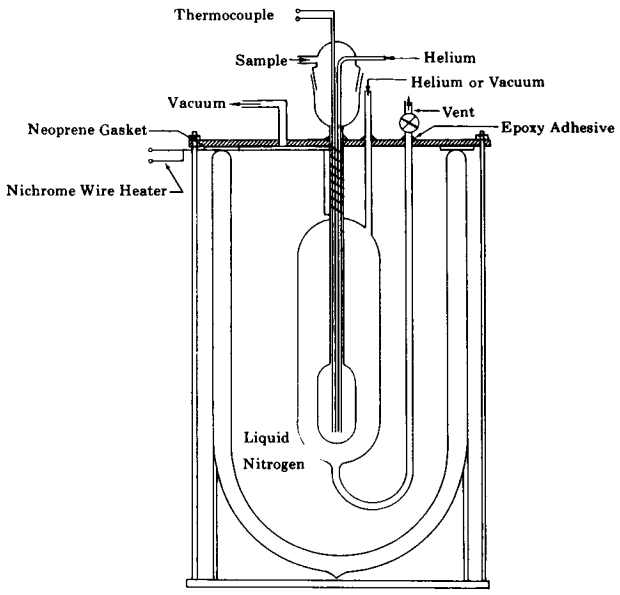

Figure B-1. Closed Freezing Point Apparatus *FD 9554*

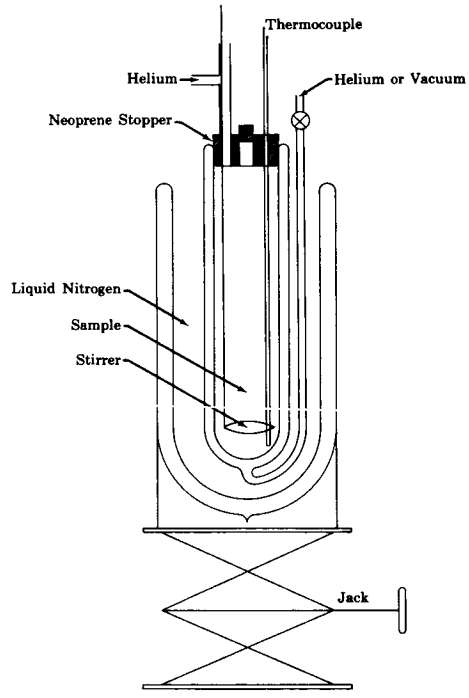

Figure B-2. *FD 9562*

Open Freezing Point Apparatus

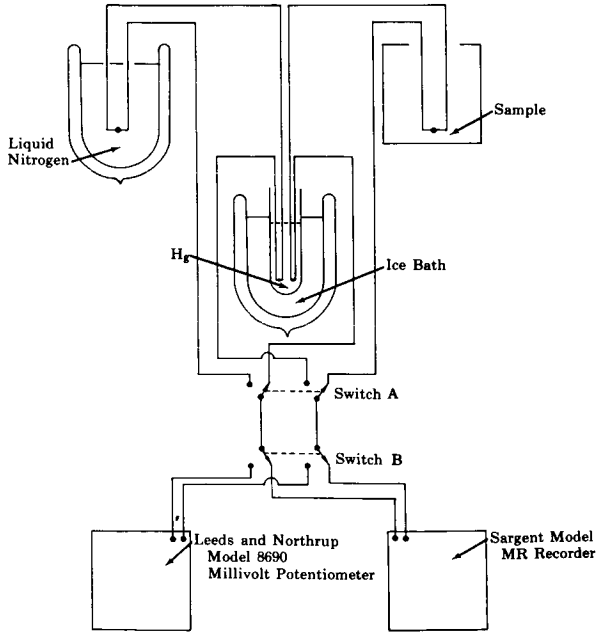

Figure B-3. Thermometry Circuit *FD 9556*

A schematic of the gas mixing apparatus is shown in figure B-4. To gasify the composition, the mixture was analyzed with a gas chromatograph. The melting point apparatus was thoroughly dried and evacuated. By surrounding the apparatus with liquid nitrogen and filling the helium jacket with helium to atmospheric pressure, the glassware was cooled to 140°R. By slowly admitting the analyzed mixture of gases, a solution of liquid methane and liquid propane was formed in the freezing point apparatus. By reducing the pressure in the helium jacket, the rate of cooling was lowered. By reducing the pressure on the liquid nitrogen, freezing points down to 125°R could be determined.

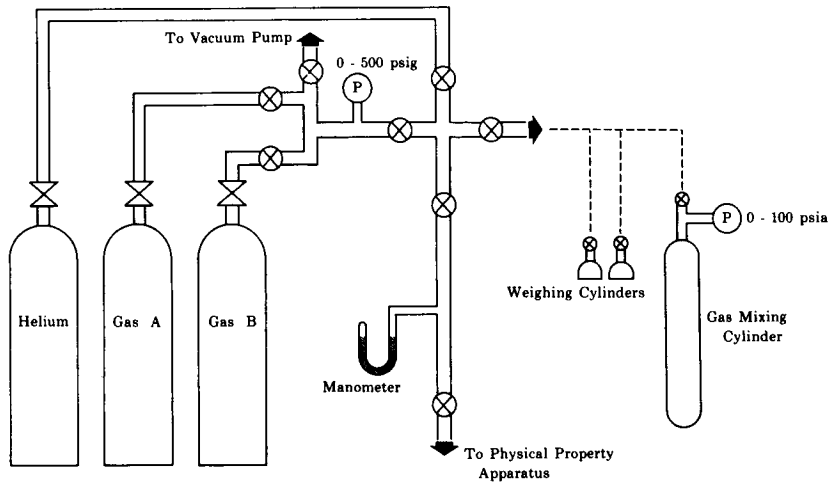

Figure B-4. Gas Mixing Apparatus *FD 9561*

At temperatures slightly below the freezing point of methane, crystals of methane formed on the walls of the container above the surface of the unfrozen solutions. This phenomenon would pose a problem for tankage when crystals would deposit on the walls above the liquid level of the fuel blend provided the temperature is below the freezing point of the vapor. This problem appears to be pronounced only in systems containing methane, since the other hydrocarbons tested have considerably lower vapor pressures near their freezing points. The eutectic point is at 126°R with 16% methane as shown in figure B-5.

(2) Methane-Ethane

A portion of the methane-ethane freezing point curve was determined by T. A. Whatley for U.T.C. in February 1964. Whatley's data did not go below 140°R. Extrapolation appeared to indicate a eutectic point of 133°R and 55% methane. By using the apparatus and procedure described for methane-ethane, the predicted eutectic point was verified experimentally as shown in figure B-6.

Figure B-5
Effect of Blending on the Freezing Point and Cooling Capacity of Hydrocarbon Fuels (Methane-Propane)

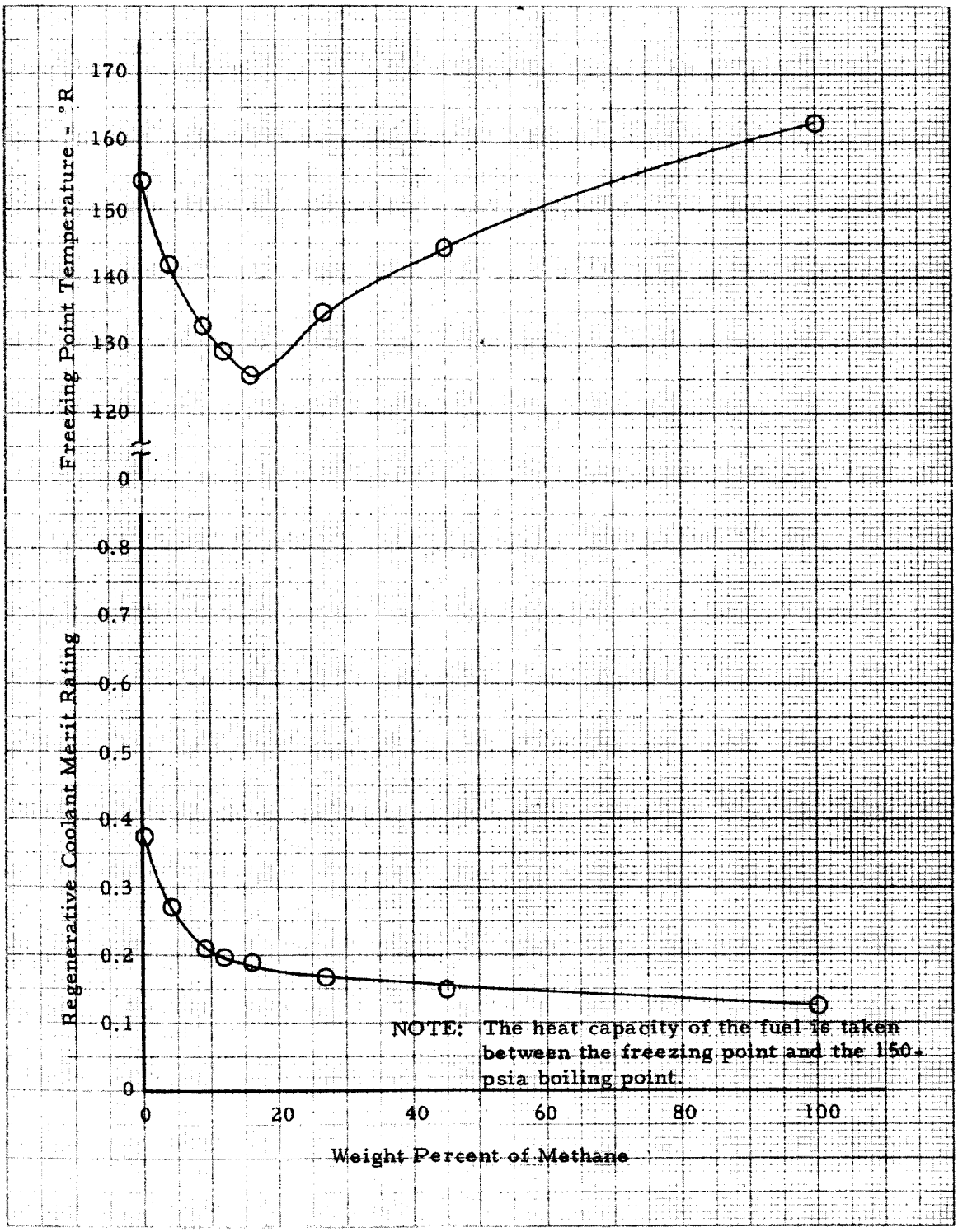

DF 33144
Sheet 5 of 8

Figure B-6
Effect of Blending on the Freezing Point and Cooling Capacity of Hydrocarbon Fuels (Methane-Ethane)

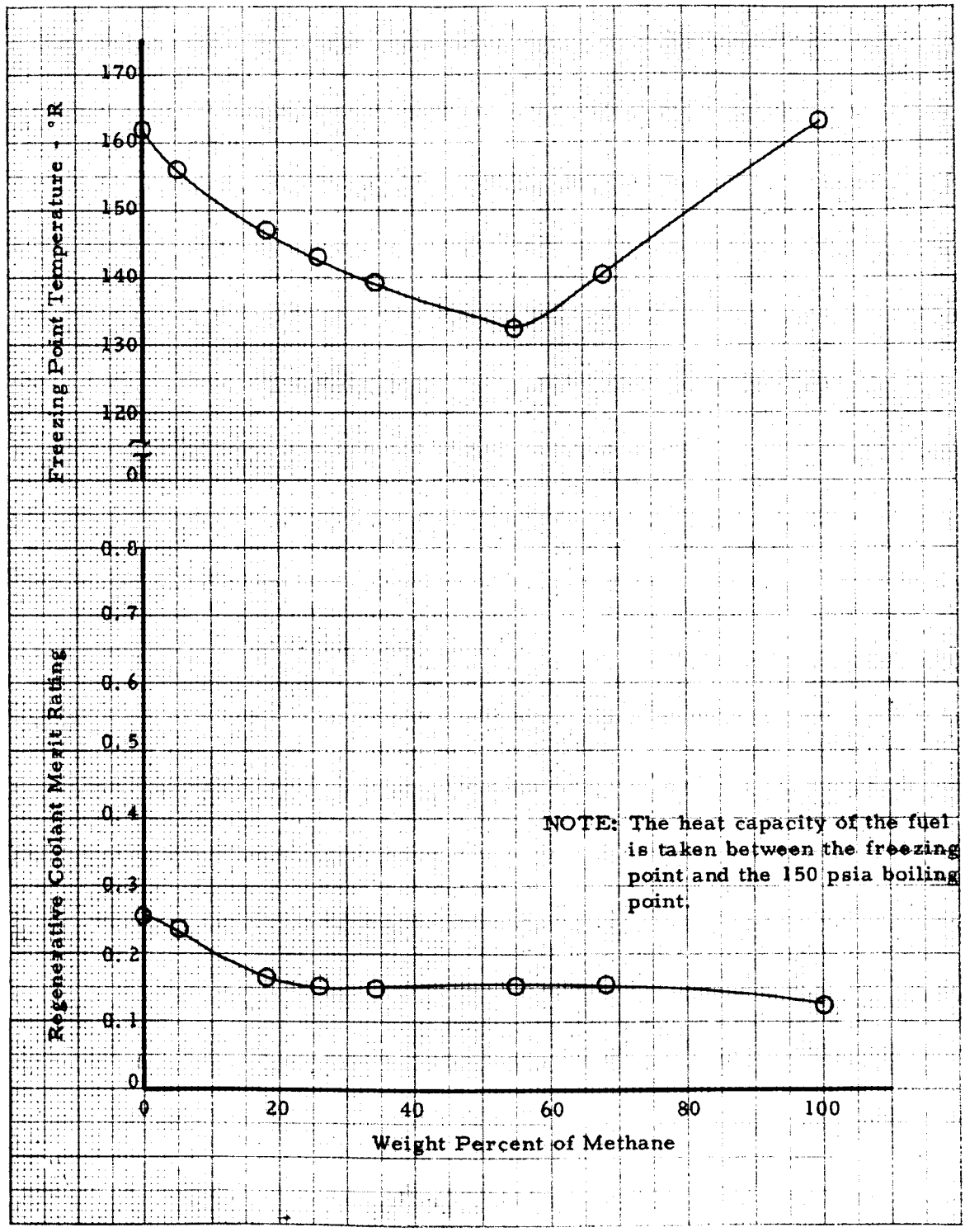

DF 33144
Sheet 2 of 8

(3) Propane-Butene-1

Samples were prepared by mixing the two compounds in the gaseous state as described in the methane-propane procedure. However, the freezing point curve could not be determined because of the glasslike behavior of Butene-1. On cooling, the solutions hardened without any inflection in the cooling curve and without any visual evidence of crystallization.

(4) Propane-Pentane

Since propane is normally a gas and pentane is normally a liquid, the preparation of these mixtures was somewhat more involved. A lightweight 30 ml metal cylinder was evacuated and submerged in liquid nitrogen. Propane gas was liquefied in the cylinder and allowed to warm to room temperature. The cylinder and its contents were weighed to 0.1 milligram. The closed melting point apparatus was evacuated and filled with helium at atmospheric pressure and cooled to 360°R. A measured volume of pentane was introduced through the tapered glass joint with a long needle syringe. The pentane was then frozen and the helium pumped off. Propane vapors from the weighed cylinder were liquefied with the frozen pentane. By noting the change in weight of the propane cylinder and the density of the pentane added volumetrically, the weight composition of the mixture was determined.

Before determining the freezing point of the mixture, the pentane was allowed to melt and thoroughly mixed with the liquid propane by bubbling helium through the solution. The eutectic point is at 148°R with 95% propane as shown in figure B-7.

(5) Butane-Pentane

These determinations followed the same procedure as described under the propane-pentane procedure. The eutectic point is at 221°R with 68.0% butane as shown in figure B-8.

(6) Propane-Propylene

A second metal weighing cylinder, similar to the propane weighing cylinder described above, was fabricated for weighing samples of propylene. Mixtures were made by liquefying quantities of the two gases from their weighing cylinders into the melting point apparatus at 160°R. The eutectic temperature was observed clearly at 137°R with 48% propane as shown in figure B-9.

Figure B-7
Effect of Blending on the Freezing Point and Cooling Capacity of Hydrocarbon Fuels (Propane-Pentane)

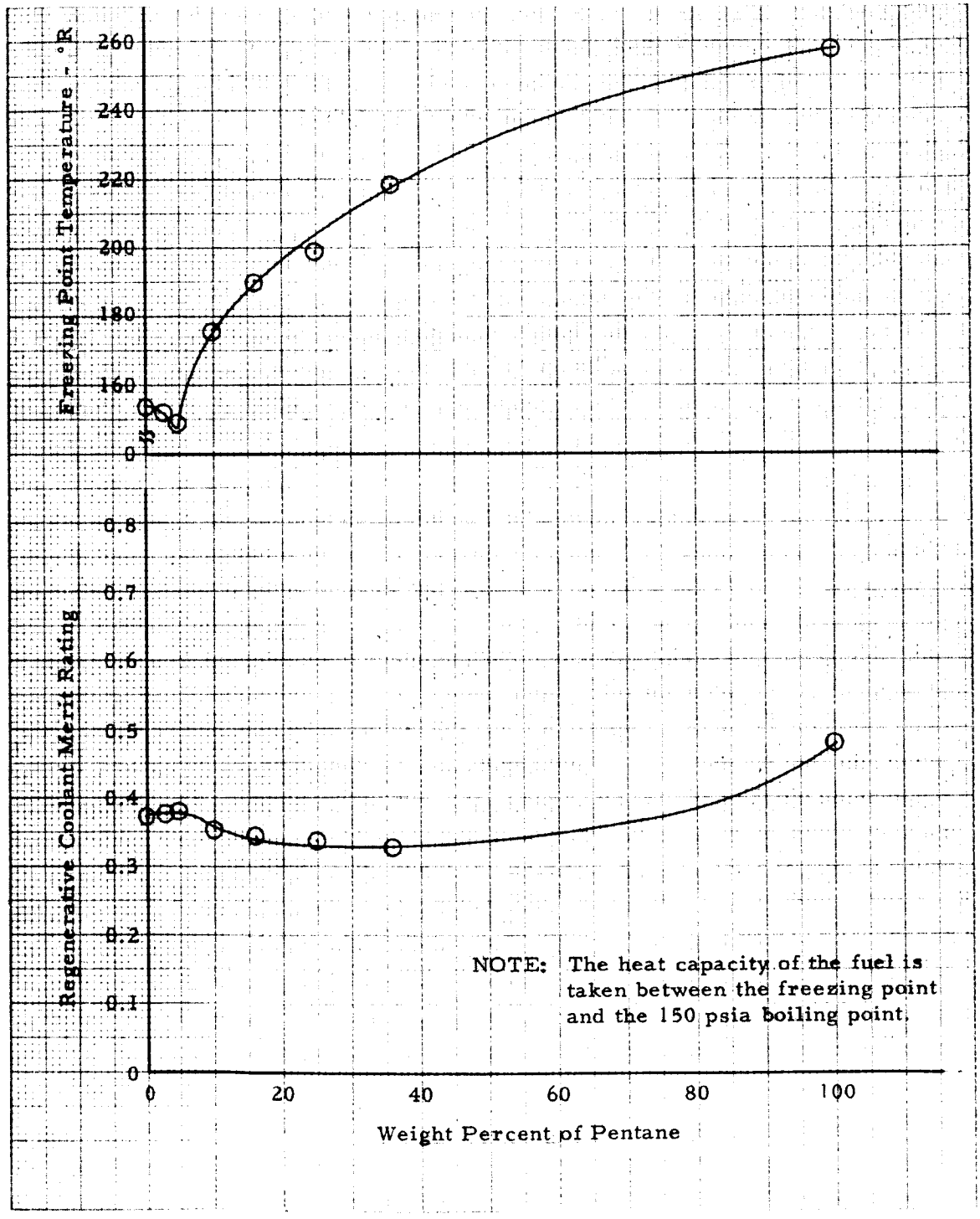

DF 33144
Sheet 1 of 8

Figure B-8
Effect of Blending on the Freezing Point and Cooling Capacity of Hydrocarbon Fuels (Butane-Pentane)

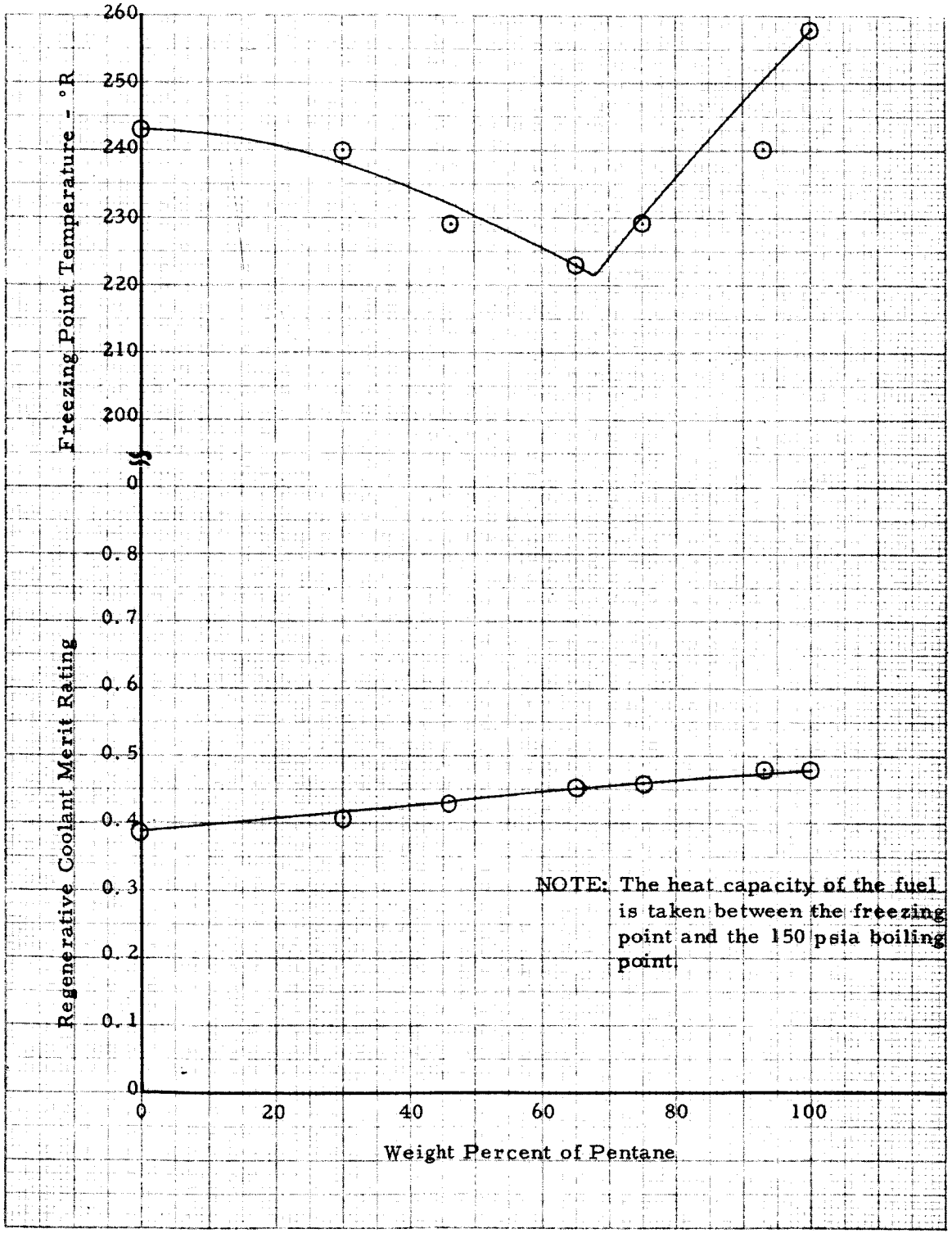

DF 33144
Sheet 6 of 8

Figure B-9
Effect of Blending on the Freezing Point and Cooling Capacity of Hydrocarbon Fuels (Propylene-Propane)

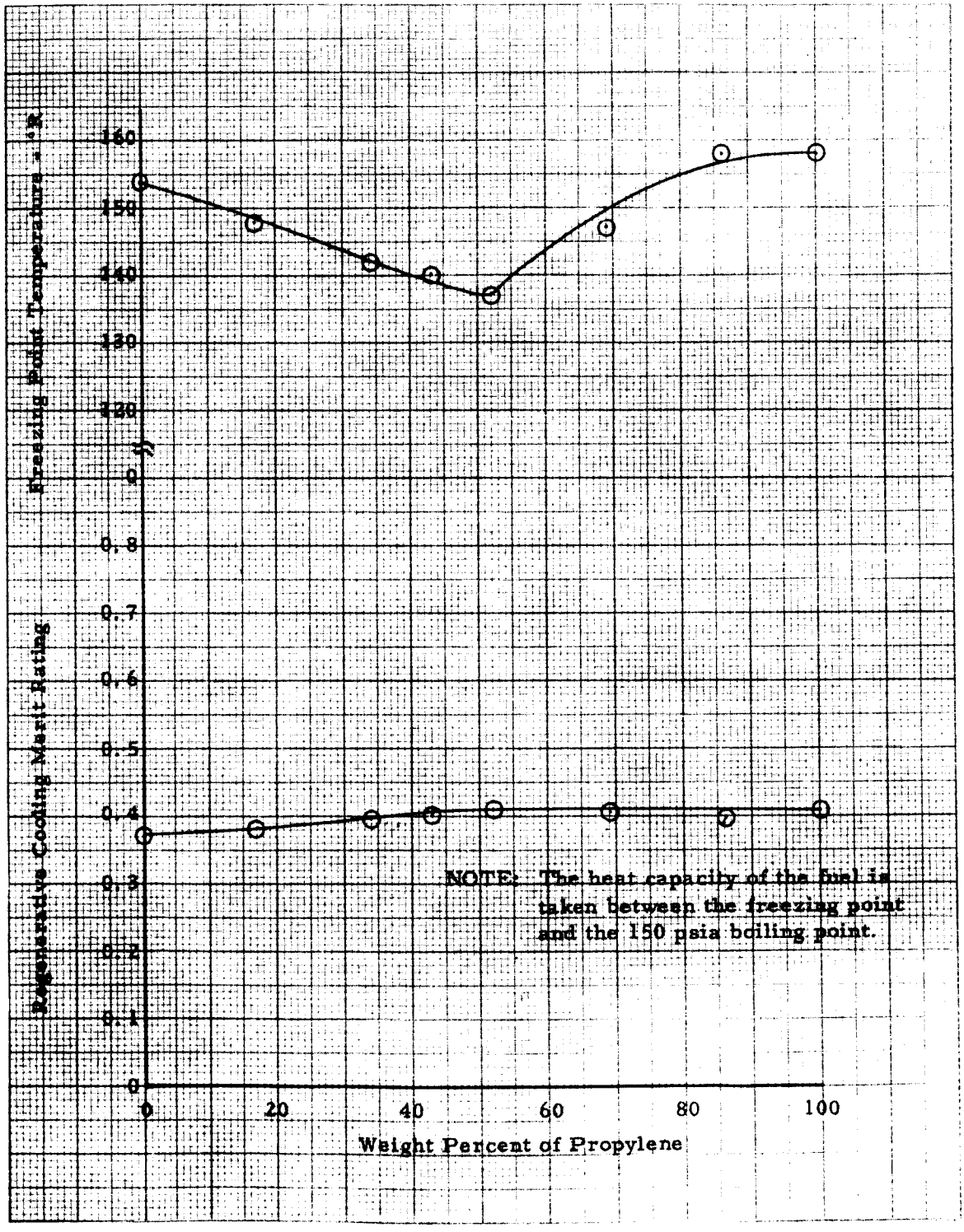

DF 33144
Sheet 4 of 8

(7) Propane-Isopentane

Since the remaining three systems (7, 8, and 9) were all composed of normal liquids, the simpler open apparatus was used to determine the freezing points. The liquids were weighed in stoppered glass containers and transferred to the freezing point apparatus under a blanket of helium. The viscosity of pentane-isopentane mixtures appeared quite low and freezing required little supercooling. The eutectic point is at 196°R with 14.0% pentane as shown in figure B-10.

(8) Methylcyclopentane-2-Methylpentane

These mixtures took considerable time to come to equilibrium because of the glasslike behavior of 2-methylpentane. The viscosity increased sharply as the freezing point was approached. The eutectic point is at 197°R with 31% methylcyclopentane as shown in figure B-11.

(9) 2-Methylpentane-Isopentane

The eutectic point could not be determined due to several indeterminate freezing points. Seeds of both materials were stirred into mixtures of 32.2, 51.6, and 66.7 percent 2-methylpentane for 1 to 2 hours without inducing crystallization. The temperatures listed for these points represent merely the point at which the solutions were so viscous that mechanical stirring became difficult. The eutectic point is estimated at 184°R with 36% 2-methylpentane as shown in figure B-12.

Figure B-10
Effect of Blending on the Freezing Point and Cooling Capacity of Hydrocarbon Fuels (Pentane-Isopentane)

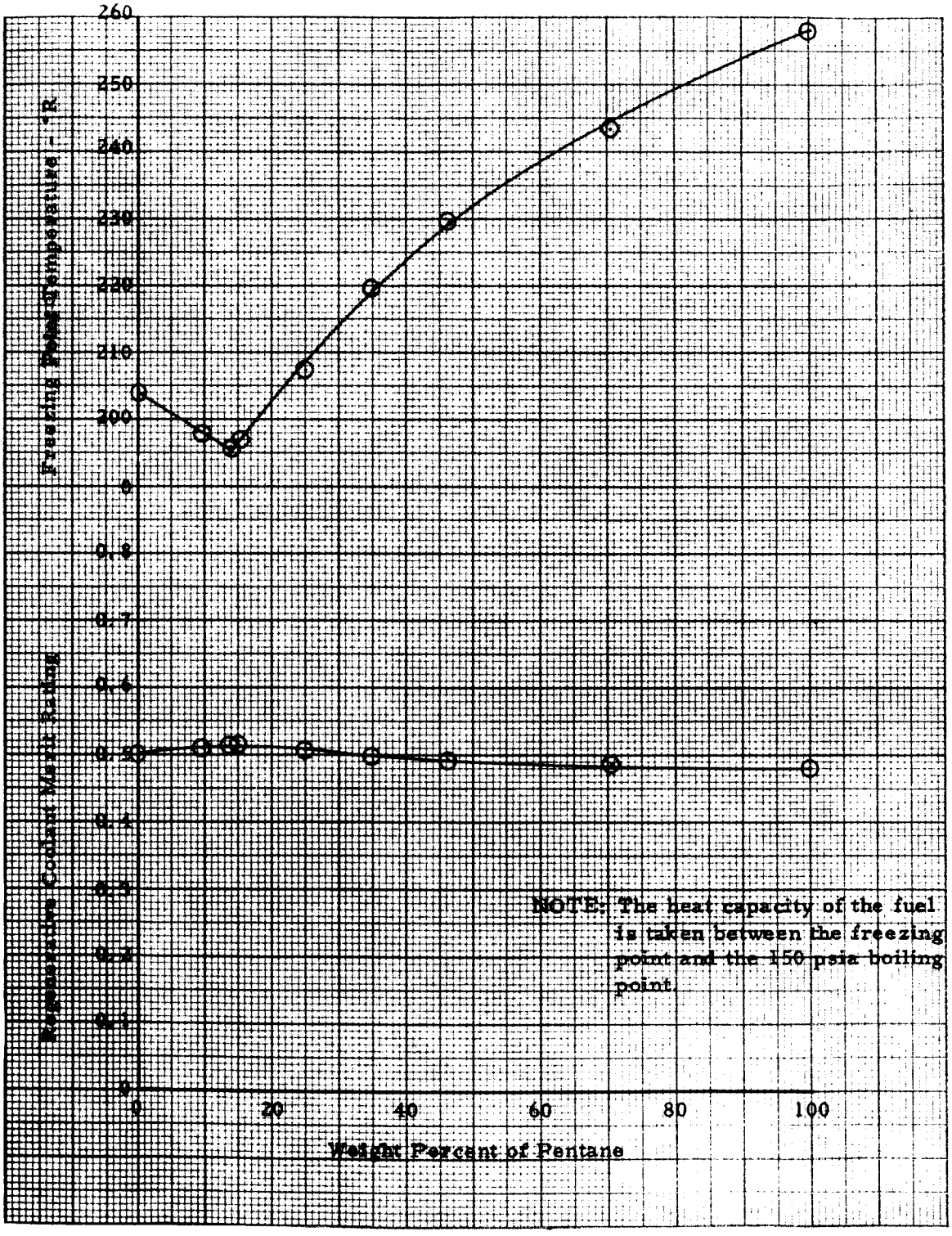

DF 33144
Sheet 3 of 8

Figure B-12
Effect of Blending on the Freezing Point and Cooling Capacity of Hydrocarbon Fuels (Isopentane-2-Methylpentane)

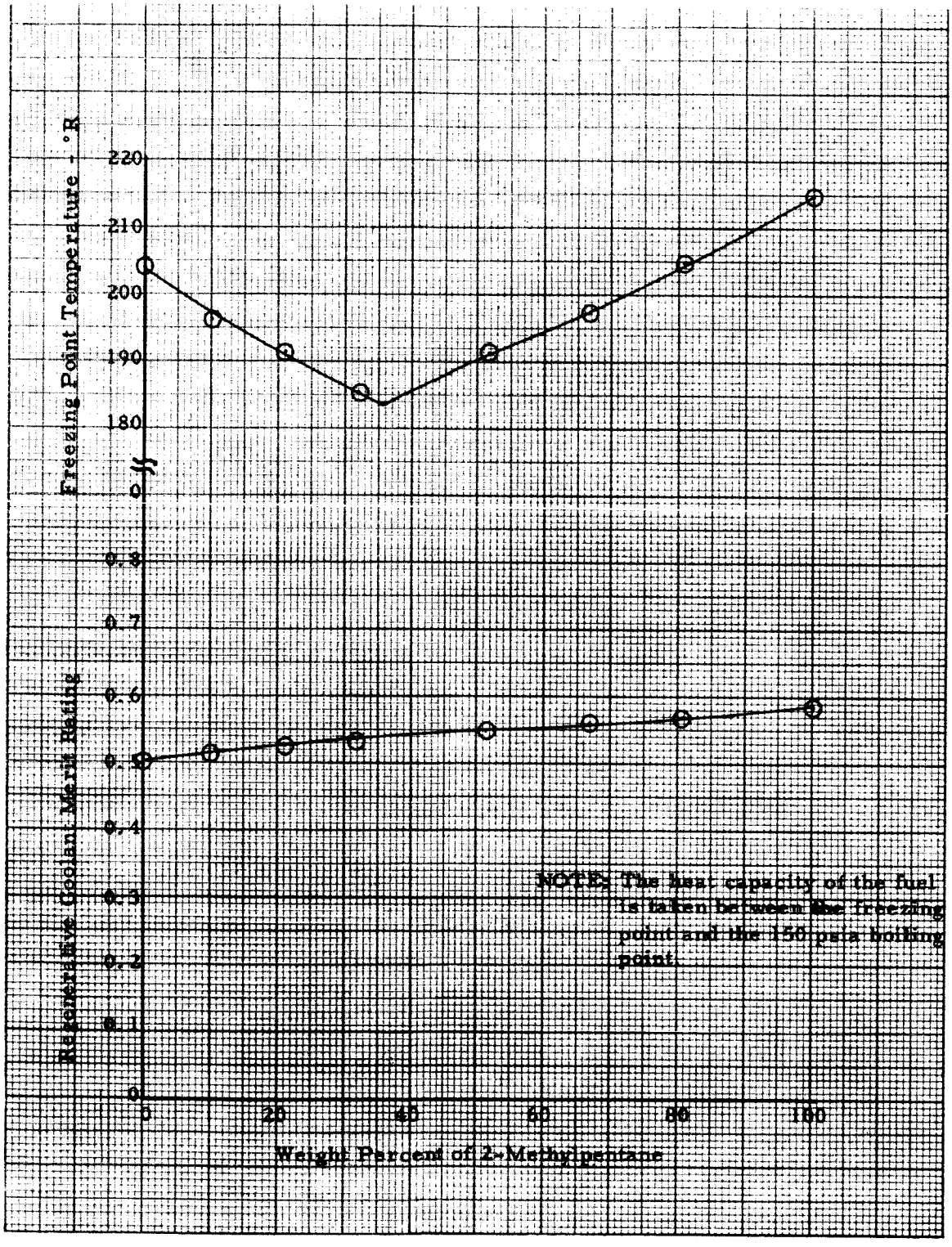

DF 33144
Sheet 7 of 8

Figure B-11
Effect of Blending on the Freezing Point and Cooling Capacity of Hydrocarbon Fuels (2-Methylpentane-Methylcyclopentane)

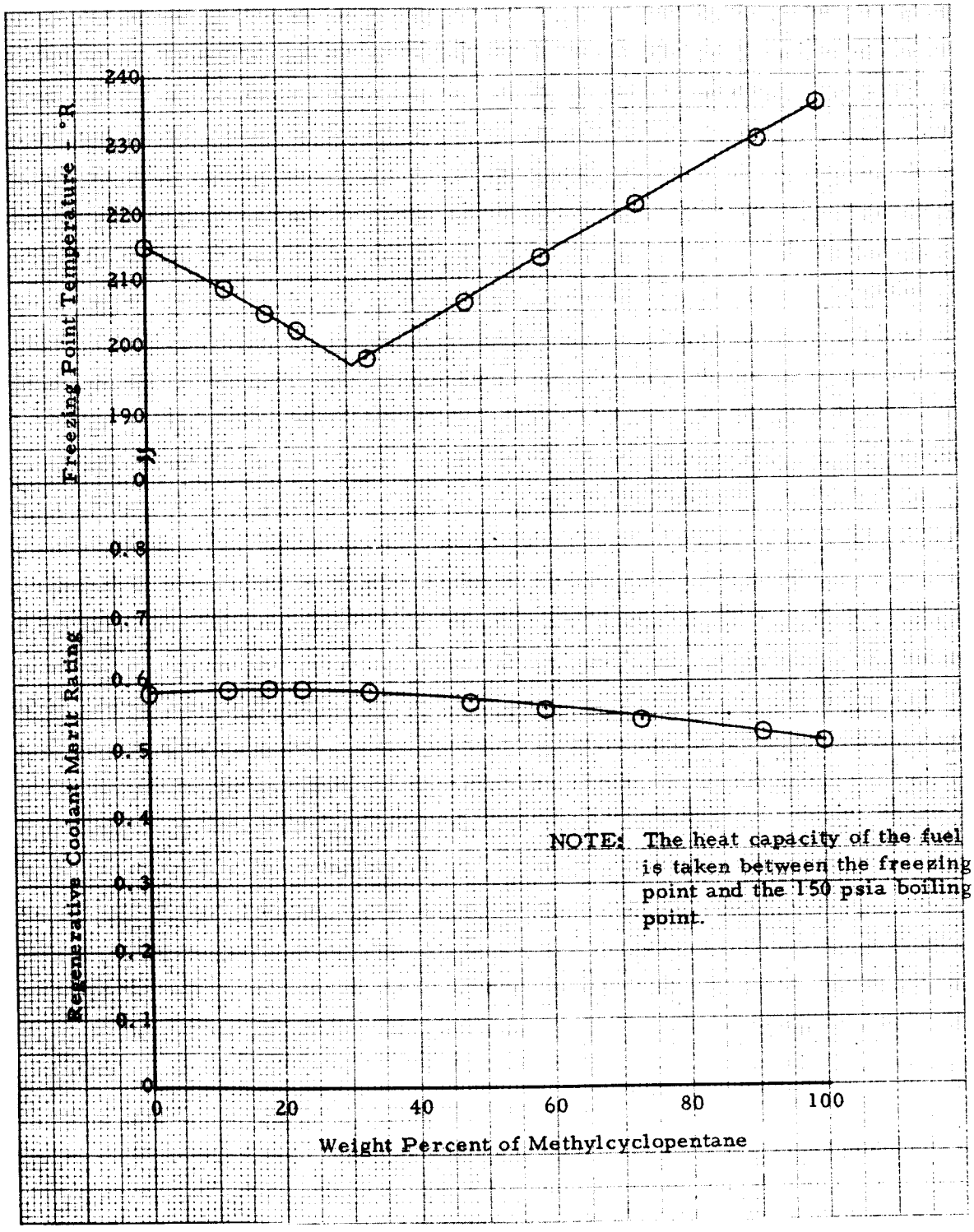

DF 33144
Sheet 8 of 8

2. *DENSITY*

a. Apparatus

A glass dewar, 7 inches long and 1 inch diameter was modified for admitting helium to the vacuum jacket (figure B-13). The dewar was fitted with a neoprene stopper with appropriate glass fittings for providing a helium blanket, and openings for the stirrer, thermocouple, and 1 ml quartz bob. The quartz bob was suspended with two feet of fine platinum wire from a one-pan substitution weighing balance. A ring stirrer was operated by an electric motor through a rotary to linear drive gear box to minimize the adverse effects of air currents on the balance.

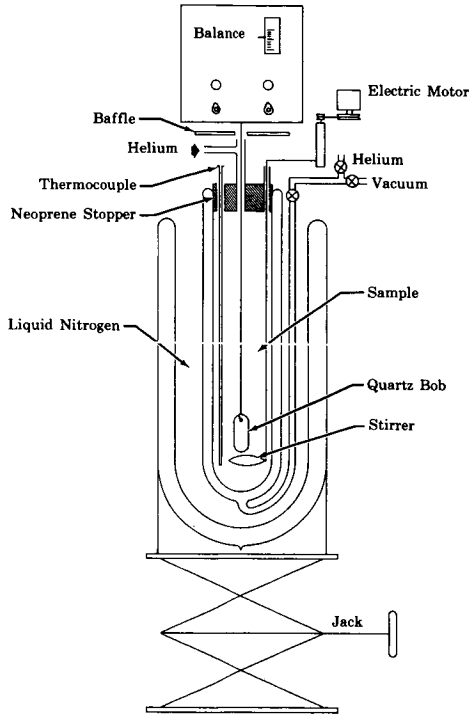

Figure B-13. Cryogenic Density Apparatus *FD 9555*

b. Procedure

The bob was weighed in water at room temperature and in air. By determining the difference in weight and the density of the water, the volume of the bob was calculated.

(1) Pentane-Isopentane

Approximately 75 ml of the pentane-isopentane eutectic solution was placed in the cryostat and cooled to the desired temperature with constant stirring. When the dewar was evacuated, the temperature remained constant for approximately five minutes, allowing sufficient time for at least two weighings of the bob. Just prior to releasing the bob for the final weighing, the stirrer and helium purges were turned off to eliminate any slight effect on the balance. Results are shown in figure B-14.

Figure B-14
Density of Pentane-Isopentane Eutectic Solution

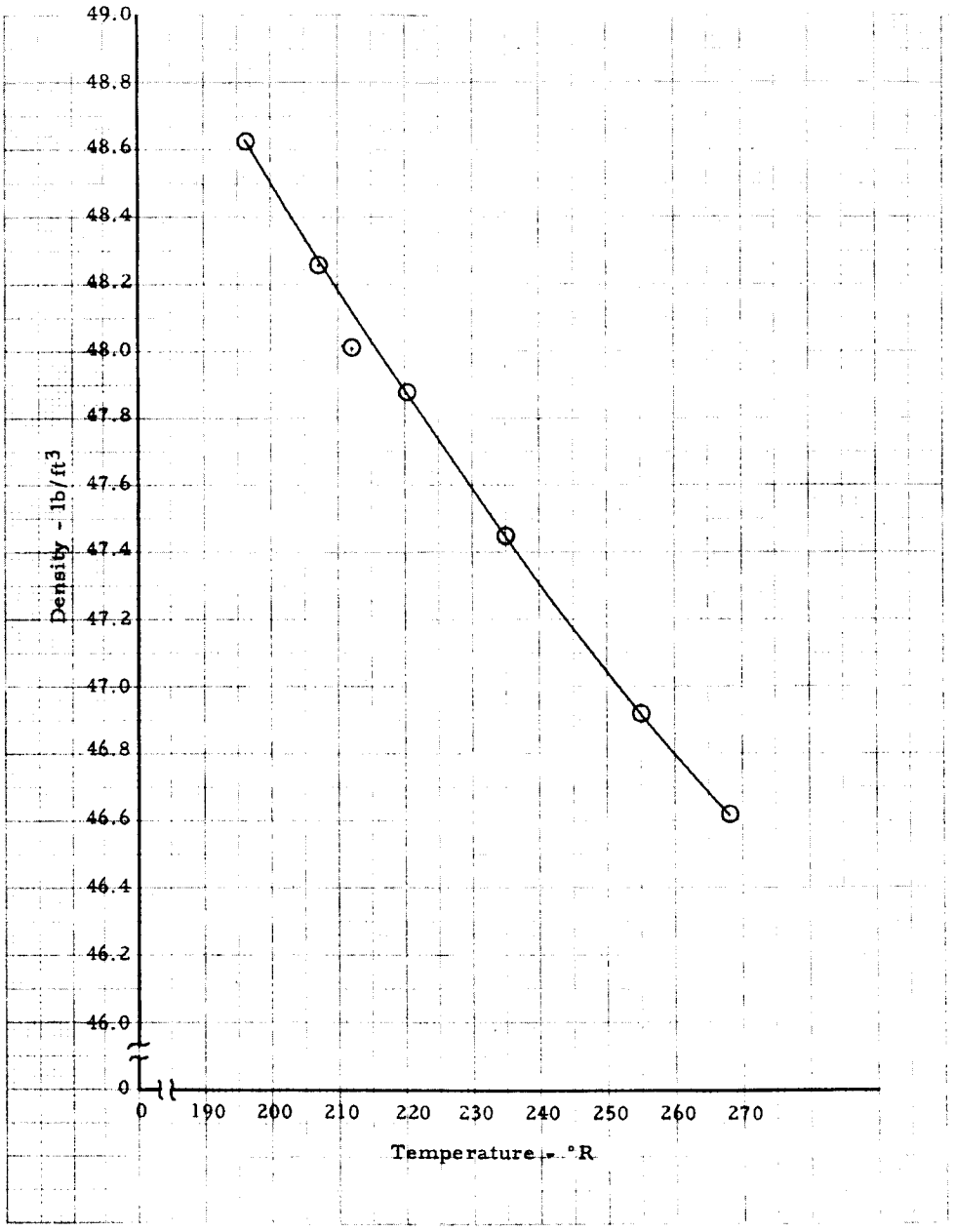

DF 34007

(2) Propane-Propylene

The dewar was fitted with a one-hole rubber stopper and evacuated. The dewar was then cooled in liquid nitrogen and filled with the propane-propylene eutectic solution using the procedure described in the freezing point determinations. After covering the sample with a helium blanket, the quartz bob, thermocouple, and stirrer were positioned in the sample. Determination of the density then proceeded as described above. Results are shown in figure B-15.

Figure B-15
Density of Propane-Propylene Eutectic Solution

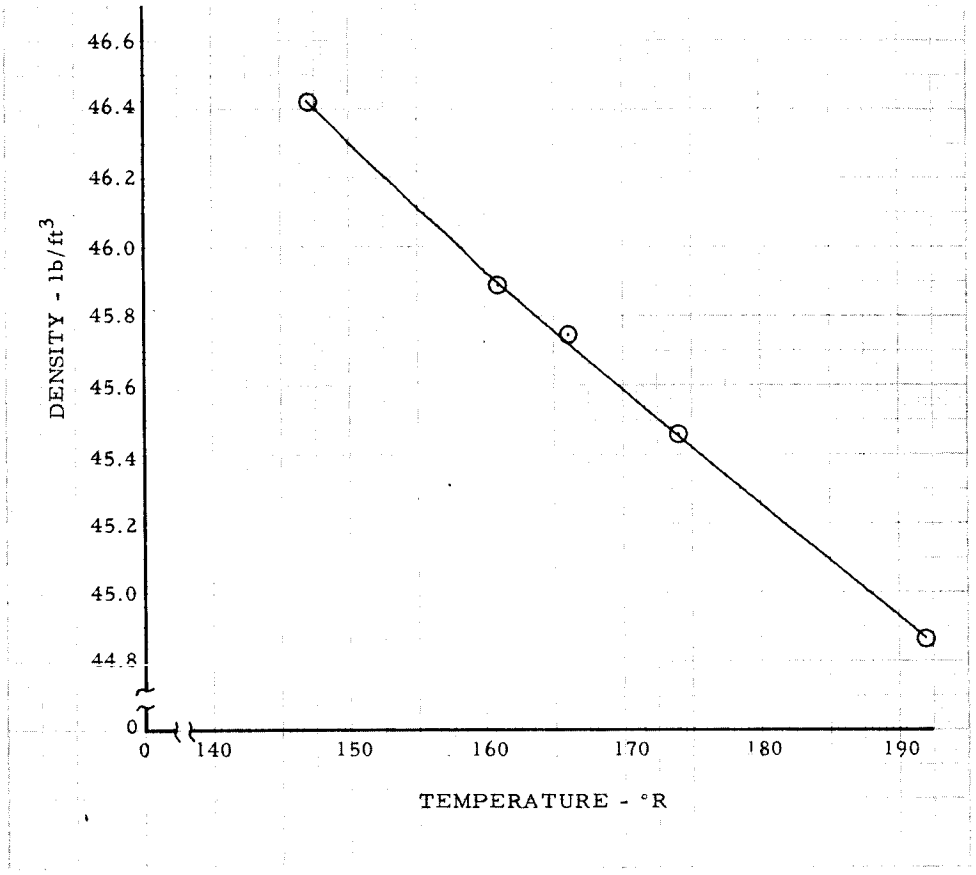

DF 34008

(3) Methylcyclopentane-2 Methylpentane

It was not possible to eliminate temperature gradients throughout the sample because of its considerably higher viscosity. By attaching the thermocouple to the ring stirrer, various temperatures throughout the sample were recorded. When the temperature variations remained with $\pm$ 1°R of the mean, the average density was determined. Results are shown in figure B-16.

3. VISCOSITY

a. Apparatus

Two stainless steel dewars, one fitting inside the other, were fitted with flanges and bolted together, (figure B-17). The cover for the inner dewar contained three round annealed glass windows bonded with silicone potting compound, an electrical feed-through, a glass sample inlet, and several tubing connections.

Four 2-volt lamps were positioned in the dewar near the viscosimeter to increase visibility.

Figure B-16
Density of Methylcyclopentane-2-Methylpentane Eutectic Solution

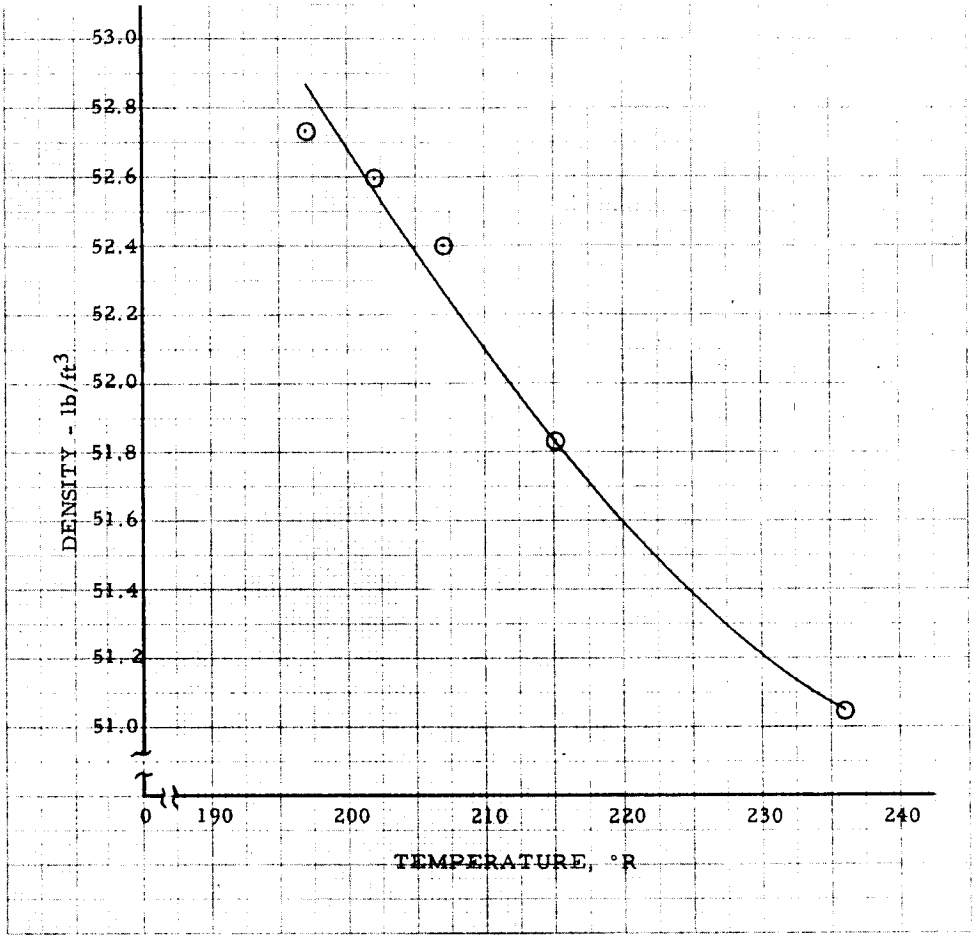

DF 34009

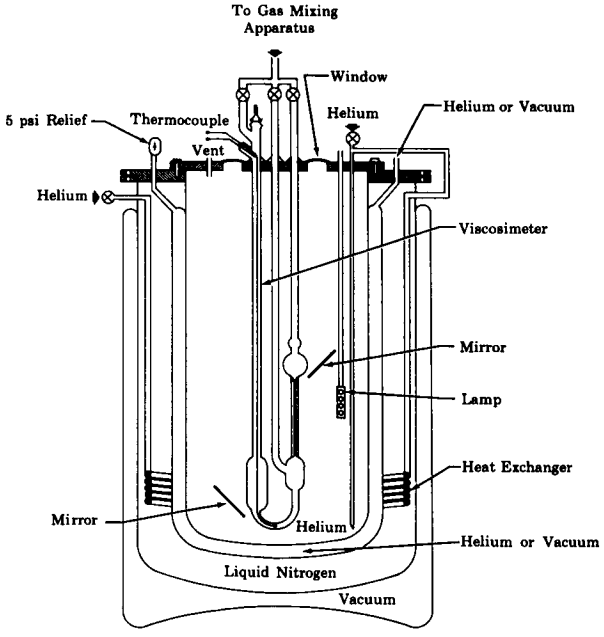

Figure B-17. Cryogenic Viscosity Apparatus

FD 9557

A helium purge was found necessary to prevent a vertical temperature gradient and the formation of frost on the mirrors. Since room temperature helium tended to warm the sample, the purge was cooled in a heat exchanger submerged in liquid nitrogen. Temperatures between 260°R and 150°R could be controlled within ± 1°R.

b. Procedure

Propane gas was used as a calibrating fluid and liquefied directly, in a size No. 1 Ubbelohde viscosimeter. The time of efflux was measured with a stopwatch by visual observation of the reflected image of the viscosimeter through the windows. Since the viscosity value found by using the tube equation supplied by the manufacturer was in good agreement with the accepted value, the decision was made to use the tubes without recalibration.

(1) Pentane-Isopentane

The apparatus was filled with helium gas at atmospheric pressure and cooled to 260°R. The sample was poured into the viscosimeter through the tapered glass cap. Trial runs in the No. 1 tube were too lengthy and a No. 2 tube was used. Viscosity measurements were completed as above and are shown in figure B-18.

Figure B-18
Viscosity of Pentane-Isopentane Eutectic Solution

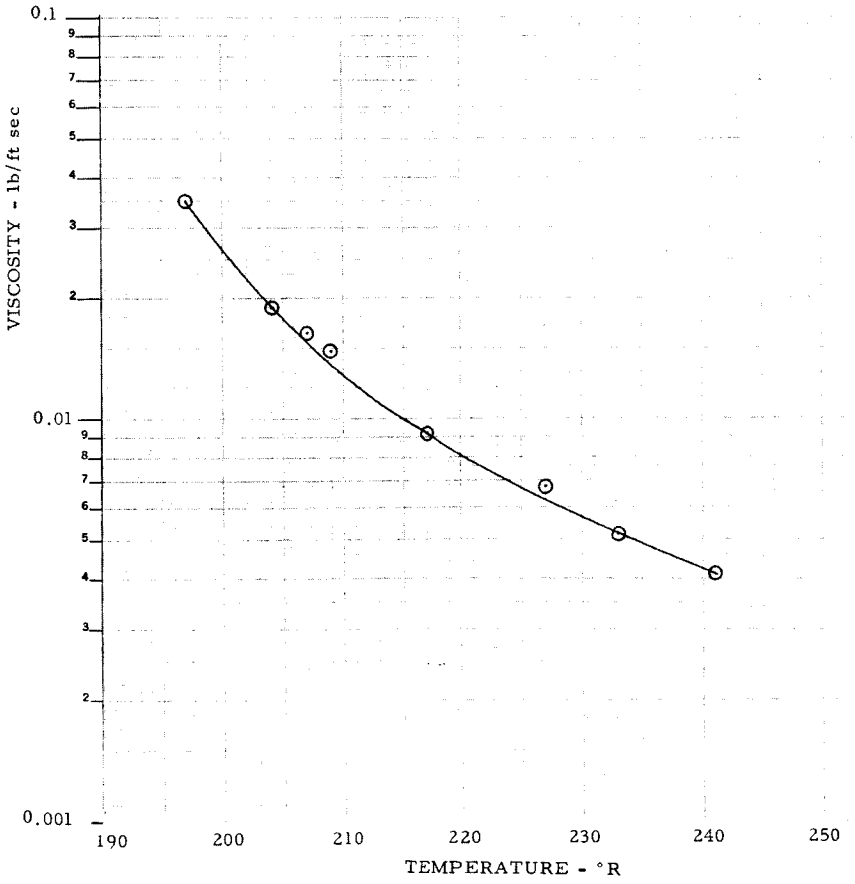

(2) Propane-Propylene

Weighed quantities of propane and propylene from the small gas weighing cylinders were transferred at room temperature into the 6 liter cylinder at 140°R. Then, by warming the 6 liter cylinder to room temperature, the eutectic solution was vaporized to produce a mixture of propane and propylene gases with the same weight composition. This gas mixture was liquefied in the viscosimeter, and the viscosity measured as described above and the data shown in figure B-19.

Figure B-19
Viscosity of Propane-Propylene Eutectic Solution

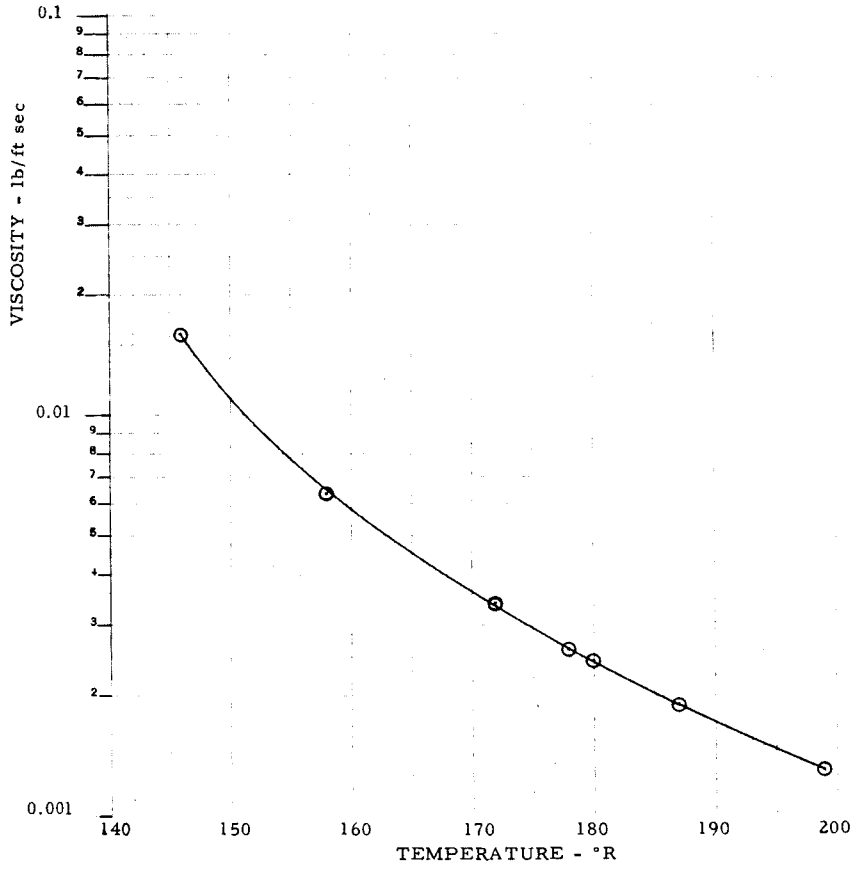

DF 34012

(3) Methylcyclopentane-Methylpentane

Since the viscosity increased sharply as the freezing point was approached, two separate determinations were required to establish consistent data. The same No. 3 tube was used for both sets of data. The data is included in figure B-20.

Figure B-20
Viscosity of Methylcyclopentane-2-Methylpentane Eutectic Solution

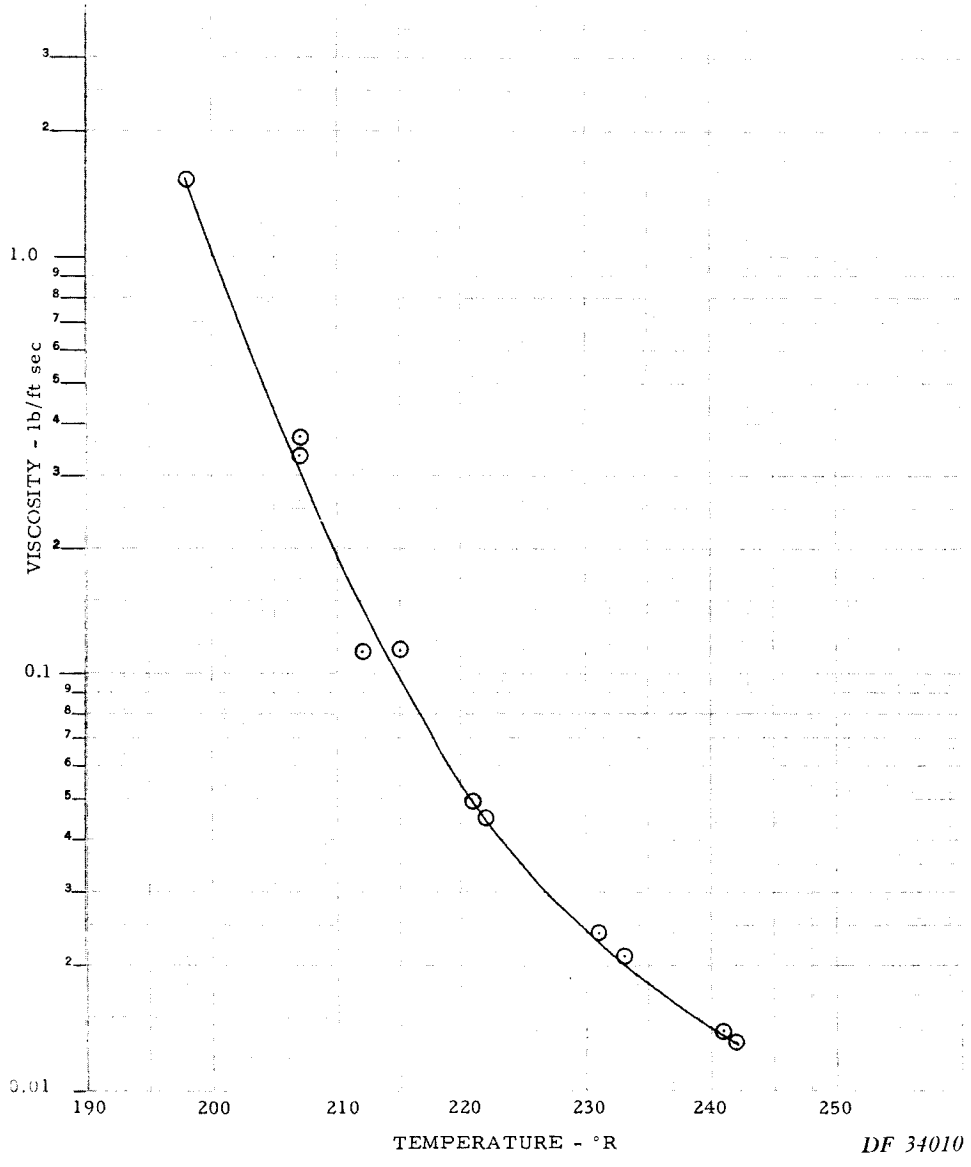

4. *VAPOR PRESSURE*

For a eutectic solution of pentane (14%)-isopentane (86%), the vapor pressure was measured at 539°R. The measured vapor pressure was 699 mm Hg (0.920 atm) compared to 697 mm Hg (0.917 atm) predicted based on the calculated vapor pressure for a true solution. The 2 mm Hg difference is within the accuracy of the experiment. It is concluded, as expected, that vapor pressure calculations based on the assumption of a true solution are sufficiently accurate for the pentane-isopentane blend, and probably for all other light hydrocarbon blends of interest.

APPENDIX C
THEORETICAL PERFORMANCE

Figures C-1 through C-20 present theoretical shifting equilibrium performance data for methane, propane, ethylene, butene-1 and a blend of 14% pentane – 86% isopentane with fluorine-oxygen (flox) blends. Flox blends range from 0 to 100% fluorine by weight. Data are based on a 100 psia chamber pressure and nozzle expansion area ratios of 40 and 60. Inlet conditions for the fuels and oxidizers were taken as liquids at their respective normal boiling points. It will be noticed that discontinuities occur in the slopes of the characteristic velocity and chamber temperature curves at the higher fluorine percentages. This discontinuity occurs at the mixture ratio where solid carbon ceases to be formed as a chamber reaction product; i.e., at mixture ratios above this point there is no solid carbon.

Thermochemical data used in the calculations are from tables published by the Joint Army-Navy-Air Force (JANAF) Thermochemical panel. These data are extended and revised quarterly. The theoretical performance values given in this appendix are based on latest JANAF data and are slightly higher (about 1.0 sec for specific impulse) than previous values because of a recent change by JANAF in the estimated heat of formation of HF. Data used in the propellant selection studies (Section III) are based on the old data; however, these data were used consistently in the propellant selection; the small differences would not affect the comparison. All data reduction decks used for analyzing the test results are based on the new data.

For simple bipropellant combinations, the theoretical vacuum specific impulse and other performance variables are usually calculated as a function of oxidizer-to-fuel ratio for a particular chamber pressure and nozzle expansion ratio. With flox-LPG combinations, the percentage of fluorine in the oxidizer is an additional variable that must be optimized to obtain maximum specific impulse. Figures C-1 and C-2 show the vacuum specific impulse for flox-methane with varying percentages of fluorine in the oxidizer. Figure C-21 shows a cross-plot of the maxima of the curves from figure C-2. Note that the percentage of fluorine in the oxidizer required for maximum specific impulse is very sharply defined. The optimum percentage of fluorine is less than 100% because oxygen releases more energy than fluorine in reaction with carbon, while fluorine releases more energy with hydrogen. At the fluorine and oxidizer-fuel ratio for maximum specific impulse, calculations show that CO and HF make up more than 99% of the reaction products at the nozzle exit. The stoichiometric equation for the oxidation of methane with fluorine and oxygen to form CO and HF is:

$$CH_4 + 2F_2 + 1/2\ O_2 \rightarrow CO + 4HF$$

The relative mole ratio of fluorine to oxygen is 4 to 1; this is equivalent to 82.6% of fluorine by weight. The peak from figure C-21 is also 82.6% fluorine. The sharp peak and the coincidence of this peak with the percentage calculated from formation equations like (C-1) have been found for all hydrocarbon fuels investigated, regardless of the chamber pressure or nozzle expansion ratio.

In figure C-22 the optimum mixture ratio for various flox-LPG combinations is plotted as a function of hydrogen-to-carbon atomic ratio. The excellent correlation obtained provides a simple means of determining the oxidizer-to-fuel ratio for maximum specific impulse for any LPG fuel or for any blend of LPG fuels. By using first a stoichiometric equation for the formation of CO and HF to determine the optimum percentage of fluorine in the oxidizer, and then using the correlation in figure C-22 to determine the optimum oxidizer-to-fuel ratio, the maximum specific impulse can be determined by calculation of a single performance point, eliminating the time and expense of constructing an extensive map of values as shown in figure C-2.

Another interesting result of the flox-LPG theoretical performance calculations is that the fluorine concentration that provides the maximum specific impulse also permits a higher engine mixture ratio than do other concentrations, as seen in figure C-2. Because the flox blends have higher densities than any of the LPG fuels, this higher mixture ratio is desired to increase propellant bulk density. For all of the combinations studied, the flox-LPG bulk density at the optimum mixture ratio is greater than the bulk density of the same fuel with fluorine at optimum mixture ratio even though fluorine itself is more dense than flox.

Figure C-1
Theoretical Performance of Fluorine-Oxygen Mixtures with Methane

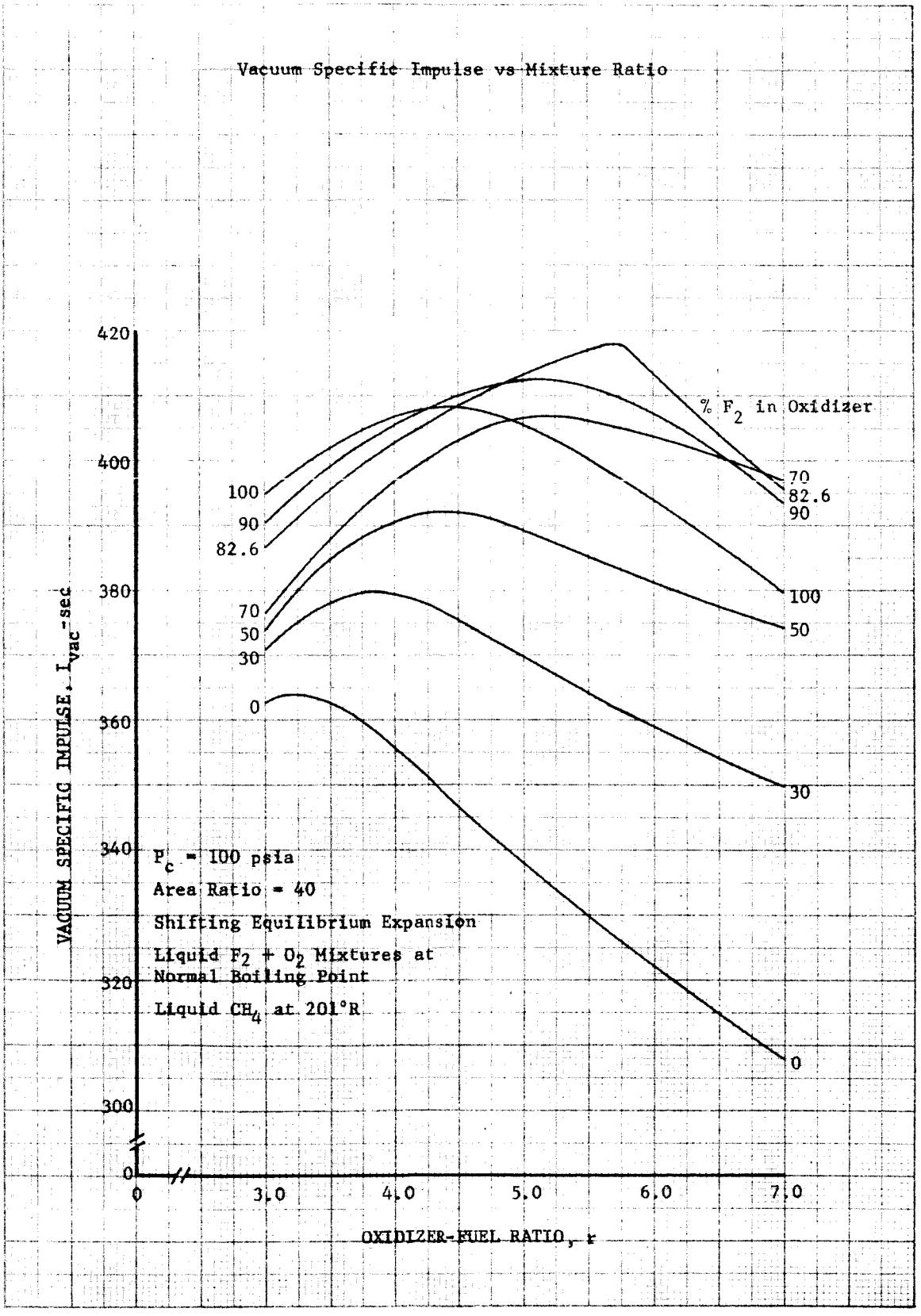

Figure C-2
Theoretical Performance of Fluorine-Oxygen Mixtures with Methane

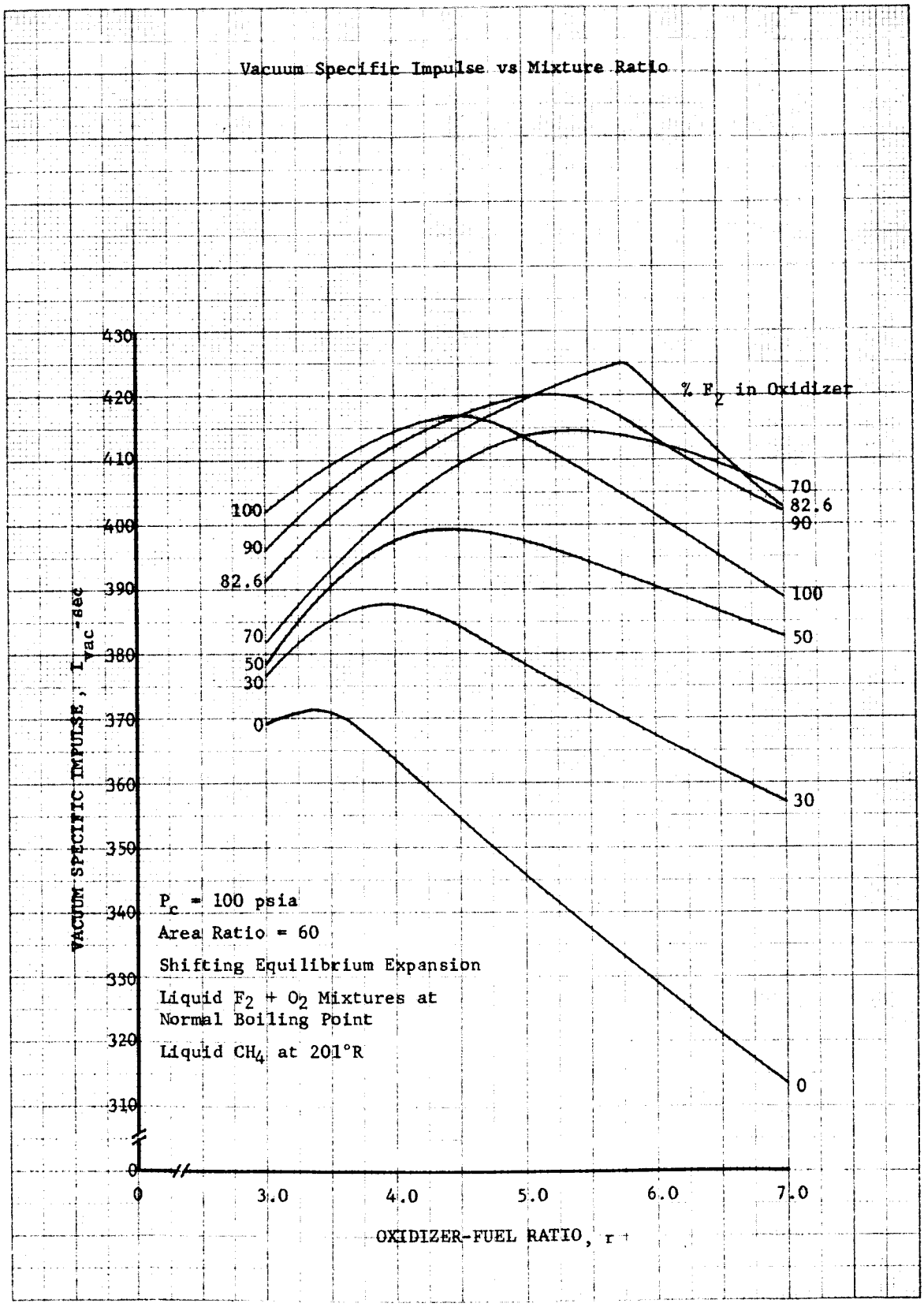

Figure C-3
Theoretical Performance of Fluorine-Oxygen Mixtures with Methane

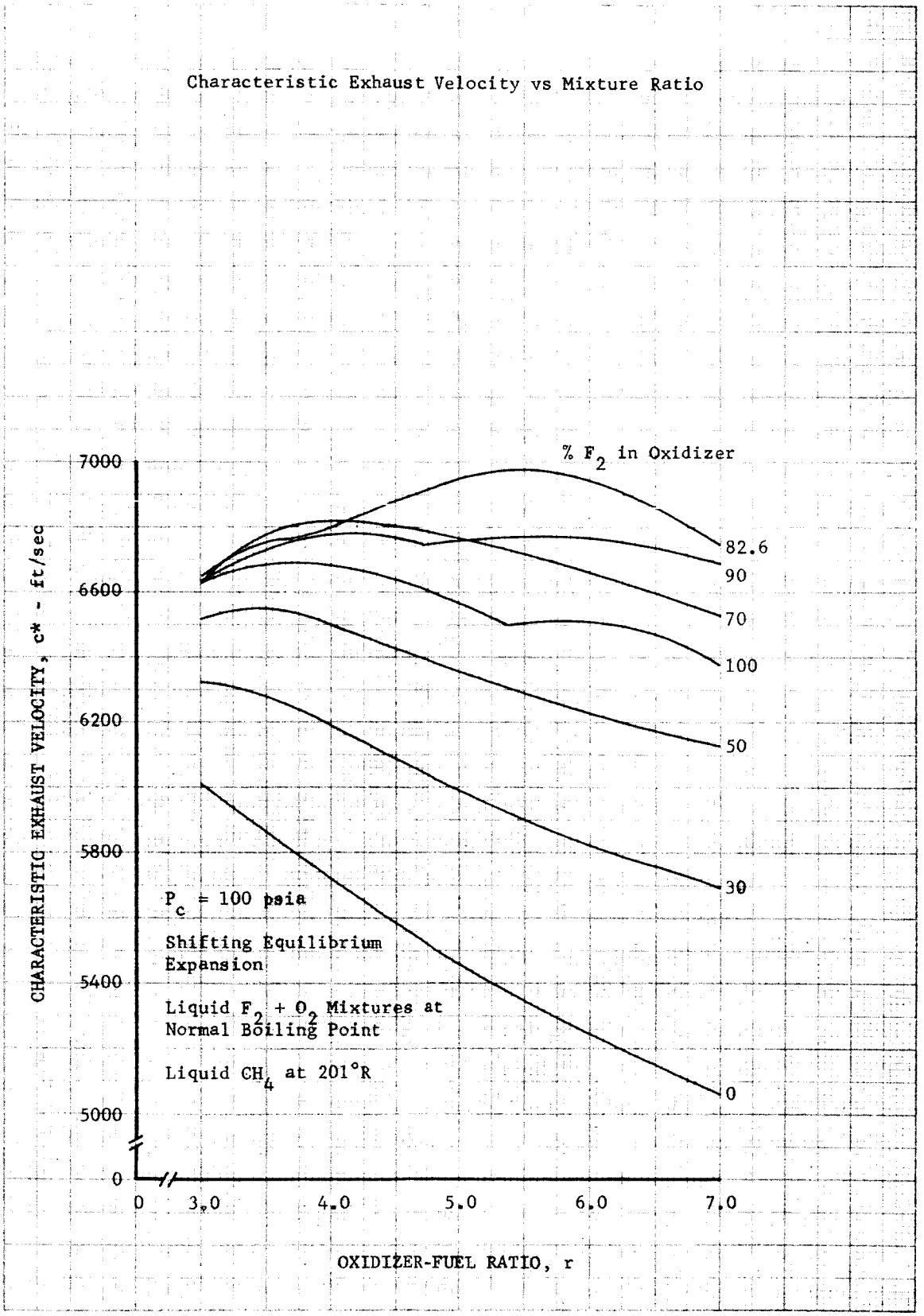

DF 32495
Sheet 3 of 4

Figure C-4
Theoretical Performance of Fluorine-Oxygen Mixtures with Methane

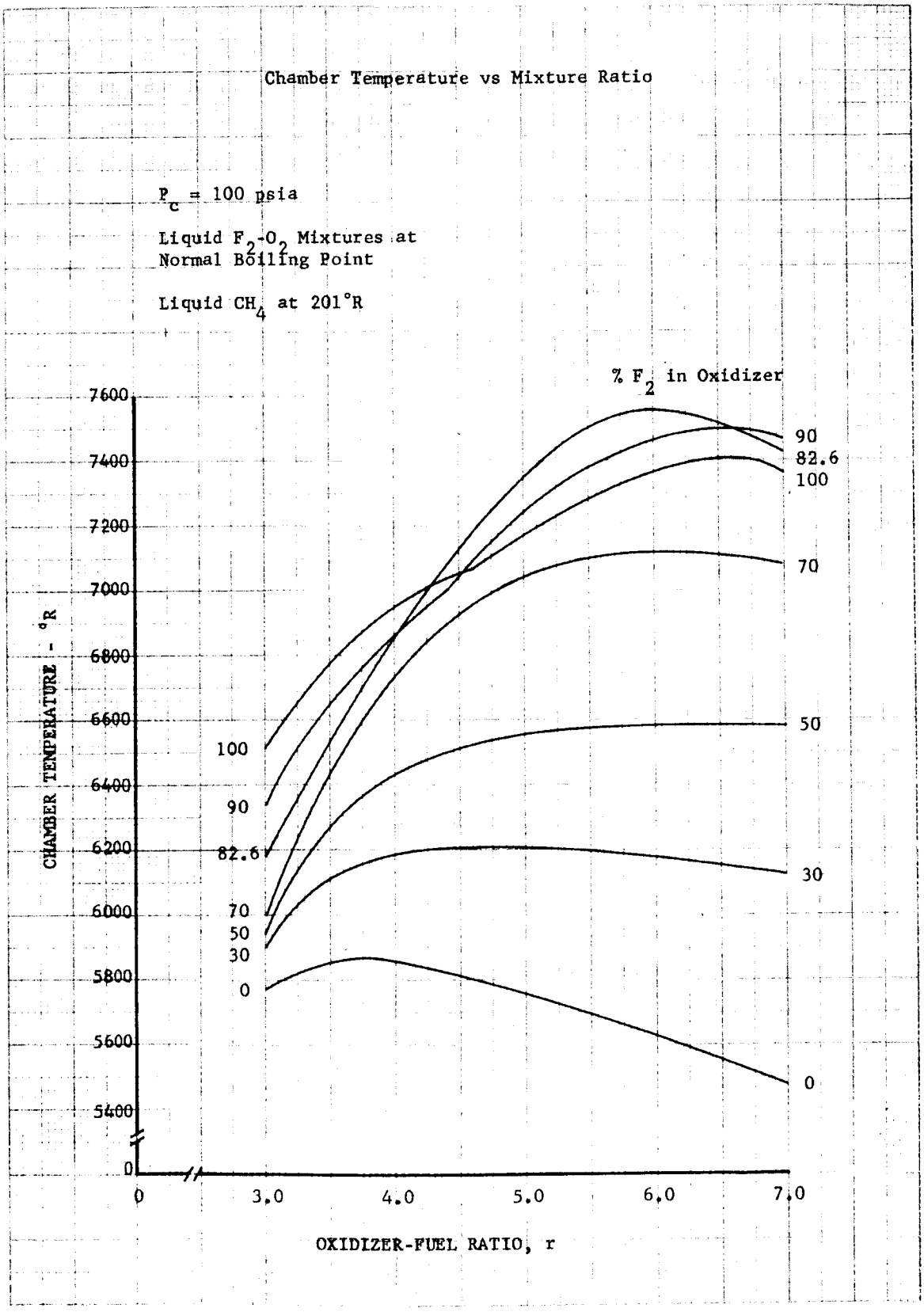

DF 32495
Sheet 4 of 4

Figure C-5
Theoretical Performance of Fluorine-Oxygen Mixtures with Propane

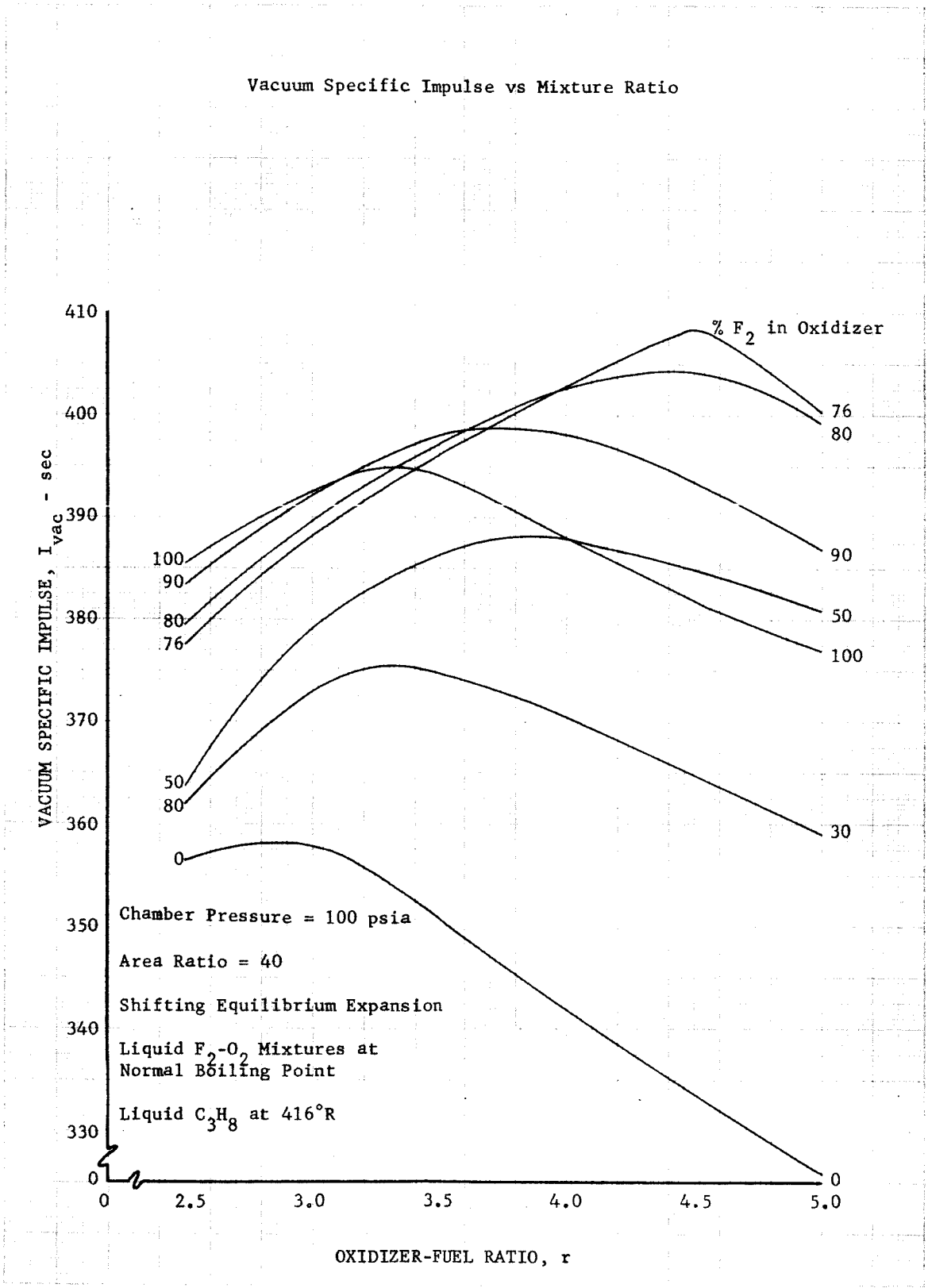

DF 32503
Sheet 1 of 4

Figure C-6
Theoretical Performance of Fluorine-Oxygen Mixtures with Propane

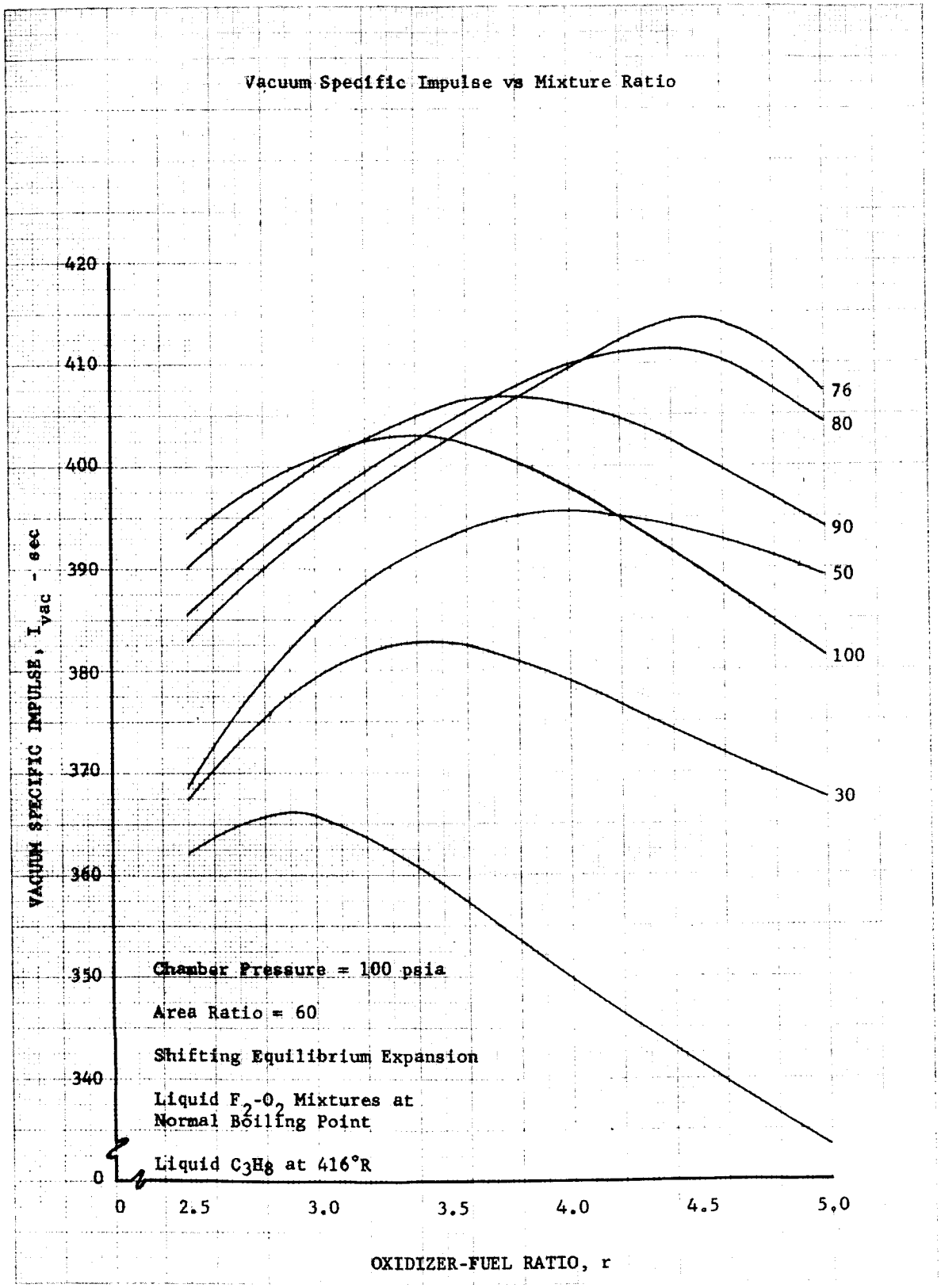

DF 32503
Sheet 2 of 4

Figure C-7
Theoretical Performance of Fluorine-Oxygen Mixtures with Propane

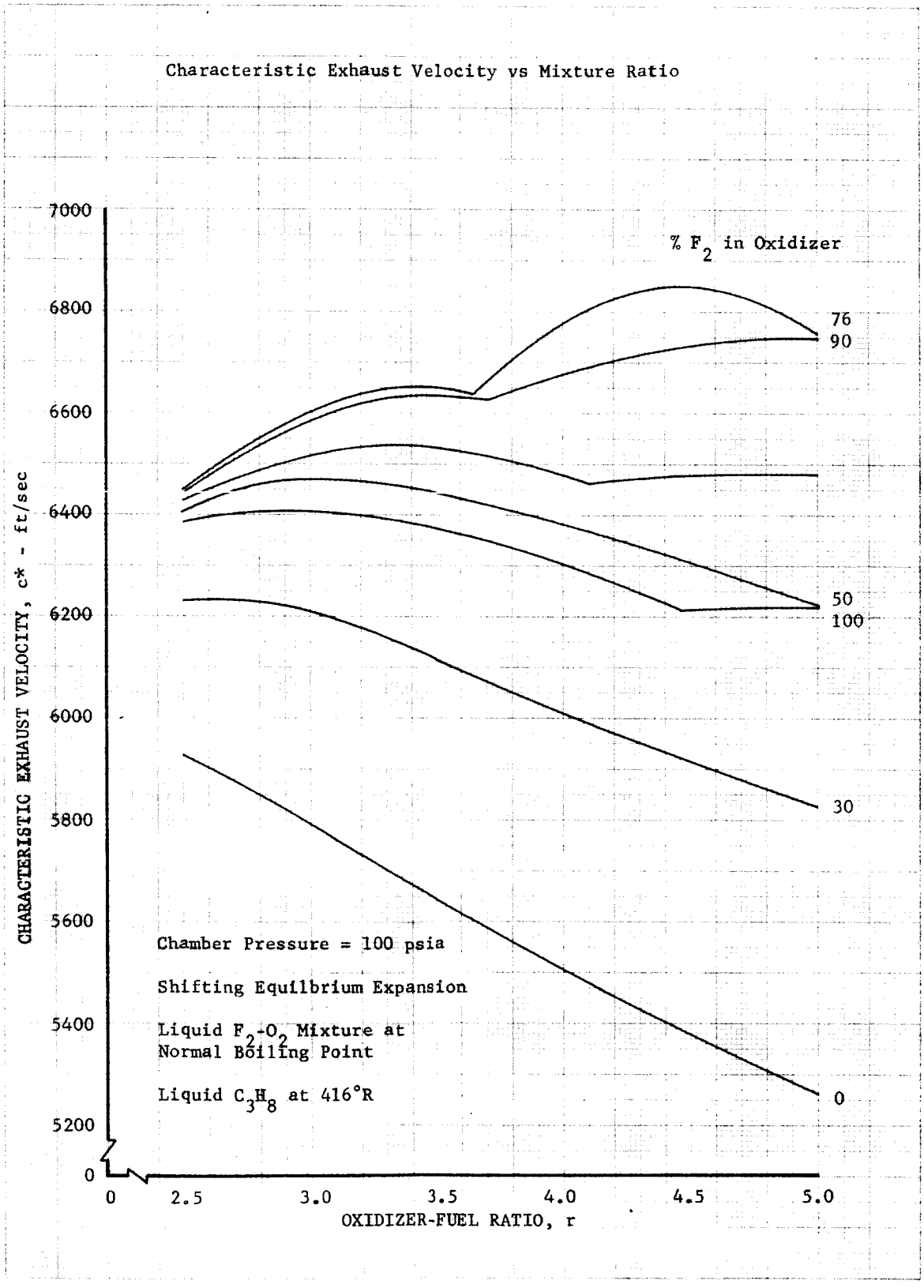

DF 32503
Sheet 3 of 4

Figure C-8
Theoretical Performance of Fluorine-Oxygen Mixtures with Propane

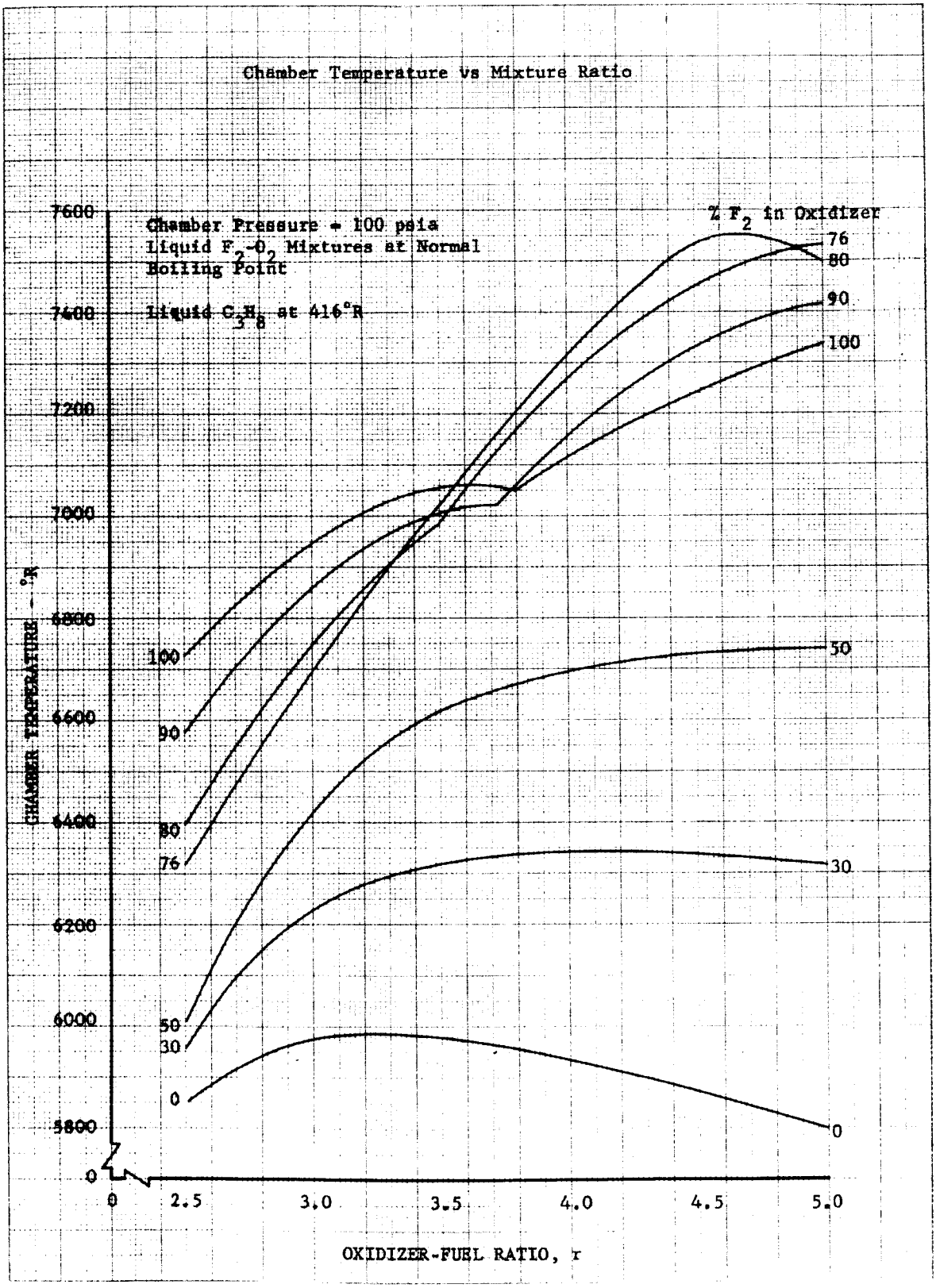

DF 32503
Sheet 4 of 4

Figure C-10
Theoretical Performance of Fluorine-Oxygen Mixtures with Ethylene

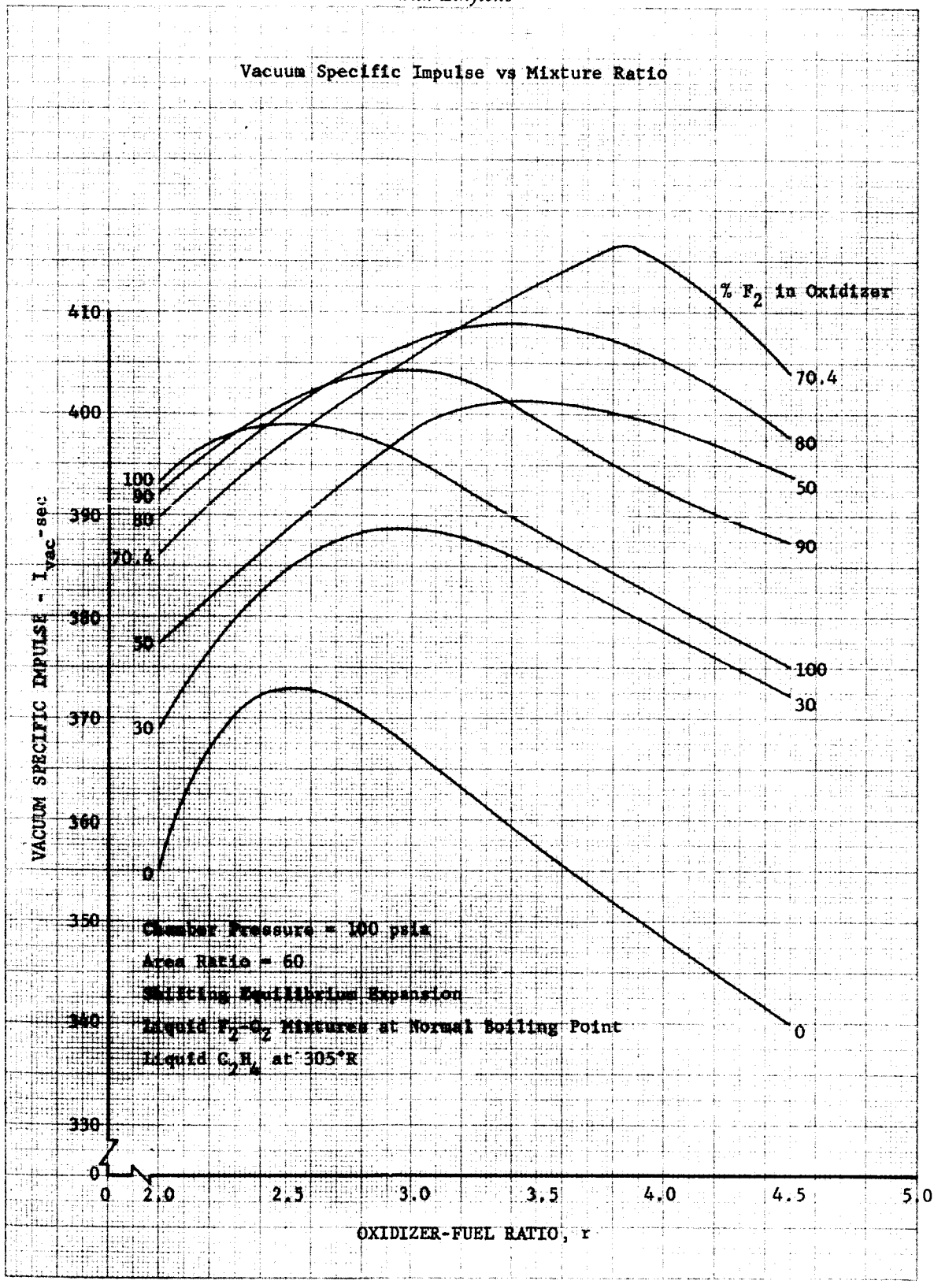

DF 32502
Sheet 2 of 4

Figure C-9
Theoretical Performance of Fluorine-Oxygen Mixtures with Ethylene

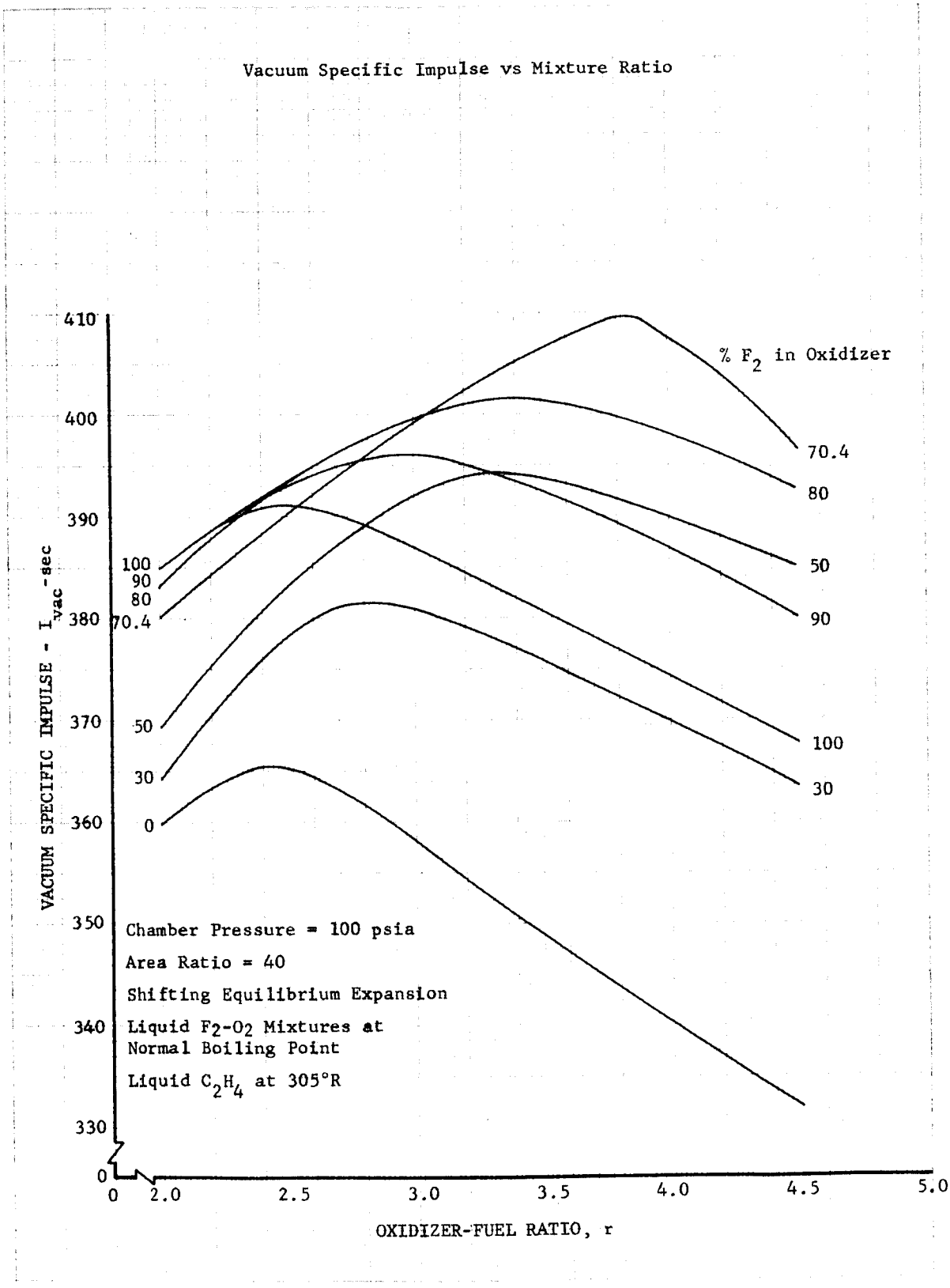

DF 32502
Sheet 1 of 4

Figure C-11
Theoretical Performance of Fluorine-Oxygen Mixtures with Ethylene

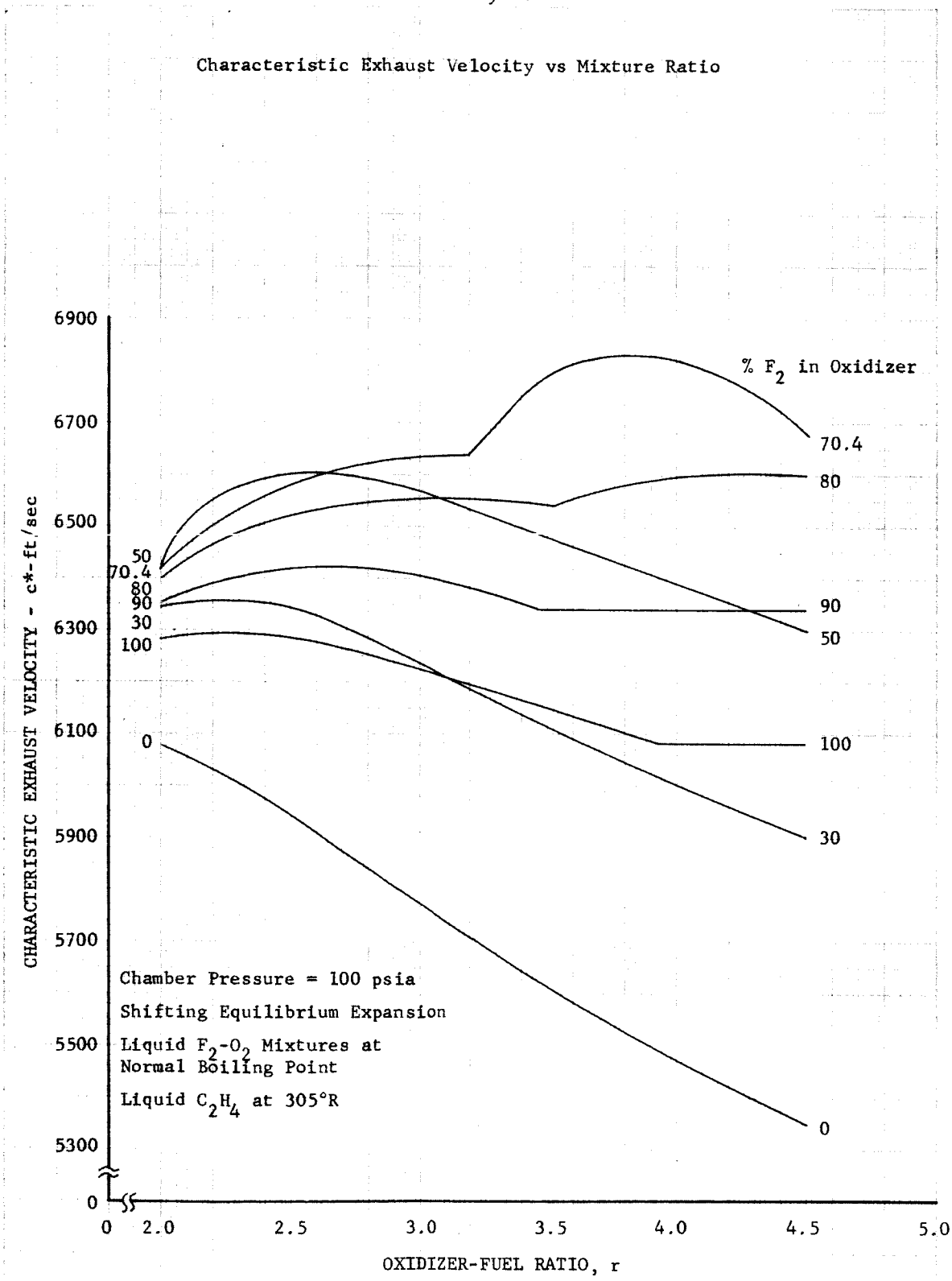

DF 32502
Sheet 3 of 4

Figure C-12
Theoretical Performance of Fluorine-Oxygen Mixtures with Ethylene

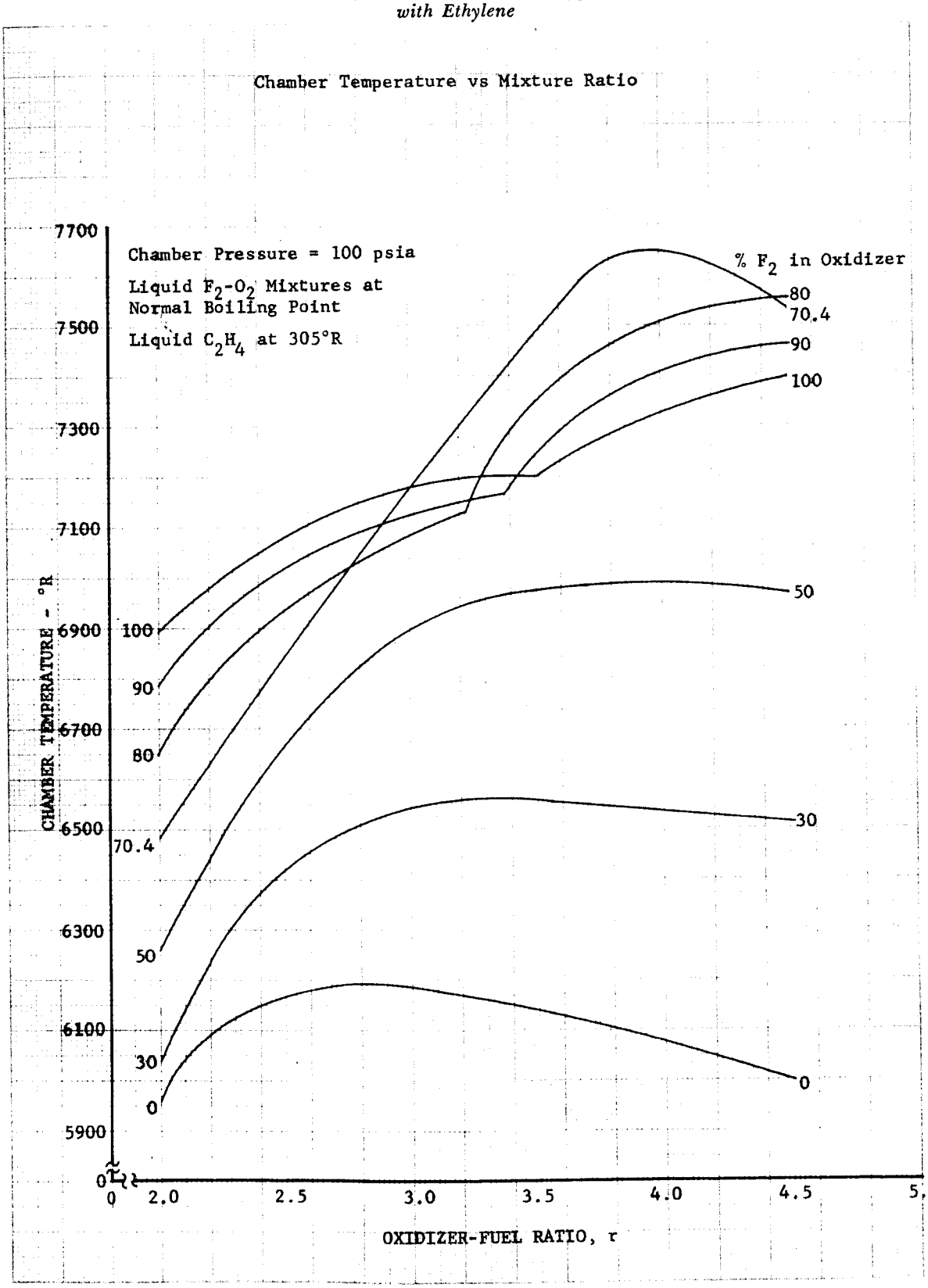

DF 32502
Sheet 4 of 4

Figure C-13
Theoretical Performance of Fluorine-Oxygen Mixtures with Butene-1

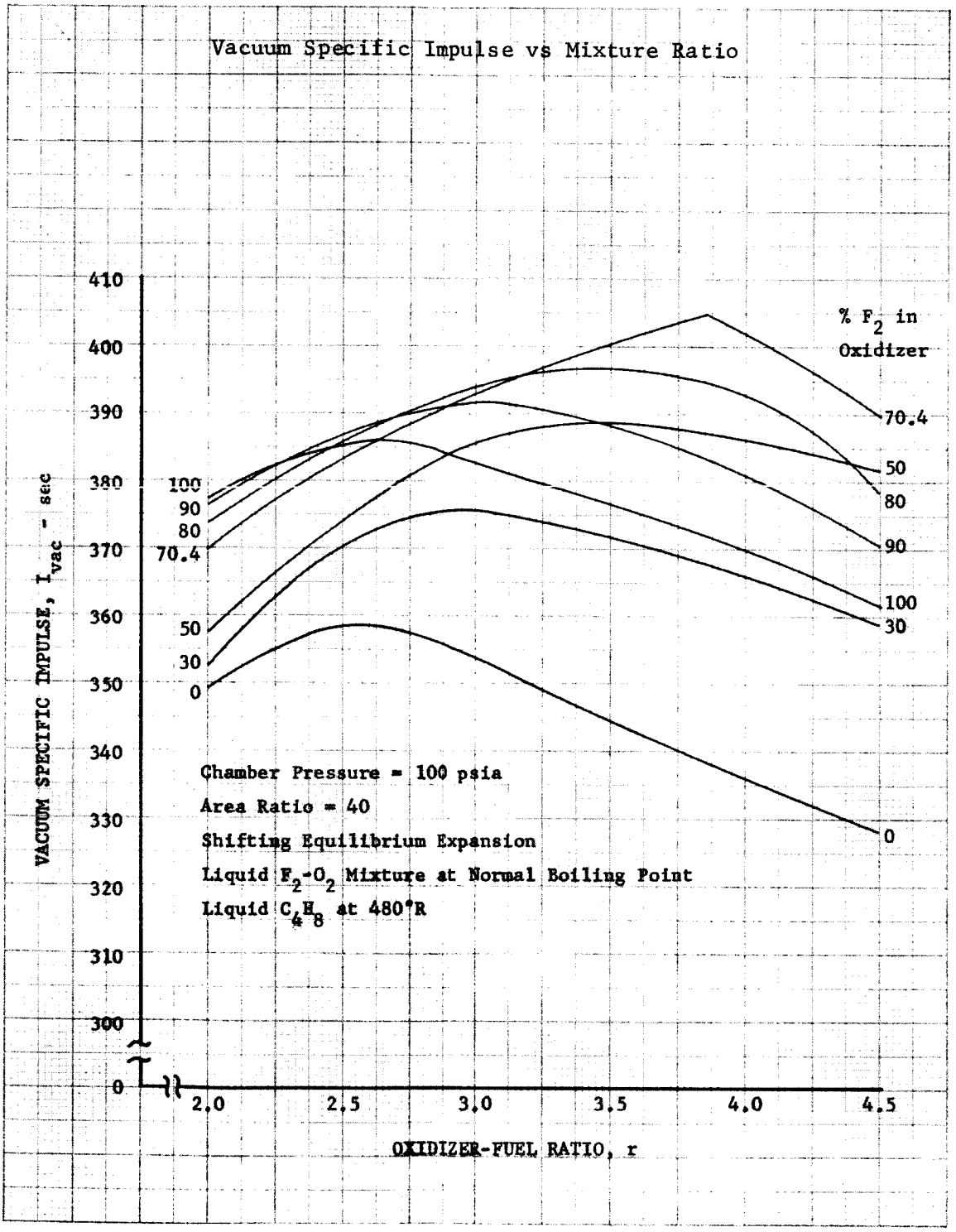

DF 37595

Figure C-14
Theoretical Performance of Fluorine-Oxygen Mixtures with Butene-1

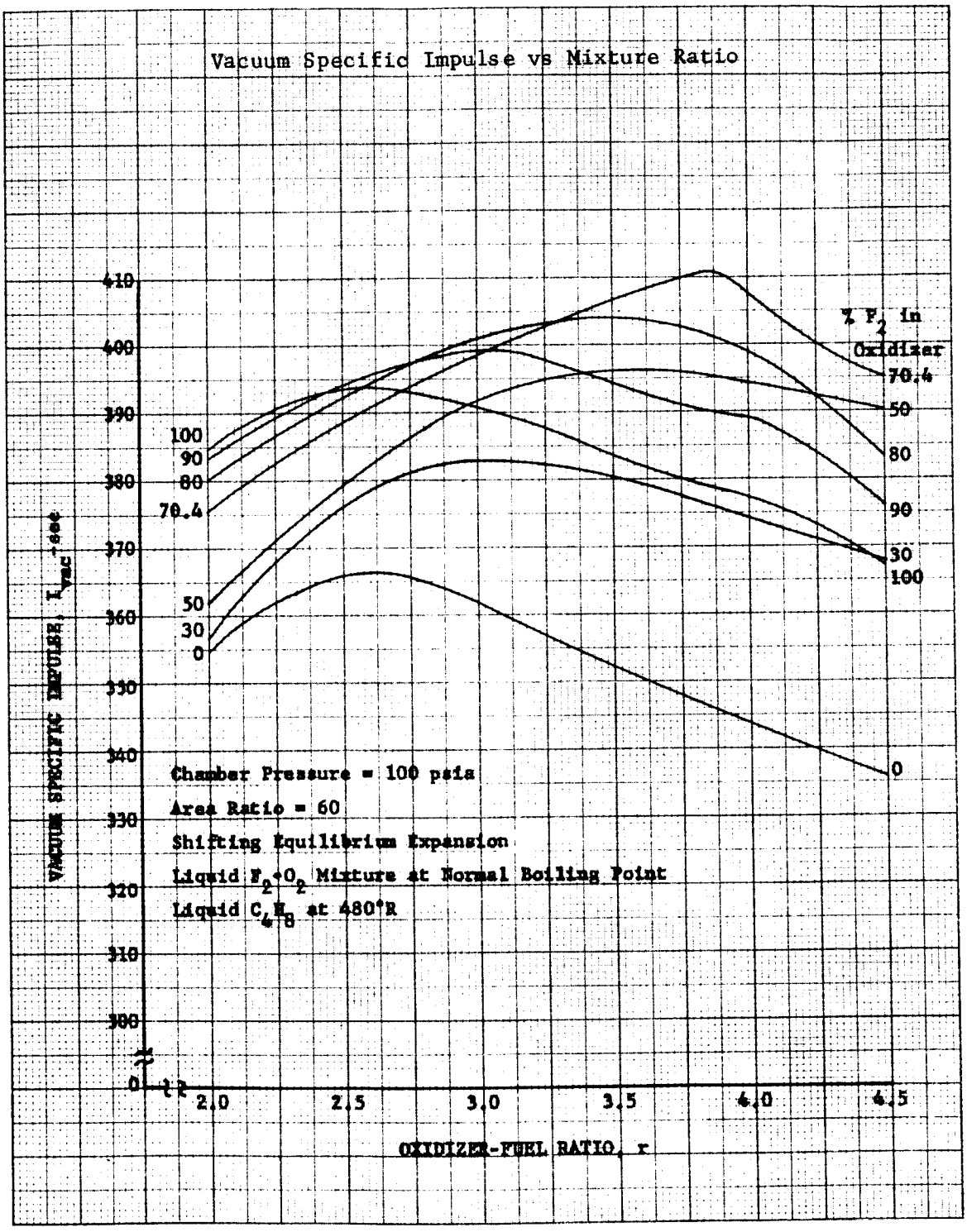

DF 37596

Figure C-15
Theoretical Performance of Fluorine-Oxygen Mixtures with Butene-1

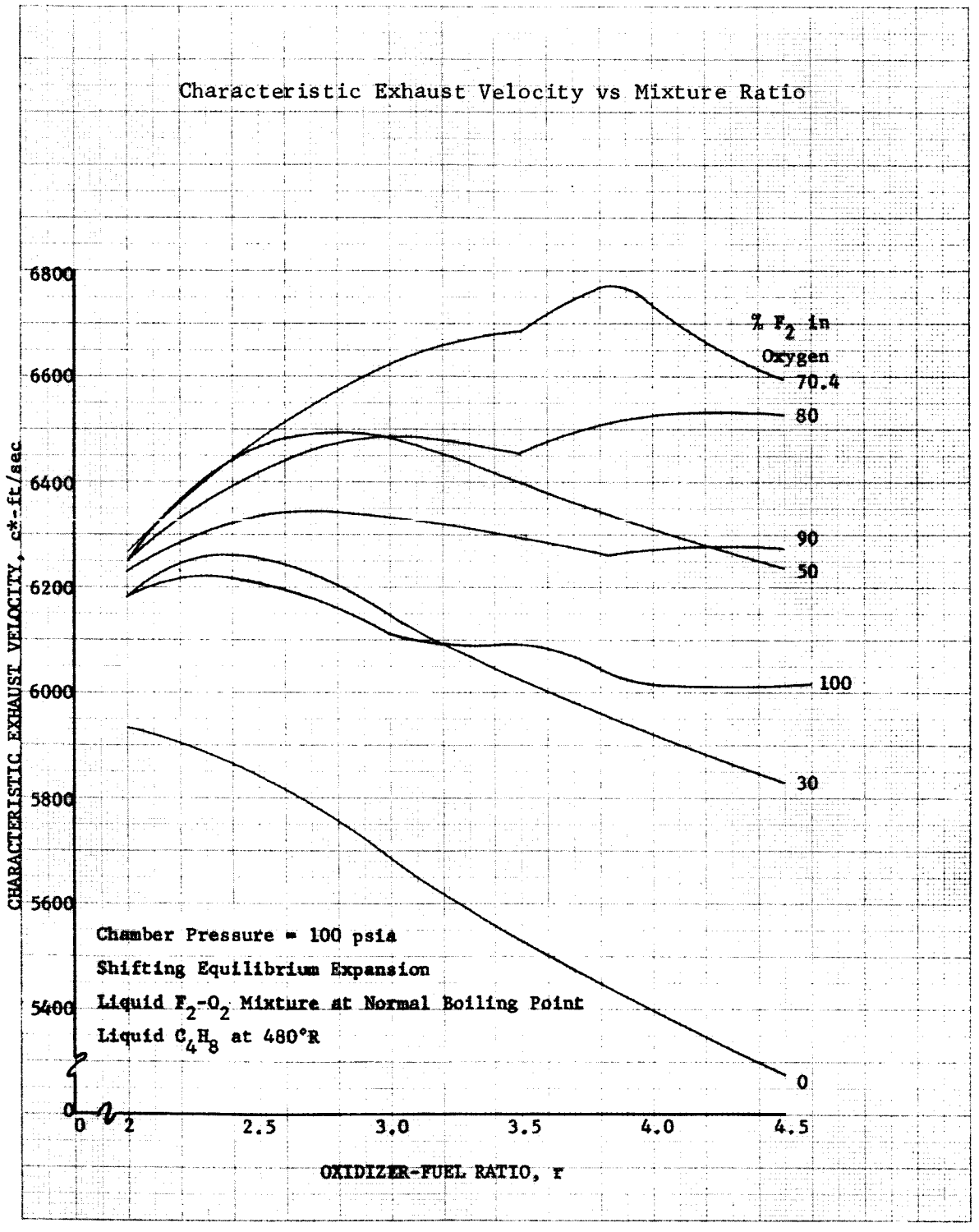

DF 37597

Figure C-16
Theoretical Performance of Fluorine-Oxygen Mixtures with Butene-1

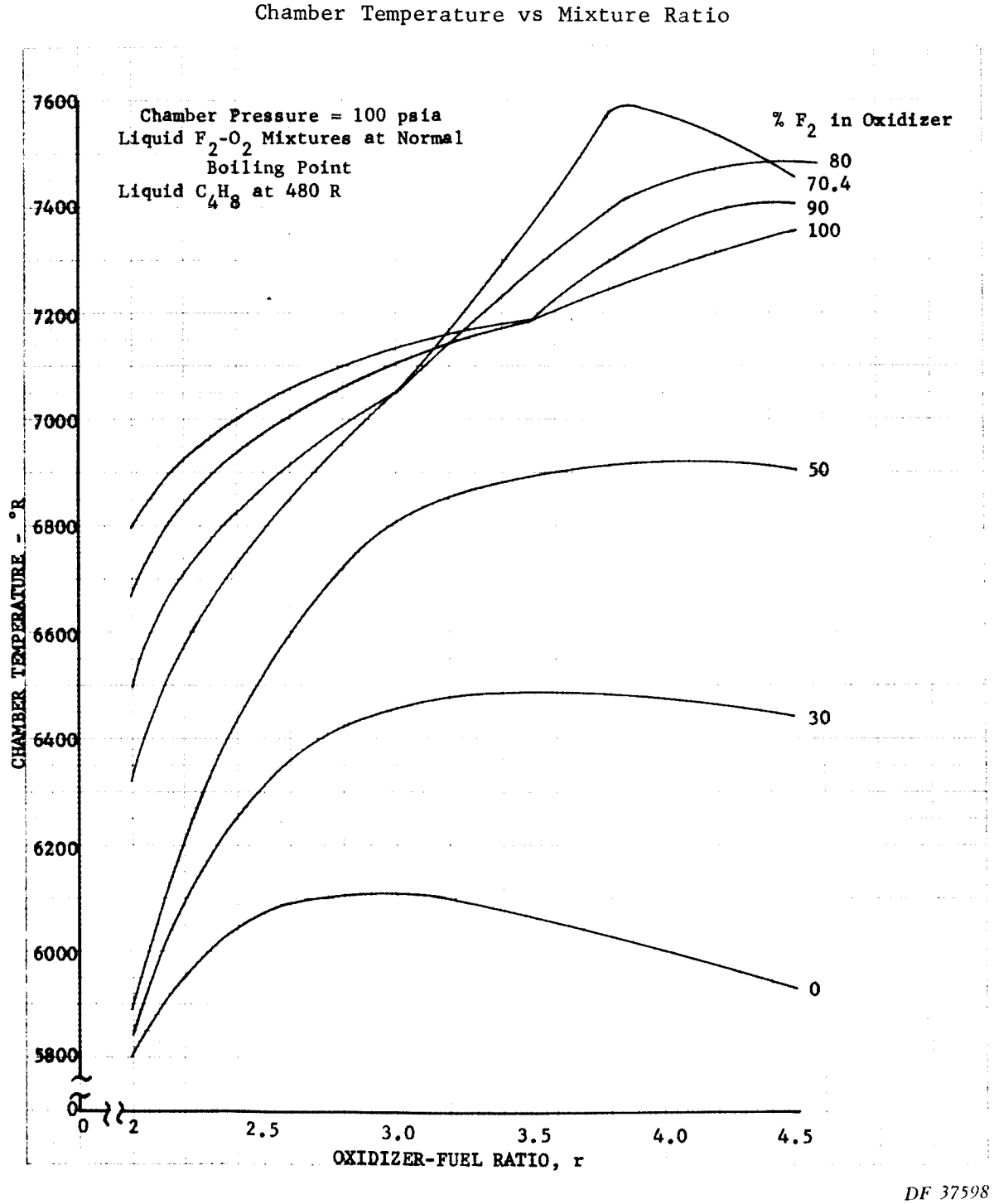

DF 37598

Figure C-17
Theoretical Performance of Fluorine-Oxygen Mixtures with 14% Pentane — 86% Isopentane

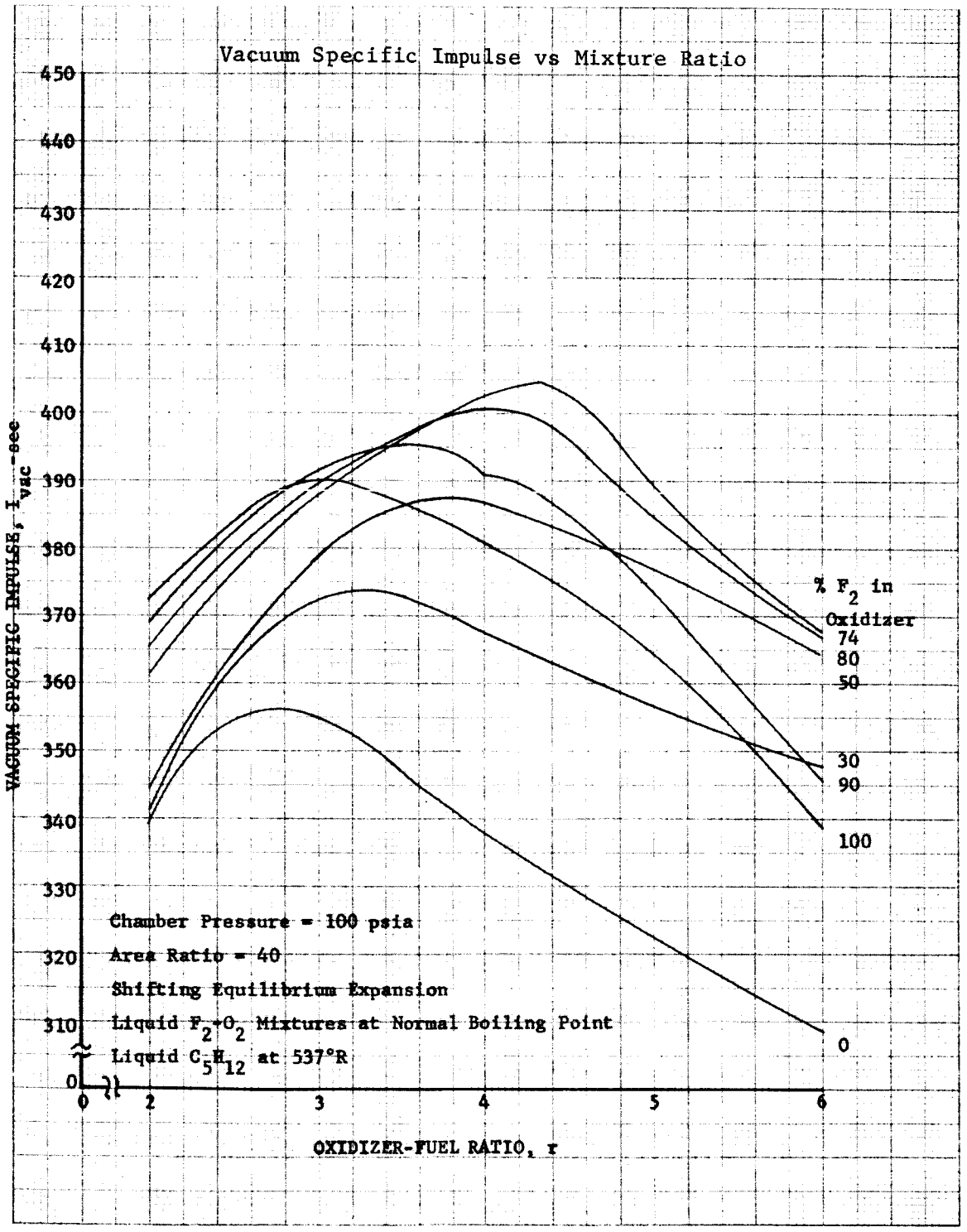

DF 37599

Figure C-18
Theoretical Performance of Fluorine-Oxygen Mixtures with 14% Pentane — 86% Isopentane

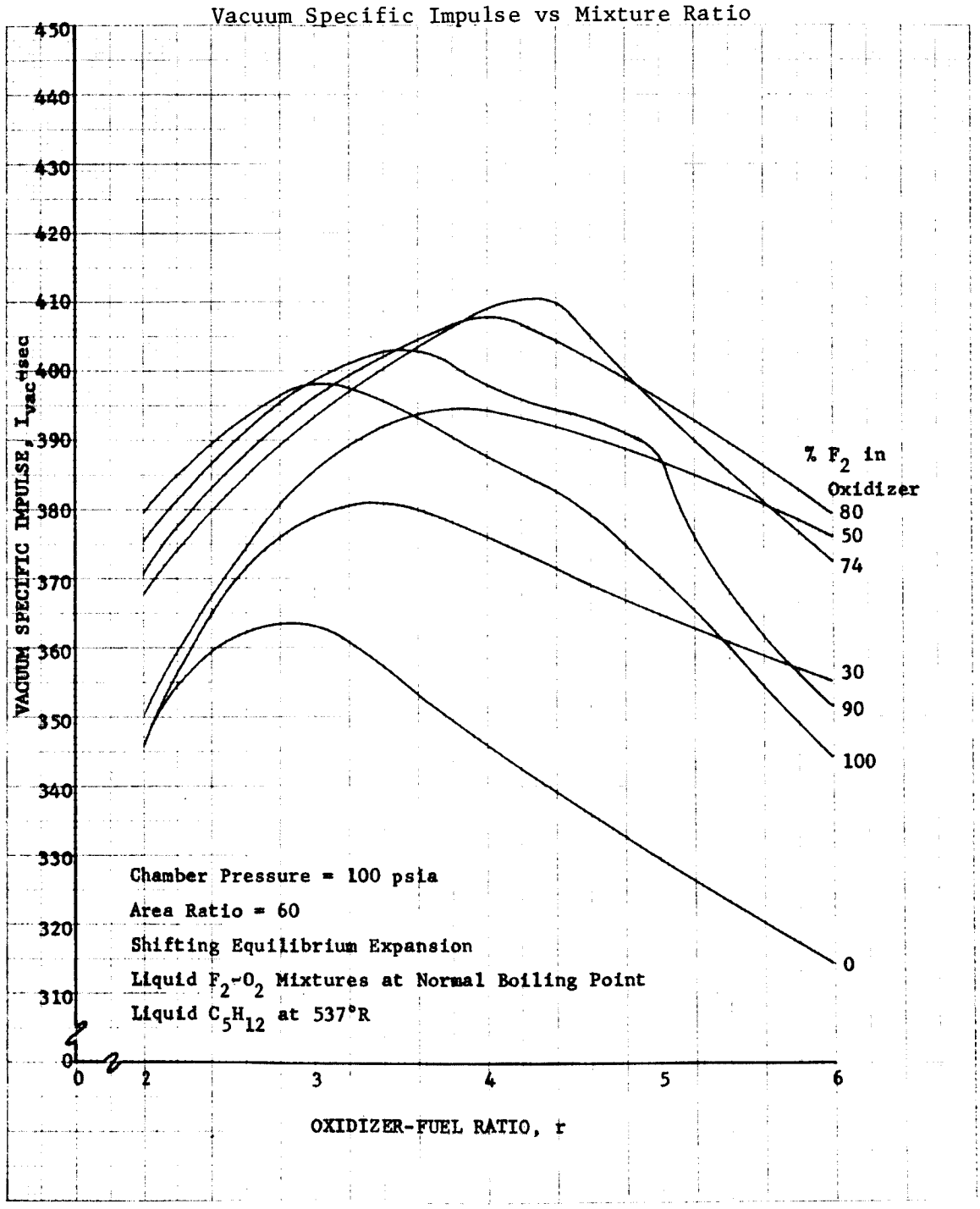

DF 37600

Figure C-19
Theoretical Performance of Fluorine-Oxygen Mixtures with 14% Pentane – 86% Isopentane

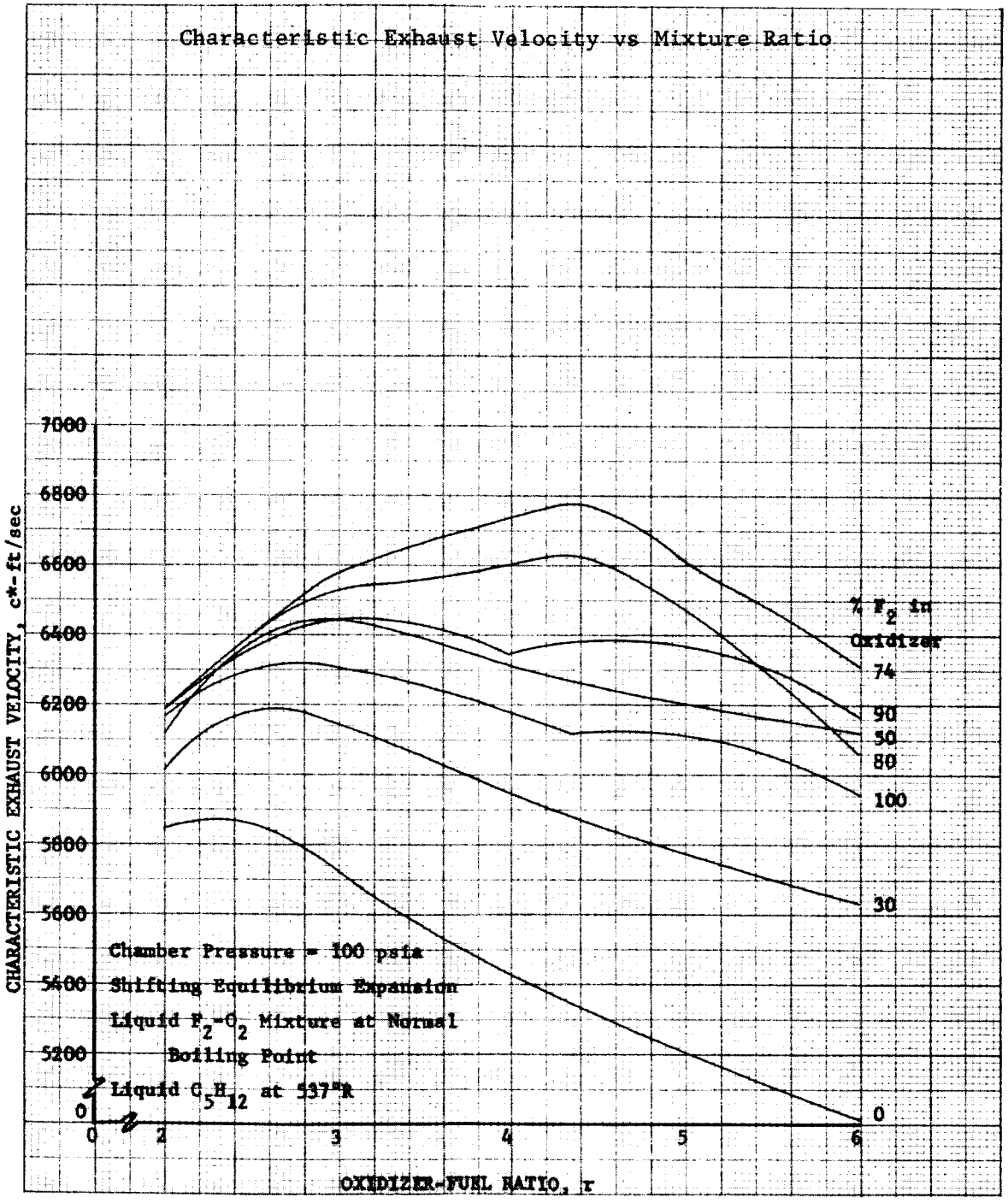

DF 37601

Figure C-20
Theoretical Performance of Fluorine-Oxygen Mixtures with 14% Pentane – 86% Isopentane

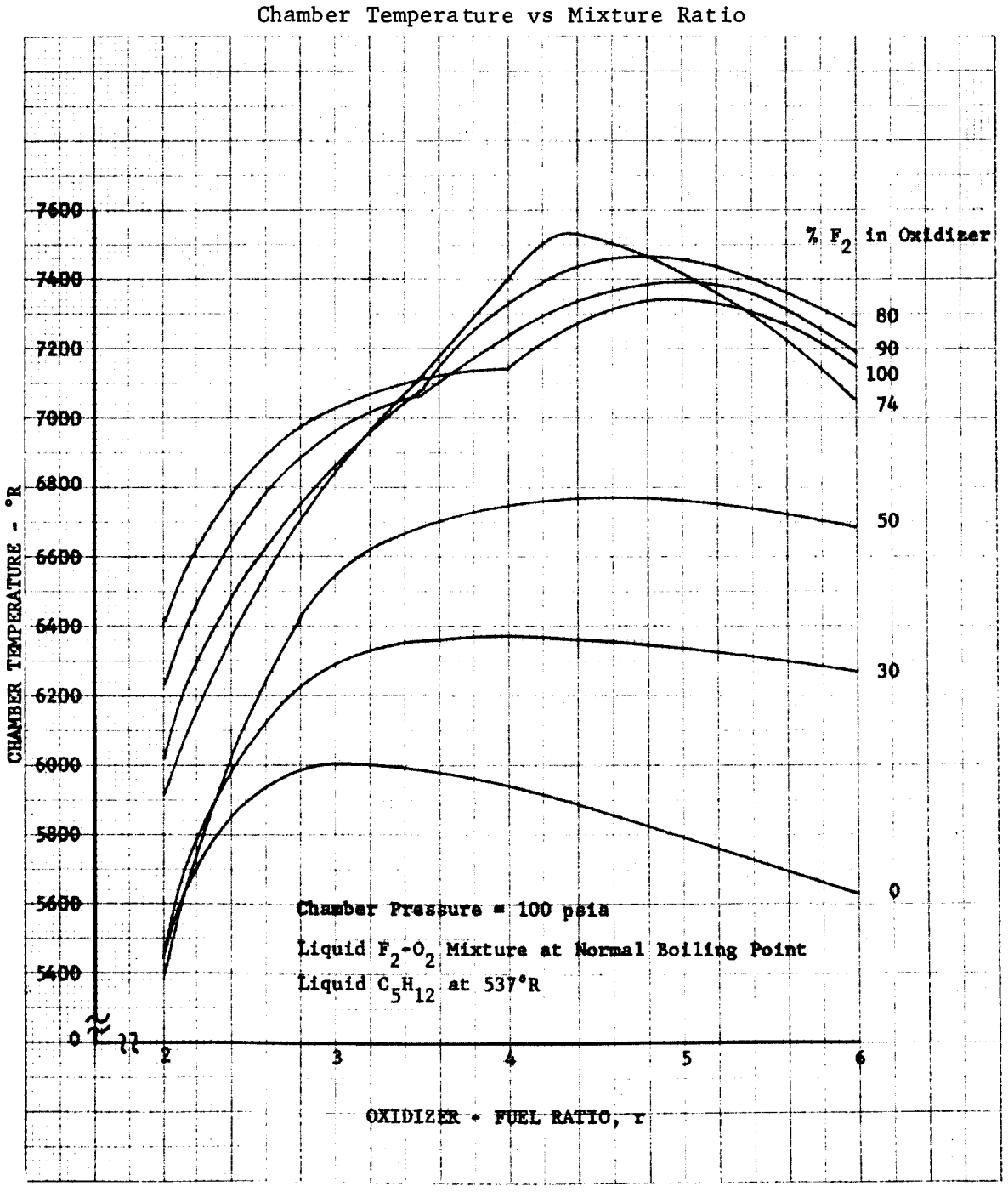

DF 37602

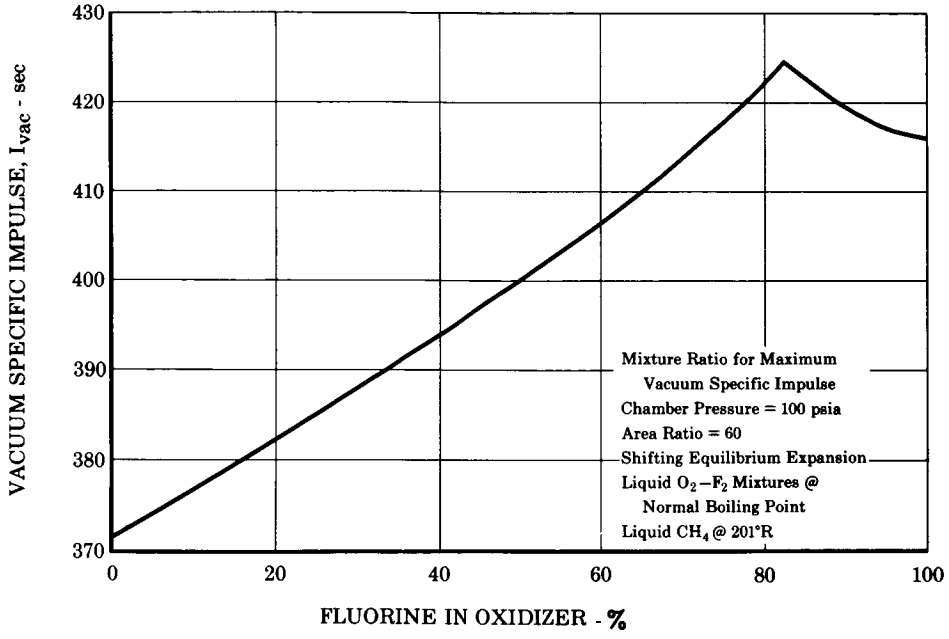

Figure C-21. Theoretical Vacuum Specific Impulse vs Percent Fluorine in Oxidizer for Flox-Methane *FD 8219*

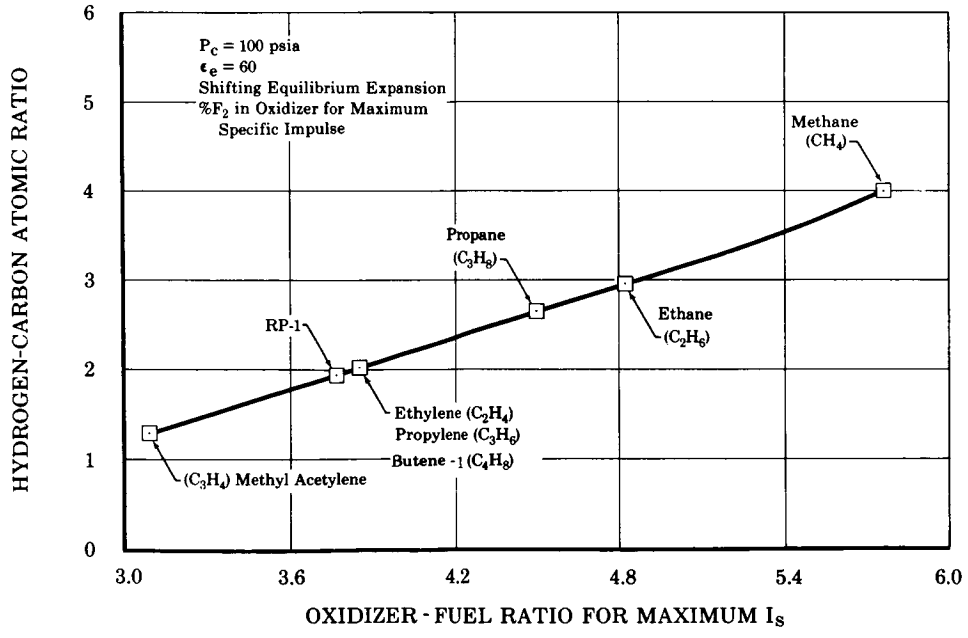

Figure C-22. Effect of Hydrogen-Carbon Ratio on Optimum Mixture Ratio *FD 8215*

APPENDIX D
HYPERGOLIC IGNITION TESTS

It is well known that light hydrocarbon fuels, such as methane and propane, will ignite hypergolically with fluorine over a wide range of temperatures, pressures, and mixture ratios. In addition, JP-4 is hypergolic with mixtures of fluorine and oxygen (Reference 1*) and hydrogen will ignite with fluorine-oxygen mixtures (Reference 2). However, it was not known if the light hydrocarbon fuels would ignite hypergolically with fluorine-oxygen mixtures over the range of physical conditions normally encountered in rocket motor applications.

An experimental program was undertaken to investigate the ignition characteristics of flox with methane, ethylene, propane, propylene, butene-1, and a eutectic blend of 14% pentane and 86% isopentane. In addition, the hypergolic ignition of gaseous hydrogen with gaseous fluorine was studied in the same ignition rig for comparison.

1. EXPERIMENTAL RIG

The basic ignition test rig, shown in figure D-1, consisted of a combustion chamber and an injector. The chamber diameter was 1.20 inches over a length of 2.60 inches from the injector face to a convergent section upstream of the chamber throat. The convergent and divergent sections approaching and leaving the 0.40-inch diameter throat were at angles of 45 and 30 degrees, respectively, with the chamber axis. The characteristic chamber length for the test rig was approximately 25 inches.

Two injectors were chosen for use with the combustion chamber. Although each differed in the manner in which the oxidizer and fuel were brought into contact within the combustion chamber, the same basic injector housing was used. The housing was fabricated with an integral cooling passage, through which liquid nitrogen could be flowed for some of the tests to prevent the liquid oxidizer from flashing to a gas or to a two-phase mixture prior to injection.

The first injector, shown in figure D-1, was a single-element concentric type. The oxidizer injection element (with swirler) and fuel annulus combination for the test rig injector was identical to an RL10 injector element except that the length/maximum diameter ratio for the fuel annulus was approximately twice that for the RL10 injector fuel annulus. Oxidizer and fuel flow areas in this injector were 0.0057 and 0.0161 in.^{2}, respectively.

* *References in this appendix are listed in paragraph 5.*

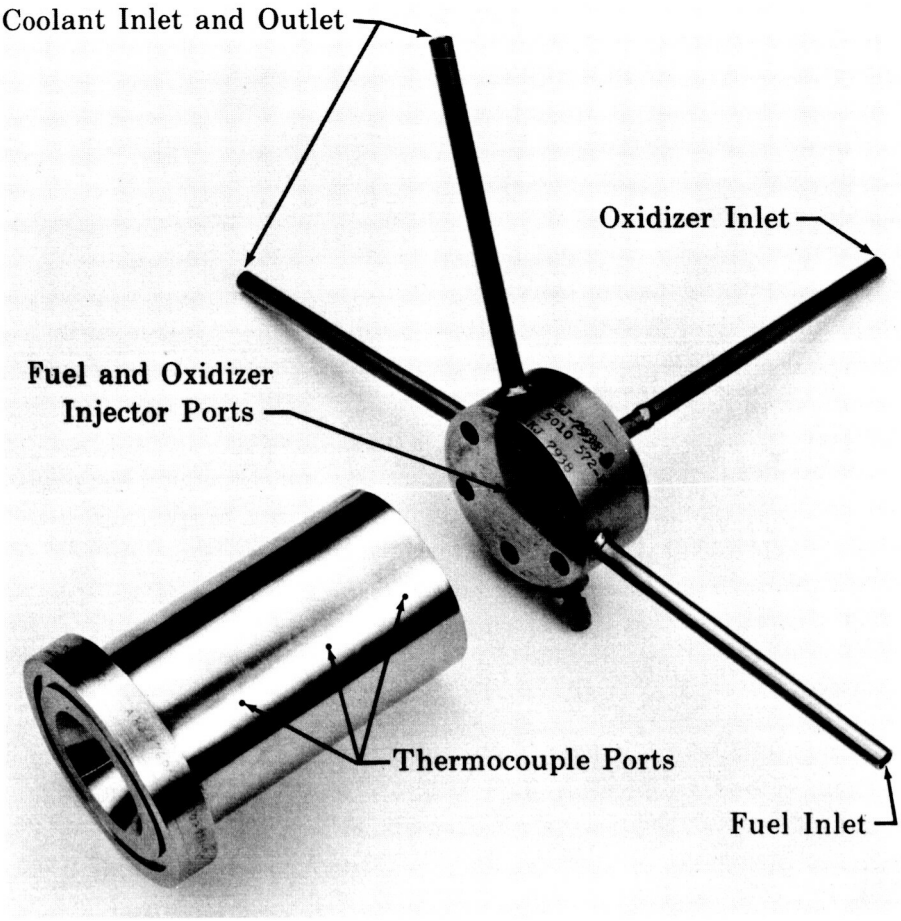

Figure D-1. Flox-Hydrocarbon Miniature Rocket Engine Ignition Tester FD 9558

The second injector was of the impingement type and is shown in figure D-2. The oxidizer injection element and injector housing were identical to the injection element and housing for the concentric injector; however, a propellant impingement plate was adapted to the face of the basic injector housing to convert the injector to one in which three fuel streams impinged upon the oxidizer stream. The total area of the fuel impingement orifices was 0.0116 in.^{2}. The fuel injection angle provided for impingement within $\frac{1}{4}$ inch of the injector face.

2. *TEST STAND AND INSTRUMENTATION*

The test stand on which the hypergolicity tests were performed is shown photographically in figure D-3 and schematically in figure D-4. For the gaseous oxidizer – gaseous fuel tests, the LN_2 heat exchanger and liquid run valves shown in figure D-4 were not required.

The test stand sensing instrumentation consisted of (1) propellant supply pressure sensors, (2) a flox mixing tank pressure sensor, (3) propellant and heat exchanger temperature sensors, and (4) propellant flow control

orifice static and differential pressure and temperature sensors. The pressure sensors were standard 4-arm bridge strain gage pressure transducers; the temperature sensors were bare-wire copper-constantan thermocouples. The recording instrumentation consisted of strip charts and a high-speed direct reading 36-channel oscillograph. Parameters needed for test stand control, as well as those parameters for which rapid response was not necessary, were recorded on strip charts; all other parameters were recorded on the oscillograph. Sequencing of the valves controlling the propellant flow into the test section and sequencing of the valves controlling the inert gas purge flow were done mechanically with a cam-operated sequencer for each test.

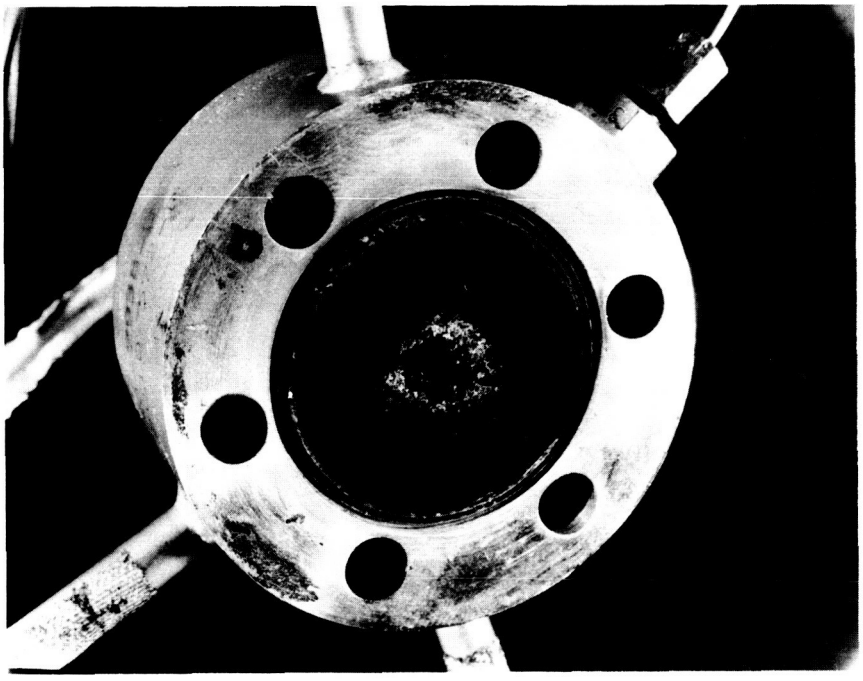

Figure D-2. Single Oxidizer Element Fuel-on-Oxidizer Impingement Injector *FE 47443*

The experimental chamber was instrumented to sense ignition and hardware temperature. Ignition was detected simultaneously by (1) two 1/16-inch bare-wire, chromel-alumel thermocouples that extended into the combustion chamber, (2) a 0-100 psig, $\frac{1}{4}$-inch, 4-arm bridge strain gage pressure transducer, and (3) a cadmium selenide photoconductive cell. Chamber wall and injector head temperatures were sensed by a 1/16-inch bare-wire, chromel-alumel thermocouple and a 1/16-inch standard contact type copper-constantan thermocouple, respectively.

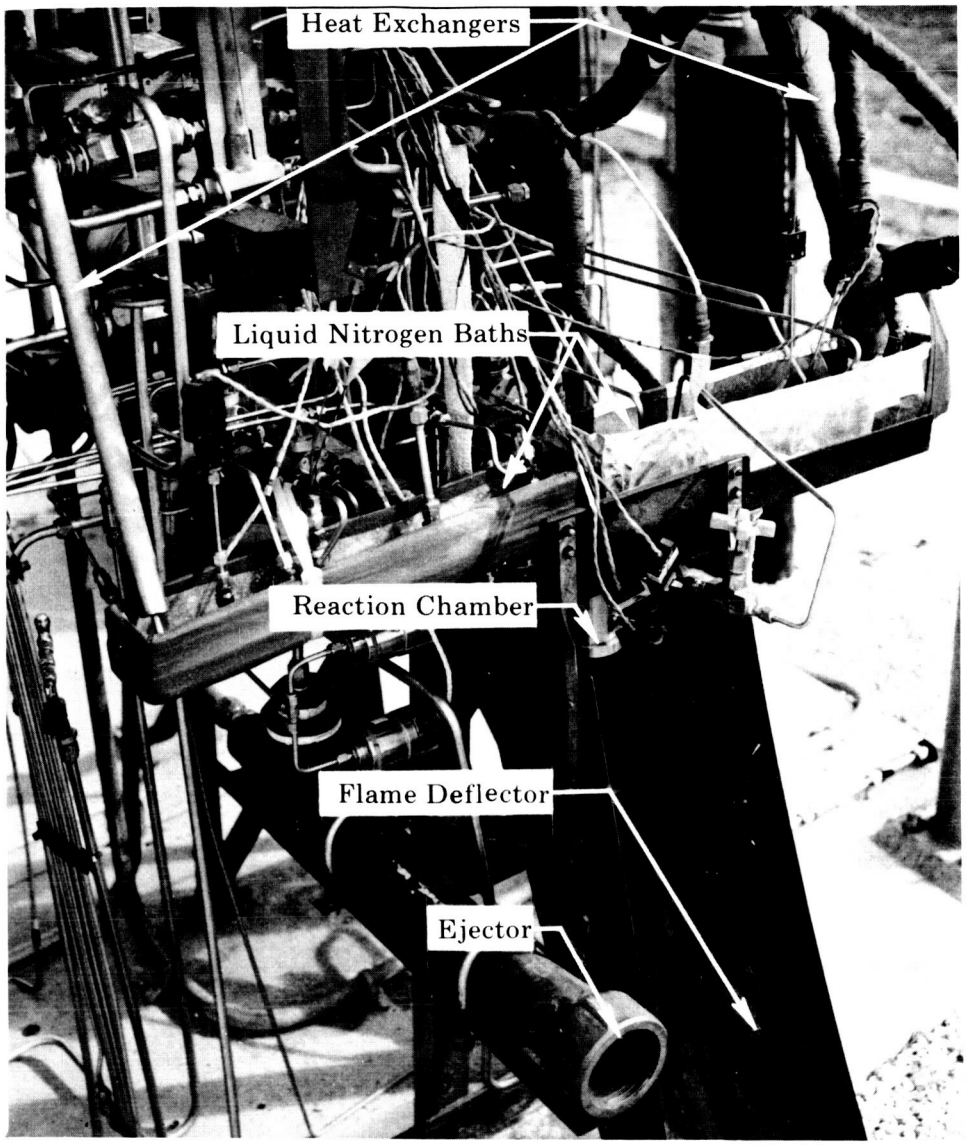

Figure D-3. Hypergolic Ignition Test Stand *FD 10624*

3. EXPERIMENTAL PROCEDURE

For the gaseous propellant tests, a supply of gaseous flox (sufficient for 3-5 tests) was first prepared by alternately introducing gaseous fluorine and oxygen into the flox mixing tank until the desired oxidizer composition, at a preselected supply or driving pressure, was obtained. The gaseous fuel supply pressure was then set with a remote-controlled pressure regulator. The test was initiated by actuating the mechanical sequencer that controlled the purge gas, propellant flow precedence and lead time, fuel lag at shutdown, and test duration time. The sequence of events for a typical test, in which fuel and oxidizer purge flows are already in process, is:

1. Close fuel purge valve and open fuel run valve simultaneously.
2. Close oxidizer purge valve and open oxidizer run valve simultaneously.
3. After approximately 100 milliseconds, close oxidizer run valve and open oxidizer purge valve simultaneously.
4. Close fuel run valve and open fuel purge valve simultaneously.

To investigate the effect of combustion chamber reduced initial pressure on ignition delay time, the chamber was equipped with a blowoff plate at the nozzle exit plane. The plate was maintained in place prior to ignition by a pressure differential across the plate caused by the action of a gaseous nitrogen ejector, as shown in figure D-4. After ignition, the pressure generated within the combustion chamber released the blowoff plate. This procedure was not successful for the reduced temperature tests because a simple pressure differential seal could not be effected with the hardware on hand after the injector and chamber were cooled down; hence, no reduced temperature – reduced pressure tests were conducted.

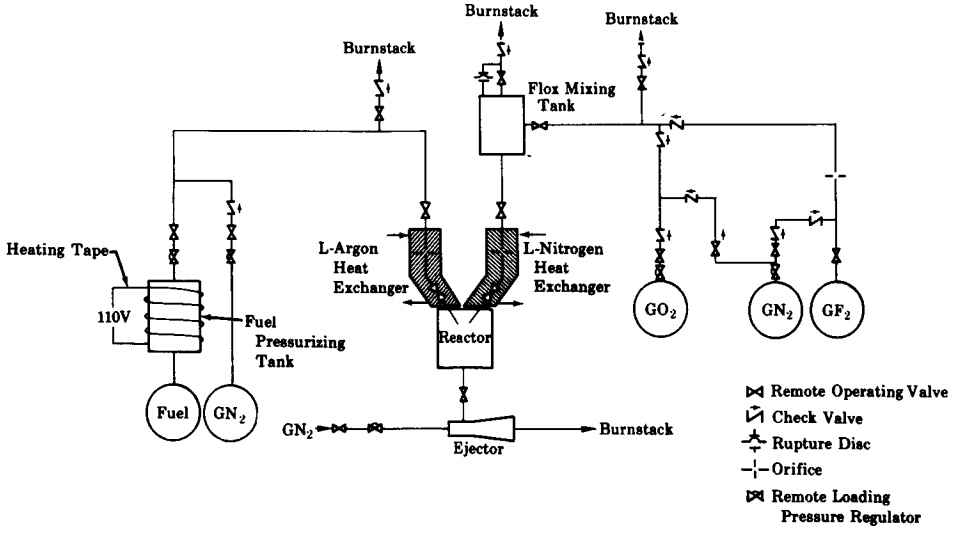

Figure D-4. Flox-LPG Ignition Test Stand Schematic *FD 9559B*

Some modifications were made to the experimental procedure to permit testing with liquid oxidizer and liquid fuel. The gaseous flox was prepared, as previously described, in the desired concentrations, and liquefied in the flox supply line within the LN_2 heat exchanger shown in figure D-4. The liquid flox was then pressurized with gaseous helium to the supply pressure necessary to give the desired flox flow rate. During the time in which liquid flox was being generated, the injector head was being cooled with liquid nitrogen. Except for butene-1 and the pentane blend, which are normally liquids at 540°R, the other hydrocarbon fuels were liquefied and pressurized in a manner similar to that used for the flox mixtures.

A change in procedure was made during the attempted liquid methane test series. The other hydrocarbon fuels investigated have relatively wide temperature bands in which the fuel could remain in the subcooled liquid phase; it was possible to liquefy them and keep them above their respective freezing temperatures. However, the liquid temperature range for methane is small and the fuel could not be kept from accidentally freezing. Therefore, the procedure used was to deliberately freeze the methane in the fuel supply line just upstream of the fuel run valve, and then to warm the line slowly until fuel flow was indicated when the fuel flow control valve was cycled rapidly. When it was apparent that liquid methane was available, the program sequencer was actuated and a test was made.

4. TEST RESULTS

Before discussing the experimental results the following definitions are made:

1. Equivalence ratio: The ratio of the stoichiometric (oxidizer/fuel) mixture ratio to the mixture ratio at ignition for the oxidizer and fuel being tested.
2. Ignition delay time: The time interval between the inception of flow of the lagging propellant at the static pressure tap of the flow controlling and measuring orifice (just upstream of the combustion chamber) and the time of the first indicated response from a reaction in the chamber as sensed and measured by the pressure, temperature or photosensor.

In figure D-5, the ignition delay time is taken as the interval between inception of oxidizer flow and the initiation of chamber temperature rise. The ignition sensors responded simultaneously in almost all tests. In the tests in which there was a difference in sensor actuation, the ignition delay time corresponding to the sensor that yielded the most rapid response was reported. Discrepancies were never more than a few milliseconds.

The transient time for propellants flowing from the static pressure tap to the combustion chamber was 1-6 milliseconds for all supply pressures. For ignition delay time comparison studies, this range of values is considered acceptable within the accuracy of an experimental system. Correcting for this transit time has no significant effect on the trends resulting from this study. Any ignition delay time that is measured for a flowing hypergolic propellant system (in other than the exact configuration in which the propellants will be used) is, of necessity, a comparative or qualitative estimate; consequently, absolute values of delay time were not considered as important as the relative value of delay time and trends resulting from a consistent experimental procedure that was used in all tests.

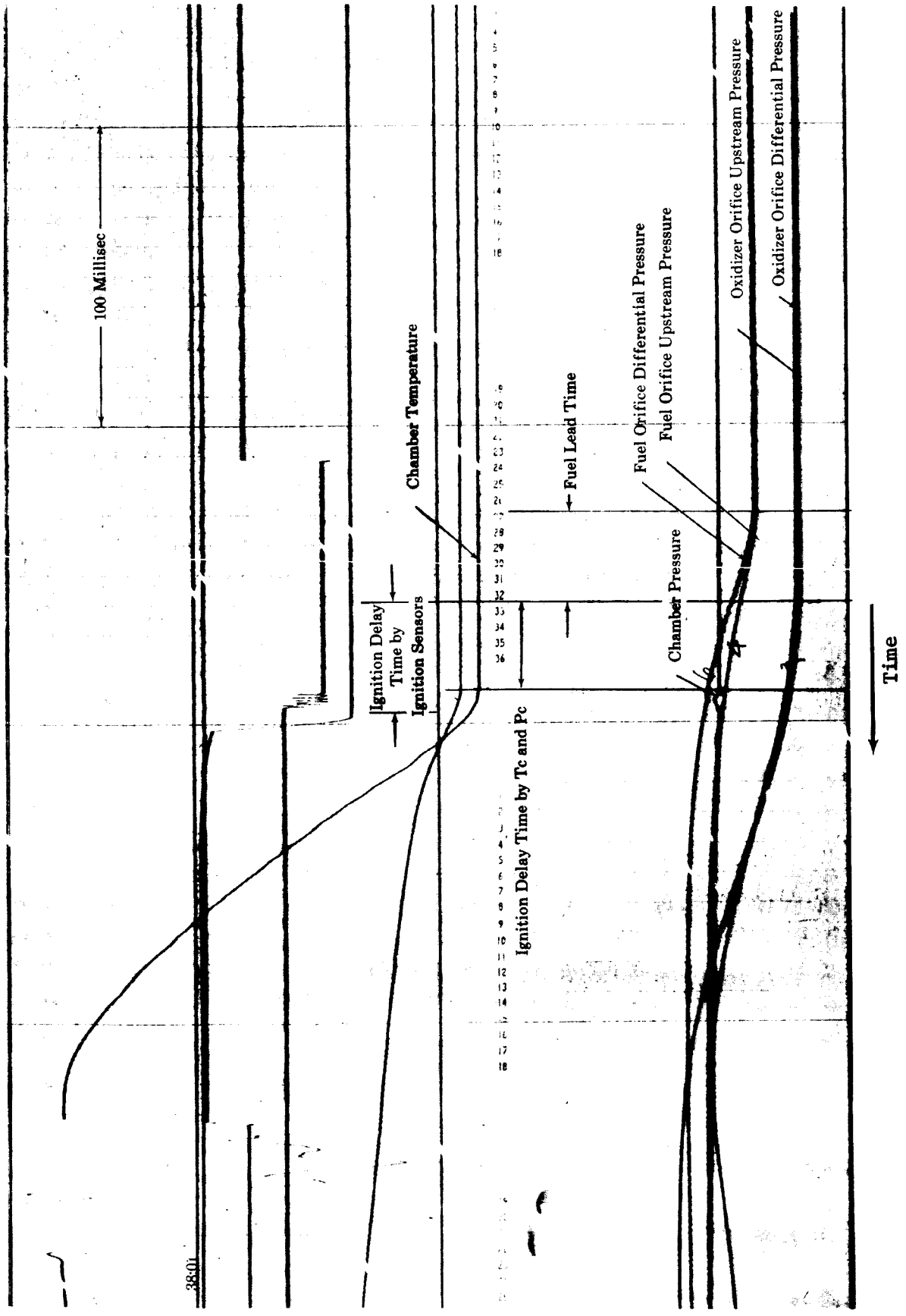

Figure D-5. Typical Ignition Test Oscillograph

A total of 161 hypergolic ignition tests was made over a wide range of operating conditions, of which 138 were made with flox and light hydrocarbons and 23 were made with fluorine and hydrogen. This total excludes cold-flow tests and tests in which there were system and instrumentation malfunctions. Results are summarized briefly in table D-1 for all fuels, and in detail in tables D-2 through D-8 by fuel type.

As shown in table D-1, test conditions were widely varied to enable an overall survey of flox-hydrocarbon hypergolicity to be made. As a result, few tests were made in which the more important parameters, such as propellant temperature, pressure and flox concentration, were identical for each fuel examined. Consequently, this study shows general trends regarding the effect of system variables on flox-hydrocarbon hypergolicity, rather than unequivocal conclusions.

a. Propellant Temperature

Except for methane, the general effect of reducing propellant temperatures was to increase the flox-hydrocarbon ignition delay time.

b. System Initial Pressure

Except for butene-1, the general effect of reducing initial chamber pressures was to decrease the flox-hydrocarbon ignition delay time. This is not considered a true pressure effect; it is attributed to reduced amounts of oxidizer and fuel purge gases being present in the combustion chamber to dilute the incoming oxidizer and fuel. The purge gases that are normally present in small amounts in the combustion chamber are largely removed by the action of the nitrogen ejector that was used to evacuate the combustion chamber prior to a reduced pressure test. The presence of purge gases has been shown in the literature to suppress, or otherwise influence, the ignition of many oxidizer-fuel mixtures. This effect is discussed in paragraph g.

c. Propellant Precedence

To reduce the ignition delay time, a fuel lead was found to be more effective than an oxidizer lead, using the concentric injector with the propellants methane and flox at fluorine concentrations of 75 and 82.6%, both propellants at a temperature of 540°R.

d. Flox Concentration

With an oxidizer lead, the general effect of increasing the fluorine concentration in the oxidizer was to decrease the flox-hydrocarbon ignition delay time. This was found to be the case in seven tests using 540°R flox and 540°R methane and in three tests using liquid flox and 540°R propylene. These tests were made at 14.7 psia using the concentric injector.

TABLE D-1. COMPARATIVE SUMMARY OF HYPERGOLICITY TEST RESULTS

Fuel	System Initial Pressure, psia		540°R OXIDIZER - 540°R FUEL Concentric Injector								140°R OXIDIZER - 540°R FUEL Concentric Injector						140°R OXIDIZER - 540°R FUEL Impinging Injector						140°R OXIDIZER - COLD FUEL Impinging Injector			
			Oxidizer Lead			Fuel Lead					Oxidizer Lead			Fuel Lead			Oxidizer Lead			Fuel Lead			Oxidizer Lead		Fuel Lead	
			FLOX CONCENTRATION (PERCENT FLUORINE IN FLUORINE-OXYGEN OXIDIZER MIXTURE)																							
			70.4	75	82.6	70.4	75-76	82.6	100		70.4	75-76	100	70.4	76	82.6	70.4	76	82.6	70.4	74	82.6	76		76	82.6
Methane	14.7	No. of Tests with Ignition		5	2		3	5							1				2			1				11
		Mean Ignition Delay Time, millisecond		345	136		48	68							1143				127			180				37
		No. of Tests with No Ignition		1	2			4				1*														1
	5.0-5.5	No. of Tests with Ignition			1			2																		
		Mean Ignition Delay Time, milliseconds			30			22																		
Ethylene	14.7	No. of Tests with Ignition				4	3							3						3						
		Mean Ignition Delay Time, milliseconds				24	11							341						176						
	5.5	No. of Tests with Ignition				2																				
		Mean Ignition Delay Time, milliseconds				6.5																				
Propane	14.7	No. of Tests with Ignition					6					1			1*			3							11	
		Mean Ignition Delay Time, milliseconds					33					160			195			422							118	
		No. of Tests with No Ignition																						1	2	
	4.5-5.5	No. of Tests with Ignition					3																			
		Mean Ignition Delay Time, milliseconds					15																			
Propylene	14.7	No. of Tests with Ignition				3	3				1		2	3**						3						
		Mean Ignition Delay Time, milliseconds				34	18				500		171	35						209						
	5.0	No. of Tests with Ignition				3																				
		Mean Ignition Delay Time, milliseconds				9																				
Butene-1	14.7	No. of Tests with Ignition	1			3	3							3			1			4						
		Mean Ignition Delay Time, milliseconds	48			37	233							531			95			309						
		No. of Tests with No Ignition															1			3						
	5.0-5.5	No. of Tests with Ignition	1			2																				
		Mean Ignition Delay Time, milliseconds	87			63																				
		No. of Tests with No Ignition				1																				
Pentane Blend	14.7	No. of Tests with Ignition																			12					
		Mean Ignition Delay Time, milliseconds																			81					
Hydrogen	14.7	No. of Tests with Ignition							23																	
		Mean Ignition Delay Time, milliseconds							16																	

*Simultaneous propellant injection.

**Includes 1 simultaneous injection test t_d = 18 milliseconds.

TABLE D-2. FLOX-METHANE HYPERGOLICITY TESTS

Test No.	Fuel Temperature (°R)	Percent F_2 in Flox Mixture	Flox Temperature (°R)	Injector Type	Chamber Initial Pressure (psia)	Lead Propellant and Lead Time (millisec)	Fuel Flow Rate at Orifice at Ignition (lbm/sec), thousandths	Oxidizer Flow Rate at Orifice at Ignition (lbm/sec), thousandths	Orifice Mixture Ratio at Ignition, ri, $(lb_m/sec)_o/(lb_m/sec)_f$	Orifice Equivalence Ratio at Ignition (r_s/r_i)	Ignition Delay (millisec)	Remarks
01	540	75	540	Concentric	14.7	F-1000	2.10	2.20	1.049	5.85	37	
02	540	75	540	Concentric	14.7	F-1000	1.79	2.98	1.663	3.68	48	
03	540	75	540	Concentric	14.7	F-1000	1.65	1.24	0.751	8.14	59	
16	540	75	540	Concentric	14.7	0-76	0.92	7.04	7.650	0.80	43	
17	540	75	540	Concentric	14.7	0-83	2.28	2.85	1.250	4.89	1505	
18	540	75	540	Concentric	14.7	0-94	—	—	—	—	—	No ignition
19	540	75	540	Concentric	14.7	0-73	1.00	7.27	7.270	0.84	11	
20	540	75	540	Concentric	14.7	0-75	1.41	8.18	5.800	1.06	43	
21	540	75	540	Concentric	14.7	0-80	0.39	8.19	21.000	0.29	123	
22	540	82.6	540	Concentric	14.7	0-80	2.76	8.89	3.220	1.86	124	
23	540	82.6	540	Concentric	14.7	0-90	—	—	—	—	—	No ignition
24	540	82.6	540	Concentric	14.7	0-110	1.36	9.63	7.090	0.85	148	
25	540	82.6	540	Concentric	14.7	0-20	—	—	—	—	—	No ignition
26	540	82.6	540	Concentric	14.7	F-26	—	—	—	—	—	No ignition
27	540	82.6	540	Concentric	14.7	F-23	2.02	3.32	1.642	3.66	54	
28	540	82.6	540	Concentric	14.7	F-20	1.71	9.38	5.490	1.09	143	
29	540	82.6	540	Concentric	14.7	F-20	—	—	—	—	—	No ignition
30	540	82.6	540	Concentric	14.7	F-25	—	—	—	—	—	No ignition
31	540	82.6	540	Concentric	14.7	F-20	—	—	—	—	—	No ignition
58	540	82.6	540	Concentric	5.0	F-96	1.75	0.76	0.435	13.90	20	
59	540	82.6	540	Concentric	5.0	F-108	1.71	0.61	0.357	16.95	23	
60	540	82.6	540	Concentric	5.5	0-20	1.53	1.42	0.929	6.46	30	
61	540	82.6	540	Concentric	14.7	F-89	1.82	2.92	1.603	3.75	60	
62	540	82.6	540	Concentric	14.7	F-120	1.71	1.05	0.615	9.79	40	
63	540	82.6	540	Concentric	14.7	F-90	1.56	1.83	1.171	5.11	43	
64	540	82.6	140	Concentric	14.7	F-207	1.84	6.20	3.370	1.83	1143	
65	540	82.6	140	Concentric	14.7	S	—	—	—	—	—	No ignition
84	540	82.6	140	Impingement	14.7	0-54	1.68	17.62	10.500	0.55	125	
85	540	82.6	140	Impingement	14.7	0-83	1.74	8.50	4.890	1.18	128	
86	540	82.6	140	Impingement	14.7	F-2	1.90	11.50	6.050	0.95	180	
105	300	82.6	140	Impingement	14.7	F-47	—	—	—	—	—	No ignition
106	290	82.6	140	Impingement	14.7	F-26	2.14	11.68	5.450	1.06	144	
197	300	82.6	140	Impingement	14.7	F-17	0.23	2.00	8.700	0.66	23	
198	300	82.6	140	Impingement	14.7	F-27	0.28	4.80	17.120	0.33	63	
199	330	82.6	140	Impingement	14.7	F-17	0.24	1.56	6.500	0.89	10	
200	350	82.6	140	Impingement	14.7	F-33	0.29	6.40	22.050	0.26	80	
201	360	82.6	140	Impingement	14.7	F-30	0.26	1.56	6.000	0.97	10	
202	280	82.6	140	Impingement	14.7	F-27	0.26	1.56	6.000	0.96	12	
203	350	82.6	140	Impingement	14.7	F-25	0.24	2.00	8.340	0.70	22	
204	310	82.6	140	Impingement	14.7	F-15	0.25	1.56	6.240	0.92	13	
205	290	82.6	140	Impingement	14.7	F-13	0.13	2.00	15.390	0.39	4	
207	290	82.6	140	Impingement	14.7	F-14	0.15	5.25	35.000	0.15	30	

S = Simultaneous

TABLE D-3. FLOX-ETHYLENE HYPERGOLICITY TESTS

Test No.	Fuel Temperature (°R)	Percent F_2 in Flox Mixture	Flox Temperature (°R)	Injector Type	Chamber Initial Pressure (psia)	Lead Propellant and Lead Time (milliisec)	Fuel Flow Rate at Orifice at Ignition (lbm/sec), thousandths	Oxidizer Flow Rate at Orifice at Ignition (lbm/sec), thousandths	Orifice Mixture Ratio at Ignition, r_i, $(lb_m/sec)_O/(lb_m/sec)_F$	Orifice Equivalence Ratio at Ignition (r_s/r_i)	Ignition Delay (milliisec)
10	540	75.0	540	Concentric	14.7	F-1000	2.40	0.96	0.400	9.65	25
11	540	75.0	540	Concentric	14.7	F-1000	2.07	0.76	0.367	10.50	4
12	540	75.0	540	Concentric	14.7	F-1000	1.91	1.55	0.811	4.74	3
35	540	70.4	540	Concentric	14.7	F-34	2.30	1.89	0.822	4.69	30
36	540	70.4	540	Concentric	14.7	F-30	2.12	1.70	0.802	4.78	28
37	540	70.4	540	Concentric	14.7	F-32	1.90	1.63	0.858	4.48	30
49	540	70.4	540	Concentric	5.5	F-65	1.81	0.43	0.238	16.15	8
50	540	70.4	540	Concentric	5.5	F-80	1.85	0.93	0.503	7.64	5
51	540	70.4	540	Concentric	14.7	F-66	1.63	0.66	0.405	9.46	12
73	540	70.4	140	Concentric	14.7	F-19	3.64	17.10	4.700	0.82	515
74	540	70.4	140	Concentric	14.7	F-42	3.52	19.60	5.570	0.69	287
75	540	70.4	140	Concentric	14.7	F-29	3.52	16.60	4.710	0.82	222
87	540	70.4	140	Impingement	14.7	F-48	3.06	18.80	6.150	1.00	199
88	540	70.4	140	Impingement	14.7	F-45	3.68	12.20	3.315	0.84	154
89	540	70.4	140	Impingement	14.7	F-33	3.00	16.60	5.540	0.70	175

TABLE D-4. FLOX-PROPANE HYPERGOLICITY TESTS

Test No.	Fuel Temperature (°R)	Percent F_2 in Flox Mixture	Flox Temperature (°R)	Injector Type	Chamber Initial Pressure (psia)	Lead Propellant and Lead Time (milliisec)	Fuel Flow Rate at Orifice at Ignition (lbm/sec), thousandths	Oxidizer Flow Rate at Orifice at Ignition (lbm/sec), thousandths	Orifice Mixture Ratio at Ignition, r_i, $(lb_m/sec)_O/(lb_m/sec)_F$	Orifice Equivalence Ratio at Ignition (r_s/r_i)	Ignition Delay (milliisec)	Remarks
4	540	75.0	540	Concentric	14.7	F-1000	2.17	1.64	0.756	6.16	25	
5	540	75.0	540	Concentric	14.7	F-1000	1.76	1.81	1.029	4.55	31	
6	540	75.0	540	Concentric	14.7	F-1000	1.65	1.65	1.000	4.66	25	
38	540	76.0	540	Concentric	14.7	F-30	1.95	1.83	0.939	4.98	38	
39	540	76.0	540	Concentric	14.7	F-36	2.08	2.41	1.160	4.02	40	
40	540	76.0	540	Concentric	14.7	F-34	1.90	2.38	1.251	3.73	40	
52	540	76.0	540	Concentric	4.5	F-85	1:76	0.58	0.330	14.20	20	
53	540	76.0	540	Concentric	5.5	F-106	1.85	0.88	0.475	9.76	10	
54	540	76.0	540	Concentric	5.0	F-104	1.78	0.58	0.745	14.40	16	
79	540	76.0	140	Concentric	14.7	0-16	1.68	12.60	7.500	0.60	160	
80	540	76.0	140	Concentric	14.7	S	2.31	13.10	5.670	0.79	195	
81	540	76.0	140	Impingement	14.7	0-85	2.71	14.50	5.350	0.84	439	
82	540	76.0	140	Impingement	14.7	0-159	2.71	16.90	6.240	0.72	349	
83	540	76.0	140	Impingement	14.7	0-88	2.67	13.20	4.950	0.91	477	
175	285	76.0	140	Impingement	14.7	F-8	—	—	—	—	—	No ignition
178	460	76.0	140	Impingement	14.7	0-4	—	—	—	—	—	No ignition
180	260	76.0	140	Impingement	14.7	F-15	—	—	—	—	—	No ignition
183	240	76.0	140	Impingement	14.7	F-21	2.15	9.00	4.190	0.92	110	
184	240	76.0	140	Impingement	14.7	F-20	2.62	8.30	3.170	0.70	131	
185	305	76.0	140	Impingement	14.7	F-29	2.65	10.60	4.000	0.89	119	
186	290	76.0	140	Impingement	14.7	F-18	2.10	12.00	5.710	1.27	138	
187	260	76.0	140	Impingement	14.7	F-14	2.00	12.00	6.000	1.33	145	
191	280	76.0	140	Impingement	14.7	F-24	2.85	9.40	3.300	0.73	192	
192	280	76.0	140	Impingement	14.7	F-19	2.53	5.80	2.295	0.51	136	
193	310	76.0	140	Impingement	14.7	F-19	2.01	10.60	5.275	1.17	88	
194	260	76.0	140	Impingement	14.7	F-37	2.19	6.40	2.920	0.65	123	
195	200	76.0	140	Impingement	14.7	F-13	1.52	7.40	4.860	1.08	56	
196	280	76.0	140	Impingement	14.7	F-14	1.59	6.90	4.340	0.96	61	

S = Simultaneous

TABLE D-5. FLOX-PROPYLENE HYPERGOLICITY TESTS

Test No.	Fuel Temperature (°R)	Percent F_2 in Flox Mixture	Flox Temperature (°R)	Injector Type	Chamber Initial Pressure (psia)	Lead Propellant and Lead Time (milliisec)	Fuel Flow Rate at Orifice at Ignition (lbm/sec), thousandths	Oxidizer Flow Rate at Orifice at Ignition (lbm/sec), thousandths	Orifice Mixture Ratio at Ignition, r_i, $(lb_m/sec)_O/(lb_m/sec)_F$	Orifice Equivalence Ratio at Ignition (r_s/r_i)	Ignition Delay (milliisec)
07	540	75.0	540	Concentric	14.7	F-1000	2.22	1.47	0.662	6.43	20
08	540	75.0	540	Concentric	14.7	F-1000	2.10	1.05	0.500	8.44	21
09	540	75.0	540	Concentric	14.7	F-1000	1.96	0.93	0.475	8.97	14
32	540	70.4	540	Concentric	14.7	F-26	2.27	2.09	0.921	4.20	34
33	540	70.4	540	Concentric	14.7	F-30	2.30	2.47	1.073	3.61	38
34	540	70.4	540	Concentric	14.7	F-25	1.96	1.74	0.889	4.36	30
55	540	70.4	540	Concentric	5.0	F-99	2.58	0.93	0.360	10.69	10
56	540	70.4	540	Concentric	5.0	F-120	2.42	1.03	0.426	9.09	8
57	540	70.4	540	Concentric	5.0	F-110	2.27	0.72	0.318	12.20	10
66	540	70.4	140	Concentric	14.7	F-21	1.35	19.40	14.380	0.27	73
67	540	70.4	140	Concentric	14.7	F-11	0.75	9.00	12.000	0.32	15
68	540	70.4	140	Concentric	14.7	S	0.72	9.68	13.440	0.31	18
69	540	74.4	140	Concentric	14.7	O-33	3.77	19.40	5.150	0.75	500
70	540	100.0	140	Concentric	14.7	O-2	3.28	15.20	4.630	0.97	150
71	540	100.0	140	Concentric	14.7	O-23	3.33	15.80	4.750	0.95	192
90	540	70.4	140	Impingement	14.7	F-20	3.41	13.90	4.075	0.95	173
91	540	70.4	140	Impingement	14.7	F-26	2.99	13.20	4.410	0.87	204
92	540	70.4	140	Impingement	14.7	F-17	3.17	14.20	4.480	0.86	249

S = Simultaneous

TABLE D-6. FLOX-BUTENE-1 HYPERGOLICITY TESTS

Test No.	Fuel Temperature (°R)	Percent F_2 in Flox Mixture	Flox Temperature (°R)	Injector Type	Chamber Initial Pressure (psia)	Lead Propellant and Lead Time (milliisec)	Fuel Flow Rate at Orifice at Ignition (lbm/sec), thousandths	Oxidizer Flow Rate at Orifice at Ignition (lbm/sec), thousandths	Orifice Mixture Ratio at Ignition, r_i, $(lb_m/sec)_o/(lb_m/sec)_f$	Orifice Equivalence Ratio at Ignition (r_s/r_i)	Ignition Delay (milliisec)	Remarks
13	540	75.0	540	Concentric	14.7	F-1000	0.75	3.53	4.700	0.91	272	
14	540	75.0	540	Concentric	14.7	F-1000	0.74	3.97	5.360	0.79	257	
15	540	75.0	540	Concentric	14.7	F-1000	0.63	4.17	6.620	0.64	168	
41	540	70.4	540	Concentric	14.7	F-20	0.52	0.61	1.172	3.28	25	
42	540	70.4	540	Concentric	14.7	F-20	0.73	0.64	0.876	4.38	39	
43	540	70.4	540	Concentric	14.7	F-25	0.63	0.79	1.253	3.04	47	
44	540	70.4	540	Concentric	14.7	0-50	0.25	0.91	3.640	1.05	48	
45	540	70.4	540	Concentric	5.0	0-76	0.10	0.79	7.900	0.49	87	
46	540	70.4	540	Concentric	5.5	F-60	0.38	0.15	0.395	9.99	53	
47	540	70.4	540	Concentric	5.5	F-63	0.77	0.25	0.324	11.60	72	
48	540	70.4	540	Concentric	5.0	F-81	—	—	—	—		No ignition
76	540	70.4	140	Concentric	14.7	F-24	0.88	16.80	19.100	0.20	253	
77	540	70.4	140	Concentric	14.7	F-23	1.24	15.50	12.500	0.31	994	
78	540	70.4	140	Concentric	14.7	F-18	0.71	16.90	23.800	0.16	347	
93	540	70.4	140	Impingement	14.7	0-29	0.67	13.60	20.300	0.20	95	
94	540	70.4	140	Impingement	14.7	0-28			—			
97	540	70.4	140	Impingement	14.7	F-57	2.26	11.67	5.160	0.75	179	
98	540	70.4	140	Impingement	14.7	F-43	1.55	7.57	4.890	0.79	57	
99	540	70.4	140	Impingement	14.7	F-24	—	—	—	—	—	No ignition
101	540	70.4	140	Impingement	14.7	F-44	—	—	—	—	—	No ignition
102	540	70.4	140	Impingement	14.7	F-74	—	—	—	—	—	No ignition
103	540	70.4	140	Impingement	14.7	F-50	1.47	10.62	7.240	0.53	878	
104	540	70.4	140	Impingement	14.7	F-60	1.67	10.90	6.530	0.59	123	

TABLE D-7. FLOX-PENTANE-ISOPENTANE BLEND HYPERGOLICITY TESTS

Test No.	Fuel Temperature (°R)	Percent F_2 in Flox Mixture	Flox Temperature (°R)	Injector Type	Chamber Initial Pressure (psia)	Lead Propellant and Lead Time (milliisec)	Fuel Flow Rate at Orifice at Ignition (lbm/sec), thousandths	Oxidizer Flow Rate at Orifice at Ignition (lbm/sec), thousandths	Orifice Mixture Ratio at Ignition, r_i, $(lb_m/sec)_O/(lb_m/sec)_F$	Orifice Equivalence Ratio at Ignition (r_s/r_i)	Ignition Delay (milliisec)
162	540	74.0	140	Impingement	14.7	F-62	3.30	4.78	1.448	3.02	60
163	540	74.0	140	Impingement	14.7	F-62	3.30	4.12	1.250	3.47	38
164	540	74.0	140	Impingement	14.7	F-62	2.89	7.58	2.620	1.66	78
165	540	74.0	140	Impingement	14.7	F-62	2.79	8.56	3.070	1.40	100
166	540	74.0	140	Impingement	14.7	F-61	2.96	6.00	2.025	2.15	92
167	540	74.0	140	Impingement	14.7	F-66	2.93	5.74	1.958	2.20	65
168	540	74.0	140	Impingement	14.7	F-60	2.74	3.40	1.240	3.50	37
169	540	74.0	140	Impingement	14.7	F-65	2.24	6.50	2.900	1.50	59
170	540	74.0	140	Impingement	14.7	F-68	2.01	1.50	0.746	5.79	27
171	540	74.0	140	Impingement	14.7	F-68	2.07	2.50	1.208	3.59	20
172	540	74.0	140	Impingement	14.7	F-57	2.11	13.20	6.250	0.70	165
173	540	74.0	140	Impingement	14.7	F-60	2.07	11.20	5.410	0.80	232

TABLE D-8. FLUORINE-HYDROGEN HYPERGOLICITY TESTS

Test No.	Fuel Temperature (°R)	Percent F_2 in Flox Mixture	Flox Temperature (°R)	Injector Type	Chamber Initial Pressure (psia)	Lead Propellant and Lead Time (milliisec)	Fuel Flow Rate at Orifice at Ignition (lbm/sec), thousandths	Oxidizer Flow Rate at Orifice at Ignition (lbm/sec), thousandths	Orifice Mixture Ratio at Ignition, r_i, $(lb_m/sec)_O/(lb_m/sec)_f$	Orifice Equivalence Ratio at Ignition (r_s/r_i)	Ignition Delay (milliisec)
110	540	100.0	540	Impingement	14.7	F-524	4.09	3.19	0.781	24.3	59
111	540	100.0	540	Impingement	14.7	F-390	4.04	1.98	0.490	38.7	49
112	540	100.0	540	Impingement	14.7	F-283	4.07	1.50	0.368	51.5	26
113	540	100.0	540	Impingement	14.7	F-234	4.01	1.48	0.369	51.4	27
114	540	100.0	540	Impingement	14.7	F-188	4.09	0.56	0.137	139.5	6
115	540	100.0	540	Impingement	14.7	F-158	4.07	0.56	0.138	139.5	7
116	540	100.0	540	Impingement	14.7	F-91	4.08	0.56	0.137	137.5	11
117	540	100.0	540	Impingement	14.7	F-66	3.13	0.56	0.179	105.5	8
118	540	100.0	540	Impingement	14.7	F-66	3.12	0.54	0.173	110.0	8
119	540	100.0	540	Impingement	14.7	F-54	2.96	0.74	0.250	76.0	26
120	540	100.0	540	Impingement	14.7	F-64	2.87	0.78	0.272	70.0	6
121	540	100.0	540	Impingement	14.7	F-68	2.07	0.77	0.372	51.2	7
122	540	100.0	540	Impingement	14.7	F-60	2.09	0.97	0.464	41.1	10
123	540	100.0	540	Impingement	14.7	F-71	2.16	0.96	0.445	42.7	5
124	540	100.0	540	Impingement	14.7	F-62	2.08	0.99	0.475	57.0	4
125	540	100.0	540	Impingement	14.7	F-48	1.54	0.89	0.578	32.8	40
126	540	100.0	540	Impingement	14.7	F-52	1.69	0.55	0.325	59.0	18
127	540	100.0	540	Impingement	14.7	F-40	1.53	0.37	0.242	83.4	10
128	540	100.0	540	Impingement	14.7	F-45	1.45	0.96	0.661	28.6	10
129	540	100.0	540	Impingement	14.7	F-39	1.13	0.83	0.735	26.0	8
130	540	100.0	540	Impingement	14.7	F-31	1.19	0.98	0.824	21.7	10
131	540	100.0	540	Impingement	14.7	F-21	1.29	0.91	0.705	27.0	9
132	540	100.0	540	Impingement	14.7	F-28	1.25	0.56	0.448	41.3	10

With a fuel lead, no general effect of increasing the fluorine concentration in the flox was apparent. With all other conditions the same (concentric injector, 14.7 psia initial pressure, 540°R flox and 540°R fuel) increasing the flox concentration decreases the ignition delay time for flox-ethylene and flox-propylene, and increases the ignition delay time for flox-methane. Because of insufficient testing at other conditions, further conclusions cannot be made.

e. Injector Type

The only tests in which a comparison between the concentric and the impinging injectors can be made were those at 14.7 psia initial chamber pressure where the oxidizer and the fuel were at 140°R and 540°R, respectively. For flox-ethylene and flox-propylene, the concentric injector was more effective than the impinging injector. For flox-methane, flox-ethylene and flox-butene-1, however, the impinging injector was more effective than the concentric injector.

f. Propellant Mixture Ratio at Ignition

From an attempt to correlate ignition delay times for each flox-fuel combination that was studied with some basic or derived parameter, it was found that under identical conditions of propellant temperature, system pressure, propellant precedence, flox concentration and injector type, a linear relationship between ignition delay time and propellant equivalence ratio at ignition was obtained for the flox-pentane blend combination as shown in figure D-6. As the equivalence ratio at ignition increased, the ignition delay time decreased.

The same general ignition delay time – equivalence ratio relationship was found for the other hydrocarbon fuels, not only when test conditions were identical within each group of flox-hydrocarbon combinations but for all tests within each fuel group regardless of fuel temperature, system pressure, propellant precedence, flox concentration or injector type. However, each fuel is influenced differently. As shown in figure D-7 for all flox-hydrocarbon combinations, and in figures D-8 through D-12 for each flox-hydrocarbon combination separately, the fuels in the order of decreasing dependency on the equivalence ratio at ignition are butene-1, methane, propane, the pentane blend, propylene and ethylene. It is also seen that the fluorine-hydrogen combination is strongly dependent on propellant equivalence ratio.

For methane, it also appears that the ignition delay time is not only a function of the equivalence ratio at ignition, but also of the fuel flow rate at ignition: at least in the tests where 140°R flox and cold fuel were used. There were not enough tests made at other temperatures over a range of flow rates to make any general conclusions regarding the effect of temperature and flow rate on ignition delay time for methane. As shown in figure D-8, where the data from all the flox-methane tests are presented, three curves appear to be possible: one at low values of fuel flow rate, one at the fuel flow rates corresponding to those of the other fuels investigated, and one at an intermediate flow rate value. This flow rate dependency was not readily evident with the other fuels tested because the flow rates throughout the test series remained nearly the same.

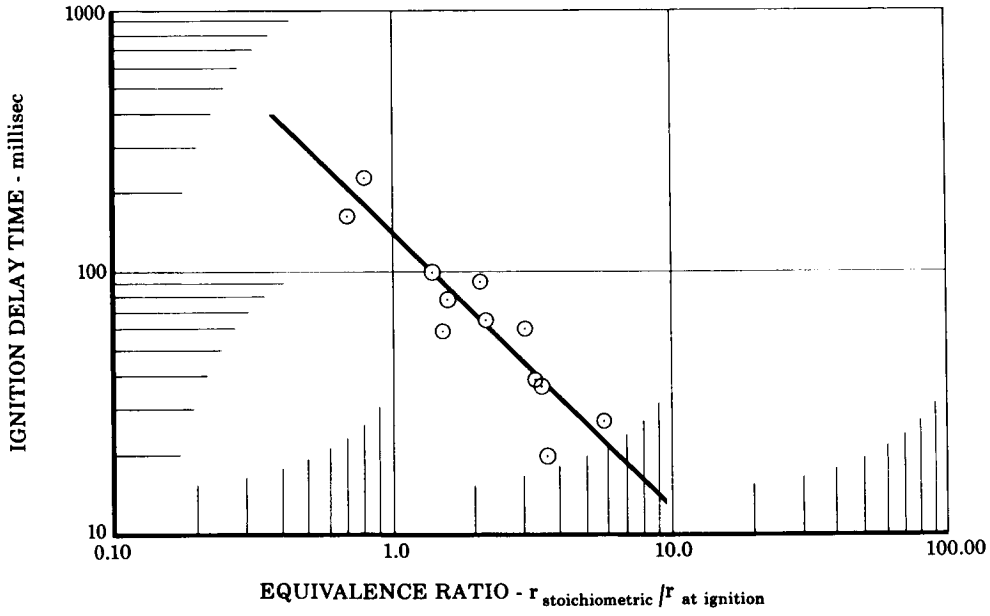

Figure D-6. Variation in Ignition Delay Time with Equivalence Ratio for 14% Pentane — 86% Isopentane Blend *FD 13040*

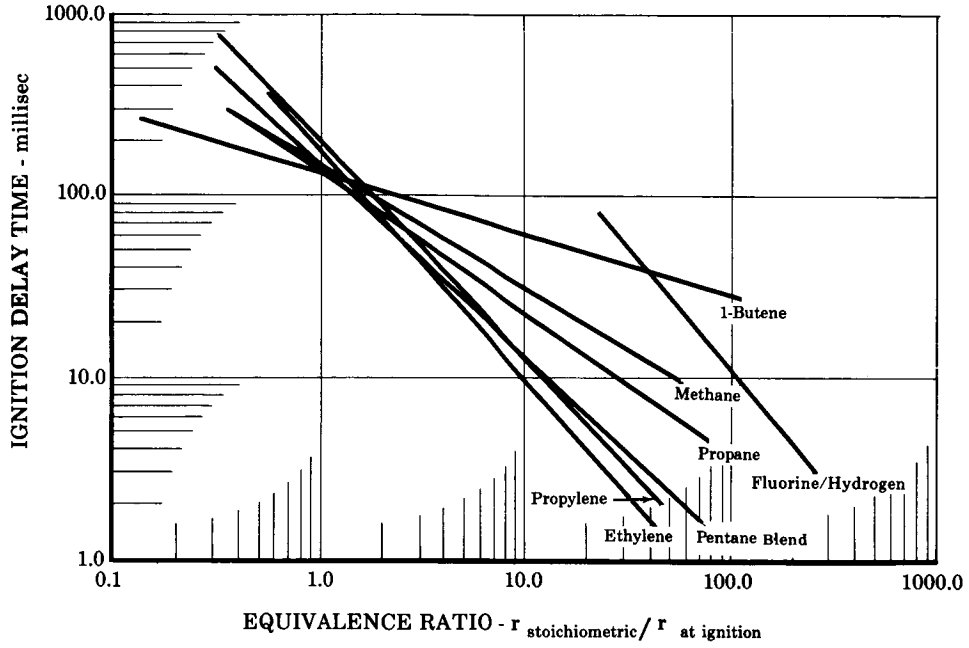

Figure D-7. Variation in Ignition Delay Time with Equivalence Ratio for Flox-Hydrocarbon Combinations FD 13044A

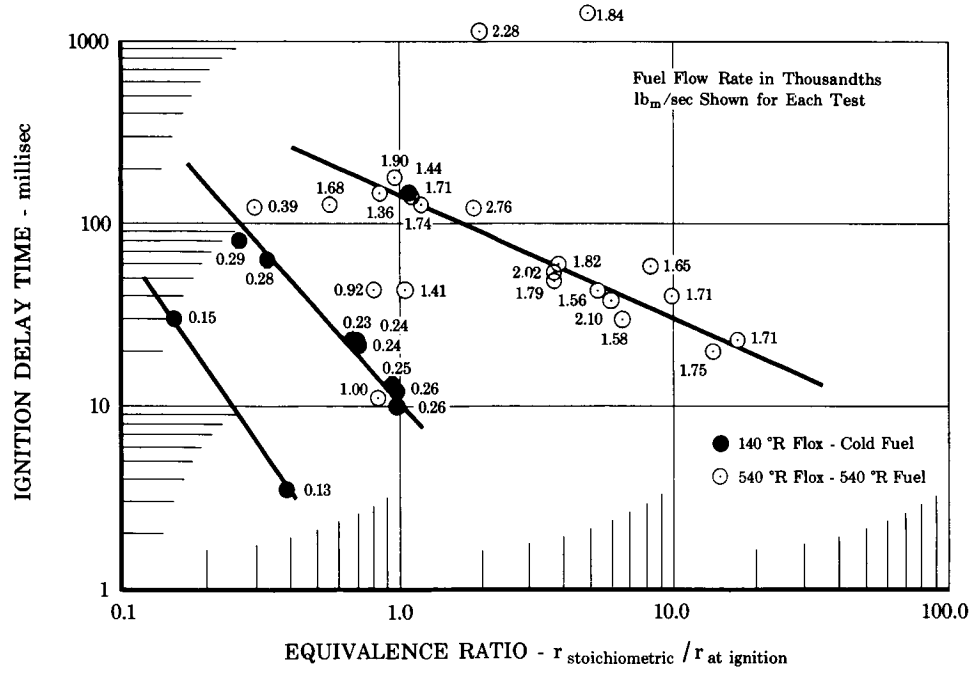

Figure D-8. Variation in Ignition Delay Time with Equivalence Ratio for Methane FD 13045A

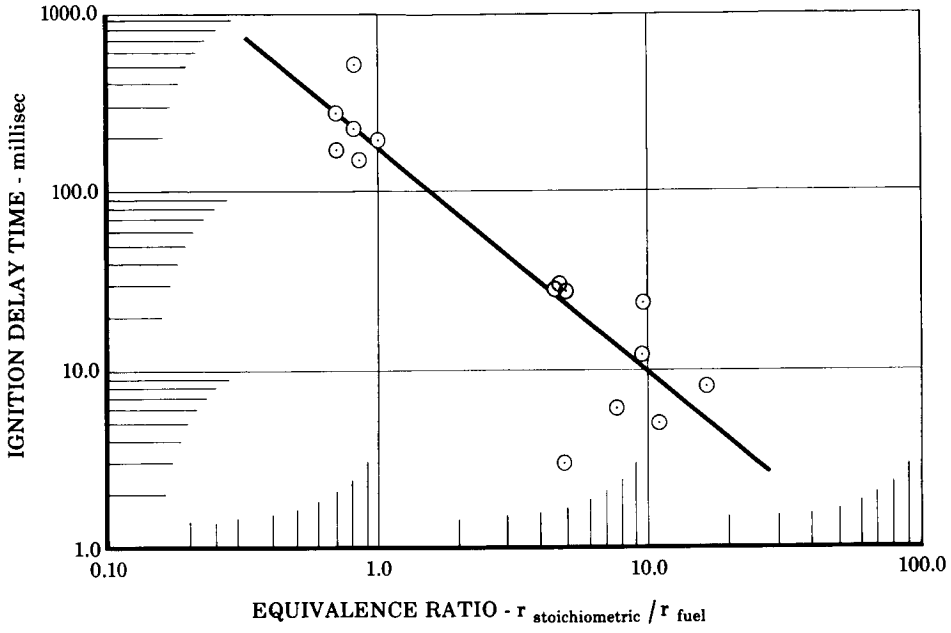

Figure D-9. Variation in Ignition Delay Time with Equivalence Ratio for Ethylene *FD 13046*

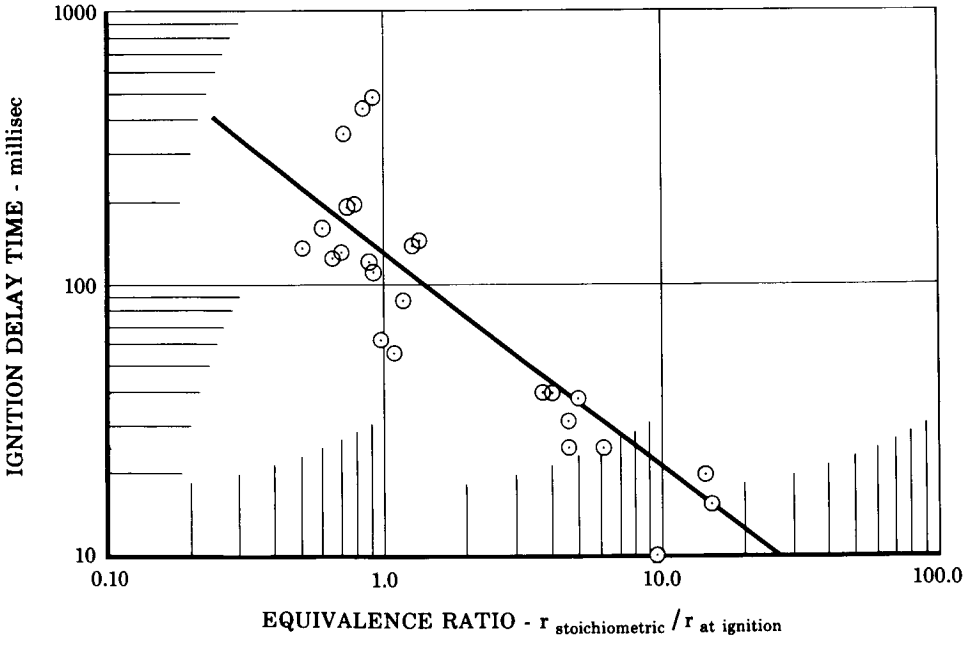

Figure D-10. Variation in Ignition Delay Time with Equivalence Ratio for Propane *FD 13043A*

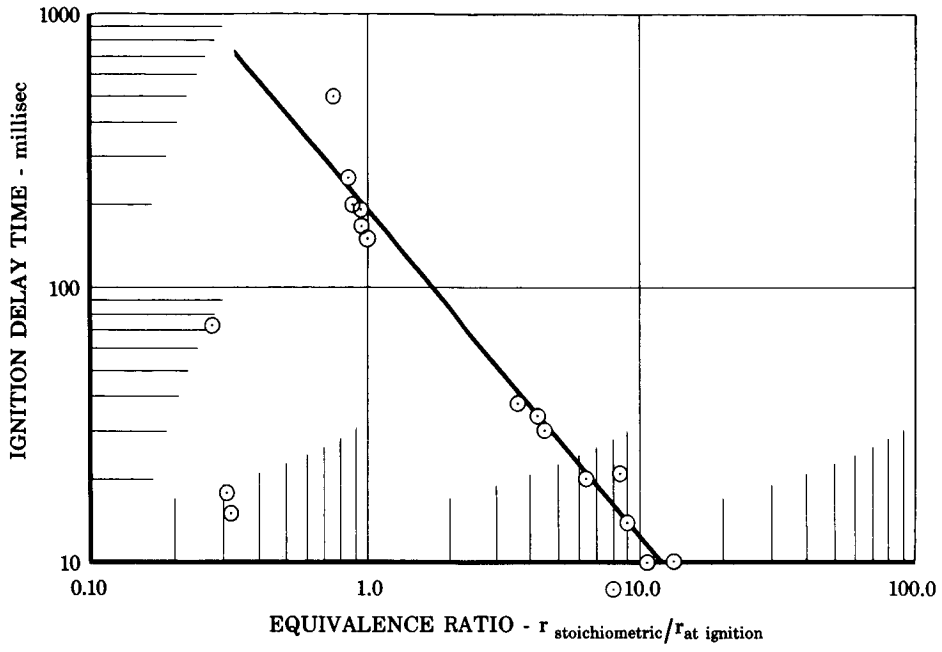

Figure D-11. Variation in Ignition Delay Time with Equivlance Ratio for Propylene *FD 13042A*

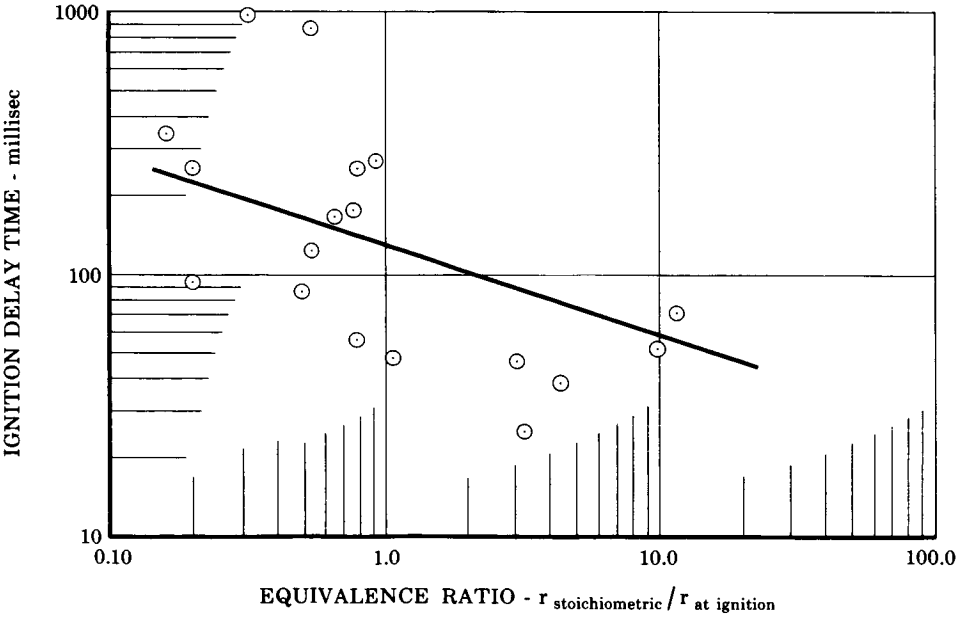

Figure D-12. Variation in Ignition Delay Time with Equivalence Ratio for Butene-1 *FD 13041*

g. Propellant Dilution

Some of the data scatter shown in the ignition delay time – equivalence ratio curves for the propellant combinations studied may be explained in part in that conditions were not exactly equivalent in the combustion chamber before the start of each test. There were some indications that the reaction in the combustion chamber is influenced by an interaction between the purge gas and the leading propellant prior to the entrance of the lagging propellant, thereby affecting the ignition delay time. Whether this interaction has a significant effect on flox-hydrocarbon hypergolicity cannot be ascertained without considerably more study. However, there is some indication in the literature (Reference 3) that a nitrogen-dilution effect on hypergolicity may exist under certain conditions for fluorine-hydrogen and flox-hydrogen mixtures.

By itself, the pressure of a purge gas (such as nitrogen or helium) in a hypergolic oxidizer-fuel mixture might not inhibit or otherwise influence the reaction. The surface-to-volume ratio of the confining reaction vessel, and the condition of the vessel inner lining also have a paramount effect. For example, the work of Coward and Jones (Reference 4) shows that the addition of increasing amounts of a chemically inert substance causes the flammability limits of a gas to vanish; however, the effectiveness of the inert substances (on a volume basis) varies as the reaction vessel dimensions change.

Work was reported by Gayle and Tubbs (Reference 5) on the effectiveness of different agents used for suppressing ignition of oxygen/RP-1 and oxygen/hydrogen mixtures under flow conditions.

The effect of purge gas on ignition delay time appeared to be demonstrated during the gaseous fluorine – gaseous hydrogen tests. Fixed purge gas rates were maintained in tests No. 110 through 118; therefore, composition of the purge gas in the chamber (nitrogen from the fuel side and helium from the oxidizer side) prior to each test should have been nearly identical. From these tests, the well-defined linear correlation of ignition delay time with equivalence ratio shown in figure D-13 was obtained. However, in the remainder of the fluorine-hydrogen tests (tests No. 119 through 132) purge-gas flow rates did not remain fixed. The consistent test procedure that was used up to this point was changed. In an attempt to conserve helium, nitrogen was substituted for the helium purge gas on the flox side until immediately prior to a test (there was a longer time period between tests as compared to the earlier tests). There is evidence that the helium purge-gas flow rate (which was reset from test-to-test during tests No. 119 through 132) was not the same as the purge-gas flow rate that existed during tests No. 110 through 118. Consequently, the concentration of the purge gas in the combustion chamber prior to

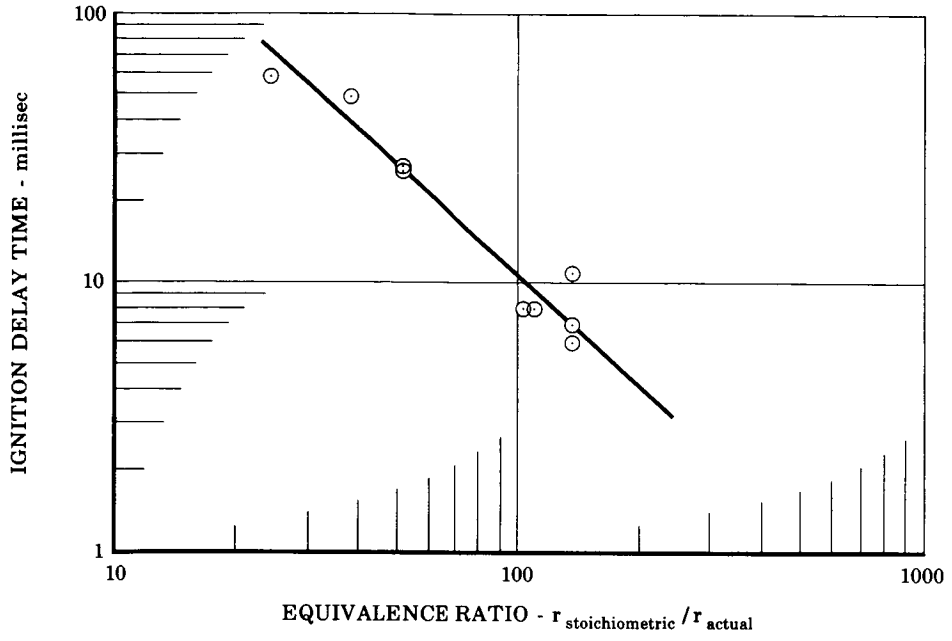

Figure D-13. Variation in Ignition Delay Time with Equivalence Ratio for Fluorine and Hydrogen for Tests No. 110 through 118 *FD 13259*

each fluorine-hydrogen test was not the same; this variation in chamber conditions may have affected the linear delay time — equivalence ratio relationship. All the data from the fluorine-hydrogen hypergolicity test series are shown in figure D-14. Although a purge dilution effect might be significant in small chemical reactors with low flow rates, such as those used in the flox hypergolicity program as well as in the referenced literature, it is unlikely that the purge gas will seriously influence the reaction induction period or ignition delay time in a large-scale propellant reaction system.

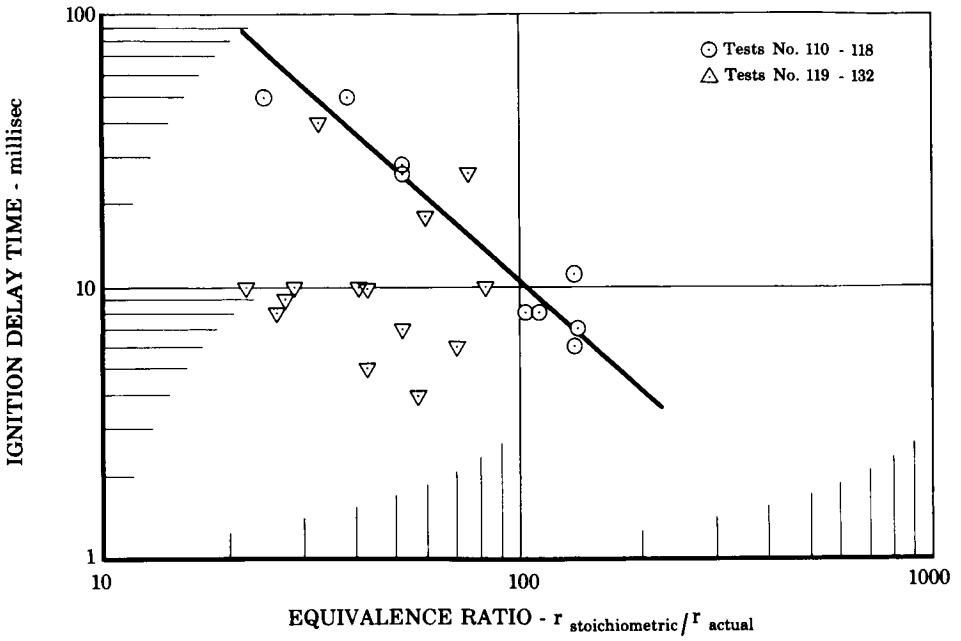

Figure D-14. Variation in Ignition Delay Time with Equivalence Ratio for Fluorine and Hydrogen *FD 13260*

5. *REFERENCES*

1. Rothenburg, E. A. and P. M. Ordin, "Preliminary Investigation of Performance and Starting Characteristics of Liquid Fluorine-Liquid Oxygen with Jet Fuel," NACA RM E53J20, January 1954.

2. Rollbuhler, R. J. and D. M. Straight, "Ignition of a Hydrogen-Oxygen Rocket Engine by Addition of Fluorine to the Oxidant," NASA TN D-1309, July 1962.

3. Levy, J. B. and B. K. W. Copeland, "The Kinetics of the Hydrogen-Fluorine Reaction – II. The Oxygen Inhibited Reaction," J1 Phys. Chem 69, No. 2, February 1965.

4. Coward, H. F. and G. W. Jones, "Limits of Flammability of Gases and Vapors," Bureau of Mines, Bulletin 503.

5. Gayle, J. B. and H. E. Tubbs, "Effectiveness of Various Agents for Suppressing Ignition of RP-1 and Hydrogen under Flow Conditions," NASA TN D-2581, January 1965.

APPENDIX E
HEATED TUBE TESTS

Heated tube heat transfer tests were conducted with six hydrocarbon fuels: (1) methane, (2) propane, (3) propylene, (4) butene-1, (5) a eutectic blend of 48% propane and 52% propylene, and (6) a eutectic blend of 14% n-pentane and 86% isopentane. Determinations of the maximum nucleate boiling heat flux, or peak heat flux, were made at fuel inlet temperatures from 160 to 520°R, subcritical and supercritical fuel inlet pressures (140 to 800 psia), and fuel inlet velocities of 1.3 to 28 ft/sec. Film boiling heat transfer coefficients were also measured for various fuel flow conditions to obtain data for prediction of wall temperatures at conditions where the maximum nucleate boiling heat flux is exceeded.

1. TEST FACILITY

A schematic of the cryogenic heated tube facility is shown in figure E-1. The system consists of a run tank, precooler, surge tank, test section, and exhaust system, as well as the required control and instrumentation systems. Electric power for heating the test section is supplied from a 100-KW alternating current variable power supply. Various coolants, such as liquid nitrogen, may be used in the precooler to lower the fuel temperature before it enters the test section tube. The surge tank serves to prevent pressure fluctuations, caused by boiling instabilities in the test section tube, from propagating upstream to the precooler, flow meter, and run tank. Figures E-2 and E-3 are photographs of the facility.

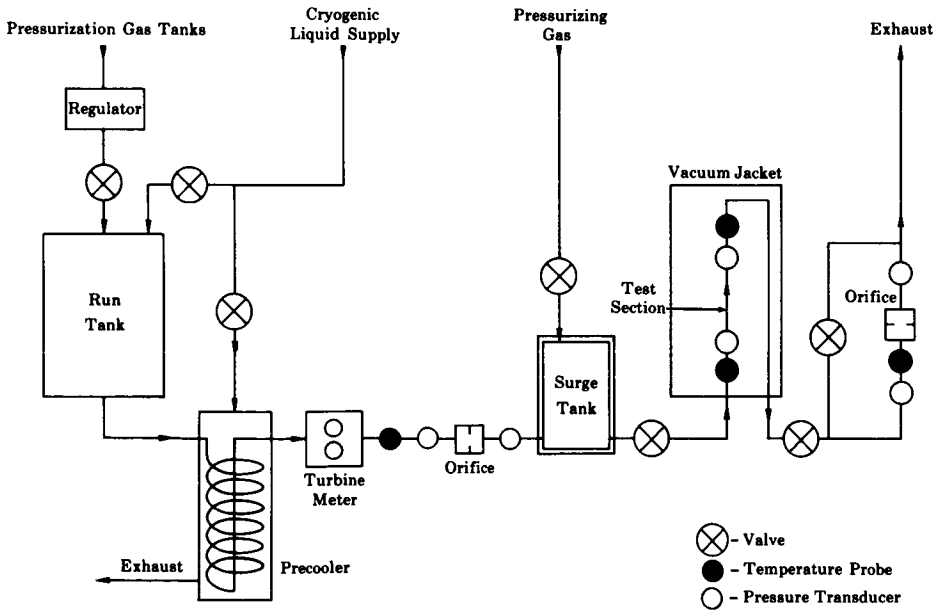

Figure E-1. Schematic of Cryogenic Heated Tube Facility *FD 7415*

A photograph of a test section tube before being instrumented and wrapped with insulation is shown in figure E-4. The 33-inch test sections were fabricated from 3/8-inch OD Inconel X 750 tubing with a wall thickness of 0.015 inch. Pressure taps were made by brazing a 1/16-inch OD tube to a bushing, which was in turn brazed onto the test section tube. A 0.020-inch diameter hole was then electro-discharge machined through the bushing and test section tube wall by passing the elox electrode through the 1/16-inch OD pressure tap tube. Electrical power was supplied to the test section tube through bus bar clamps that attached to the copper bushings on both ends of the tube. The test section was instrumented with 16 chromel-alumel thermocouples and 9 voltage taps.

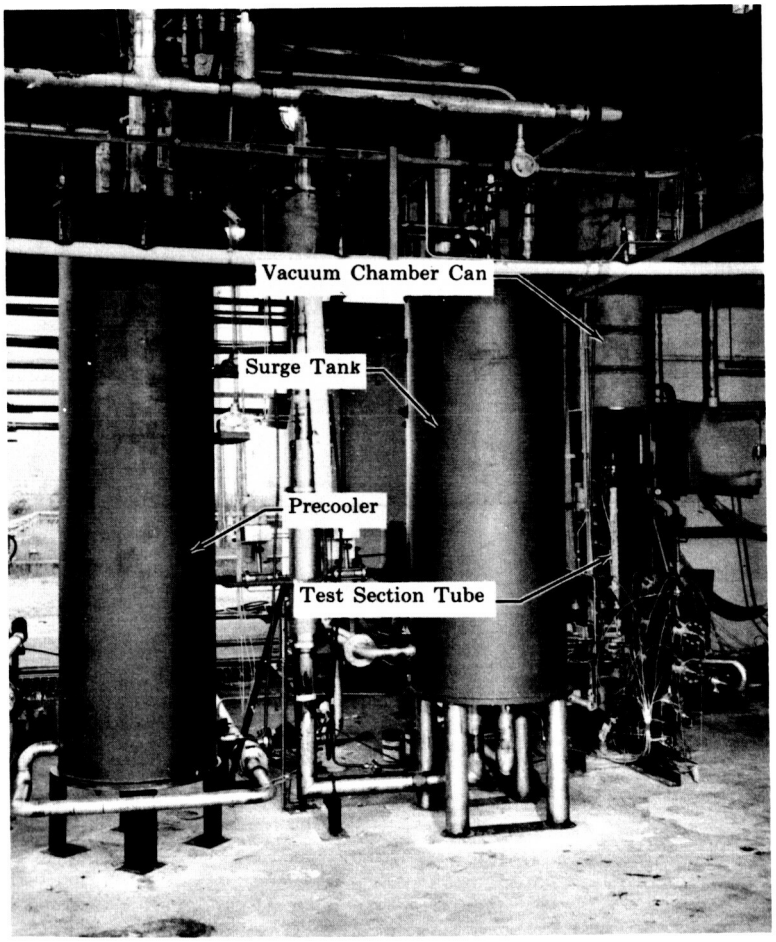

Figure E-2. Cryogenic Heated Tube Test Facility *FD 9552*

Figure E-5
Maximum Nucleate Boiling Heat Flux for Methane

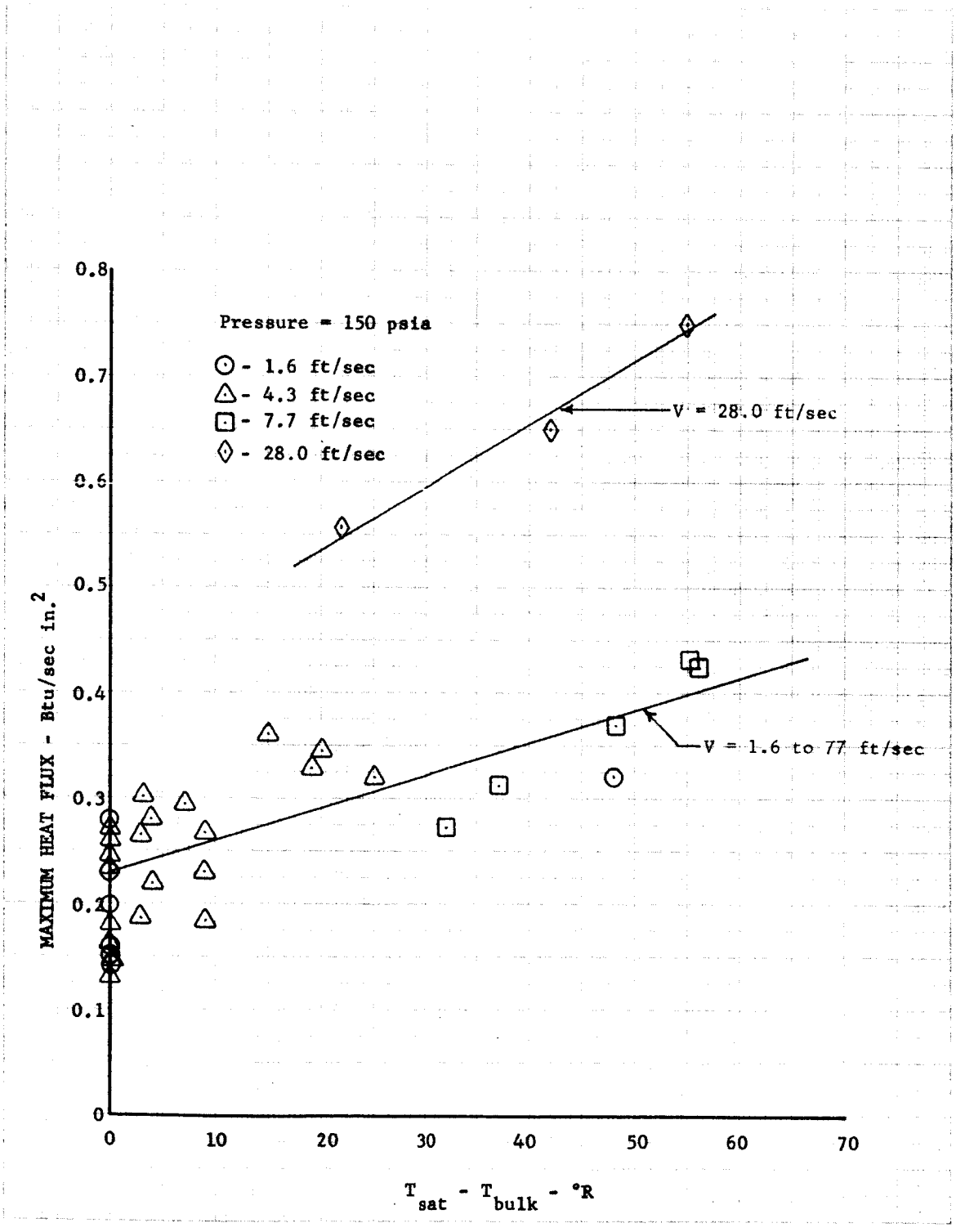

DF 35309

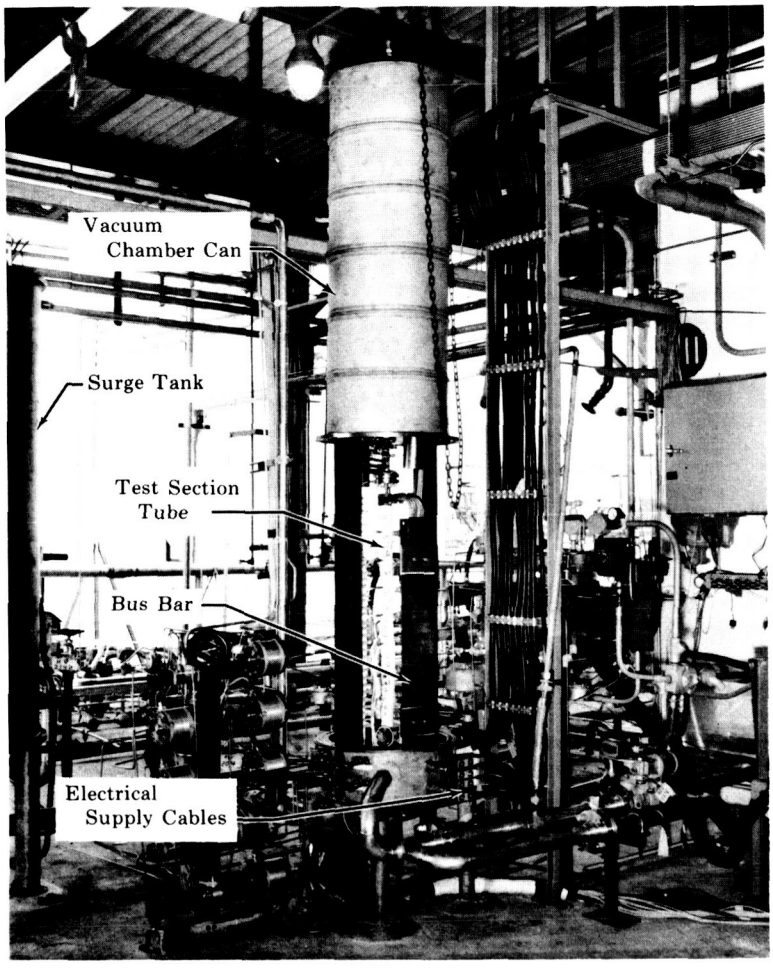

Figure E-3. Test Section Tube Chamber FD 9551

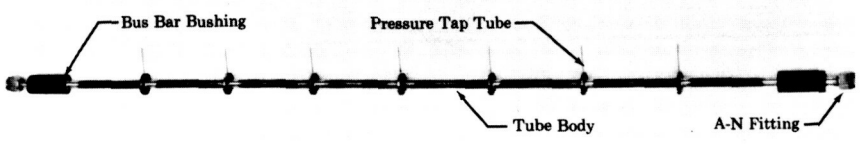

Figure E-4. Cryogenic Test Section Tube FD 9553

2. *MAXIMUM NUCLEATE BOILING HEAT FLUX DATA*

Graphs of maximum nucleate heat flux vs the degree of local subcooling for all six fuels are shown in figures E-5 through E-10. All of these graphs are for a pressure of 150 psia and show lines of constant fuel inlet velocity. The trends regarding the effect of velocity and subcooling on the maximum nucleate heat flux as evidenced by these graphs agree with similar data for other fluids with one exception — the data for methane does not exhibit a velocity effect on the maximum heat flux for the velocity range of 1.6 to 7.7 ft/sec. Data were not obtained for maximum nucleate heat fluxes for methane at degrees of subcooling as high as those obtained for the other hydrocarbons tested because the difference between the saturation temperature and the freezing temperature is much smaller than that of the other hydrocarbons tested. Consequently, most of the data obtained was at low values of subcooling and much of it was for no subcooling.

Figure E-6
Maximum Nucleate Boiling Heat Flux for Propane

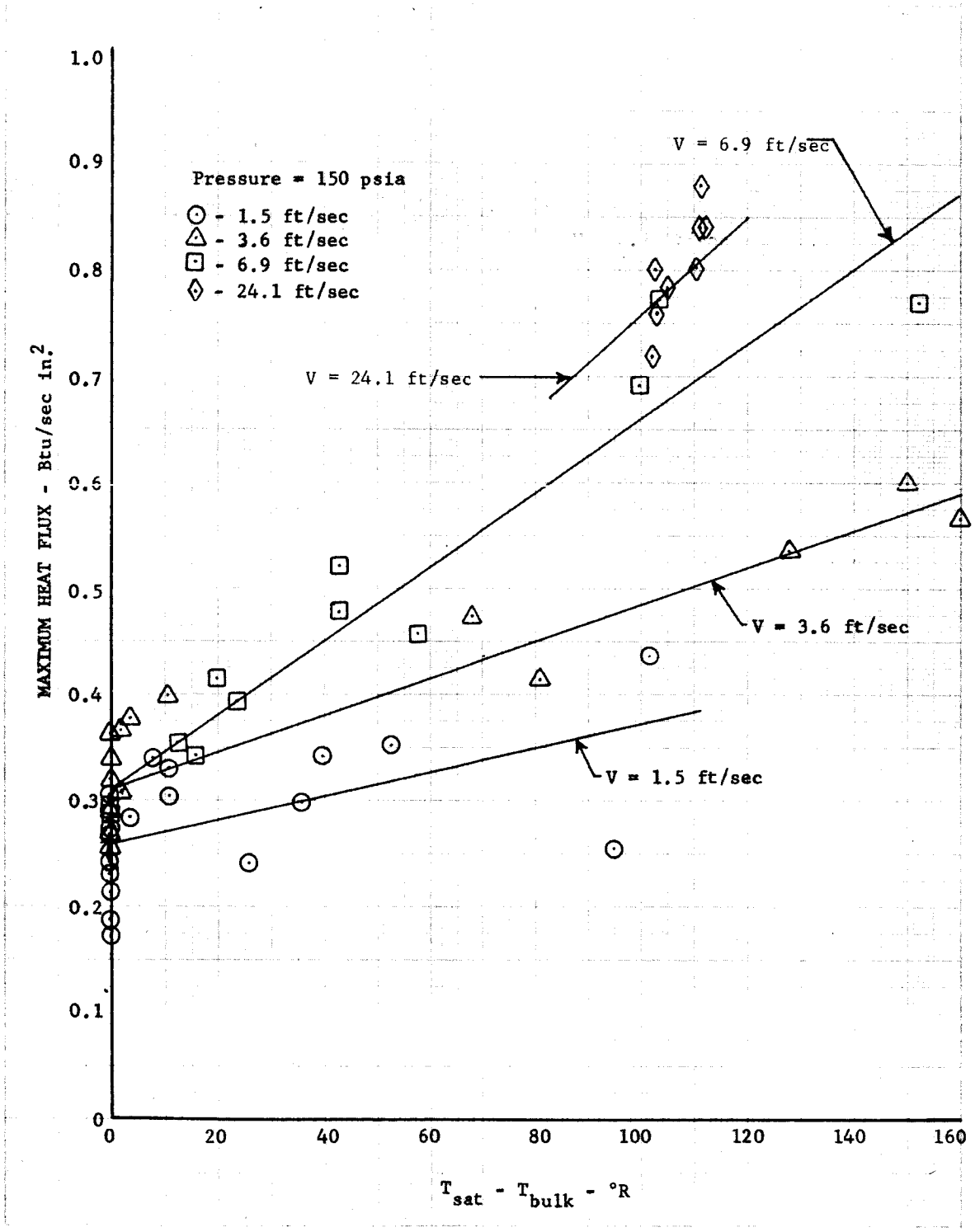

DF 34832
Sheet 2

Figure E-7
Maximum Nucleate Boiling Heat Flux for Butene-1

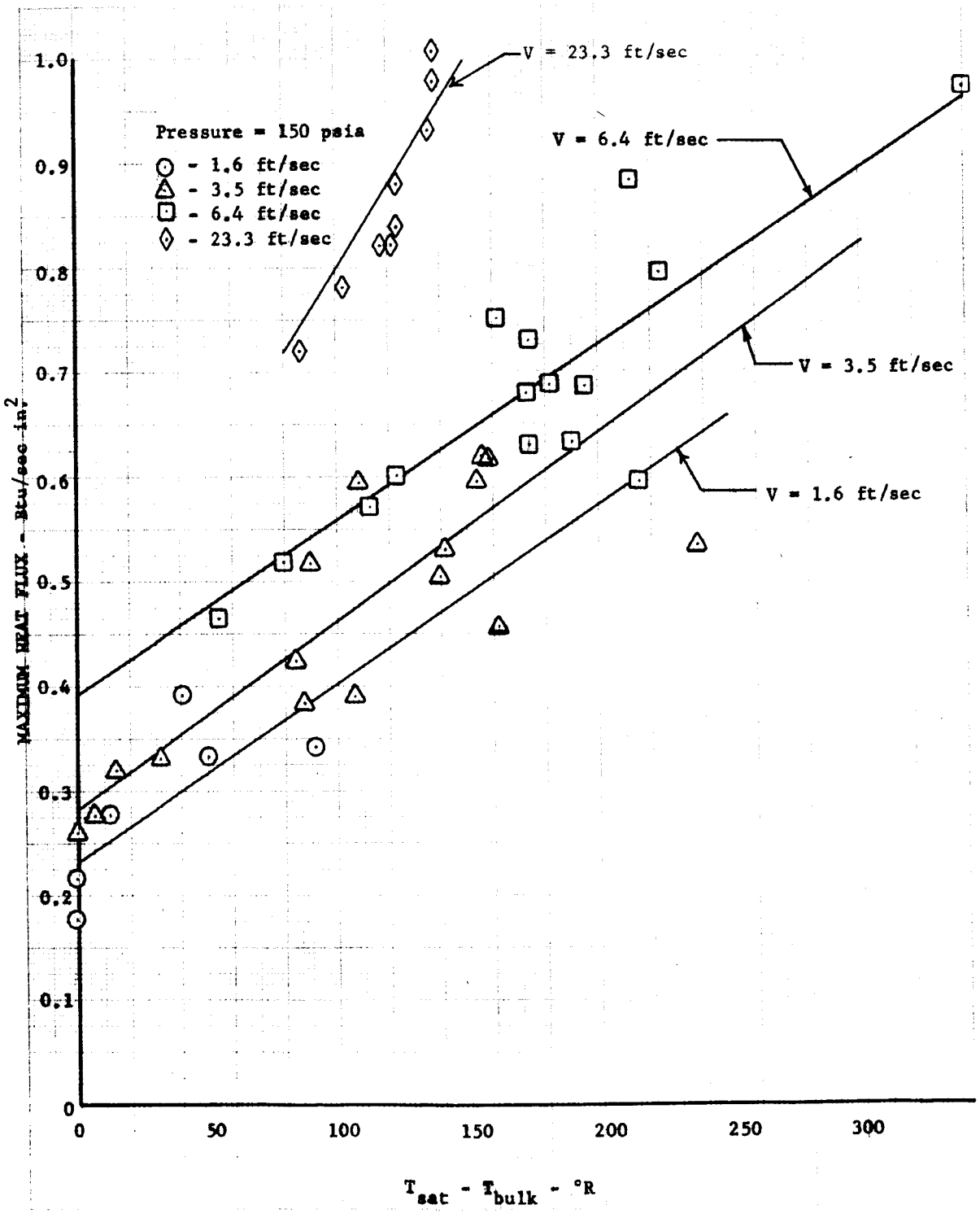

DF 34832
Sheet 1

Figure E-8
Maximum Nucleate Boiling Heat Flux for 0.14 Pentane-0.86 Isopentane Blend

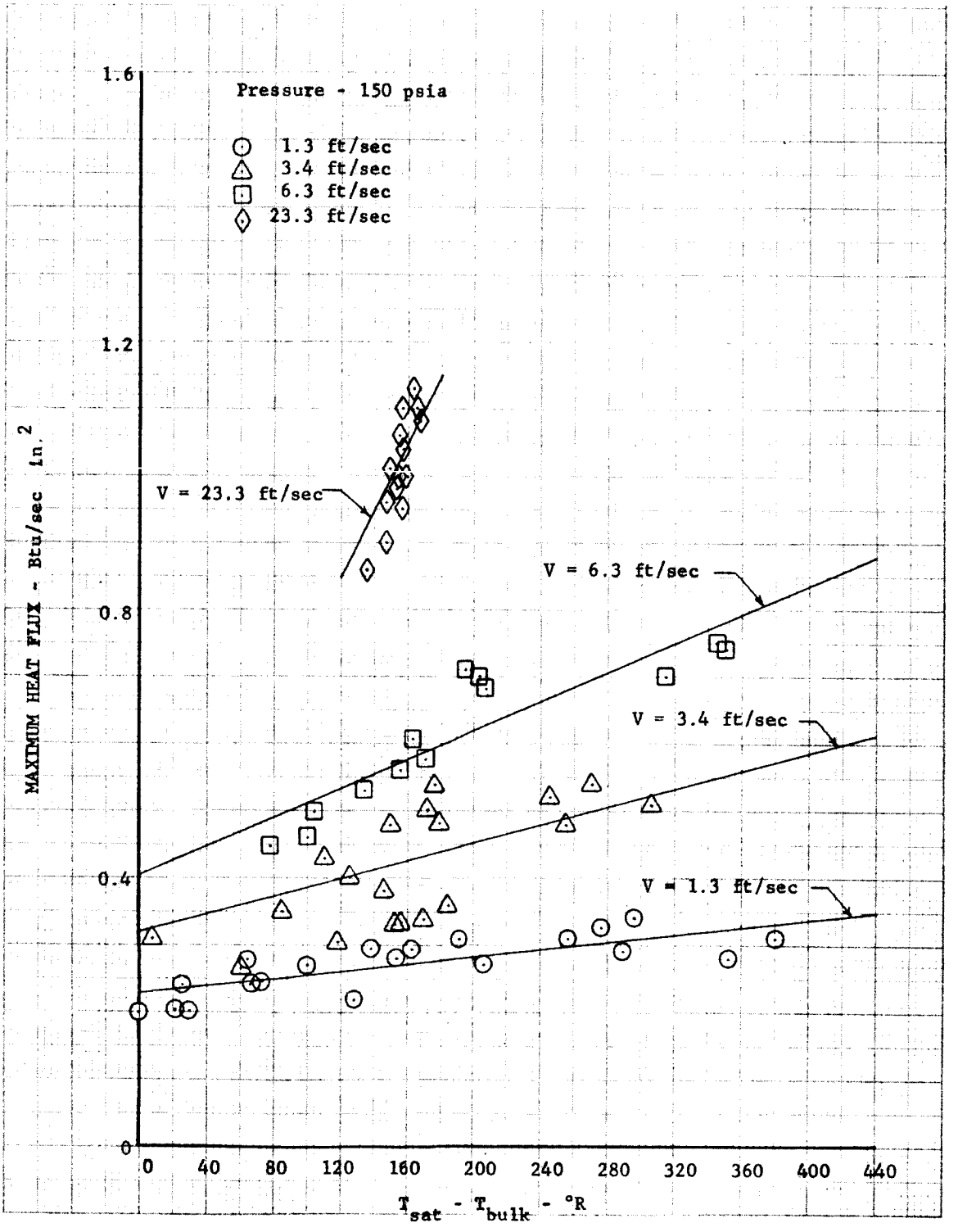

DF 35544

Figure E-9
Maximum Nucleate Boiling Heat Flux for Propylene

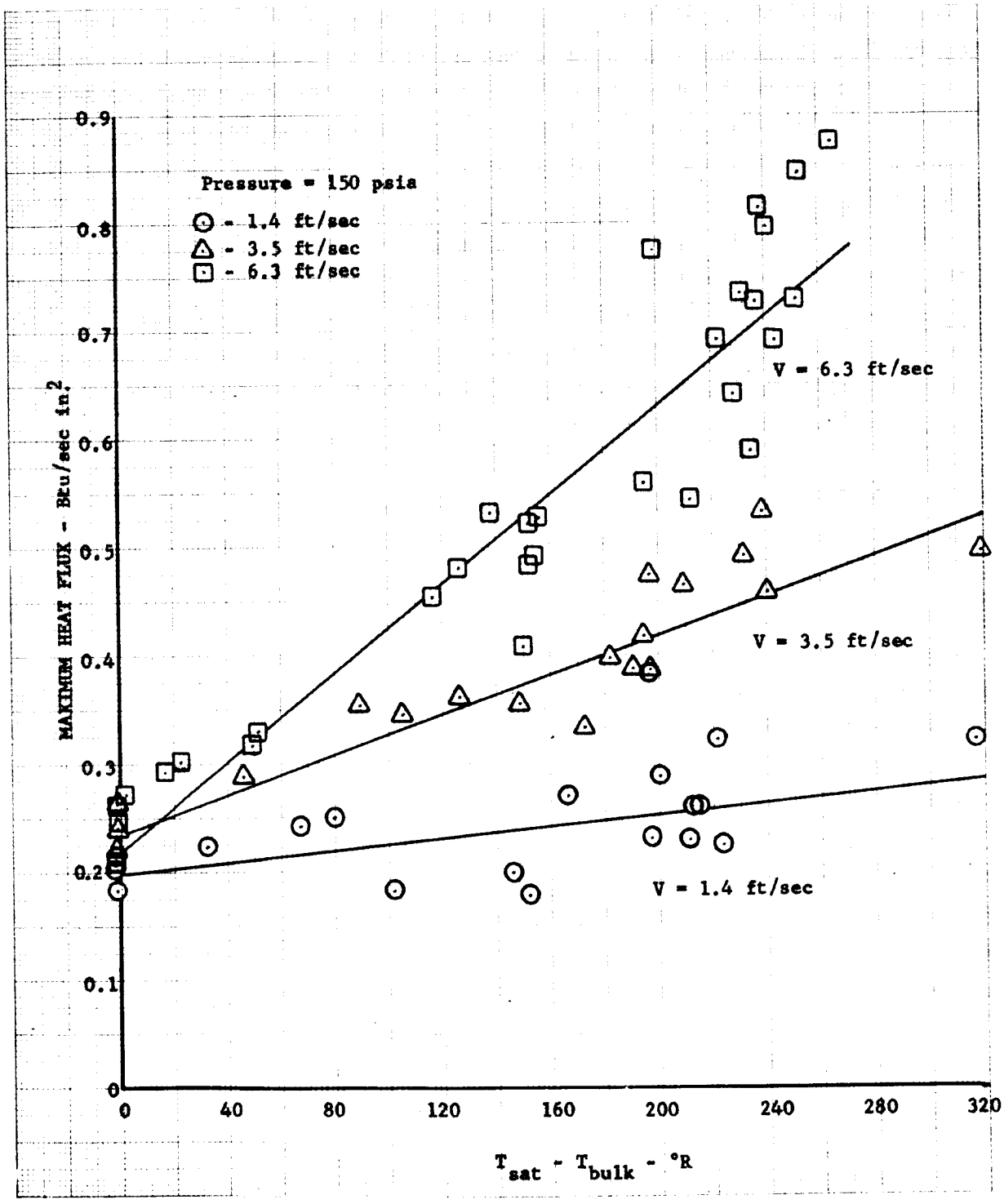

DF 35404

Figure E-10
Maximum Nucleate Boiling Heat Flux for 0.48 Propane-0.52 Propylene Blend

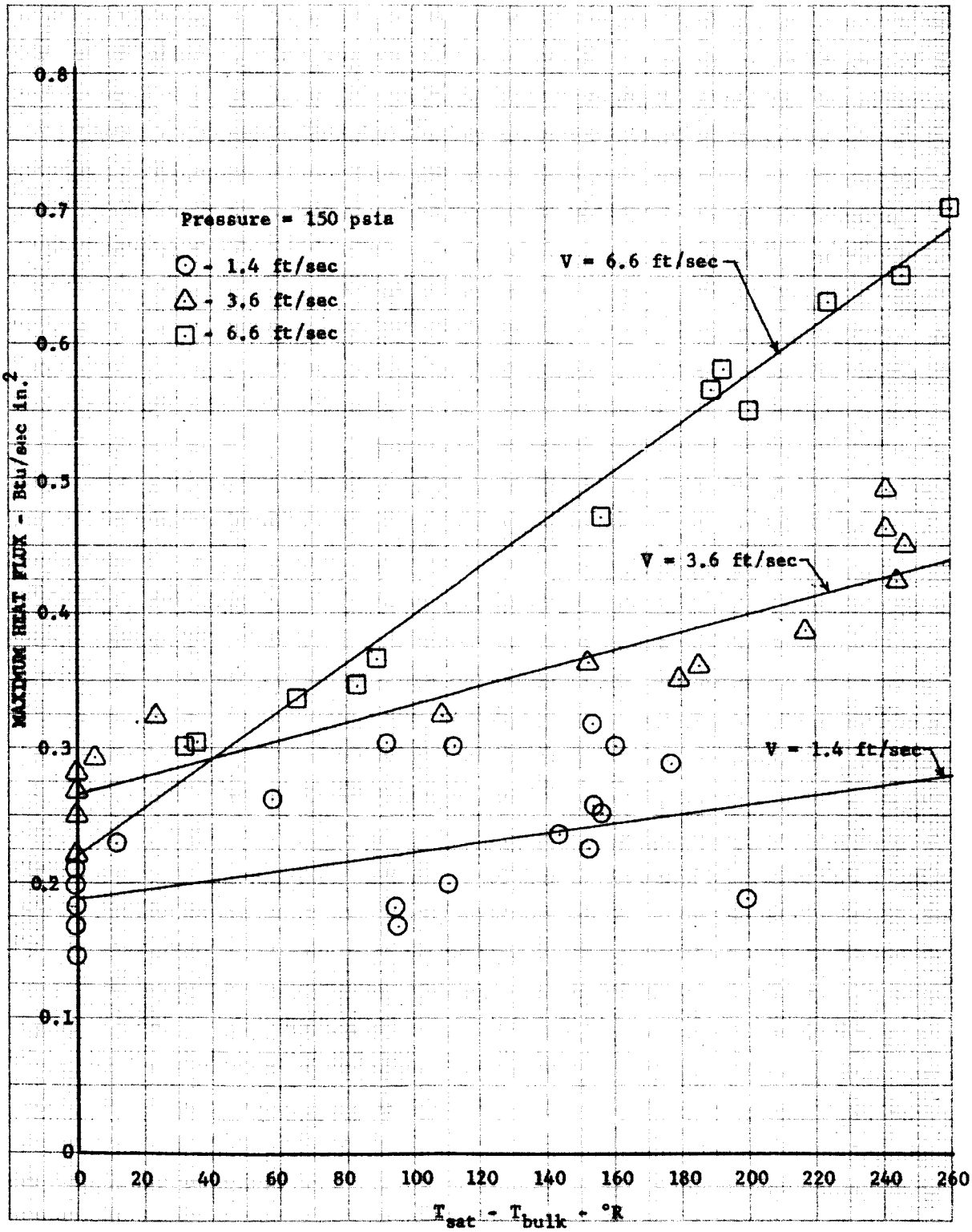

DF 35840

Equations which represent the experimentally measured maximum nucleate heat flux as a function of velocity and degree of subcooling were formulated for each of the fuels tested. These equations are valid only over the range of velocities from 1.0 to 8.0 ft/sec and for a pressure of 150 psia.

The equations are of the form

$$q_{max} = A + B\,(T_s - T_b)$$

where:

q_{max} = Maximum nucleate heat flux
T_s = Fluid saturation temperature
T_b = Fluid bulk temperature
A = Function of velocity or a constant
B = Function of velocity

The final equation for each of the hydrocarbon fuels is:

$$q_{max} = (a + bV) + (c + dV)\,(T_s - T_b)$$

where q_{max} is in Btu/sec in.^{2} and V is in ft/sec.

The constants for each of the fuels are as follows:

	a	b	c	d
Propane	0.2702	0.	−0.0003192	0.0005607
Butene-1	0.1933	0.02355	0.001643	0.00005175
Propylene	0.2255	0.	−0.0004152	0.0003921
Methane	0.2279	0.	0.003159	0.
48% Propane-52% Propylene	0.2180	0.	−0.00004694	0.0002750
14% Pentane-86% Isopentane	0.1883	0.032	0.	0.000204

Further tests were made with methane, propane, butene-1, and a 14% pentane-86% isopentane blend at a higher velocity of approximately 25 ft/sec and at pressures other than 150 psia. Each of these fuels was tested with a single inlet temperature, which resulted in the narrow spread of the data in figures E-5 through E-8. The effect of velocity on the maximum nucleate boiling heat flux can be better discerned from figures E-11, E-12, and E-13 for butene-1, propane and the pentane blend. It is evident that the effect of velocity is not linear, but becomes less at higher velocities for all three fuels. Hence, an extrapolation of the equations for the maximum nucleate heat flux as a function of the degree of subcooling and velocity, as presented above could result in large errors at velocities higher than 8 ft/sec.

Figure E-11
Maximum Nucleate Boiling Heat Flux for Butene-1
(Bulk Temperature = 535°R, Pressure = 150 psia)

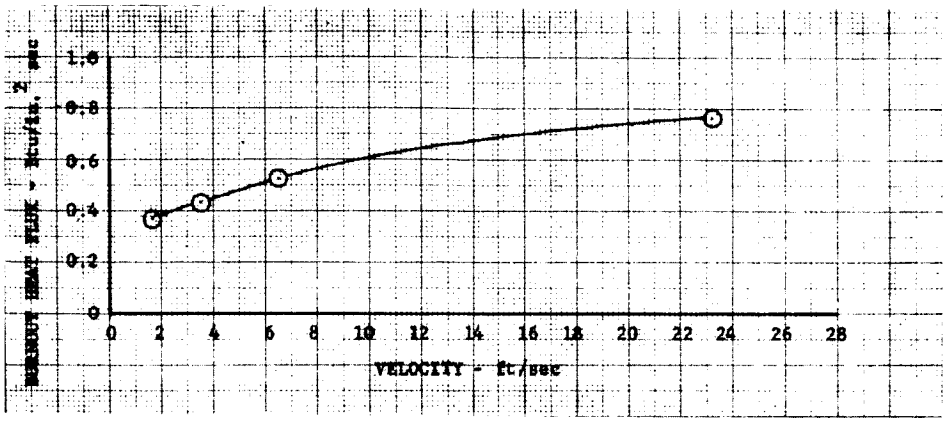

Figure E-12
Maximum Nucleate Boiling Heat Flux for Propane
(Bulk Temperature = 430°R, Pressure = 150 psia)

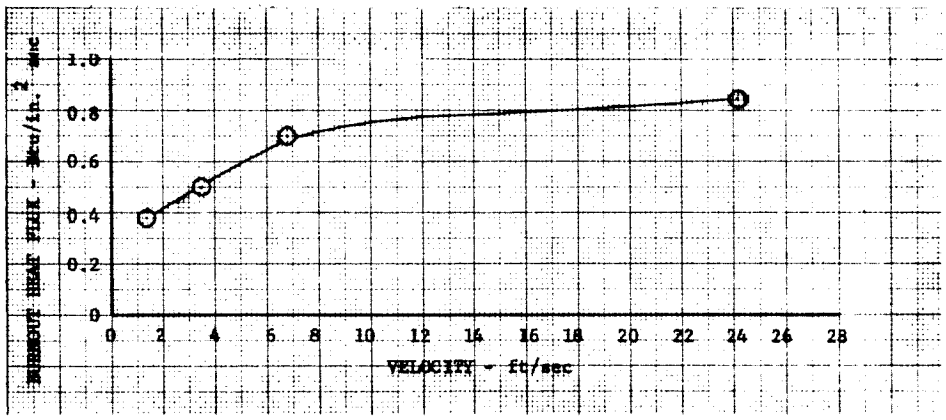

Figure E-13
Maximum Nucleate Boiling Heat Flux for Pentane-Isopentane Blend (Bulk Temperature = 553°R, Pressure = 150 psia)

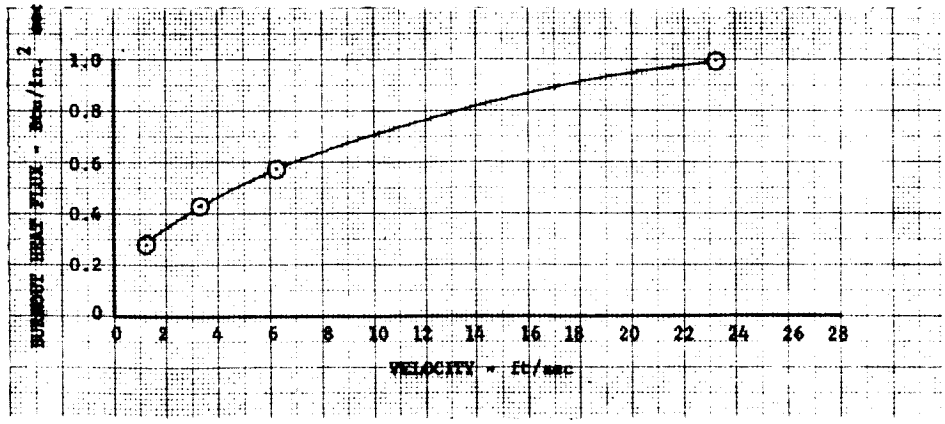

The effect of pressure on the maximum nucleate heat flux for butene-1, methane and the pentane blend can be seen in figures E-14, E-15, and E-16. The maximum heat flux is called peak flux in these figures since they include data at supercritical pressures where nucleate boiling per se does not occur. However, at the supercritical pressures a peak heat flux did exist which, if exceeded, would result in a sudden increase in wall temperature of several hundred degrees, depending on the exact conditions. This suggests that a heat transfer mechanism similar to that for subcritical boiling exists for the supercritical state, at least over a limited range of conditions. For test conditions in the critical region, moderate differences in bulk and wall temperatures, yielding large differences in bulk and wall fluid density could result in a simulation of subcritical film boiling, with a low density vapor blanket on the wall and high density bulk liquid conditions. Similar results have been reported for supercritical heat transfer to hydrogen by Hendricks et al (Reference 1).

It has been established in the heat transfer literature that there is an optimum pressure, relative to the critical pressure, at which the peak heat flux reaches a maximum value. There is, however, disagreement as to the exact value of this optimum relative pressure and this value may depend upon the test fluid and conditions. Figure E-14 and E-16 reveal that the optimum pressure is a function of velocity and that it increases with velocity. The same results are reported by Noel (Reference 2) in work with ammonia. The data points in figures E-14, E-15, and E-16 are connected by dashed lines due to the uncertainty of the exact shape of the curve.

3. FILM BOILING DATA

Film boiling data were obtained for both subcooled fluid and the two-phase region. Some difficulty was encountered in trying to correlate both the subcooled and the two-phase film boiling data by the same techniques.

Results of efforts to correlate film boiling data for both of the above mentioned fluid conditions are presented in figures E-17, E-18, E-19, and E-20 for methane, propane, butene-1, and the pentane blend. The heat transfer coefficient is plotted versus the quality parameter (ϕ) for constant values of inlet liquid velocity or mass flow per unit area where:

$$\phi = \frac{H - H_l}{H_g - H_l}$$

and

H = Local fluid enthalpy

H_l = Saturated liquid enthalpy

H_g = Saturated vapor enthalpy

Negative values of ϕ represent subcooled film boiling while values of ϕ greater than zero represent film boiling in the two-phase region. Coefficients for the saturated vapor have been calculated for methane and propane at the same values of mass flow per unit area as the experimental data. These calculated coefficients are plotted in figures E-17 and E-18. The curve for the experimental data would be expected to pass through these points.

Figure E-14
Peak Heat Flux for Butene-1
(Bulk Temperature = 535°R)

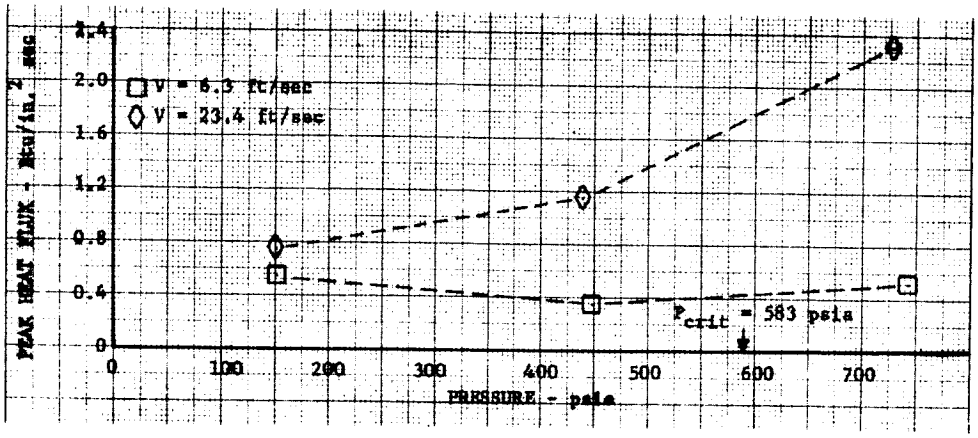

Figure E-15
Peak Heat Flux for Methane
(Bulk Temperature = 270°R)

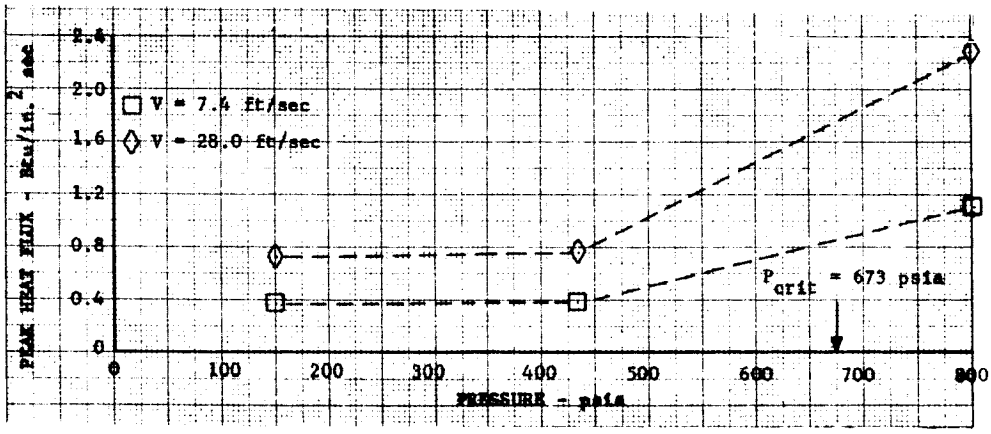

Figure E-16
Peak Heat Flux for 0.14 Pentane — 0.86 Isopentane
Blend (Bulk Temperature = 553°R)

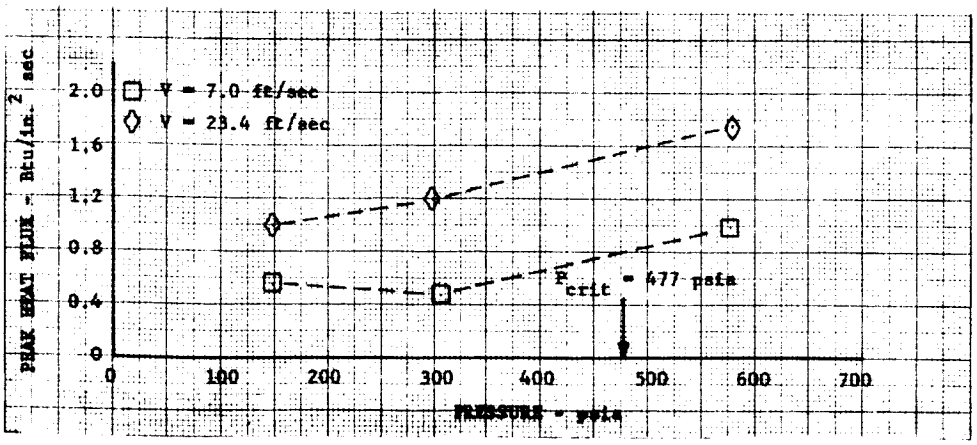

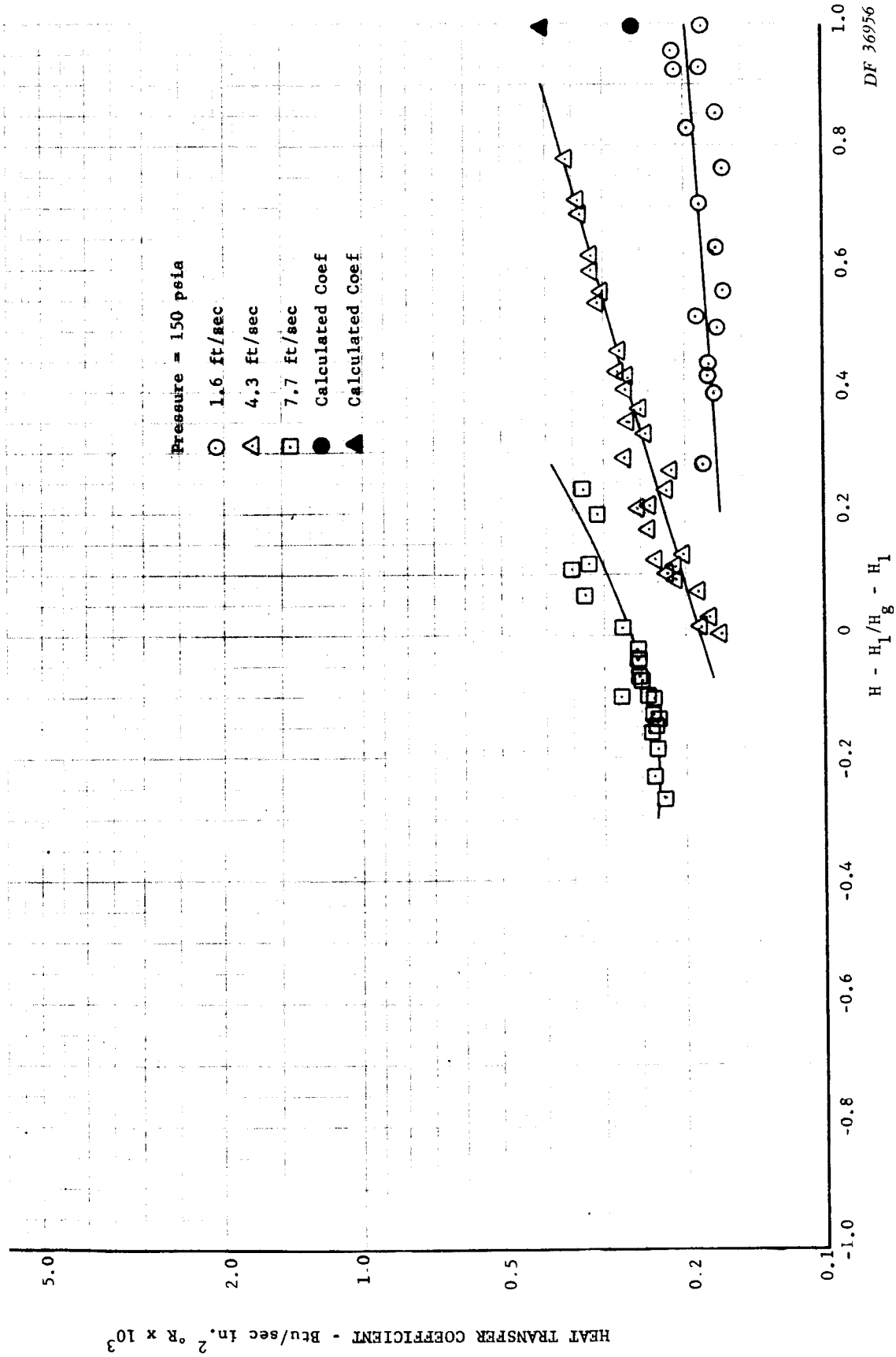

Figure E-17
Methane Film Boiling Data

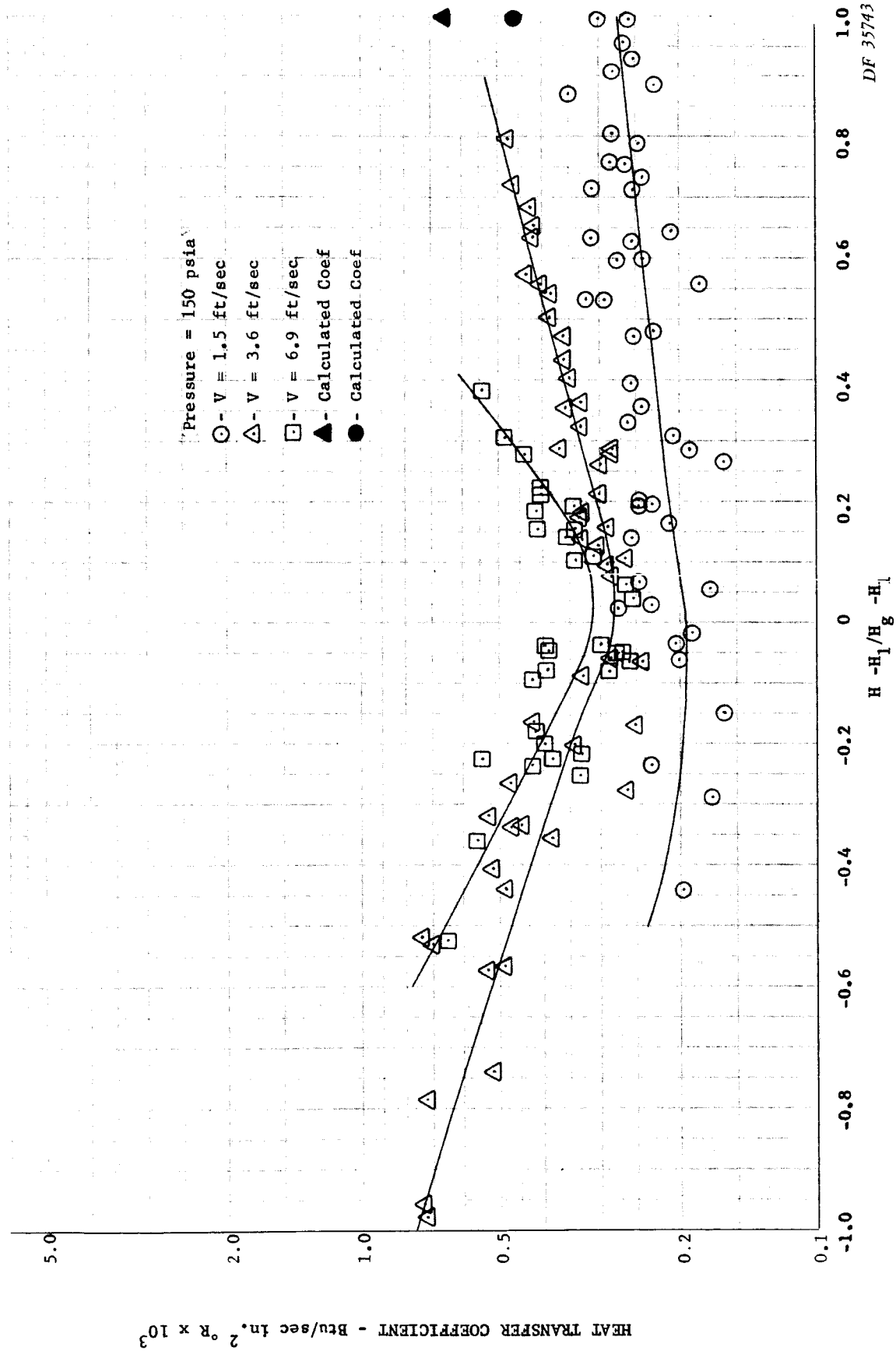

Figure E-18
Propane Film Boiling Data

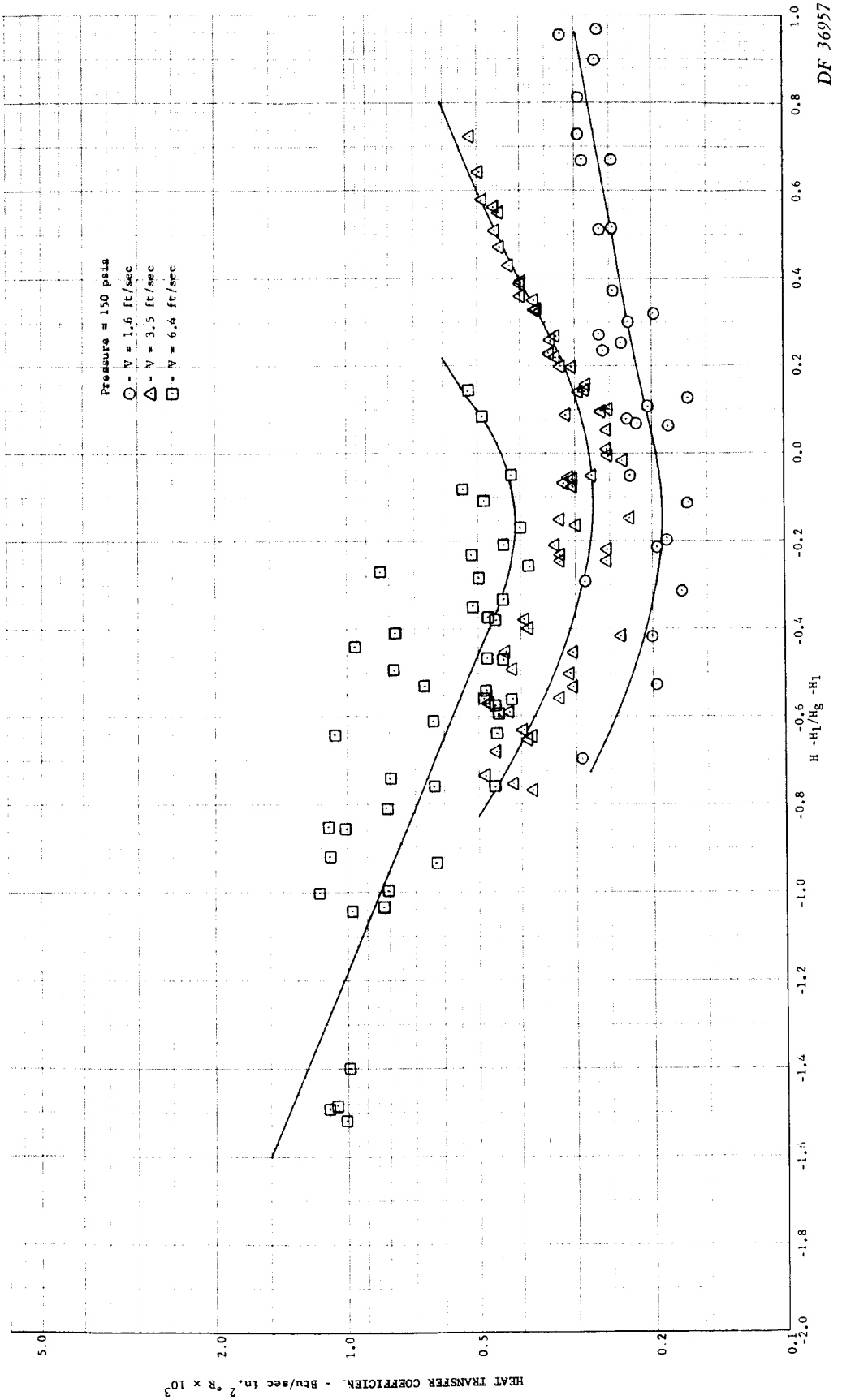

Figure E-19
Butene-1 Film Boiling Data

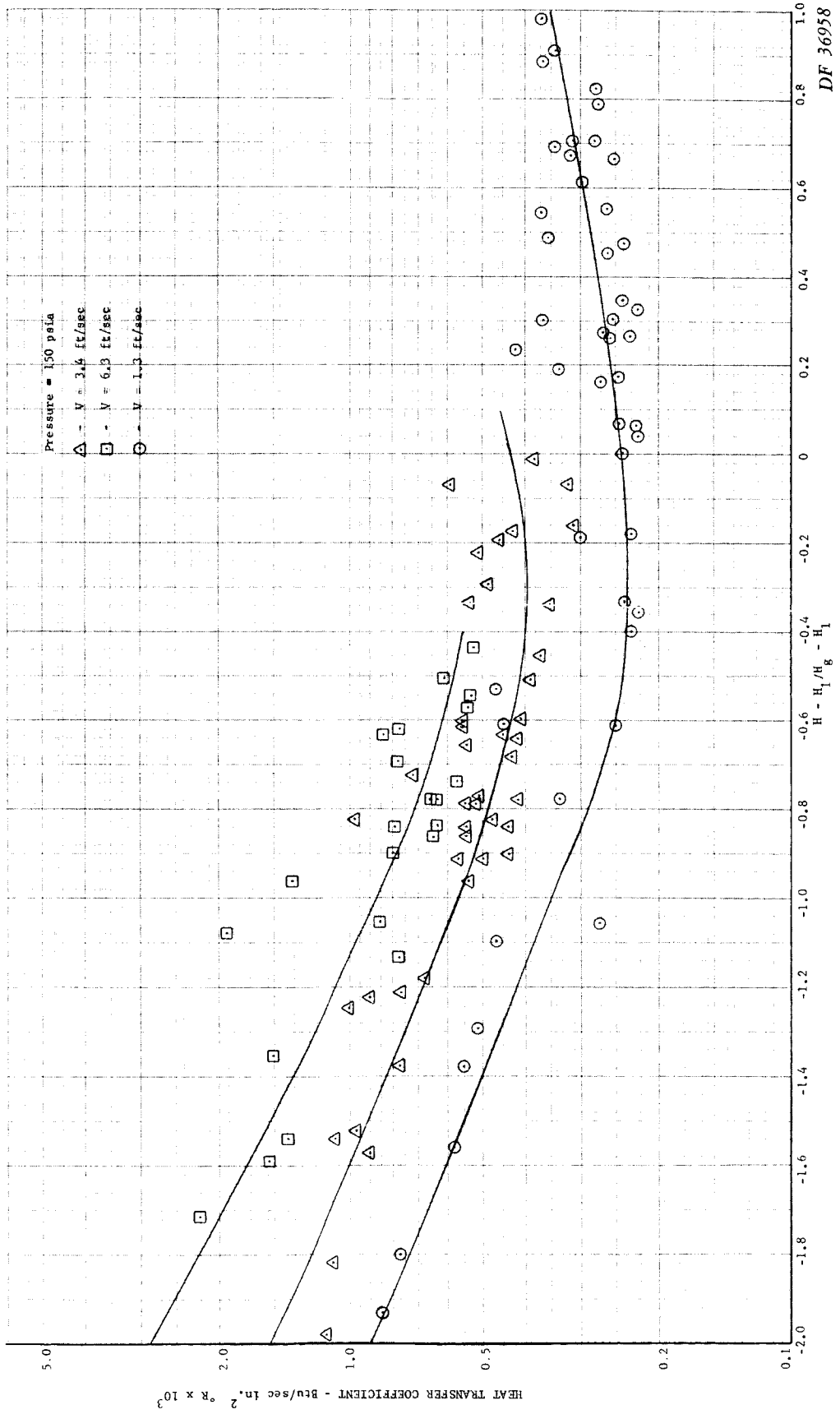

Figure E-20
0.14 Pentane-0.86 Isopentane Blend Film Boiling Data

Figures E-17 through E-20 show that, for values of ϕ between zero and one, the experimental data points group closely along lines of constant inlet velocity; however, for values of ϕ less than zero there is considerably more data scatter. The scatter appears to increase as the fluid state approaches saturated liquid. In addition, there is more data scatter over the entire range of ϕ for the lowest mass velocity; this is caused by increased experimental error in measuring the lowest mass flow rates.

A general correlation of film boiling data for several fluids at various pressures, temperatures, mass velocities, and qualities has been obtained by von Glahn (Reference 3). This correlation was satisfactory for film boiling in the two-phase region where there was net vapor generation as the fluid moved through the tube, but it did not apply to subcooled film boiling where the bulk temperature was less than the saturation temperature and no net vapor generation occurred. Experimental data for propane, methane, butene-1, and the pentane blend have been correlated using the parameters developed in Reference 3, and are shown in figures E-21, E-22, E-23, and E-24.

The film vaporization parameter X_F is defined as

$$X_F = \frac{4qL/GDH_{fg}}{1 - X_c}$$

where:

q = Heat flux

L = Length along heated tube measured from the "burnout" location

G = Mass velocity

D = Inside tube diameter

H_{fg} = Latent heat of vaporization

X_c = Fluid quality at the "burnout" location

The experimental Nusselt number is

$$Nu_{exp} = h_{exp} \left(\frac{D}{K}\right)$$

and the calculated Nusselt number is

$$Nu_{calc} = 0.023 \, (Re)^{0.8} \, (Pr)^{0.4}$$

Figure E-21
Film Boiling Correlation, Propane Data

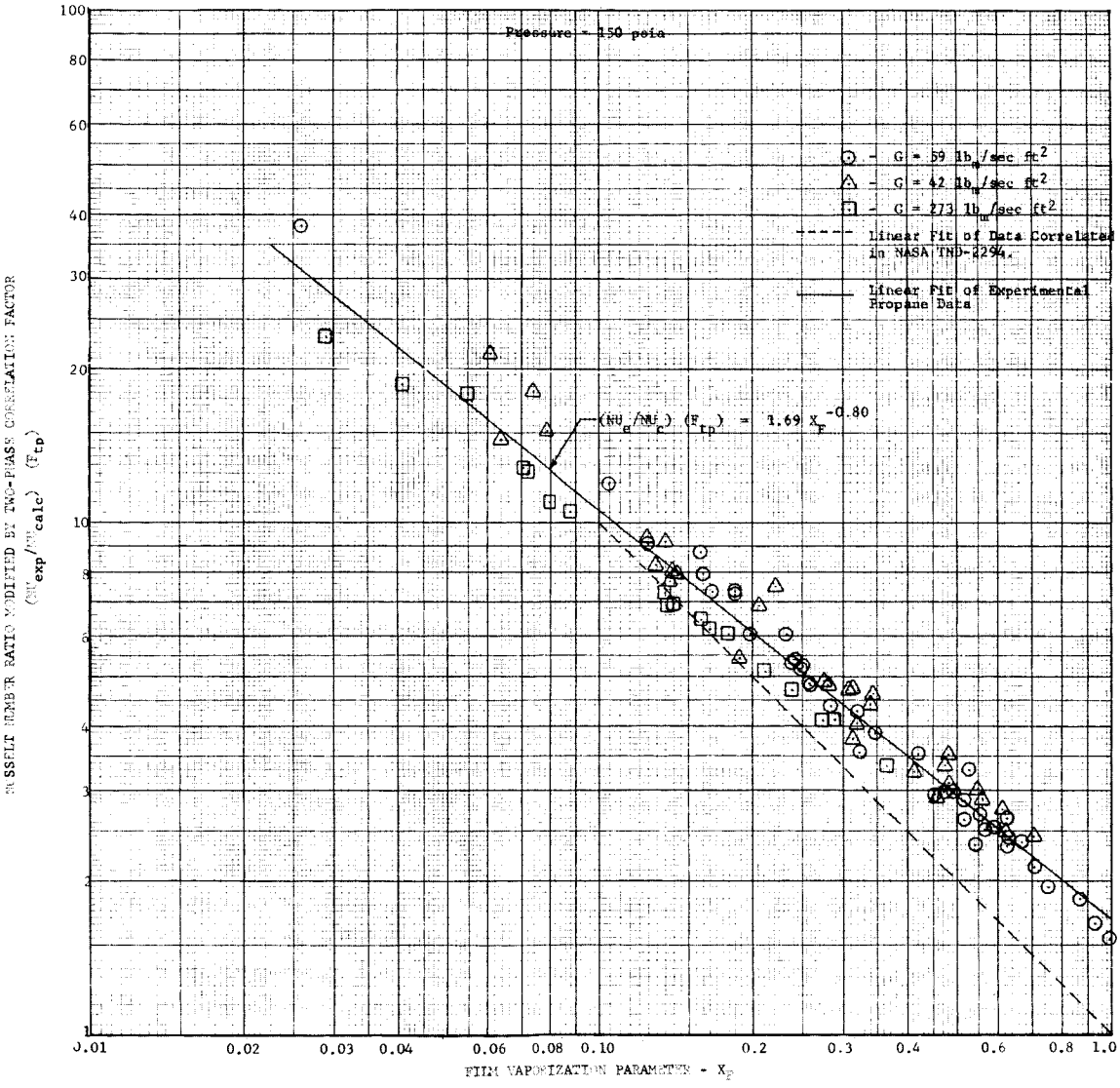

DF 36980

Figure E-22
Film Boiling Correlation, Methane Data

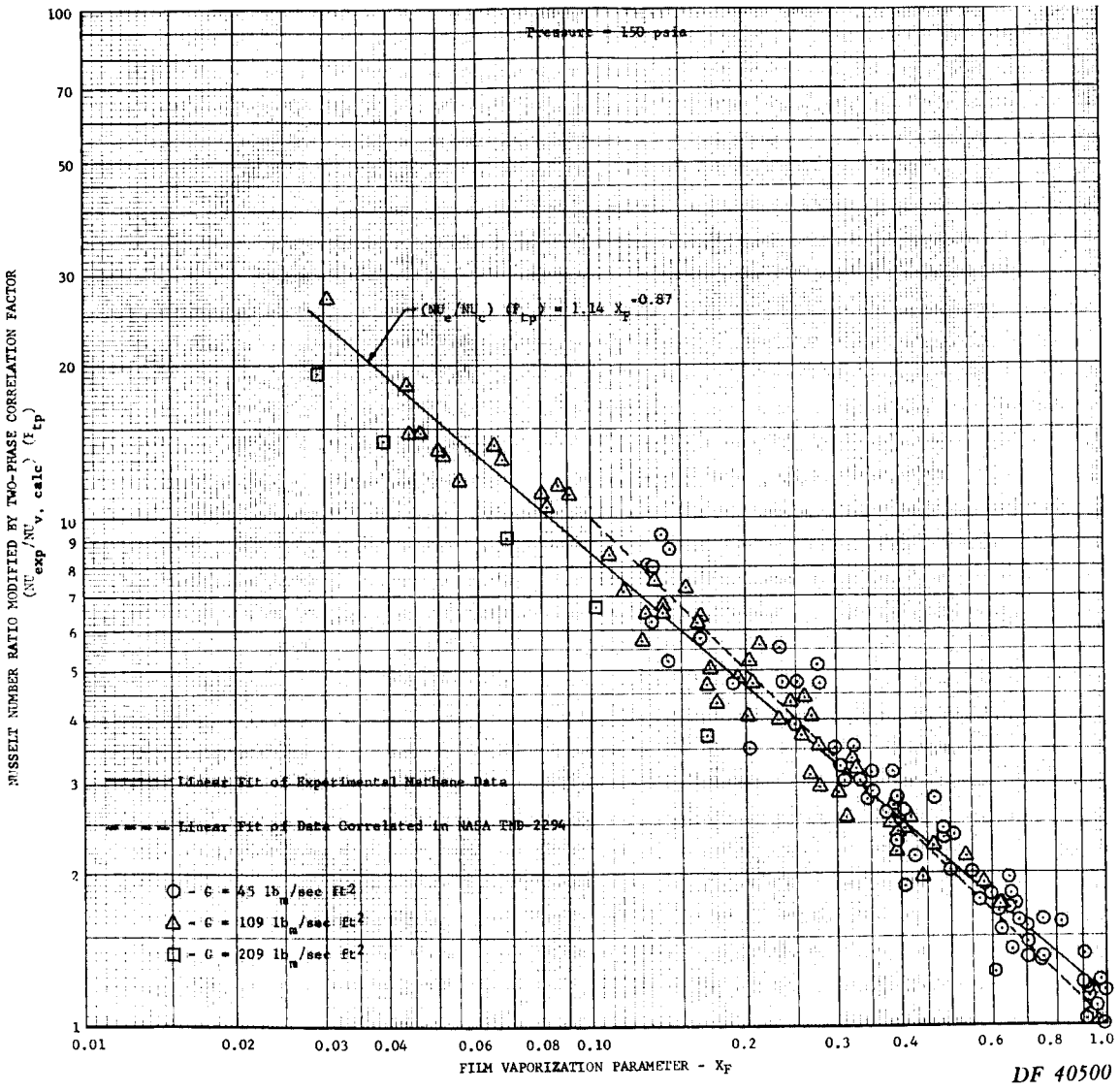

DF 40500

Figure E-23
Film Boiling Correlation, Butene-1 Data

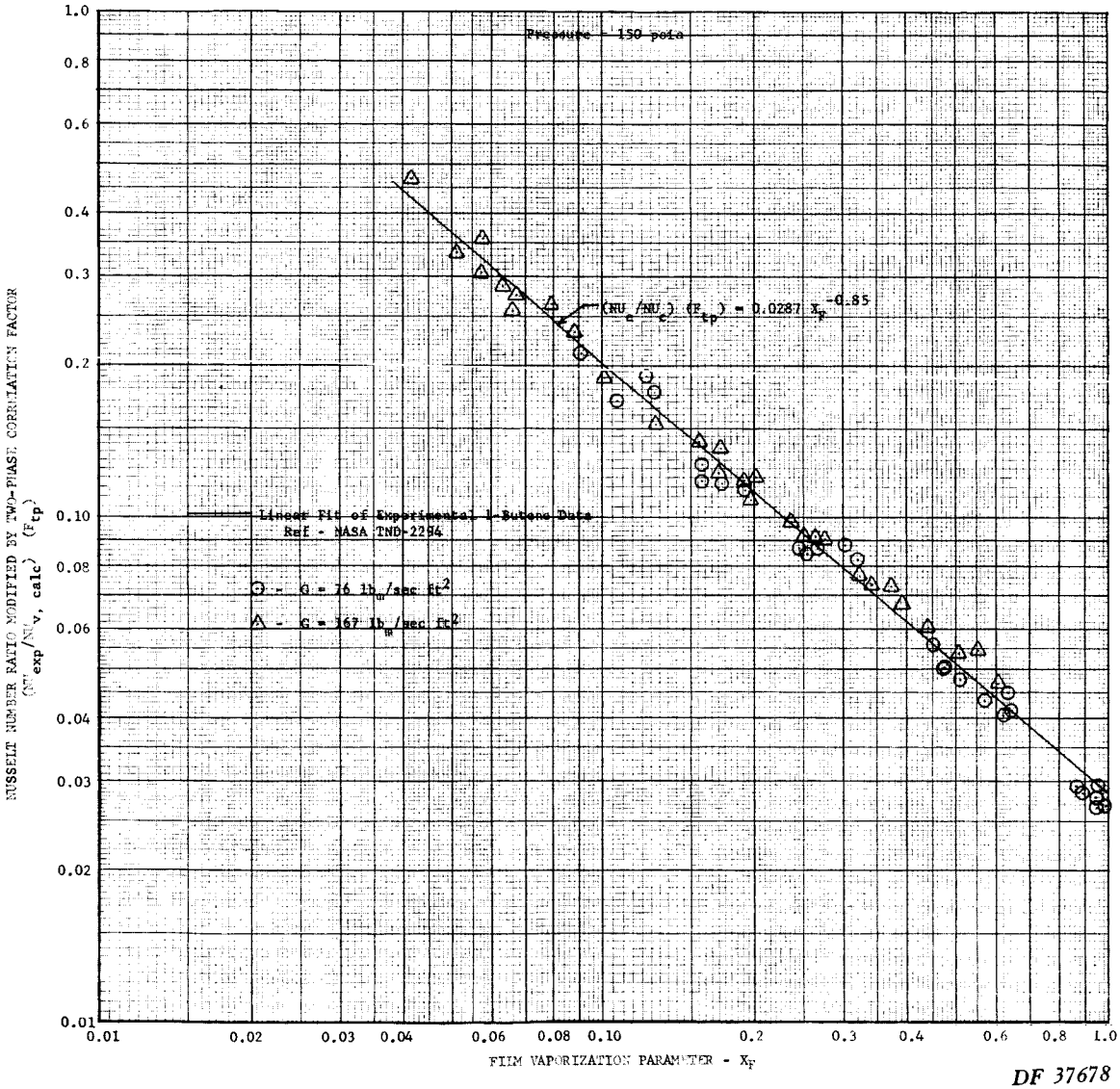

DF 37678

Figure E-24
Film Boiling Correlation, 0.14 Pentane-0.86 Isopentane Blend Data

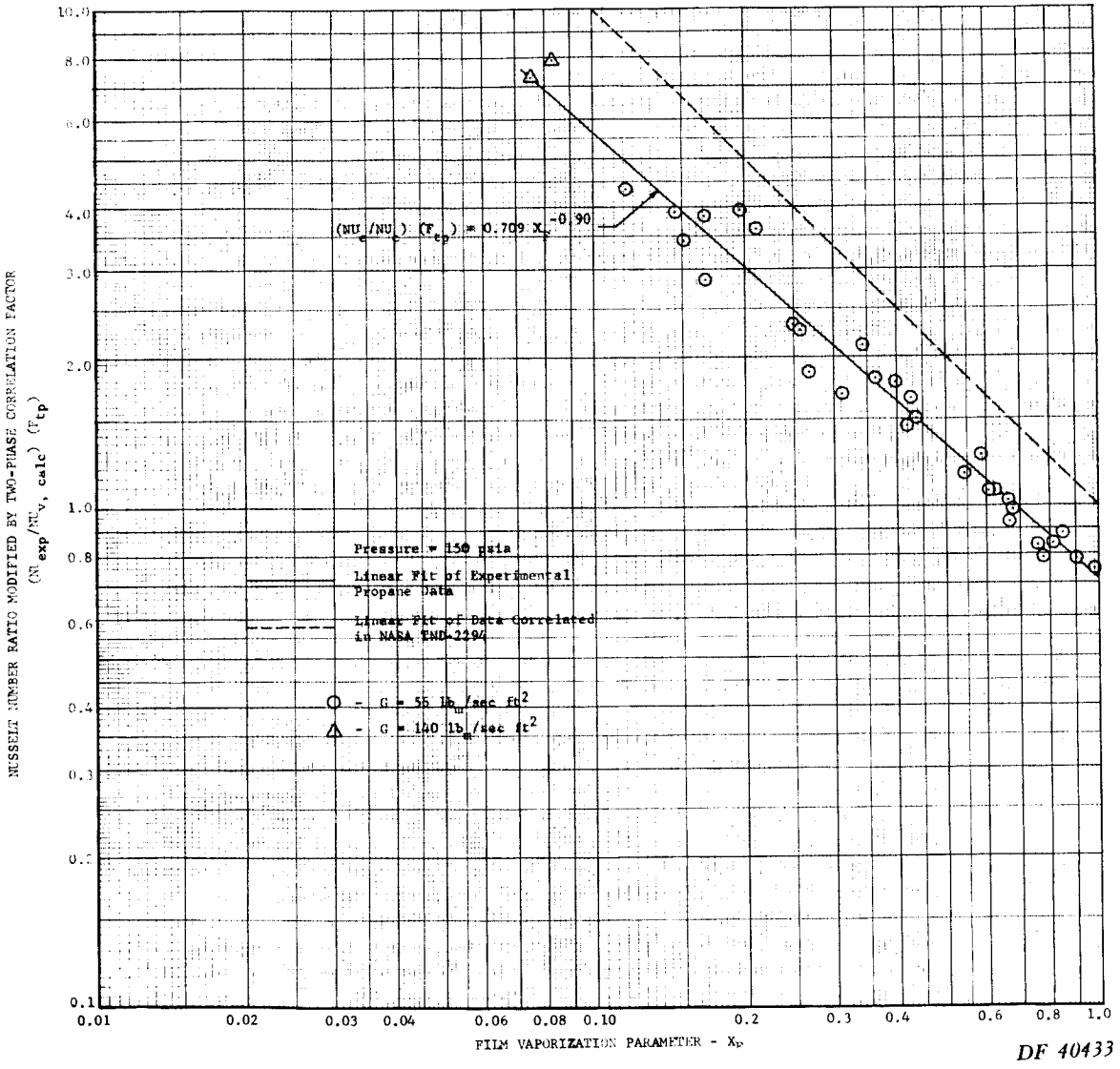

DF 40433

All properties are evaluated for the saturated vapor at the saturation temperature. The two-phase correlation factor (F_{tp}), is a complicated empirical factor involving transport properties, thermodynamic properties, Reynolds number, heat flux and the film vaporization parameter. The data in figures E-21 to E-24 group closely along a single line for each fuel. However, the "best fit" lines for each of the four fuels and a linear "best fit" of the data correlated in Reference 3 do not coincide. The methane data groups closest to the correlation line in Reference 3, while the butene-1 data is considerably lower. Most of the differences between the "best fit" lines for each fuel are probably due to an uncertainty in property values, particularly surface tension. Surface tension is a strong variable in the correlation presented in Reference 3, and experimental data for surface tension was scarce for many of the hydrocarbons tested, especially butene-1.

4. REFERENCES

1. Hendricks, R. C., R. W. Graham, Y. Y. Hsu, and A. A. Medeiros, "Correlation of Hydrogen Heat Transfer in Boiling and Supercritical Pressure States," ARS Journal, February 1962, Vol. 32.

2. Noel, M. B., "Experimental Investigation of the Forced Convection and Nucleate Boiling Heat-Transfer Characteristics of Liquid Ammonia," JPL Technical Report No. 32-125.

3. von Glahn, Uwe H., "A Correlation of Film-Boiling Heat Transfer Coefficients Obtained with Hydrogen, Nitrogen, and Freon 113 in Forced Flow," NASA TN D-2294, May 1964.

APPENDIX F
DISTRIBUTION LIST

National Aeronautics and Space Administration
Lewis Research Center
21000 Brookpark Road
Cleveland, Ohio 44135

Attn: Contracting Officer, MS 500-210	1
Liquid Rocket Technology Branch. MS 500-209	8
Technical Report Control Office, MS 5-5	1
Technology Utilization Office, MS 3-16	1
AFSC Liaison Office, MS 4-1	2
Library	2
Office of Reliability & Quality Assurance, MS 500-203	1
Arthur N. Curren, MS 6-1	1
Harold Valentine, MS 501-2	1
Joseph N. Sivo, MS 501-2	1

National Aeronautics & Space Administration — 2
Washington, D. C. 20546
Attn: Code RPX

Scientific and Technical Information Facility — 6
P. O. Box 5700
Bethesda, Maryland 20014
Attn: NASA Representative Code CRT

National Aeronautics and Space Administration — 1
Ames Research Center
Moffett Field, California 94035
Attn: Library

National Aeronautics and Space Administration — 1
Flight Research Center
P. O. Box 273
Edwards, California 93523
Attn: Library

National Aeronautics and Space Administration — 1
Goddard Space Flight Center
Greenbelt, Maryland 20771
Attn: Library

National Aeronautics and Space Administration — 1
Langley Research Center
Langley Station
Hampton, Virginia 23365
Attn: Library

National Aeronautics and Space Administration — 1
Manned Spacecraft Center
Houston, Texas 77001
Attn: Library

National Aeronautics and Space Administration — 1
George C. Marshall Space Flight Center
Huntsville, Alabama 35812
Attn: Library

National Aeronautics and Space Administration — 1
Western Operations
150 Pico Boulevard
Santa Monica, California 90406
Attn: Library

National Aeronautics and Space Administration — 1
John F. Kennedy Space Center
Cocoa Beach, Florida 32931
Attn: Library

Jet Propulsion Laboratory — 1
4800 Oak Grove Drive
Pasadena, California 91103
Attn: Library

U. S. Department of the Interior — 1
Bureau of Mines
4800 Forbes Avenue
Pittsburgh, Pennsylvania 15213
Attn: M. M. Dolinar, Repts Librarian
Explosives Research Center

Office of the Director of Defense Research & Engineering — 1
Washington, D. C. 20301
Attn: Dr. H. W. Schulz, Office of Asst. Dir. (Chem. Technology)

RTD(RTNP) — 1
Bolling Air Force Base
Washington, D. C. 20332

Arnold Engineering Development Center — 1
Attn: AEOIM
Air Force Systems Command
Tullahoma, Tennessee 37389

AFSC(SCLT/Captain S. W. Bowen) — 1
Andrews Air Force Base
Washington, D. C. 20332

AFRPL (RPR) — 1
Edwards, California 93523

AFRPL(RPM) — 1
Edwards, California 93523

AFFTC (FTAT-2) — 1
Edwards AFB, California 93523

Office of Research Analyses (OAR) — 1
Attn: RRRT
Holloman Air Force Base, New Mexico 88330

Air Force Office of Scientific Research — 1
Washington, D. C. 20333
Attn: SREP, Dr. J. F. Masi

AFRPL (RPC) — 1
Edwards, California 93523

Wright-Patterson Air Force Base, Ohio 45433 — 1
Attn: AFML (MAAE)

Wright-Patterson Air Force Base, Ohio 45433 — 1
Attn: AFML (MAAM)

Commanding Officer — 1
Ballistic Research Laboratories
Aberdeen Proving Ground, Maryland
Attn: AMXBR-1
21005

APPENDIX F DISTRIBUTION LIST (Continued)

Department of the Army
U. S. Army Materiel Command
Washington, D. C. 20315
Attn: AMCRD-RC — 1

Commanding Officer
U. S. Army Research Office (Durham)
Box CM, Duke Station
Durham, North Carolina 27706 — 1

U. S. Army Missile Command
Redstone Scientific Information Center
Redstone Arsenal, Alabama 35808
Attn: Chief, Document Section — 1

Bureau of Naval Weapons
Department of the Navy
Washington, D. C. 20360
Attn: DLI-3 — 1

Bureau of Naval Weapons
Department of the Navy
Washington, D. C. 20360
Attn: RMMP-2 — 1

Bureau of Naval Weapons
Department of the Navy
Washington, D. C. 20360
Attn: RMMP-4 — 1

Bureau of Naval Weapons
Department of the Navy
Washington, D. C. 20360
Attn: RRRE-6 — 1

Commander
U. S. Naval Missile Center
Point Mugu, California 93041
Attn: Technical Library — 1

Commander
U. S. Naval Ordnance Laboratory
White Oak
Silver Spring, Maryland 20910
Attn: Library — 1

Commander
U. S. Naval Ordnance Test Station
China Lake, California 93557
Attn: Code 45 — 1

Commander (Code 753)
U. S. Naval Ordnance Test Station
China Lake, California 93557
Attn: Technical Library — 1

Superintendent
U. S. Naval Postgraduate School
Naval Academy
Monterey, California 93900 — 1

Commanding Officer
Office of Naval Research
1030 E. Green Street
Pasadena, California 91101 — 1

Director (Code 6180)
U. S. Naval Research Laboratory
Washington, D. C. 20390
Attn: H. W. Carhart — 1

Director
Special Projects Office
Department of the Navy
Washington, D. C. 20360 — 1

Commanding Officer
U. S. Naval Underwater Ordnance Station
Newport, Rhode Island 02844
Attn: W. W. Bartlett — 1

Commander
U. S. Naval Weapons Laboratory
Dahlgren, Virginia 22448
Attn: Technical Library — 1

Aerojet-General Corporation
P. O. Box 296
Azusa, California 91703
Attn: Librarian — 1

Aerojet-General Corporation
11711 South Woodruff Avenue
Downey, California 90241
Attn: F. M. West, Chief Librarian — 1

Aerojet-General Corporation
Attn: Technical Library 2484-2015A
P. O. Box 1947
Sacramento, California 95809 — 1

Aeronautical Division Philco Corporation
Ford Road
Newport Beach, California 92600
Attn: Dr. L. H. Linder, Manager
Technical Information Department — 1

Aeroprojects, Inc.
310 East Rosedale Avenue
West Chester, Pennsylvania 19389
Attn: C. D. McKinney — 1

Aerospace Corporation
P. O. Box 95085
Los Angeles, California 90045
Attn: Library-Documents — 1

Allied Chemical Corporation
General Chemical Division
P. O. Box 405
Morristown, New Jersey 07960
Attn: Security Office — 1

Celanese Corporation of America
Box 3049
Asheville, North Carolina 28802 — 1

American Cyanamid Company
1937 W. Main Street
Stamford, Connecticut 06902
Attn: Security Officer — 1

APPENDIX F DISTRIBUTION LIST (Continued)

IIT Research Institute — 1
Technology Center
Chicago, Illinois 60616
Attn: C. K. Hersh, Chemistry Division

ARO, Inc. — 1
Arnold Engrg. Dev. Center
Arnold AF Station, Tennessee 37389
Attn: Dr. B. H. Goethert
Chief Scientist

Atlantic Research Corporation — 1
Shirley Highway and Edsall Road
Alexandria, Virginia 22314
Attn: Security Office for Library

University of Denver — 1
Denver Research Institute
P. O. Box 10127
Denver, Colorado 80210
Attn: Security Office

Battelle Memorial Institute — 1
505 King Avenue
Columbus, Ohio 43201
Attn: Report Library, Room 6A

Bell Aerosystems — 1
Box 1
Buffalo, New York 14205
Attn: T. Reinhardt

The Boeing Company — 1
Aero Space Division
P. O. Box 3707
Seattle, Washington 98124
Attn: Ruth E. Peerenboom (1190)

Chemical Propulsion Information Agency — 1
Applied Physics Laboratory
8621 Georgia Avenue
Silver Spring, Maryland 20910

Propulsion Engineering Division — 1
(D.55-11)
Lockheed Missiles & Space Company
1111 Lockheed Way
Sunnyvale, California 94087

Douglas Aircraft Company, Inc. — 1
Santa Monica Division
3000 Ocean Park Boulevard
Santa Monica, California 90405
Attn: Mr. J. L. Waisman

The Dow Chemical Company — 1
Security Section
Box 31
Midland, Michigan 48641
Attn: Dr. R. S. Karpiuk, 1710 Building

E. I. duPont deNemours and Company — 1
Eastern Laboratory
Gibbstown, New Jersey 08027
Attn: Mrs. Alice R. Steward

Esso Research and Engineering Company — 1
Special Projects Unit
P. O. Box 8
Linden, New Jersey 07036
Attn: Mr. D. L. Baeder

Ethyl Corporation — 1
Research Laboratories
1600 West Eight Mile Road
Ferndale, Michigan 48220
Attn: E. B. Rifkin, Assistant Director,
Chemical Research

General Dynamics/Astronautics — 1
P. O. Box 1128
San Diego, California 92112
Attn: Library and Information Services (128-00)

Hercules Powder Company — 1
Allegany Ballistics Laboratory
P. O. Box 210
Cumberland, Maryland 21501
Attn: Library

Institute for Defense Analyses — 1
400 Army-Navy Drive
Arlington, Virginia 22202
Attn: Classified Library

Lockheed Propulsion Company — 1
P. O. Box 111
Redlands, California 92374
Attn: Miss Belle Berlad, Librarian

Marquardt Corporation — 1
16555 Saticoy Street
Box 2013 – South Annex
Van Nuys, California 91404

Minnesota Mining & Manufacturing Company — 1
900 Bush Avenue
St. Paul, Minnesota 55106
Attn: Code 0013 R&D
VIA: H. C. Zeman, Security Administrator

North American Aviation, Inc. — 1
Space & Information Systems Division
12214 Lakewood Boulevard
Downey, California 90242
Attn: Technical Information Center
D/096-722 (AJ01)

Rocket Research Corporation — 1
520 South Portland Street
Seattle, Washington 98108

Rocketdyne — 1
6633 Canoga Avenue
Canoga Park, California 91304
Attn: Library, Department 596-306

Rohm and Haas Company — 1
Redstone Arsenal Research Division
Huntsville, Alabama 35808
Attn: Librarian

APPENDIX F DISTRIBUTION LIST (Continued)

Space Technology Laboratory, Inc. 1
1 Space Park
Redondo Beach, California 90200
Attn: STL Tech. Lib. Doc. Acquisitions

Texaco Experiment Incorporated 1
P. O. Box 1-T
Richmond, Virginia 23202
Attn: Librarian

Thiokol Chemical Corporation 1
Alpha Division, Huntsville Plant
Huntsville, Alabama 35800
Attn: Technical Director

Thiokol Chemical Corporation 1
Elkton Division
Elkton, Maryland 21921
Attn: Librarian

Thiokol Chemical Corporation 1
Reaction Motors Division
Denville, New Jersey 07834
Attn: Librarian

Thiokol Chemical Corporation 1
Rocket Operations Center
P. O. Box 1640
Ogden, Utah 84401
Attn: Librarian

Thiokol Chemical Corporation 1
Wasatch Division
P. O. Box 524
Brigham City, Utah 84302
Attn: Library Section

United Aircraft Corporation 1
Corporation Library
400 Main Street
East Hartford, Connecticut 06118
Attn: Dr. David Rix

United Aircraft Corporation 1
Pratt & Whitney Fla. Res. & Dev. Ctr.
P. O. Box 2691
W. Palm Beach, Florida 33402
Attn: Library

United Aircraft Corporation 1
United Technology Center
P. O. Box 358
Sunnyvale, California 94088
Attn: Librarian

General Electric Company 1
Apollo Support Department
P. O. Box 2500
Daytona Beach, Florida 32015
Attn: C. Day

British Defence Staff, British Embassy 1
3100 Massachusetts Avenue
Washington, D. C. 20008
Attn: Scientific Information Officer
VIA: National Aeronautics and Space Administration
Washington, D. C. 20546
Attn: Office of International Programs

Defence Research Member 1
Canadian Joint Staff (W)
2450 Massachusetts Avenue
Washington, D. C. 20008
VIA: National Aeronautics and Space Administration
Washington, D. C. 20546
Attn: Office of International Programs

Department of Commerce 1
Office of Export Control
Washington, D. C.
Attn: Chief, Chemistry & Fuels Section
Paul M. Terlizzi

AFRPL (RPCL) 1
Edwards, California 93523

Callery Chemical Company 1
Research and Development
Callery, Pennsylvania 16024
Attn: Document Control

FMC Corporation 1
Chem. Research & Development Center
P. O. Box 8
Princeton, New Jersey 08540
Attn: Security Officer

Ethyl Corporation 1
P. O. Box 3091
Baton Rouge, Louisiana 70805

Hynes Chemical Research Corp. 1
308 Bon Air Avenue
Durham, North Carolina 27704

Olin Mathieson Chemical Corporation 1
Research Library 1-K-3
275 Winchester Avenue
New Haven, Connecticut 06511
Attn: Mail Control Room
Mrs. Laura M. Kajuti

Pennsalt Chemicals Corporation 1
Technological Center
900 First Avenue
King of Prussia, Pennsylvania 19406

Purdue University 1
Lafayette, Indiana 27907
Attn: M. J. Zurcrow

Commanding Officer 1
Picatinny Arsenal
Liquid Rocket Propulsion Laboratory
Dover, New Jersey 07801
Attn: Technical Library

General Electric Company 1
Missile & Space Division
Re-Entry System Department
3198 Chestnut Street
Philadelphia, Penna.
Attn: D. W. Bahr
A. D. Cohen